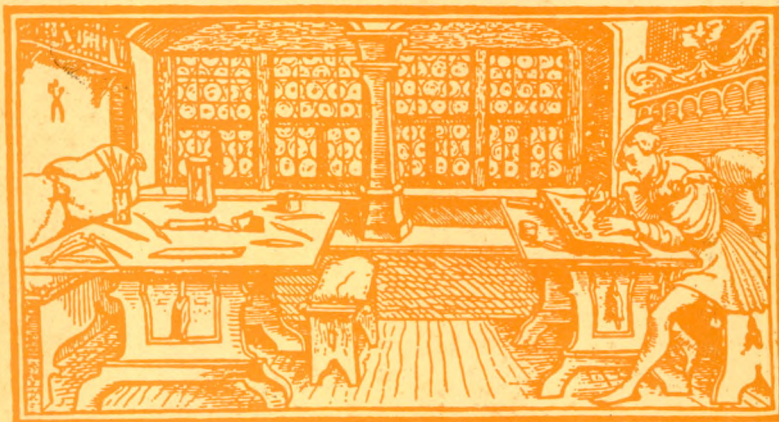


STUDIA

UNIVERSITATIS
BABES-BOLYAI

C h e m i a

C L U J - N A P O C A 1 9 9 6



**EDITORIAL BOARD OF
STUDIA UNIVERSITATIS BABEȘ-BOLYAI CHEMIA**

EDITOR - IN - CHIEF: Prof. dr. SORIN MAGER

EDITORIAL BOARD: Prof. dr. IOAN A. SILBERG
Prof. dr. ȘERBAN AGACHI
Prof. dr. IOAN BALDEA
Prof. dr. EMIL CORDOȘ
Prof. dr. MIRCEA DIUDEA
Prof. dr. LIVIU ONICIU
Prof. dr. IONEL CĂTĂLIN POPESU
Prof. dr. IOAN SILAGHI-DUMITRESCU
Prof. dr. CRISTIAN SILVESTRU
Prof. dr. MIRCEA VLASSA
Prof. dr. EUGENIA GAVRILĂ
Prof. dr. NICU DULĂMIȚĂ

EXECUTIVE EDITOR: Prof. dr. LUMINIȚA SILAGHI-DUMITRESCU

STUDIA
UNIVERSITATIS BABES-BOLYAI

CHEMIA

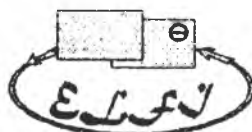
2

1996

Special Issue

Dedicated to

**“ Electrochemistry - a Frontier Field of Theoretical
and Practical Interest” - ELFI'96**



31st October - 3rd November 1996

- CLUJ-NAPOCA -

SECTIONS

of the Symposium



**"ELECTROCHEMISTRY
a FRONTIER FIELD of
THEORETICAL and PRACTICAL INTEREST"**

① Electrosyntheses

② Electroanalytical Chemistry

**③ Corrosion, passivation and electro-
chemical metal deposition**

**④ Bioelectrochemistry and
Environmental electrochemistry**

**⑤ Electrochemical conversion and
Electrochemical engineering**

STUDIA UNIVERSITATIS BABES-BOLYAI

CHEMIA

Redacția: 3400 CLUJ-NAPOCA, str. M.Kogălniceanu, 1 • Tel. ...

SUMAR - CONTENTS

S. TORII, Generation and synthetic use of reactive Transition Metal Complexes in Electrolysis Systems.....	1
D. FLONER, J. P. HURVOIS, P. JEGO, C. MOINET, Cellule a circulation a electrodes poreuses. Applications en electrosynthese organique et Organometallique.....	6
J. P. CAIRE, Prometheus: A simple cod for modelling thermal and current distribution problems.....	23
D. BRITZ, Recent advances in electrochemical digital simulation.....	31
G. INZELT, The origin and mechanism of electrochemical oscillations.....	47
M. JITARU, J. LESSARD, D. ALOWY, Heterogeneous triple bond electroreduction of saturated and unsaturated nitriles.....	70
M. UNGUREANU, E. SAINT-AMAN, I. ION, A. POPESCU, T. VISAN, J. C. MOUTET A. C. ION, Electrochemical recognition od Group I or II metal cations by redox active ionophores in homogeneous solutions or by functionalized modified electrode.....	79
M. JITARU, C. MOINET, M. DARABANTU, Electrochemical behaviour of a new ozazolidine derivative, intermediate in the chloromycetine synthesis.....	89
V. DANCIU, V. COSOVEANU, D. LEMNARU, A. M. MARTRE, G. MOUSSET, Electrochemical and structural characterization of Ti/TiO ₂ electrodes obtained by thermal methods and tested in the electrod reduction of 4.4'-dinitrostilbene-2.2'-disulfonic acid (DNSS).....	96
A. M. MARTRE, S. LEMANCEAU, G. MOUSSET, V. COSOVEANU, V. DANCIU, Reduction selective de Molecules Polyfonctionnelles psr des complexes du titane(III) electrogenerers en milieux aqueux et non aqueux.....	106
I. IVANOV, St. RASHKOV, Electroextraction of zinc from sulphate electrolytes containing manium, antimony and nickel ions.....	122
T. I. BREV, St. RASHKOV, Processes during the electrorefining and electrowinning of lead.....	138

D. A. LOWY, M. JITARU, B. C. TOMA, I. A. SILBERG, L. ONICIU, The electrosynthesis of propionitrile on the pilot plant scale.....	15
D. TKALENKO, N. CHIMLENKO, T. VISAN, M. TKALENKO, C. GHIGA, Rate-Determining steps in the electroreduction of complex oxyanions in molten salts.....	15
I. A. SILBERG, F. CIOMOS, I. SILAGHI-DUMITRESCU, Ion molecule interaction in organic electrochemical systems. III. Acrylonitrile-quaternary ammonium cations adducts and their possible implications in electrohydrodimerization processes.....	16
H. HAIDUC, P. ILEA, A. NICOARA, S. DORNEANU, L. ONICIU, Kinetic study of copper electrocrystallization.....	17
L. DIMA, D. BUGHIU, L. ANICAL, C. TRIFU, Current-concentration correlation for anodic dissolution of zinc in sulphate electrolytes.....	18
L. ANICAL, T. VISAN, A. MEGHEA, C. TRIFU, Electrochemical colouring of anodized aluminium in AgNO ₃ based electrolytes.....	19
D. A. LOWY, H. O. FINKLEA, Electrochemical investigation of ionically assembled multilayer systems.....	20
C. I. SEMIONESCU, AI. DUCA, M. GROVU-IVANOIU, I. CIANGA, M. GRIGORAS, Electrochemical polymerization of some monomers with thiophene units and Schiff base structure.....	21
S. COLDEA, The Electrostatic Properties of a Multispecies Ionospheric Plasma.....	22
M. SIMA, M. BUDA, Cyclic Voltammetry of Poly-orto-Metoxyaniline Films.....	22
I. LEOCA, O. POGACEANU, I. C. STEFAN, E. CORDOS, The influence of the lipophilic salt added to the PVC-based membranes upon the response of a magnesium-selective electrode.....	23
I. LEOCA, I. C. STEFAN, E. CORDOS, The response of a modified PVC-Based pH electrode.....	24
A. FODOR, L. MURESAN, A. SUTEU, I. C. POPESCU, Electrochemical study of vanadium containing Keggin-type heteropolytungstate and heteropolymolybdate acids.....	24
S. K. KOVACH, Yu. M. STASYUK, V. V. PANYKO, Electrochemical processes at the Cu ₆ PS ₅ I electrolyte interfase.....	25
M. BUDA, N. IBRIS, M. PALI, T. VISAN, Cyclic voltametry of powder sulfide ores dissolution.....	25
D. BUGHIU, M. BUDA, L. DIMA, Anodic behaviour of zinc in cyanide solutions.....	26
E. M. PICA, M. JITARU, I. MARIAN, N. SANTA, Electrochemical Characterization of Some Metal Phthalocyanines Electrodes.....	28
L. BENEA, O. MITOSERIU, M. LAKATOS-VARSANY, Electrodeposition of Zirconium oxide and silicon carbide with nickel.....	28
E. M. RUS, D. CONSTANTIN, The Effect of Antimony on Electrochemical Behaviour of Lead/Acid Grids.....	31
D. CONSTANTIN, L. ONICIU, E. M. RUS, The Electrochemical Behaviour of Sintered Cadmium Electrodes in Alkaline Electrolyte.....	32
L. ONICIU, S. AVRAM, G. TARALUNGA, L. D. BOBOS, C. S. BOLLA, Cathode Materials from Lithium Batteries Characterized by Cyclic Voltammetry.....	33
V. VOINA, L. MURESAN, L. ONICIU, The Electrochemical Behaviour of Zinc in KOH Solutions, Under Potentiodynamic Technique (RDE).....	34

**PRESENTATION OF THE SYMPOSIUM
"ELECTROCHEMISTRY - A FRONTIER FIELD OF THEORETICAL AND
PRACTICAL INTEREST"**

Under the patronage of "Babes-Bolyai" University of Cluj-Napoca, the Cluj - Branch of the Roumanian Academy of Science and the Ministry of Research and Technology took place between 31st October - 3rd November 1996, the International Symposium "Electrochemistry - a Frontier Field of Theoretical and Practical Interest" - ELFI, initiated and organized by the Group of Chemical Research from the Faculty of Chemistry and Chemical Engineering.

There were three main goals of this symposium: to bring together the Roumanian electrochemists, to give the possibility of revealing the value of the Roumanian electrochemical school to foreign scientists and, last but not least, the presentation of our University and country.

The ELFI - Symposium is meant to continue the Roumanian Electrochemical National Seminary and more, to become a correspondent event for the Journées d'Electrochimie in our region. In order to ensure the proper conditions for this complementarity it is intended to schedule the ELFI - Symposium every two years, in the Central and Eastern European countries under the high patronage of ISE, in the years that alternate with those of the Journées d'Electrochimie.

In 1996 at ELFI participated 124 scientists from 14 countries. We were honored to have among our guests 20 great foreign scientists like Prof. Sigeru Torii (Japan), Prof. Claude Moinet and Prof. Guy Mousset (France), Prof. Luigi Campanella (Italy), Prof. Jean Lessard (Canada), Prof. Dieter Britz (Denmark), Prof. Gyorgy Inzelt (Hungary) a.s.o. The full papers were refereed by the Scientific Board of the ELFI and those accepted are published in the present issue of the journal "Studia Universitatis Babes-Bolyai - Chemia".

The first impact of this international meeting is the agreement of Prof. Torii, Lessard and Inzelt for the scientific cooperation with the Group of Chemical Research. We hope also that the publications of the papers of well-known scientists in the field of electrochemistry will increase the quality and the recognition of our journal

Executive Editor

Dr. Luminița Silaghi-Dumitrescu

GENERATION AND SYNTHETIC USE OF REACTIVE TRANSITION METAL COMPLEXES
IN ELECTROLYSIS SYSTEMS

Sigeru Torii

*Department of Applied Chemistry, Faculty of Engineering,
Okayama University, Okayama 700, Japan*

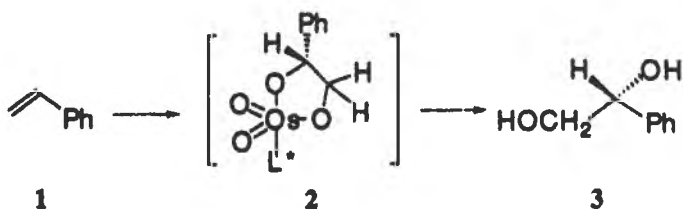
The metal complexes generated in electrooxidation and reduction media are expected to exhibit unusual behavior due to the unique phenomena in the vicinity of the electrode surface, which may enable us to open a promising entry to a new mode of metal-catalyzed reactions. Mean while, asymmetric synthesis by the aid of homogeneous metal catalysts with well designed chiral ligands is a challenging subject in modern organic chemistry. Only a few electrochemical versions have, however, been envisioned presumably because of lack of the suitable mediatory systems. This paper deals with Os and Mn complexes recycling in the electrooxidative media together with their application for the synthesis of *l*-shikonin. The former opened new mode of Pd-catalyzed reactions and the later allow us to realize electrochemical asymmetric dehydroxylation and epoxidation of olefins.

(1) Electrochemical Os-Catalyzed Asymmetric Dihydroxylation of Olefins:

Notable success of chiral ligands for Os-catalyzed asymmetric dihydroxylation of olefins stimulates further development as an electrochemical process, which could be encountered:

- (1) minimum use of co-oxidant $[K_3Fe(CN)_6]$ for potassium osmate,
- (2) decreasing use of the amount of $K_2OsO_2(OH)_4$,
- (3) finding novel co-oxidant systems.
- (4) performing in an undivided cell.

As a preliminary study, we investigated the above two beginning items.¹ Recently, the effective chiral ligands for enantioselective dihydroxylation of olefins have intensively been investigated. Among the reported asymmetric dihydroxylation systems, the superiority of a $H_2O/t\text{-BuOH}-K_3Fe(CN)_6/K_2CO_3$ system with chiral ligands, *i.e.*, dihydroquinidine (DHQD) and/or dihydroquinine (DHQ) derivatives, has been mentioned.² Herein we disclose a preliminary studies on the electrochemical Os-catalyzed asymmetric dihydroxylation of olefins with Sharpless' ligands (L^*).



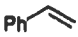
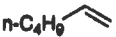

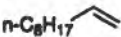


As shown in Table I, the reconfirmative attempt for Sharpless' chiral diol synthesis on styrene was fully successful by obtaining 97.2 % ee in 88 % conversion yield (Scheme 1). Our initial efforts were focused on the chiral Os-complex assisted electrosynthesis to examine mediator activity by employing 0.3 equivalent (10 weight %) of potassium ferricyanide as a co-oxidant. The mixture was electrolyzed in an undivided cell equipped with two Pt-electrodes under a constant current of 2 mA/cm² under vigorous stirring (applied voltage: 1.0–3.0 V). Happily enough, after passage of 2.33 F/mol of electricity, we could obtain the desired diol 3 in very high values both on % ee and conversion yield (Table I, Run A), clearly demonstrating that the chiral induction system together with the co-oxidant does work under the employed electrolysis conditions. Further reducing the amount of the co-oxidant [K₃Fe(CN)₆] to 0.1 equivalent did not give any change on the asymmetric induction as well as the conversion yields (Table I, Run B). Under a similar electrolysis conditions, small change in the yields has been found when the amount of the co-oxidant was diminished to 0.05 mmol. We obtained the diol 3 in 95.3 % ee and 82 % conversion yield. It is worthy to note that both potassium chloride and potassium bromide are also effective as co-oxidants in the absence of K₃Fe(CN)₆. The electrolysis systems of K₂OsO₂(OH)₄/KCl and/or K₂OsO₂(OH)₄/KBr afforded ca. 92 – 93 % ee at room temperature in spite of their inferior conversion yields (ca. 48 ~ 65%).

Next attempt was to clarify the limitation of reducing the amount of potassium osmate in the electrolytic recycling system. The result obtained by use of one-fourth amount of the Os-catalyst (Table I, Run C) demonstrates that asymmetric dihydroxylation of styrene proceeded still in high yield of enantiomeric excess (ca. 99 % ee). However, the decrease of the conversion yield down to 72 % should be improved. The efficient formation of chiral osmate ester 2 in an electrolytic bulk solution may reflect high values of enantiomeric excess in every electrolysis conditions (Runs A, B, and C). Enantiomeric excesses obtained in the electrolytic asymmetric dihydroxylation of various olefins under the typical experimental conditions are summarized in Table II. The relatively better % ee and conversion yield are obtained in respects to the figures reported in the literatures.²

Table I Chiral Os-Complex Assisted Electrosynthesis of Chiral Diol from Styrene

Conditions	Reexam. Sharpless' Conditions	Electrolysis Run		
		A	B	C
Styrene	1	1	1	1
<i>t</i> -BuOH	5	5	5	5
H ₂ O	5	5	5	5
K ₂ CO ₃	3	3	3	3
(DHQD) ₂ PHAL	0.01	0.01	0.01	0.01
K ₂ Os(CN) ₆	3	0.3	0.1	0.1
K ₂ OsO ₂ (OH) ₄	0.002	0.002	0.002	0.0005
Electricity (F/mol)	-	2.33	2.33	2.33
Time (h)	-	31.2	31.2	31.2
Temp. (°C)	0	0	0	0
Conv. Yield, (%)	88	95	95	72
% ee	97.2	97.2	97.3	99.0

Table II Chiral Os-Complex Assisted Electrosynthesis of Chiral Diols

Olefin	Conv. %	Yield, %	Ee, %	Config.	Obs[α] _D
	95	97.3	R(-)	-63.4	
	71.2	84.1	R(+)	+14.1	
	75	86.4	R(-)	-29.1	
	87.0	86.3	R(-)	-29.1	
	69 (93, GC)	91.8	R(+)	+10.9	
	92.8	90.3	R(-)	-13.1	
	97.0	100	RR(+)	+91.0	

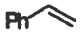



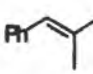

In continuation of our research in asymmetric dehydroxylation reactions, we found that iodine and iodine-iodide combinations are efficient co-oxidant for the osmate recycling.³ Namely, iodine-assisted chemical and electrochemical asymmetric dihydroxylation of various olefins in I₂-K₂CO₃-K₂OsO₂(OH)₄ and I₂-K₃PO₄/K₂HPO₄ systems with Sharpless' ligand provided the optically active glycols in excellent yield and high enantiomeric excess. Iodine (I₂) was used stoichiometrically for the chemical dehydroxylation, and good results were obtained with nonconjugated olefins in contrast to the case of potassium ferricyanide as a co-oxidant. The potentiality of I₂ as a co-oxidant under stoichiometric conditions has been proven to be effective as an oxidizing mediator in electrolysis systems (Table III). Iodine-assisted asymmetric electro-dihydroxylation of olefins in either a *t*-BuOH/H₂O(1/1)-K₂CO₃/(DHQD)₂PHAL-(Pt) or *t*-BuOH/H₂O(1/1)-K₃PO₄/K₂HPO₄/(DHQD)₂PHAL-(Pt) system in the presence of potassium osmate in an undivided cell. Irrespective of the substitution pattern, all the olefins afforded the diols in high yields and excellent enantiomeric excess (Table IV).

Table III Chiral Os-Complex Assisted Electrosynthesis of Chiral Diol from Styrene **Table IV Chiral Os-Complex Assisted Electrosynthesis of Chiral Diols**

Conditions	Electrolysis Run	
	D	E
Styrene	1	1
<i>t</i> -BuOH	5	5
H ₂ O	5	5
K ₂ CO ₃	3	-
(DHQD) ₂ PHAL	0.01	0.01
K ₂ O ₈ O ₂ (OH) ₄	0.002	0.0005
I ₂	0.5	0.5
K ₂ HPO ₄ /K ₂ HPO ₄	-	1.2/1.8

Electricity (F/mol)	2.33	2.33
Time (h)	31.2	31.2
Temp. (°C)	0	0

Conv. Yield, (%)	93.7	96.0
% ee	97.9	97.1

Olefin	Conv. Yield, %	Ee. %	Config.
	96.0	97.1	R
	87.6	>99	R
	87.6	>99	R
	92.9	97.3	RR
	86.0	87.0	R
	88.2	>99	RR

(2) Electrochemical Mn-Catalyzed Asymmetric Epoxidation of Olefins:

We have also examined electrochemical asymmetric epoxidation by using Jacobsen-Katsuki type manganese complexes. Some typical examples are listed in Table V. Under the lower temperature, both conversion yields and enantiomeric excess values are improved.

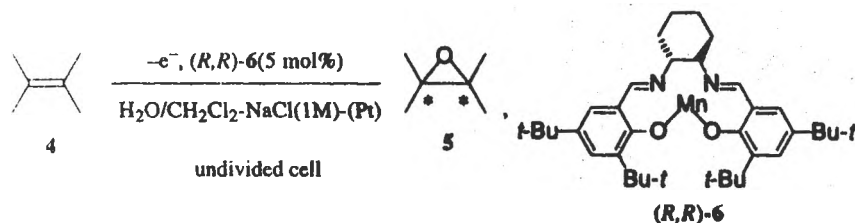

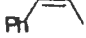
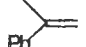
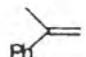
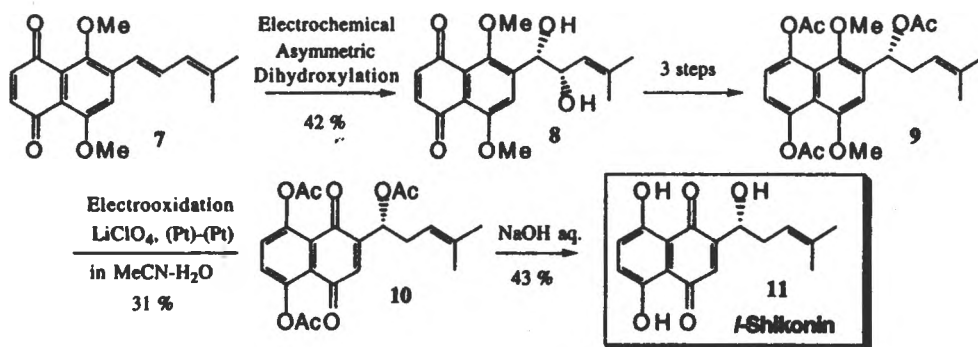


Table V Asymmetric Electro-Epoxidation of Olefins with Mn-Complexes

Entry	Substrate	Temp., °C	Epoxide, 6 Yield, %	ee, %	Config.
1		0	70	86	1 <i>R</i> , 2 <i>S</i>
2		room temp.	57	81	1 <i>R</i> , 2 <i>S</i>
3		0	65	63	R
4		room temp.	44	47	R

(3) Synthesis of *l*-shikonin Involving Electrochemical Asymmetric Dihydroxylation Reaction:

The novel I_2 -mediated asymmetric dihydroxylation reactions could be used successfully for the synthesis of *l*-shikonin as shown below.⁴



REFERENCES

- 1) S. Torii, P. Liu, and H. Tanaka, *Chem. Lett.*, **1995**, 319.
- 2) K. B. Sharpless, *J. Org. Chem.*, **54**, 2263, **1989**; P.-O. Norrby, H. C. Kolbe, and K. B. Sharpless, *J. Am. Chem. Soc.*, **116**, 8470, **1994**, and references cited therein.
- 3) S. Torii, P. Liu, N. Bhuvanewari, Christian Amatore, and Anny Jutand, *J. Org. Chem.*, **61**, 3055, **1996**.
- 4) S. Torii and K. Akiyama, to be published.

**CELLULE A CIRCULATION A ELECTRODES POREUSES.
APPLICATIONS EN ELECTROSYNTHESE ORGANIQUE ET ORGANOMETALLIQUE.**

Didier Floner, Jean Pierre Hurvois, Patricia Jégo, Claude Moinet.

*Laboratoire "Electrochimie et organométalliques".
Université de Rennes I, campus de Beaulieu, 35042 Rennes Cedex (France)*

RESUME

L'utilisation, en électrosynthèse organique et organométallique, de cellules à circulation à électrodes poreuses de grande surface spécifique (feutre de graphite) permet de réduire ou d'oxyder, avec une bonne sélectivité des substrats variés avec des taux de transformation élevés (>95 %) après un seul et bref passage (quelques secondes) à travers l'électrode. Le produit résultant qui, dans certains cas, possède une durée de vie limitée peut alors être utilisé dès la sortie de l'électrode poreuse dans une réaction chimique ou électrochimique sur une seconde électrode poreuse (cellule "redox"). Diverses applications montrant l'intérêt du procédé soit en électrolyse directe, soit en électrolyse indirecte utilisant un médiateur (catalyseur) dans un procédé bi-phasique ex-cell sont présentées. Par ailleurs, des électrodes poreuses modifiées dans la masse par greffage de complexes organométalliques ont été élaborées pour des applications en électrocatalyse réalisées en cellule à circulation.

INTRODUCTION

L'avantage d'une cellule d'électrolyse fonctionnant avec un seul passage de la solution à travers une électrode poreuse de grande surface spécifique est d'isoler rapidement de l'électrode le produit formé avec un bon rendement. La durée d'une électrolyse dépend en effet de la surface spécifique A/V (A: surface active de l'électrode, V: volume de la solution en électrolyse), et cette

durée est d'autant plus faible que la surface spécifique est plus élevée. Des électrodes poreuses utilisées sans recyclage de la solution peuvent présenter de très grandes surfaces spécifiques: la surface active A est d'autant plus importante que l'électrode est plus divisée et le volume à considérer est celui contenu à l'intérieur de cette électrode. Le feutre de graphite est, parmi les matériaux poreux conducteurs, celui qui possède l'une des surfaces spécifiques les plus élevées. Il est ainsi possible, sur feutre de graphite, de réduire ou d'oxyder des substrats variés avec des taux de transformation élevés (> 95%) après un seul et bref passage (quelques secondes) à travers l'électrode. Le produit résultant qui, dans certain cas, possède une durée de vie limitée peut être mis en oeuvre dès la sortie de l'électrode poreuse dans une réaction chimique ou électrochimique sur une seconde électrode poreuse (cellule "redox"). Par rapport aux techniques d'électrolyse classiques, l'utilisation d'électrodes poreuses sans recyclage permet ainsi de diminuer notablement l'échelle de temps. L'échelle de temps est, en effet, un paramètre très important en électrochimie organique ou organométallique, tout particulièrement lorsque des réactions chimiques interviennent parallèlement aux réactions électrochimiques (mécanismes EC, ECE,.....).

Cependant, une électrode poreuse ne peut-être utilisée dans toutes les électrolyses. Des difficultés techniques peuvent apparaître soit en présence d'espèces insolubles qui colmatent l'électrode (substrat initial ou produit), soit en présence de dégagement gazeux trop importants qui perturbent l'écoulement de la solution et provoquent une mauvaise répartition des potentiels de travail à l'intérieur de l'électrode poreuse.

RESULTATS ET DISCUSSION

1-Principe des cellules d'électrolyse à une ou deux électrodes poreuses

1.1-Montage à une électrode poreuse

Le schéma de principe à une électrode poreuse équipée de deux contre-électrodes est représentée sur la figure 1.

Les contre-électrodes disposées en amont et en aval dans des compartiments séparés par des membranes anioniques ou cationiques, sont de mêmes sections que l'électrode poreuse et parallèles aux faces d'entrée et de sortie de celle-ci. La mise en place de deux contre-électrodes en

amont et en aval assure une répartition des potentiels de travail suffisamment étroite [1-3] pour permettre une bonne sélectivité de la réaction électrochimique (cf. § 2.1.1).

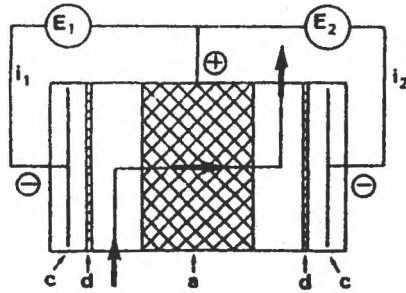


Fig. 1- Schéma de principe d'une cellule à une anode poreuse disposée entre deux contre-électrode.
 (a) anode poreuse; (c) contre-électrodes; (d) membranes
 E_1, E_2 : alimentations stabilisées; i_1, i_2 : intensité des courants
 → sens de circulation de l'électrolyte

L'intensité du courant d'électrolyse est la somme des intensités des courants amont et aval ($i = i_1 + i_2$); elle est maintenue constante pendant toute la durée de l'électrolyse et elle est déduite de la loi de Faraday en considérant la concentration de l'espèce électroactive, le débit de la solution et le nombre de faradays échangés dans la réaction électrochimique.

1.2- Montage à deux électrodes poreuses consécutives de polarité opposées (cellule "redox").

Le montage, schématisé sur la figure 2, à deux électrodes poreuses consécutives de polarités opposées séparées par un isolant poreux de faible épaisseur, permet d'effectuer une seconde réaction électrochimique immédiatement après la première. La méthode est d'un intérêt certain lorsque l'espèce produite sur la première électrode poreuse est peu stable.

La présence de deux contre-électrodes en amont et en aval et de trois circuits d'électrolyse assure d'une part, une bonne répartition des potentiels de travail à l'intérieur des électrodes poreuses et permet d'autre part, d'ajuster les intensités des courants de réduction et d'oxydation aux quantités d'électricité mises en jeu respectivement dans les réactions cathodique et anodique. Dans le cas particulier de la figure 2:

$$i_{\text{red}} = i_1 + i_2 \quad i_{\text{ox}} = i_2 + i_3$$

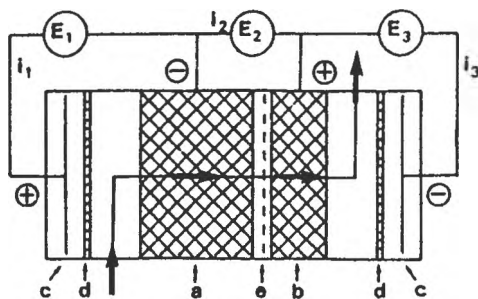


Fig 2-Schéma de principe d'une cellule "redox" à circulation à deux électrodes poreuses consécutives (a) cathode poreuse; (b) anode poreuse; (c) contre-électrodes; (d) membranes; (e) isolant poreux; E_1, E_2, E_3 : alimentations stabilisées; i_1, i_2, i_3 : intensités des courants.
 ➔ sens de circulation de l'électrolyte.

Cependant, et en particulier lorsque la quantité d'électricité qui intervient au niveau de la seconde électrode poreuse est inférieure à celle mise en jeu sur la première électrode poreuse, l'expérience montre que le troisième circuit d'électrolyse peut-être supprimé ($i_3 = 0$)

2-Exemples d'applications.

A l'échelle du laboratoire nous avons construit et utilisé des cellules équipées d'électrodes de 4 - 5,2 ou 8 cm de diamètre et de 0,6 ou 1,2 cm d'épaisseur. Les concentrations en substrat dans divers solvants aqueux ou non aqueux varient généralement de 10^{-3} à $2 \cdot 10^{-2}$ mol l^{-1} et les débits de solution sont d'environ $12 \text{ cm}^3 \text{ mn}^{-1}$ pour une électrode de 8 cm de diamètre.

2.1- Electrosynthèses directes sur feutre de graphite.

2.1.1- Montage à une électrode poreuse.

Diverses oxydations ou réductions électrochimiques ont été réalisées sur électrode en feutre de graphite sans recyclage de la solution. Elles concernent la réduction de nitrobenzènes en phénylhydroxylamines [4], de nitroporphyrines en hydroxylaminoporphyrines ou en aminoporphyrines [5], de thiazines substituées [6] ou l'oxydation de dihydropyridines [7-9], de dihydrobenzazépines [10], d'indazolinone [11,12], d'urazoles [12], de phthalhydrazides [12] ou des tous complexes $\text{Cr}(\text{CO})_5\text{X}^-$ ($\text{X} = \text{CN}, \text{I}$) [13].

Les quelques exemples qui suivent illustrent les possibilités offertes par les cellules à électrode poreuse.

Le voltammogramme cyclique de la dihydrobenzo(c)-[2,7]naphtyridine présente en milieu tampon acétique ($\text{CH}_3\text{CO}_2\text{H}$ 0,5 M + $\text{CH}_3\text{CO}_2\text{Na}$ 0,5 M) deux pics d'oxydation successifs (pic A : $E_{pA1} = 0,78$ V ECS; pic B : $E_{pA2} = 0,98$ V ECS) (figure 3, courbe a). La première oxydation à 2F par mole intervient au niveau du cycle pyridinique (réaction 1) alors que la seconde concerne la fonction amino. En contrôlant rigoureusement l'intensité du courant et la vitesse d'écoulement de la solution, l'électrolyse en cellule à circulation [8] sur anode en feutre de graphite permet d'oxyder sélectivement au niveau du pic A comme le montre le voltammogramme de la solution obtenue en sortie de cellule ; le pic A a totalement disparu sans que le pic B soit affecté (figure 3, courbe b). Après électrolyse l'aminonaphtyridine N-oxyde est isolée avec un rendement de 65 %.

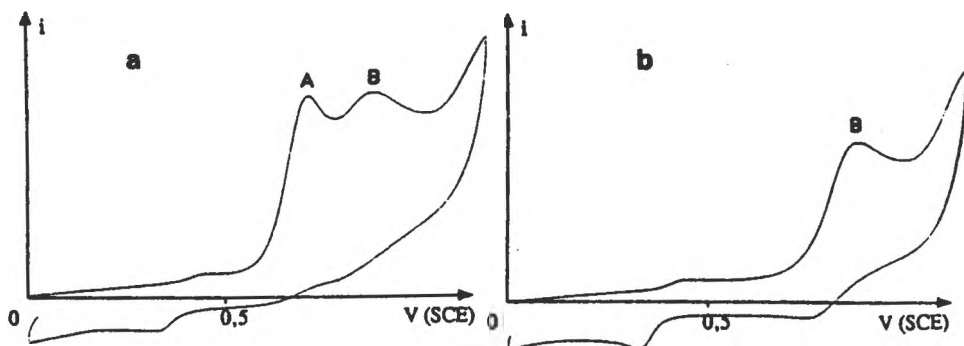
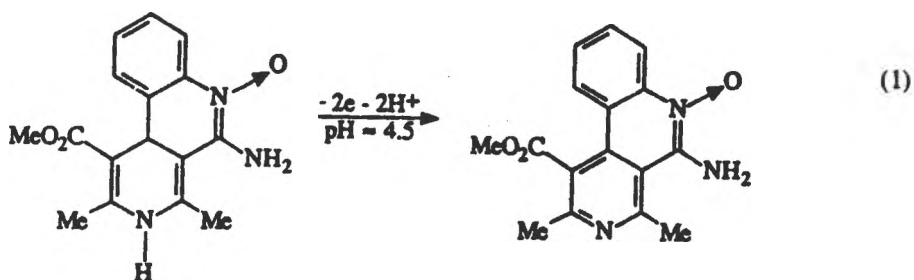
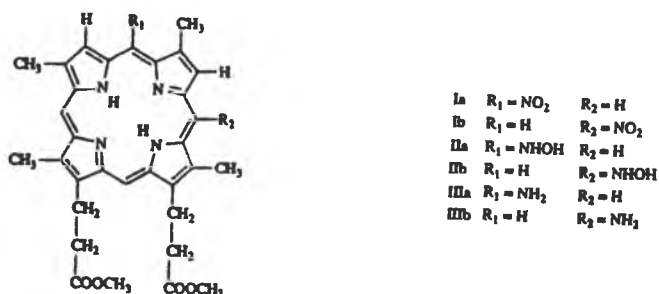


Fig.3 - Voltammogrammes cycliques de la dihydrobenzo (c)-[2,7] naphtyridine.

Electrode : carbone vitreux; tampon acétique 0,5 M + éthanol 1-1; vitesse de balayage $0,1 \text{ Vs}^{-1}$
a - avant oxydation; b - après oxydation sur feutre de graphite.

La parfaite efficacité du dispositif à une électrode poreuse localisée entre deux contre-électrodes se traduit donc par un taux de transformation élevé après un seul passage de la solution dans l'électrode et par une bonne répartition du potentiel de travail dans l'anode poreuse qui conduit à une sélectivité élevée.

La réduction électrochimique du mélange d' α et β -nitrodeutéroporphyrines Ia et Ib n'est réalisable qu'en milieu méthanol à 3 % d'acide sulfurique.



Les produits de réduction (hydroxylamines IIa et IIb, amines IIIa et IIIb) étant peu stables dans ce milieu ne peuvent être préparés dans une cellule à électrode plane, la durée de l'électrolyse étant trop importante.

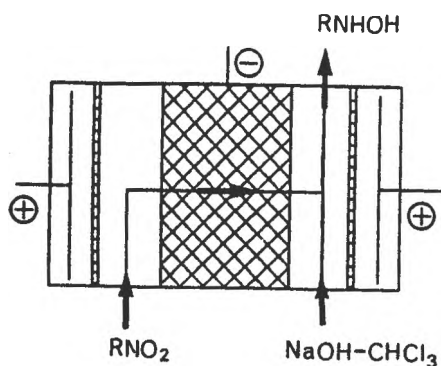
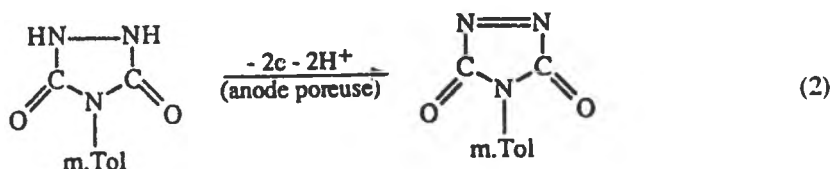


Fig.4 - Réduction de nitrodeutéroporphyrines en milieu méthanol à 3% d'acide sulfurique sur cathode poreuse en feutre de graphite. Neutralisation et extraction en continu en sortie d'électrode.

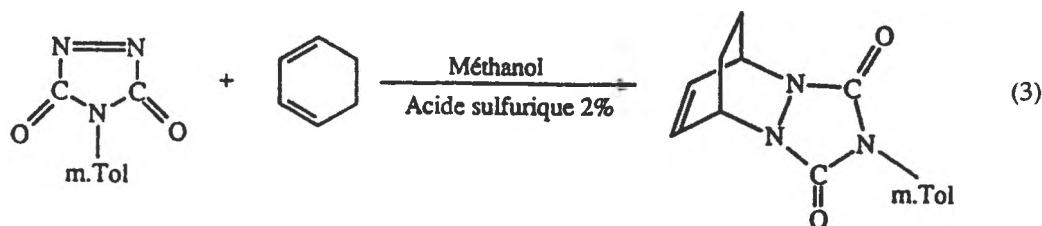
Par contre, la réduction sur cathode poreuse en feutre de graphite suivie d'une neutralisation par de la soude et une extraction en continu par du chloroforme soit en sortie de cellule (préparation de l'amine) soit en sortie d'électrode (préparation de l'hydroxylamine) (figure 4) permet

d'isoler, après purification, le mélange d'hydroxylamines IIa et IIb avec un rendement de 24 % et le mélange d'amines IIIa et IIIb avec un rendement de 64 % [5]. Tous les essais de préparation de ces composés par réduction chimique ont échoué.

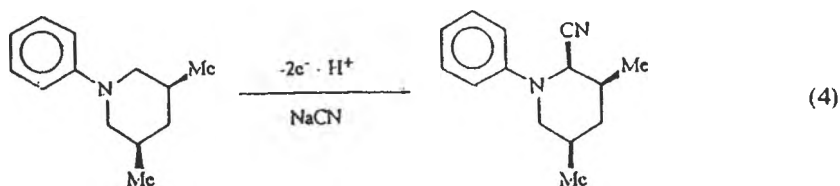
Les 1,2,4-triazoline-3,5 diones substituées en position 4 sont des espèces à fort pouvoir diénoophile mais elles sont très sensibles aux attaques nucléophiles. Ainsi, la 4-m.tolyl-1,2,4-triazoline-3,5 dione obtenue par oxydation à 2 F par mole, sur anode en feutre de graphite, de la 4-m.tolyl-1,2,4-triazolidine-3,5-dione en milieu méthanol à 2 % d'acide sulfurique évolue rapidement et ne peut être isolée du milieu réactionnel [12].



Cependant, l'addition de 1,3-cyclohexadiène à la solution électrolysée en sortie d'électrode poreuse permet de piéger la quasi totalité de l'espèce diénoophile et d'isoler l'adduit de Diels-Alder avec un rendement de 87 % [12].

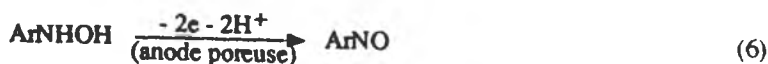


L'oxydation sur anode poreuse en feutre de graphite de 1-benzazépines [14], de tétrahydroquinolines ou de N-phényl-pipéridines en présence d'ions cyanures dans le méthanol conduit aux α -aminonitriles correspondants. Ainsi, l'oxydation à 2F par mole de la N-phényl-3,5-diméthylpipéridine en présence d'un excès d'ions cyanures (8 parts pour 1 part d'amine) en solution dans le méthanol additionné d'acétate de lithium 0.3 M fournit stéréosélectivement la N-phényl-2-cyano-3,5-diméthylpipéridine avec un rendement de 70 %.

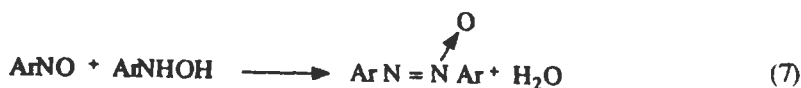


2.1.3 - Montage à deux électrodes poreuses consécutives.

L'exemple type d'utilisation d'une cellule à deux électrodes poreuses consécutives de polarités opposées est la synthèse de nitrosobenzènes à partir des composés nitrés correspondants selon la suite de réactions de réduction et d'oxydation [3,15-20].



L'oxydation, sur la seconde électrode, de la phénylhydroxylamine formée sur la première électrode est suffisamment rapide et complète pour éviter toute formation d'azoxybenzènes par condensation :

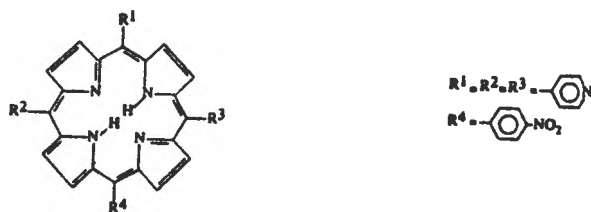


En outre, l'oxydation intervenant aussitôt après la réduction, une stabilité limitée de la phénylhydroxylamine produite sur la cathode poreuse (durée de vie de quelques dizaines de secondes) n'empêche cependant pas la synthèse de dérivés nitrosés avec des rendements élevés [3]. Par exemple, des nitrosobenzènes difficiles à obtenir par les méthodes chimiques classiques (substituants amides ou esters en position ortho [18] on été préparés, avec des rendements généralement supérieurs 90 %, en milieu alcool-tampon acétique, dans une cellule à deux électrodes poreuses et à une contre-électrode localisée en amont (*cf.* figure 2 avec $i_3 = 0$). Pour une intensité des courants identique dans

les deux circuits d'électrolyse ($i_1 = i_2$), le courant d'oxydation qui est la moitié du courant de réduction est en accord avec le bilan faradique au niveau de chaque électrode poreuse.

Une répartition différente des intensités dans les deux circuits ($i_2 = i_1/3$) ne permet d'oxyder, sur l'anode poreuse, que 50 % de la phénylhydroxylamine produite sur la cathode et la réaction (7) qui se produit en dehors de la cellule, fournit le dérivé azoxybenzène avec des rendements élevés. Cette méthode appliquée au (cyclopentadiène fer nitrobenzène)⁺ en milieu tampon acétique-alcool a conduit au complexe (di-cyclopentadiényl fer azoxybenzène)²⁺ avec un rendement de 66% [20].

Un second exemple rend compte de la souplesse du procédé "redox". Le polarogramme de la 5-(4-nitrophényl)-10,15,20-tris(4-pyridyl)porphyrine (nitroporphyrine), en milieu H₂SO₄ 0,5 M présente plusieurs vagues de réduction successives attribuées à la fonction nitro et au cycle porphyrinique de sorte que la réduction de la fonction nitro ne peut être réalisée sans affecter le macrocycle porphyrinique. Par ailleurs la forme réduite du macrocycle subit un réarrangement irréversible rapide. Les synthèses de l'aminoporphyrine et de la nitrosoporphyrine ont cependant pu être effectuées dans une cellule "redox" [19].



Dans le premier cas, l'intensité du courant sur la cathode poreuse calculée pour correspondre à 11F par mole de substrat permet de réduire à la fois le groupement nitro en fonction amino et partiellement le macrocycle. La réoxydation à 5,5 F par mole du macrocycle réduit intervient immédiatement sur l'anode poreuse et il est possible d'isoler l'aminoporphyrine avec un rendement de 80 %.

Dans le second cas, pour des intensités des courants imposées respectivement en réduction et en oxydation à 5,5 F et 3,5 F par mole de nitroporphyrine, le rendement en nitrosoporphyrine isolée après purification est de 68 %.

2.2- Electrosynthèses indirectes.

L'électrolyse indirecte réalisée selon le procédé schématisé sur la figure 5 permet de surmonter les difficultés liées à la faible solubilité des substances organiques en milieux aqueux ou hydroorganiques et à la mauvaise conductibilité électrique des milieux organiques.

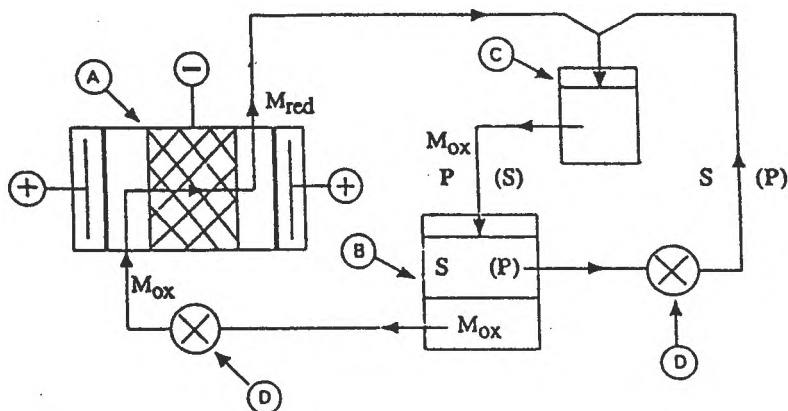
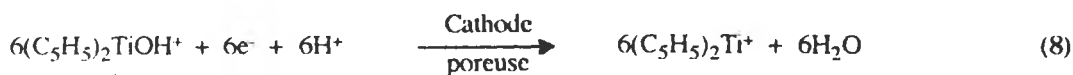


Fig.5 - Schéma de principe d'une électroréduction indirecte.

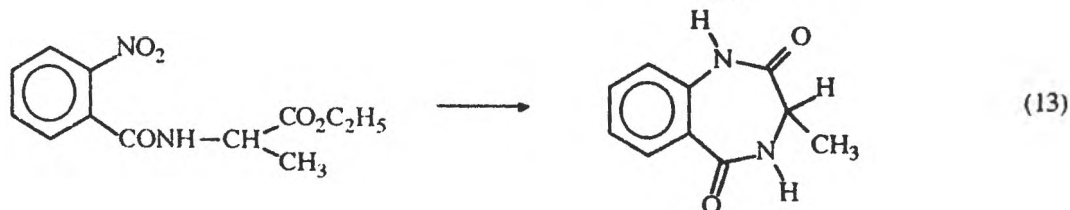
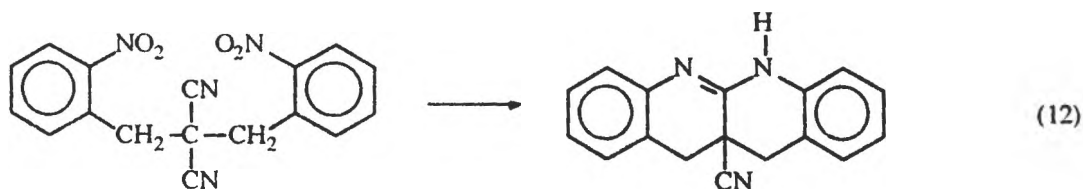
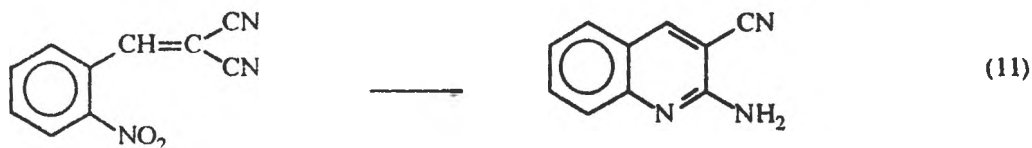
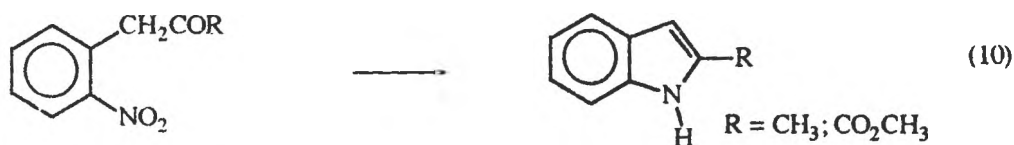
A- cellule d'électrolyse à cathode poreuse; B- réservoir - décanteur; C- réacteur; D- pompes.
 M_{red} , M_{ox} : médiateur rédox en phase aqueuse; S: substrat en milieu organique; P: produit.

Le médiateur appartenant à un couple redox soluble dans l'eau sous ses deux formes traverse l'électrode poreuse et réagit, en dehors de la cellule, avec le substrat organique en solution dans un solvant organique non miscible à l'eau. La phase aqueuse étant continuellement recyclée dans la cellule, le médiateur peut être utilisé en quantité catalytique par rapport au substrat.

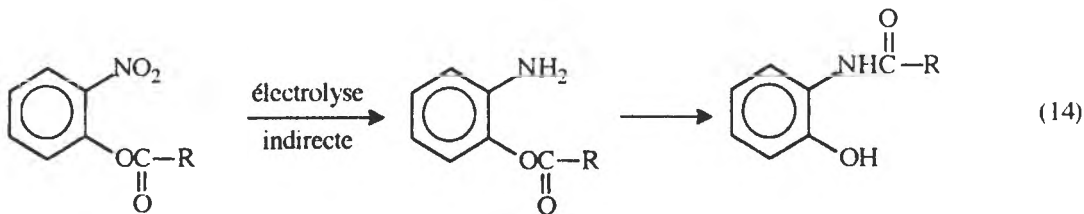
La méthode a été développée pour réduire des nitrobenzènes en solution dans le dichlorométhane ou le toluène par le complexe $(C_5H_5)_2 Ti^+$ mis en oeuvre comme médiateur en milieu aqueux acide (H_2SO_4 1N). Les composés nitrés sont transformés sélectivement en amines correspondantes et la forme réoxydée du complexe $(C_5H_5)_2 Ti OH^+$ est réduite sur une cathode poreuse en feutre de graphite par recyclage de la phase aqueuse jusqu'à complète réduction du composé nitré [21-23]. Le complexe $(C_5H_5)_2 Ti OH^+$ est initialement formé par hydrolyse acide de $(C_5H_5)_2 Ti Cl_2$ [24].



Le procédé a été étendu à la synthèse de différents hétérocycles azoté par réduction de nitrobenzènes substitués en ortho par des groupements carbonyle, ester ou nitrile. Par exemple :



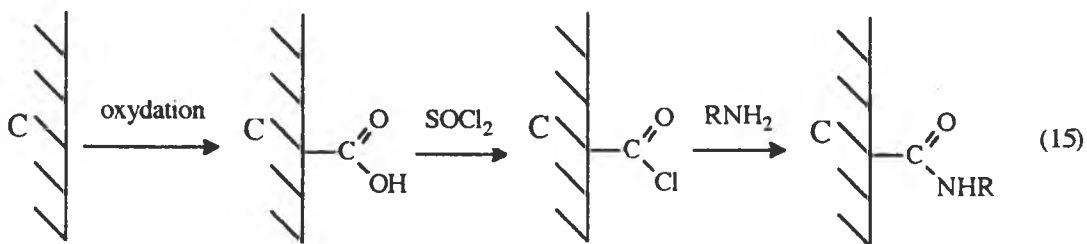
Il a été montré [23] qu'une réaction de transposition intervient lors de la réduction indirecte d'esters ou de carbonate dérivés de l'o-nitrophénol



2.3-Electrodes en feutre de graphite modifié.

Les électrodes modifiées ont, la plupart du temps, été élaborées pour leurs propriétés électrocatalytiques. Le greffage de catalyseurs dans la masse d'une électrode en feutre de graphite a été envisagé pour des applications dans les cellules à circulation à électrodes poreuses.

La méthode générale qui permet le greffage, par liaison covalente, d'un catalyseur à la surface du graphite met en oeuvre la suite de réactions :



Divers auteurs ont effectué la première étape d'oxydation par chauffage du graphite sous oxygène ; dans les mêmes conditions opératoires, le feutre de graphite étant inerte, l'oxydation a été réalisée, en présence d'une solution aqueuse de KNO_3 , par électrolyse [25] dans une cellule à circulation.

L'homogénéité du greffage dans la masse de l'électrode a été contrôlée par voltammétrie cyclique (figure 6) après réaction de la 1-ferrocényléthylamine sur le chlorure d'acide produit dans la seconde étape de fonctionnalisation.

Le taux de greffage (de l'ordre de 4×10^{-6} mole par cm^3 de feutre) est déduit de mesures coulométriques réalisées à potentiel contrôlé : il existe une bonne corrélation entre le résultat coulométrique et l'intensité des courants déduits des voltammogrammes cycliques.

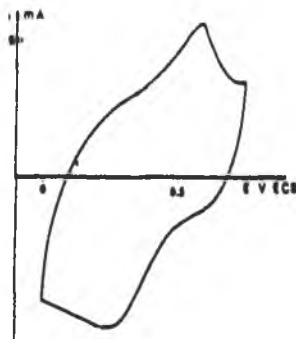
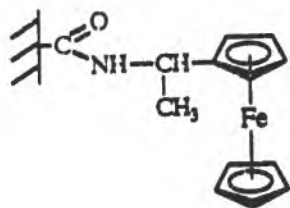


Fig.6 - Voltammogramme cyclique d'un feutre de graphite après greffage de la 1-ferrocényléthylamine; H_2SO_4 1N; vitesse de balayage $0,01 \text{ Vs}^{-1}$

La stabilité de l'électrode modifiée a été vérifiée après oxydation catalytique, dans une cellule à circulation, d'ions cyanures ou d'acide ascorbique ; le taux de greffage reste pratiquement inchangé après plusieurs milliers de cycles.

La méthode mise au point pour le greffage d'aminoferrocènes dans la masse du feutre de graphite a pu être généralisée à d'autres composés organométalliques (complexes aminés du ruthénium; aminoporphyrines métallées, complexes cationiques du fer).

CONCLUSION

Les cellules à électrodes poreuses de grandes surfaces spécifiques, fonctionnant avec un seul passage de la solution dans les électrodes, sont d'un grand intérêt en synthèse organique et leur utilisation doit permettre la préparation de produits difficiles, voire impossibles à obtenir par les méthodes chimiques ou électrochimiques classiques. En effet, la transformation électrochimique rapide (quelques secondes) et pratiquement totale (>95 %) d'un substrat organique ou organométallique conduit à la synthèse d'intermédiaires très réactifs, à durée de vie limitée, directement utilisables dès la sortie de l'électrode poreuse. Par ailleurs, la modification par greffage dans la masse d'électrodes poreuses adaptées aux cellules d'électrolyse à circulation ouvre des perspectives dans le domaine de l'électrocatalyse.

Le procédé à électrodes poreuses apparaît d'autant plus prometteur à grande échelle après adaptation d'une cellule filtre-pressé à ce type d'électrodes dont la section est de 400 cm^2 [26]. Les taux de transformation observés sont tout à fait comparables à ceux obtenus avec les cellules de laboratoire de petites tailles (15 à 50 cm^2) avec des productivités de plusieurs dizaines de grammes par heure. Des applications en chimie fine apparaissent donc tout à fait envisageables.

PARTIE EXPERIMENTALE

Préparation de la dihydro(c)-[2,7]naphtyridine et de l' amino-naphtyridine N-oxyde [8].

Une solution constituée de 1 litre du mélange tampon acétique ($\text{CH}_3\text{CO}_2\text{H}$ $0,5\text{M}$ + $\text{CH}_3\text{CO}_2\text{Na}$ $0,5\text{M}$) + éthanol (1-1 en volume) contenant 1g ($3,2 \text{ mmoles}$) de 3-cyano-5-méthoxycarbonyl-2,6-diméthyl-4 (o-nitrophényl)-1,4-dihydropyridine percole une cathode poreuse en feutre de graphite (diamètre $5,2 \text{ cm}$, épaisseur $1,2 \text{ cm}$) avec un débit de $5 \text{ cm}^3 \text{ mn}^{-1}$. L'intensité de 102 mA ($i_1 = 68 \text{ mA}$ dans le circuit amont, $i_2 = 34 \text{ mA}$ dans le circuit aval) est imposée pour correspondre à une réduction à 4F de la fonction nitro. Après cyclisation complète de la phénylhydroxylamine à 5°C , la dihydro(c)-[2,7] naphtyridine est oxydée sur une anode en feutre de graphite. Pour un débit de $5 \text{ cm}^3 \text{ mn}^{-1}$, l'intensité du courant (51 mA : $i_1 = 34 \text{ mA}$, $i_2 = 17 \text{ mA}$) est calculée pour une oxydation à 2F par mole. Après évaporation de l'éthanol; addition de NaHCO_3 à la phase aqueuse et extraction par CH_2Cl_2 , la phase organique est séchée sur MgSO_4 avant d'être évaporée sous pression réduite. Le résidu est purifié par chromatographie sur silice (éluant CH_2Cl_2 /méthanol 5%). Le rendement est de 65% . $F = 230^\circ\text{C}$.

Préparation des meso hydroxylamino et meso-aminodeuteroporphyrines [5].

Une solution de $0,1 \text{ g}$ du mélange des nitroporphyrines Ia et Ib dans 200 cm^3 de méthanol contenant 3% d'acide sulfurique concentré percole une cathode poreuse en feutre de graphite avec un débit de $6,2 \text{ cm}^3 \text{ mn}^{-1}$. L'intensité du courant est de 34 mA ($i_1 = 23 \text{ mA}$, $i_2 = 11 \text{ mA}$). Un mélange d'une solution aqueuse de soude $0,5 \text{ M}$ et de chloroforme est introduit dans le compartiment en sortie d'électrode pour neutraliser d'une part, et extraire d'autre part, les produits formés. Après lavage de la phase organique par de l'eau et évaporation sous pression réduite, le résidu est purifié sur plaque de silice (éluant CHCl_3 /méthanol 2%). Rendement 24% .

Pour l'électrosynthèse des dérivés amino, une solution de 1g du mélange de nitroporphyrines Ia et Ib dans 350 cm^3 de méthanol contenant 3% d'acide sulfurique percole une cathode poreuse en feutre de graphite avec un débit de $5,8 \text{ cm}^3 \text{ mn}^{-1}$. L'intensité du courant est 266 mA ($i_1 = 176 \text{ mA}$, $i_2 = 90 \text{ mA}$). La solution est neutralisée en sortie de cellule par NaOH 1M et extraite par du chloroforme. Après lavage de la phase organique par de l'eau et évaporation sous pression réduite, le résidu est purifié sur plaque de silice (éluant CHCl_3 /méthanol 2%). Rendement 64% .

Préparation de la 5,8-dihydro-5,8-éthano-2-m.tolyl-5-triazolo [1,2a] pyridazine-1,3-(2H)-dione [12].

Une solution de 955 mg (5 mmoles) de m.tolylurazole dans 200 cm^3 de méthanol contenant 2% d'acide sulfurique concentré percole une anode poreuse en feutre de graphite. Pour un débit de $10 \text{ cm}^3 \text{ mn}^{-1}$, l'intensité du courant (804 mA : $i_1 = 536 \text{ mA}$, $i_2 = 268 \text{ mA}$) est imposée pour

une oxydation à 2F par mole. Une solution de 600 μl (6 mmoles) de 1,3-cyclohexadiène dans 100 cm^3 de méthanol est injectée dans le compartiment en sortie d'électrode poreuse. Après addition d'eau à la phase organique obtenue, évaporation du méthanol et d'une partie de l'eau puis addition de Na_2CO_3 , la phase aqueuse résiduelle est extraite par de l'éther. Après séchage de l'éther sur MgSO_4 puis évaporation sous pression réduite, le résidu est purifié par chromatographie sur colonne de silice (éluant : dichlorométhane). Rendement 87 %. $F = 176\text{-}178^\circ\text{C}$.

Préparation de la N-phényl-2-cyano-3,5-diméthylpipéridine.

Une solution de 0,78 g (4,1 mmoles) de N-phényl-3,5-diméthylpipéridine dans 700 cm^3 de méthanol contenant 0,3 mol l^{-1} en $\text{CH}_3\text{CO}_2\text{Li}$ et 1,6 g (33 mmoles) de NaCN percole une anode poreuse avec un débit de 5 ml mn^{-1} . L'intensité du courant 120 mA ($i_1 = 80$ mA, $i_2 = 40$ mA) est imposée pour correspondre à une oxydation à 2F par mole.

Après évaporation sous pression réduite du méthanol puis addition de 100 cm^3 d'eau, la solution est extraite par le dichlorométhane. Le solvant séché sur MgSO_4 est évaporé sous pression réduite. Le résidu est purifié sur colonne de silice (éluant éther-éther de pétrole 80-20). Rendement 70 %.

Préparation du complexe (di-cyclopentadiényl fer azoxybenzène)²⁺ [20]

Une solution de 0,5 g (1,3 mmole) du cation (cyclopentadiényl fer nitrobenzène)⁺ dans 250 cm^3 du mélange tampon acétique ($\text{CH}_3\text{CO}_2\text{H}$ 2,5 M + $\text{CH}_3\text{CO}_2\text{Na}$ 2,5 M) + éthanol (1/4 volume) percole une cathode poreuse puis une anode poreuse avec un débit de 5,6 $\text{cm}^3 \text{mn}^{-1}$. Les intensités des courants à la cathode (231 mA) et à l'anode (58 mA) sont imposées pour correspondre à une réduction à 4F par mole du composé nitré et une oxydation à 2F de 50 % de phénylhydroxylamine formée intermédiairement. La solution en sortie de cellule est maintenue sous courant d'azote pendant 6 h avant d'être additionnée de quelques gouttes d'une solution aqueuse de HPF_6 à 60 %.

Après évaporation de l'alcool sous pression réduite, le précipité rouge est isolé par filtration et rincé plusieurs fois à l'éther. Rendement 66 %.

Préparation de la 5-(4-aminophényl)-10,15,20-tris(4-pyridyl)porphyrine et de la 5-(4-nitrosophényl)-10,15,20-tris(4-pyridyl)porphyrine [19].

Une solution de 0,5 g de 5-(4-nitrophényl)-10,15,20-tris(4-pyridyl)porphyrine dans 500 cm^3 d'acide sulfurique 1N percole une cathode poreuse puis une anode poreuse avec un débit de 5 $\text{cm}^3 \text{mn}^{-1}$. Pour l'électrosynthèse de l'amine, les intensités des courants pour la réduction et l'oxydation sont respectivement 134 mA et 67 mA. Pour l'électrosynthèse du dérivé nitrosé, les intensités des courants pour la réduction et l'oxydation sont respectivement 67 mA et 43 mA. Après chaque électrolyse, la solution est neutralisée par NaOH 1N puis extraite par le chloroforme. Après lavage par de l'eau et séchage sur MgSO_4 le solvant organique est évaporé sous pression réduite ; le résidu est purifié sur plaque de silice (éluant chloroforme/méthanol 3 %). Rendements : 80 % en amine, 68 % en dérivé nitrosé.

Réduction indirecte d'un nitrobenzène [22]

Avant l'électrolyse (cf. figure 5), 200 cm^3 d'une solution aqueuse de H_2SO_4 1N additionnée de 0,5 g de $(\text{C}_5\text{H}_5)_2\text{TiCl}_2$ et 200 cm^3 de dichlorométhane contenant 1g d'1-nitrobenzène sont introduits dans le réservoir décanteur B maintenu sous azote. Pendant l'électrolyse la phase aqueuse percole la cathode poreuse en feutre de graphite avec un débit de 8 $\text{cm}^3 \text{mn}^{-1}$. L'intensité du courant (130 mA : $i_1 = 90$ mA, $i_2 = 40$ mA) est calculée pour correspondre à la réduction complète de $(\text{C}_5\text{H}_5)_2\text{TiOH}^+$ après chaque passage dans l'électrode poreuse. La solution réduite en sortie de cellule et la phase organique du dérivé nitré sont envoyées et mises en contact sous une forte agitation dans le réacteur C. Le mélange réactionnel est continuellement recyclé jusqu'à réduction complète du composé nitré.

L'aniline obtenue est généralement contenue dans la phase aqueuse acide. Après neutralisation par de la soude 1N, la phase aqueuse est extraite par de l'éther; après séchage sur MgSO_4 , la phase étherée est évaporée sous pression réduite. Le résidu est purifié par chromatographie sur colonne de silice.

Greffage de la 1-ferrocényléthylamine sur feutre de graphite.

Une solution aqueuse de KNO_3 (2 mol l^{-1}) percole, avec un débit de $15 \text{ cm}^3 \text{ min}^{-1}$, une anode poreuse en feutre de graphite (diamètre 5,2 cm, épaisseur 0,9 cm) localisée entre deux contre-électrodes placées en amont et en aval. Une intensité du courant d'oxydation de 2,4 A est imposée pendant 30 mn (le sens de circulation de l'électrolyte est inversé après 15 mn). Après électrolyse, le dispositif est rincé par de l'eau, de l'acétone et du toluène avant de faire circuler dans le feutre une solution de chlorure de thionyle (15 g) dans le toluène (300 cm^3) maintenu à 30-40°C pendant 3 h. Après un nouveau rinçage par de l'éther puis du toluène, une solution de 0,69 g (3 mmoles) de 1-ferrocényléthylamine dans 300 cm^3 de toluène à 30-40°C percole le feutre de graphite pendant 3h. L'électrode est ensuite rincée par du toluène, de l'éther puis de l'eau.

L'efficacité et l'uniformité du greffage sont contrôlés par voltammétrie cyclique réalisée sur des disques de 8 mm de diamètre prélevés à différents endroits du feutre. L'électrolyte est une solution aqueuse de H_2SO_4 1N.

BIBLIOGRAPHIE

- [1] - Ng P.K., *J. Electrochem. Soc.*, *128*, **1981**, 792.
- [2] - Pollard R, Trainham J.A., *J. Electrochem. Soc.*, *130*, **1983**, 1531.
- [3] - Lamoureux C., Moinet C., Tallec A., *Electrochim. Acta*, *31*, **1986**, 1.
- [4] - Moinet C., Raoult E., *Bull. Soc. Chim. Fr.*, *128*, **1991**, 214.
- [5] - Moinet C., Autret M., Floner D., Le Plouzenec M., Simonneaux G., *Electrochim. Acta*, *39*, **1994**, 673.
- [6] - Bujoli B., Jubault M., Moinet C., Tallec A., *Electrochim. Acta*, *35*, **1990**, 809.
- [7] - Hurvois J.P., Moinet C., Tallec A., *Electrochim. Acta*, *38*, **1993**, 1775.
- [8] - David J.Y., Hurvois J.P., Tallec A., Toupet L., *Tetrahedron*, *51*, **1995**, 3181.
- [9] - Hurvois J.P., Tallec A., Toupet L., *Bull. Soc. Chim. Fr.*, *129*, **1992**, 406
- [10] - Kharraz B., Uriac P., Toupet L., Hurvois J.P., Moinet C., Tallec A., *Tetrahedron*, *51*, **1995**, 9611.
- [11] - Guilbaud-Criqui A., Moinet C., *Bull. Soc. Chim. Fr.*, *130*, **1993**, 101.
- [12] - Lorans J., Thèse Rennes 1996.
- [13] - Fehlhammer W.P., Fritz M., Floner D., Moinet C., *Electrochim. Acta*, sous presse.
- [14] - Hurvois J.P., Michel S., Legall E., Moinet C., Tallec A., *Liebigs Annal.*, sous presse.
- [15] - Lamoureux C., Moinet C., *Bull. Soc. Chim. Fr.*, *125*, **1988**, 59.
- [16] - Gault C., Moinet C., *Tetrahedron*, *45*, **1989**, 3429.
- [17] - Lamoureux C., Moinet C., Tallec A., *J. Appl. Electrochem*, *16*, **1986**, 819.

- [18] - Guilbaud-Criqui A., Moinet C., Bull. Soc. Chim. Fr., 129 ,1992, 295; 130, 1993, 10
130, 1993, 164.
- [19] - Moinet C., Simonneaux G., Autret M., Hindré F., Le Plouzenec M., Electrochim. Acta,
,1993, 325.
- [20] - Guennec N., Moinet C., J. Organometal. Chem., 465 ,1994, 233; 487, 1995, 177.
- [21] - Moinet C., Floner D., Jan T., Novel Trends in Electroorganic synthesis (Edited by S. Tori
p. 177, Kodansha, Tokyo ,1995.
- [22] - Floner D., Laglaine L., Moinet C., Electrochim. Acta, sous presse.
- [23] - Jan T., Floner D., Moinet C., Electrochim. Acta, sous presse.
- [24] - Valcher S., Mastragostino M., J. Electroanal. Chem., 145 ,1967, 219.
- [25] - Wu H.M., Olier R., Jaffredic N., Clechet P., Nyamis A., Martelet C., Electrochim. Acta, 3
1994, 327.
- [26] - Moinet C., Rapport au contrat EDF 01/L 94-2J 6962, Janvier 1993.

PROMETHEUS: A SIMPLE CODE FOR MODELLING THERMAL AND CURRENT DISTRIBUTION PROBLEMS

J.P. CAIRE

Laboratoire d'Electrochimie et de Physicochimie des Matériaux et des Interfaces
UMR 5651 INPG-CNRS associée à l'UJF
E.N.S. d'Electrochimie et d'Electrometallurgie, BP.75,
38402 Saint Martin d'Hères (France)

Abstract

A general purpose software is presented for predicting the secondary current distributions coupled with thermal transfers in an electrolyser looked as an equivalent network of discrete resistors. This easy-to-use package was made for designing of cells characterised by a complex geometry. Such a software appears to be an efficient tool for helping the initial conception of an electrochemical cell devoted to a given industrial working target.

I. INTRODUCTION

The prediction of thermal and current density distributions in an electrochemical cell is an important step for designing pertinent industrial devices. Solving such a problem could often be performed through experiments but this way is both expensive and time consuming. Then numerical modelling appears generally to provide a better approach. Some analytical evaluations of the current distribution are available for quite simple geometrical cell configurations (1-6). However numerical computations are obviously required for determining thermal and current density in electrolyzers characterised by both a complex geometry and non-linear boundary conditions at electrolyte-electrode interfaces.

As pointed out by PRENTICE and TOBIAS (7) in a general survey of the numerical methods devoted to current distribution problems in electrolyzers, most methods were known since the 1960's : Green's functions, perturbation, straight lines, co-ordinate inversion, variational methods, orthogonal collocation, finite elements and finite-differences methods. However only the last two methods are able to treat realistic current distribution problems in electrolyzers having a complex geometry as most industrial cells. These methods are used by the few commercial codes including CAD tools which were developed in the recent years for treating such modelling. However such sophisticated codes are expensive and require both a powerful computer and a specific training for the user. On the opposite, the purpose clearly defined in the present work was to propose a simple software conceived to be used on a standard personal computer by a designer without any peculiar knowledge or training.

II. THE METHOD OF RESISTANCES

The numerical method chosen here for computing the current and potential distributions is the method of resistances which was previously employed by several authors to solve different classes of discrete problems.

This method is derived from the finite difference method and uses a two-dimension resistive network. The main idea consists in dividing the cell into a mesh of parallelepipedic $dX.dY$ elements centred on a node linked by four crosswise resistances to the neighbouring nodes as shown on figures 1-2 :

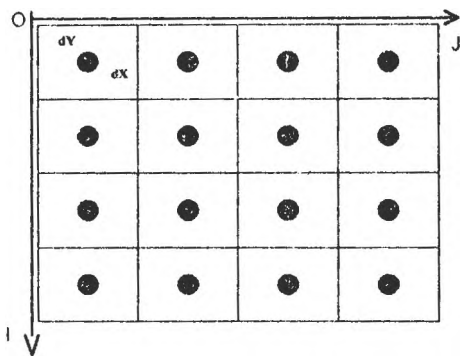


Figure 1: The resistive network

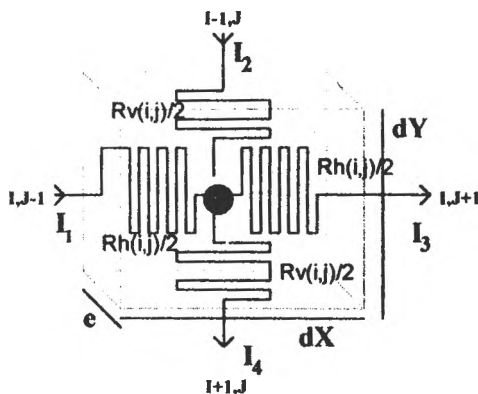


Figure 2: A mesh (I,J) and the equivalent resistors

The definition of each resistive element implies to specify both horizontal resistances R_h and vertical ones R_v as:

$$R_h[i,j] = \frac{\rho_h[k] \cdot dX}{e \cdot dY} \quad R_v[i,j] = \frac{\rho_v[k] \cdot dY}{e \cdot dX} \quad (1)$$

from the horizontal and vertical resistivities $\rho_h[k]$, $\rho_v[k]$ of a given medium k and the width e of the differential element $dX.dY$. It could be easy to demonstrate that the choice of the width has no influence on the calculations of current densities and potentials (8).

For determining the primary distribution of currents and potentials in an electrochemical cell, such a description allows to take into account in an easy way the non isotropic resistive properties of materials in the cell. Particularly it permits to consider transitions between different media : for example, electrolyte-electrode interfaces or electrolyte-cell walls transitions. Hence the whole electrolyzer can be replaced by a one network of resistances only differing by their values.

Then, after defining the boundary conditions of Dirichlet, the calculations leading to the local primary current and potential values in a cell are reduced to the determination of

electrical characteristics in an electrical network for which the classical OHM law can be applied for any node (I,J) to compute the four currents I_k :

$$I_k = \frac{V_{i,j-1} - V_{i,j}}{[R_h(i,j) + R_h(i,j-1)]/2} = \frac{V_{i,j-1} - V_{i,j}}{R_h} \quad (2)$$

as well as the KIRCHHOFF law:

$$I_1 + I_2 = I_3 + I_4 \quad (3)$$

Practical calculations are performed according to the following iterative steps:

- Step 1: Potential Initialisation for all the nodes of the network,
- Step 2: Currents Calculation for all the nodes from the Ohm law [equation (2)],
- Step 3: Determination of the deviation to the Kirchhoff law at each node from the residual defined as $RES = (I_1+I_2) - (I_3+I_4)$,
- Step 4: Correction of potentials by a relaxation method at each node but the points where the Dirichlet conditions apply, from:

$$V[i,j] = V[i,j] + Res/[R_1^{-1} + R_2^{-1} + R_3^{-1} + R_4^{-1}] \quad (4)$$

- Step 5: Iteration from step 2 until:

$$\left| \text{Max} \left[Res/[R_1^{-1} + R_2^{-1} + R_3^{-1} + R_4^{-1}] \right] \right| \leq \varepsilon \quad \forall i,j \quad (5)$$

ε being the desired numerical potential accuracy.

For determining the secondary current distribution, polarisation overpotentials η have to be taken into account. The resistance method is quite able to solve this problem by defining, between the electrolyte and an electrode, an interfacial variable resistor depending on local current density:

$$R_{equiv} = \frac{\eta[i]}{i} \quad (6)$$

corresponding to the resistive scheme of figure 3.

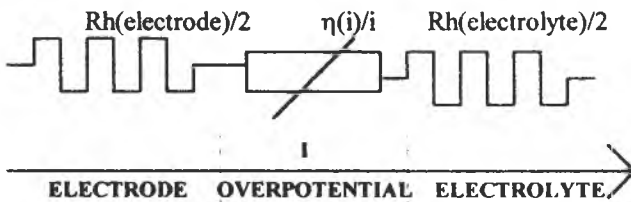


Figure 3: Equivalent circuit for electrode overpotential

Then calculations imply an extra iterative loop in the previous computing scheme because of the unknown values of the interfacial resistances except in the special case when $\eta(i)/i$ is constant.

III. THE THERMAL DISTRIBUTION

The thermal distribution is based on a simple analogy between the thermal and electrical flows. Then the cell is simulated using an equivalent mesh of thermal resistors as shown on figure 4.

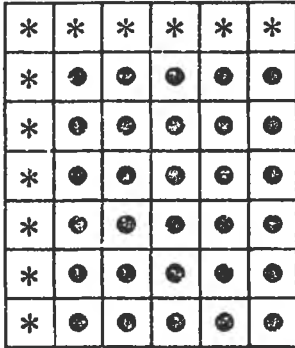


Figure 4: Thermal mesh

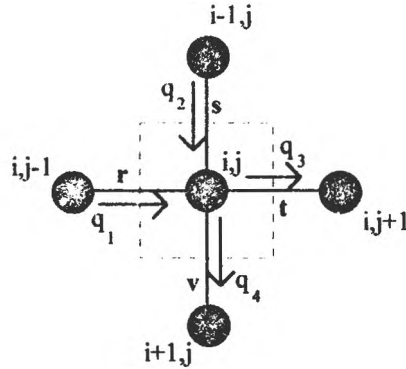


Figure 5: A mesh used in thermal computation

We suppose that the inner points are only submitted to thermal transfers by conduction and that the boundary nodes (the star points) are submitted to both convection and radiation phenomena. The resistors related to these points are computed in a different manner (9)

For thermal transfer by conduction with thermal sources, the Kirschoff law reads as:

$$q_{i,j} + \sum_{\substack{k \in \{i-1, i+1\} \\ l \in \{j-1, j+1\}}} \frac{T_{k,l} - T_{i,j}}{R_{(i,j),(k,l)}} = 0 \quad (7)$$

with :

* $q_{i,j}$ = thermal flow

* $R_{(i,j),(k,l)}$ = thermal resistor

The mathematical treatment is similar to the potential computation, but the Fourier boundary conditions requires some more iterations to obtain a good convergence.

IV. THE SOFTWARE

The software presented here extensively uses the mouse capabilities and runs on simple PC micro computers only equipped with 2 Mo RAM and VGA graphical output. The code was written in Borland TurboPascal[®].

The mesh resistor is made automatically from the matrix of pixels appearing on the computer screen.

The acquisition of the cell geometry is made from a simple two-dimensional plan by using an A4 scanner or by use of the design capabilities of Microsoft PaintBrush[®]. Then the different parts of the cell (electrolyte, anodes, cathodes, cell, insulating gas, bus bar etc...) appearing on the screen are identified by clicking the mouse and painting them with specific colours. At last the resistivity to be attributed to each colour is extracted from an internal data file which may be extended if necessary. At least the user has to define with two mouse clicks the lines (or the curves) where a potential is imposed (the so-called mathematical conditions of Dirichlet).

From this step, all operations are performed in an automatic mode. Calculations concerning either the primary or the secondary current distribution in a cell are short enough to allow a fast checking of numerous geometric configurations and electric working conditions. Typically - when using an IBM PS/2 equipped with 80386 SX and 80387 processors - computation times, for a cell such as the one presented here and described by a mesh of 100x50 nodes, are about 3 minutes for having a final 0.1 % relative precision on the potential. It grows up to 47 minutes for a 0.001 % numerical precision.

At the end of these computations, the corresponding equipotential curves and current lines can be drawn on the screen and printed or plotted on external outputs. Moreover the user can explore with the mouse any peculiar region of interest in the cell to obtain the local potential and current. Moreover our code gives an estimation of anodic and cathodic cell currents obtained by summing the individual currents on every node where a potential was primarily imposed as a boundary condition.

The thermal flows and isotherms are then computed in a next iterative process using the current density file obtained in the preceding step.

V. SOME SIGNIFICANT RESULTS OBTAINED FOR A HULL CELL

Figure 6 presents a primary distribution map as obtained from a screen copy for a simple Hull cell containing a highly resistive electrolyte. Figure 7 shows a secondary potential curved calculated along an horizontal section of the same cell containing a hypothetical electrolyte with anodic and cathodic overpotentials.

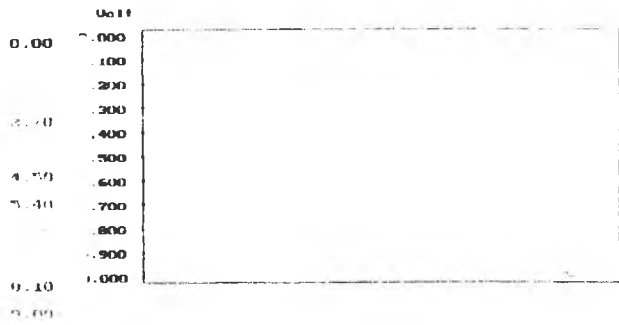
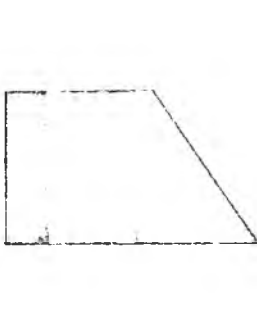


Figure 6: Primary distribution map

Figure 7: Secondary distribution

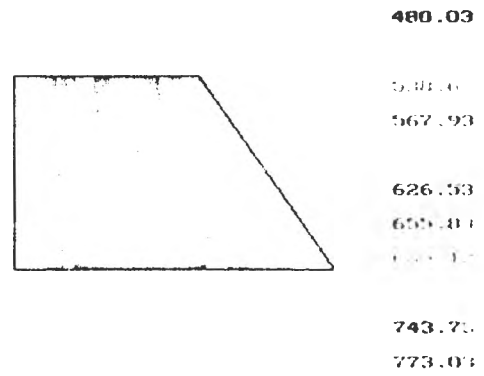
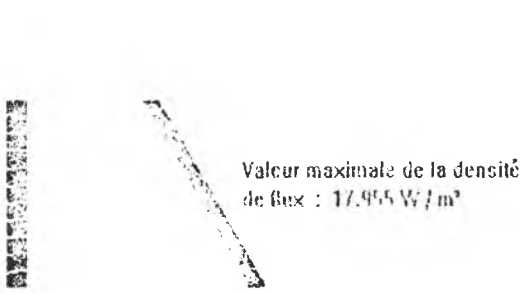


Figure 8: Thermal flows vectors

Figure 9: Thermal map

Figures 8-9 present some thermal results obtained for a Hull cell when taking into account the thermal losses generated inside the electrolyte by Joule effect and the convection effect at the electrodes, the horizontal edges being insulated. Thermal flows are expressed in Watts/m² and temperatures in K.

The thermal flows vectors are directed outward the cell since the thermal sources (Joule effect) are calculated from the currents computed in the electrolyte whereas the thermal wells (convection and radiation) are placed at the external border of electrodes.

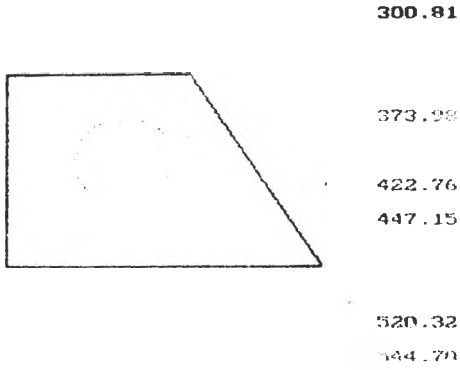


Figure 10: Thermal map (conduction+convection +radiation)

Figure 10 shows the isotherms computed in the case where convection and radiation are present on each side of the cell. These figures are easily interpreted by any user.

IV. CONCLUSIONS

The software presented here for determining two-dimensional primary and secondary current and potential distributions coupled with thermal phenomena in electrolysers is able to give helpful informations for designing industrial cells in which electrolyte flowing has no primordial effect. Moreover the modelling capabilities of such a software allow to easily analyse the impact of geometrical modifications of a cell design in order to decrease the overall cell voltage, to obtain a suitable current distribution and to insure a satisfying functioning for electrodes.

On the other hand, the study of the influence of hydrodynamics on the cell behaviour requires to interface this software to another one devoted to turbulent or not turbulent flow simulation.

RECENT ADVANCES IN ELECTROCHEMICAL DIGITAL SIMULATION

by Dieter Britz

*Kemisk Institut, Århus Universitet, 8000 Århus, Denmark.
Email: britz@kemi.aau.dk*

ABSTRACT

Until recently, several problems in the digital simulation of electrochemical systems have appeared intractable. These problems are described. They concern numerical stability and response to initial discontinuities, fast homogeneous chemical reactions leading to very thin reaction layers, coupled terms in the governing equations for complex multi-species mechanisms, general efficiency concerns and difficulties of programming, especially with sophisticated schemes. Most of these problems have been to a great extent eliminated by recent advances, which are described. These include stability studies (resulting in some surprises as well as insights), adaptive point grid distribution, the block-tridiagonal solution of coupled systems of linear equations, implicit methods and how to prevent error oscillation, the handling of two-dimensional systems such as ultramicrodisc electrodes and recently appearing commercial simulation packages.

INTRODUCTION

What we call digital simulation, that is, the numerical solution of the partial differential equations (*pdes*) for diffusion, became widely known among electrochemists after the paper by Feldberg and Auerbach (1964) and in particular, the Feldberg chapter (1967) in Vol. 3 of *Electroanalytical Chemistry*, edited by Bard. The first electrochemist, however, to use the technique (without a computer) was Randles (1949). Randles refers to the classical paper of Emmons (1944). In fact, the method was described by Courant, Friedrichs and Lewy (1928) and can be traced back further to Richardson (1911). All these older workers (but not Feldberg) used what Britz (1988b) calls the "point method", in which the underlying *pde* is approximated in terms of finite differences between points in time and space. Feldberg, however (1964, 1967) chose to use volume elements (boxes) instead, where the second Fick diffusion equation (Fick 1855) is never used; instead, Fick's first equation is used to express fluxes of material between boxes. The difference between the two

approaches has been discussed (Britz 1980, 1988b) and in the present work, only the mathematically more conventional point method will be used.

Before the description of recent advances in this field, a brief description must be given of the simplest method of implementing simulation. Assume a single electroactive species A, reduced at the electrode in a cell where diffusion can be modelled as a one-dimensional, semi-infinite diffusion system. This leads to the *pde*, Fick's second equation of diffusion,

$$\frac{\partial c}{\partial t} = D \frac{\partial^2 c}{\partial x^2} \quad (1)$$

where c is the concentration of substance A (varying in time and space), t is the time, x the distance from the electrode and D the diffusion coefficient of A. In the explicit method, time is (usually) represented at points $t = 0, \delta t, 2\delta t, 3\delta t, \dots, n_t \delta t$ (n_t being the number of time steps taken); and space x by points at $x = 0, h, 2h, \dots, (n_x+1)h$. It is convenient to use index i for the points along x , that is, $i = 0, 1, 2, \dots, n_x+1$ and at a given time t to designate a given concentration $c(t,x)$ as c_i , and the next concentration at that point but at the next time level $t+\delta t$, as c'_i . Obvious discretisation of equ(1) for all c'_i then leads to the explicit equations, for all c'_i :

$$c'_i = c_i + \frac{D\delta t}{h^2} (c_{i-1} - 2c_i + c_{i+1}) \quad (2)$$

Note that there are two spatial points where this equation cannot be applied: at $i = 0$ and $i = n_x+1$, being respectively the inner and outer boundaries. The outer boundary is most often given as a fixed concentration equal to the initial bulk concentration of A. The inner boundary is determined by the kind of experiment to be simulated. There are, mathematically, two main classes of boundary conditions: Dirichlet and Neumann. With the former, concentration *values* at $x = 0$ are given in some way; with Neumann, also called derivative boundary conditions, one is given some expression in $\partial c(t,0)/\partial x$ and this must itself be discretised as was equ(1). It turns out that in most realistic applications of digital simulation, derivative boundary conditions are

given (Butler-Volmer or quasireversible systems) and it is also these that are the more troublesome (see below).

What has just been described was standard practice until the 1970's, despite some obvious known limitations. Thus, the method is numerically stable only for $\lambda \leq \frac{1}{2}$, where $\lambda = D\delta t / h^2$. This restricts the choice of both δt and h . Generally, one wants h rather small, so this implies a small δt or a large number of time steps, leading to long computation times. Worse, the explicit scheme is not very accurate, being first order in time (it is in fact the Euler method known from ordinary differential equations, *ode*'s). The reason is that the discretisation is a two-point forward difference. Despite these shortcomings, the explicit method was widely used until fairly recently, although improvements have long been known. Thus, Crank & Nicolson (1947) presented an implicit scheme that was thought to be stable for all λ and is of second order accuracy in both time and space. A possibility for instability of this scheme has recently been found (Bieniasz et al 1995a) but this is difficult to attain in practice. In 1974, Joslin & Pletcher suggested the use of unequal intervals in the x -direction, packing points more closely near the electrode. Feldberg (1981) improved that scheme by using a better expansion function. This almost demands an implicit scheme such as Crank-Nicolson, since the point nearest to the electrode is likely to be at a distance that will render the factor $\lambda > \frac{1}{2}$. Nevertheless, not very much happened in the field until the 1990's, when a succession of new techniques has made many advances and made possible simulations that were regarded as too challenging before then. These will be described in what follows.

It should be mentioned that there are alternative schemes to the finite difference method. One of them is orthogonal collocation (Whiting & Carr 1977, Pons 1984, Speiser 1996), described by Villadsen & Stewart (1967). This can be classed as a finite element technique and has generally not been extensively adopted by electrochemists.

PROBLEMS REQUIRING SOLUTIONS

In recent years, electroanalytical chemistry has made strong moves into the field of complex reaction mechanisms involving several - sometimes many - reacting species. Digital simulation is required here both to confirm suggested mechanisms and to find the rates of individual reactions. This area has been helped by the advent and spread of the ultramicroelectrode, which has superseded hydrodynamic voltammetry systems such as the rotating electrode for these studies. These simulations are very challenging in several ways and have presented the following problems:

- Numerical stability and response to transients
- fast homogeneous chemical reactions and the resulting thin reaction layers
- coupled reaction mechanisms
- multidimensional systems
- efficiency, choice of method
- programming complexity.

These problems are interrelated and most remedies handle several of them. We shall discuss the problems first, before outlining solutions.

Numerical stability and response:

As noted above, the explicit method is stable only for $\lambda \leq \frac{1}{2}$; as will be seen below, it is essential to use unequal intervals and the limit on λ makes this method practically useless. The Crank-Nicolson method (CN) is stable for all λ in the sense that errors will (almost) always be damped out. However, as pointed out by Feldberg & Goldstein (1995), CN suffers from the defect that it shows strong error oscillations, sometimes (for very large λ) persisting throughout a simulation, in response to a sharp initial transient such as obtains with a pulse technique. This weakness is well known to mathematicians (Smith 1985, Pearson 1965, Richtmyer & Morton 1967); on the other hand, Gresho & Lee (1981) point out that such response oscillations may be preferable to a smooth but possibly erroneous response. Furthermore, one can argue (Britz & Østerby 1994) that the oscillations can be eliminated by subdividing

the first steps into a sequence of suitably spaced smaller steps, as was done by Pearson (1965). Some workers nevertheless prefer a method that does not have this problem and one of these is the adaptation of the BDF scheme (backward differentiation formula) known in the area of *odes* since 1952 (Curtiss & Hirschfelder 1952), suggested by Richtmyer (1957) for use in *pdes*, and recently adopted by electrochemists for the first time (Mocak & Feldberg 1994, Feldberg & Goldstein 1995, Rudolph 1995); these workers call it FIRM (fully implicit Richtmyer method). This method will be described below. It can be regarded as an extension of the backward difference scheme of Laasonen (1949), see below also.

In recent years, two-dimensional systems are seeing increasing use (ultramicroelectrodes as points, bands and arrays of these) and simulations are appearing. Beyond rather old work on the stability of these, not including homogeneous chemical reactions, there have been no stability studies and these need doing. For example, Britz (1996a) found, in simulating the microdisc electrode, not only the expected instabilities when using the explicit method, but unexpectedly possible instability also for the CN method. This needs to be studied.

Fast homogeneous reactions

Fast chemical reactions taking place in bulk solution present two kinds of severe challenges to simulation. The first is that for substances generated at the electrode but used up chemically away from it, form a reaction layer (usually) near the electrode. The faster the reaction, the thinner this layer becomes. Wiesner (1947) showed that for a first order reaction, the characteristic thickness μ of the layer is given by

$$\mu = (D/k)^{\frac{1}{2}} \quad (3)$$

with D the diffusion coefficient and k the reaction rate constant. An accurate simulation must place at least a few points within the layer; about 10 might be regarded as sufficient (Britz 1988b). This means in practice that unequal intervals must be used. The question then remains of how to implement them. The second problem is that homogeneous chemical reactions often lead to coupled governing equations, that is, in a system of such equations, some involve concentration terms for more than one species. If one is using an implicit scheme, this creates the

problem of how to solve the system of linear equations upon discretisation. For a single species, this is a tridiagonal system; for a coupled multispecies system, banded equation systems arise.

Multidimensional systems

Until recently, commonly used electrodes have tended to be simplified in their modelling to a one-dimensional geometry. With the edge effects appearing at the ultramicrodisc electrodes, this is no longer possible. Since these are now very popular, it becomes increasingly necessary to do simulations in at least two dimensions, and a number of papers have appeared on the subject. Here, even without coupled homogeneous chemical reaction systems, and even for a single species, the use of implicit methods leads to banded systems of equations to be solved. Implicit methods are important, because even with reasonable point spacing in two dimensions, a large number of points must be involved, so that much computer time can be required and something more efficient than the explicit method is needed. If homogeneous reactions are involved as well, the situation becomes worse. Some progress has been made here, as will be described below.

Efficiency, choice of method

As systems to be simulated become more demanding, especially as they extend to two or more dimensions, computer time increases. More efficient algorithms then become desirable.

Programming

As with efficiency, as simulation becomes more complex, it also becomes more difficult to do the computer programming. If one is attempting to fit kinetic parameters to experimental data and is unsure of the precise mechanism, one may wish to try out several. It is then tedious to write several different programs, especially as a new complex program inevitably requires debugging. Not every electrochemist enjoys this sort of work or the time it takes from actual laboratory work.

SOLUTIONS TO THE PROBLEMS

Stability, step response

Until recently, stability studies have been largely lacking. We know the stability condition for the explicit method for the simple *pde*, equ(1) (that is, $\lambda \leq 1/2$) and have tended to take for granted the unconditional stability of CN and the Laasonen methods. These assumptions were examined only recently by Bieniasz (1993a). Using the von Neumann method of analysis and for the first time including a homogeneous chemical reaction term, he studied the stability of a number of methods in detail, among them the explicit scheme, the Runge-Kutta method (Britz 1988a), DuFort-Frankel (1953), Crank-Nicolson (1947) and the method due to Saul'yev (1964). This was followed by a matrix stability analysis of these methods Bieniasz et al 1995a, 1995b, 1995c), where an unexpected possibility of an instability of CN was found (Bieniasz et al 1995a), as well as for the Saul'yev method (Bieniasz et al 1995c). These instabilities, however, occur only under circumstances difficult to attain in practice. The stability of the recently popular BDF method (Mocak & Feldberg 1994, Feldberg & Goldstein 1995) has been examined by Britz (1996b), also taking homogeneous chemical reaction terms into account, using the von Neumann method. The work on stability continues, and must now be extended into two- and three-dimensional systems, where some surprises may await. Thus, as mentioned above, Britz (1996a) found what may be an instability in a disc simulation, using CN.

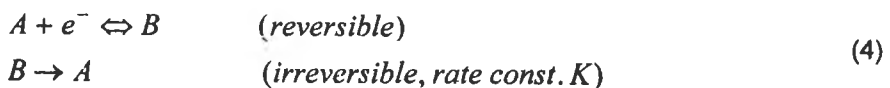
Fast homogeneous reactions

The problem of the reaction layer requires the use of unequal intervals (Britz 1988b). These were suggested first by Pao & Daugherty (1969) (not in electrochemistry), then by Joslin & Pletcher (1974) and what may be the best (fixed) stretching function, by Feldberg (1981), the exponentially expanding sequence of box widths (in fact the same function as used by Pao & Daugherty 1969). If one uses points, this translates into a transformation function with some very convenient properties (Britz 1987, 1988b). In orthogonal collocation, the points are more or less closely packed near the electrode (Whiting & Carr 1977) and if even closer packing is required (very fast chemical rates, thin reaction layer), Hertl & Speiser (1987)

suggested spline collocation. Both these approaches have an important drawback: the spacing of the points is determined before the simulation and is then fixed in time. This means that if the reaction layer undergoes marked changes in characteristic thickness during the simulation, then for some of the time at least, the point distribution is unsuitable (and needs to be predicted before the simulation). Furthermore, there are systems where a more or less thin layer appears away from the electrode (Bieniasz 1994c). All of these problems are solved elegantly by Bieniasz (1993b, 1994a, 1994b, 1994c), using the adaptive grid strategy, in which points are moved at every iteration, so as to ensure an optimal spacing, taking the momentary concentration profile(s) into account. The scheme can easily handle time-varying reaction layers (Bieniasz 1994b, 1994c), layers away from the electrode (Bieniasz 1994c) and even - when applied to time intervals - discontinuities in time (Bieniasz 1994b). No other scheme is able to do all this. As with many other algorithms, a stability study has yet to be made, however.

With unequal intervals and especially when using adaptive grids, reaction rates up to the theoretical (diffusion) limit can now be accommodated (Bieniasz 1993b, 1994a, 1994b, 1994c, Rudolph 1995). The problem can therefore be regarded as essentially solved.

Similarly, the problem of coupled systems has been solved, at least for one-dimensional systems. Up until 1991, electrochemical simulators tended to reject the efficient implicit algorithms such as CN for such systems, because the resulting systems of equations correspond to pentadiagonal or, worse, banded systems, not amenable to the simple Thomas algorithm for solving a tridiagonal equation system for a single species (Thomas 1949, Britz 1988b). For example, the relatively simple catalytic mechanism,



whose governing equations are, for unequal intervals and using the transformation due to Feldberg (1981) and Pao & Daugherty (1969), $Y = \ln(1 + \alpha X)$:

$$\begin{aligned}\frac{\partial C_A}{\partial T} &= a^2 \exp(-2Y) \left(\frac{\partial^2 C_A}{\partial X^2} - \frac{\partial C_A}{\partial Y} \right) + KC_B \\ \frac{\partial C_B}{\partial T} &= a^2 \exp(-2Y) \left(\frac{\partial^2 C_B}{\partial X^2} - \frac{\partial C_B}{\partial Y} \right) - KC_B\end{aligned}\quad (5)$$

gives rise to the discrete systems

$$\begin{aligned}C'_{A,i-1} + a_1(i)C'_{A,i} + a_k(i)C'_{B,i} + a_2C'_{A,i+1} &= b_{A,i} \\ C'_{B,i-1} + [a_1(i) - a_k(i)]C'_{B,i} + a_2C'_{B,i+1} &= b_{B,i}\end{aligned}\quad (6)$$

for all i in the Y -space, with the coefficients a and b depending on the particular implicit method used. The dashes, as in C'_A , indicate as yet unknown values at the next time point (Britz 1988b). Clearly, no matter how one arranges the unknowns vectors \bar{C}'_A and \bar{C}'_B , it is not possible to obtain a tridiagonal system. Rudolph (1991) showed how to cast system (6) into a tridiagonal system of equations in vectors and coefficient matrices, which can then be solved by a straightforward method analogous to the Thomas algorithm. Equ (6) becomes

$$\bar{C}'_{i-1} + A_1(i)\bar{C}'_i + \bar{A}_2(i)\bar{C}'_{i+1} = \bar{B}_i\quad (7)$$

where now A_1 is the coefficient matrix $\begin{bmatrix} a_1(i) & a_k(i) \\ 0 & a_1(i) - a_k(i) \end{bmatrix}$ and A_2 and B are coefficient vectors. It turns out that this, now called the Rudolph method, was developed by mathematicians and engineers as early as 1974 (Greenfield 1974) and is referred to as the block-tridiagonal method (Hindmarsh 1977). Once one has programmed a particular mechanism, the program is relatively easy to adapt to another mechanism (if one programs with some care); however, while this method solves the problem of coupled reaction systems for one-dimensional geometries, it does not help with multidimensional ones, even in the absence of coupled reactions.

Another method of solving the problem (Britz 1996a) recognises that we now have more powerful and fast computers with large memories; that it may therefore no longer be pressing to use efficient algorithms. Britz therefore

proposed (1996a) simply to solve the large system of equations (6) as a matrix problem, using available software such as LU-decomposition. It turns out that in some cases, where the matrix can be LU-decomposed beforehand (being invariant in time, as in fact seen in equ(7)), this "brute force" method can be quite efficient. Furthermore, as will be seen below, it may be the preferred method where the Rudolph method cannot be used.

Multidimensional systems

The ultramicrodisc electrode is that which is seeing the most vigorous developments now. Heinze (1981) was the first to attempt to simulate the simple potential step experiment at this electrode. This was subsequently solved semi-analytically (arriving at series solutions or asymptotic solutions for very short and very long times) (Oldham 1981, Aoki & Osteryoung 1981, Aoki 1993). However, there are no solutions for those cases of greatest interest which involve chemical reactions, nor is there much hope for this in the future, so that simulation must be resorted to. Due to the two-dimensional diffusion field, this presents several difficulties. The flat circular disc embedded flush in an insulating plane has the following governing equation for simple one-species diffusion:

$$\frac{\partial c}{\partial t} = D \left(\frac{\partial^2 c}{\partial z^2} + \frac{\partial^2 c}{\partial r^2} + \frac{1}{r} \frac{\partial c}{\partial r} \right) \quad (8)$$

where z is the distance normal to the disc and r is radial distance from the axis normal to the disc centre. To sample this space sufficiently densely, a large number of points is required, leading to considerable computation times. The problem is compounded by the fact that there is a singularity around the disc edge and points need to be spaced more closely there for accuracy. Both these problems were solved by using a conformal map, by Michael & Wightman (1989), later improved by Verbrugge & Baker (1992). In this latter form, the semi-infinite (z,r) space is mapped into the closed (Γ,θ) space, by the relations

$$\frac{r}{r_0} = \cos(\theta) \cosh\left(\frac{\Gamma}{1-\Gamma}\right)$$

$$\frac{z}{r_0} = \sin(\theta) \sinh\left(\frac{\Gamma}{1-\Gamma}\right)$$
(9)

with r_0 the disc radius. Concentration c is normalised to $C = c/c_{\text{bulk}}$ and time t to $T = tD/r_0^2$; the new diffusion equation is then

$$\frac{\partial C}{\partial T} = \frac{1}{\sin^2 \theta + \sinh^2\left(\frac{\Gamma}{1-\Gamma}\right)} \left\{ \frac{\partial^2 C}{\partial \theta^2} - \tan \theta \frac{\partial C}{\partial \theta} + (1-\Gamma)^4 \frac{\partial^2 C}{\partial \Gamma^2} \right. \\ \left. + \left[(1-\Gamma)^2 \tanh\left(\frac{\Gamma}{1-\Gamma}\right) - 2(1-\Gamma)^3 \right] \frac{\partial C}{\partial \Gamma} \right\} \quad (10)$$

Although this appears more complicated than the original equation (8), the new equation has the advantage of strongly unequally spaced points with equal spacing in Γ and θ , and they are spaced in a convenient way, that is, closely where they need to be, near the disc and around the disc edge. Verbrugge & Baker (1992) found, and Britz (1996a) confirmed, that a 30*30 grid of internal points in (Γ, θ) space gives sufficient accuracy in simulation. In the Britz (1996a) work, roughly 4-decimal accuracy was obtained for the current integrated over the disc at steady state for a 30*30 point grid.

Another difficulty appears, however. In order to ensure stability, it is clearly necessary to use an implicit scheme to simulate this system. Heinze (1981) used the alternating direction implicit scheme (ADI) (Douglas 1955, Peaceman & Rachford 1955) but this has its limitations. A true implicit scheme is desirable. However, even in the absence of a multi-species mechanism with homogeneous chemical reactions, equation (10) leads to a banded discrete equation system, no matter in what order one arranges, for example, the 30*30 grid points (Γ -row order or θ -column order). Equation (11) discretises to a 5-point second derivative at every (Γ, θ) point and inevitably, points from neighbouring rows and columns must be involved. This leads to a matrix with a tridiagonal structure plus diagonals at some distance from the centre, on either side. If now, more than one species is involved, the problem becomes worse. The Rudolph method (1991), discussed above, cannot be applied here. A simple solution to this was proposed by Britz (1996a): accept the problem and simply

solve the system of linear equations by the usual matrix solvers, by "brute force". Rather large matrices are obtained. For example, in the case of the 30×30 grid, this leads to an approximately 900×900 matrix. However, this can be easily handled by small work stations of today and it was found that reasonably short computation times result (12 min for a simple potential step simulation). Given that in that case, the matrix bandwidth was only about 60 (out of a row length of 900), considerable savings in computer time are possible by using special solvers that take the structure into account. An approach to this has already been made by Compton et al (1995), using the strongly implicit procedure (SIP) of Stone (1968) provided by the commercial NAG subroutine package. We can now expect real mechanistic simulations of ultramicrodisc experiments.

Efficiency, choice of method

So far, the simulation schemes all have some drawbacks. As we have seen, explicit schemes are inefficient due to their stability requirement. The Crank-Nicolson method seems to be a method of choice; like other implicit schemes it is (almost) unconditionally stable (Bieniasz et al 1995a did find a case of CN instability but also found that it is difficult to enter the condition in practice; in fact, they had to resort to some tricks to show the instability). However, CN is well known for its sensitivity to initial discontinuities (Gresho & Lee, 1981 explain why). Thus, a CN simulation tends to produce initial oscillations around the true solution for a potential step simulation. This has led Mocak & Feldberg (1994) and Feldberg & Goldstein (1995) to propose what they call FIRM (fully implicit Richtmyer method). It was invented in 1952 by Curtiss & Hirschfelder for *odes* and suggested for use in solving *pdes* by Richtmyer (1957). Among mathematicians, it has the name BDF (backward differentiation formula) and is one of a number of methods using more than two time levels (Mocak & Feldberg (1994) and Feldberg & Goldstein (1995) suggest 5 or 6). The method does possess remarkable stability (Britz 1996b) and insensitivity to initial transients. The difference between BDF and CN in this respect is due to differences in their error propagators, as discussed by Gresho & Lee (1981), who argue that perhaps an oscillating error is not a bad thing, that "it may be

telling us something". BDF, furthermore, has a problem: how to start the simulation. If more than one known, past, row of values must be known, one must devise some scheme for the first few iterations, where these are not available. Feldberg & Goldstein (1995) employ a crude strategy, of taking the initial ($T = 0$) values also as those of further "past" values, and simply begin the simulation. They find that this leads to certain errors that can be compensated away by an arbitrary shift in the T value later assigned to time, by $\frac{1}{2}\delta T$. Such arbitrary shifts have been argued against (Britz 1988b) in another context and are difficult to justify, being quite empirical. An alternative and rational scheme was used by Britz (1996a). For the first iteration, only two T -levels are used. This corresponds to the fully implicit Laasonen scheme (1949). Then one expands to three levels, then to four, and so on until reaching the wanted number of levels. This has not been fully explored yet.

It seems that CN would be preferable, avoiding the BDF start-up problem; and there is a way of avoiding the excessive oscillation with initial discontinuities. The optimal strategy may be to subdivide the first step, or first few steps, into a number of smaller steps in time. This was used in a simple form by Pearson (1965) and, as an exponentially expanding series of δT steps by Britz & Østerby 1994 and Britz (1996a). It eliminates the persistent oscillations with CN.

Other efficient algorithms recently suggested include orthogonal collocation (Villadsen & Stewart 1967, Whiting & Carr 1977, Hertl & Speiser 1987); the Saul'yev method (Saul'yev 1964, Britz et al 1990, Bieniasz & Britz 1993) and recently the adaptation of the "finite analytic method" of Chen (1980, 1981) by a Chinese team (Jing et al 1996a, 1996b, further papers are in progress), which appears to be extraordinarily efficient.

Finally, we mention a thorough study of accuracy, using contour plots in $(\delta T^{-1}, \lambda)$ space, by Britz & Nielsen (1991). Such a study can assist in finding the optimal parameters for a given simulation.

Programming vs commercial packages

The average electrochemist might prefer to spend his/her time in the laboratory and not coding simulation programs. In recent years, a number of

more or less general purpose simulation packages have become available. These were reviewed thoroughly by Speiser (1996). There are, at the time of writing, only two that deserve attention: the DigiSim2 package of Rudolph & Feldberg (Rudolph et al 1994, Rudolph 1995) and Elsim by Bieniasz (1992, 1996). DigiSim2 (now released as V2.1) is specific to cyclic voltammetry and easy to operate, while Elsim has a more abstract, mathematical, approach and can handle a very wide range of experiments (it is also much cheaper). It is, however, correspondingly more difficult to master. Clearly, this is the future of simulation. The recent advances discussed above will become internal to such commercial packages and the electrochemist will be able to simulate without first having to learn computer programming.

Acknowledgements

The author thanks Professor Oniciu and Dr. Jitaru, both of Cluj, Romania, for the opportunity to present this paper at their ELFI symposium at Cluj in October/November 1996, and Drs. Bieniasz (Cracow) and Feldberg (Long Island) for stimulating interchange during manuscript preparation.

References

- Aoki K. & Osteryoung J. (1981) *J. Electroanal. Chem.* **122**, 19.
- Aoki K. (1993) *Electroanalysis* **5**, 627.
- Bieniasz L.K. (1992) *J. Electroanal. Chem.* **340**, 19.
- Bieniasz L.K. & Britz D. (1993) *Acta Chim. Anal.* **278**, 59.
- Bieniasz L.K. (1993a) *J. Electroanal. Chem.* **345**, 13.
- Bieniasz L.K. (1993b) *J. Electroanal. Chem.* **360**, 119.
- Bieniasz L.K. (1994a) *J. Electroanal. Chem.* **374**, 1
- Bieniasz L.K. (1994b) *J. Electroanal. Chem.* **374**, 23
- Bieniasz L.K. (1994c) *J. Electroanal. Chem.* **379**, 71
- Bieniasz L.K., Østerby O. & Britz D. (1995a) *Comput. Chem.* **19**, 121.
- Bieniasz L.K., Østerby O. & Britz D. (1995b) *Comput. Chem.* **19**, 351.
- Bieniasz L.K., Østerby O. & Britz D. (1995b) *Comput. Chem.* **19**, 357.

- Bieniasz L.K. (1996) *J. Electroanal. Chem.* **404**, 195.
- Britz D. (1980) *Anal. Chim. Acta* **122**, 331.
- Britz D. (1987) *Anal. Chim. Acta* **193**, 277.
- Britz D. (1988a) *J. Electroanal. Chem.* **240**, 17.
- Britz D. (1988b) *Digital Simulation in Electrochemistry*, Springer, Berlin.
- Britz D., Marques da Silva B., Avaca L.A. & Gonzalez E.R. (1990) *Acta Chim. Anal.* **239**, 87.
- Britz D. & Nielsen M.F. (1991) *Coll. Czech. Chem. Commun.* **56**, 20.
- Britz D. (1993) *J. Electroanal. Chem.* **352**, 17.
- Britz D. & Østerby O. (1994) *J. Electroanal. Chem.* **368**, 143.
- Britz D. (1996a) *J. Electroanal. Chem.* **406**, 15.
- Britz D. (1996b) *Comput. Chem.*, in press.
- Chen C.-J. & Li P. (1980) ASME Paper 80-HT-86, 1
- Chen C.-J., Naseri-Neshat H. & Ho K.-S. (1981) *Num. Heat Transf.* **4**, 179.
- Compton R.G., Dryfe R.A.W., Wellington R.G. & Hirst J. (1995) *J. Electroanal. Chem.* **383**, 13.
- Courant R, Friedrichs K & Lewy H. (1928) *Math. Ann.* **100**, 32
- Crank J. & Nicolson P. (1947) *Proc. Cambridge Phil. Soc.* **43**, 50.
- Curtiss C.F. & Hirschfelder J.O. (1952) *Proc. Nat. Acad. Sci. US* **38**, 235.
- Douglas Jr. J. (1955) *J. Soc. Ind. Appl. Math.* **3**, 42.
- DuFort E.C. & Frankel S.P. (1953) *Math. Tables Aids Comput.* **7**, 135.
- Emmons H.W. (1944) *Quart. Appl. Math.* **2**, 173
- Feldberg S.W. & Auerbach C. (1964) *Anal. Chem.* **36**, 505.
- Feldberg S.W. (1967) in *Electroanal. Chem.* (Ed.: A.J. Bard), Marcel Dekker, New York **3**, 199.
- Feldberg S.W. (1981) *J. Electroanal. Chem.* **127**, 1.
- Feldberg S.W. & Goldstein C.I. (1995) *J. Electroanal. Chem.* **397**, 1.
- Fick A. (1855) *Pogg. Ann.* **94**, 59.
- Greenfield P.F. (1974) *Simulation* **22**, 152.
- Gresho P.M. & Lee R.L. (1981) *Computers Fluids* **9**, 223.
- Hertl P. & Speiser B. (1987) *J. Electroanal. Chem.* **217**, 225.
- Heinze J. (1981) *J. Electroanal. Chem.* **124**, 73.

- Hindmarsh A.C. (1977) Rept. UCID-30150, LLL.
- Jin B., Qian W., Zhang Z. & Shi H. (1996a) *J. Electroanal. Chem.* **411**, 19.
- Jin B., Qian W., Zhang Z. & Shi H. (1996b) *J. Electroanal. Chem.* **411**, 29.
- Joslin T & Pletcher D. (1974) *J. Electroanal. Chem.* **49**, 171.
- Laasonen P. (1949) *Acta Math.* **81**, 309.
- Michael A.C. & Wightman R.M. (1989) *J. Electroanal. Chem.* **267**, 33.
- Mocak J. & Feldberg S.W. (1994) *J. Electroanal. Chem.* **378**, 31.
- Oldham K. *J. Electroanal. Chem.* **122**, 1.
- Pao Y.-H. & Dougherty R.J. (1969), Boeing Sci. Res. Lab. Rept. DI-82-0822
- Peaceman D.W. & Rachford H.H. (1955) *J. Soc. Indust. Appl. Math.* **3**, 28.
- Pearson C.E. (1965) *Math. Comput.* **19**, 570.
- Pons S. (1984) *Electroanal. Chem. (Ed.: A.J. Bard)* **13**, 115.
- Randles J.E.B. (1948), *Trans. Faraday Soc.* **44**, 327
- Richardson L.F. (1911) *Phil. Trans.* **A210**, 307
- Richtmyer R.D. (1957) *Difference Methods for Initial-Value Problems*, Interscience, New York.
- Richtmyer R.D. & Morton K.W. (1967) *Difference Methods for Initial-Value Problems*, Interscience, New York.
- Rudolph M. (1991) *J. Electroanal. Chem.* **314**, 13.
- Rudolph M., Reddy D.P. & Feldberg S.W. (1994) *Anal. Chem.* **66**, 589A.
- Rudolph M. (1995) in *Physical Electrochemistry* (Ed.: I. Rubinstein), Marcel Dekker, New York, 81.
- Saul'yev V.K. (1964) *Integration of Equations of Parabolic Type by the Method of Nets*, Pergamon Press, New York.
- Smith G.D. (1985) *Numerical Solution of Partial Differential Equations*, 3rd Ed., Oxford University Press, Oxford. 1st & 2nd Eds. 1965 & 1974, resp.
- Speiser B. (1996) *Electroanal. Chem. (Eds.: A.J. Bard & I. Rubinstein)* **19**, 1.
- Stone H.L. (1968) *SIAM J. Num. Anal.* **5**, 530.
- Thomas L.H. (1949) *Elliptic Problems in Linear Difference Equations over a Network*, Watson Scientific Computing Lab, Columbia University, New York.
- Verbrugge M.W. & Baker D.R. (1992) *J. Phys. Chem.* **96**, 4572.
- Villadsen J.V. & Stewart W.E. (1967) *Chem. Eng. Sci.* **22**, 1483.
- Whiting L.F. & Carr P.W. (1977) *J. Electroanal. Chem.* **81**, 1.
- Wiesner K. (1947) *Chem. Listy* **41**, 6.

THE ORIGIN AND MECHANISM OF ELECTROCHEMICAL OSCILLATIONS

György Inzelt

*Department of Physical Chemistry, Eötvös Loránd University
Budapest 112, P.O.Box 32, H-1518, Hungary*

ABSTRACT

Since the first report (Fechner, 1828) on the electrochemical oscillation much effort has been made to gain a deeper understanding of this spectacular phenomenon. The key question concerning the origin and mechanism of this type of chaotic behaviour is the elucidation of the events occurring at the electrode surface. Researchers working in this field generally agree that the galvanostatic potential oscillation or the potentiostatic current oscillation are closely related to the formation and decomposition of an inhibiting surface layer, which may consist of chemisorbed species (e.g. $-\text{COOH}$, $=\text{CO}$, $-\text{CH}_2\text{OH}$) in the case of the oxidation of organic compounds or insoluble salt during the dissolution of metals (e.g. CuCl). Less frequently, periodic changes of the solution composition in the double layer or rearrangement of the atoms on the metal surface have also been considered.

The application of new and powerful in-situ techniques, such as quartz crystal microbalance (EQCM), radiotracer and probe beam deflection, has opened up new vistas concerning these issues.

In this paper beside a general overview the results obtained by using these methods will be presented and discussed.

INTRODUCTION

Since the first report on electrochemical oscillations [1] more than 150 years ago, much effort has been expended to gain a deeper understanding of this exotic phenomenon [2-4]. Periodical behaviour can also be observed in other branches of science. For instance, in biology the classical example is the periodical, interconnected variation of the populations of antelopes and lions and the amount of grass in the savannah of Africa. The biological clock in our life is also well known and probably related to some periodical chemical/biological changes. In a wider outlook the oscillatory behaviour belongs to the group of chaotic phenomena or - in other name - to dynamical collective systems. It has been recognized that in science as in life a chain of events can have a point of crisis that could magnify small changes. For example, in meteorology it is called Butterfly Effect, because a small effect - that with

some exaggeration may cause even a butterfly - can cause thunderstorms and blizzards in other places. Although this type of thinking is a little bit strange for us since we have been educated on Newton's second law, however, we may find it even in the folklore. The well known English children verse says:

" For want of a nail, the shoe was lost;
For want of a shoe, the horse was lost;

.....
For want of a battle, the kingdom was lost!"

After this short wandering in "foreign waters" we will return to chemistry.

In Figure 1 a classification is given showing the two main classes, i. e. the homogeneous and the heterogeneous oscillations. In fact, the homogeneous, Belousov-Zhabotinskii reaction [5,6] led a renaissance of the study of the oscillation reactions at about three decades ago. Now it has become a mature science including the studies on pattern formation and fractals. Figure 2 shows the main features of electrochemical oscillations.

Because of the great diversity of the systems it is better if we focus on a given system, i.e. the galvanostatic potential oscillations that arise during the electrooxidation of small organic molecules such as formic acid [2-4, 7, 9, 11-14] or alcohols [2-4, 7-10] at a platinum electrode in acid media. In our studies beside the detection of the periodical changes of the potential three powerful in-situ techniques such as radiotracer [8], quartz crystal microbalance [10, 11, 13-15] and probe beam deflection [12] methods have been applied that may supply direct evidences on the events occurring at the surface and its vicinity.

RESULTS AND DISCUSSION

Does the oscillations originate from the external circuit or is it an inherent property of the processes occurring at the electrode surface ?

Twenty years ago it was a subject of debate, although in many cases rest potential oscillations at open-circuit have been observed.[2] . Our idea was to imitate galvanostatic potential oscillations observed in the course of anodic oxidation of organic molecules. It was assumed that the origin of galvanostatic potential oscillations is rooted in the very nature of the electrode process and not in the behaviour of electrical circuit. In this case the only role of the external circuit is to ensure the constant flux of electrons to or from the electrode. This may, however, be realised by an appropriate redox system too, i.e., by coupling the anodic oxidation

process by the cathodic process of the redox system at open circuit conditions. In order to imitate galvanostatic conditions the rate of the cathodic process should be constant in a wide potential range. This may be realised in the case of a limiting current. For example, in the case of Ce^{4+} -ions present in not too high concentrations a cathodic diffusion limiting current may be attained at potentials where the oxidation of the different organic compounds takes place. In Figure 3 potential oscillations observed in the presence of different organic compounds and Ce^{4+} -ions at a platinum electrode are shown. These experiments provided the first direct experimental evidence that the role of the external circuit may be excluded [7,9]. Later it was also demonstrated that surface mass oscillation may occur even if the potential oscillation is negligible at open-circuit condition [15].

After exclusion of the possible role of the external circuit, the question arises what processes at the electrode surface are responsible for the periodic potential oscillations. During the oxidation the organic substance may participate in the processes as follows.

i) Chemisorption involving dehydrogenation, the rupture of bonds, possibly splitting of the molecule and considerable charge transfer. Essentially, this is also an oxidation process.

ii) Oxidation of the products of chemisorption and removal of the oxidation products from the electrode surface.

iii) Oxidation of the organic molecule yielding some definite end-product, which proceeds on the free sites not involved in the chemisorption.

The oxidation of the chemisorbed species (e.g. $-COOH$, $=CO$, $-CH_2OH$) leading to CO_2 takes place only above certain potential values, so that at potentials more negative than these, the surface is virtually completely covered with chemisorbed molecules. This chemisorbed layer forms a barrier to reactions of type iii) and behaves as a passive layer. Accordingly, the oxidation of the chemisorbed layer increases the reaction rates, because it increases the number of free sites. A change in the coverage with chemisorbed molecules affects therefore the rate of processes proceeding by the route iii). In steady state under galvanostatic conditions the total current (I) is distributed between three processes described above:

$$I = I_a + I_1 + I_2 \quad (1)$$

where I_a , I_1 and I_2 are the currents corresponding to chemisorption, to the oxidation of chemisorbed molecules and to the oxidation process taking place at the free sites, respectively. In steady-state all three partial currents are constant. In the case of

potential oscillations all these partial currents are time and, of course, potential dependent and the charging/discharging current $C(dE/dt)$ should also be taken into consideration:

$$I = I_a(E,t) + I_1(E,t) + I_2(E,t) + C(dE/dt) \quad (2)$$

To this equation the variation of the coverage by the chemisorbed molecules ($d\theta/dt$) with time must be added. Now, we may understand the origin of the periodical changes of potential at constant current.

Because we apply (force) a constant reaction rate (current) on the system the electrode reaction should maintain it. Consequently, the potential will increase when the number of free sites - where the main reaction occurs - diminish. Eventually, the potential range will be reached where the chemisorbed species will be oxidised. Then, the potential will decrease because the reaction can proceed unhindered, i. e. with high enough reaction rate also at low potentials. As the chemisorption will poison the surface the whole process starts again. All these are nicely manifested in the cyclic voltammograms of small organic compounds (formic acid, alcohols) as shown in Figure 4. During the positive-going scan much smaller current can be observed than during the reverse scan, i. e. since we cleaned the surface (at positive potentials) the reaction rate will be higher at lower potentials. (Because the reaction results in CO_2 and $HCOOH$ cannot be reduced in this potential range no cathodic wave can be observed.) This mechanism that involves the formation and decomposition of an inhibiting surface layer is valid not only in the case of the oxidation of small organic molecules but also in many cases of other electrochemical oscillations. For instance, during the dissolution of metals an insoluble salt (e.g. $CuCl$) can be formed that depending on the rate of transport processes in the solution will leave the surface in a soluble form ($CuCl_2$). It should be mentioned, however, that other mechanisms and explanations also exist. In the course of reduction of anions (e.g. $S_2O_8^{2-}$) the mass transport limitations and the repulsive interactions may lead to oscillations. Based on the observations obtained for heterogeneous gas reactions the surface reconstruction may play a pivotal role.

Nevertheless, monitoring the surface mass changes, i. e. the variation of the coverage seems to be of utmost importance. Electrochemical quartz crystal microbalance [10,11] is just the right tool for obtaining such information without disturbing the primary experimental conditions.

What happens on the surface of electrode?

We have assumed that the formation and decomposition of chemisorbed surface layer govern the whole oscillation phenomenon. If we assume monolayer coverage, i.e. about 10^{-9} - 10^{-10} mol cm^{-2} and if an average molar mass 40 is taken, it means a mass change 4×10^{-8} - 4×10^{-9} g during the formation or removal of this layer. By the help of an electrochemical quartz crystal microbalance (EQCM) 1 Hz change can be measured with high accuracy. It corresponds to 5.1 ng and 1.3 ng mass changes when AT-cut crystals (geometrical surface area : 0.3 cm^2) with 5 MHz and 10 MHz characteristic frequencies are used, respectively. Because we want to measure even lesser mass changes than that corresponds to a monolayer it is advisable to increase the sensitivity. Therefore we used platinized platinum in order to increase the real surface area without increasing the geometrical one. This crystal works reasonable well as can be seen in Figure 5. Figure 5 shows a cyclic voltammetric and a simultaneously obtained EQCM curve for a platinized platinum electrode in contact with $1 \text{ mol dm}^{-3} \text{ H}_2\text{SO}_4$. The EQCM response also involves three distinct regions. At low potentials the ionisation of adsorbed hydrogen occurs, accompanied by a slight increase in frequency (small mass decrease). In the double layer region frequency decrease can be observed which is due to the potential-dependent sorption of anions and water molecules. At higher potentials the frequency decreases (the mass increases) more substantially due to the formation of platinum oxides. All these processes reversible as expected.

If we add formic acid to the solution and apply a constant current a slow increase of potential and a frequency decrease (mass increase) can be observed, that indicates the accumulation of chemisorbed species on the surface (Figure 6). Then the periodical formation and removal of the blocking layer at the surface causes an oscillation in the potential. Eventually, as the potential further increases, all the chemisorbed species will be oxidised and platinum oxide will be formed. We selected a typical pattern for the illustration of the oscillation phenomena, including its birth and ceasing. Depending on the conditions (current density, electrolyte and substrate concentration, stirring, temperature etc.), the oscillation can be maintained for a long time, even with disturbing the system as will be illustrated below.

If we add Cu^{2+} -ions to the solution oscillations can be observed further on, however, the pattern of the oscillation and the period time will change as shown in Figure 7. Cu^{2+} -ion has been selected because the underpotential deposition of copper and the dissolution of adatoms occur in the potential range of the oscillation. In this way the sensitivity of our frequency measurement may also be amplified due to the deposition and removal of coppers atoms that having relatively high molar mass.

The deposition of copper indicates the amount of free sites on the surface, however, this process also influences the oscillation as seen in Figure 7.

The amplitude of the potential oscillation remains practically the same, but the period time - after some delay - gradually decreases. The mass changes become also higher and follow the potential oscillation pattern. A continuous frequency decrease is superimposed on the oscillation pattern indicating a progressing increase of the surface coverage. As the potential decreases the mass on the surface increases (the frequency decreases) and vice versa. The period time become shorter and shorter upon adding more and more Cu^{2+} -ions to the solution (Figs. 7a and b). Even more interesting oscillation patterns develop as the Cu^{2+} -ion concentration is further increased (Figs. 7c and d). As can be seen in Fig. 7d between two oscillations having high potential amplitude (similar to those observed without Cu^{2+} -ions or at low Cu^{2+} concentrations) an other periodical pattern of low-amplitude appears. Because the lower potential limit of small oscillation does not reach the potential region of UPD of Cu^{2+} -ions, the frequency response is also small, however, the frequency changes nicely follow the changes of the potential. Later this bifurcation pattern (mixed-mode oscillation) turns into a simple relaxation oscillation again (Fig. 7e). Interestingly enough further increasing the concentration of Cu^{2+} -ions at constant formic acid concentration only the small-amplitude oscillation at higher potential can be observed (Fig. 7f), and eventually the oscillation comes to an end when, at high potential the chemisorbed species are removed from the surface by oxidation and the formation of platinum oxides on the surface begins.

Owing to the high complexity of the system the explanation of the behaviour observed is difficult. However, it seems to be evident that Cu^{2+} discharge takes place at the free sites of the surface and the whole phenomenon is governed by the accumulation and oxidation of chemisorbed species originated from reaction between formic acid and the active sites of platinum metal. A concurrent adsorption (chemisorption) of Cu^{2+} -ions and formic acid, and the oxidation of coppers adatoms, which takes place at lower potential than that of the chemisorbed organic species, should certainly considered. For the description of the phenomena observed it may be assumed that, beside the principal feedback mechanism which involves the non-linear and autocatalytic reaction between strongly bound species originating from the chemisorption of formic acid at the platinum surface and the adsorbed hydroxyl radicals or water molecules, another non-linear feedback mechanism prevails. In our case - because the mixed-mode oscillation pattern arose upon addition of Cu^{2+} -ions - a reaction sequence should be considered in which Cu-adatoms and Cu^{2+} -ions partake. It may be a reaction between Cu-adatoms and hydroxyl radicals on the

surface, which also produced at least two vacant sites, thus increasing the reaction rate. Of course, other effects should also be taken into account. For instance, the slow recovery of the diffusion layer or the time dependent shape of the concentration profile can also be considered as the reason for the mixed-mode or chaotic oscillations. It should be mentioned that the density fluctuation near to the electrode surface may slightly affect the frequency response.

In respect of the effect of Cu^{2+} -ions on the period time, it should be taken into account that the formation of Cu -adatoms is in fact a reduction process, while the chemisorption of formic acid is an oxidation. These processes take place practically simultaneously at low potentials. Therefore, the spontaneous reduction of Cu^{2+} -ions causes a virtual increase in the current because it consumes electrons. The increase in the galvanostatic current density causes a decrease of the period time of oscillation, thus the effect observed may be explained in terms of these two simultaneous reactions described above.

Although EQCM is a powerful tool to follow the surface mass changes it is difficult to distinguish between the contributions of chemisorption and ionic adsorption to the total mass change. Using labelled anions the anion adsorption on the free sites becomes visible as presented in Figure 8.

Figure 8 shows that the potential oscillation and the adsorption of chloride ions occurring simultaneously [8]. The rapid decrease of the potential is followed by a fast decrease of the adsorption. As the potential increases again the adsorption does the same but much slower. It may be due to the slow adsorption (and/or diffusion) rate or the slowness of the oxidation of chemisorbed particles which occupy the adsorption sites. (The addition of alcohol or aldehyde to the solution decreases the amount of chloride ions adsorbed on the electrode surface in equilibrium at a given potential as it was proved separately in potentiostatic experiments.) The results of radiotracer experiments attest our model based on the crucial role of chemisorption but also draw our attention to the fact that the ionic adsorption may also contribute to the total mass change observed during the EQCM experiments.

What happens in the solution ?

It has been shown before that the EQCM method, especially, proved to be very useful in monitoring the surface mass changes, however, the periodical changes of the frequency response may be converted to mass changes by using the Sauerbrey equation, only if the density and viscosity fluctuations close to the electrode surface are unimportant or play a minor role. The frequency response of the quartz crystal is proportional to the product of square roots of the density and

viscosity of the solution in contact with the electrode. While substantial viscosity changes are not expected, the density changes may contribute to the frequency response. The latter effect may be of importance even if the formation and removal of chemisorbed molecules involves less than a monolayer-equivalent amount of molecules on the surface during a given potential oscillation. The effects of mass changes and density fluctuations cannot be separated in the case of EQCM measurements.

The probe beam deflection (PBD) technique [12] has been applied in order to obtain information about the concentration gradient changes during cyclic voltammetry. This is an optical in-situ technique for monitoring the refractive index gradient which is directly linked to the concentration profiles established at the electrode/electrolyte interface during electrochemical reactions.

Figure 9 shows a typical pattern of the simultaneous oscillations of the potential and PBD signal obtained at a current density of 2 mA cm^{-2} in a 5 M HCOOH solution using 1 M HClO_4 as the supporting electrolyte. Although the PBD signal nicely follows the potential oscillations, a continuous increase in its mean value can be observed. The fast increase in the beginning of the experiments and the smaller changes afterwards are due to the continuous build up of the concentration gradient near the electrode surface under conditions of constant current and unstirred conditions. The oscillation period and the potential amplitude increase with time. The oscillations come to an end when the potential reaches a high positive value (about $1 \text{ V vs. Pd(H}^+/\text{H}_2)$). At this point a decrease of the PBD signal can be observed together with a fast potential increase. When the potential-time curve levels off at 1.25 V , the PBD signal starts to increase again. During the oscillations - an enlarged part of Fig. 9 is shown in Fig. 10 - the maxima of the potential coincide with the minima of the PBD signal, while a maximum of the PBD signal appears a few seconds after the potential minimum independent of the period or amplitude of the oscillations. Similar oscillation patterns were recorded at other HCOOH concentrations and current densities.

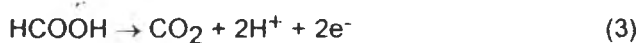
A quantitative evaluation of the data is difficult, although we may conclude that the periodical PBD changes occur simultaneously with the potential oscillations, not only at the electrode surface, but also in the solution layer close to the electrode, i.e. some micrometers away from the solid surface. The PBD technique only detects the overall refractive index gradient, which is generated by the sum of all components.

The exact value of the concentration dependence of the refractive index $\partial n/\partial c$ for CO_2 is not known, however, it was demonstrated that it is a negative and by analogy

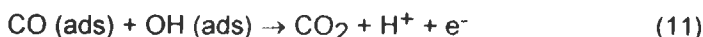
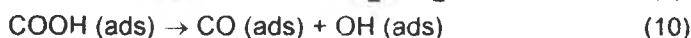
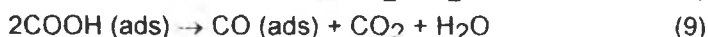
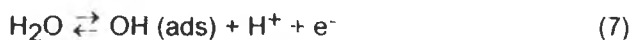
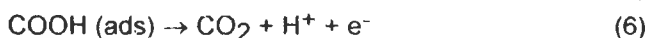
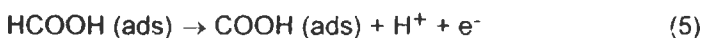
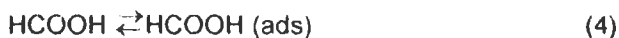
with common gases like Ar, H₂, N₂ and O₂ it is probably relatively large ($\partial n/\partial c$ for H⁺ in HClO₄ = 6.4X10⁻³ vs $\partial n/\partial c$ for O₂ = -14 4x10⁻³)

Using a reasonable mechanism and parallel experiments with the same electrolyte without HCOOH it is possible to find a rational interpretation of the obtained probe beam deflection during the potential oscillation experiments

Two main oxidation products can be considered to be generated in the solution, i.e. CO₂ and H⁺, according to the overall reaction of formic acid oxidation



Even taking into account the adsorption/chemisorption processes, CO₂ and H⁺ are the major final products



Since the water is formed in stoichiometric amounts together with CO₂ (Eqs. (8), (9)) we expect that it will only have a very small influence on the magnitude of the CO₂ gradient at the electrode but not change the PBD signal significantly. In fact, we should focus our attention on the reactions described by Eqs. (3), (5)-(7), and (11).

In order to gain some insight into the changes of the PBD signal occurring during the galvanostatic potential oscillations, we examine the PBD response obtained while recording cyclic voltammograms when the platinum electrode was in contact with 1 M HClO₄ solution (Fig. 11.) and 1 M HClO₄ + 5 M HCOOH solution (Fig. 12.), respectively. The features in the PBD scans shown in Fig. 11. are readily understood in terms of H⁺ generation and consumption. During the oxidation of H₂O, OH(ads) formation and oxide formation (Eq. (7)), the generation of protons leads to an increased acid concentration in the electrolyte next to the electrode surface, causing a negative beam deflection (deflection towards the electrode). Conversely, the beam

deflection is positive during oxide reduction (OH(ads) and H₂O formation), where protons are consumed.

In the presence of formic acid the PBD response is somewhat more complicated (Fig.12.). During the positive-going scan practically no change in the PBD signal is observed at potentials up to 0.8 V. At somewhat higher potentials (0.9 V) there is a small decrease of the signal followed by a step-like increase (at 1.02 V) occurring in parallel with a small anodic current peak in the cyclic voltammogram. At higher positive potentials (~1.3 V) a substantial increase in the PBD signal occurs. The small decrease in the signal at the foot of the voltammetric wave (0.8 V) coincides with the oxide formation on the Pt electrode giving rise to the generation of H⁺ (reaction (7)). The negative deflection however is suppressed, by direct oxidation of formic acid from the solution at the platinum oxide layer and the formation of CO₂. This leads then to a positive deflection since $(\partial n/\partial c)_{CO_2}$ is negative. We assume that the solubility of CO₂ is high enough to avoid bubble formation at the electrode surface.

During the negative-going scan, first a decrease in PBD signal is observed, because of reduced CO₂ evolution subsequently the PBD signal increases again as a consequence of both the consumption of H⁺-ions for the Pt oxide reduction and the direct oxidation of formic acid at the clean surface, which takes place with a very high rate and leads to H⁺ and CO₂ generation.

Bearing the above interpretation in mind, we now return to the evaluation of the PBD during the electrochemical oscillations depicted in Figs. 9 and 10. At the lower potentials (part with slow potential change) the PBD signal shows a maximum. In this part the oxidation of the formic acid takes place at the clean electrode surface, similar to the back scan in Figure 11, where we have a pronounced maximum in the same potential region. Here the potential change is slow, since the reaction is fast in this range. However, the surface is slowly poisoned due to the adsorption of CO and other reaction products. In order to keep the current constant, the overpotential to drive this reaction is increasing as the surface is poisoned. If the reaction product(s) would remain the same we would expect a constant concentration gradient and constant beam deflection. With increasing potentials however, the probe beam deflection decreases after a relative flat maximum, which is most probably due to an increasing formation of protons and poisoning species instead of CO₂. In addition to formic acid oxidation at the free sites, a charging of the double layer also takes place. In fact, it has been shown that the CO₂ production decreases as the potential increases further, since the main reaction (CO₂ formation) becomes more and more inhibited at the poisoned surface.

At the upper potential limit of the oscillations, the oxidation of the chemisorbed species occurs according to Eqs. (6), (8) and (14) and the electrode is cleaned. At this cleaned surface the oxidation of the formic acid and CO₂ generation is fast again. This results in a decreased overpotential and lower electrode potential and the PBD signal is expected to increase until the electrode surface is poisoned again.

The oscillation ends with a large increase of the potential, which first leads to a decreasing PBD signal. At this point the electrode is blocked for formic acid oxidation and the current is maintained by oxide formation (H⁺ generation) giving rise to the steep potential increase. Once the potential is high enough (>1.3 V) the PBD signal is increasing again, which can be explained by the generation of CO₂ by fast formic acid oxidation, now taking place on the oxide layer.

The results imply that the electrochemical (heterogeneous) oscillations lead to periodical homogeneous changes even relatively far from the solid surface, i.e. the effect spreads beyond the double layer region. The time-dependent changes in solution composition may in turn affect the parent heterogeneous oscillations.

Effect of current density, capacitance and temperature

The increase of current density leads to a decrease of period time (Figure 13) [16]. It should be, however, mentioned that there is only a relatively narrow range of current that can be investigated because both at low and high current values a steady state develops. Although the explanation of the effect of current density is not straightforward in the first approach it can be interpreted at least qualitatively as follows. As more charges is forced through the system - under identical conditions (concentration, stirring rate etc.) - all charge consuming processes (see eqs (1) and (2)) may be faster. It is especially true for the oxidation of chemisorbed molecules and the charging/discharging of the double layer (see later). Because these two processes are above all responsible to the steepness of both the increasing and decreasing parts of the potential vs. times curves it is understandable that the period time will change in the direction observed.

The whole effect is even more striking if we increase the capacitance of the electrode.

The capacitance of the electrode should also affect the whole oscillation phenomenon because a part of the charge forced galvanostatically through the system will be consumed by the periodical charging/discharging of the double layer. Therefore, it is of interest to study the effect of electrode capacitance on the oscillation. The electrode capacitance can be varied by using electrodes of different

surface area, i.e. either increasing the geometric area or the roughness factor of the electrode. However, in this case the charge consumed by the oxidation reactions will also be increased. Therefore, we used a different approach to investigate this problem [14].

First, we investigated the electrosorption and the oscillation phenomena using a slightly platinized platinum electrode. (The increase of the roughness factor is desirable to measure reliable values for the frequency changes.) Then a poly(aniline) (PANI) layer was deposited by electropolymerization of aniline on half of the geometric area of the electrode. Because the reversible oxidation/reduction reactions of poly(aniline) at proper conditions (current density, solution composition) take place in the same potential region where the oscillation occurs, the electrochemically active polymer layer behaves as a pseudocapacitance. It consumes a well-defined amount of charge, i.e. it acts as a well-defined capacitance and its value can be determined in a separate experiment. Another advantage is the easy change of the value of the capacitance by varying the thickness of the polymer layer. Furthermore, at suitably selected conditions the charging/discharging processes of poly(aniline) are accompanied by the sorption/desorption of substantial amounts of counterions. In this way an enhanced frequency (mass) oscillation may be detected. It should also be mentioned that a new spectacular oscillation phenomenon can also be observed because a periodical colour change (yellow \leftrightarrow green) can also be seen beside the potential and frequency (mass) oscillation.

Fig.14 shows a typical pattern for the effect of electrode capacitance. It is nicely seen that the poly(aniline) pseudocapacitance alters the period time, but not the amplitude of the potential oscillation.

This effect can be explained in terms of equation (2) and on the basis of the model described therein. In the first approximation the increase of the period time may be explained as follows. In the case of the platinum electrode the total capacitance (C) is equal to the double-layer capacitance (C_{dl}) of the electrode, while in the presence of PANI the pseudocapacitance (C_{PANI}) should be added: $C = C_{dl} + C_{PANI}$.

Because $C_{PANI} > C_{dl}$ and the potential amplitude is practically the same in both cases a decrease of the period time should be observed. (There is no reason to assume that the other terms in equation (2) change because - as mentioned - the oxidation of formic acid takes place at the platinum surface.) This assumption is supported by the fact that the character of the $E-t$ curve does not change. If our conception is correct, there should be a direct proportionality between C and the period time (τ) and the product $C(dE/dt)$ should be approximately constant.

A detailed study [14] has proved that the assumption on the inverse proportionality of C and (dE/dt) is valid, i.e. $-I_a - I_1 - I_2 = C(dE/dt) \approx \text{constant}$ and the value of C determines the period time. Of course, one should not forget that $I_2 \gg I_a + I_1 + C(dE/dt)$ except for a short period of time when $I_2 \approx I_1$ (the rapid oxidation of chemisorbed species at high potential raises I_1 to a comparable value) and during the fast potential decrease when the effect of $C(dE/dt)$ term and possibly I_a may be substantial.

With the help of an appropriate electrochemical pseudocapacitance (eg thick PANI film) very high period time can be achieved and according to our experience, the stability of the oscillation is also better.

Temperature also influences the oscillations as seen in Figure 15. As temperature increases the period time also increases and the potential amplitude of oscillation will be higher [16]. Although the satisfactory explanation of this effect requires further studies a closer look at the temperature dependence of the cyclic voltammograms may reveal some points (Figure 16). With increasing temperature the rates of all oxidation processes increase. We may assume that the temperature coefficient of the main oxidation reaction at the free sites through loosely adsorbed species is higher than that of other processes. At constant current this reaction will consume most of the charge forced through the system. It is also well seen in Figure 16 that the cyclic voltammetric waves become wider with increasing temperature, i.e. it is not surprising that the potential spans a wider range in the course of oscillation. Because we do not know the potential dependence of the rate of the processes taking place during the adsorption and oxidation of formic acid a well-established interpretation of the phenomena observed is not possible at present, however, this preliminary results - which are the first ones of this kind - may open new vistas in the research of this field.

In this paper I tried to recapitulate the main features of our knowledge on electrochemical oscillations. I trust that this summary will be helpful for my fellow-colleagues and initiate further studies in this very attractive and spectacular field of electrochemistry.

ACKNOWLEDGEMENTS

I express my gratitude to Professor G. Horányi with whom I started to study the oscillating electrochemical systems and also to the colleagues - in particular to V Kertész - who have participated in this research.

Financial support from the National Scientific Research Fund (OTKA - TO1498) and from the Hungarian Ministry of Education and Culture (MKM - 379/1995) is gratefully acknowledged.

This paper is based on my plenary lecture delivered at the first ELFI Symposium, Cluj - Napoca, 1996. I would like to thank the organizers for the invitation and especially to Dr. M. Jitaru whose enthusiasm and hard work made the conference successful.

REFERENCES

- [1] G. Th. Fechner, *Schweigg. J.f. Chemie Physik*, **53 (1828)** 129.
- [2] J. Wojtowicz, *Oscillatory behaviour in electrochemical systems*, in J.O'M. Bockris and B.E. Conway (Eds.), *Modern Aspects of Electrochemistry*, Vol.8., Chap.2, Plenum Press, New York (1972).
- [3] U.F. Franck, *Faraday Symp. Chem. Soc.*, **9 (1974)** 137.
- [4] J.L. Hudson and T.T. Tsotsis, *Chem. Eng. Sci.*, **49 (1994)** 1493.
- [5] S.K. Scott, *Oscillations, waves, and chaos in chemical kinetics*, Oxford University Press (1994)
- [6a] B. P. Belousov, *Sbornik Referator po Radiatsionni Medicine, Medgiz, Moscow*, p 145 (1958)
- [6b] A.M. Zhabotinskii, *Dokl. Akad. Nauk USSR*, **157 (1969)** 392.
- [7] G. Horányi, G. Inzelt and E. Szetey, *J. Electroanal. Chem.*, **81 (1977)** 395.
- [8] G. Horányi and G. Inzelt, *J. Electroanal. Chem.* **87 (1978)** 423.
- [9] G. Horányi, G. Inzelt and E. Szetey, *Acta Chim. Acad. Sci. Hung.*, **97 (1978)** 299.
- [10] G. Inzelt, V. Kertész and G. Láng, *J. Phys. Chem.*, **97 (1993)** 6104.
- [11] G. Inzelt and V. Kertész, *Electrochim. Acta*, **38 (1993)** 2385.
- [12] V. Kertész, G. Inzelt, C. Barbero, R. Kotz and O. Haas, *J. Electroanal Chem.*, **392 (1995)** 91.
- [13] G. Inzelt and V. Kertész, *Electrochim. Acta*, **40 (1995)** 221.
- [14] G. Inzelt and V. Kertész, *Electrochim. Acta*, **42 (1997)** 229.
- [15] G. Inzelt, *J. Electroanal. Chem.*, **348 (1993)** 465.
- [16] G. Inzelt and V. Kertész, unpublished results

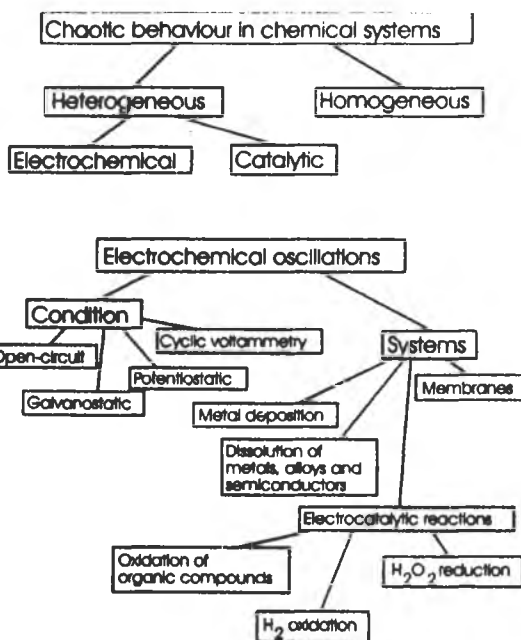


Figure 1: Classification of the oscillation in chemical systems.

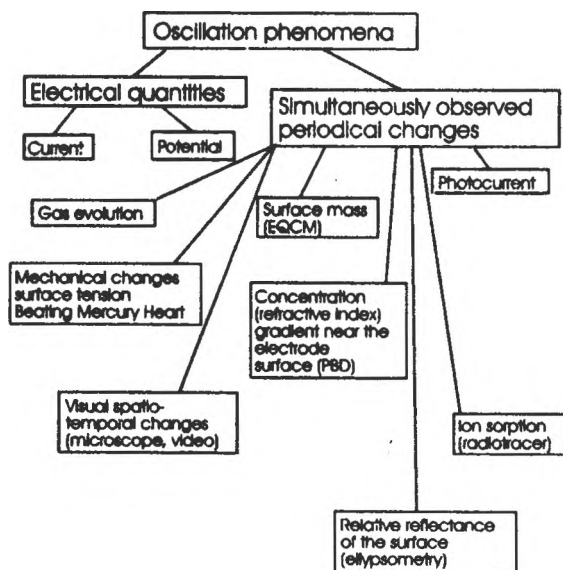


Figure 2: Periodical phenomena observed so far in electrochemistry and studied by the methods indicated in the figure.

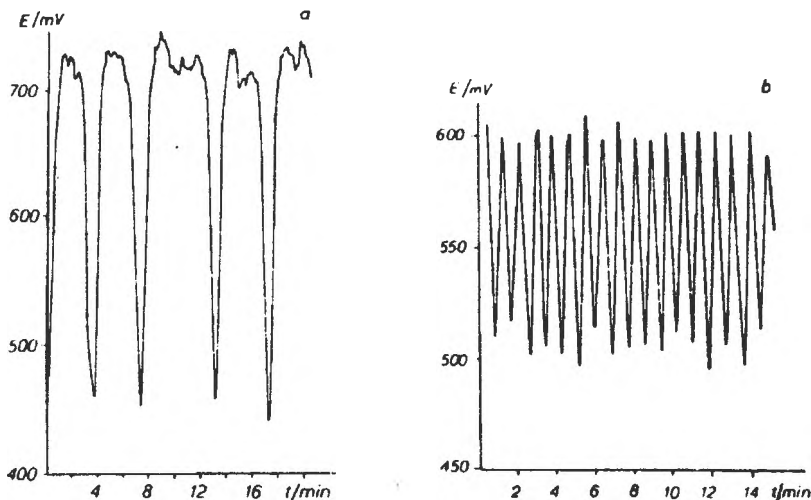


Fig. 3. Oscillations of the rest potential of platinized platinum electrodes.
 a) HO-CH₂-COH (0.5 mol dm⁻³) + Ce⁴⁺ (2.5x10⁻² mol dm⁻³);
 b) HO-CH₂-OH (0.8 mol dm⁻³) + Ce⁴⁺ (2.5x10⁻² mol dm⁻³).

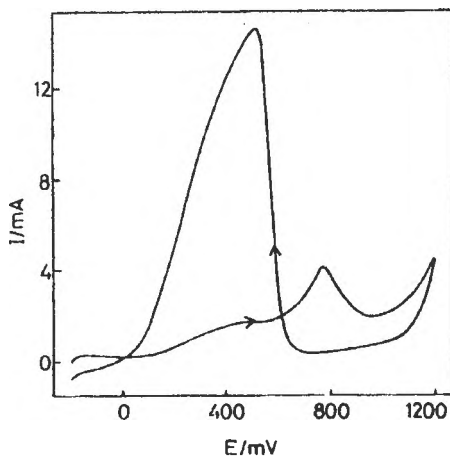


Figure 4. Cyclic voltammogram obtained for 1 mol dm⁻³ HClO₄ solutions containin 0.5 mol dm⁻³ 2-propanol at a platinized platinum electrode. The geometrical area is 0.3 cm², the roughness factor is 400, and the scan rate is 10 mV s⁻¹.

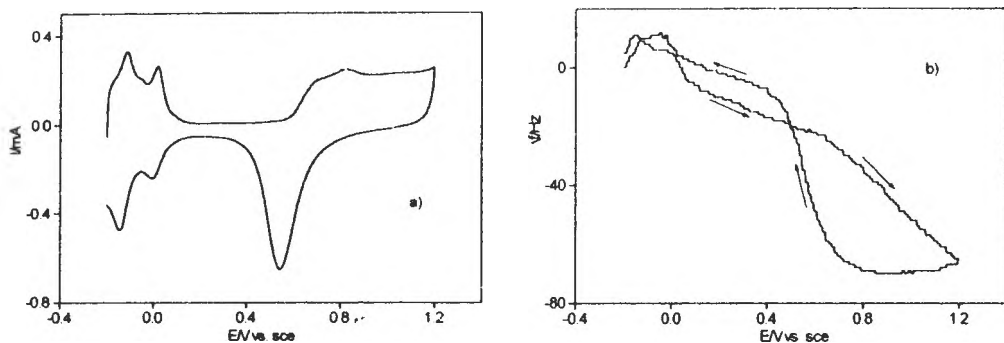


Figure 5. Cyclic voltammetric (a) and EQCM (b) responses obtained for a platinumized platinum electrode in contact with $1 \text{ mol dm}^{-3} \text{ H}_2\text{SO}_4$ solution. Scan rate is 10 mV s^{-1} .

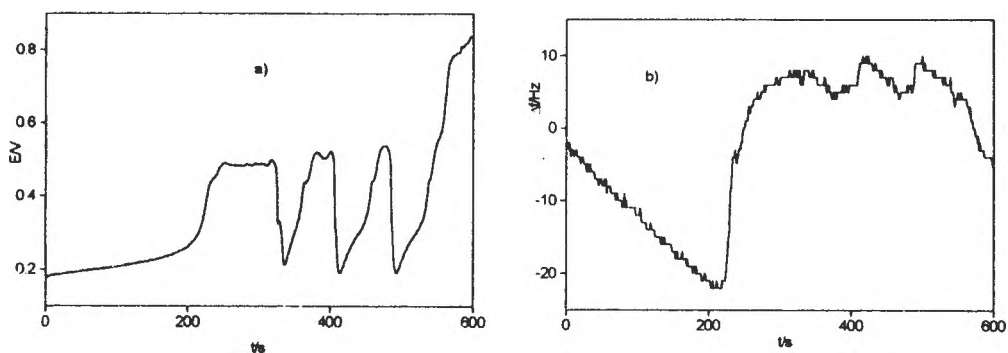


Figure 6. Potential (a) and frequency (b) changes during the galvanostatic oxidation of formic acid at a platinumized platinum electrode. Current: 0.5 mA . Solution: $0.6 \text{ mol dm}^{-3} \text{ HCOOH}$.

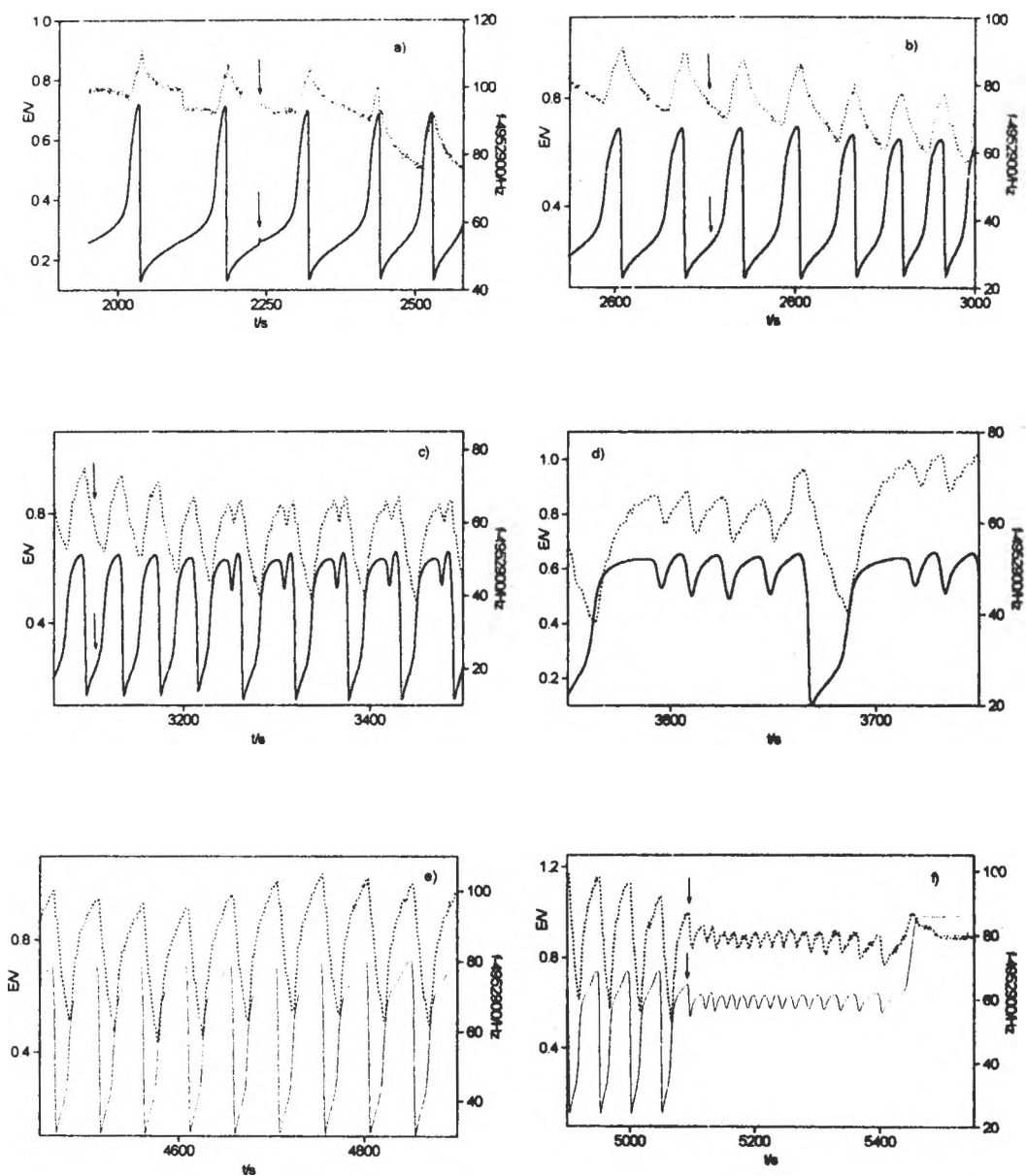


Figure 7. Effect of Cu^{2+} ions on the potential (continuous line) and frequency (points) changes in the course of the galvanostatic oxidation of formic acid at Pt/Pt. Current: 0.5 mA. Solution: 0.6 mol dm^{-3} HCOOH. CuSO_4 stock solution was added to the solution phase at the moments indicated by the arrows. Final concentrations of Cu^{2+} -ions were (a) 3×10^{-3} ; (b) 5×10^{-3} ; (c)-(e) 7×10^{-3} ; and (f) 10^{-2} mol dm⁻³.

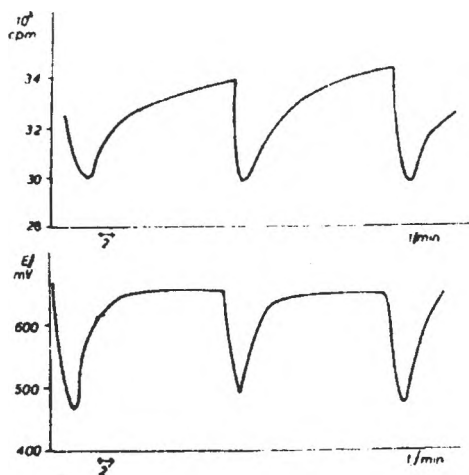


Fig. 8. Potential oscillations and periodical changes in the count rate (i.e. Cl-adsorption) in the course of electrooxidation of glyoxal under galvanostatic experimental conditions.

$i = 0.3 \text{ mA}$; glyoxal conc. $= 0.4 \text{ mol dm}^{-3}$.

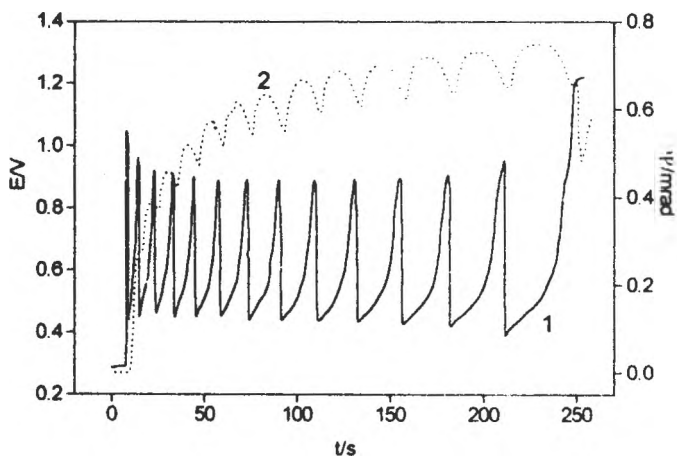


Figure 9. Typical oscillation patterns for galvanostatic oxidation of formic acid in $1 \text{ mol dm}^{-3} \text{ HClO}_4$ at a platinized platinum electrode: (1) potential (solid line), (2) PBD signal (dotted line). The current density was 2 mA cm^{-2} , the concentration of HCOOH was 5 mol dm^{-3} .

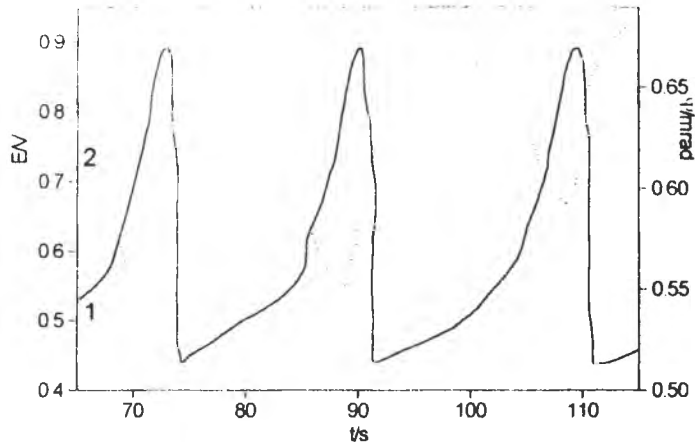


Figure 10. An enlarged part of the oscillation pattern shown in Fig. 9: (1) potential (solid line), (2) PBD signal (dotted line).

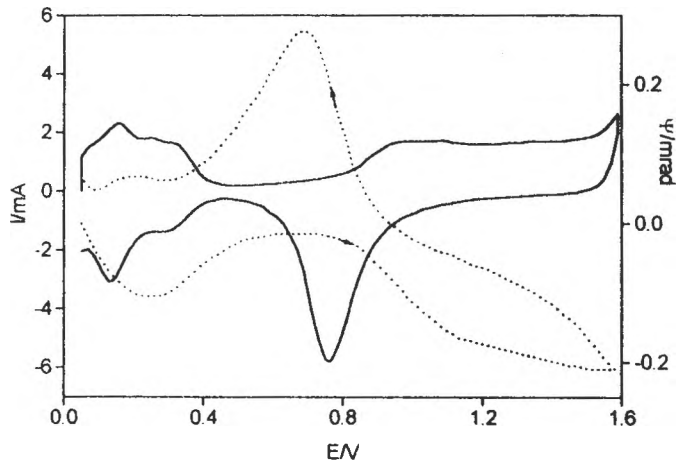


Figure 11. Cyclic voltammogram (solid line) and the simultaneously detected beam deflection (dotted line) for $1 \text{ mol dm}^{-3} \text{ HClO}_4$ solution at a platinum electrode. The roughness factor was ca. 17, and the scan rate was 100 mV s^{-1} .

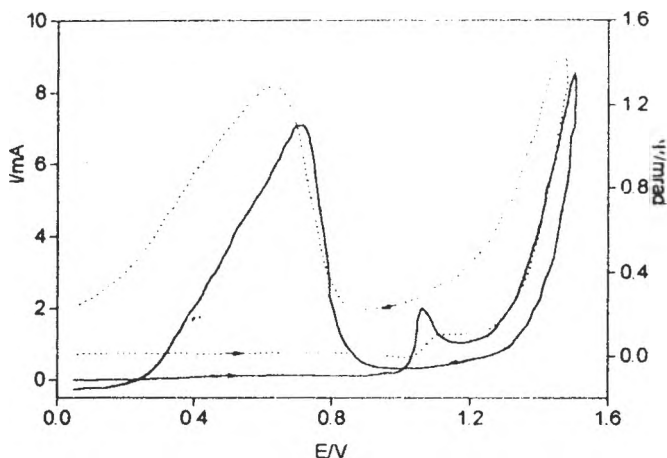


Figure 12. Cyclic voltammogram (solid line) and the simultaneously detected beam deflection (dotted line) for a solution containing 1 mol dm⁻³ HClO₄ and 5 mol dm⁻³ formic acid. Other conditions as in Fig. 11.

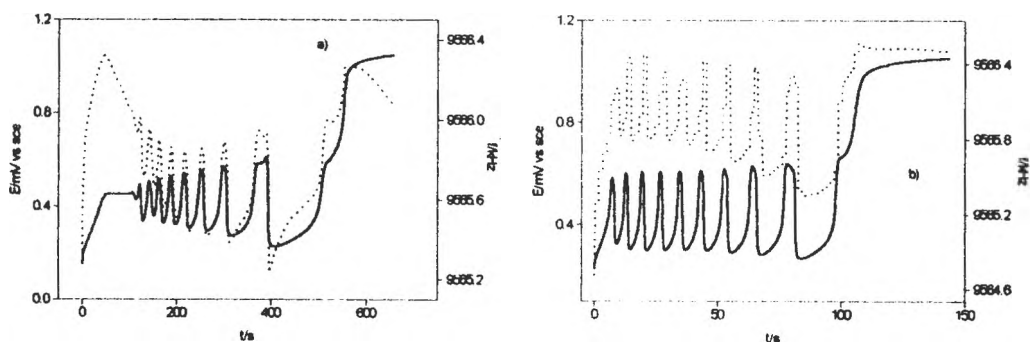


Figure 13. Dependence of the period time on the current. Current values are (a) 5×10^{-4} and (b) 1×10^{-3} mA. System: 0.8 mol dm⁻³ formic acid + 1 mol dm⁻³ HClO₄, Pt-electrode.

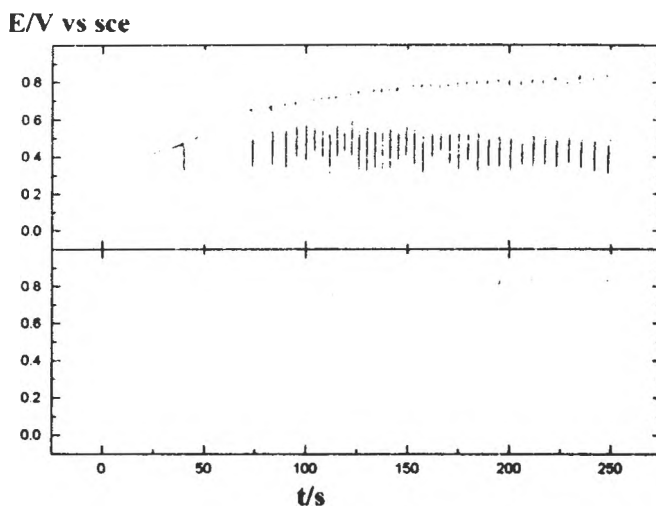


Figure 14: The effect of poly(aniline) pseudocapacitance on the period time of oscillations. Solution: $1 \text{ mol dm}^{-3} \text{ HCOOH} + 1 \text{ mol dm}^{-3} \text{ HClO}_4$. Temperature: $70 \text{ }^\circ\text{C}$. Current: 0.7 mA . Upper curve: Pt-electrode, lower curve: Pt-electrode partially covered with PANI.

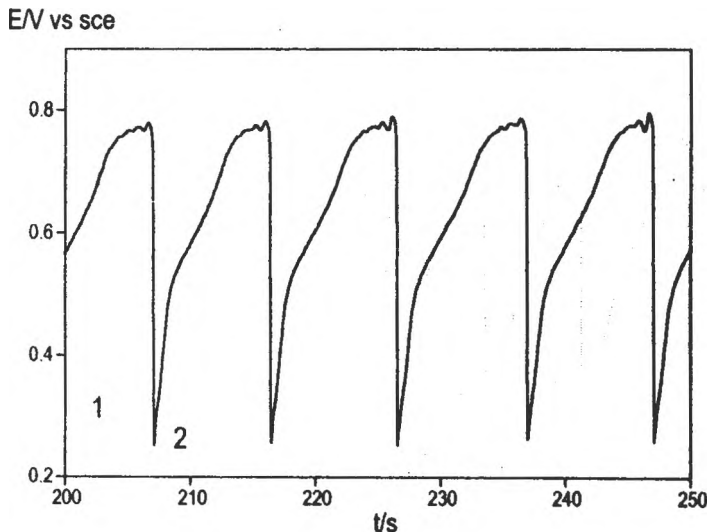


Figure 15: Effect of temperature on the oscillation. Solution: $0.7 \text{ mol dm}^{-3} \text{ HCOOH} + 1 \text{ mol dm}^{-3} \text{ HClO}_4$. Current: 0.5 mA . Electrode: platinized platinum. Temperatures are (1) $50 \text{ }^\circ\text{C}$ and (2) $70 \text{ }^\circ\text{C}$.

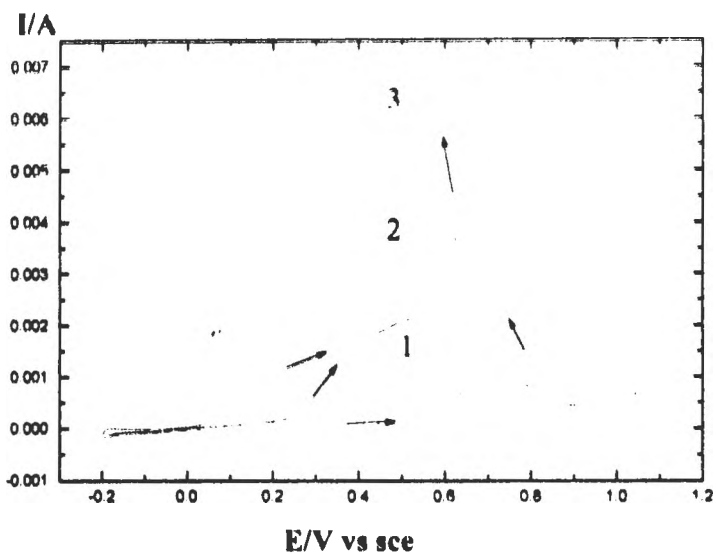


Figure 16: Effect of temperature on the cyclic voltammetric curve of formic acid.
 Solution: $0.7 \text{ mol dm}^{-3} \text{ HCOOH} + 1 \text{ mol dm}^{-3} \text{ HClO}_4$. Electrode: platinumized platinum.
 Scan rate : 50 mV s^{-1} . Temperatures are (1) $30 \text{ }^\circ\text{C}$, (2) $40 \text{ }^\circ\text{C}$ and (3) $60 \text{ }^\circ\text{C}$.

HETEROGENEOUS TRIPLE BOND ELECTROREDUCTION
OF SATURATED AND UNSATURATED NITRILES

Maria Jitaru

*Babes-Bolyai University
Chemistry Research Group
St. Arany Janos No.11, RO-3400 Cluj-Napoca, Romania*

Jean Lessard

*Université de Sherbrooke
Département de Chimie
Sherbrooke (Québec) J1K 2R1, Canada*

Daniel A. Lowy

*Babes-Bolyai University, Department of Physical Chemistry
Present address: The University of Memphis,
Department of Chemistry, Memphis, TN 38152-6060, USA*

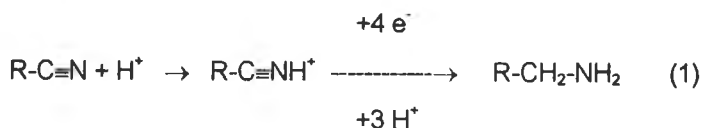
ABSTRACT. - An account on the electroreduction of acrylonitrile to allyl amine (AA), and of the catalytic electrohydrogenation of adiponitrile to hexamethylenediamine (HMDA) is made. In both syntheses porous nickel Raney electrodes were used as the cathode. The preparation procedure of the electrodes involves the co-deposition [1] and electrochemical co-deposition of Ni/Zn and Ni/Al mixtures, followed by the chemical activation of the electrode surface, in alkaline media. An improved adherence and compactness of the metallic deposits were achieved by treating the electrode surface with an aqueous surfactant solution. The effects of current density, supporting electrolyte composition, pH and temperature on product selectivity were investigated. When the synthesis of AA was performed in neutral supporting electrolyte, in the temperature range from 288 to 293 K and at current densities not exceeding 70 mA cm^{-2} , current yield: up to 95% were reached. Also, HMDA was obtained with good selectivities ($\geq 85\%$) in a filterpress type cell, in neutral supporting electrolytes, at temperatures from 275 to 283 K.

Key words: electroreduction, catalytic electrohydrogenation, Raney nickel electrodes, hexamethylene diamine, allylamine, adiponitrile, acrylonitrile.

INTRODUCTION. The use of Raney-nickel as the cathode material was mentioned several years ago [2], but the last ten years have seen an increasing number of papers on this subject [3] which demonstrate its use-fullness for the hydrogenation of

organic compounds. The catalytic Raney-nickel cathodes could be prepared by co-deposition of Ni/Zn or Ni/Al mixtures on nickel plate or on nickel wire-net [1] and by electro co-deposition of Ni/Zn alloy in a bath containing metal ions [4,5].

The primary use of the reparative nitrile reduction is the synthesis of amines. Saturated aliphatic nitriles may be electrochemically reduced to imines and amines [6], while saturated aliphatic dinitriles can yield diamines or aminonitriles [7]. The latter are important for synthesising lactam precursors of nylon, i.e. polyamide 6. Unsaturated nitriles are prone to undergo more various electroreduction processes, that may affect the heterogeneous triple bond or the homogeneous double bond only, or both the C=C and the C≡N bonds [8]. Two main mechanisms are known for nitrile reduction: (i) *electrocatalytic hydrogenation*, on cathodes with low hydrogen overpotential [9], e.g., Ni or Pd black, that promote the reduction by electrocatalytically generated hydrogen [10], and (ii) *electroreduction* on metals with high hydrogen overpotential [11]. Nitrile electroreduction is customarily performed in strongly acidic medium, in water or in mixed aqueous-alcohol solution [12], according to the general scheme shown in Eq.1. It was suggested that the protonation takes place at the nitrogen atom, and is the rate determining step [13,14].



Intensely studied is the selective electroreduction of acrylonitrile (AN) to allylamine (AA). Allylamine is important as an intermediate for pharmaceutical and organic syntheses [15], in the preparation process of colour toners [16], and in the manufacturing of silver halide photographic material [17]. Although AA is a compound in great demand for the chemical industry, literature data reveal that serious problems are experienced in both its chemical and electrochemical synthesis. The faradaic yield attained in the electrolytic process is modest and the selectivity is unsatisfactory [18]. Also, the activity of the otherwise efficient spongy Ni, Pd and Cu cathodes is lost rapidly under continuous use [19]. Porous Pt electrodes were found active, but they drive the reduction of nitriles to alkanes [20]. The use of rotating electrodes for indirect electrochemical amine synthesis [21] is still in the incipient stage. Several side reactions may also occur.

The thermodynamic data for AcN electroreduction were calculated [22], table 1, from bond energies and were adjusted with the dissociation energies of the water molecules involved in reaction.

Table 1: Thermodynamic data for AcN electroreduction to AA, PA and PN [22].

Product	Number of e ⁻	ΔG°_f (S) [KJ/mol]	ΔG°_f (P) [KJ/mol]	ΔG° [KJ/mol]	E° [V/ SHE]
CH ₂ = CHCH ₂ NH ₂	4	195.3	132.8	- 63.0	+ 0.177
CH ₃ CH ₂ - C = N	2	195.3	89.2	- 187.3	+ 0.971
CH ₃ CH ₂ CH ₂ NH ₂	6	195.3	97.8	- 98.3	+ 0.170

In this paper the selectivity control of the electroreduction and/or electrocatalytic hydrogenation of the nitrile group to amines is addressed. Our interest is focused mainly on both the electroreduction/electrocatalytic hydrogenation of AD to HMDA, and the electroreduction of AN and PN to PA.

EXPERIMENTAL. Acrylonitrile (99.5%, Combinatul Chimic Pitesti, Pitesti, Romania) was distilled from Na₂CO₃, and then stored over 3A molecular sieves. Adiponitrile was obtained in our laboratory by the electrohydrodimerization of AN, according to a patented procedure [23]. The 95% AD was purified by vacuum distillation at 1 torr to provide 99.5% pure product. Propionitrile was synthesized by the non-dimerizing electroreduction of AN [23 - 28]. After separation from the aqueous supporting electrolyte, PN was purified by distillation from Na₂CO₃, and stored over 3A molecular sieves. Orthophosphoric acid (Merck, Darmstadt, Germany), boric acid (Reactivul, Bucharest, Romania), glacial acetic acid (Fisher Scientific), sodium hydroxide (Malinckrodt), and potassium chlorides (Aldrich) were used as received. Porous cathodes of Ni/Zn and Ni/Al were obtained by co-deposition and by electrochemical co-deposition of Ni and Zn and of Ni and Al, respectively, followed by an activation process performed in alkaline media (30% NaOH solution in water), at 343 K [5]. Two procedures were applied: (i) co-deposition performed in homogeneous solution (sodium sulphate or chloride electrolyte), Table 2 and (ii) co-deposition accomplished in a suspension of hydroxides, Table 3. Typical current densities used were from 15 to 80 mA cm⁻², at temperatures of 288 ± 2 K.

Table 2: Composition of the electrolytic bath (g/L) and conditions for Ni / Zn alloy electrodeposition performed in homogeneous solution.

NiSO ₄ · 7H ₂ O	80	S _{cathode} (cm ²)	15
ZnSO ₄ · 7H ₂ O	40	S _{anode} (cm ²)	10 - 12
NaOH	12 - 28	i (mA/cm ²)	20 - 80
Gelatine	0.3	Temp (°C)	70
Zaharine	5-10	Time (h)	6 - 8

Table 3: Composition of the electrolytic bath⁺ (g/L) and conditions for Ni /Zn alloy electrodeposition performed in a suspension of hydroxides.

NiCl ₂	60	S _{cathode} (cm ²)	15
ZnSO ₄	30	S _{anode} (cm ²)	10 - 12
NH ₄ Cl	280	i (mA/cm ²)	15 - 80
H ₃ BO ₃	20	Temp (°C)	25 - 50
ZnAc ₂	25	Time (h)	5 - 8

20-80 mL PEG and 15-40 mL Dextrin were added.

Microphotographs of the Ni Raney cathodes were taken before and after their chemical activation by using a Tesla type BS 340 scanning electronic microscope with a resolution of 4 nm. The magnetite anode (metallic iron coated with an Fe₃O₄ layer) was obtained by heating the metallic iron electrode, for 2 hours at 633 K, in the presence of steam [29]. A 100 nm thick magnetite layer was formed at the iron surface.

The voltammetric curves were recorded with a PAR 362 Polarograph equipped with three electrodes cell (Ni Raney cathode, glassy carbon or magnetite counter-electrode and a saturated calomel reference electrode).

The undivided filterpress type cell [30] for preparative scale synthesis was equipped with a porous Ni Raney cathode and a magnetite anode. The frames of the reactor were manufactured from stainless steel, while the spacers and the insulation elements were made of silicon rubbers, resistant towards AN [31]. A peristaltic pump ensured linear circulation speeds of the supporting electrolyte in the range from 0.1 to 1.0 m s⁻¹. A thermostatic separation vessel completed the installation. Electroreduction experiments were performed under potentiostatic and quasi-isothermal conditions, at 288 ± 2 K. Typical current densities were in the range of 15-80 mA cm⁻².

RESULTS AND DISCUSSION. The composition of the obtained cathodes had a Ni/Zn ratio in the range from 9:1 to 7: 1, **Table 4**.

Table 4: Characteristics of the porous cathodes Ni/ Zn, before and after activation.

No	i $\frac{mA}{cm^2}$	η_F (%)	Ni (%)		Zn (%)		δ (μm)	S _{spec} $\frac{m^2}{g}$
			before	after activation	before	after activation		
1.	20	80.2	43.2	54.2	56.8	45.8	24	22
2.	40	76.0	45.5	55.5	54.5	44.5	52	25
3.	80	61.6	46.4	53.6	53.6	46.4	60	29
4.	20	73.4	22.5	26.2	77.5	43.2	32	16
5.	40	65.8	34.6	35.4	65.4	44.6	45	19
6.	80	46.3	44.8	47.4	55.2	42.6	49	20

* S_{spec}. was determined by BET method and composition by AA.

The activation process increases the Ni content of the deposit formed on the electrode surface. Coarse pores and cracks are developed during leaching, **Figure 1**.

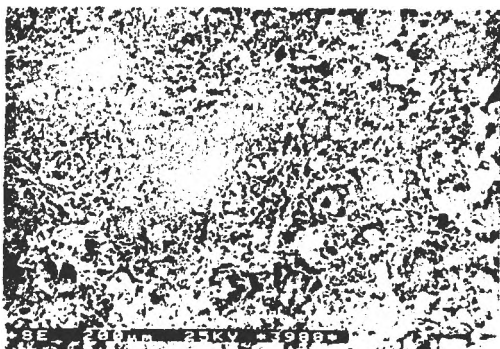
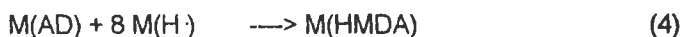
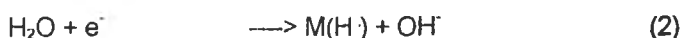


Figure 1.

SE photomicrograph of one Ni Raney cathode after activation

This rough surface of the electrode is essential for the high catalytic activity in the hydrogen discharge reaction [5,32]. The spongy Ni deposit formed *in situ* is able to adsorb atomic hydrogen, and the interface becomes saturated with hydrogen. A schematic of the possible mechanism of electrohydrogenation of AD is shown in Eqs.2-5, where M represents the cathode with electrocatalytic properties. First, adsorbed atomic hydrogen is generated by the electroreduction of water molecules (Eq.2); in a simultaneous process (Eq.3) AD is adsorbed to the cathode surface. Next, the adsorbed substrate molecules, noted as $M(AD)$, are hydrogenated with the atomic hydrogen, and adsorbed HMDA is formed (Eq.4), which eventually desorbs from the electrode surface (Eq.5).



Several secondary reactions may occur: the atomic hydrogen adsorbed to the electrode surface can be released under the form of molecular hydrogen or can reduce AD to 6-aminocapronitrile. A similar reduction mechanism can be conceived for the formation of AA.

All experiments were carried out in the galvanostatic conditions and the Ni Rane electrodes were saturated with hydrogen, before the electrochemical hydrogenation of AN or AD.

The dependence of the faradaic yield (r_F) on the pH of the supporting electrolyte and on the temperature was investigated for both the electrohydrogenation of AN to AA (Figure 2 and 3.) and of AD to HMDA (Figure 4 and 5.) respectively. As seen in Fig.2 AA is obtained with current yields up to 95% at $pH\ 7 \pm 0.5$, while propylamine formation is favoured by acidic pH values. The optimal temperature for AA synthesis is below 29°K, at higher temperature values the undesired hydrolysis of AN is intensified (Fig.3.) Also, to avoid hydrogen evolution, the current density should be maintained at values not exceeding $70\ mA\ cm^{-2}$.

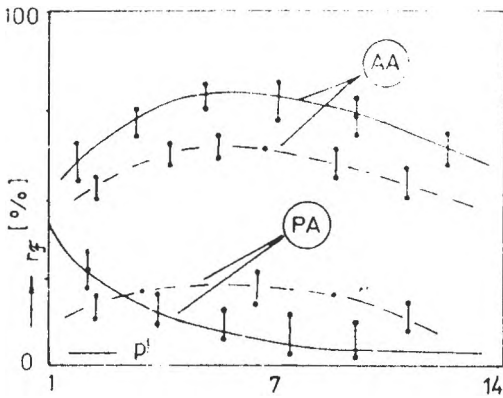


Fig. 2. The influence of pH on the r_F of AA and PA formation (at 50 mA cm^{-2} and $293 \pm 1 \text{ K}$)

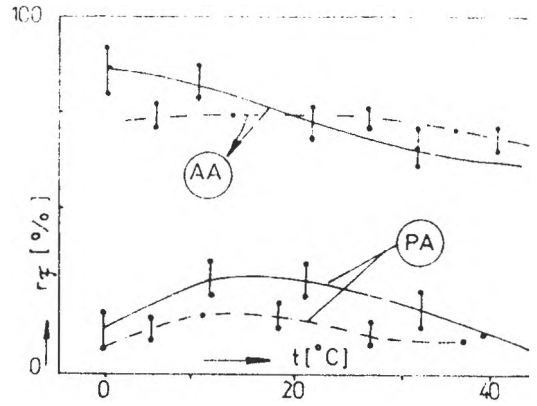


Fig. 3. Dependence of r_F of AA and PA formation on the temperature (at 50 mA cm^{-2} and $\text{pH } 7 \pm 0.2$)

AA - allylamine; PA -propylamine;
for the cathodes obtained by electrodeposition (- -) and by codeposition (---).

The selectivity for the HMDA formation for the current density bigger than 100 mA/cm^2 increases, when the AmCN formation is smaller than 10-12 %, **Figure 4.**

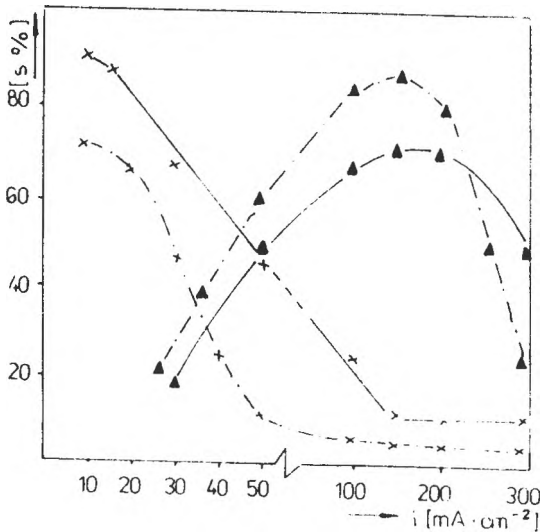


Figure 4. Dependence of S (%) on the current density
• - HMDA; x - AmCN;
(—) for the cathodes obtained by co-deposition and (- -) for the cathodes obtained by electrochemical co-deposition

Approximately neutral supporting electrolytes have proven useful for the selective electrohydrogenation of AD to HMDA. In **Figure 5** the optimal pH range for HMDA production is from pH 5 to 8. Though the selectivity is good (up to 85%), the formation of 6-amino-capronitrile (Am-CN) cannot be completely avoided. The synthesis of HMDA can be conducted at basic pH values, as well. A decrease of the faradaic yield can be, however observed ($r_F = 41.2\%$, at $\text{pH } 10 \pm 1$, and $r_F = 32.6\%$, at $\text{pH } 12 \pm 1$). Temperature values in the proximity of the freezing point of water (from 275 to 279 K) are recommended, **Figure 6**. At temperatures above 283 K the faradaic yield decreases, due to the enhancement of the hydrolysis of the starting material (AD). Simultaneously, at temperatures ≥ 293 K there is a significant increase in the concentration of the side-product, AmCN, formed by the incomplete electrohydrogenation of AD.

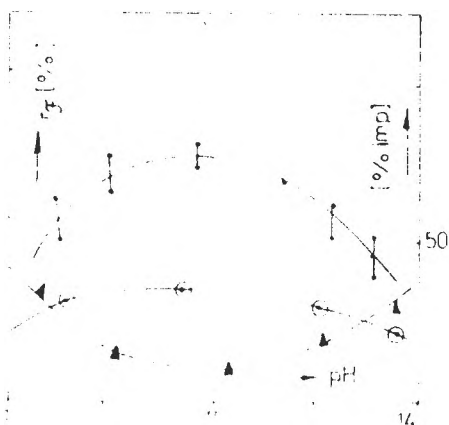


Fig.5. The influence of pH on the r_F of HMDA formation (at 50 mA cm^{-2} and $275 \pm 1 \text{ K}$)
 ○ - HMDA; ▽ - AmCN; o - hydrolysis products

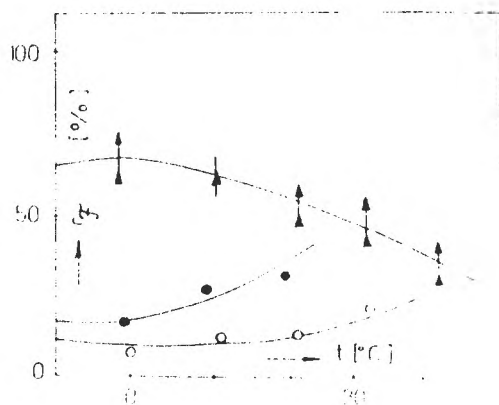


Fig.6. Dependence of r_F of HMDA on the temperature (130 mA cm^{-2} and $\text{pH } 4 \pm 1$); ▽ - HMDA; ○ - AmCN; o - hydrolysis products

CONCLUSIONS. A modified procedure for obtaining Raney Ni cathodes was described. By using a new activation procedure Ni Raney electrodes with good physico-mechanical characteristics and an improved electrocatalytic activity were obtained. Allylamine was

obtained on these electrodes with current yields up to 95%. Another successful application of such Ni Raney electrodes is the selective electrochemical synthesis of HMDA from AD. In our experiments HMDA was obtained with selectivity up to 85 %, and very satisfactory current efficiencies (> 52 %)

ACKNOWLEDGEMENTS

This work was supported by a grant from the National Council of the Scientific Research . The Ministry of Research and Technology and the PHARE financial supports are also appreciated.

REFERENCES

1. A.K.Cheong, Y.Bolduc, J.Lessard, *Can.J.Chem.*, **71**, **1993**, 1850-56.
2. B.Sakurai and T.Arai, *Bull. Chem. Soc. Jpn*, **1955**, **28**, 93.
3. J.C.Moutet, in *Organic Preparations and Procedures Int.*, **1992**, **24**, 309-25.
4. G.Belot, S. Desjardins and J.Lessard, *Tetrahedron Lett.*, **1984**, **25**, 5347
5. M. Jitaru, D. A. Lowy, Electrohydrogénation d'adiponitrile sur des électrodes Ni Raney obtenues par électrodéposition et activation, Journées d'Electrochimie, 29 may-1 june, Strasbourg (France) **1995**
6. M. R. Riffi, in: N. L. Weinberg (Ed.), *Techniques of electroorganic synthesis*, Part 2, Wiley Interscience, New York, 1974, Ch.8.
7. Y. Song and P. N. Pintauro, *J. Appl. Electrochem.*, **21**, **1991**, 21
8. M. Jitaru, L. Oniciu, I. A. Silberg, *Rev. Roum. Chim.*, **34**, **1989**, 537.
9. V. Khrishnan, A. Muthukumarau, K. Raghupathy, H. V. K. Udupa, *Trans. SAEST* **13** (1978) 161; *Chem. Abstr.*, **91**, **1974**, 4634b.
10. V. Khrishnan, K. Raghupathy, H. V. K. Udupa, *J. Electroanal. Chem. Interfacial Electrochem.*, **88**, **1978**, 433.
11. H. Kita, *J. Electrochem. Soc.*, **113**, **1966**, 1095.
12. H. Wenker, *J. Am. Chem. Soc.*, **57**, **1935**, 772.
13. O. Manousek, P. Zuman, *Chem. Commun. (London)*, **1965**, 158.
14. P. Zuman, *The elucidation of organic electrode processes*, Academic Press, New York, London, 1969, pp.95-6.
15. (a) S. Budavari (Ed.), *The Merck Index*, 11th edn., Merck & Co., Rahway, N.J., 1989, pp.49; (b) Ch. R. Taylor, A. D. Cale, Jr., H. F. Stauffer, Jr., *U. S. Pat.*, **1992**, **5,095,014**; *Chem. Abstr.*, **116**, **1992**, 255466n; (c) W. Schwab, H. Anagnostopoulos, E. Porsche-Wiebkking, J. Grome, *Eur. Pat. Appl.*, **1991**, **451,790**; *Chem. Abstr.*, **116**, **1992**, 83658h
16. Y. Okamoto, Sh. Chiiba, T. Makita, *Jpn. Kokai Tokkyo Koho*, **1991**, **03,267,9474**; *Chem. Abstr.*, **116**, **1992**, 245255d.
17. Y. Usagawa, T. Sanpei, A. Onodera, *Jpn. Kokai Tokkyo Koho*, **1992**, **04,56,949**; *Chem. Abstr.*, **116**, **1992**, 265513e.
18. A. P. Tomilov, S. G. Mairanovskii, M. Ya. Fioshin, V. A. Smimov, *Electrochemistry of Organic Compounds*, Halsted Press, Jerusalem, London (1972) pp 268-80.

19. G. Trumpler, R. Schmid, *Helv. chim. Acta*, **40**, **1957**, 1940.
20. S. Wasmus, W. Vielstich, *J. Electroanal. Chem.*, **345**, **1993**, 323.
21. H. V. K. Udupa, *Stud. Org. Chem. (Amsterdam)* **1987**, 30 (*Recent Adv Electroorg. Synth.*), p.423-31; *Chem. Abstr.*, **108**, **1988**, 94136x.
22. D. A. Lowy, M. Jitaru, B. C. Toma, I. A. Silberg, L. Oniciu, *Ind. J. Chem Technol.*, **4**, **1997**, 18.
23. L. Oniciu, I. A. Silberg, F. Ciomos, M. Jitaru, P. Popescu, D. A. Lowy, O. H Oprea, *Romanian Pat.*, **1986**, 88417; *Chem. Abstr.*, **107**, **1987**, 25114f.
24. L. Oniciu, D. A. Lowy, M. Jitaru, *Bul. Electrochem.*, **4**, **1988**, 1040.
25. L. Oniciu, I. A. Silberg, D. A. Lowy, M. Jitaru, F. Ciomos, *Stud. Univ. Babes-Bolyai, Chemia*, **31**, 1986, 80.
26. L. Oniciu, D. A. Lowy, M. Jitaru, I. A. Silberg, B. C. Toma, *Rev. Roum. Chim.*, **32**, **1987**, 701.
27. L. Oniciu, D. A. Lowy, M. Jitaru, I. A. Silberg, B. C. Toma, I. Baldea, *Rev. Chim. (Bucharest)*, **39**, **1988**, 219.
28. (a) L. Oniciu, D. A. Lowy, M. Jitaru, B. C. Toma, *Stud. Univ. Babes-Bolyai, Chemia*, **33**, **1988**, 87; (b) L. Oniciu, D. A. Lowy, M. Jitaru, B. C. Toma, *Extended Abstracts of the 40th Meeting of ISE*, Kyoto, Japan, **1989**, Vol. 2, pp. 877.
29. D. A. Lowy, *Ph.D. Thesis*, Babes-Bolyai University, Cluj, Romania, 1991
30. (a) L. Oniciu, I. A. Silberg, V. Toc, F. Ciomos, O. H. Oprea, D. A. Lowy, M. Jitaru, *Romanian Pat.*, **1987**, RO 91208.; *Chem. Abstr.* **107**, **1987**, 245181r; (b) L. Oniciu, I. A. Silberg, F. Ciomos, D. A. Lowy, M. Jitaru and O. H. Oprea, *Romanian Pat. RO 91210* (1987); *Chem. Abstr.*, **107**, **1987**, 245180q; (c) M. Jitaru, B. C. Toma, M. Toma, D. A. Lowy, *Bull. Electrochem.*, **11**, **1995**, 573.
31. L. Oniciu, D. A. Lowy, O. H. Oprea, I. A. Silberg, Z. Csipor-Fazakas, *Mater. Plast. (Bucharest)*, **21**, **1984**, 146.
32. M. Jitaru, J. Lessard, D. A. Lowy, Microstructure et activité electrocatalitique des électrodes Ni-Raney, *Proceedings of the ELFI Symposium*, Cluj-Nappoca, Romania, October 31- November 3, 1996, pp.28.
33. P.Chambion, L.Roger and J.Lessard, *Can.J.Chem.*, **73**, **1995**, 804-15.

ELECTROCHEMICAL RECOGNITION OF GROUP I OR II METAL CATIONS
BY REDOX-ACTIVE IONOPHORES
IN HOMOGENEOUS SOLUTIONS OR BY FUNCTIONALIZED MODIFIED
ELECTRODE

Mihaela Ungureanu, Eric Saint-Aman*, Ion Ion, Angela Popescu, Teodor Visan,
Jean-Claude Moutet* and Alina Catrinel Ion

Faculty of Industrial Chemistry, Politehnica University Bucharest, Roumania

**LEOPR, Université Joseph Fourier, Grenoble, France*

ABSTRACT

Two series of functionalized ferrocenes (Fc_1 and Fc_2) were synthesized and studied as redox-active ionophores. Ferrocene bis-amide derivatives (Fc_1) present properties of Li^+ electrochemical recognition in solution, but sterical constraints due to the immobilization onto the electrode surface by its pyrrole derivative electropolymerization mask the complexation effect. Ferrocene crown ethers (Fc_2) complex Ba^{2+} very selectively. Ba^{2+} is electrochemically recognized in solution as well as on the modified electrode by polypyrrole derivatives.

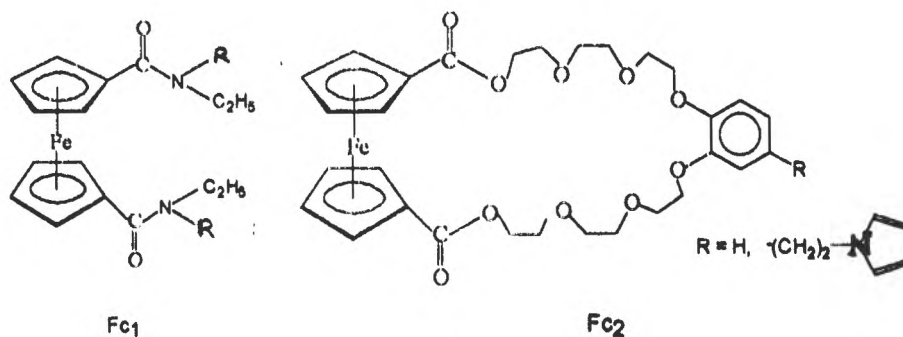
INTRODUCTION

The redox-active ionophores are molecules capable to bind selectively guest species. This complexation can be electrochemically detected by a change in the electroactivity of the redox center and has applications in electrochemical sensor technology.¹

An important step in succeeding an electrochemical sensor is its immobilization on the electrode surface if the electrochemical recognition properties could be transferred from the solution to the electrode/solution interface. Numerous binding sites have been

ELECTROCHEMICAL RECOGNITION BY REDOX-ACTIVE IONOPHORES

synthesized principally starting from macrocyclic ligands, but other groups such as bis-amides have been tested successfully. In this regard, redox centers such as transition metal complexes and organometallic compounds appear very attractive taking into account the wide variety of complexes, their good stability, and the large scale of available formal potentials. In particular, ferrocene bis-amide, ferrocene crown ethers, and cryptand derivatives exhibit remarkable complexation and recognition properties towards Group I and II metal cations.⁷ In this paper we present comparatively the selective complexation properties of two series of functionalized ferrocenes (Fc_1 and Fc_2).



EXPERIMENTAL

The synthesis and characterization of the ferrocene derivatives Fc_1 and Fc_2 have been performed.^{3,5}

Electrochemical cell and instrumentation is described elsewhere.⁶ All experiments were run at room temperature under argon atmosphere in a dry glovebox. Potentials are referred to a Ag/0.01 M AgNO₃ + 0.1 M TBAP/CH₃CN reference electrode. The working electrode was a Pt disk (5 mm diameter) polished with 1 μ m diamond paste.

All metal ions were added as perchlorates or tetrafluoroborates. Addition of salts was performed by adding small volumes of concentrated stock solution to the electrolyte. Tetra-n-butylammonium perchlorate (TBAP), obtained from Fluka was purified using the procedure described before.⁶ Tetra-n-butylammonium tetrafluoroborate (TBABF₄) was prepared from tetra-n-butylammonium hydrogensulfate and sodium tetrafluoroborate.⁷

RESULTS AND DISCUSSION

Electrochemical study of Fc_1

The cyclic voltammogram of Fc_1 ($R = H$) in $CH_3CN + 0.1 M TBABF_4$ is characterized by a reversible wave at $E_{1/2} = 0.30 V$ corresponding to the redox ferrocene/ferricinium couple (Fig.1, curve 1). The addition of increasing amounts of Li^+ caused a shift to positive potentials (Fig.1, curves 2-4) and a decrease in the intensity of the redox wave along with the appearance of a new redox wave of increasing intensity at a more positive potential ($E_{1/2} = 0.70 V$).

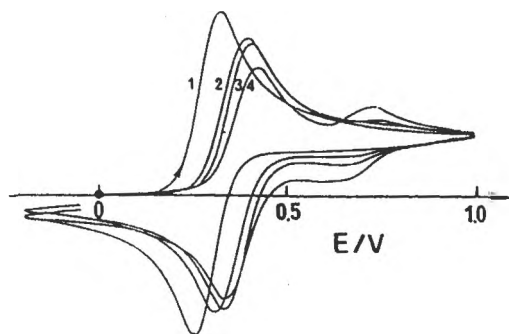


Fig. 1. Cyclic voltammograms of Fc_1 ($R = H$) in $CH_3CN + 0.1 M TBABF_4$ with different amounts (equivalents) of $LiBF_4$: 0 (1); 0.5 (2); 1 (3); 4 (4); 0.1 V/s.

This results confirm Beer's findings who established the formation of complexes between $Fc_{1,H}$ and Li^+ .⁶ The shift in potential for the initial wave was attributed to the formation of a labile complex $(Fc_{1,H})_2Li^+$ and the new wave was related to the formation of $Fc_{1,H}Li^+$ complex:



The cyclic voltammograms of $Fc_{1,P}$ ($R = pyrrole$) in $CH_3CN + 0.1 M TBABF_4$ (or TBAP) exhibited the regular reversible wave corresponding to the ferrocene/ferricinium system at $E_{1/2} = 0.3 V$ at the same potential as $Fc_{1,H}$ ($R = H$), followed at higher potential by the reversible oxidation of the pyrrole group (1.3 V). Repeated scans over 0 to 0.95 V

range led to the growth of a polymer film on the electrode. The continuous growth of the film on each cycle is accompanied by a shift of ≈ 100 mV in the formal potential until a stabilized value is reached. Poly($\text{Fc}_{1,P}$) films were also grown in potentiostatic conditions, by oxidation at 0.8–1 V, using millimolar solutions of $\text{Fc}_{1,R}$ in acetonitrile containing 0.1 M TBAP. The electropolymerization was carried on until the desired charge ($Q_p = 0.2$ –5 mC) was passed. For each specific charge between 0.2 and 2 mC reproducible films have been obtained having the same apparent surface concentration of ferrocene (Γ) within 10 %.

After transfer of the electrode in a pure electrolyte, the cyclic voltammogram shows the electrochemical response of the modified electrode owing to the ferrocene/ferricinium system in the film at $E_{1/2} = 0.4$ V.

In the presence of Li^+ a positive shift of 110 mV in the $E_{1/2}$ of the redox wave corresponding to $\text{Fc}_{1,P}/\text{Fc}_{1,P}^+$ has been found in the presence of an excess of Li^+ ion confirming the complexation properties of the bis-tertiary amide group in $\text{Fc}_{1,H}$ and $\text{Fc}_{1,P}$.

The influence of Li^+ ion on the electropolymerization of $\text{Fc}_{1,P}$ was studied, too. Films were prepared in solutions having various Li^+ concentrations and transferred in $\text{CH}_3\text{CN} + 0.1$ M TBAPF₄. The evolution of the deposition efficiency in the presence of increasing amounts of Li^+ in the polymerisation solution is depicted in Fig. 2.

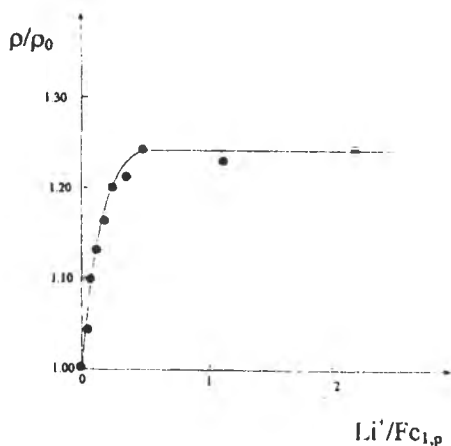


Fig. 2. Variation of deposition efficiency vs. LiBF_4 concentration in the preparation solution of poly($\text{Fc}_{1,R}$) containing also $\text{CH}_3\text{CN} + 0.1$ M TBAP + 1 mM $\text{Fc}_{1,P}$ at constant potential of 0.85 V electropolymerization charge: 1 mC; ρ_0 and ρ are respectively, the deposition efficiencies in the absence and in the presence of Li^+ .

A limiting value of 37.5% was reached for a $\text{Li}^+/\text{Fc}_{1,P}$ ratio higher than 0.5 in the preparation solution, confirming the previously reported stoichiometry for the complex. One can assume that the complexation of $\text{Fc}_{1,P}$ with Li^+ is favored in the polymerization, which is presumable initiated via intramolecular coupling in the $\text{Fc}_{1,P} \text{Li}^+$ complex rather than via intermolecular coupling.

In conclusion, two different processes cause a positive shift in the formal potential of the $\text{Fc}_{1,P}/\text{Fc}_{1,P}^+$ redox couple. Both Fc_1 species present properties of Li^+ electrochemical recognition in solution. For $\text{Fc}_{1,P}$, sterical constraints due to the immobilization on to the electrode surface by its pyrrole derivative mask the complexation effect.

Electrochemical study of Fc_2

A series of different ferrocene crown ether macrocycles have been investigated by CV in acetonitrile solution with 0.1 M TBAP as supporting electrolyte, and tested in complexation. For 2 oxygen member ring no complexation appears, and for 4 oxygen member ring only a weak complexation with Li^+ and Na^+ was noticed. Only for 6 oxygen member ring ($\text{Fc}_{2,H}$) a strong complexation of Ca^{2+} and Ba^{2+} was observed. The CV curve is characterized by a quasi-reversible redox wave at $E_{1/2} = 0.53 \text{ V}$ ($\Delta E_p = 100 \text{ mV}$ at 0.1 V s^{-1}). The current associated with the new redox couple increases linearly with the concentration of Ba^{2+} cation until a full equivalent has been added (Fig. 3).

Then the original wave disappears and the new redox couple reaches full development. These findings suggest the formation of a 1:1 complex between Ba^{2+} and $\text{Fc}_{2,H}$. Formation of this complex has been corroborated by UV-VIS and $^1\text{H-NMR}$ spectrophotometric studies.

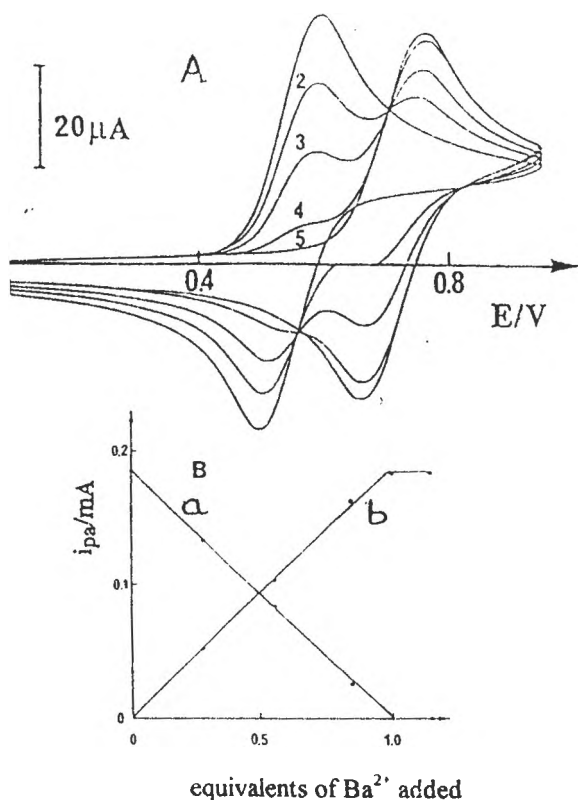


Fig. 3. (A) Cyclic voltammograms of $\text{Fc}_{2,\text{H}}$ (3.7 mM) in $\text{CH}_3\text{CN} + 0.1 \text{ M TBAP}$ at different ratios $\text{Ba}^{2+}/\text{Fc}_{2,\text{H}}$: 0 (1); 0.28 (2), 0.56 (3); 0.84 (4); 1 (5); (B) Oxidation peak current vs. Ba^{2+} concentration for the free (curve a) and complexed (curve b) $\text{Fc}_{2,\text{H}}$; 0.1 V/s.

The selectivity of the complexation process towards group I and II metal cations was judged from CV and UV-VIS experiments. Li^+ and Mg^{2+} cations have no effect on the electrochemical behaviour of $\text{Fc}_{2,\text{H}}$. Moreover the addition of increasing amounts of Na^+ and K^+ cations to solutions of Fc_2 results in a continuous positive shift in potential of the ferrocene wave but no new redox couple is observed. The shift of the positive potential reached a maximal value of 50 mV in the presence of at least 5 equivalents of Na^+ or K^+ cations. Like Ba^{2+} the addition of Ca^{2+} cations causes two wave behaviour with the rise of a new less reversible redox wave ($E_{1/2} = 0.53 \text{ V}$, $\Delta E_p = 120 \text{ mV}$ at 0.1 V s^{-1}) at the expense of the original ferrocene/ferrocinium wave. The formation of a $\text{Fc}_{2,\text{H}}\text{Ca}^{2+}$ complex having 1:1 stoichiometry was confirmed by UV-VIS titration. $\Delta E_{1/2}$ between free and Ca^{2+} complexed $\text{Fc}_{2,\text{H}}$ is smaller (120 mV) than with Ba^{2+} (160 mV) indicating a lower stability constant for Ca^{2+} complex compared with Ba^{2+} complex. The crown ether $\text{Fc}_{2,\text{H}}$ cavity provides an optimal spatial fit for the Ba^{2+} guest cation. Thus, $\text{Fc}_{2,\text{H}}$ appears to be an attractive redox switchable ionophore for the construction of electrochemical sensory devices.

ELECTROCHEMICAL RECOGNITION BY REDOX-ACTIVE IONOPHORES

The $\text{Fc}_{2,R}$ ($R = \text{pyrrole}$) electrochemical behaviour was also investigated in $\text{CH}_3\text{CN} + 0.1 \text{ M TBAP}$. The CV curve is characterized by a quasi-reversible redox wave at 0.53 V corresponding to the ferrocene/ ferricinium couple. This wave is followed at higher potential by a large peak ($E_{p,a} = 0.97 \text{ V}$) which is due to the irreversible oxidation of both the pyrrole group and benzocrown ether moiety of $\text{Fc}_{2,P}$. It was established that the electrooxidative polymerization of functionalized pyrrole is an effective method for carrying out the coating of electrode surface by non-passivating polymer layers containing redox-active centers. The growth of $\text{poly}(\text{Fc}_{2,P})$ films on Pt electrode was accomplished either by repeated CV scans or controlled potential electrolysis at 0.8 V . The resulting modified electrodes transferred to clean CH_3CN electrolyte exhibit a stable electrochemical response for immobilized $\text{Fc}_{2,P}$ at the formal potential of 0.56 V (Fig. 4, curve 1; p_a^f and $p_c^f =$ anodic and cathodic peaks of the free ferrocene).

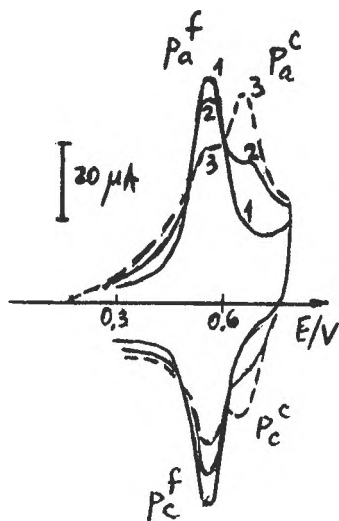


Fig. 4. CV of a $\text{poly}(\text{Fc}_{2,P})$ modified electrode (1mC) in $\text{CH}_3\text{CN} + 0.1 \text{ M TBAP}$; $[\text{Ba}^{2+}]$: 0 (1); 10^{-6} (2); $2 \cdot 10^{-6}$ (3) M; 0.1 V/s .

In the presence of increasing amounts of Ba^{2+} a new redox wave rises at $E_{1/2} = 0.7 \text{ V}$ (Fig.4, curves 2 and 3; p_a^c and $p_c^c =$ anodic and cathodic peaks of the complexed ferrocene) at the expense of the original redox wave at $E_{1/2} = 0.53 \text{ V}$. For $\text{Ba}^{2+}/\text{Fc}_{2,P}$ ratio greater than 1 only the second wave remained. This suggests the formation of a 1:1 complex between $\text{Fc}_{2,P}$ and Ba^{2+} , like its pyrrole-free analogue. This process was additionally confirmed by UV-VIS spectrophotometric studies. A two-wave behaviour was also noticed by adding increasing amounts of Ca^{2+} cations to an electrolytic solution of $\text{Fc}_{2,P}$. The decrease of the free $\text{Fc}_{2,P}$ wave and the appearance of a new redox wave at $E_{1/2} = 0.65 \text{ V}$ can be associated with the formation of 1:1 $\text{Fc}_{2,P}\text{Ca}^{2+}$ complex.

However, competitive complexation experiments have shown that the receptor $\text{Fc}_{2,1}$ exhibit a large selectivity for Ba^{2+} against Ca^{2+} . Addition of Ba^{2+} to an electrochemical solution of $\text{Fc}_{2,1}$ Ca^{2+} resulted in a gradual positive shift of the redox wave from 0.65 V up to 0.7 V. This potential was reached when one equivalent of Ba^{2+} was added. The addition of 10 equivalents of Ca^{2+} to this solution did not cause any change in the CV curve. These result indicates that Ba^{2+} takes gradually the place of Ca^{2+} in the complex and confirms the selectivity of the benzocrown ether structure towards Ba^{2+} complexation.

$\text{Fc}_{2,1}$ retains its recognition properties after its electropolymerization. This is demonstrated by the changes in the electrochemical response of the poly($\text{Fc}_{2,1}$) modified electrode studied by CV in $\text{CH}_3\text{CN} + \text{TBAP}$ electrolyte in the presence of increasing amounts of $\text{Ba}(\text{ClO}_4)_2$ (Fig. 4). The addition of Ba^{2+} results in the appearance of a new redox wave ($E_{1/2} = 0.68$ V) at the expense of the regular wave for the immobilized $\text{Fc}_{2,1}$ ($E_{1/2} = 0.56$ V). Analysis of the peak currents for ferrocene signal free and complexed as a function of Ba^{2+} concentration gives a calibration curve (Fig.5 curve 1) which is characterized by a linear increase at low Ba^{2+} concentration ($< 10^{-6}$ M) to reach a plateau at about $2 \mu\text{M}$ Ba^{2+} concentration for thin films (Fig.5). The slope of the calibration curve increases when the film thickness decreases.⁹

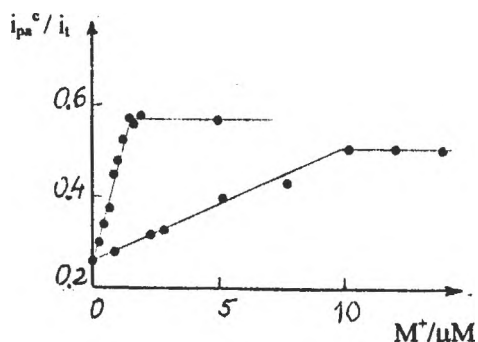


Fig. 5. Calibration curve for Ba^{2+} (1) and Ca^{2+} (2) recorded on poly($\text{Fc}_{2,1}$) modified electrode; $i_t = i_{pa}^c + i_{pa}^o$; $\Gamma = 2 \cdot 10^{-9}$ mol/cm².

As in homogenous solution, a two-wave electrochemical behaviour was observed with

poly($\text{Fc}_{2,P}$) in the presence of Ca^{2+} . The $E_{1/2}$ for the poly($\text{Fc}_{2,P}$ Ca^{2+}) redox system (0.66 V) is very close to that for the poly $\text{Fc}_{2,P}$ Ba^{2+} redox system (0.68 V).

Competitive complexation experiments were not possible. However, the slopes of the calibration curves (Fig.5, curve 2) show that poly($\text{Fc}_{2,P}$) is less sensitive to Ca^{2+} than to Ba^{2+} (Fig.5, curve 1). In addition we found that poly($\text{Fc}_{2,P}$) was insensitive to other group I and II metal cations such as Li^+ , Na^+ , K^+ and Mg^{2+} .

In conclusion, the electrochemical polymerization of the pyrrole substituted ferrocene crown ether leads to a polymer film modified electrode showing remarkable behaviour for the amperometric recognition and titration in an organic solvent of Ca^{2+} and Ba^{2+} among the alkaline and alkaline earth metal cation.

Acknowledgements: The authors thank Dr. A. Deronzier for fruitful discussions and laboratory facilities and "Région Rhône-Alpes" for partial financial support through TEMPRA program.

References

1. P. D. Beer, *Adv. Inorg. Chem.* 39 (1992) 79.
2. Z. Chen, A.J. Pilgrim and P.D. Beer, *J. Chem. Soc., Faraday Trans.* 91 (1995) 4331.
3. J.-C. Moutet, E. Saint-Aman, M. Ungureanu and T. Visan, *J. Electroanal. Chem.* 410 (1996) 79.
4. J.-C. Moutet, E. Saint-Aman, I. Ion, *J. Electroanal. Chem.* 415 (1996) 187.
5. A. Ion, I. Ion, A. Popescu, M. Ungureanu, J.-C. Moutet and E. Saint-Aman, *J. Electroanal. Chem.*, in press.
6. A. Deronzier, J.-C. Moutet and E. Saint-Aman, *J. Electroanal. Chem.* 327 (1992) 147.
7. E. Saint-Aman, M. Ungureanu, T. Visan and J.-C. Moutet, *Elchim. Acta*, in press.

ELECTROCHEMICAL RECOGNITION BY REDOX-ACTIVE IONOPHORES

8. P.D. Beer, H. Sikanyika, C.Blackburn and J.F. McAleer, *J. Organomet.Chem.* 350 (1988) C15; P.D. Beer, A. Keefe, H. Sikanyika, C.Blackburn and J.F. McAleer, *J. Chem.Soc. Dalton Trans.* (1990) 3289.
9. A. Ion, I. Ion, A. Popescu, M. Ungureanu, J.-C. Moutet and E. Saint-Aman, *J. Chem. Commun.*, submitted.

**ELECTROCHEMICAL BEHAVIOUR OF A NEW OXAZOLIDINE
DERIVATIVE, INTERMEDIATE IN THE
CHLOROMYCETINE SYNTHESIS**

Maria Jitaru^a, C. Molnet^b and M. Darabantu^a

^a "Babes-Bolyai" University, Cluj-Napoca
Faculty of Chemistry and Chemical Engineering
St. Arany Janos No.11,RO- 3400 Cluj-Napoca, Roumania

^b University of Rennes I
Laboratory of Electrochemistry and Organometallics
Campus of Beaulieu, 35042 Rennes, France

ABSTRACT

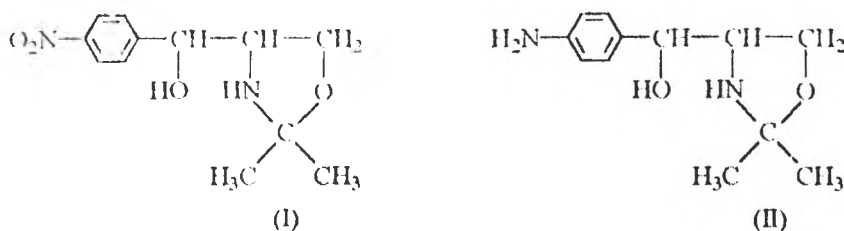
The 2R(S)-2,2 dimethyl-4-[(4-nitrophenyl)-1,3-oxazolidine (I) was prepared by the reaction between *threo* 2-amino-1-(4-nitrophenyl)-propane -1,3-diol and acetone[1]. The electrochemical reducibility of (I) was studied in hydroalcoholic (0.1 M Bu₄NBF₄ and/or H₂SO₄), in DMF (0.1 M Bu₄NBF₄) and in DMF- water solution. In aqueous solutions the polarographic reduction of (I) to 2R(S) -2,2 dimethyl-4-[(4-aminophenyl) -1,3-oxazolidine (II) occurs in a single four-electron step and in the presence of 10-30% DMF the separation of two waves can be observed. The pH-dependence of the half-wave and peak potentials was discussed. A new preparative scale electrochemical method for the synthesis of (II) is described. The UV-Vis and IR spectroscopic characteristics of (I) and (II) and the results of CG-SM methods proved the conservation of the oxazolidine ring during electrosynthesis. Due to their biological activity (I) and (II) are of interest for the pharmaceutical industry.

Key-words : electroreduction, organic electrosynthesis, nitroderivatives, DME polarography, cyclic voltammetry.

INTRODUCTION

The electroreduction of nitroarenes has been investigated since the beginning of the twentieth century, but there is still scientific and practical interest in this field [2-5]. Thus, the electrochemical reduction of (I) to (II)

proved to be an advantageous synthetic route to obtain an intermediate for the chloromycetine preparation [6]. In this case, the interest is the conservation of the oxazolidine ring during the electro-synthesis [7].



The heterogeneous $-N=O$ bond of nitro [8,9] and nitroso [10] derivatives is reducible by polarography, in both aqueous and non-aqueous solution. It is widely accepted that the reducibility of $-NO_2$ group depends on the molecular skeleton [11,12], the composition of electrolyte - pH [12] co-solvent and presence of the surfactants [13,14] - electrocatalytic activity of the electrodes [15], current density and potential [16].

EXPERIMENTAL

Synthesis of (I)

The reaction between *threo* 2-amino-1-(4-nitrophenyl)-propane-1,3-diol and $(CH_3)_2CO$ is carried out in aqueous solutions and has been reported previously [1].

Chemicals and solutions for electrochemical determinations

DMF, alcohol, and water were purified by vacuum and atmospheric distillation respectively, and cooling under argon to exclude oxygen.

For the polarographic and cyclic voltammetric measurements all chemicals were obtained from Fluka Chemical Company, except (I) which was prepared according to Darabantu's method [1]. 0.1 M Stock solution of (I) was prepared in DMF and stored in the dark.

Buffer solutions used in the specific pH range were Britton-Robinson type. All pH measurements were carried out in aqueous media before the eventual addition of DMF. In mixtures with organic co-solvents pH values of the aqueous component (before addition of organic solvent) were measured.

Polarography

Polarographic curves were recorded with a Taccussel Polarograph and registered with X-Y Recorder BD 90 Kipp and Zonen. An electrolytic cell (Kalousek cell) with a liquid junction was used. All the solutions were deoxygenated (A_r 99.9%) for 4 min., before the recording of the current-voltage curves.

Cyclic voltammetry

The voltammetric curves were recorded with a PAR 362 Polarograph HMDE and SMDE cell, PARC 303A type, with a glassy carbon counter-electrode and a saturated calomel reference electrode (SCE).

Spectroscopic measurements

To confirm the structure of (I) and (II), the IR spectra were recorded, using a FT-IR Nicolet 205 and Karl-Zeiss Jena UR 20 spectrophotometer in the $250\text{-}4000\text{ cm}^{-1}$ range and Perkin-Elmer 204B analyser. The samples were introduced as KBr pellets and nujol. The UV spectra were recorded with a Hewlett-Packard 8452 A spectrophotometer.

CG-SM determinations

The analysis of the mixture after the electrosynthesis were carried out with an Perkin-Elmer 990 Gas-Chromatograph linked with a Mass-Spectrometer type Varian Mat 311.

Preparative scale electrosynthesis

Electrochemical reduction of (I) on Hg was made under potentiostatic conditions using a Potentiostat PRT 20-2 (0.5-2A) and 1G5-N Integrator (0.1-10A), in both aqueous solution and water : DMF mixture.

RESULTS AND DISCUSSIONS

1. In aqueous buffered solutions (pH=1-14) a single four-electron wave is observed. The polarographic limiting current is depending on the concentration of (I) between 10^{-4} - 10^{-3} M, (figure1).

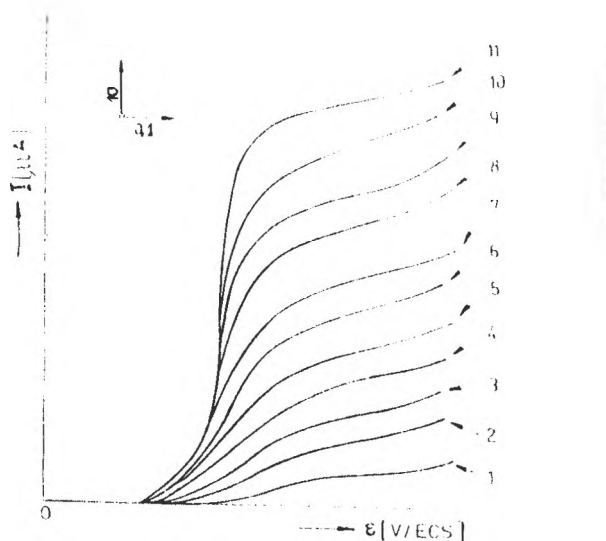


Figure 1.

Polarographic curves of (I) in Britton - Robinson aqueous solution (pH=2.5) ; concentrations of (I) : from 1×10^{-4} M (curve 1) to 1.1×10^{-3} M (curve 11).

2. In the hydroalcoholic medium the absorption of the R-NHOH intermediate takes place for the $E = -0.7\text{ V/ SCE}$, when a single adsorption maximum is observed (figure 2).

At the more positive potentials (I) is still adsorbed, because of the interaction of the π electrons of the rings with the positively charged surface [13].

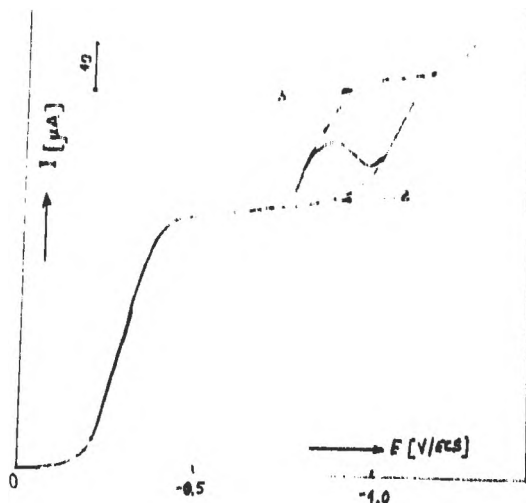


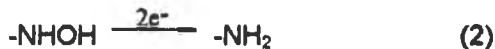
Figure 2.

Polarogrammes of (I) in hydroalcoholic solution (H_2SO_4 2.5M : EtOH=1 : 4); $E_0 = 0.4$ V/SCE ; $E_1 = -1.2$ V/SCE; $v=5\text{mv/sec}$; $s=1\text{mA}$; $\tau = 2$ sec.; $t = (20 \pm 0.5)^\circ\text{C}$.

3. For the first half-wave potential, $E_{1/2} = -0.28$ V/SCE, the limiting current, $i_L = 70\mu\text{A}$ is due to -NO reduction:



At $E_{1/2} = -1.05$ V/SCE the limiting current, $i_L = 35\mu\text{A}$ is attributed to bielectronic reduction of the hydroxylamine intermediate:



4. As is expected [8-10], the half-wave potentials, $E_{1/2}$, of the first step of the reduction of the nitro group are shifted to more negative values with increasing pH, figure 3, curve 1, and corresponds to a four-electron process.

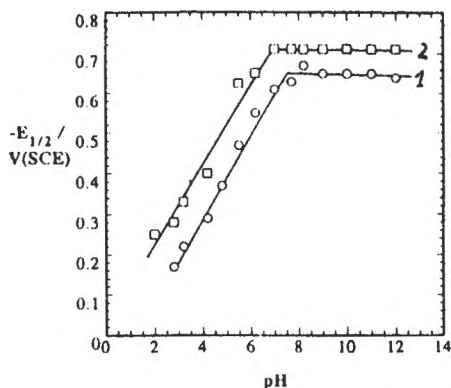


Figure 3.

Dependence of polarographic half-wave potentials upon pH in aqueous solution (curve 1) and in water : 20% DMF solution (curve 2); concentration of (I) 5×10^{-4} M.

5. In DMF : 0.1 M Bu_4NBF_4 solution, the first one-electron reversible process:



was observed, figure 4, both on glassy carbon and Hg electrodes, according to Stradins [9].

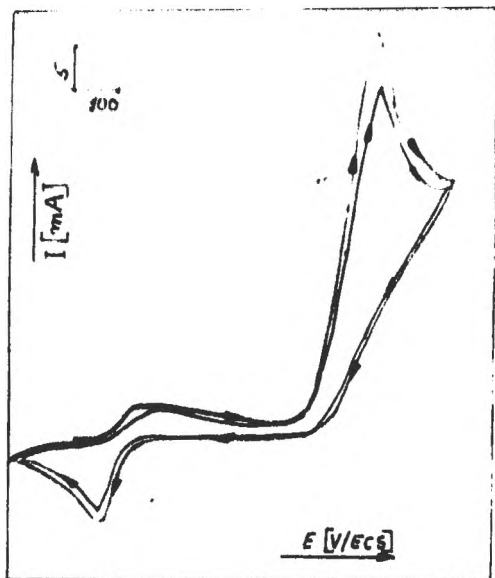


Figure 4.

Voltammogram of (I) in DMF (0.1 M Bu_4NBF_4) on Hg ; $E_0 = 0$; $E_r = -1.6$ V/SCE ; 5×10^{-4} M (I) ; $v = 100$ mv/sec.

Even in the presence of small quantities of water the reduction of $-\text{NHOH}$ to $-\text{NH}_2$ is possible, figure 5, what is proved by the new reduction peaks in the more negative region of potentials.

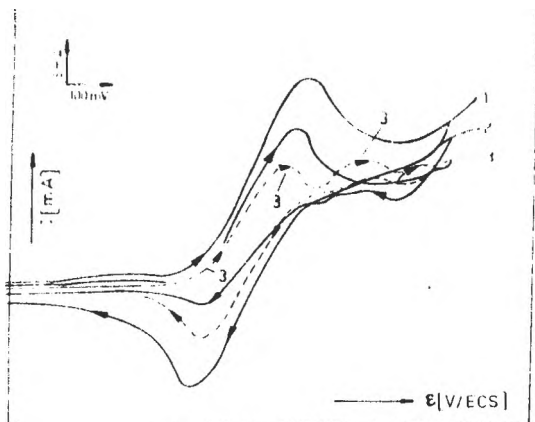
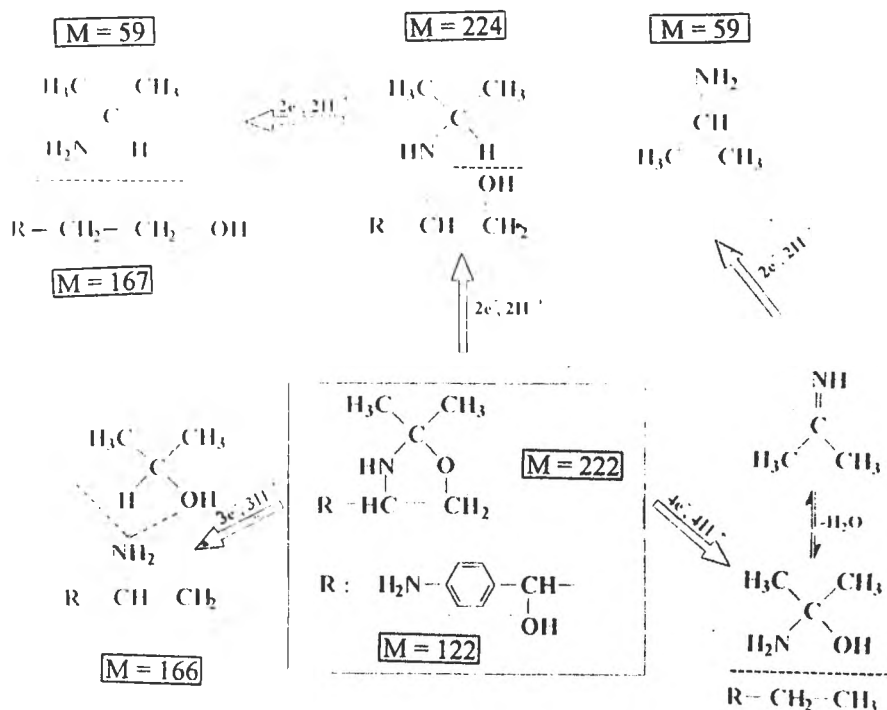


Figure 5.

Electrochemical behaviour of (I) in the presence of 5% water for the different scan rates : curve 1-200 mv/sec. ; curve 2-100 mv/sec. curve 3 - 50 mv/sec.

6. During the electrosynthesis in aqueous solution it can undergo oxazoline ring opening (Scheme 1). Such a process has been proposed to account for the changes in composition of products of electrolysis of (I).



In addition to the nitro group reducibility the self-condensation can occur, for the $pH > 8$. Faster self-condensation reactions can play a role during electrosynthesis and result in the formation of new waves on polarographic curves or/and new voltammetric peaks, corresponding to reduction or condensation products [15].

In the presence of 10-25% DMF the oxazolinic structure is conserved and (II) was obtained with $r_{ch} = 78\%$ and $r_F = 80\%$.

ACKNOWLEDGMENTS

This work was supported by a grant from the Roumanian Academy of Science. The support of the Ministry of Research and Technology is also appreciated.

We express our gratitude to M. Pierre Hurvois of Rennes I University, for the scientific discussions.

REFERENCES

1. M. Darabantu, S. Mager, Camelia Puscas, M. Bogdan, Eleonora Cotoră, G. Ple and I. Bratu, *Rev. Roum. Chim.*, 1994, **39**(6),955-65.

1. G. Ple and I. Bratu, *Rev. Roum. Chim.*, 1994, **39**(6),955-85.
2. B. S. Jensen, and V. D. Parker, *J. Chem. Soc. Chem. Commun.*, 1974,**30**.
3. I. Rubinstein, *J. Electroanal. Chem.*, 1985, **183**, 379.
4. L. Onichu, Maria Jitaru, G. Bocsa, *Electrocataliza*, Ed. Stiintifica si Enciclopedica, Bucuresti 1991, p. 305 - 311.
5. P. Pouillon, A. M. Martre and P. Martinet, *Electrochim. Acta*, 1982, **27**, 853.
6. V. I. Isagulyants and V. R. Melikien, *Khim. Farm. Zh.*, 1971, **8** (10), 35-6.
7. Maria Jitaru, C. Molnet, M. Darabantu and Cecilia Cristea, *Symposium "Electrochemistry a Frontier Field of Theoretical and Practical Interest"*, 31 October-3 November 1990, Cluj-Napoca, Romania, p.29.
8. W. Kemula and T. M. Krygowski, "Encyclopedia of the Electrochemistry of the Elements, vol. XIII", M. Dekker, New York, 1979, p.77-130.
9. Ya. Stradins, "Polarography of Nitrocompounds", Publ. House of the Latvian S. S. R., Riga, 1961, p.166
10. Maria Jitaru, B. C. Toma, Mariana Toma and D. A. Lowy, *Bull. of Electrochem.*, 1986, **11** (12),573-77.
11. A. Darchen, C. Molnet, *J. Electroanal. Chem.*, 1969, **81**, 373.
12. C. Karakus, P. Zuman, *J. of Electroanal. Chem.*, 1996, **396**, 599-605.
13. E. Lavtron, R. Meunier-Prest and R. Lacasse, *J. of Electroanal. Chem.*, 1994, **378**, 263-74.
14. B. Kastening and L. Hollek, *J. Electroanal. Chem.*, 1970, **27**, 355.
15. P. Zuman, Z. Fijalek, Dragica Dumanovic and Desanka Suanjlevich, *Electroanalysis*, 1992, **4**, 763-94.
16. C. Nishirara and H. Shindo, *J. Electroanal. Chem.*, 1987,**221**, 245.
17. M. Jitaru, C. Molnet, *Can. J. Chem.*, *in print*

ELECTROCHEMICAL AND STRUCTURAL CHARACTERIZATION OF Ti/TiO₂
ELECTRODES OBTAINED BY THERMAL METHODS AND TESTED
IN THE ELECTROREDUCTION OF 4,4'-DINITROSTILBENE-2,2'-DISULFONIC
ACID (DNSS)

Virginia Danclu, Veronica Coşoveanu, Diana Lemnaru, Anne-Marie Martre*,
G. Moussat *

*"Babes-Bolyai" University, Faculty of Chemistry and Chemical Engineering,
Team of Chemical Research 11, Arany Janos, 3400 Cluj-Napoca, Roumania*

** "Blaise Pascal" University, UMR 6504 : S.E.E.S.I.B Team of
Electrosynthesis and Bioorganic Electroanalysis, 24 Avenue des Landais,
63177 Aubiere Cedex, France*

ABSTRACT

Ti/TiO₂ electrodes are obtained by thermal methods. The best conditions of preparation were determined from the influence of roughening and number of thermal cycles on the structure and electrocatalytic properties of the TiO₂ coat. Structural analysis of electrodes was performed by scanning electron microscopy with X-ray detection and by X-ray diffraction. The results proved that the TiO₂ layer formed on the electrode's surface has not a homogeneous structure. However, the crystalline anatase form prevails. Electrocatalytic activity of the prepared electrodes was studied by cyclic voltammetry. The influence of pH, number of thermal cycles and sweep rate on the peak of cathodic current was also investigated. The behaviour of these electrodes in the electroreduction of DNSS confirms their electrocatalytic activity. The products of the electroreduction were determined photodensitometrically.

KEY WORDS: electroreduction, electrocatalytic activity, nitroderivatives, Ti/TiO₂

INTRODUCTION

The electrochemical reduction of nitrocompounds is of great interest because it considerably avoids environmental pollution. It also has a better selectivity than the chemical reduction. Direct electroreduction of some aromatic nitrocompounds by using metal and graphite cathodes in H₂SO₄ and HCl media, stops at phenylhydroxylamine. Thus yields of amines and their current efficiency are low so that isolation requires additional operations [1].

An indirect electrochemical method is in use to increase the current efficiency and the yield of products. By *in situ* regeneration of Ti³⁺ from the Ti⁴⁺ salt on a copper

cathode, aromatic nitrocompounds could be conveniently reduced to their corresponding amines [2,3,4]. The main problems raising within this technique were the hydrolysis of Ti^{4+} and Ti^{3+} salts in low acidity media as well as the recovery of soluble aromatic amines from the salty solutions.

A more efficient redox catalytic process to obtain aromatic amines would involve the use of thermally deposited Ti^{4+}/Ti^{3+} redox species, as redox mediators. Beck and Gabriel [5] developed a titanium dioxide coated titanium electrode, a stable Ti^{4+}/Ti^{3+} redox electron carrier, which had been used in the reduction of nitrocompounds.

P.N. Anantharaman and co-workers [6-9] started the study of catalytic redox behaviour of titanium dioxide coated titanium electrode in the absence or presence of some nitrocompounds, by using cyclic voltammetry as well as preparative scale experimental techniques. This electrode behaves as an efficient heterogeneous redox electron carrier, thus nitrocompounds can be catalytically reduced with a high current efficiency. The described method to obtain aromatic amines is an environmentally friendly technique, so that it can be commonly adopted to prepare various nitrocompounds.

Our work consists in the electrochemical and structural characterization of Ti/TiO_2 electrodes obtained by thermal methods. The obtained electrodes were tested for the indirect electroreduction of DNSS. Results are reported below.

1. ELABORATION OF TITANIUM DIOXIDE COATED TITANIUM ELECTRODES

In order to obtain Ti/TiO_2 electrodes, a thermal method was used. It involves two steps: (1) a roughening of the titanium electrode, to assure a good adherence of TiO_2 layer and (2) thermal treatment to obtain the TiO_2 layer.

1.1. Roughening of titanium electrodes

According to scanning electron microscopy images for sample no.2 (Figure 1) and sample no.3 (Figure 2), an increase of immersion time of the metal in acid mixture, from 30 to 60 min., leads to the appearance of holes in its surface. Same heterogeneous surface is obtained when increasing the hydrochloric acid concentration - see sample no.4 (Figure 3).

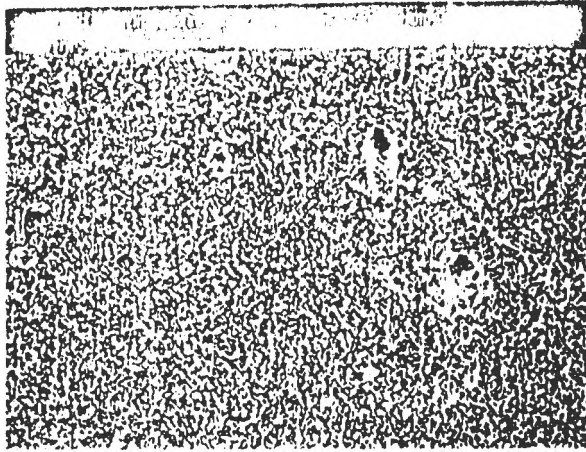


Figure 1 SEM for sample no.1

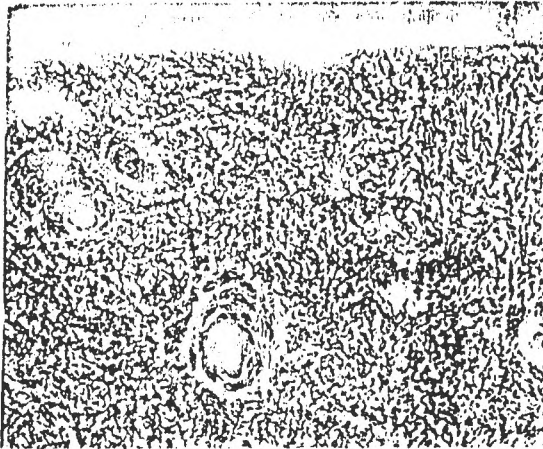


Figure 2. SEM for sample no. 2

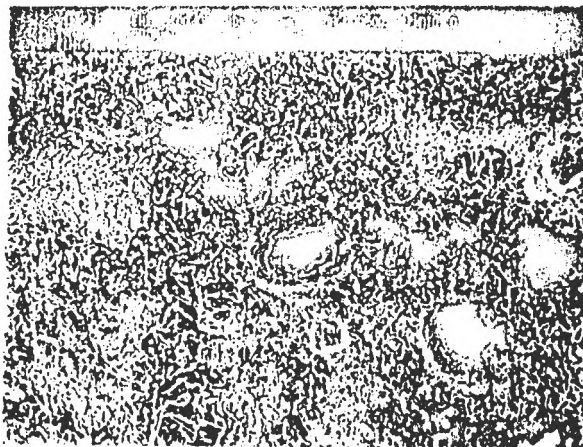


Figure 3. SEM for sample no. 3

1.2. Coating of titanium with TiO₂ by thermal method

The TiO₂ coated titanium electrodes were prepared by following the standard procedure developed by Beck et al. [5] although slight changes were made.

2. STRUCTURAL CHARACTERIZATION OF Ti/TiO₂ ELECTRODES

Scanning electron microscopy with X-ray detection (SEM-RX) and X-ray diffraction were used to characterize the layer's structure.

2.1. Scanning electron microscopy with X-ray detection

The SEM-RX images of samples 9 (fig.4) and 10 (fig.5) show that by increasing the number of thermal cycles the surface becomes more homogeneous.

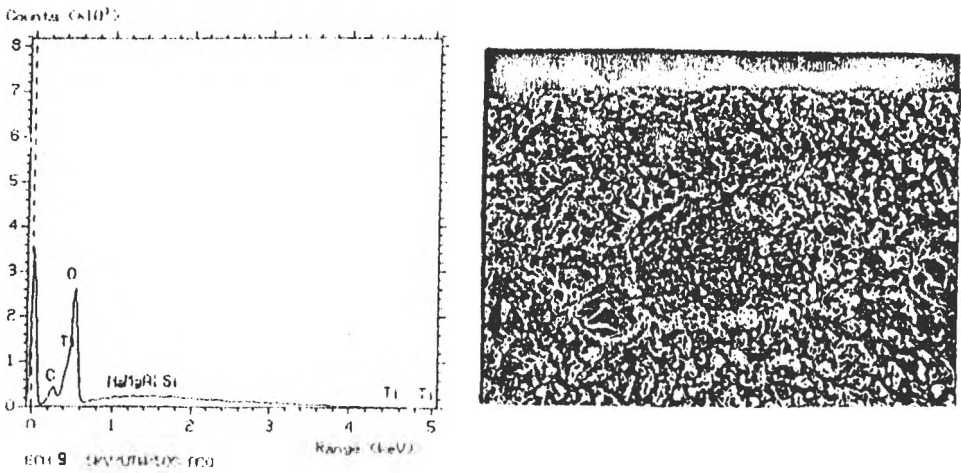


Figure 4. SEM and RX for sample No. 9 (5 thermal cycles) :

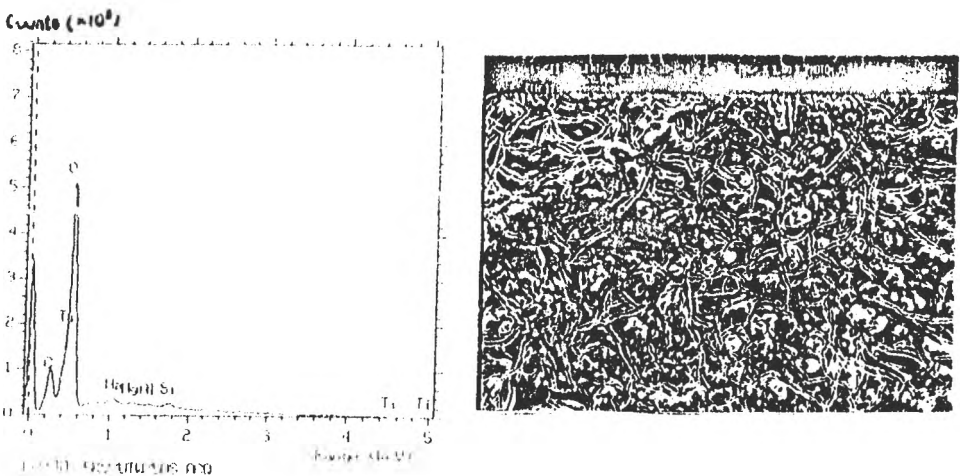


Figure 5. SEM and RX for sample No.10 (10 thermal cycles) :

Analysis by SEM and RX detection shows that the greater number of thermal cycles the thicker the TiO₂ layer is.

2.2. X-ray diffraction

According to X-ray diffraction diagrams, even if the TiO₂-anatase form prevails, the obtained TiO₂ layer has not an homogeneous structure.

3. ELECTROCHEMICAL CHARACTERIZATION AND THE TEST OF Ti/TiO₂ ELECTRODES

The redox behaviour of Ti/TiO₂ electrodes was studied by cyclic voltammetry in order to evaluate the influence of: pH (fig.6), sweep rate (fig.7) and number of thermal cycles (fig. 8).

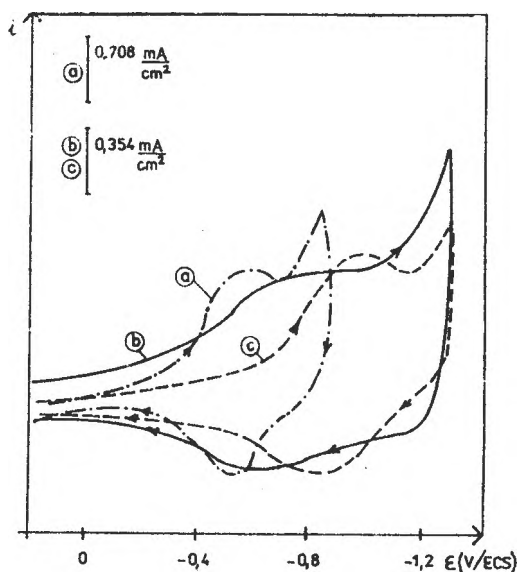


Figure 6. Cyclic voltammograms on Ti/TiO₂ thermally coated electrode (10 cycles) in (a) 1M H₂SO₄, (b) 0.1M Na₂SO₄ and (c) 1M NaOH at $v = 100 \text{ mV s}^{-1}$

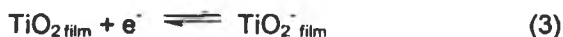
At constant sweep rate, the cathodic current peak ($i_{p,c}$) decreases in the following order : $i_{p,c} (\text{H}_2\text{SO}_4) > i_{p,c} (\text{NaOH}) > i_{p,c} (\text{Na}_2\text{SO}_4)$. The cathodic peak potential ($E_{p,c}$) shifts towards the negative domain when increasing pH. The ΔE_p values grow while decreasing $i_{p,c}$ in the following order : $\Delta E_p (\text{H}_2\text{SO}_4) < \Delta E_p (\text{NaOH}) < \Delta E_p (\text{Na}_2\text{SO}_4)$. The maximum $i_{p,c}$ occurs at 1.0 M concentration when H₂SO₄ is used. In strong acidic media, damage of the electrode because of cathodically induced dissolution, may take place:



The sensitivity of Ti/TiO₂ electrodes to pH derives from the equilibrium and transport properties of protons in the oxide film. Protonation and OH⁻ ion adsorption occurs in acidic and basic media, according to the following equilibrium:



Electroreduction of the oxide film requires the diffusion of a counter-ion (H⁺) from the electrolyte to the interface, and further into the oxide layer. This permits the charge neutralization within the film:



In acid media, the proton diffusion takes place efficiently by a "surface Grothus" mechanism [10]. In alkaline media, adsorbed OH⁻ ions aid proton transfer by extracting them from the hydroxide layer or the adsorbed water molecules. The proton transport is less efficient in neutral media. Hence, acid media were chosen for further redox catalytic studies.

Figures 7 and 8 show voltammograms recorded to study redox behaviour of the species present on the electrode's surface in 1M H₂SO₄, at various sweep rates (fig. 7) and for different Ti/TiO₂ electrodes (fig. 8):

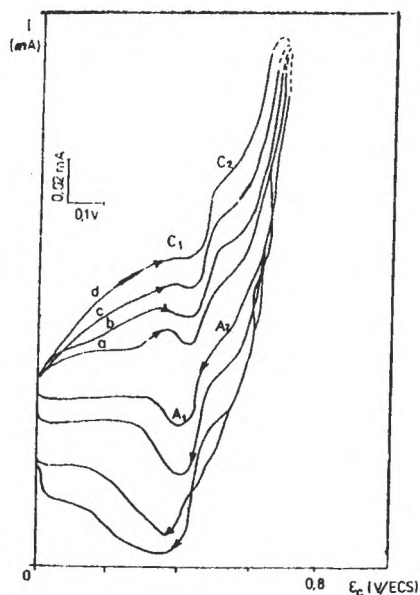


Figure 7. Cyclic voltammograms on Ti/TiO₂ electrodes in 1 M H₂SO₄. Sweep rate: (a) 50, (b) 100, c) 200, (d) 300 mV · s⁻¹

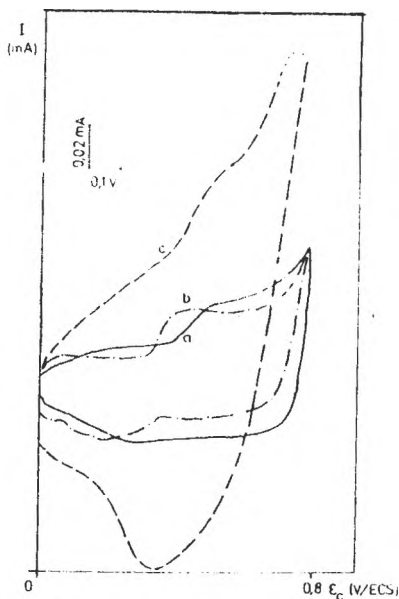


Figure 8. Cyclic voltammograms on Ti/TiO₂ electrodes in 1 M H₂SO₄. Sweep rate : 200 mV · s⁻¹; (a) 5, (b) 8, (c) 10 thermal cycles

Well defined reversible redox peaks also appear by increasing the number thermal cycles. At sweep rates $v \geq 0.05 \text{ V sec}^{-1}$, two cathodic waves C_1 ($\epsilon_c = 0.3$ – 0.39 V/SCE) and C_2 ($\epsilon_c = 0.49$ – 0.52 V/SCE) are observed. During reverse scan two anodic waves A_1 ($\epsilon_a = 0.35$ – 0.40 V/SCE) and A_2 ($\epsilon_a = 0.56$ – 0.57 V/SCE) are observed also. Earlier reports [6-10] suggest that the first cathodic wave C_1 is due to the following reduction:



and the second cathodic wave C_2 , which occurs at slightly higher negative potentials is due to the following one:



4. BEHAVIOUR OF Ti/TiO₂ ELECTRODES IN THE ELECTROREDUCTION OF THE DNSS

4.1. Cyclic voltammetry

Details regarding instrumentation, cell and electrodes employed in the cyclic voltammetry studies are the same as those reported in the experimental part.

A DNSS solution with a concentration of 1mM in 1M H₂SO₄ is used.

The cyclic voltammograms for a Ti/TiO₂ electrode, in the absence and presence of DNSS, are shown in fig. 9. It may be observed that the presence of DNSS leads to a simultaneous increase of the cathodic and decrease of the anodic peak heights.

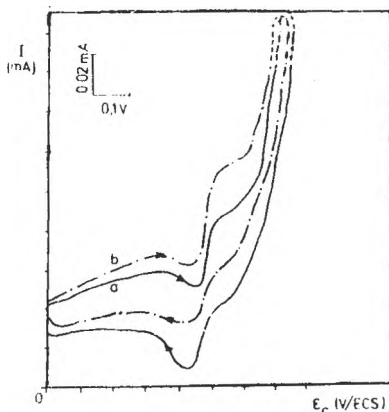
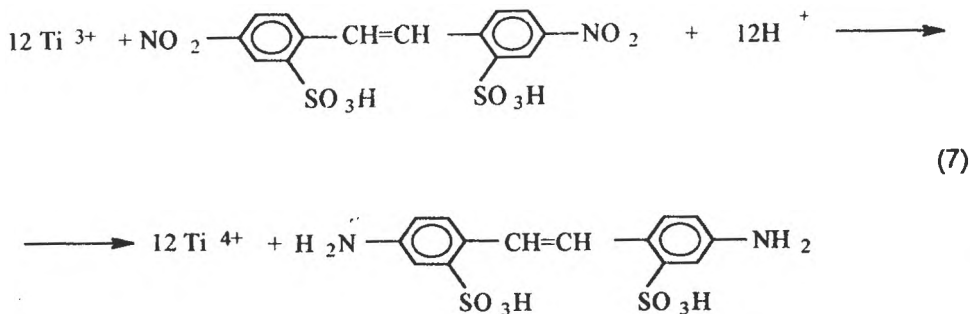


Figure 9 Typical cyclic voltammogram obtained on Ti/TiO₂ electrode in 1 M H₂SO₄; (a) in the absence, (b) in the presence 1 mM DNSS. Sweep rate : 50 mVs⁻¹ :

This clearly demonstrates the catalytic regeneration of Ti^{4+} at the electrode's surface. It is due to a fast reaction between Ti^{3+} and the dinitro - compound:



The most plausible explanation of the Ti^{3+} concentration decrease in the presence of DNSS, is given by a heterogeneous chemical reaction as shown in equation (7).

In conclusion, the cyclic voltammetry have revealed that the Ti/TiO_2 electrode is a good heterogeneous redox catalytic electrode for the reduction of DNSS.

4.2 Galvanostatic electrolysis

Table 3 Reduction of DNSS to DASS

Cathode: Ti/TiO_2 ; anode : Pb; catholyte : 1M H_2SO_4 , $4.6 \cdot 10^{-3}$ DNSS;
anolyte : 1M H_2SO_4 ; T = 293⁰K.

nr.crt.	i (A dm ⁻²)	S _{sp} (cm ⁻¹)	m _{DNSS} (g)	r _F (%)	r _{ch} (%)
1	1.77	0.11*	0.2	91.99	83.05
2	2.66	0.11*	0.2	88.56	75
3	3.55	0.11*	0.2	56.66	38.35
4	2.62	0.04	0.2	78.14	58.23
5	2.62	0.14	0.2	95.23	88.70

* geometrical surface; net type electrode

From Table 3 one may conclude that, the higher the current density, the more competitive the hydrogen emission. Thus, current efficiency decreases (experiments no.1-3). A higher specific surface promotes redox reaction and increases current efficiency (experiments no. 4-5).

CONCLUSIONS

1. Ti/TiO₂ electrodes were obtained by thermal method. SEM, SEM-RX and X-ray diffraction were used to emphasize the importance of operating conditions as roughening and number of thermal cycles upon the structure and quality of the TiO₂ deposit.

2. The deposited TiO₂ layer on the electrode's surface is more homogeneous and more compact after its roughening in 12.5% HCl + 7.5% H₂C₂O₄, for 30 min. and thermal coating during 5-10 thermal cycles.

3. The electrocatalytic properties of the TiO₂ layer were evidenced not only by cyclic voltammetry but also by preparative electroreduction of DNSS to DASS. Hence, by using a Ti/TiO₂ cathode and a 1M H₂SO₄ catholyte, for a current density of 2.62 A·dm⁻² and a specific surface of 0.14 cm⁻¹, a yield as well as a current efficiency of 95% and 88.7% respectively, were obtained for DASS.

EXPERIMENTAL

Roughening of titanium electrodes

A titanium foil, 0,5mm thick, 99,7% and a titanium rod 6,35 mm diameter, 99,99% (Aldrich) were utilized.

Roughening of titanium electrodes was carried out in various HCl-H₂C₂O₄ mixture, for different periods of immersion, at the boiling temperature of 80 - 90°C (table 1). Scanning electron microscopy (SEM) was used to characterize the titanium surface.

Table 1 Roughening conditions

Composition of roughening medium		Immersion period	No. of sample	Reference
% HCl	% H ₂ C ₂ O ₄			
15	5	30	1, 7, 8	-
15	5	60	4, 5, 6	-
12.5	7.5	60	3, 11, 12	-
12.5	7.5	30	2, 9, 10	-
20	-	30	13	{1}

Coating of titanium with TiO₂ by thermal method

The roughened metal was dipped into a solution of 0.05 M titanylacetylacetonate (Aldrich) in iso-propanol containing 7.5% vol. HNO₃ (GR grade quality). Then drying at 100-110°C for 10 min. The metal strip was heated at 500-550°C for 25 min., for an oxide layer to form. The described coating and drying cycle was repeated 5, 8 or 10 times in order to obtain a good electrocatalytic TiO₂ - layer.

Scanning electron microscopy with X-ray detection

Instrumentation : Leica Cambridge Instruments S380 microscope; secondary electron detector; Oxford Link RX detector

Operating parameters : - electron source with thermoelectronic emission;
- acceleration voltage 5 kV;
- RX analysis by energy selection;
- ultra thin window for light element detection;
- data acquisition time 50 sec.

Observations : - the image of each sample was increased 500 times;
- titanium from the metallic support could not be differentiated from titanium of the TiO₂ layer so that light elements as C, Si, Al, Mg, Na were also detected.

X-ray diffraction

Instrumentation : D 520 Siemens Diffractometer

Cyclic voltammetry

Cyclic voltammetric measurements were performed in a typical one compartment glass cell. An aqueous SCE and a platinum foil served as reference and counter electrodes, while a Ti/TiO₂ electrode (area of 0.07 cm²) served as working electrode. A Wenking potentiostat (model HP 172), a voltage scan generator and an X-Y recorder (Endim 620) were also employed. The experiments were carried out in 1M H₂SO₄, 1M Na₂SO₄ and 1M NaOH solutions, at 20^oC. The solutions were thoroughly deoxygenated by purging the cell system with pure argon. A DNSS solution with a concentration of 1 mM was used. The supporting electrolytes are prepared from double-distilled water and H₂SO₄, Na₂SO₄ or NaOH of GR grade quality 4,4'-dinitrostilbene-2,2'-disulfonic acid was from TCI and 4,4'-diamino-2,2'-disulfonic acid from Lancaster.

Galvanostatic electrolysis studies

Preparative experiments were carried out in a divided glass cell. A solution of 4,6·10⁻³ in 2M H₂SO₄ was used as catholyte. The anolyte was a 2M H₂SO₄ solution. Two types of Ti/TiO₂ electrodes were used as cathode:

- a net - electrode, with a geometrical surface of 11.25 cm²,
- a plate - electrode, with a surface area of 4.2 cm².

A lead sheet was used as anode. The glass cell was thermostated at 20^oC. The catholyte was stirred by means of a glass stirrer and degassed with pure Ar. Galvanostatic conditions of 1.75 - 4 A·dm⁻² were assured.

Dosage of 4,4'-diaminostilben-2,2'-disulfonic acid (DASS) was made by thin layer chromatography and an original photodensitometric method [11].

REFERENCES

1. F. Goodrige, M.A. Hamilton, *Electrochem. Acta*, **25** (5), 481 (1980)
2. M. Noel, P.N. Anantharamen, H.V.K. Udupa, *J. Appl. Electrochem*, **12**, 291(1982)
3. A. M. Martre, V. Danciu, G. Mousset *Can. J. Chem.* **71**, 1136 (1993)
4. A. M. Martre G. Mousset, V. Cosoveanu, V. Danciu *New J. Chem.* **18**, 1221 (1994)
5. F. Beck, W. Gabriel, *Angew. Chem. Int.*, **24**, 771-772 (1985)
6. P.N. Anantharamen. D. Vasudevan, S. Cheilamal, *J. Appl. Electrochem.*, **21**, 839 (1991)
7. D. Vasudevan, P.N. Anantharamen, *J. Appl. Electrochem*, **24**, 559 (1994)
8. P.N. Anantharamen, M. Noel, C. Ravichandran, *J. Appl. Electrochem*, **369**, 217 (1994)
9. M. Noel, C. Ravichandran, P.N. Anantharamen, *J. Appl. Electrochem*, **25**, 690 (1995)
10. P.N. Anantharamen, M. Noel, C. Ravichandran, *J. Appl. Electrochem.*, **26**, 195 (1996)
11. V. Coşoveanu, V. Danciu, G. Câmpan, A.-M. Martre, G.Mousset, S. Gocan, *J. of Chromatography A*, **727**, 342-349 (1996)

REDUCTION SELECTIVE DE MOLECULES POLYFONCTIONNELLES PAR DES COMPLEXES DU TITANE (III) ELECTROGENERES EN MILIEUX AQUEUX ET NON AQUEUX.

Anne-Marie Martre, Séverine Lemanceau, Guy Mousset

*Université Blaise Pascal de Clermont-Ferrand Formation associée au CNRS :
Synthèse, Electrosynthèse et Etude de Systèmes d'Intérêt Biologique
Equipe d'Electrochimie Organique
24, Avenue des Landais - 63177 AUBIERE Cedex (France)*

Veronica Cosoveanu, Virginia Danciu

*Faculty of Chemistry and Chemical Engineering
University Babes-Bolyai - Group of Chemical Research
11 Arany Janos street - 3400 CLUJ-NAPOCA (Romania)*

ABSTRACT

La réduction de dérivés dinitrés et de cétones est étudiée en milieux aqueux et non aqueux. En milieu aqueux acide, les réductions électrochimiques du 4,4'-dinitrodibenzyle et de l'acide 4,4'-dinitrostilbène 2,2'-disulfonique sont réalisées sur différentes électrodes métalliques. Dans chaque cas, il est montré le rôle du système rédox Ti^{3+}/Ti^{2+} sur les produits formés. Ce travail a été développé en milieu aprotique DMF. Des études analytiques par voltammétrie cyclique et par spectroscope de résonance paramagnétique électronique, réalisées sur les dérivés dinitrés et la fluorénone, mettent en évidence les possibilités de réduction électrocatalytique par un complexe de titane, le dichlorure de titanocène. Les résultats préliminaires d'électrosynthèse sont indiqués.

Dans le cadre de recherches effectuées depuis quelques années sur la réduction de dérivés dinitrés aromatiques en diamines ou en monoamines, nous nous sommes déjà intéressés au 4,4'-dinitrodibenzyle (DNDB) et à l'acide 4,4'-dinitrostilbène 2,2'-disulfonique (DNSS). Sur électrode de mercure, nous avons précisé leurs caractéristiques électrochimiques dans plusieurs milieux, l'importance des phénomènes d'adsorption à la surface de l'électrode et l'influence d'additions de molécules tensio-actives (1,2). Nous avons également comparé leurs réductions électrochimiques (par transfert direct d'électrons ou en présence d'un couple rédox) et chimiques par un réducteur préalablement électrogénéré (2-4). L'intérêt industriel des amines correspondantes a orienté nos recherches vers l'utilisation d'électrodes solides mieux adaptées que le mercure aux technologies de synthèses (5-7).

Le présent travail concerne les réductions du 4,4'-dinitrodibenzyle et de l'acide 4,4'-dinitrostilbène-2,2'-disulfonique dans de nouvelles conditions expérimentales. D'une part, l'influence du couple rédox Ti^{3+}/Ti^{4+} sur la nature des produits formés par réduction électrochimique est examinée en milieu aqueux acide, sur plusieurs matériaux d'électrode (étain, monel, plomb, mercure). D'autre part, la très faible solubilité du DNDB dans l'eau ou dans le mélange hydroalcoolique nous a conduit à envisager la réduction dans un milieu non aqueux, le diméthylformamide (DMF), en présence d'un complexe de titane, le dichlorure de titanocène (Cp_2TiCl_2). Nous abordons également la réduction catalytique de dérivés carbonylés dans les mêmes conditions.

A. MILIEUX AQUEUX ACIDES

Influence du couple Ti^{3+}/Ti^{4+} sur la nature des produits formés par réduction électrochimique sur différentes électrodes.

Les milieux acides choisis sont respectivement H_2SO_4 5N / EtOH 50/50 à 60°C pour le DNDB en raison de sa très faible solubilité dans l'eau et H_2SO_4 2,5N à 30°C pour le DNSS plus soluble. Des études analytiques préalables, dans les conditions des réductions préparatives (électrochimique à potentiel constant ou chimique), sont nécessaires pour connaître les caractéristiques électrochimiques de chacun des dérivés dinitrés et du couple rédox utilisé. Dans ces solutions acides, seule l'électrode de mercure - pour laquelle la limite cathodique est à environ -1,0 V/ECS - permet une étude satisfaisante. Nous rappelons le comportement électrochimique du sulfate de titanyle $TiOSO_4$, promoteur du couple Ti^{3+}/Ti^{4+} et celui des dérivés dinitrés qui ont déjà fait l'objet d'études antérieures (1-4).

Les courbes des Fig. 1A et 1B permettent de comparer les réductions de chaque dérivé dinitré à ceux du couple rédox dans les conditions des électrolyses. Les écarts relatifs de leurs potentiels, en particulier celui de la réduction des hydroxylamines, laissent prévoir des effets différents sur les mécanismes et par conséquent sur la nature des produits de réduction. Nous avons montré précédemment l'influence de l'électrolyte et de la concentration en alcool sur la réduction des ions Ti^{4+} : l'acide H_2SO_4 étant complexant, il y a formation d'espèces

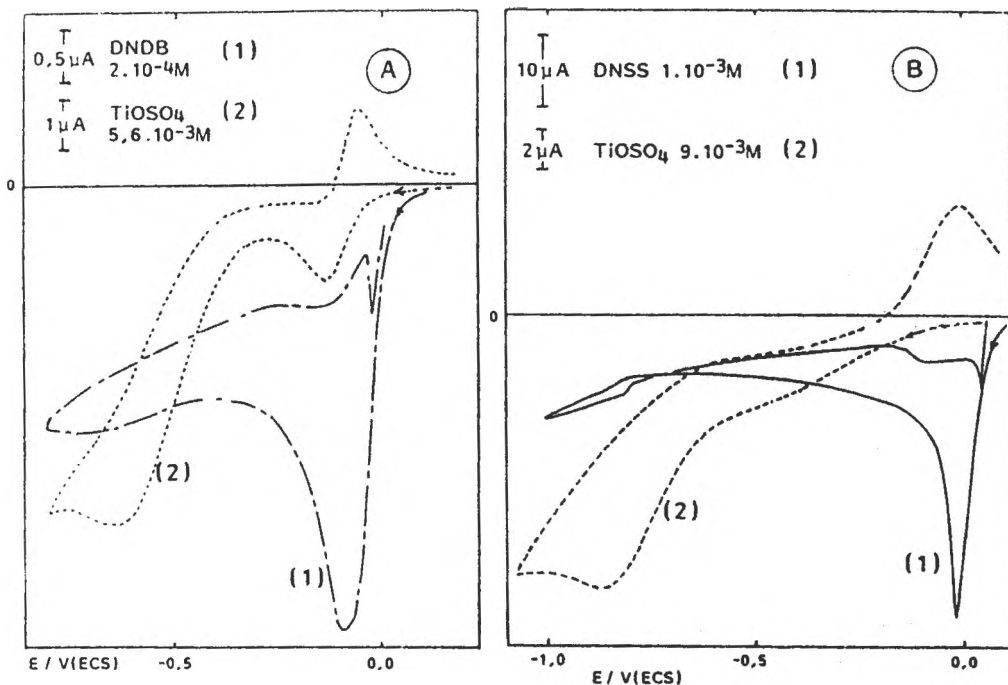


Fig. 1. Voltammogrammes de réduction sur électrode de mercure, $\nu = 0,1 \text{ V} \cdot \text{s}^{-1}$.
 (A): milieu H_2SO_4 5N / EtOH 50/50 à 60°C . (B): milieu H_2SO_4 2,5N à 30°C .

en équilibre dans la solution dont la nature et les proportions relatives dépendent, entre autres paramètres, de l'acidité et de la température (3, 8-11). Le mécanisme global de cette réduction met en jeu un électron par molécule

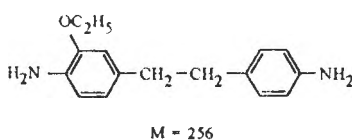
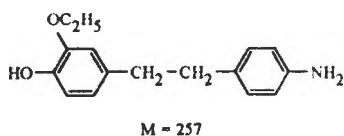
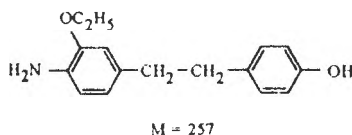
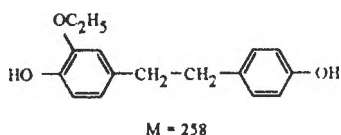


La réduction des dérivés dinitrés est classique et conduit globalement à la diamine correspondante avec formation intermédiaire de dihydroxylamine. La réaction globale met approximativement en jeu douze électrons. Sur les voltammogrammes, les pics de faible intensité, vers 0,0 V et -0,8 V, sont de nature capacitive et délimitent la zone d'adsorption / désorption du dérivé nitré et (ou) de ses produits de réduction comme il a été montré par des mesures tensammétriques (1a,2).

Les électrolyses à potentiel constant ont été réalisées sur quatre électrodes : mercure, étain, monel et plomb. L'influence de la nature de l'électrode sur la

réduction de dérivés nitrés a déjà fait l'objet de quelques travaux (12-17). Suivant les matériaux, sur lesquels la réduction des ions H^+ en hydrogène est plus ou moins difficile, on peut envisager des mécanismes différents d'électronation-protonation ou d'hydrogénation électrocatalytique (18-21). Les concentrations les plus souvent employées sont de 1×10^{-3} M pour le DNDB et de 2×10^{-3} M pour le DNSS.

Les tableaux 1 et 2 résument les principaux résultats des électrolyses et le rôle de $TiOSO_4$ sur la nature des produits formés. En ce qui concerne le DNDB, sur électrodes de mercure et d'étain, il y a formation de dérivés mono- et dihydroxylés et éthoxylés de formules :



Pour les molécules de masses $M = 257$ et $M = 256$, on pourrait envisager des structures N-éthoxylées. Le spectre de masse indique l'existence d'un fragment à

$m/z = 134$ correspondant à l'ion radical favorable à la substitution sur le noyau aromatique

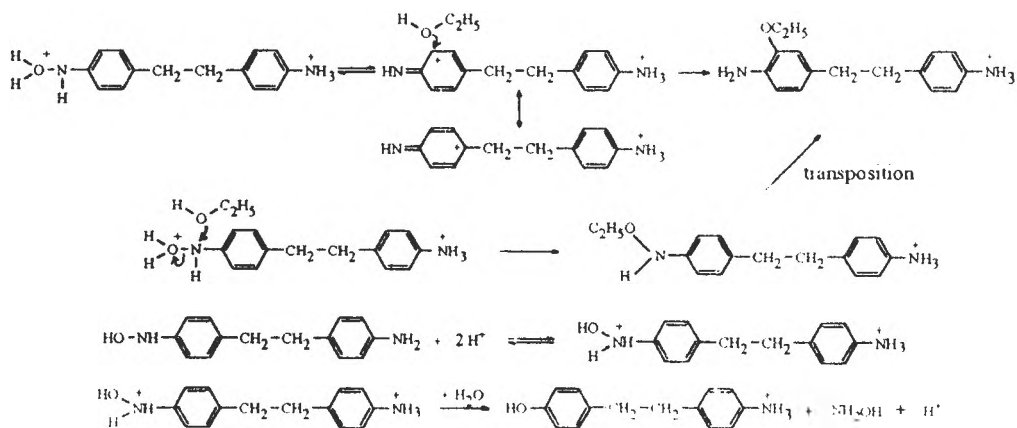


Tableau 1 : Produits de réduction du DNDB en milieu H_2SO_4 5N/EtOH 50/50 à 60°C

Matériau d'électrode	Médiateur	DADB %	composé amino-hydroxylé	composé dihydroxylé	composés éthoxylés	DNDB
<i>mercure</i>	sans	75	9	2	-	traces
	TiOSO ₄	92	-	-	-	traces
<i>monel</i>	sans	45	-	-	-	55
	TiOSO ₄	90	-	-	-	traces
<i>étain</i>	sans	50	18	8	15	traces
	TiOSO ₄	90	-	-	-	traces

DADB : 4,4'-diaminodibenzyle

Tableau 2 : Produits de réduction du DNSS en milieu H_2SO_4 2,5N à 30°C

Matériau d'électrode	Potentiel d'électrolyse	Produits formés	en présence de TiOSO ₄
<i>mercure</i>	- 0,05 V	DASS 90 %	sans effet
<i>plomb</i>	- 0,60 V	DASS + quelques % de ANSS et DHSS	sans effet
<i>monel</i>	- 0,30 V	DASS + traces de ANSS et DHSS + DNSS	DASS + traces de DHSS
<i>étain</i>	- 0,65 V	DASS + quelques % de ANSS et DHSS	sans effet

DASS : acide diaminostilbène disulfonique
ANSS : acide amino-nitrostilbène disulfonique

DHSS : dihydroxylarr...ne

Quelle que soit l'électrode, on note une amélioration sensible de la concentration en DADB en présence de TiOSO_4 ainsi que la disparition des produits secondaires qui permet d'obtenir la diamine très pure avec un rendement de l'ordre de 90 %.

Dans le cas du DNSS, plus soluble en milieu aqueux que le DNDB, sur cathode de mercure, le DASS est le seul produit de réduction, de l'ordre de 90 %. L'utilisation d'électrode solides permet également cette synthèse avec un bon rendement mais parfois il y a formation en faibles quantités de dihydroxylamine, de dérivé amino-nitré et de dérivé dinitré non réduit. La présence de TiOSO_4 a peu d'effet ou favorise la formation de DASS plus pur.

Sélectivité de la réduction chimique par le réducteur Ti^{3+} électrogénéré.

Le réducteur Ti^{3+} est électrogénéré à partir de TiOSO_4 en milieux H_2SO_4 5N / EtOH 50/50 et H_2SO_4 . Des travaux antérieurs (2, 3) ont déjà permis de mettre en évidence la sélectivité de la réduction chimique par Ti^{3+} . Selon la valeur du rapport des concentrations Ti^{3+} /dérivé dinitré, les composés amino-nitrés ou diaminés peuvent être préparés et nous avons déterminé les meilleures conditions de synthèse des composés mono-aminés. Pour le rapport Ti^{3+} /dérivé dinitré égal à 6/1, le rapport du dérivé amino-nitré sur le dérivé diaminé est respectivement égal à 78/22 dans le cas du DNDB et à 85/15 dans celui du DNSS.

B. MILIEU NON AQUEUX

La faible solubilité dans l'eau du DNDB ainsi que de nombreux dérivés carbonylés nous a incités à développer cette étude en milieu aprotique, le diméthylformamide (DMF). Dans ce cas, les ions Ti^{3+} sont électrogénérés à partir du dichlorure de titanocène (Cp_2TiCl_2).

Etude voltammétrique

Sur la figure 2 sont représentés les voltammogrammes en milieu DMF du sel de titane Cp_2TiCl_2 , des deux dérivés dinitrés DNDB et DNSS ainsi que celui d'une

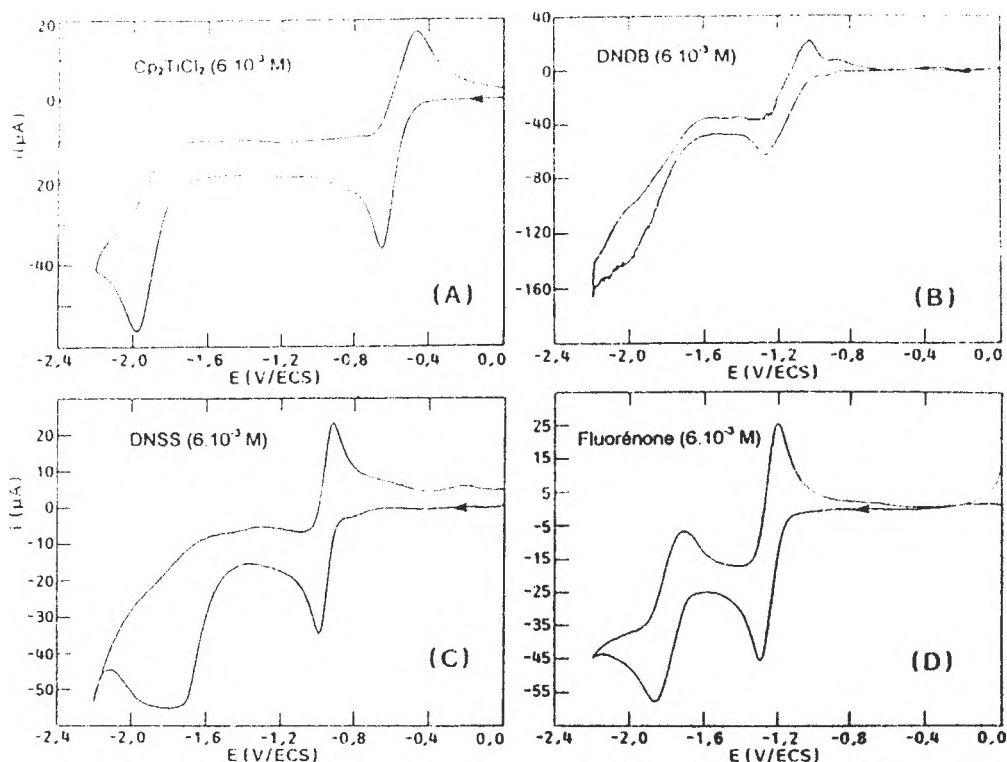


Fig. 2. Voltammogrammes de réduction en milieu DMF/ Bu_4NBF_4 0,1 M sur électrode de carbone vitreux, $v = 0,02 \text{ V.s}^{-1}$.

cétone, la 9-fluorénone. Le composé Cp_2TiCl_2 présente deux étapes de réduction (Fig. 2A). La première est réversible et monoélectronique, elle conduit à Cp_2TiCl . La seconde, à potentiel plus négatif, est irréversible et conduit à Cp_2Ti (22-25). La réduction des dérivés dinitrés est classique (Fig. 2B et 2C). La première étape réversible met en jeu deux électrons et correspond à la formation du radical anion de chaque fonction NO_2 et la deuxième irréversible qui fait intervenir au total six électrons, correspond à la formation de la dihydroxylamine. La fluorénone (Fig. 2D) est réduite en deux étapes réversibles monoélectroniques correspondant successivement à la formation du radical anion et du dianion. Les principales caractéristiques électrochimiques de ces composés sont résumées dans le tableau 3.

Tableau 3 : Potentiels de réduction des composés et quantités d'électricité mises en jeu.

Composés	1ère étape		2ème étape	
	Ep (V/ECS)	Nombre d'électrons	Ep (V/ECS)	Nombre d'électrons
Cp ₂ TiCl ₂	- 0,65	1	- 2,00	1
DNDB	- 1,26	2	- 2,06	6
DNSS	- 0,99	2	- 1,80	6
Fluorénone	- 1,30	1	- 1,90	1

Comportement électrochimique en présence de Cp₂TiCl₂

Des additions successives de dérivés dinitrés à une solution de Cp₂TiCl₂ s'accompagnent d'une part, d'une diminution jusqu'à la disparition de la réversibilité de la réaction Ti(IV) - Ti(III) et d'autre part, de la formation d'une prévalgue de réduction du dérivé dinitré (Fig. 3A). On peut faire l'hypothèse d'un complexe dérivé dinitré - Ti(III) plus facilement réductible que la fonction -NO₂ seule (26). Le radical anion associé à Ti(III) est alors plus facilement réductible et un second transfert d'électron régénérant Ti(IV) peut intervenir ce qui explique la perte de réversibilité de la première étape de réduction de Cp₂TiCl₂.

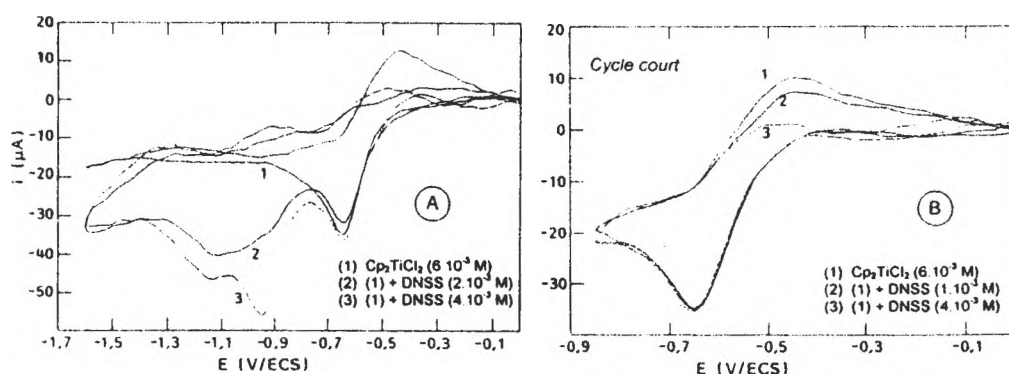
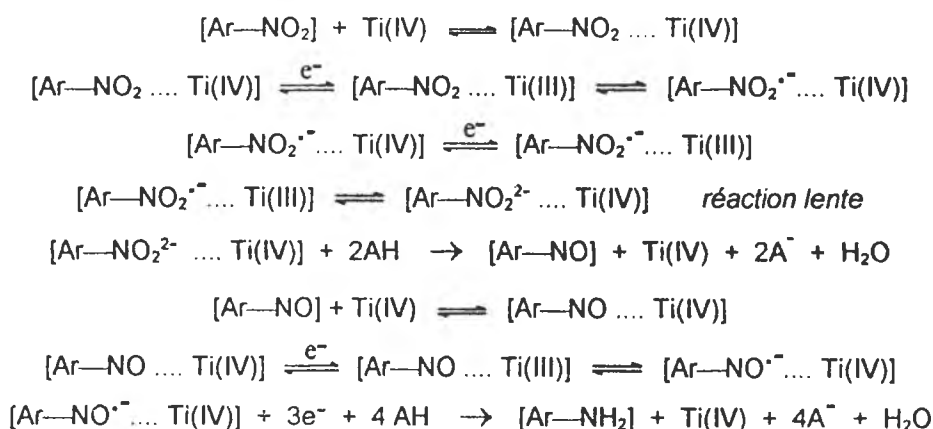


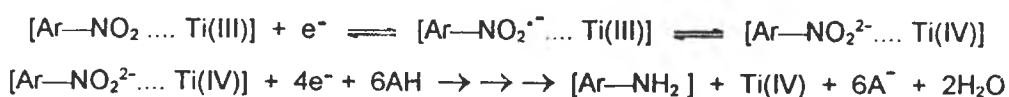
Fig. 3. Voltammogrammes de réduction du DNSS en présence de Cp₂TiCl₂ en milieu DMF/Bu₄NBF₄ 0,1 M sur électrode de carbone vitreux, $\nu = 0,02 \text{ V.s}^{-1}$.

Le pouvoir catalytique du système rédox Ti(III)/Ti(IV) devrait se traduire sur les voltammogrammes par l'augmentation de l'intensité du pic correspondant à la réduction de Ti(IV) et par la décroissance du pic de réoxydation. Sur les voltammogrammes à cycle court (Fig. 3B), avec arrêt du balayage en potentiel juste après la réduction de Ti(IV), on note une nette perte de réversibilité qui est d'autant plus forte que la concentration en dérivé dinitré augmente. Par contre, l'intensité du pic de réduction n'augmente pas de manière sensible, ce qui montre que la réduction du groupement nitré par Ti(III) est très lente. De plus, l'hypothèse d'une association entre Ti(IV) et le dérivé nitré peut correspondre à une modification du coefficient de diffusion du sel de titane. Les différentes réactions peuvent se faire suivant les mécanismes :

Première étape :



Deuxième étape :



Dans le cas de la fluorénone ajoutée à une solution de Cp_2TiCl_2 (Fig. 4A), des remarques similaires aux précédentes peuvent être faites : la réversibilité de la réduction de Ti(IV) diminue sans toutefois disparaître même lorsque le cycle de balayage est court (Fig. 4B), cela signifie que le transfert d'électrons à partir de Ti(III) est plus difficile, ce qui est logique compte tenu des potentiels de réduction de

la fluorénone et du DNDB et surtout du DNSS. De plus, le pic de réduction de la fluorénone se scinde en deux pics irréversibles, le premier pouvant être attribué comme pour les dérivés nitrés à la présence d'un complexe cétone - sel de titane (III).

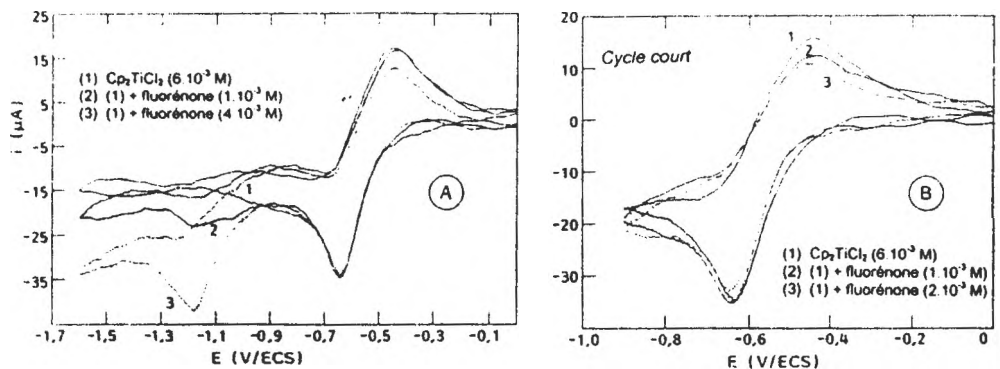


Fig. 4. Voltammogrammes de réduction de la fluorénone en présence de Cp_2TiCl_2 en milieu DMF/Bu_4NBF_4 0,1 M sur électrode de carbone vitreux, $v = 0,02 V.s^{-1}$.

Influence d'un donneur de protons

En présence d'un donneur de protons tel que l'hydrogénosulfate de tétrabutylammonium ($Bu_4N(HSO_4)$), les voltammogrammes relatifs aux dérivés dinitrés montrent un effet catalytique plus important (Fig. 5A et 5B).

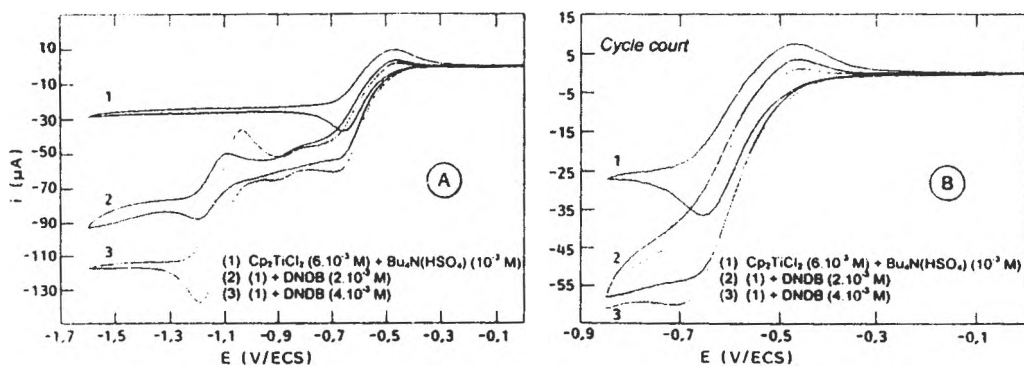
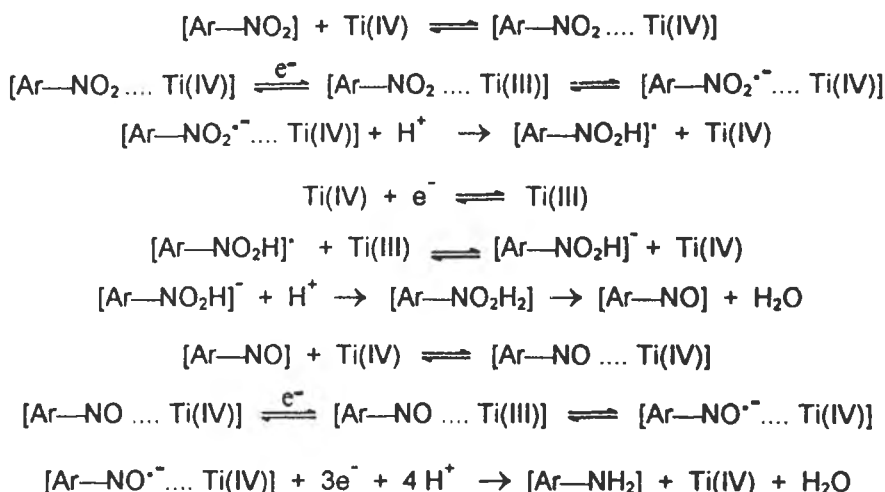


Fig. 5. Influence d'un donneur de protons, le $Bu_4N(HSO_4)$ sur les voltammogrammes de réduction du DNDB en présence de Cp_2TiCl_2 en milieu DMF/Bu_4NBF_4 0,1 M sur électrode de carbone vitreux, $v = 0,02 V.s^{-1}$.

En effet, l'intensité du pic de réduction de Ti(IV) augmente notablement en fonction de la concentration en dérivé dinitré (courbes 2 et 3). De plus, sa réversibilité diminue avec l'augmentation en dérivé nitré même lorsque le balayage en potentiel est limité à la première étape de Cp_2TiCl_2 . On peut supposer que dans ces conditions, il y a compétition entre l'association du radical anion du dérivé nitré avec Ti(III) ou Ti(IV) et la protonation qui conduit au radical neutre plus facilement réductible par Ti(III) que le dérivé nitré lui-même. A chaque étape, Ti(IV) est régénéré et sa réduction est à nouveau possible dans un cycle catalytique. Le mécanisme réactionnel peut être représenté par les relations globales :



Etude par résonance paramagnétique électronique (R.P.E.)

L'électroréduction de dérivés nitrés et de cétones aromatiques conduit à la formation de radicaux anions qui peuvent être caractérisés par RPE. Dans le cas du DNDB, les spectres (Fig. 6) montrent dans un premier temps la disparition lente du signal de Ti(III) sans que celui du radical anion du DNDB n'apparaisse (spectres a et b). Ensuite, si l'intensité d'électrolyse est plus élevée, le radical anion du dérivé nitré est formé électrochimiquement et se complexe avec Ti(III) en entraînant la disparition rapide de ce dernier (spectres c et d). En présence de sel de titane, le spectre du radical anion du DNDB est sensiblement modifié et l'intensité de certaines raies est plus importante (spectre d) que celles du radical anion obtenu en

absence de Cp_2TiCl_2 (spectre e). Ceci peut s'expliquer par son association avec Ti(III) . L'évolution des deux spectres est en accord avec les résultats des voltammétries cycliques.

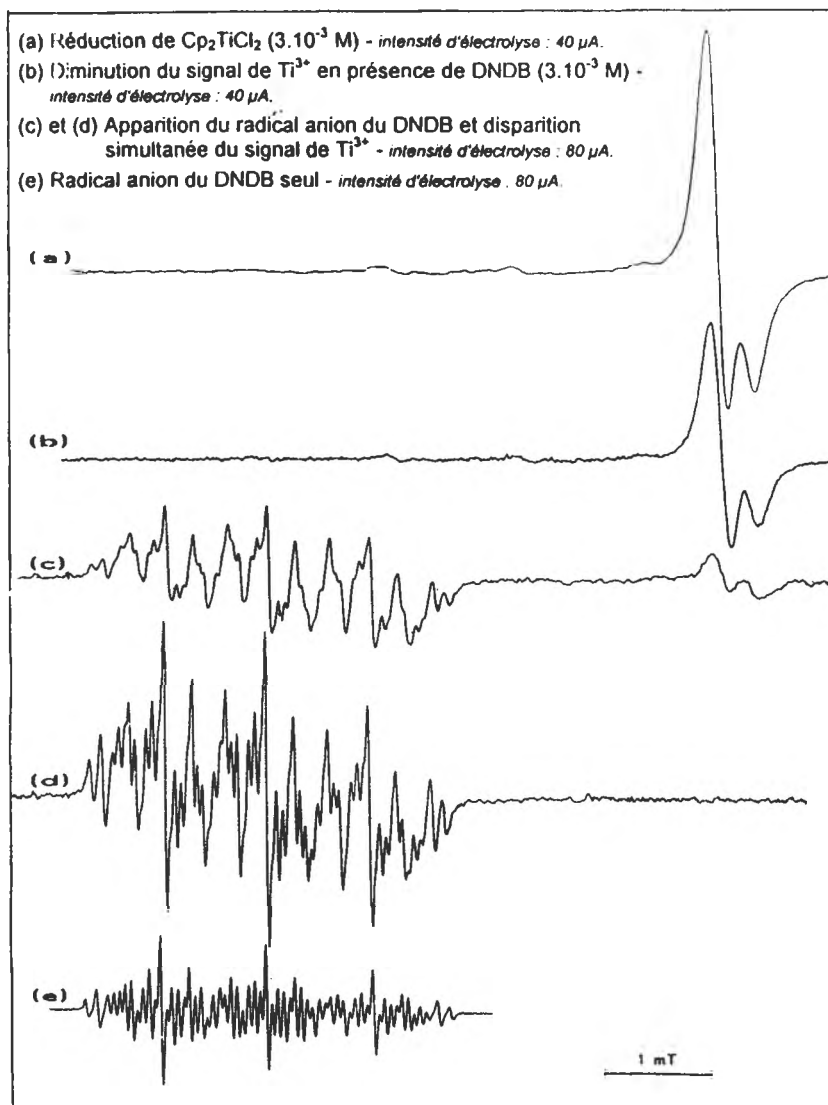


Fig. 6. Spectres de RPE en milieu DMF. Electrolyses à intensité constante de Cp_2TiCl_2 et évolution des signaux en présence de DNDB.

L'électroréduction du DNSS réalisée en présence de Cp_2TiCl_2 , "in situ" dans le spectromètre RPE, montre la formation du radical anion du DNSS et la disparition du signal de l'ion Ti(III) (Fig. 7, spectres a et b), signe d'un complexe dérivé nitré Ti(III) qui se réduit plus facilement. De plus, on voit apparaître des raies supplémentaires qui correspondent au composé amino-nitré (ANSS) (spectre b). Cela confirme la présence d'un complexe [1,1] dérivé nitré - Ti(III) qui permet l'obtention de produits mono-aminés. Les spectres c et d représentent ceux de radical anions du DNSS et du ANSS seuls en solution (2).

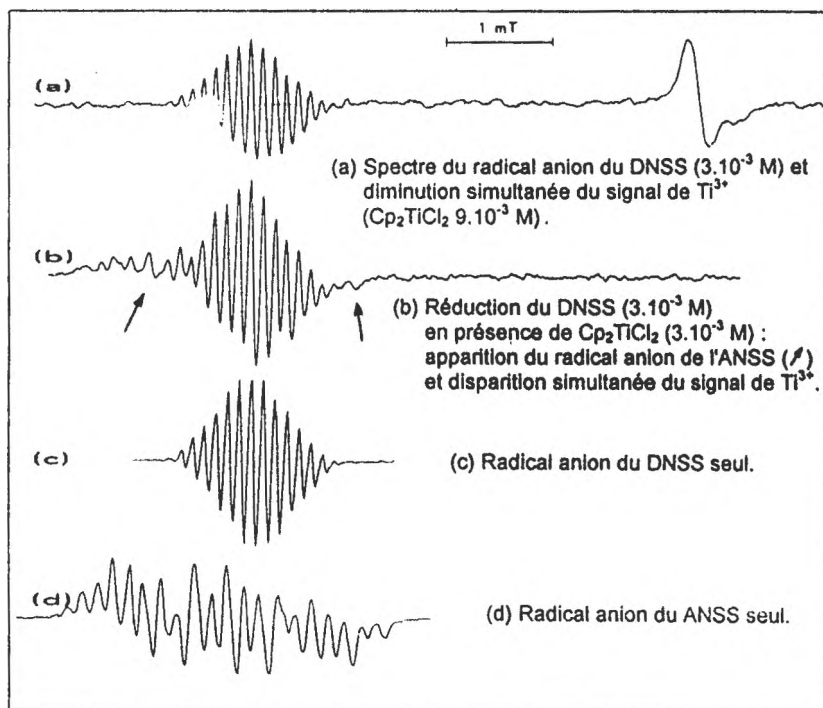


Fig. 7. Spectres de RPE en milieu DMF. Electrolyses à intensité constante.
 (a) et (b) évolution des signaux de Cp_2TiCl_2 et de DNSS en mélange.
 (c) Radical anion du DNSS ; (d) Radical anion du ANSS.

Dans le cas de la fluorénone, le potentiel de réduction est plus négatif que celui des composés dinitrés et le transfert d'électrons à partir de Ti(III) rendu plus difficile se traduit en RPE par l'existence simultanée des spectres de l'ion Ti(III) et du radical anion de la fluorénone (Fig. 8, spectre a). La comparaison des spectres a et b n'indique pas de modifications dues à la présence de Cp_2TiCl_2 .

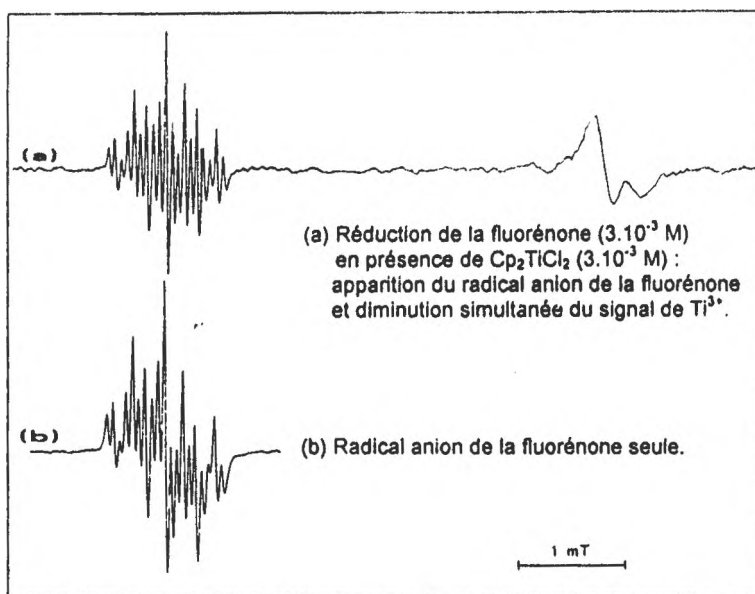


Fig. 8. Spectres de RPE en milieu DMF.
 (a) Electrolyses à intensité constante d'une solution de Cp_2TiCl_2 et de fluorénone.
 (b) Radical anion de la fluorénone seule.

Electrolyses préparatives

Les électrolyses préparatives sont réalisées à potentiel constant $E = -0,8$ V(ECS) qui est le potentiel de réduction du sel de titane, à la température ambiante, en solution DMF/ Bu_4NBF_4 0,1 M sur cathode de mercure avec des concentrations en dérivés carbonylés de 2×10^{-3} M en présence de Cp_2TiCl_2 4×10^{-3} M.

Plusieurs essais effectués avec le DNDB conduisent à une réduction sélective mais partielle. En effet, le seul produit obtenu est le composé amino-nitré (ANDB) avec un rendement de 30 %. Des expériences complémentaires, avec d'autres paramètres sont envisagées pour tenter d'améliorer cette valeur. Les premiers résultats indiquent toutefois que Ti(III) électrogénéré ne doit se complexer qu'avec une seule fonction NO_2 en raison d'un effet d'encombrement stérique.

Dans le cas de la fluorénone, la réduction est également lente et partielle. Trois produits sont présents en fin de réaction. Deux sont identifiés comme étant le

fluorénol et la fluorénone non réduite. Le troisième n'a pas encore été isolé mais la chromatographie sur couche mince laisse penser qu'il s'agit du pinacol.

Comme en milieu aqueux acide dans lequel nous avons montré la sélectivité de la réduction chimique des dérivés dinitrés par Ti(III) et défini les conditions de synthèse des composés mono-aminés, en milieu aprotique, la réduction électrocatalytique par Ti(III) apparaît également sélective et adaptée à la préparation de ces composés. Afin de compléter les résultats, d'autres travaux dans ce domaine sont en cours.

REFERENCES

1. V. Danciu, A.M. Martre, P. Pouillen et G. Mousset. *Electrochim. Acta* (1992) **37**, (a) 1993 ; (b) 2001.
2. A.M. Martre, G. Mousset, V. Cosoveanu et V. Danciu. *New J. Chem.* (1994) **18**, 1221.
3. A.M. Martre, V. Danciu et G. Mousset. *Can. J. Chem.* (1993) **71**, 1136.
4. A.M. Martre, G. Mousset, V. Cosoveanu et V. Danciu. *Can. J. Chem.* (1996) **74**, 1409.
5. L. Oniciu, I.A. Silberg, V. Danciu, M. Olea et S. Bran. *36th Meeting of International Society of Electrochemistry, Salamanca, Spain* (1985).
6. V. Danciu, I.A. Silberg, O.H. Oprea et L.A. Oniciu. Rom RO 94157 (CI C 07C87/14) 30/07/88, Appl. 122483, 07/03/86. *Chem. Abstracts.* 114:163704u.
7. L. Oniciu, M. Olea et V. Danciu. *Rev. Chim. (Bucharest)* (1990) **41**, 779.
8. G.M. Habashy. *Collect. Czech. Chem. Commun.* (1960) **25**, 3166 et *J. Electroanal. Chem.* (1964) **8**, 237.
9. L. Kisova, S. Sotkova et I. Komendova. *Collect. Czech. Chem. Commun.* (1994) **59**, 1279.
10. V.H. Kelsall, D.J. Robbins et W. Wang. *Electrochem. Eng. Energy [Proc. Eur. Symp. Electr. Eng.]*, 3rd 1994, Editeurs : F. Lapique, A. Storck et A. Wragg , Plenum Press New-York (1995), pp. 129-140.
11. I. Cservenyak, G.H. Kelsall et W. Wang. *Electrochim. Acta* (1996) **41**, 563.
12. J. Chon et W. Paik. *Bull. Korean Chem. Soc.* (1981) **2**, 1.
13. A.A. Konarev, V. Kh. Katunin, L.S. Pomogaeva, I.A. Avrutskaya et M. Ya. Fioshin. *Elektrokhimiya* (1984) **20**, 204.
14. I. Rubinstein. *J. Electroanal. Chem.* (1985) **183**, 379.
15. A. Davidovic, D. Davidovic et I. Tabakovic. *J. Serb. Chem. Soc.* (1991) **56**, 677

16. K. Filipiak, T. Paryczak et B. Grzelak. *Zesz. Nauk.-Politech. Lodz., Chem.* (1991) **616**, 367.
17. G. Kokkinidis, A. Papoutsis et G. Papanastasiou. *J. Electroanal. Chem.* (1993) **359**, 253.
18. J. Chaussard, R. Rouget et M. Tassin. *J. Appl. Electrochem.* (1986) **16**, 803.
19. J.C. Moutet. *Organic Preparations and Procedures Int.* (1992) **24**, 309.
20. B.J. Coté, D. Despres, R. Labrecque, J. Lamothe, J.M. Chapuzet et J. Lessard. *J. Electroanal. Chem.* (1993) **353**, 219.
21. J. Lessard, G. Belot, Y. Couture, S. Desjardins et C. Roy. *Int. J. Hydrogen Energy* (1993) **18**, 681.
22. S. Valcher et M. Mastragostino. *J. Electroanal. Chem.* (1967) **14**, 219.
23. R.G. Doisneau et J.C. Marchon. *J. Electroanal. Chem.* (1971) **30**, 487.
24. E. Laviron, J. Besançon et F. Huq. *J. Organomet. Chem.* (1978) **159**, 279.
25. R.J. Johnston, R.E. Borjas et J.L. Furilla. *Electrochim. Acta* (1995) **40**, 473.
26. C. Moinet, D. Floner et T. Jan. dans *Novel Trends in Electroorganic Synthesis, Proceedings of the Second International Symposium on Electroorganic Synthesis, Kurashiki 1994*, éd. S. Torii, Kodansha Tokyo (1995) p. 177.

ELECTROEXTRACTION OF ZINC FROM SULPHATE ELECTROLYTES CONTAINING GERMANIUM, ANTIMONY AND NICKEL IONS

I. IVANOV, ST. RASHKOV¹

ABSTRACT. The effect of several organic compounds of the process of reverse dissolution of zinc during the electrowinning from sulphuric acid zinc sulphate electrolytes containing metal impurities has been investigated. It was established that the inhibiting action of hydroxyethylated-2-butyne-1,4-diol (EEA) in the presence of Ge^{4+} and Sb^{3+} , of triethyl-benzyl-ammonium chloride (TEBA) in the presence of Ni^{2+} and of their combination (IT-85) under the simultaneous addition of all three metal ions, was the strongest when the inhibitors were introduced in the electrolyte before or simultaneously with the addition of the metal impurities. The addition of the inhibitor IT-85 leads to the stoppage of reverse dissolution of zinc, when the process has already started. In the presence of the inhibitors smooth zinc deposits with fine grain structure without corrosion pits and pitting defects on the surface and without dendritic growth at the cathode edges were obtained.

As a result of optical in situ investigations of the growth rate of hydrogen bubbles during the electrowinning of zinc from Ni^{2+} - containing electrolytes and in the presence of an inhibitor, a relationship has been established between the shape of the hydrogen bubbles and the duration of the "induction period". It has been found that during the "induction period" hydrogen bubbles alter their shape from spherical at the beginning to cupola-shaped at the end, thus increasing by 10-12 times the extent of the screening of the cathode surface beneath. Experimental confirmation is presented for the validity of the proposed physical model for the nature of the "induction period".

INTRODUCTION

The reverse dissolution of zinc during the electrowinning from sulphuric acid zinc sulphate solution in the presence of Ge^{4+} , Sb^{3+} and Ni^{2+} leads to a decrease in current efficiency of zinc, increases the specific electric power consumption and the cathodic deposits become brittle and corroded. The highly rough surface or deposit leads to the oxidation of zinc, which in turn increases the amount of peeled off metal and correspondingly reduces the amount of smelted metal [1-34]. The present investigation studies the effect exerted by several inhibitors upon the zinc electrowinning process in the presence of Ge^{4+} , Sb^{3+} and Ni^{2+} in amounts surpassing the critical concentrations, in effort to eliminate their harmful effect.

¹ Institute of Physical Chemistry, Bulgarian Academy of Sciences, Sofia 1113, Bulgaria.

EXPERIMENTAL

The alteration of zinc current efficiency was determined by measuring the volume of hydrogen gas was reduced to normal conditions and current efficiency of hydrogen (CEH) was calculated according to Faraday's laws. The current efficiency of zinc (CEZ) was evaluated as the difference (100-CEH) in percents.

The apparatus used (Fig.1) resembled the technological electrolyte entered in upper vessel, than transferred to working cell 2, equipped with a glass bell connected to a burette 6. The aluminium cathode was suspended under the bell. The bell and the burette were filled with electrolyte by a water jet vacuum pump. Hydrogen evolved during the electrodeposition process displaced the solutions in the burette, thus providing data for its volume. The solution in the working cell overflowed to a second (lower) vessel, from where the pump returned it to the upper vessel. The acid and zinc concentration were kept constant due to the relatively large (21), of circulating electrolyte. Zinc was electrowinned galvanostatically at a current density $5A.dm^{-2}$. The anodes were platinum stripes. The quantity of electricity passed was checked with a coulometer and temperature was kept constant at $36-38^{\circ}C$ with a thermostat. Zinc electrowinning was carried out using an industrial electrolyte containing ($g.l^{-1}$): sulphuric acid 125-130, zinc 50-55, manganese 5-6. To this electrolyte were added $Ge^{4+} - 0,6mg.l^{-1}$, $Sb^{3+} - 0,55mg.l^{-1}$ and $Ni^{2+} - 9mg.l^{-1}$ separately or in combination.

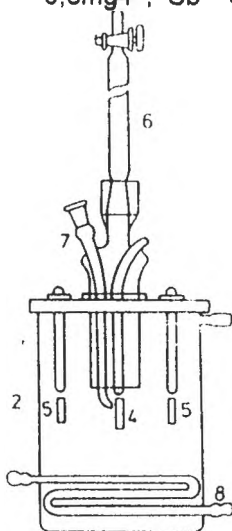


Fig. 1. The apparatus used: 2-electrolytic cell; 4-cathodes; 5-anodes; 6-burette; 7-Luggin capillary; 8-heater.

RESULTS AND DISCUSSION

1. Inhibiting the reverse dissolution of zinc in the presence of germanium ions.

In the presence of Ge^{4+} ($0,6 \text{ mg}\cdot\text{l}^{-1}$) in the electrolyte, as shown by curve 1 in Fig.2, the CEH increases rapidly up to 76% within 5,5 hours. Hydrogen evolution is intensive and often the zinc deposit peels off from the aluminium cathode, falls on the bottom and is completely dissolved. After 5,5 hours electrowinning, only a thin, corroded zinc layer remains on the cathode, which is very brittle and breaks during stripping off.

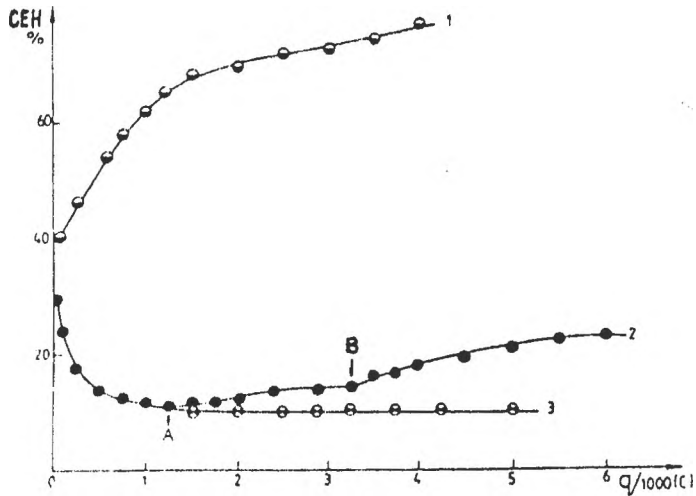


Fig. 2. CEH vs. quantity of electricity flown - q (Coulombs): curve 1 - electrolyte containing Ge^{4+} ($0,6 \text{ mg}\cdot\text{l}^{-1}$) - point A and inhibitor EAA ($5 \text{ ml}\cdot\text{l}^{-1}$) - point B; curve 3 - electrolyte with no additives.

In the case of deposition from germanium-free electrolytes CEH is rapidly decreased and reaches a value of only 10% (Fig. 2, curve 2). After the addition of $5 \text{ ml}\cdot\text{l}^{-1}$ of a 30% solution of the inhibitor hydroxyethylated-2-butynediol-1,4 denoted as EEA (curve 2, point A) and of Ge^{4+} at a concentration $0,6 \text{ mg}\cdot\text{l}^{-1}$ (point B), CEH slowly increases up to 22%, but a reverse dissolution of zinc does not occur. The zinc deposit obtained is compact, smooth, with no pits on the surface and dendrites protruding from the edges. The zinc deposit is readily peeled off from the aluminium substrate.

The SEM micrograph 1, shot at magnification 1000 shows the surface morphology of zinc deposited from a pure electrolyte. The characteristic hexagonal flat layered zinc crystallites are readily seen.

ELECTROEXTRACTION OF ZINC

The addition of Ge^{4+} at a concentration of $0.25 \text{ mg}\cdot\text{l}^{-1}$ leads to a rapid dissolution of the zinc crystallites at the edges and their hexagonal shape disappears, acquiring rounded appearance (micrograph 2). In the presence of EAA in the electrolyte zinc is deposited with a considerably more fine-grain structure as compared with deposits obtained from pure electrolytes and partial recovery of crystallite shape is observed, as well as the layered structure (micrograph 3).



SEM micrograph 1: Morphology of zinc deposited from a pure electrolyte. Magnification 1000x; **SEM micrograph 2:** Morphology of zinc deposited in the presence of Ge^{4+} ($0,25 \text{ mg}\cdot\text{l}^{-1}$). Magnification 1000x.



SEM micrograph 3: Morphology of zinc deposited in the presence of Ge^{4+} ($0,6 \text{ mg}\cdot\text{l}^{-1}$) and inhibitor EAA ($5 \text{ ml}\cdot\text{l}^{-1}$).

In the presence of antimony ions were obtained similar dependencies.

2. Inhibiting the reverse dissolution of zinc in the presence of nickel ions.

A characteristic feature of the effect exerted by Ni^{2+} is, that it appears when concentration 10-20 times higher as compared with those of Sb^{3+} and Ge^{4+} and the "induction period" are reached. During this period zinc is deposited at a high current yield and after that a rapid dissolution occurs, accompanied with ample hydrogen evolution.

Our investigation provided evidence that EEA does not inhibit satisfactorily the reverse dissolution process of zinc in the presence of Ni^{2+} , therefore some other organic compounds were tested. Among the latter, best results were displayed by triethyl-benzyl-ammonium chloride, further denoted as TEBA.

The relationship CEH vs. q in the presence of Ni^{2+} ($9 \text{ mg}\cdot\text{l}^{-1}$) in the electrolyte is shown by Fig. 3, curve 1.

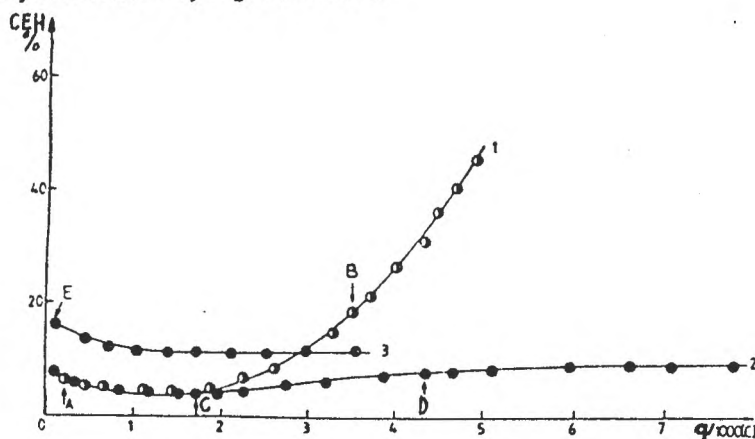


Fig. 3. CEH vs. quantity of electricity flow $-q$ (Coulombs): curve 1 - electrolyte containing Ni^{2+} ($9 \text{ mg}\cdot\text{l}^{-1}$) - point A and inhibitor TEBA ($100 \text{ mg}\cdot\text{l}^{-1}$) - point B; curve 2 - electrolyte containing inhibitor TEBA ($100 \text{ mg}\cdot\text{l}^{-1}$) - point C and Ni^{2+} ($9 \text{ mg}\cdot\text{l}^{-1}$) - point D; curve 3 - electrolyte containing Ni^{2+} ($9 \text{ mg}\cdot\text{l}^{-1}$) and inhibitor TEBA ($100 \text{ mg}\cdot\text{ml}^{-1}$) - point E.

It can be noted that following an induction period of 1.5 hours, the CEH increases rapidly, due to the start of reverse dissolution. The addition of TEBA at concentration $100 \text{ mg}\cdot\text{l}^{-1}$ (point B) does not cause a suppression of the reverse dissolution process, due to the addition of Ni^{2+} - ions (point A). However, if the inhibitor is added to the solution (point C) before the addition

of Ni^{2+} (curve 2, point D), reverse dissolution does not occur and a smooth deposit at high current efficiency is obtained. Reverse dissolution does not occur also in cases when Ni^{2+} and inhibitor are simultaneously added to the solution (curve 3, point E). The surface morphology of Zn, deposited from electrolytes containing Ni^{2+} is similar to the shown by micrograph 2, while Zn deposited from solutions containing Ni^{2+} and inhibitor TEBA has a morphology similar to the one shown by micrograph 3.

3. Inhibiting the reverse dissolution of zinc in the case of the simultaneous presence of germanium, antimony and nickel ions.

It is well known that the effect of positive metal ions on the zinc deposition process is enhanced if they are simultaneously present in the electrolyte. The CEH vs. q in the case of simultaneous presence of all three ions in the electrolyte for zinc electrowinning and the IT-85 inhibitor (containing $300 \text{ g}\cdot\text{l}^{-1}$ EAA and $20 \text{ g}\cdot\text{l}^{-1}$ TEBA) is shown in Fig. 4, curve 1.

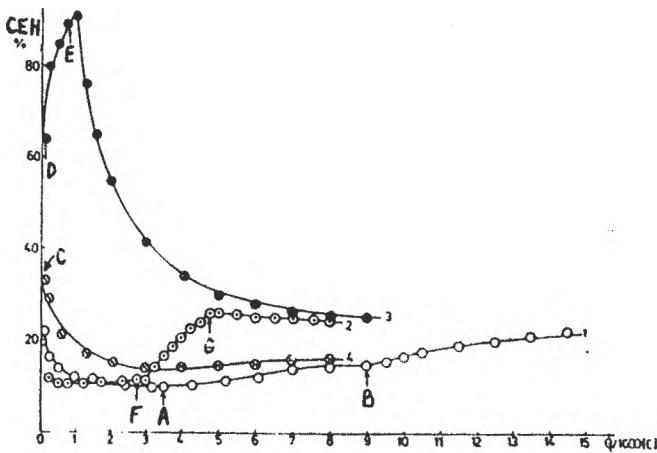


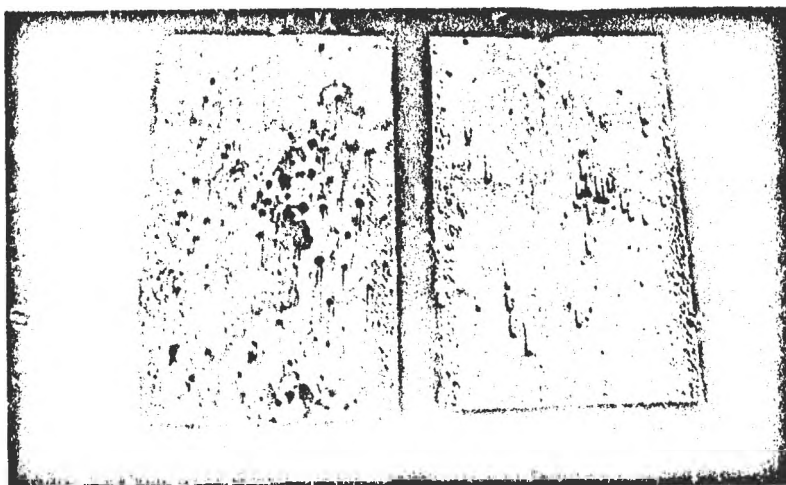
Fig. 4. CEH vs. quantity of electricity flow - q (Coulombs): curve 1 - electrolyte containing inhibitor IT-85 ($\text{ml}\cdot\text{l}^{-1}$) - point A and Sb^{3+} ($0,6 \text{ mg}\cdot\text{l}^{-1}$), Ge^{4+} ($0,6 \text{ mg}\cdot\text{l}^{-1}$), Ge^{4+} ($0,6 \text{ mg}\cdot\text{l}^{-1}$) and Ni^{2+} ($9 \text{ mg}\cdot\text{l}^{-1}$) - point B curve 2 - electrolyte containing Sb^{3+} ($0,6 \text{ mg}\cdot\text{l}^{-1}$), Ge^{4+} ($0,6 \text{ mg}\cdot\text{l}^{-1}$) and Ni^{2+} ($9 \text{ mg}\cdot\text{l}^{-1}$) - point F and inhibitor IT-85 ($5 \text{ ml}\cdot\text{l}^{-1}$) - point G curve 3 - electrolyte containing Sb^{3+} ($0,6 \text{ mg}\cdot\text{l}^{-1}$), Ge^{4+} ($0,6 \text{ mg}\cdot\text{l}^{-1}$) and Ni^{2+} ($9 \text{ mg}\cdot\text{l}^{-1}$) - point D and inhibitor IT-85 ($5 \text{ ml}\cdot\text{l}^{-1}$) - point E curve 4 - electrolyte containing Sb^{3+} ($0,6 \text{ mg}\cdot\text{l}^{-1}$), Ge^{4+} ($0,6 \text{ mg}\cdot\text{l}^{-1}$) Ni^{2+} ($9 \text{ mg}\cdot\text{l}^{-1}$) and inhibitor IT-85 ($5 \text{ ml}\cdot\text{l}^{-1}$) - point C.

It can be noted that the CEH during the electrowinning of zinc from pure electrolytes rapidly decreases to 10%. The additions of $5 \text{ ml}\cdot\text{l}^{-1}$ inhibitor (point A) and the simultaneous addition of Ge^{4+} , Sb^{3+} and Ni^{2+} in the above -

mentioned concentrations (point B) leads only to an increase of CEH, without exhibiting a reverse dissolution process of the deposited zinc. In case the ions of these metals and the IT-85 inhibitor are added to the electrolyte at the early stage of the electrodeposition process (curve 4, point C), the CEH is decreased to 16% and no further changes are observed.

The case when the reverse dissolution process has already started is of special interest. Curve 3 shows that after the impurities have been added (point D), the CEH rapidly within one hour increases to 92%. The addition of inhibitor IT-85 in the above - mentioned concentration (point E) leads to the stoppage of the reverse dissolution of zinc and the CEH is reduced to approximately 24%.

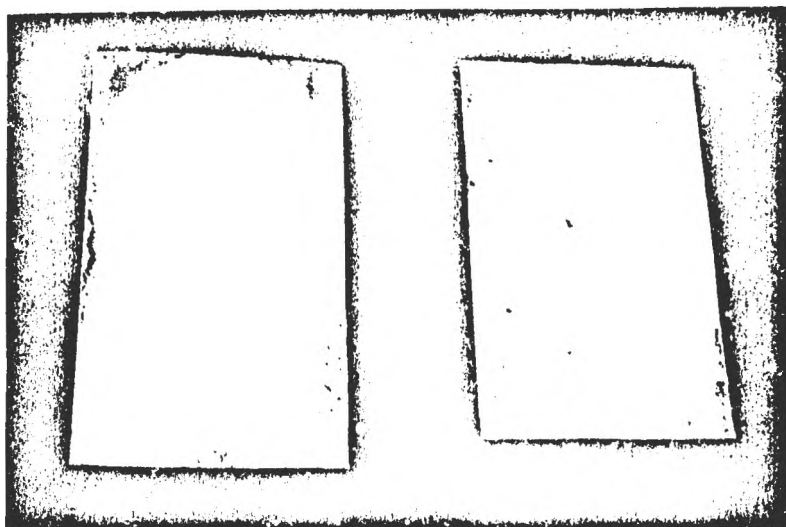
The case when impurities are introduced in the electrolyte after the aluminium cathode is covered with electrodeposited zinc is shown in the same figure, curve 2. The additives are introduced at the started concentration (point F) and the increase of the CEH is considerably slower as compared with the previous case. When the complex additive IT-85 at concentration $5 \text{ ml}\cdot\text{l}^{-1}$ is introduced (point G) a gradual decrease of the CEH down to 22% is observed and this trend is continued. Tests carried out under the conditions similar to industrial electrowinning are shown in micrograph 4. The electrodeposition is carried out from an electrolyte containing metal ions in concentrations as follows (in $\text{mg}\cdot\text{l}^{-1}$): Ge^{4+} - 0,15; Sb^{3+} - 0,15; Ni^{2+} .



Micrograph 4: The surface of a zinc cathode deposited in electrolyte containing ($\text{mg}\cdot\text{l}^{-1}$): Ge^{4+} - 0,15; Sb^{9+} - 0,15; Ni^{2+} - 3 and Co^{2+} - 5. Electrodeposition duration 8 hours.

4. The deposit obtained after 8 hours is very thin, breaks easily when stripped of and as shown by the micrograph, heavily corroded, sometimes the pits reaching the aluminium surface.

Electrowinned zinc deposited from an industrial electrolyte containing the same metal ions in the same concentrations and the IT-85 inhibitor ($0,5 \text{ ml}\cdot\text{l}^{-1}$) is shown by micrograph 5. It can be noted that the zinc deposit is compact, smooth, with no traces of reverse dissolution on the surface and no dendrite growth at the edges.



Micrograph 5. The surface of a zinc cathode deposited in electrolyte containing ($\text{mg}\cdot\text{l}^{-1}$): Ge^{4+} - 0,15; Sb^{3+} - 0,15; Ni^{2+} - 3 and Co^{2+} - 5 and inhibitor IT-85 ($5 \text{ ml}\cdot\text{l}^{-1}$). Electrodeposition duration 8 hours.

5. The relationship between the growth of hydrogen bubbles and the process of redissolutions of zinc in the presence of nickel ions.

It was noted that the redissolution of zinc in the presence of Ni^{2+} - ions begins after a period of time, named "induction period". We have obtained that there is a relationship between the process of reverse dissolution of zinc in presence of Ni^{2+} - ions and its inhibition and the process of hydrogen bubble growth and detachment from the electrode surface. This process was investigated in situ by photography. A Zeiss optical microscope was used at magnifications of 32,50 and 100 x.

The specially designed glass cell was provided with two plane - parallel glass windows for illumination and photography of the cathode (Fig.5).

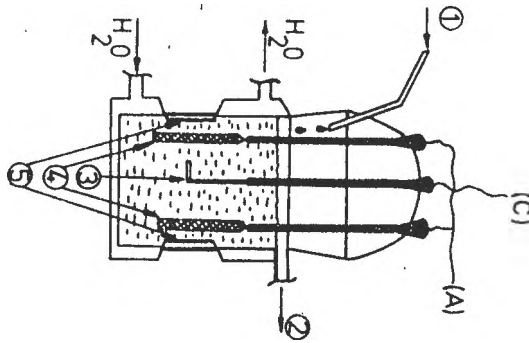


Fig. 5. Laboratory electro-winning cell. 1 - solution feeder; 2 - cell overflow; 3 - aluminium cathode; 4 - Pb (1% Ag) anodes; 5 - plane parallel glasses; (A) Anode; (C) Cathode.

The base electrolyte used has the following composition (in $\text{g}\cdot\text{l}^{-1}$): sulphuric acid - 130, zinc - 50 and manganese - 5. To the base electrolyte was added NiSO_4 , so that the concentration of nickel ions was $10 \text{ mg}\cdot\text{l}^{-1}$. On Fig.6 is shown a gas bubble on the metal surface and its; wetting angle (θ), height (h), radius ® and gas bubble - surface contact circle diameter (d).

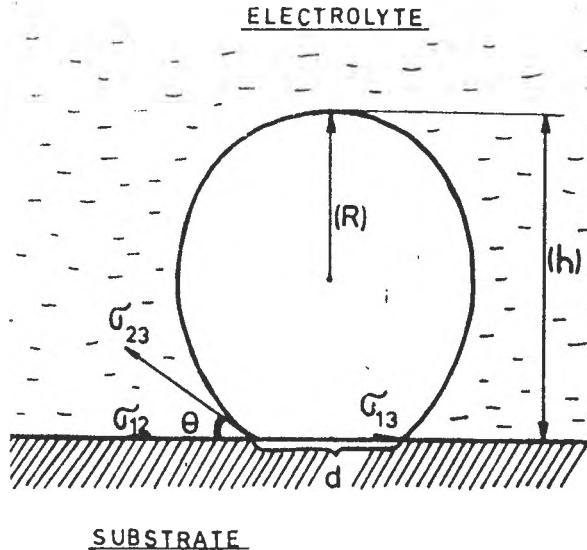


Fig. 6. Equilibrium state of a gas bubble upon a solid surface.

ELECTROEXTRACTION OF ZINC

The change of the wetting angle, θ , with electrolysis time, T , in the base electrolyte (curve 2) and in the nickel containing electrolyte (curve 1) is shown in Fig.7. It is noted that during the introduction period, θ increases and reaches a maximum value (about $20\text{-}23^\circ$) is maintained during the entire duration of the electrolysis ($T = 6\text{h}$), both in the basic electrolyte (curve 2) and in the nickel + inhibitor-containing electrolyte (curve 2).

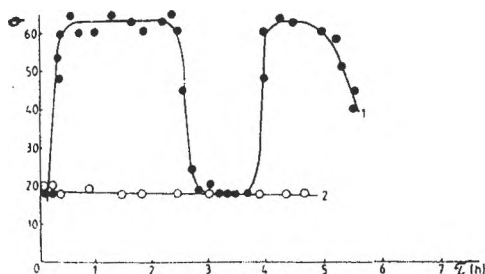


Fig. 7. Time dependence of the mean wetting angle, of hydrogen bubbles established in (curve 1) basic electrolyte with $10\text{ mg}\cdot\text{l}^{-1}\text{ Ni}^{2+}$, (curve 2) basic electrolyte with $10\text{ mg}\cdot\text{l}^{-1}\text{ Ni}^{2+}$ and $5\text{ ml}\cdot\text{l}^{-1}$ inhibitor IT-85, (curve 2) basic electrolyte. $I = 5\text{ A}\cdot\text{dm}^{-2}$.

It becomes possible to determine, from continuous photography of the electrode surface, the magnitudes θ_c , h_c and D_c , for a separate hydrogen bubble during its growth. The values corresponding to the moment when the bubble is detached from the cathode are denoted as critical values in the text. (θ_{crit} , h_{crit} , D_{crit}) respectively.

The change in h_{crit} and D_{crit} of hydrogen bubbles is plotted against the duration of electrolysis in Fig. 8. In the case of the base electrolyte (curve 4) and in electrolytes containing nickel with an inhibitor (curve 3) h_{crit} increases gradually with time and reaches $180\text{-}200\ \mu\text{m}$, in the presence of only nickel (curve 1) h_{crit} and D_{crit} decrease abruptly from about 350 and 250 to about $60\ \mu\text{m}$ during the transition from the induction period to the active "self-dissolution stage".

The similar character of the changes of h_{crit} and D_{crit} (curve 1 and 2) θ (curve 1 of Fig. 7) reflects the pronounced change of the hydrogen bubbles at the end of the induction period.

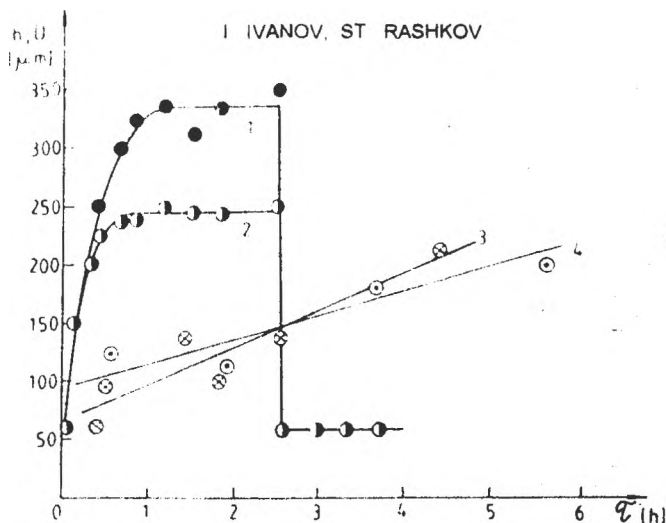


Fig. 8. Time dependence of the critical height, h_{crit} , of the hydrogen bubbles obtained in: (curve 1) basic electrolyte with $10 \text{ mg}\cdot\text{l}^{-1}$ (curve 2) basic electrolyte with $10 \text{ mg}\cdot\text{l}^{-1} \text{ Ni}^{2+}$ and inhibitor IT-85 $5 \text{ ml}\cdot\text{l}^{-1}$, (curve 3) basic electrolyte with $10 \text{ mg}\cdot\text{l}^{-1} \text{ Ni}^{2+}$ and inhibitor IT-85 $5 \text{ ml}\cdot\text{l}^{-1}$, (curve 4) basic electrolyte and of the critical diameter D_{crit} of the hydrogen bubbles obtained in: (curve 2) basic electrolyte with $10 \text{ mg}\cdot\text{l}^{-1} \text{ Ni}^{2+}$, $I = A\cdot\text{dm}^{-2}$.

In this respect it appeared interesting to establish the relationship between the mean attachment time, τ_i , of hydrogen bubbles and duration of electrolyses. These results are presented in Fig. 9. They show that at the end of the induction in a nickel containing solution (curve 1) τ_i decreases abruptly from 20-25 minutes to a few seconds during the zinc "dissolution" process.

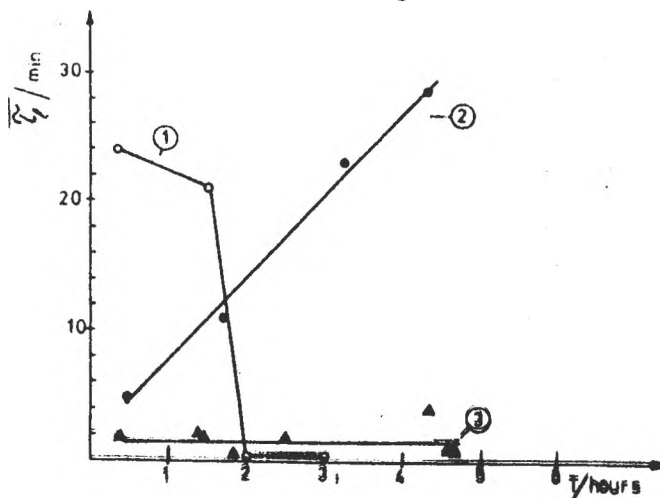


Fig. 9. Time dependence of the mean attachment time, τ_i , of the hydrogen bubbles obtained in: (curve 1) basic electrolyte with $10 \text{ mg}\cdot\text{l}^{-1} \text{ Ni}^{2+}$, (curve 2) basic electrolyte and (curve 3) basic electrolyte with $10 \text{ mg}\cdot\text{l}^{-1} \text{ Ni}^{2+}$ and inhibitor IT-85 $5 \text{ ml}\cdot\text{l}^{-1}$, $I = 5 \text{ A}\cdot\text{dm}^{-2}$.

ELECTROEXTRACTION OF ZINC

The result presented above show that at the end of the induction period (after about 2h of deposition) hydrogen bubbles have a maximum wetting angle (Fig. 7, curve 1), maximum height and diameter (fig. 8, curve 1 and 2) and maximum attachment time (Fig. 9, curve 1), which abruptly decrease during the process of active "self-dissolution". The general conclusion, based on the results shown in Figs 7, 8 and 9 suggests that two completely different cases of hydrogen bubble growth are observed. In the first case in the base electrolyte and inhibitor containing electrolytes, hydrogen bubbles grow only in height, retaining approximately constant wetting angle, θ and gas bubble-surface contact circle diameter, d . Therefore the bubble remain approximately spherical during their attachment time (Fig. 10a). In the second case, observed in Ni^{2+} - containing electrolytes, the growing bubbles simultaneously experience a change in both θ and d during the induction period. The initial spherical shape changes to a cupola shape with maximum screening effect of the electrode surface under bubbles.

Consequently, during the induction period, hydrogen bubbles with a mean attachment time longer than 20 min develop a diameter of contact area with the cathode 10-12 times larger than bubbles formed at an identical time in the base electrolyte, or in inhibitor containing electrolytes. This is obviously a result mainly of the change in θ , which leads to the alteration of the hydrogen bubble shape from spherical at the beginning of the induction period to cupola-shape at the end of it. (Fig. 10b).

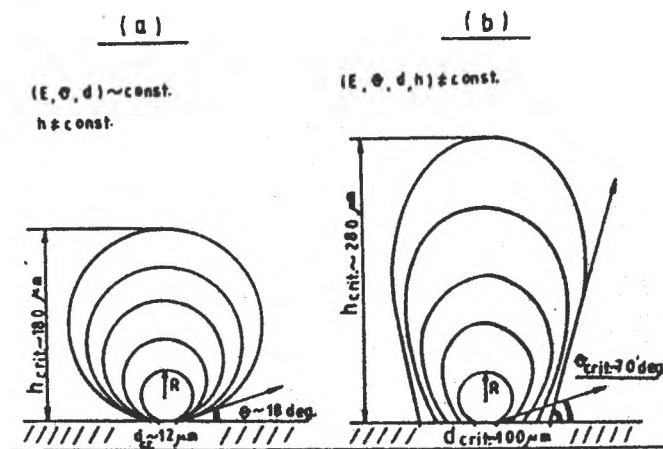


Fig. 10. Schematic representation of the growth of the hydrogen bubbles established in: (a) basic electrolyte or in electrolyte containing inhibitor IT-85 and $10 \text{ mg} \cdot \text{l}^{-1} \text{ Ni}^{2+}$.

A logical conclusion is that the cathode surface, thus screened by the bubble (Fig. 10b) is no longer in electrical contact with the electrolyte, so the cathodic protection is lost. Under these condition the screened zinc under the hydrogen bubble reaches a corrosion potential. On the other hand, reference data shows that the zero charge potential of zinc ($E_{zc} = -1.40 V_{SSE}$) in sulphuric acid is approximately equal to its corrosion potential in these electrolytes ($E_{cor} = -1.40 V_{SSE}$). This enhances the formation of hydrogen bubbles with a maximum wetting angle or with maximum screening effect (Figs. 10b and 11). This is a prerequisite for the start of the active dissolution of the deposited zinc under the bubbles (Fig. 12). Thus, the effect of the surfactant (inhibitor) can be explained by the strongly accelerated rate of hydrogen bubble growth. Thus, hydrogen bubbles grow up to their critical sizes 7-8 times faster, reducing their attachment time. As a result their local screening effect is completely eliminated and the surface is void of pitting defects (Fig. 13).



Fig. 11. Photograph of hydrogen bubbles formed during deposition in basic electrolyte containing $10 \text{ mg} \cdot \text{l}^{-1} \text{ Ni}^{2+}$, $T = 1 - 10 - 133 - 172 \text{ min}$.

ELECTROEXTRACTION OF ZINC

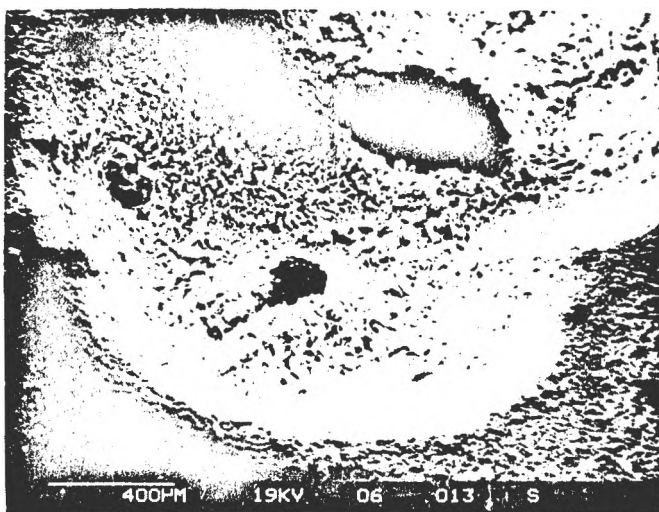


Fig. 12. Photograph of pitting defect and reverse dissolution of the deposited zinc under the hydrogen bubble.



Fig. 13. Photograph of hydrogen bubbles formed during deposition in basic electrolyte containing 10 mg·l⁻¹ Ni²⁺ and 5 ml·l⁻¹ inhibitor IT-85.

CONCLUSIONS

1. It was established that the inhibiting action of hydroxyethylated-2-butene-1,4-diol (EEA) in the presence of Ge^{4+} and Sb^{3+} , of triethyl-benzylammonium chloride (TEBA) in the presence of Ni^{2+} and their combination (IT-85) under the simultaneous addition of all three metal ions, was the strongest when the inhibitors were introduced in the electrolyte before or simultaneously with the addition of the metal impurities. The addition of the inhibitor IT-85 leads to the stoppage of the reverse dissolution of zinc, when the process has already started.

2. In the presence of the inhibitors, smooth zinc deposits with fine grain structure without corrosion pits and pitting defects on the surface and without dendritic growth and the cathode edges were obtained.

3. It is shown that a characteristic features of hydrogen bubbles is the pronounced increase of their wetting angle, θ , which result in a 10-12-fold larger diameter of the circle of the contact area with the cathode. As a result of the altered shape on the hydrogen bubbles from spherical at the beginning of the induction period to cupola-shaped at the end, the screening effect upon the cathode is also increased by an order of magnitude, thus allowing the zinc under the bubbles to reach its corrosion potential. Under these conditions, in the absence of cathodic protection, nickel codeposited with zinc forms a galvanic pair zinc-nickel, which explained the corrosion pits under the hydrogen bubbles.

REFERENCES

1. Pecherskaia, A.G., Stender, V.V., *Zs. Prikladnoi Him*, 1950, 23, 920.
2. Turomshina, U.F., Stender, V.V., *Zs. Prikladnoi Him*, 1955, 28, 372.
3. Turomshina, U.F., Stender, V.V., *Zs. Prikladnoi Him*, 1955, 28, 467.
4. Nikiforov, A.F., *Ukr. Him. Zs.*, 1959, 25, 18.
5. Znamensky, G.N., Serebritsky, V.M., *Ukr. Him. Zs.*, 1965, 31, 703.
6. Znamensky, G.N., Beziyazikov, B.N., *Ukr. Him. Zs.*, 1965, 38, 361.
7. Klimenko, V.L., *Tsevtnie Metalli*, 1952, 5, 29.
8. Sheka, Z.A., *Ukr. Him. Zs.*, 1956, 22, 394.

ELECTROEXTRACTION OF ZINC

9. Salin, A.A., Fuman, N.I., *Tsvetnie Metalli*, 1953, 4, 31.
10. Sheka, Z.A., Karlisheva, K.F., *Dokl. An. SSSR*, 1956, 103, 126.
11. Zsurin, A.I., Piunonen, S.P., *Trudi Leningr. Politehn. Inst.*, 1957, 188, 204.
12. Levin, A.I., Pomosov, O.V., Krimakova, E.E., Falicheva, V.I.,
Zs. Prikl. Him., 1958, 31, 581.
13. Zosimovich, D.P., Bogatova, N.F., *Zs. Fiz. Him.*, 1959, 33, 1324.
14. Shteingart, G.M., *Tsvetnie Metalli*, 1954, 5, 31.
15. Kiriakov, G.Z., Bainetova, F.K., *Trudi Inst. Him. Nauk AN Kazah SSR*, 1960,
6, 86.
16. Klimentko, V.L., *Tsvetnie Metalli*, 1971, 11, 17.
17. Kiriakov, G.Z., *Dokl. AN SSSR*, 1954, 94, 1067.
18. Kiriakov, G.Z., Bainetova, F.K., *Izv. Kazah SSR, ser. Him.*, 1958, 1, 20.
19. Bundzse, V.G., Kiriakov, G.Z., *Izv. Kazah SSR, ser. Him.*, 1958, 2, 18.
20. Levin, A.I., *Tsvetnie Metalli*, 1980, 8, 12.
21. Kolevatova, V.S., Levin, A.I., *Zs. Prikl. Him.*, 1954, 27, 456.
22. Kolevatova, V.S., *Patent SSSR*, 1979, 699, 036.
23. Gabitov, Zs. Sh., Shlemova, O.G., *Patent SSSR*, 1981, 865, 988.
24. Fulman, N.I., *Patent SSSR*, 1978, 567, 746.
25. Fratesi R., G. Roventi, M. Maja, N. Penazzi, *J. Appl. Electrochem.*, 1980,
10, 765.
26. Maja M., S. Pozzoli, *Chimie ind.*, 1969, 51, 113.
27. Steinveit G., H. Holtan, Jr., *J. Electrochem. Soc.*, 1960, 107, 247.
28. Robinson J.D., J.T. O'Keefe, *J. Appl. Electrochem.*, 1976, 6, 1.
29. Barisin, D., C. Jelacic, *Anti-Corrosion*, July, 4, 1982.
30. Morrison M R., J.D. MacKinnon, *7th Canadian Metal Chemistry Conference*,
Kingston, Ontario, June 22-24, 1983.
31. J.T. O'Keefe, *International Conference on the Application of Polarization*
Measurements in the Control of Metal Deposition, May 4-7, 1982, Victoria, British,
Columbia, Canada, 1982.
32. Kerby, R.C., *ibid.*
33. J.D. MacKinnon, L.P. Fenn, *J. Appl. Electrochem.*, 1984, 14, 467.
34. Heimada S.O., *Pat. USA 4 243 499*, 1981.

PROCESSES DURING THE ELECTROREFINING AND ELECTROWINNING OF LEAD

Tsvetan Dobrev and Stephan Rashkov

Institute of Physical Chemistry, Bulgarian Academy of Sciences, Sofia 1113, Bulgaria

ABSTRACT

The influence of the composition of fluorosilicate electrolytes on the character of anodic and cathodic processes during galvanostatic deposition under (DC) and polarity reversal current (PRC) regimes is investigated.

It is established that during the process of lead electrorefining from concentrated electrolyte without applying PRC at c.d. $i=3\text{A/dm}^2$, after 60-80 hours of the 95 hour long operation cycle, a limiting anodic polarization barrier value ($\Delta\varphi_{\text{ACR}}=200\text{mV}$) is attained. In this case bismuth and antimony start actively to dissolve from the anodes and are deposited onto the cathode, while under PRC conditions $\Delta\varphi_{\text{ACR}}$ is not reached even after 95 hours. The cathodic deposits are round-shaped crystal grains and display pronounced epitaxial growth. Spectral analysis show that Sb is the main impurity of cathodic lead instead of Bi

During the electrowinning of lead, without using H_3PO_4 as inhibitor of $\beta\text{-PbO}_2$ parasitic deposition onto the inert graphite anodes, it is established that a critical value of the anodic potential ($\varphi_{\text{ACR}}=1430\text{-}1500\text{ mV/SCE}$) exists, under which $\beta\text{-PbO}_2$ is not deposited. When H_3PO_4 is present, $\beta\text{-PbO}_2$ is not deposited onto the graphite anodes at any values of the anodic potential.

INTRODUCTION

1. ELECTROREFINING OF LEAD

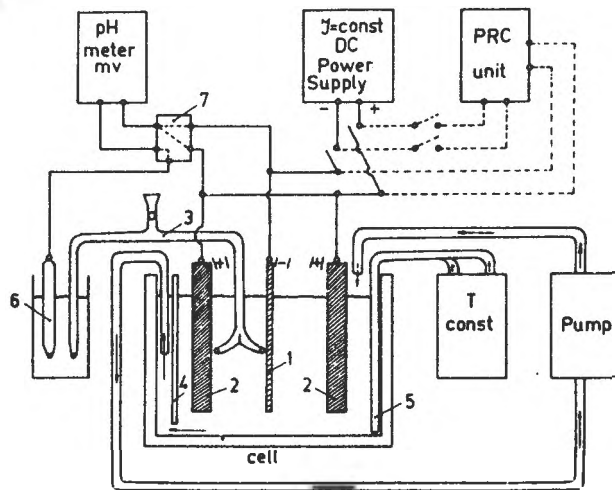
The most known in the literature and applied industrial technologies is the Betts' process [1-6]. It uses a fluorosilicate electrolyte containing 70g/l Pb in the form of PbSiF_6 , 90g/l H_2SiF_6 and some of the following organic additives: glue, lignin sulphate, aloin, etc. The Betts' process ensures deposition of high purity grade lead (99.99%) and a stable anodic slime, but the cathodic current densities used are rather modest - $i_k=1.2\text{-}2.2\text{A/dm}^2$, mainly due to early reaching of the anodic polarization limit of 200mV, when bismuth in the raw lead anode starts dissolving and is deposited onto the cathode [1,5]. The improvement of the influence of the process is related with the increase of Pb concentration in the electrolyte, application of polarity reversal current (PRC), use of various organic additives, increase of electrolyte temperature, more intensive stirring, bipolar deposition technologies, ultrasonic enhancement of the process, etc.[1, 4, 7, 8, 9].

EXPERIMENTAL

On the basis of existing literature data about this problem, we carried out studies in an effort to intensify the lead electrorefining process. A suitable electrochemical cell was made of plexiglass, designed as shown in Fig. 1.

Fig.1. Block diagram of the cell

- 1 - cathode,
- 2 - anodes,
- 3 - Luggin capillary,
- 4 - transversal partition plate,
- 5 - tubular heat exchanger for temperature control,
- 6 - reference electrode,
- 7 - switch.



The formulation of the electrolyte in g/l was as follows: Pb (as $PbSiF_6$) - 115 to 125, H_2SiF_6 - 95 to 105, glue - 2, lignin sulphonate - 2. The temperature of the electrolyte was within the range 39-43°C and stirring by circulation ensured a flow rate of 1-2 cell volumes per hour. When no PRC was applied (DC) $i_k=i_A=1-3A/dm^2$ while with current reversal of 10 cycles/min.[8] (at cathodic period 5.5 seconds and anodic period 200 milliseconds) c.d. up to 6 A/dm^2 was reached. The distance between the cathode and anode was 32-33 mm. The anodes were made of raw lead, while the cathode substrate was lead foil 0.5-0.6 mm thick, purity grade 99.99% at working area 1.26 dm^2 (7x9 cm) and volume of the electrolyte was 1.7 litres.

In order to maintain the same coverage throughout the experiments, growth was restricted to a fixed number of cycles (50). The obtained MHCf-modified electrodes were rinsed thoroughly with distilled water and then, they could be used for testing or stored in air.

RESULTS AND DISCUSSION

Lead electrorefining

We established during the electrorefining process that anodic polarization ($\Delta\phi_A$) is considerably increased mainly as a result of the ohmic drop (IR) in the anodic slime while the decrease of the cathodic polarization ($\Delta\phi_K$) is due to the coarser grain size of the lead deposit. The limiting anodic polarization (Fig.2, $\Delta\phi_{Ac}$) in the case of DC operation regime is attained after approximately the initial 60

ELECTROREFINING AND ELECTROWINNING OF LEAD

hours of the 95 hour long operation cycle (curve 1), while $\Delta\phi_{ACr}$ under PRC conditions is not reached even after 95 hours (curve 2).

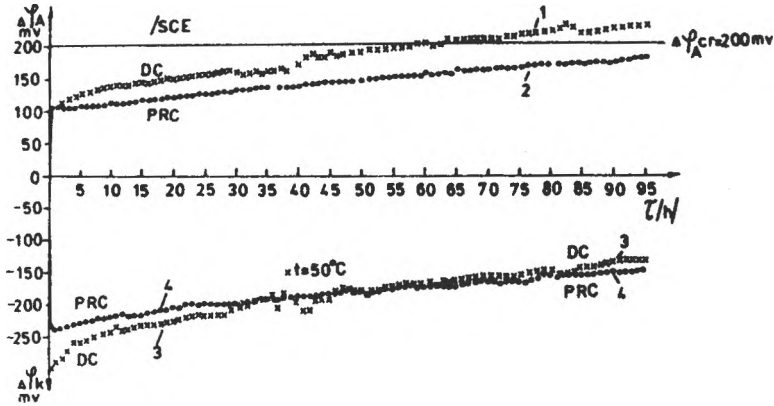


Fig.2. $\Delta\phi_A$ vs τ traced under continuous operation regime at $i_K=i_A=3\text{ A/dm}^2$: curves 1 and 3 (sample 23) - DC; curves 2 and 4 (sample 22) - PRC

In both DC and PRC regimes, a gradual increase of $\Delta\phi_A$ is observed (curves 1 and 2), while $\Delta\phi_K$ decreases (curves 3 and 4) in an almost parallel way, and as a result the cell voltage (U) displayed no substantial deviations throughout the 95 hour long cycle. In addition to the effect of polarity reversal, $\Delta\phi_{ACr}$ is also affected by the initial active/passive state of the anodes. If the process starts with passivated anodes, it ends in the same state. In this case, even reversal can not eliminate the surpassing of the 200mV barrier (Fig.3, curve 1). If the anodes are not passivated in the beginning, they remain in active state up to the end of the process (curves 2 and 3).

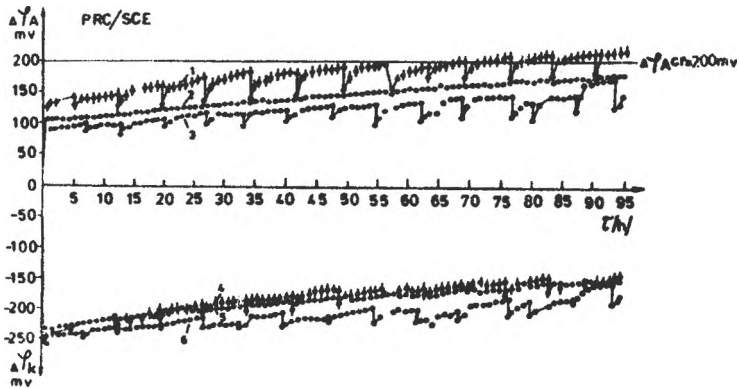


Fig.3. $\Delta\phi_A$ vs τ and $\Delta\phi_K$ vs τ curves traced under polarity reversal conditions at $i=3\text{ A/dm}^2$.

Curve 1 (sample 25) - interrupted cycle with partial passivated anodes; curve 2 (sample 22) - uninterrupted cycle; curve 3 (sample 21) - interrupted cycle; curves 4 (sample 25) and 6 (sample 21) - interrupted cycle; curve 5 (sample 22) - uninterrupted cycle.

Direct visual observations and inspection with a binocular lens of the samples deposited at 3 A/dm^2 during a 95 hours long cycle, as well as photographs suggest the following conclusions:

-the appearance of the lead deposits obtained after 95 hours in the absence of polarity reversal (Fig.4(23) and 4(23')) and in the presence of reversal (Fig.5(22) and 5(22')) is visually almost the same. They are compact with a light gray shades;

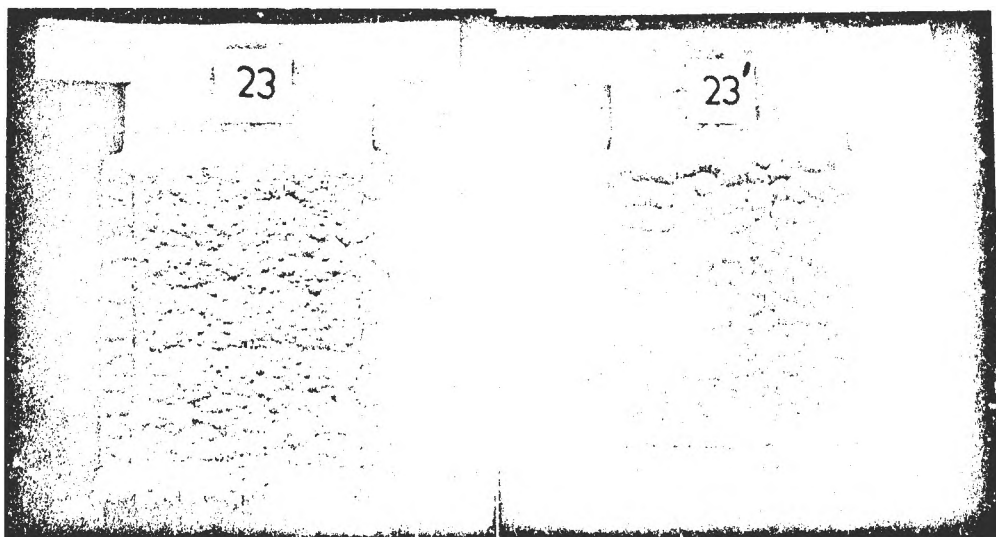


Fig.4. Lead deposit on a lead cathodic substrate after 95 hours uninterrupted deposition cycle at 3 A/dm^2 without polarity reversal: picture 23 - the smooth side of the cathodes; picture 23' - the rough side.

- deposits plated onto lead substrates are characterized by well shaped edges, especially at the lower corners of the cathodes. No needle-shaped crystallites are present - the growth mode is rounded dendrites. The effect of the substrate roughness upon the deposit is not diminished when the thickness increases with time, but just a reversly it is enhanced, i.e. epitaxial growth is very pronounced (Fig.4(23'), Fig.5(22'));

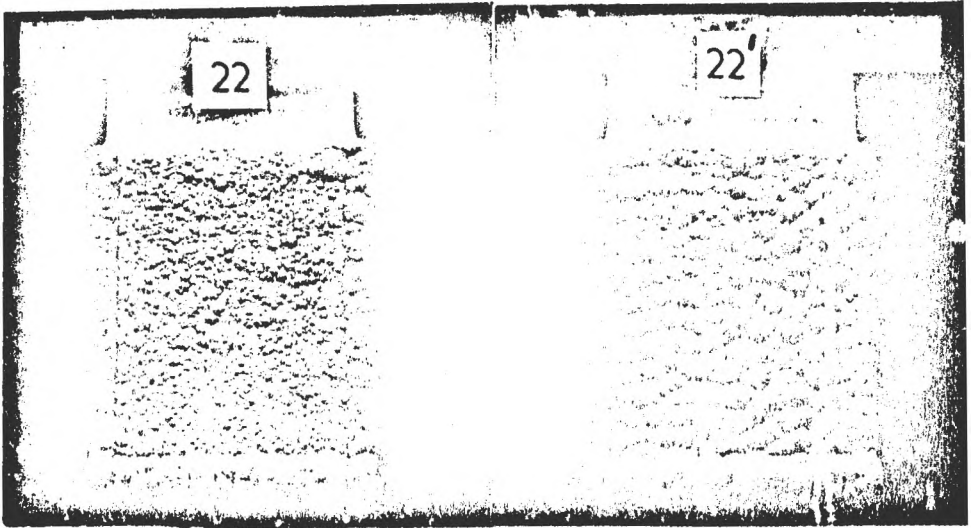


Fig.5. Lead deposit on a lead cathodic substrate after 95 hours uninterrupted cycle at 3 A/dm^2 with polarity reversal: picture 22 - the smooth side of the cathode; picture 22' - the rough side

- as a rule the deposits are round-shaped, 1 to 10 mm crystal grains appear, gradually severing from each other as the deposition cycle increases its duration (Fig.6(20') and 6(19', analog of the 21')). In the case of smoother substrates, these effects are not so pronounced (Fig.4(22) and Fig.5(23)).

The anodic slime obtained is dark, bluish-brown, adhering to the anode, remaining bound to it even after 125 hours deposition.

Data obtained after long-term investigations corresponding of the industrial electrorefining duration (4 night and day cycles) were used for the calculation of the specific energy costs (E_{CE}), according to equation (1); cathodic current efficiency (η_{cCE}), according to equation (2), and for defining the purity of the deposited lead by a spectral analysis (Tabl.1 and Tabl.2).

$$(1) \quad E_{CE} = \frac{U \cdot I \cdot \tau}{\Delta G} \quad [\text{Wh/kg}],$$

where: U - a cell voltage, [V]; I - current, [A]; τ - duration of electrorefining, [h]; G - the quantity of lead deposited during the run τ [kg].

$$(2) \quad \eta_{cCE} = \frac{\Delta G}{\Delta G_T} \cdot 100 = \frac{\Delta G}{I \cdot \tau \cdot Q_{Pb/Pb^{2+}}} \cdot 100 \quad [\%],$$

TSVETAN DOBREV AND STEPHAN RASHKOV

where: G_{τ} - theoretical quantity of Pb which could be deposited within τ , in [kg];
 $Q_{Pb/Pb^{2+}}$ - the electrochemical equivalent of the Pb $\Rightarrow 2e^{-} + Pb^{2+}$ reaction equal to 3.866 [g/Ah] or 3.866×10^{-3} [kg/Ah]

If DC and PRC are compared it becomes clear, that the specific cost of energy during PRC deposition is average approximately 30-50% more than of DC (Table 1).

The impurities are concerned at sample 20(DC) it has as far as included about 56% more Sb than sample 21(PRC) (Table 2). This could be explained by the fact that at the end of the 95-hour cycle $\Delta\phi_A(20) = 240 \text{ mV} > 178 \text{ mV} = \Delta\phi_A(21)$. Samples 22(PRC) and 23(DC) are different from samples 20 and 21, both the uninterrupted of the cycle, and the activity of the anodes at the beginning of deposition. While in the case of samples 20 and 23 then were in a passive state, leading to a very high anodic polarization in the beginning, strongly favouring the dissolution of Bi and Sb from the anodes and their deposition onto the cathode. During the first 35 minutes $\Delta\phi_A$ of sample 22 was 330-440 mV, then the anodes were activated and the potential was normalized and at the 95th hour was 174 mV.

Table 1. Conditions for electrorefining and results

Conditions and results	Sample No					
	20	21	22	23	24	25
	2	3	4	5	6	7
Operating temperature, °C	40±1.5	"	41±1.5	"	"	"
Duration of 1 cycle, hours	95	"	"	"	"	"
Geometrical area of Pb cathode, dm ²	1.26	"	"	"	"	"
Cathodic current density, A/dm ²	3	"	"	"	"	"
Current, A	3.78	"	3.80	"	"	"
DC/PRC	DC	PRC	"	DC	"	PRC
Daily regime in one cycle	interr.	"	uninter	"	inter.	"
Character of interrupting	daily weigh.	"	"	"	without	"
Deposited Pb during 1 cycle (96hs), kg	1.3795	1.2953	1.2999	1.3914	1.3902	1.2946
Cathodic crt. yield, η_{cct}	99.37	93.26	93.14	99.70	99.61	92.76
Energy costs, wh/kg	108.6	129	147	98.6	95.6	166

Sample 23 in the first 10 minutes displayed $\Delta\phi_A$ 470 mV after that the anodes were activated and normalized and at the 95th hour the potential was 228 mV.

ELECTROREFINING AND ELECTROWINNING OF LEAD

Table 2. Grade (level) of the purity of the Pb deposited, in %

Impurity	Sample* No					
	20 DC	21 PRC	23 DC	22 PRC	24 DC	25 PRC
1	2	3	4	5	6	7
Sb	0.0028	0.0018	0.0420	0.0640	0.0730	0.0360
Cu	0.0003	0.0003	0.0003	0.0012	0.0004	0.0003
Ag	<0.00004	=>	=> =>	=>	0.00008	0.00017
Bi	<0.0006	0.0006	0.0044	0.0072	0.0089	0.0039
Total impurities	0.00374	0.00274	0.04674	0.07244	0.08238	0.04037
Pb purity	99.99	99.99	99.95	99.93	99.92	99.96
Anode conditions $\Delta\phi_A$ (95h), mV	Active 240	Active 178	Passive 10 min 228	Passive 35 min 174	Active 210	Partial passive 220

*Each result is the average value of two parallel determinations (x70 grams cathodic Pb per every) of the sample impurities.

The analysis of the results of samples 24 and 25 it can be concluded that under equal conditions (i , $t^{\circ}C$, $\Delta\phi_A$) the quantity of impurities, mainly Sb and Bi, is substantially less during the PRC regime (s.25), independent of the partial passive state of the anode (established at the end of the cycle), influenced on the $\Delta\phi_A$ during the process: $\Delta\phi_A(25) = 220$ mV and $\Delta\phi_A(24) = 210$ mV (s.25) Sb and Bi are preferentially dissolved from the cathode, which in turn leads to their general reduction in the cathodic lead.

In summary can be stated that the impurity of the cathodic lead is affected not only by Bi but also by Sb, since in all cases Sb is about one order of magnitude more than Bi.

The experimental investigations performed for electrorefining lead from the concentrated electrolytes shows that both at PRC and DC regimes the process can be intensified by 40-50%. An important result in this respect could be obtained by working in a potentiostatic operation regime within the 200 mV anodic polarization limit, which ensures high purity grade of the cathodic lead deposit, together with using various organic additives, and applying PRC.

II. ELECTROWINNING OF LEAD

INTRODUCTION

Electrowinning of lead is carried out like electrorefining in a fluoroarsenate electrolyte, using insoluble graphite, titanium or platinum anodes and stainless steel or lead cathodes at a DC [10, 11, 13] or at a PRC [12]. Another substantial difference during electrowinning is the formation of parasitic PbO_2 upon the insoluble graphite anodes. Phosphorus- or As-containing compounds are added to the electrolyte in order to suppress this process [11, 12, 14].



Fig.6. Lead deposit onto a rough substrate after 95 hours uninterrupted cycle at 3 A/dm^2 : picture 6a (sample 20') - without polarity reversal; picture 6b (sample 19', similar to 21') - with polarity reversal. The crystal grains are larger and prone to separation. Magnification 5x.

ELECTROREFINING AND ELECTROWINNING OF LEAD

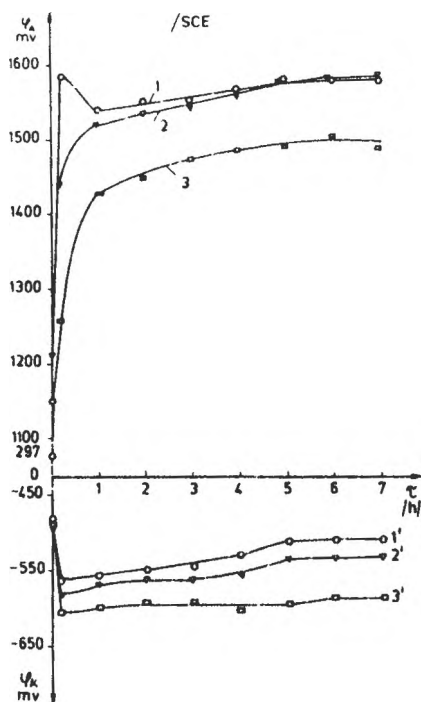


Fig.7. Potential vs time (φ/τ) curves traced without polarity reversal at 2 A/dm^2 , without H_3PO_4 :
 φ_A/τ - with fresh graphite anodes (curve 1);
 φ_A/τ - with fresh lead cathodes for fresh lead cathodes for each curve.

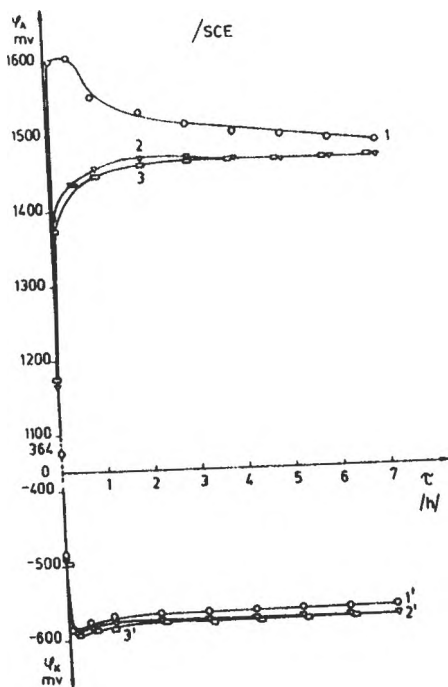


Fig.8. Potential vs time (φ/τ) curves traced without polarity reversal at 2 A/dm^2 , with H_3PO_4 :
 φ_A/τ - with fresh graphite anodes (curve 1);
 φ_A/τ - with fresh lead cathodes for fresh lead cathodes for each curve.

Since electrorefining and electrowinning are quite similar processes, we carried out laboratory studies in an effort to elucidate the effect of several additives upon the character of the anodic processes during electrowinning of lead, by using the same cell and the principle wiring diagram as in the electrorefining investigations (Fig. 1), at a suitable change of the electrode mount [15, 16].

EXPERIMENTAL

The initial composition of the electrowinning electrolyte was the following in g/l. Pb (as $PbSiF_6$) - 100 H_2SiF_6 - 80 to 90. The temperature of the electrolyte was within the range 39-42°C, distance between anode/cathode 30-32 mm. Graphite anodes and lead foil cathodic substrates were used.

RESULTS AND DISCUSSIONS

Lead electrowinning

When 2 g/l glue was added to the electrolyte and circulation at a rate of 1-2 volumes per hour it was established that in the absence of H_3PO_4 (Fig. 7) or in the presence at concentration 1.8 g/l (Fig. 8) the anodic potential (φ_A) of the plateau is 1500 mV/SCE. In the first case (Fig. 7) β - PbO_2 is deposited in stoichiometric amounts (Fig. 9) onto graphite anodes. The latter is a hard, brownish-black glassy deposit, with crater-shaped densely and uniformly distributed pits with diameters 0.05-1.4mm, strongly adhering to the substrate (Fig. 10). It was also established that $\Delta\varphi_A$ has a value from 2 to 4 times higher than $\Delta\varphi_K$, i.e. $\Delta\varphi_{AB}$ the power consumption determining factor in the electrowinning of lead as it is in electrorefining.



Fig.9. Graphite anodes with a β - PbO_2 coating, formed in an electrowinning electrolyte without H_3PO_4 . Left - integral anode; right - anode with a slot for the Luggin capillary. Scale 1:1.

ELECTROREFINING AND ELECTROWINNING OF LEAD

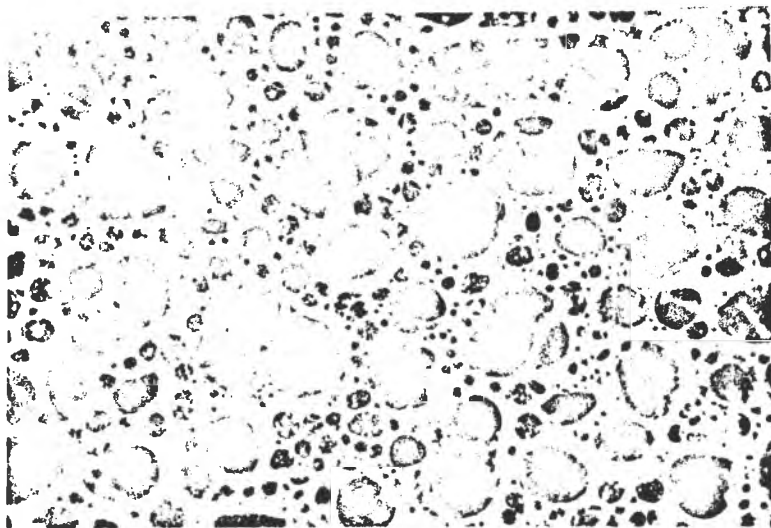


Fig.10. Micrograph of a β - PbO_2 coating on graphite anodes with dimensions of the craters 0.05-1.4 mm. Magnification 12x.

In order to clarify the conditions leading to the deposition of the parasitic β - PbO_2 , we tested different versions of the deposition process: with and without circulation of the electrolyte, in the presence or absence of H_3PO_4 , in electrolytes containing organic additives or in their absence, applying DC or PRC regimes. It was established that in the absence of H_3PO_4 the factor for the deposition of β - PbO_2 is φ_A . A treshold value of this potential exists which when surpassed, deposition of β - PbO_2 onto the graphite anodes starts. This treshold value is within the range 1430-1500 mV/SCE.

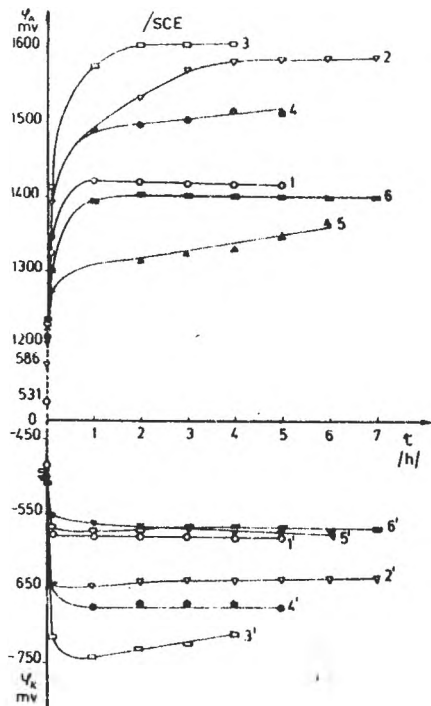


Fig.11. Potential vs time (φ/τ) curves, traced in the absence of H_3PO_4 , used graphite anodes at c.d. as follows: curve 1 - 2 A/dm², curve 2 - 3 A/dm², curve 3 - 4 A/dm², curve 4 - 2 A/dm², curve 5 - 1 A/dm², curve 6 - also 1 A/dm², but without circulation.

A very convenient illustration of this presumption is shown in Fig. 11 in the case when polyethylene glycol 6000 0.1 g/l + glue 1g/l are present in the electrolyte and PRC is applied at a rate of 5 cycles per minute [12] together with circulation. Initially at 2 A/dm² (curve 1), β -PbO₂ is not deposited onto the anodes, but once deposited at higher c.d., (curve 2 and 3), if again we apply the same low c.d. of 2 A/dm² β -PbO₂ starts depositing (curve 4). It should be noted that in the latter case (curve 4, $\phi_A = 1500$ mV) the anodic potential displayed a value by 100 mV more positive than in the case of curve 1.

It is also established that the ϕ_0 value of graphite electrodes with and without β -PbO₂ in the presence of additives (glue-lignine sulphonate) in the electrolyte becomes by 90-100 mV more positive as compared with the value in additive-free solutions, and in the case of lead electrodes the difference is 30-50 mV in the positive direction. Parallel tests with and without circulation of the electrolyte and in the presence of additives provided evidence that all types of electrodes - graphite, PbO₂ and lead - display ϕ_0 by 5-7 values mV more negative in the presence of circulation as compared with those in electrolytes without circulation.

The cathodic lead obtained displayed a purity grade of 99.9% and some of the parameters are given below (Table 3).

The results obtained provide evidence to conclude that the electrochemical cell, the circuit diagram and the layout used are useful and convenient for the investigation of the lead electrowinning process. The relationship between ϕ_A and the deposition of β -PbO₂ onto to graphite anodes suggests that more detailed studies are required for the clarification of the effect exerted by PRC, area and type of anodes, as well as organic additives upon the anodic process.

Table 3. Experimental data

Conditions	Cat. current efficiency η_{CCE} , %	Anodic current efficiency, % (parasitic β -PbO ₂)	E _{SE} wh/kg
1. DC at 2A/dm ²			
- without H ₃ PO ₄	96.5-98	up to 100 ^x	590
- with " "	" "	1 - 2	570
2. PRC			
- without H ₃ PO ₄ at 2A/dm ²	78	55 ^{xx}	700-800
- " " " "	78	1-2 ^x	"
- " " " 4 "	91	75 ^{xxx}	"
- with H ₃ PO ₄ " 2 "	77.5	1 - 2	720-750
- " " " 3.5 "	84	1 - 2	"
3. US Patent [11]	96-98	1 - 2	700

^x $\phi_A = 1450-1550$ mV/SCE; ^{xx} $\phi_A = 1500$ mV; ^{xxx} $\phi_A = 1400$ mV.

ELECTROREFINING AND ELECTROWINNING OF LEAD

The authors express their thanks to senior research associates Dr. Enchev, Dr. Iliev and Eng. Starev from the Inst. of Non-Ferrous Metals - Plovdiv for the helpful cooperation.

REFERENCES

1. C.J. Krauss, and R.C. Kerby, *Process Metallurgy Series No. 3*, 1984, 24.
2. D.L. Thomas, C.J. Krauss and R.C. Kerby, *TMS Paper Selection A81-6* Met.Soc.of AIME, Warrendale, PA 15086, 1981.
3. R.C. Kerby and H.E. Jackson, *Metal Soc. of CIMM, Annual Volume 1978*, 125
4. C.J. Krauss, *JOM*, November 1976, 4.
5. R.C. Kerby, *Can.Patent 1 126 684*, Aug. 17, 1982
6. P. Doby, *JOM*, April 1982, 56.
7. R.C. Kerby, *US Patent 4 177 117*, Dec. 4, 1979
8. R.C. Kerby and C.J. Krauss, *US Patent 4 416 746*, Nov. 22, 1983
9. R. Walker, *Hydrometallurgy*, 1979, 4, 209.
10. R.D. Prengaman and H.B. McDonald, *US Patent 4 229 271*, Oct. 21, 1980.
11. E.R. Cole, A.Y. Lee and D.L. Paulson, *US Patent 4 272 340*, Jun. 9, 1981
12. I. Enchev, L. Starev, E. Iliev, St. Rashkov, Ts. Dobrev, *Authorship Certificate* Bulgaria, reg. No. 89565/89, 1989.
13. O. Marco and Fr. Pierluigi, *Deutsches Patent 3 637 270 A 1/86*, 1986.
14. R.D. Prengaman and H.B. McDonaki, *US Patent 4 230 545*, oct. 28, 1980.
15. Ts. Dobrev, St. Rashkov, *Bulgarian Chemical Communications, No.2*, 1992, 205.
16. Ts. Dobrev, St. Rashkov, *Ided*, No.2, 1992, 215.

THE ELECTROSYNTHESIS OF PROPIONITRILE ON THE PILOT PLANT SCALE

Daniel A. Lowy^{*}, Maria Jitaru^{**}, Bogdan C. Toma^{**}, Ioan A. Silberg[†] & Liviu Oniciu^{**}

^{*}"Babes-Bolyai" University, Department of Physical Chemistry, Str. Arany János No. 11, RO-3400 Cluj-Napoca, Romania

Present address: The University of Memphis, Department of Chemistry, Campus Box 526060, Memphis, TN 38152-6060, USA¹

^{**}"Babes-Bolyai" University, Chemical Research Group

[†]"Babes-Bolyai" University, Department of Organic Chemistry

^{**}"Babes-Bolyai" University, Department of Physical Chemistry

The non-dimerizing electroreduction of acrylonitrile yields propionitrile (PN) with an almost quantitative selectivity and current yields up to 96%. The electrochemical PN manufacturing was applied on the pilot plant scale. The reactor incorporated 7 undivided pressfilter type cells, operated simultaneously, each of them equipped with a Pb vs. PbO₂ electrode pair. The anode was formed in situ, by the anodic oxidation of lead, in neutral phosphate buffer solution. Each electrode had a surface area of 0.21 m². As PN formation is kinetically favored over adiponitrile, the yield of PN raises with increasing current densities (*j*). However, the optimal current density was found in the range from 90 to 130 mA cm⁻². Endurance tests are reported for a continuous operation of the pilot plant over 7-days. Over this time period the specific material consumptions is of 1.12-1.15 kg AN (kg PN)⁻¹, while the power usage is 1.70 x 10⁴ kJ kg⁻¹. The annual productivity of this type of plant is 6.53 x 10³ kg, at *j* = 100 mA cm⁻², and can be increased significantly at greater current densities.

Keywords: Propionitrile, acrylonitrile, adiponitrile, electroreduction, organic electrosynthesis, preparative electrosynthesis.

¹ Author to whom correspondence should be addressed

Propionitrile manufacturing by the non-dimerizing electroreduction of acrylonitrile

Propionitrile is a compound highly demanded by industry¹. It is used as a non-protic electrolyte for zinc-bromine batteries, as a solvent for various organic syntheses, and as a reaction intermediate in the manufacturing of propyl amines^{1,2}. In a large-scale industrial procedure adiponitrile (AD) is obtained by the reductive dimerization of acrylonitrile (AN) *via* the Baizer reaction³. During this process, AN also undergoes a complementary reaction which yields propionitrile (PN). Surprisingly, the latter process, has been almost ignored, regardless of its possible industrial applications¹. In order to make PN electrosynthesis economically as advantageous as the manufacturing of AD, the cell voltage had to be reduced significantly. Also, the most important electrochemical, chemical, electrical and physical parameters controlling PN production had to be optimized by means of systematic studies^{1,4-8}.

In this paper we report technological data on the manufacturing of propionitrile at the pilot plant scale. Dependence of the yield of PN on the current density is shown and endurance tests for a continuous operation of the pilot plant over a 7-day period are discussed. The specific material- and energy consumptions, and the annual productivity of the plant are calculated.

Experimental procedure

The electrochemical plant. The schematic of the pilot plant is shown in Fig.1. The supporting electrolyte was prepared in vessel 101 by dissolving potassium phosphates (Ph) in de-ionized water (DIW). Acrylonitrile (AN), the organic raw material, was pumped (with pump P1) from container 102 into the measuring vessel 103. Next, the suspension of AN in aqueous supporting electrolyte was prepared in vessel 104. A hydraulic pump (P2) ensured the forced convection of the electrolyte

(previously cooled with the heat exchanger 201) through the electrochemical reactor (ER). The upward linear velocity of the supporting electrolyte through the cell was of $1.0 \pm 0.1 \text{ m s}^{-1}$. Vessel (104) is used also to degas the suspension, the anodic gases being exhausted through two heat exchangers (202 and 203), cooled with water and with brine, respectively. A separation vessel (105) continuously removed the organic phase, which was stored in the reservoir 106. Temperature (temperature indication, T), flow rates (flow control, F), liquid level (L), and pressure (P) were continuously monitored. A previously described electrochemical reactor (ER) was used^{9,10}. It incorporated seven undivided pressfilter type cells that were operated simultaneously.

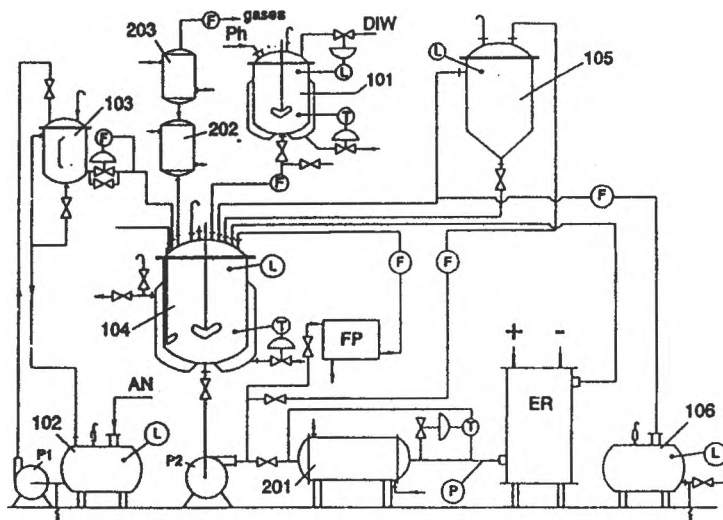


Figure 1: Schematic of the pilot plant used for PN manufacturing (see explanations in text)

The electrodes had a surface area of 2100 cm^2 and were connected to a stabilized current source, able to deliver currents up to 1 kA at cell voltages of 30-32 V. The cathode potential was controlled with respect to saturated calomel electrodes brought into the proximity of the working electrodes *via*

Luggin capillaries. A high purity bulk lead cathode (99.99%) was used in conjunction with a PbO_2 -coated lead anode. The anode was obtained by the *in situ* formation of a 1-3 mm thick compact PbO_2 layer at the lead surface¹⁰⁻¹². The procedure was based on the anodic oxidation of the lead in concentrated aqueous phosphate buffer (pH 7, ionic strength: 1.19)^{11,12}, at current densities of approximately 20 mA cm^{-2} . The Pb surface was previously cleaned with aqueous acetic acid solution (20 wt.%). Neutral aqueous potassium phosphate buffer was used as the supporting electrolyte for PN synthesis. To this, 20 vol.% of AN was added, and the suspension of AN in the aqueous phase was electrochemically reduced under potentiostatic conditions, at $295 \pm 2 \text{ K}$.

Analytical control. The reduction products were analyzed by gas-chromatography according to a previously published method¹³. The composition of the evolved gas mixture (CO_2 , O_2 and H_2) was monitored with an Orsat apparatus.

Results and Discussion

Endurance studies. As seen in Fig. 2, the product yield for PN, raised with the increasing current density. This is due to the slight kinetic preference of NDE the of AN to PN over AD formation. In the same figure the variation of the current efficiency, *CE*, with the current density, *j*, is shown.

As seen from Fig.2, at $j > 60 \text{ mA cm}^{-2}$ the CE improves with increasing current density, and reaches a limiting plateau in the range from 90 to 130 mA cm^{-1} . At current densities greater than 140 mA cm^{-2} CE drops significantly, due to cathodic hydrogen evolution. On the other hand, below 80 mA cm^{-2} the productivity of the pilot plant becomes insufficient.

Endurance tests were performed over a 7-day period of continuous operation of the pilot plant.

Both the current density and the selectivity of PN, S_{PN} , had steady values (Fig.3).

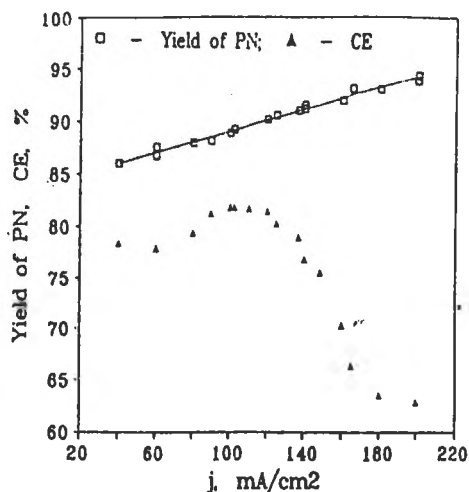


Fig. 2: Plot of the yield of PN and current efficiency (CE) of the process with respect to the current density, j .

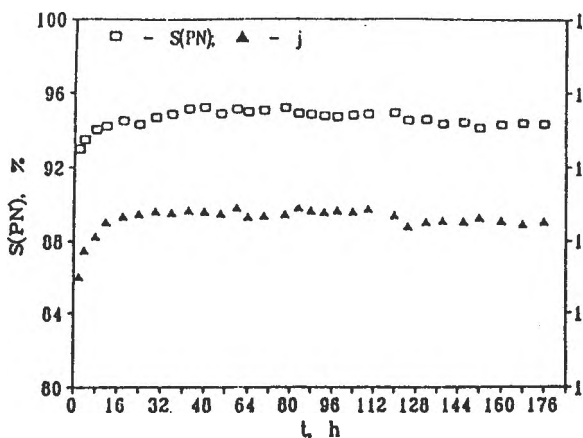


Fig.3: Endurance tests performed over a 7-day period: plot of the selectivity, $S(PN)$ to and of j (secondary y axis) vs. time

By definition, $S_{PN} = [PN] / ([PN] + [AD])$, where: $[PN]$ and $[AD]$ are the concentrations of PN and AD in wt%. After 100 hours of functioning there was a gradual increase of the CO_2 content of the gas mixture obtained by the anode reaction. This increase in CO_2 ranged from the initial 0.2 vol% to the final 3.5 vol%. Carbon dioxide was formed by the anodic oxidation of AN in the undivided cell, a process which was enhanced by the "aging" of the supporting electrolyte. In order to avoid the undesired CO_2 formation, the supporting electrolyte should be replaced by freshly prepared phosphate buffer after each operation period of about 120 hours.

Productivity and power usage. At the average cell voltage of $E_{cell} = 3.5$ V, one can assume typical product yields of 90%, and a current efficiency of 80%. For the continuous operation of the cell at an average current density of 100 mA cm^{-2} ($I = 210$ A) over a time period of one year ($t = 250$ days (year^{-1})), the productivity of the pilot plant can be derived from Faraday's law. For a reactor with 7

cells the calculated productivity is $6.53 \times 10^3 \text{ kg (year)}^{-1}$. From the material balance¹⁴, the specific material consumption of $1.12 \text{ kg AN (kg PN)}^{-1}$ was calculated. As the process is performed in an undivided cell, approximately 1.2 wt% of the electrochemically converted AN is oxidized to carbon dioxide. Using the values listed above the power usage is $1.70 \times 10^4 \text{ kJ kg}^{-1} = 4.73 \text{ kWh kg}^{-1}$. Thus the power usage during the electrolysis (performed at ambient temperatures) is less than the heats involved in a conventional catalytic reduction. Also, this power usage is less than that for AD production in the divided cell process¹⁵.

Conclusion

Based on several preliminary studies, the electrochemical propionitrile synthesis was applied on the pilot plant scale. Selective and energetically convenient operating conditions were found, specific matter and energy consumptions were calculated, and the endurance of the electrodes was studied. The annual productivity of the pilot plant can be significantly increased by increasing the current density, e.g. at 200 mA cm^{-1} the productivity becomes $1.3 \times 10^4 \text{ kg (year)}^{-1}$. However, at higher current densities problems related to the corrosion of the electrodes become more significant. All the technological data reported here are useful for the scale up of the propionitrile electrosynthesis from the pilot plant scale to commercial production.

References

1. L. Oniciu, D. A. Lowy, M. Jitaru, *Bull. Electrochem.*, **4**, 1988, 1041.
2. (a) Y. Kato, K. Fukumoto, *Jpn. Kokai Tokkyo Koho*, 1994, JP 06 09,549; *Chem Abstr.*, **121** 1994, 108496x; (b) J. N. Rubin, J. C. Norenbug, *Eur. Pat. Appl.*, 1994, EP 605,822; *Chem. Abstr.*, **121**, 1994, 107981q; (c) M. Constantini, D. Manaut, D. Michelet, *Eur. Pat. Appl.*, 1994, EP 606,182; *Chem. Abstr.*, **121**, 1994, 157286n.

3. (a) M. M. Baizer, *J. Electrochem. Soc.*, **111**, 1964, 215; (b) M. M. Baizer, J. D. Anderson, *J. Electrochem. Soc.*, **111**, 1964, 226; (c) M. M. Baizer, *French Patent*, 1964, 82591; (d) M. M. Baizer, *Chemtech.*, **10**, 1980, 161; (e) M. M. Baizer, *Tetrahedron Lett.*, **1983**, 973.
4. L. Oniciu, I. A. Silberg, D. A. Lowy, M. Jitaru, F. Ciomos, *Stud. Univ. Babes-Bolyai, Chemia*, **31**, 1986, 80.
5. L. Oniciu, D. A. Lowy, I. A. Silberg, M. Jitaru, B. C. Toma, *Rev. Roum. Chim.*, **32**, 1987, 701.
6. L. Oniciu, D. A. Lowy, M. Jitaru, I. A. Silberg, B. C. Toma, I. Baldea, *Rev. Chim. (Bucharest)*, **39**, 1988, 219.
7. L. Oniciu, D. A. Lowy, M. Jitaru, B. C. Toma, *Stud. Univ. Babes-Bolyai, Chemia*, **33**, 1988, 87.
8. D. A. Lowy, *The Non-Dimerizing Electroreduction of Unsaturated Nitriles*, Ph.D. Dissertation, "Babes-Bolyai" University, Cluj, Romania, 1991.
9. L. Oniciu, I. A. Silberg, F. Ciomos, M. Jitaru, P. Popescu, D. A. Lowy, O. H. Oprea, *Romanian Pat.*, 1986, RO 88417, 1986; *Chem. Abstr.*, **107**, 1987, 25114f.
10. L. Oniciu, I. A. Silberg, V. Toc, F. Ciomos, O. H. Oprea, D. A. Lowy, M. Jitaru, *Romanian Pat.*, 1987, RO 91208; *Chem. Abstr.*, **107**, 1987, 245181r.
11. L. Oniciu, I. A. Silberg, F. Ciomos, D. A. Lowy, M. Jitaru, O. H. Oprea, *Romanian Pat.*, 1987, RO 91210; *Chem. Abstr.*, **107**, 1987, 245180q.
12. M. Jitaru, B. C. Toma, M. Toma, D. A. Lowy, *Bull. Electrochem.*, **11**, 1995, 573.
13. D. A. Lowy, I. A. Silberg, L. Oniciu, *Rev. Chim. (Bucharest)*, **36**, 1985, 354.
14. D. A. Lowy, M. Jitaru, B. C. Toma, I. A. Silberg, L. Oniciu, *Ind. J. Chem. Tech.*, **4**, 1997, 18.
15. D. E. Danly, C. J. H. King, *Industrial Electroorganic Chemistry*, in *Organic Electrochemistry*, edited by Lund H & Baizer M M, 3rd edition, Marcel Dekker, New York, 1991, p.1325.

RATE-DETERMINING STEPS IN THE ELECTROREDUCTION
OF COMPLEX OXYANIONS IN MOLTEN SALTS

D. TKALENKO^a, N. CHMILENKO^b, T. VISAN^c,
M. TKALENKO^a and C. GHIGA^d

^a National Technical University of Ukraine, Dept. Technical Electrochem., 37 Pobeda prospect, 252056 Kiev, Ukraine.

^b Inst. Gen. Inorg. Chem., 32-34 Palladina prospect, 252680 Kiev, Ukraine.

^c "POLITEHNICA" University, Dept. Appl. Phys. Chem. & Electrochem., 132 Calea Grivitei, Bucharest, Roumania.

^d Academy of Economic Studies, Dept. Industr. Technol., 6 Piata Romana, Bucharest, Roumania.

ABSTRACT

It was shown that the use of classical Heyrovsky-Illkovic, Kolthoff-Lingane and Frumkin-Bagotskiy equations for experimental I-E polarization curves may lead to a number of wrong conclusions. In order to prove the reversibility of NO_3^- reduction in single nitrate melts new I-E equations were established for experiments in LiNO_3 , NaNO_3 and KNO_3 , respectively. The addition of nitrite ions, acetamide (or carbamide) and alkaline-earth cations in alkali-metal nitrate melts was also discussed.

INTRODUCTION

During the investigation of electrode processes in oxyanionic molten salts, the anomalous phenomenon of cathodic corrosion of some metals (Ni, Fe, Co, Cu, Ti, Al) and their alloys was observed. This behaviour is very important from practical point of view, especially because the use of nickel, stainless steels or carbon steels as primary containment materials in solar power plants or molten salt fuel cells. The isothermal corrosion tests of various ferrous materials in the heat transfer fluid have shown that after exposure to molten nitrates the attack of metal is always accompanied by formation of soluble or weak-soluble products. The cathodic corrosion is certainly related to the cathodic discharge of oxygen-containing anions (NO_3^- , OH^- , CO_3^{2-} , PO_4^{3-} , BO_3^-) at metal/melt interface. According to the majority of authors [1, 2] the completely different electrochemistry of nitrate ion discharge in various nitrate melts is related to the chemistry of oxides; the formation of high-oxidation state oxides (peroxides, superoxides) can be limited or favoured by the presence of various acid species.

Despite the large number of publications dealing with the mechanism and kinetics of oxyanion reduction in molten salts, the question of rate determining step of such processes is still to be clarified. In order to prove this, the present paper analyses some of our own experimental data referring to the nitrate ion reduction in alkali metal nitrates and discusses several diagnostic criteria of reversibility.

Usually, in molten salts the electrode processes occur reversibly without the influence of chemical reactions and/or adsorption and the electrochemical rate is determined on the whole by reactant supply or product removal (mass transport steps).

EXPERIMENTAL

Steady-state polarization measurements, chronopotentiometric and cyclic voltammetry experiments were performed by usual technique, in a conventional electrochemical cell [3, 5]. Various working electrodes (Pt, Ni, Fe, Co and their alloys) were used, whereas the reference electrode was an Ag wire immersed in the melt with Ag^+ cation ($\text{KNO}_3 + 0.03 \text{ M AgNO}_3$ molten system). The reference compartment was separated from the main one by a glass tube.

RESULTS AND DISCUSSION

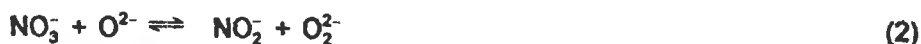
There are several methods for establishing the rate-determining step and the degree of electrode reaction reversibility. Among them, the method using the agreement/disagreement of experimental current-potential curve with certain kinetic equations as a reversibility criterion is the most commonly employed.

We noticed that in the case of nitrate ion reduction in various oxyanionic melts the use of classical Heyrovsky-Ilkovic, Kolthoff-Lingane and Frumkin-Bagostskiy equations for experimental i - E polarization curves may lead to a number of wrong conclusions. Therefore, we have tried to establish new i - E equations starting from the Nernst equation which depends for each particular system on the nature of reactants involved in the reaction and the products formed.

Numerous electrochemical investigations have shown that during the reduction of NO_3^- anion, nitrite and oxide ions result as initial products, according to the process:



The oxide ions produced in the process (1) may convert in the subsequent reactions:



Obviously, the stability of all three ionic forms of oxygen (O^{2-} , O_2^{2-} and O_2^-) depends on the nature of metal cations present in the melts as well as the oxobasicity (oxoacidity) character of the other added substances.

Shibata [7] and Johnson [8] have confirmed by chemical and electrochemical measurements that in individual alkali metal nitrates, the production of peroxide prevails over the superoxide one in molten NaNO_3 , whereas the superoxide is dominant

in KNO_3 melt. In molten LiNO_3 it has been reported the cathodic formation of lithium oxide Li_2O only

Some authors [9] have shown that the slope of the linearized cathodic polarization curve for a molten alkali-metal nitrate does not comply with the prelogarithmic factor of the equation:

$$E = \text{const} - \frac{2.3RT}{2F} \lg i \quad (4)$$

derived from Heyrovski-Ilkovic equation for low current densities. In their opinion this means that the cathodic reduction process of the NO_3^- ion is irreversible. However, we have succeeded to develop a mathematical model by which it can be demonstrated that the cathodic polarization curves for single LiNO_3 , NaNO_3 and KNO_3 melt should be respectively described by the following equations:

$$E = E^\circ - \frac{2.3RT}{2F} \lg \left(\frac{i}{2F} \right)^2 \frac{\delta^2}{D_{\text{O}^{2-}} D_{\text{NO}_3^-}} = \text{const} - \frac{2.3RT}{F} \lg i \quad (5)$$

$$E = \text{const} - \frac{3}{2} \times \frac{2.3RT}{F} \lg i \quad (6)$$

$$E = \text{const} - \frac{2.3RT}{F} \lg \frac{i^3}{(i_d - i)^2} \quad (7)$$

where: E is the electrode potential; E° – the standard electrode potential; i and i_d – the current and the diffusion limited current, respectively, d – the thickness of Nernst diffusion layer; D_i – the diffusion coefficients for i ion. The other symbols have their usual meanings.

As an example it will be considered the case of nitrate ions NO_3^- reduction in LiNO_3 melts, where cathodic process (1) takes place without the formation of peroxide and superoxide combinations.

The expression of Nernst equation can be used to describe the experimental electrode potential:

$$E = E^\circ - \frac{2.3RT}{2F} \lg \frac{a_{\text{NO}_2} a_{\text{O}^{2-}}}{a_{\text{NO}_3^-}} \quad (8)$$

where: a_i is the thermodynamic activity of the ions involved in the electrochemical reaction.

As the nitrate is the solvent electrolyte, the NO_3^- activity $a_{\text{NO}_3^-} = 1$. Assuming an ideal

behaviour, the above equation becomes:

$$E = E^{\circ} - \frac{2.3RT}{2F} \lg C_{\text{NO}_2^-} C_{\text{O}^{2-}} \quad (9)$$

where E° is the formal electrode potential and C_i denotes the concentration of ions at the electrode surface

According to the Fick's law the diffusion fluxes for NO_2^- and O^{2-} ions resulted from the reaction (1) have the following expressions:

$$\frac{i}{2F} = -\frac{D_{\text{NO}_2^-}}{\delta} (C_{\text{NO}_2^-} - C_{\text{NO}_2^-}^*) \quad (10)$$

$$\frac{i}{2F} = -\frac{D_{\text{O}^{2-}}}{\delta} (C_{\text{O}^{2-}} - C_{\text{O}^{2-}}^*) \quad (11)$$

In pure nitrate melts the equilibrium concentration for NO_2^- and O^{2-} in the electrolyte bulk ($C_{\text{NO}_2^-}^*$ and $C_{\text{O}^{2-}}^*$) are very close to zero. Thus, by neglecting them in the concentration differences and substituting $C_{\text{NO}_2^-}$ and $C_{\text{O}^{2-}}$ one obtains:

$$E = E^{\circ} - \frac{2.3RT}{2F} \lg \left(\frac{i}{2F} \right)^2 \frac{\delta}{D_{\text{O}^{2-}}} \frac{\delta}{D_{\text{NO}_2^-}} \quad (12)$$

Considering the same value for the diffusion constant D/δ of NO_2^- and O^{2-} ions, the final expression of the electrode potential can be written as:

$$E = E^{\circ} - \frac{2.3RT}{F} \lg i - \frac{2.3RT}{F} \lg \frac{\delta}{2FD} = \text{const} - \frac{2.3RT}{F} \lg i \quad (13)$$

It results that the potential-current density dependence is linear in E - $\lg i$ coordinates, having a $2.3 RT/F$ (123 mV at 350°C) slope value.

In lithium nitrate-nitrite melts a more simple equation might be written, considering that the thermodynamic activities of NO_3^- and NO_2^- components are equal one another. In such a case, because the electrode potential is described with Nernst equation in the form:

$$E = E^{\circ} - \frac{2.3RT}{2F} \lg C_{\text{O}^{2-}} \quad (14)$$

the expression for the polarization curve takes the form:

$$E = E^{\circ} - \frac{2.3RT}{2F} \lg i - \frac{2.3RT}{2F} \lg \frac{\delta}{2FD_{\text{O}^{2-}}} \quad (15)$$

This equation may be written in a simpler form:

$$E = \text{const} - \frac{2.3RT}{2F} \lg i \quad (16)$$

where the prelogarithmic factor is equal to $2.3RT/2F$. Similar deductions of $i - E$ dependencies were achieved for NaNO_3 and KNO_3 melts taking into account the occurrence of O_2^{2-} and O_2^- ions (eqs. 6 - 7)

Figures 1-3 show the linear dependence in the appropriate coordinates.

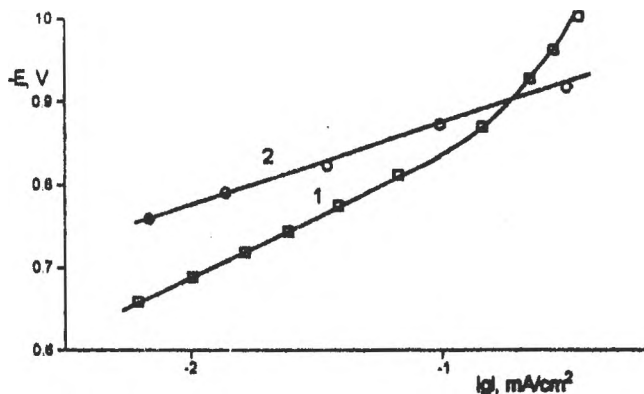


Fig. 1. $E - \log i$ dependence at 350°C for NO_3^- ion cathodic discharge in LiNO_3 single melt (1) and $\text{LiNO}_3 - 0.2\text{M LiNO}_2$ mixture (2). Scan rate: 80 mV s^{-1} ; Pt electrode.

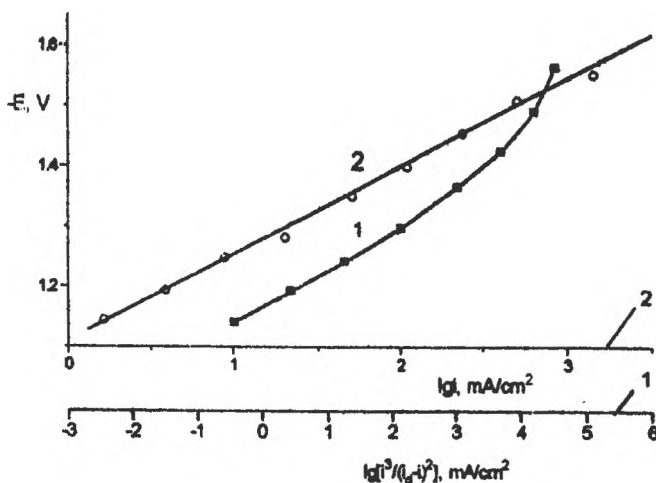


Fig. 2. The analysis of cathodic potentiodynamic curves at 360°C for NaNO_3 melt in the coordinates: $E - \log i$ (curve 1) and $E - \log \frac{i^3}{(i_a - i)^2}$ (curve 2). Scan rate: 80 mV s^{-1} ; Pt electrode.

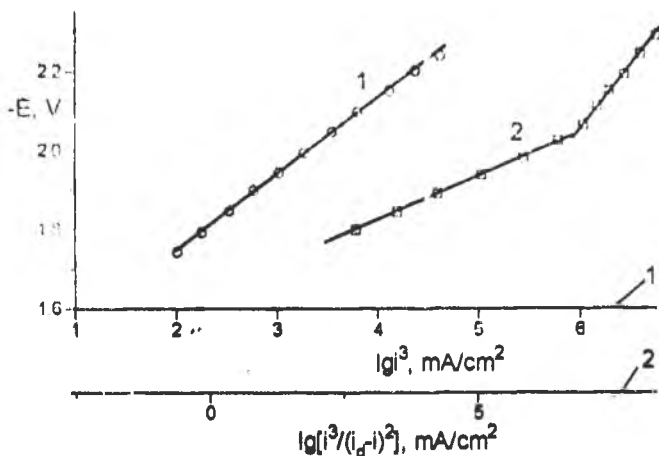


Fig.3. The analysis of cathodic potentiodynamic curves at 360°C for KNO₃ melt in the coordinates: $E - \log i^3$ (curve 1) and $E - \log \frac{i^3}{(i_0 - i)^2}$ (curve 2). Scan rate: 80 mV s⁻¹; Pt electrode.

The slopes of polarization curves in semilogarithmic coordinates to each individual melt agree totally with the prelogarithmic factors of the equations (5)-(7). It has therefore been concluded that a specific reversibility criterion may be applied in the kinetic interpretation of nitrate ion reduction using single alkali-metal nitrate melt. At the same time it might be considered that the process is not controlled by the charge transfer step.

During an electrolysis experiment in the alkali metal nitrate melt oxide ions produced by the principal electrochemical reduction process (1) may give rise to simple alkali metal oxide precipitate or formation of peroxide or superoxide compounds. A number of electrochemical studies (cyclic voltammetry, chronoamperometry and chronopotentiometry) have also been conducted by us [4,5,10] on different materials (Pt, Fe, Ni, Co and their alloys) in single or binary (equimolar NaNO₃ - KNO₃ and LiNO₃ - KNO₃ melts) nitrate melts, confirming the accepted results in the literature of alkali metal oxides production. As an example, the Fig.4 exhibits the cathodic branches of several cyclic voltammetric curves recorded on Pt electrode in various NaNO₃ - KNO₃ melts at 400°C. Well defined cathodic peaks have been found and a continuous shift of their potentials has been invariably observed during the transition from single KNO₃ (without cathodic peak) to single NaNO₃. Note that the NaNO₃ - KNO₃ melt having

about 10% mole NaNO_3 has already got the same peak potential and peak current values as for equimolar mixture of NaNO_3 - KNO_3 or pure NaNO_3 . We have also found a cathodic shift of peak potential with increasing scan rate, although the formation of sodium peroxide Na_2O_2 and oxide Na_2O (which is more stable and less soluble species at such high temperature) is diffusion-controlled, in agreement with recent Singh's works [1,2]. The experiments carried out in LiNO_3 - KNO_3 equimolar melt at 190°C on graphite electrode have revealed the cathodic formation of Li_2O , emphasized by the occurrence of a well defined cathodic peak and a corresponding anodic peak of Li_2O dissolution. The deposition of less soluble Li_2O product, firmly covering the electrode surface leads to the decreasing of electron transfer process; in this way, the continuous diminishing of cathodic peak of Li_2O formation is explained.

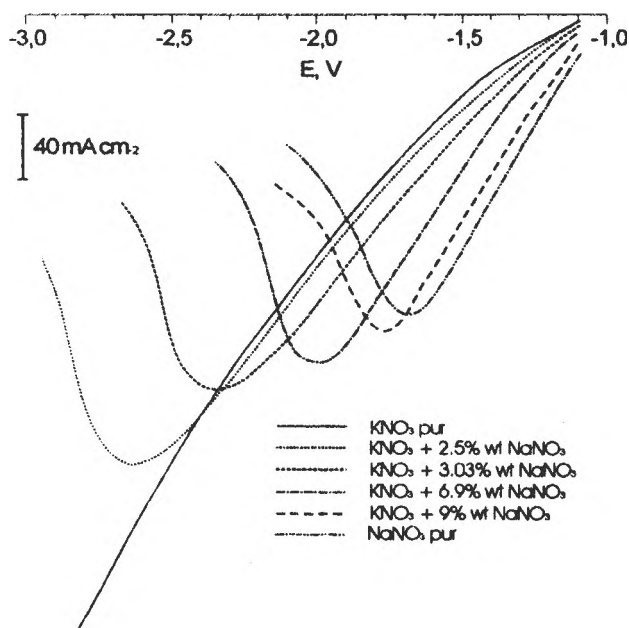


Fig. 4 Cathodic branches of cyclic voltammograms on Pt electrode (400°C) individual KNO_3 , NaNO_3 melts and in molten KNO_3 with various NaNO_3 weight percentages.

The addition of acetamide or carbamide have been studied by cyclic voltammetry. It was observed that the presence of these compounds has caused a shift in the cathodic wave towards positive potentials as well as a substantial increase in the cathodic current. This effect has been easily explained by the fact that the organic

additives interact with oxide ions, decreasing their concentration both in the melt bulk and in the electrode layer and intensifying the reduction process of NO_3^- ion.

As it was pointed out above the cathodic reaction in nitrate systems can be regarded as consisting in a charge transfer step followed by neutralization reaction of resulted oxygen ion; the cathodic process in the nitrate melts containing alkaline-earth cations (Ca^{2+} , Sr^{2+} or Ba^{2+}) may therefore be represented by a EC scheme [11]:



where k_f and k_b are the rate constants of direct and reverse first order chemical reactions and Z denotes the product of conversion. According to the acid-base theory of Lux and Flood [11] the oxide ion O^{2-} is a very strong base and cations such Ca^{2+} (generally, alkaline-earth cations) are strong acids; hence the equilibrium constant, $K=k_f/k_b$ of the second step in EC mechanism (precipitation of alkaline-earth oxides) could have very high values. This means that cathodic peaks on cyclic voltammograms involving NO_3^- reduction (and subsequent neutralization of O^{2-} ion) are not necessarily accompanied by anodic peak occurrence corresponding to opposite electrochemical reaction. The behaviour of investigated melts containing alkaline-earth cations [3,12] could be readily compared with the diagrams described in Nicholson's paper [11], e.g. cyclic voltammograms having $K\sqrt{a/l} = 50$ (where, $a = nFv/RT$ and $l = k_f + k_b$). Moreover, the overall cathodic process was considered moderately irreversible and kinetic information could be obtained [3].

CONCLUSIONS

It has been demonstrated using potentiodynamic polarization curves and cyclic voltammetry data that the cathodic processes of NO_3^- ion in molten alkali nitrates occurs reversible, so that the charge transfer rate is generally higher than the rate of mass transport. Nevertheless, in several cases, the overall process with formation of a less soluble product might be interpreted as quasireversible or even irreversible process

REFERENCES

1. I.B. Singh, S. Sultan and K. Balakrishnan, *Electrochim. Acta*, **38**, **1993**, 2611
2. I.B. Singh, S. Sultan and K. Balakrishnan, *Electrochim. Acta*, **40**, **1995**, 1755
3. S. Sternberg and T. Visan, *Electrochim. Acta*, **26**, **1981**, 75.
4. S. Sternberg, C. Ghiga and T. Visan, *Electrochim. Acta*, **36**, **1991**, 655
5. D.A. Tkalenko, "Electrochemistry of nitrate melts", Kiev, 1983, Naukova Dumka Press, p. 88, 93.
6. C. Ghiga and T. Visan, "Natl. Conf. Chem. Chem. Eng., Bucharest, Oct. 20-21, 1995" Vol 3-II, p. 326.
7. S. Shibata and M.P. Sumino, *Electrochim. Acta*, **20**, **1975**, 871.
8. K.E. Johnson and P.S. Zacharias, *J. Electrochem. Soc.*, **124**, **1977**, 448.
9. S.B. Aganesova and V.P. Yurinskiy, *Elektrokhimiya Rasplav. Solei i Metallov (Trudy Leningr. Polytekh. Inst.)*, **348**, **1976**, 44.
10. S. Sternberg, T. Visan, V. Petrescu and A. Cotarta, "Proc. of the 2nd Roum. Symp. of Appl. Electrochem.", Timisoara, Oct. 4-5 1985", Vol. 1, p. 122.
11. R.S. Nicholson and I. Shain, *Anal. Chem.*, **36**, **1964**, 706.
12. T. Visan, C. Matei, and M. Buda, "Natl. Conf. Chem. Chem. Eng., Bucharest, Oct. 29-30, 1993", Vol. 4, p. 1169.

ION MOLECULE INTERACTION IN ORGANIC ELECTROCHEMICAL SYSTEMS III. ACRYLONITRILE - QUATERNARY AMMONIUM CATIONS ADDUCTS AND THEIR POSSIBLE IMPLICATIONS IN ELECTROHYDRODIMERIZATION PROCESSES

I.A.SILBERG, FLORENTINA CIOMOS, I.SILAGHI-DUMITRESCU
*"Babes-Bolyai" University, Faculty of Chemistry and Chemical Engineering,
11 Arany Janos str., 3400 Cluj-Napoca*

ABSTRACT

The interaction between the voluminous cation of Romegal (a quaternary ammonium salt) and acrylonitrile (ACN) was investigated by NMR spectra and quantum-mechanical calculations.

A pronounced shift of proton signals of ACN was observed upon addition of the surfactant; a notable deshielding effect appears for the proton adjacent to the CN group as compared to the proton in the *trans* position vs.the CN group.The proton situated in *cis* with respect to the CN group is only slightly affected.

An attempt was made to evaluate the coupling of the cationic compound to the negative part of ACN dipole, located at the N atom.We concluded that the molecular associations with predominant electrostatic character between ACN and the quaternary ammonium salt are stable enough to allow the recording of NMR signal shifts.It is assumed that similar molecular associations are responsible for the selectivity of the electrohydrodimerization of ACN to adiponitrile.

INTRODUCTION

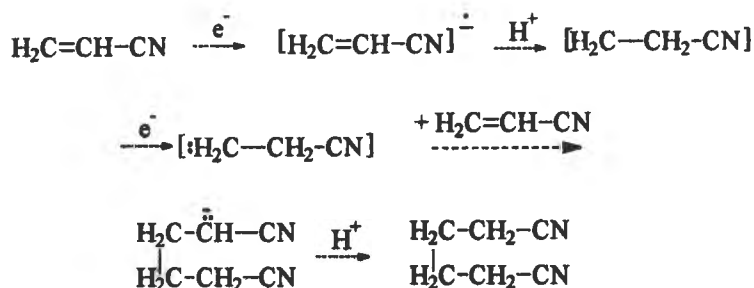
It is a well-known fact that through the electrohydrodimerization of the acrylonitrile adiponitrile is obtained, a key-intermediate in making the polyamid 6,6, the original nylon.

The electrohydrodimerization process takes place on cadmium or lead electrodes (metals with a high overpotential, thus the cathode electrons pass to the organic molecule rather than to the protons) using a phosphate buffer (pH=7). Also, besides the electrolyte, the conducting solution must contain a surface active quaternary ammonium salt. In the absence of the last one the process takes place with formation of propionitrile.



It is important to find the nature of the processes that occur during the electroreduction of the acrylonitrile in a system containing a quaternary ammonium salt. The literature data [1-3] provides only a single hypothesis: it is supposed that the metallic surface of the cathode attracts both the cation of the quaternary ammonium salt and the hydrophobic medium or long-chain alkyl radicals. Therefore, in the vicinity of the electrode, a region with a relatively low water content is formed preventing, at least partly, the access of the protons to the active negatively charged intermediate species and minimizing the yield of the side reaction of formation of the propionitrile (to under 5%). Definitely, this interpretation partially explains the process, but the reaction leading to adiponitrile suggests that the protons cannot be totally excluded from the reaction scheme. The stoichiometry difference (1 H⁺ for electrohydrodimerization, 2 H⁺ for reduction of an acrylonitrile molecule) is not big enough to justify the above hypothesis, or to present it as the only possible one. Our previous research work has demonstrated that the phase transfer catalysis, represents the phenomenon that brings the acrylonitrile anion

(generated by cathode reduction) from the aqueous phase to the acrylonitrile drops, facilitating the Michael-addition, the most important step towards the doubling of the molecule:



If we symbolize the quaternary ammonium salt in the usual way, Q^+X^- , $[\text{CH}_2-\text{CH}_2\text{CN}]^-\text{Q}^+$ will be transferred in the nonpolar medium. This way the Q^+ cation will be found both in the aqueous phase where it reacts with the solvated acrylonitrile (with a saturation concentration of about 7%) and in the dispersed acrylonitrile drops, where it gets due to the interphasic transfer. This way, all the steps of the electrohydrodimerization process (starting with the transfer towards the electrode, adsorption on it and continuing with the electronations, protonations and the formations of the new C-C bond) are affected by the interaction of the acrylonitrile molecule with the cations of the quaternary ammonium salt. Fig.1 briefly shows the pattern for the phase transfer catalysis.

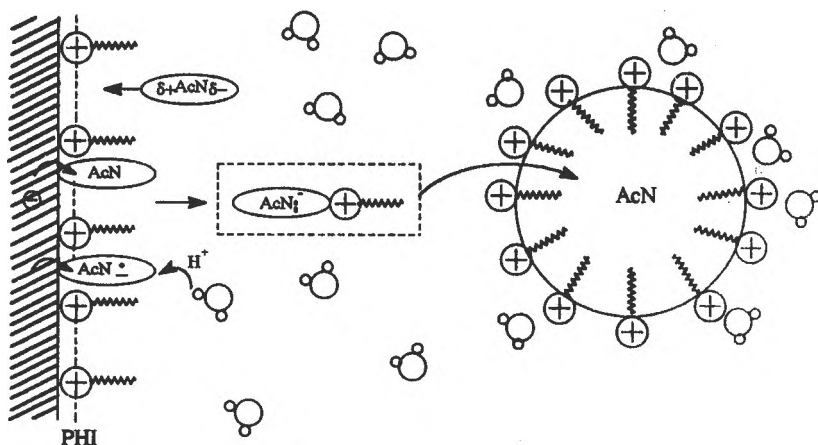


Fig.1. The pattern of the phase transfer catalysis ACN = acrylonitrile, AcNH^+ is the anion $[:\text{CH}_2-\text{CH}-\text{CN}]^-$, $\text{O} \cdots \text{O}$ = the water dipole, \oplus wavy = RCM

ION MOLECULE INTERACTION IN ORGANIC ELECTROCHEMICAL

We tried to find the nature of the bond formed between the cationic tenside and the neutral acrylonitrile molecule ACN, on the one hand, and the formed anionic species (ACN:⁻) on the other.

EXPERIMENTAL

NMR is a very sensitive and accurate method for emphasizing the structure changes and the local electron densities, that are to be found in organic molecules due to the changes of the media which they are placed in.

The 300 MHz NMR spectrum of acrylonitrile in heavy-water medium was recorded, using Romegal CM - a cationic surface - active agent (of industrial use) with C₁₂ - C₁₄ chain bonded to a nitrogen atom quaternarized with methyl radicals. This way, the three protons of the acrylonitrile become a readable AMX system (Fig.2)

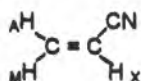


Fig.2 Structure of AMX system

RESULTS AND DISCUSSION

A comparison between the rigorously calculated literature data and our experimental data, emphasizes the fact that the second order rezidual character (which appears in infinitesimal differences between the coupling constants) can be ignored (the more so as we used deuterium oxide, an unusual solvent for this kind of experiments). [4]

		Observed
J _{AM}	0,91	very small
J _{AX}	17,92	17,86
J _{MX}	11,75	11,81

After adding Romegal CM in quantities in usual electrosynthesis (approx. 1% in the water-acrylonitrile mixture), characteristic shifts of the peaks of the three protons (very coherent for the various components of the AMX multiplets) are observed, together with a light smoothing-off of the spectrum (due to the loss of sensitivity because of the increase in viscosity of the solution).

When the solution was nearly saturated with the cationic surface agent, the M and X protons, (placed in a *cis* mutual position far from the CN group of the molecule, were subject to bigger shifts and were better distinguished, while the A proton, due to compensation effects, reoccupied its initial position (see Table I and Table II).

These experimental facts prove that, on the approach of the Q⁺ cation to the acrylonitrile molecule, the molecule is polarized in a highly specific manner, generating obvious differences between the two parts of it (placed on the two sides of the double-bond plan)

Table I. Observed chemical shifts

Sample	A		M		X			
	Hz							
Acrylonitrile	1922,92	1905,06	1878,14	1866,33	1766,95	1756,01	1745,24	1737,43
Q ⁺ added	1927,31	1909,48	1884,18	1872,37	1773,42	1781,39	1755,41	1743,54
Q ⁺ in excess	1922,92	1905,06	1884,25	1872,43	1775,13	1763,32	1757,27	1745,46

Table II Differences in chemical shifts

	A		M		X					
	media									
Q ⁺ added	+4,39	+4,40	+6,04	+6,04	+6,21	+6,15	+6,17	+6,11	+6,16	+6,16
Q ⁺ in excess	0	0	+6,11	+6,10	+8,08	+8,08	+8,03	+8,03	+8,05	+8,05

These differences in chemical shifts show the changes in charge-density because of the approach of the cation of the surface-active agent to the nitrile molecule. The geometrical characteristics of this approach are to be determined. From the literature data either the π electrons of the double-bond, or the CN group (with its negative end, at the nitrogen atom) of acrylonitrile can accept electrons (fig.3).

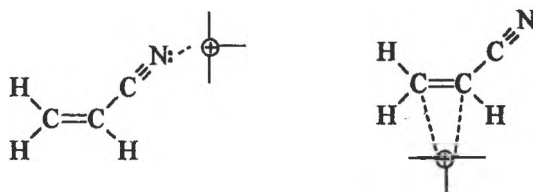


Fig.3 Possible ways of RCM bounding

In order to solve this problem we made quantum-mechanical calculations MNDO [5], in two different variants. Figures (4-6) represent the geometric configuration and the optimized charge densities for the acrylonitrile (fig.4), the situation of the approach of a positive charge (conventionally, we operated with an H⁺ ion) to the double bond (π^2 complexed) (fig.5) and that with the charge placed to the nitrogen atom (on the prolonged axis of the CN group) (fig.6). There is an excellent agreement between the NMR experimental data (for the differentiated chemical shift) and the polarization differences calculated for the third situation (fig.6). There is an excellent agreement between the NMR experimental data (for the differentiated chemical shift) and the polarization differences calculated for the third situation (fig.6). Case two leads to a different set of relations between protons. Thus, both in proton NMR and in calculation the M and X protons undergo large influences (X higher than M as expected) and A experiences smaller ones. We can now consider a proven fact that the acrylonitrile bonds the cationic tenside to the nitrogen atom of the nitrile group.

ION MOLECULE INTERACTION IN ORGANIC ELECTROCHEMICAL

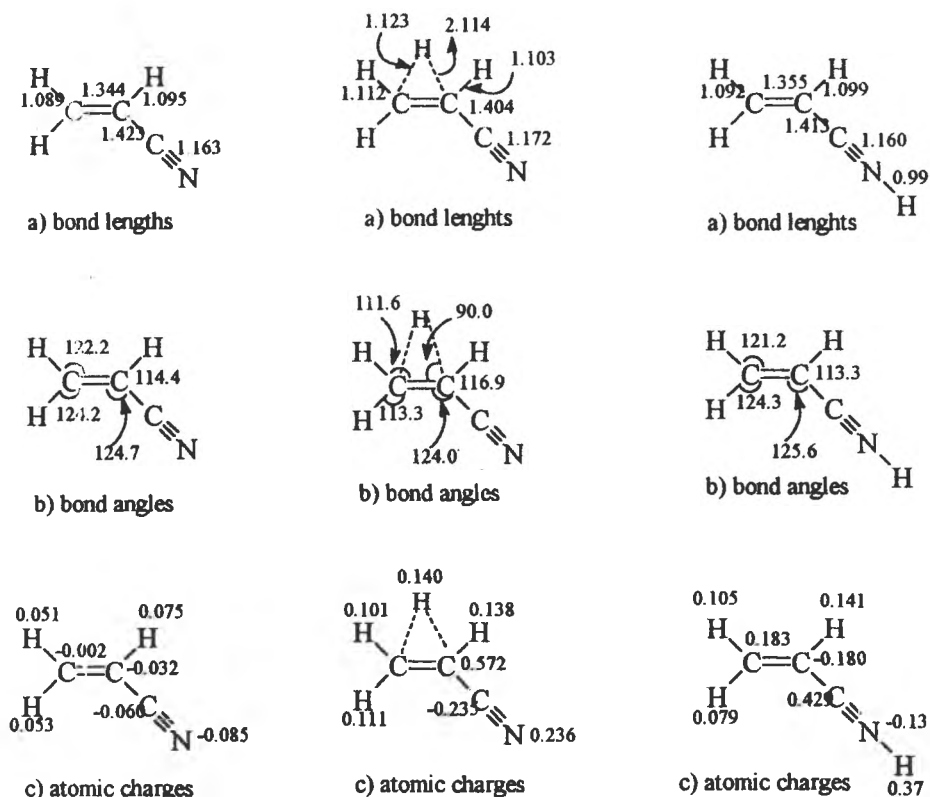


Fig.4 The acrylonitrile molecule

Fig.5 The approach of a positive charge to the π -olefine bond in the acrylonitrile molecule

Fig.6 Placing a charge in the vicinity of the nitrogen atom of the acrylonitrile molecule

CONCLUSION

The results of our work show strong displacement of the peak signals of the three protons of the acrylonitrile. The highest deshielding is that of the proton adjacent to the nitrile group, then that of the *trans*-proton relative to the nitrile group. The least affected is the proton placed in *cis* position (again, relative to the nitrile group).

Thus we have demonstrated the linking of the cationic compound at the negative end of the acrylonitrile dipole (f.e. the nitrogen atom).

Therefore we have demonstrated the existence of a mainly electrostatic molecular associations between the acrylonitrile and the quaternary ammonium salt, long-lived and

stable enough to be recorded and to influence the selectivity of the electrohydrodimerization of the acrylonitrile.

ACKNOWLEDGEMENT

We would like to thanks to Dr.M.T.Caprolu and Mr.Calin Deleanu for preliminary recordings of NMR spectra of ACN In presence of tensides.

REFERENCES

1. M.M.Balzer, C.Danly, *Chemistry and Industry*, 1987, 104, 32.
2. F.Beck, Erdgas Erdoel Kohle, *Petrochem*, 1988, 41, 287.
3. F.Ciomos, *Thesis*, University Babes-Bolyai, Faculty of Chemistry and Chemical Engineering, 1991.
4. I.A.Silberg, *NMR Spectrometry of the organic compounds*, Ed.Dacia, Cluj, 1978.
5. M.I.S.Dewar, W.Thiel, *J.Am.Chem.Soc.*, 1977, 99, 3899.

KINETIC STUDY OF COPPER ELECTROCRYSTALLIZATION

H. Haiduc,

SC "ELMET SA, RO-3400 Cluj-Napoca, Romania

P. Ilea*, A. Nicoara, S. Dorneanu and L. Oniclu

Facultatea de Chimie si Inginerie Chimica, Universitatea Babes-Bolyai,

RO-3400 Cluj-Napoca, Romania

* author to whom correspondence should be adressed

Abstract

The kinetics of the nucleation and growth of copper by means of potential step technique was studied. The electrolyte was a $\text{CuSO}_4 - \text{H}_2\text{SO}_4$ aqueous solution. Some parameters like electrode material (Pt, TiO_2/Ti , stainless steel and vitreous carbon) and potential step values (380 - 800 mV) were investigated. Steady state nucleation rate and nuclei density were calculated, for a 0.05 M $\text{CuSO}_4 - 1 \text{ M H}_2\text{SO}_4$ aqueous solution. The activation energy of nucleation stage by means of the steady state nucleation rate obtained at several different temperatures was calculated.

INTRODUCTION

Qualitatively, electrocrystallization involves a number of distinct steps [1], as follows: solvated ion diffusion from the solution bulk to the electrode surface, charge transfer, partial or complete loss of the solvating sphere, surface diffusion of ad-atoms, nucleation, incorporation of ad-atoms on lattice sites and development of crystallographic and morphological characteristics of the deposit. Characteristics of the deposit (porosity, smoothness, brightness) strongly depend on the initial stages of the process. Most of authors [2-7] consider that nucleation is one of the most important stages of electrocrystallization. The study of nucleation kinetics generally starts from the distinction between two types of mechanisms: instantaneous and progressive nucleation. In practice, potential step technique is often used to diagnose the nucleation type [8,9].

The aim of this paper is to study the influence of the substrate type and the value of applied potential step, concerning copper nucleation, and estimation of nucleation kinetic parameters.

GENERAL CONSIDERATIONS

In the nucleation stage, germs of nucleation are formed on the so called active sites [10,11,12]. The electrode material capacity to provide active sites for nucleation are given by [13]: epitaxial compatibility between substrate and depositing metal, finishing degree of electrode surface and experimental conditions. New formed germs have a great degree of instability [1]. Part of them grows up and the other dissolve. Over the critical size, the germs become stable. Around of each nucleus are diffusion zones with hemispherical symmetry. The following equation gives the total current density for nucleation and growth [6].

$$i(t) = zF c \pi (2D)^{3/2} (Mc / \rho)^{1/2} \int_0^t (t-u)^{1/2} \frac{dN}{du} du \quad (1)$$

where $i(t)$ is the instantaneous current density, z - ion charge, F - Faraday number, c - molar concentration of electroactive species, D - diffusion coefficient, M/ρ - molar volume, t - time, u - time of birth of a critical nucleus, N - number density of nuclei at time t .

Solving this integral for limiting conditions of instantaneous nucleation ($N = N_0$) and progressive nucleation ($N = AN_0t$) we obtain:

-for progressive nucleation

$$i(t) = \frac{2}{3} zFc\pi(2D)^{3/2} (Mc/\rho)^{1/2} AN_0t^{3/2} \quad (2)$$

-and for instantaneous nucleation

$$i(t) = zFc\pi(2D)^{3/2} (Mc/\rho)^{1/2} N_0t^{1/2} \quad (3)$$

where: A is the nucleation rate constant reported at an active site, N_0 - maximum number density of nuclei at certain experimental conditions

Estimation of the nucleation type is made according to the type of dependence $i = f(t^n)$. An $i = f(t^{3/2})$ dependence shows a progressive nucleation, and an $i = f(t^{1/2})$ dependence indicates an instantaneous mechanism.

As nuclei are growing, it appears interference of the diffusion zones and finally overlaps of the neighboring nuclei, to be seen as coalescence of the growing clusters [14] (see fig. 1). It is time when individual diffusion zones of hemispherical symmetry turn in a joint diffusion zone of plane symmetry. That is why the validity of equations 1 - 3 is affected.



Figure1. Interference of the diffusion zones and overlap of the neighboring nuclei.

Gunawardena et al. [3] proposed the following equations considering interference of the diffusion zones, overlap of the neighboring nuclei and diffusive transport.

-for progressive nucleation

$$i(t) = \frac{zFcD^{1/2}}{(\pi t)^{1/2}} \left[1 - \exp\left(\frac{-AN_0\pi k' Dt^2}{2}\right) \right] \quad (4)$$

-and for instantaneous nucleation

$$i(t) = \frac{zFcD^{1/2}}{(\pi t)^{1/2}} [1 - \exp(-N\pi kDt)] \quad (5)$$

KINETIC STUDY OF COPPER ELECTROCRYSTALLIZATION

where:

$$k' = 4 / 3(8\pi cM / \rho)^{1/2} \text{ and } k = (8\pi cM / \rho)^{1/2}.$$

Deriving equations 4,5 and equalizing with zero we obtain the current maximum coordinates, i_m and t_m . These, together with product expression $i_m^2 t_m$ are given in Table 1.

Table 1. Expressions resulting from the analysis of the current maximum for instantaneous and progressive nucleation.

instantaneous nucleation	progressive nucleation
$t_m = 1.2564/N kD \quad (6)$	$t_m = (4.6733/AN_o k'D)^{1/2} \quad (7)$
$i_m = 0.6382zFDc(kN)^{1/2} \quad (8)$	$i_m = 0.4615zFD^{3/4}c(k'AN_o)^{1/4} \quad (9)$
$i_m^2 t_m = 0.1629(zFc)^2 D \quad (10)$	$i_m^2 t_m = 0.2598(zFc)^2 D \quad (11)$

The product $i_m^2 t_m$ does not contain the k , k' , A , N parameters and therefore a convenient diagnostic criterion for the particular form of nucleation occurred. The product depends only on concentration and diffusion coefficient, offering therefore distinction, very easy to verify, between instantaneous and progressive types (Is given by the numerical coefficient).

EXPERIMENTAL CONDITIONS

The nucleation of copper from $CuSO_4 - 2 M H_2SO_4$ aqueous solutions was studied potentiostatically. The concentration range was 3.17 - 40 g/L Cu. All solutions were prepared from analytical grade reagents and distilled water.

The experimental setup consisted of: a three-electrode cell, a potentiostat and a data acquisition system. The working electrodes were made of stainless steel (0.031 cm^2), TiO_2/Ti (0.071 cm^2), Pt (0.008 cm^2) and vitreous carbon - VC (0.062 cm^2). To ensure reproducibility between experiments, the exposed surface was polished to a grinding paper (800 and 1200) and well washed with distilled water. The counter electrode was a platinum band with a surface of 5 cm^2 . A saturated calomel reference electrode (SCE) was used, connected to the main cell through a Luggin capillary adjacent to the working electrode. All potentials are in respect with the SCE and overpotentials were calculated using the Nernst equation.

A PS3 Forschungsinstitut Meinsberg, Dresden (Germany) potentiostat connected with a personal computer Olivetti AT 486 DX by a National Instruments AT M10 16F acquisition board was used for experimental data acquisition. The kinetics of copper nucleation was studied with single negative potential steps within -380 and -600 mV, recording in each case the current transients. The rest potential, between two running measurements, was +300 mV vs. SCE.

The working temperature was within 20 and 47.

RESULTS AND DISCUSSION

Value of potential step

A family of current transients obtained at different potential steps is shown in Fig. 2. The potential step values, in mV, are given beside corresponding current transients. The shape of these experimental transients suggests that they can be analyzed according to the theoretical model proposed by Gunawardena et al. [3]. For an accurate analysis we must remove nonfaradaic current corresponding to the charging of electric double layer. That can be done by subtracting the nonfaradaic current from the current recorded in the working solution. Nonfaradaic current was recorded in a 2 M H₂SO₄ aqueous solution experiment. Unfortunately, it is impossible to remove completely the nonfaradaic current, because capacitance of double layer is different in - working and H₂SO₄ solution - just because of the presence of copper ions.

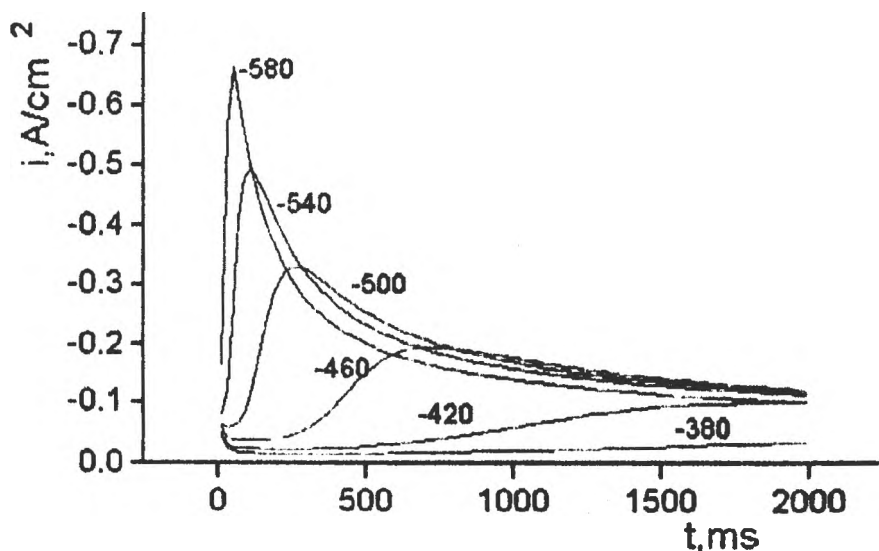


Figure 2. Potentiostatic current transient for the electrodeposition of copper on Pt from 40 g/L CuSO₄ - 2 M H₂SO₄ aqueous solution at the potentials indicated in mV vs. SCE.

After the rapid double layer charging the current tends to zero and then, it follows a rising part due to the growth of the new phase and/or the increasing number of nuclei. As those grow, the coalescence of the neighboring diffusion fields with localized spherical symmetry give rise to a current maximum, and then the current decays, approaching a Cottrell dependence [6] (see eq. 12). In fact, equations 4 and 5 tend to Cottrell equation at sufficient large times.

$$i(t) = \frac{zFcd}{(\pi t)^{1/2}} \quad (12)$$

KINETIC STUDY OF COPPER ELECTROCRYSTALLIZATION

Electrode material

To study the influence of the substrate material on the nucleation rate of copper experiments on platinum (Fig. 2), stainless steel (Fig. 3) and TiO_2/Ti (Fig. 4) electrodes were made.

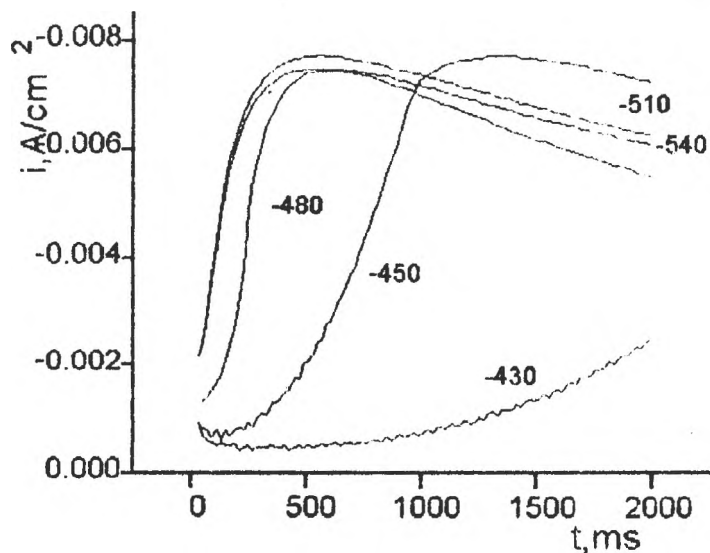


Figure 3. Potentiostatic current transient for deposition of copper on stainless steel from 40 g/L CuSO_4 - 2 M H_2SO_4 aqueous solution at the potentials indicated in mV vs. SCE.

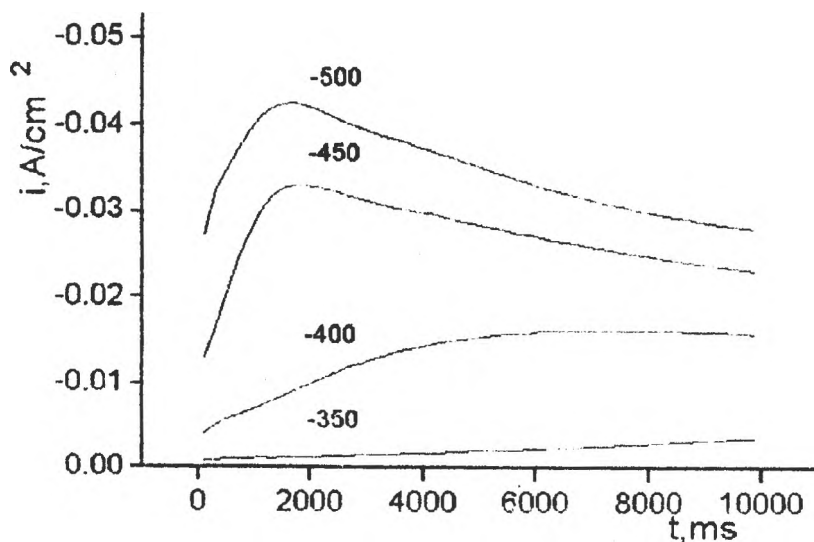


Figure 4. Potentiostatic current transient for electrodeposition of copper on TiO_2/Ti from 40 g/L CuSO_4 - 2 M H_2SO_4 aqueous solution at the potentials indicated in mV vs. SCE.

Both depositing rate and process evolution strongly depend on the electrode material, i.e., substrate type. Nucleation rate on platinum is greater with one magnitude order than onto TiO₂/Ti and with two magnitude orders than onto stainless steel. In the case of copper nucleation on platinum and TiO₂/Ti the process evolution is common, and diffusion control after 1.5 - 2 s and more than 10 s, respectively is reached. At the nucleation on stainless steel the value of the current maximum is the same disregarding the potential step value.

Determination of nucleation type. Calculation of A and N

It was used the test based on product $i_{m}^2 t_m$ for determination of nucleation type (see Tab.1), working with a 0.05 M CuSO₄ - 2 M H₂SO₄ solution. Diffusion coefficient from the decaying current after the maximum (when diffusion control is installed) using the Cottrell equation was calculated[15-17]. The obtained value was $D = 7.02 \cdot 10^{-6} \text{ cm}^2 \text{ s}^{-1}$. In the experimental conditions the value of the product $i_{m}^2 t_m$ is:

-for instantaneous nucleation:

$$i_{m}^2 t_m = 1.064 \cdot 10^{-4} \text{ A}^2 \text{ cm}^4 \text{ s} \quad (13a)$$

-and for progressive nucleation:

$$i_{m}^2 t_m = 1.697 \cdot 10^{-4} \text{ A}^2 \text{ cm}^4 \text{ s} \quad (13b)$$

disregarding electrode material.

Nucleation on vitreous carbon is presented in the following section.

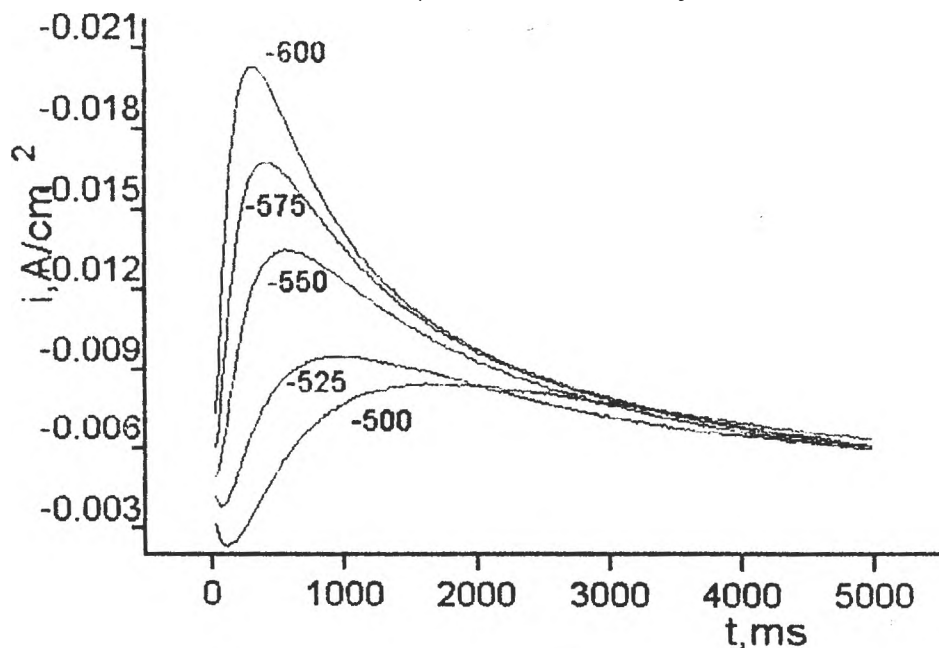


Figure 5. Potentiostatic current transient for the electrodeposition of copper on VC from 0.05 M CuSO₄ - 2 M H₂SO₄ aqueous solution at the potentials indicated in mV vs. SCE

KINETIC STUDY OF COPPER ELECTROCRYSTALLIZATION

Table 2. Calculated parameters for the nucleation of copper on VC from 0.05 M CuSO₄ - 2 M H₂SO₄ aqueous solution.

E/SCE (mV)	Over- potential (mV)	t_m (s)	i_m (Acm ⁻²)	$10^7 i_m^2 t_m$ (A ² cm ⁻⁴ s)	N (10 ⁶ cm ²)	N ₀ (10 ⁶ cm ²)
-500	-255	1.61	0.00848	1.157	0.38	0.35
-525	-280	0.99	0.00952	0.997	0.61	0.42
-550	-305	0.55	0.01351	1.003	1.10	0.76
-575	-320	0.43	0.01675	1.205	1.41	1.15
-600	-355	0.31	0.02002	1.242	1.95	1.64

From the $i_m^2 t_m$ values it can be observed, in this case, nucleation was in essence instantaneous. In column 6 are given the values for the nuclei density, calculated from current maximum, and in column 7 are the values for maximum nuclei density, calculated from the slope of $i(t) = f(t^{1/2})$. Values of N, calculated for entirely instantaneous nucleation, are smaller than those calculated from current maximum. This means that there are nuclei appearing after the potential step input, meaning that nucleation is mostly instantaneous but a small amount of progressive nucleation also appears.

In the following, we present the data obtained at nucleation of copper on platinum.

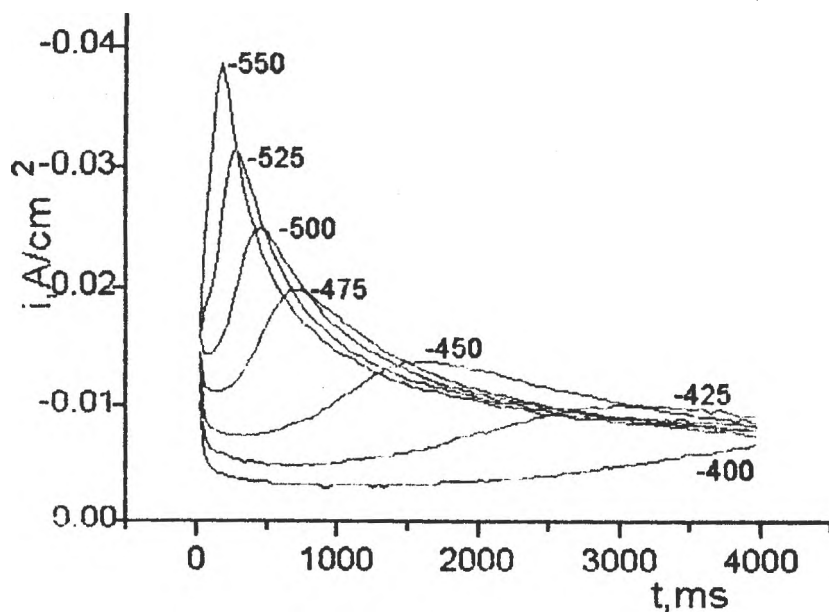


Figure 6. Potentiostatic current transient for the electrodeposition of copper on Pt from 0.05 M CuSO₄ - 2 M H₂SO₄ aqueous solution at the potentials indicated in mV vs. SCE.

Table 3. Calculated parameters for the nucleation of copper on Pt from 0.05 M CuSO₄ - 2 M H₂SO₄ aqueous solution.

E/ECS (mV)	Overpotential (mV)	t _m (s)	10 ⁷ i _m ² t _m (A ² cm ⁴ s)	AN ₀ (10 ⁶ cm ⁻² s ⁻¹)	N ₀ (10 ⁶ cm ⁻²)	A (s ⁻¹)
400	-155	-	-	-	-	-
-425	-180	2.98	2,016	0,20	0,35	0,57
-450	-205	1.62	1,935	0,68	0,64	1,06
-475	-230	0.70	1,730	3,65	1,48	2,47
-500	-255	0.46	1,838	8,46	2,26	3,74
-525	-280	0.26	1,554	26,48	3,99	6,64
-550	-305	0.18	1,682	55,25	5,77	9,58

In this case we have to deal with progressive nucleation. We can obtain the nucleation rate, AN₀ from the slope of the straight $l(t) = f(t^{3/2})$ (column 5, table 3). Calculation of N₀ (column 6) is possible because even in the case of progressive nucleation there is a moment when germination is repressed (after the overlap of diffusion zones), therefore nucleation becomes instantaneous [6]. Nucleation is not entirely progressive, but is prevailing. It can be observed that A and N₀ are growing together with potential step value, the growth of A being double in comparison with N₀. This means that A is more sensitive at potential step applied than N₀.

At small potential step current maximum is flat, so that is the reason for the first measurements is not so exact in both of cases (see Tab.2 and 3).

Activation energy of nucleation

The possibility to determine nucleation rate constant allowed us to calculate activation energy of nucleation. The method consists in determination of rate constant at several temperatures, and using a $\ln A = f(1/T)$ plot, the activation energy being calculated by the Arrhenius theory. This treatment has a physical meaning only in case of progressive nucleation, when there is a pure rate constant. This happens at copper nucleation on platinum. We worked at four different temperatures, and recorded current transients are shown in fig.7.

Table 4. Calculated parameters for the nucleation of copper on Pt from 0.05 M CuSO₄ - 2 M H₂SO₄ aqueous solution, at different temperatures.

T (K)	10 ⁴ *i _m ² t _m calculated (A ² cm ⁴ s)	10 ⁴ *i _m ² t _m experimental (A ² cm ⁴ s)	AN ₀ (10 ⁷ cm ⁻² s ⁻¹)	N ₀ (10 ⁶ cm ⁻²)	A (s ⁻¹)
302	1,63	1,56	4,385	2,246	19,52
311	2,15	2,09	5,318	2,190	24,28
316	2,47	2,32	10,018	2,700	37,10
320	2,89	2,61	13,543	2,900	46,70

KINETIC STUDY OF COPPER ELECTROCRYSTALLIZATION

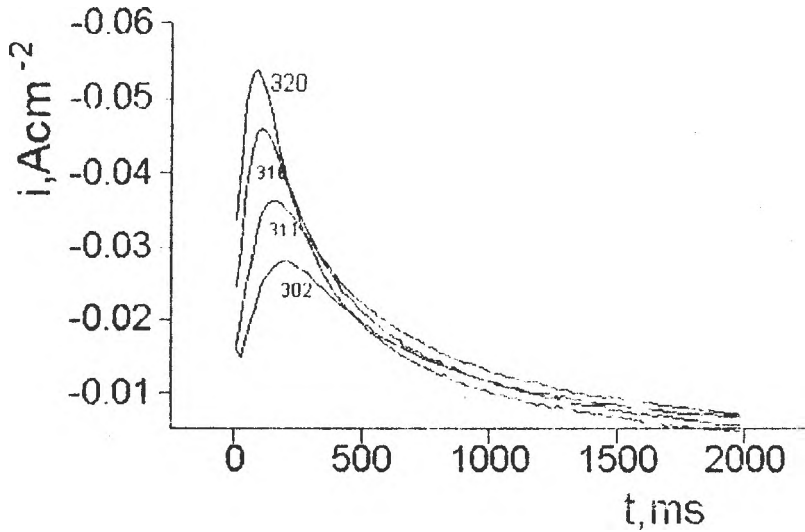


Figure 7. Potentiostatic current transient for the deposition of copper on Pt from 0.05 M CuSO_4 - 2 M H_2SO_4 aqueous solution, at different temperatures indicated in K.

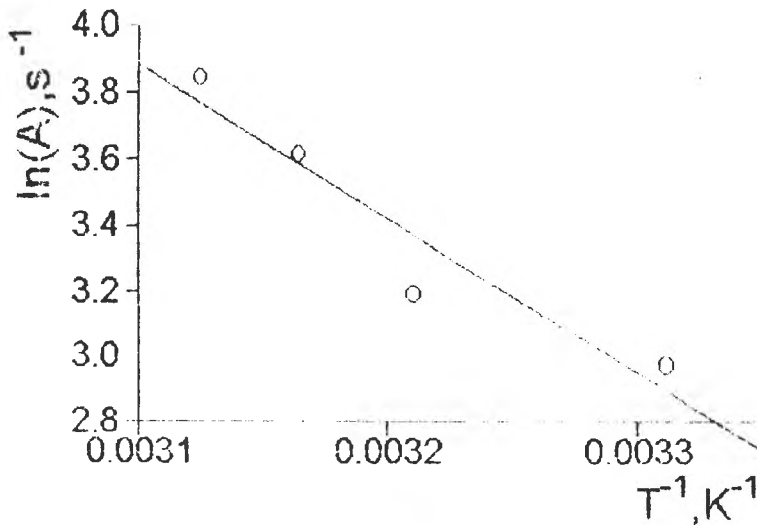


Figure 8. Arrhenius representation of $\ln A = 1/(1/T)$ for copper nucleation on platinum (see fig 7).

Activation energy obtained is 37 024 kJ/mole.

From the data presented in Table 4, columns 5 and 6, it can be seen that A is growing with temperature much faster than N_0 . It is a similar situation with that found at variation of A and n_0 with potential step value.

CONCLUSIONS

Electronucleation of copper on foreign substrate is strictly dependent from substrate nature. This influences both nucleation rate and nucleation mechanism. This dependence comes from epitaxial compatibility between depositing species and substrate.

The nucleation of copper on vitreous carbon was found to be mostly instantaneous, and on platinum mostly progressive. It is important to say that complete distinction between these two types of nucleation was not possible to be done. There are authors who consider this distinction forced [5].

We calculated A and N and/or N_0 , and their values were not found to be strictly specific for copper. They change with: electrode material and it's finishing degree, potential step value, copper concentration and working temperature.

Obviously, A and N and/or N_0 are growing together with potential step value and temperature. The constant rate grows faster than nuclei density. That means, in much forceful conditions the number of active sites grows reasonable while the reactivity of an active site grows much quickly. The limiting growth of nuclei density is according to a finite surface area of the electrode

REFERENCES

1. R.Greef, R.Peat, L.M. Peter, D.Pletcher and J.Robinson, *Instrumental Methods in Electrochemistry, Chapter 9 Electrocrystallisation*, Ellis Horwood Limited, Chichester, 1985.
2. J.O'M.Bockris and G.A.Razumney, *Fundamental Aspects of Electrocrystallisation*, Plenum Press, New York, 1967.
3. G.Gunawardena, G.Hills, I.Montenegro and B.Scharifker, *J. Electroanal. Chem.*, 1982, **138**, 225.
4. R.Winand, *Hydrometallurgy*, 1992, **29**, 567.
5. B.Scharifker and C.Hills, *Electrochim. Acta*, 1983, **28**, 879.
6. J.Wijenberg, *J. Electroanal. Chem.*, 1987, **236**, 1.
7. E.B.Budevski in B.F.Conway, J.O'M.Bockris, E.Yeager and S.U.M.Khan (Eds.), *Comprehensive Treatise of Electrochemistry*, Vol. 7, Plenum, New York, 1983.
8. H.R.Thiirk and J.A.Harrison, *Guide to the Study of Electrode Kinetics, Chapter 3 Electrocrystallisation*, Academic Press, London, 1972.
9. R.Varma and J.R.Selman, *Techniques for Characterization of Electrodes and Electrochemical Processes, Chapter 15. Techniques for Nucleation Analysis in Metal Electrodeposition*, J. Wiley & Sons, Inc., New York, 1991.
10. R.Winand, *J. Appl. Electrochem.*, 1991, **21**, 377.
11. W.K.Burton, K.Cabrera and F.C.Frank, *Nature*, 1949, **163**, 398.

KINETIC STUDY OF COPPER ELECTROCRYSTALLINATION

12. M.Sanchez Cruz, F.Alonso and J.M.Palacios, *J. Appl. Electrochem.*, 1993, **23**, 364.
13. Al.Milchev, *Electrochim. Acta*, 1983, **28**, 947.
14. M.Y.Abyaneh, *Electrochim. Acta*, 1982, **27**, 1329.
15. A.J.Bard and L.R.Faulkner, *Electrochemical Methods. Fundamentals and Applications*, J. Wiley & Sons, inc., New York, 1980.
16. C.M.A. Brett and A.M.O. Brett, *Electrochemistry Principles, Methods and Applications, Part I, Cap. 5 Mass Transport*, Oxford University Press, 1993.
17. I. Oniciu and E.Constantinescu, *Electrochimie și Coroziune*, Editura Didactică și Pedagogică, București, 1982

Current - concentration correlation for anodic dissolution of zinc in sulphate electrolytes

L. Dimă, D. Bughiu, L. Anicai, C. Trifu

Department of Electrochemical Technologies and Products, Research and Development Institute for Electrical Engineering, ICPE-SA, Splaiul Unirii 313, 74204, Bucharest, Romania

ABSTRACT

The paper gives a mathematical equation that correlates the limiting dissolution current and the concentration of zinc and sulphate anions, and the working temperature.

EXPERIMENTAL

The working electrode consisted of a 99.99% Zn rod, insulated with inert resin (active surface area 0.636 cm^2). The reference electrode was a saturated calomel electrode (SCE), and as counterelectrode a platinum gauze was used ($\sim 20 \text{ cm}^2$).

As sulphate electrolytes we used ZnSO_4 solutions with different concentrations (0.5, 0.75, 1, 1.5 and 2M) and Na_2SO_4 solutions (0.5, 0.75, 1, 1.25 and 1.5M), as well as their combinations (analytical grade reagents). The working temperature was 20, 40 and 60°C .

The potentiodynamic polarization curves were drawn using a scan rate of 500 mV/min. The electrochemical measurements were performed using a TACUSSEL potentiostat, model PRT-20, voltmeter for monitoring the polarization potential and a milliamperemeter.

RESULTS AND DISCUSSIONS

An example of polarization curves is shown in Fig. 1. The anodic limiting dissolution current decreases as the Zn^{2+} concentration and temperature increases. The anodic limiting dissolution current corresponds to the first maximum on the polarization curve. The dependencies of the anodic limiting dissolution currents on the Zn^{2+} concentration (c), sulphate concentration and temperature are shown in figs. 2, 3 and 4.

A first way for correlation the obtained data is to correlate the anodic limiting dissolution current (i) with the free anion concentration (sulphate concentration, h), Zn^{2+} concentration (c) and temperature. All concentrations are in mol/L. At a given free anion concentration, h, the i vs. c dependence is a straight line having the general form $i = b \times c + a$, where b are the slopes in figs. 2, 3 and 4, and a are the X-intercepts from the same figures. Both a and b depend on the free anion concentration, h and temperature.

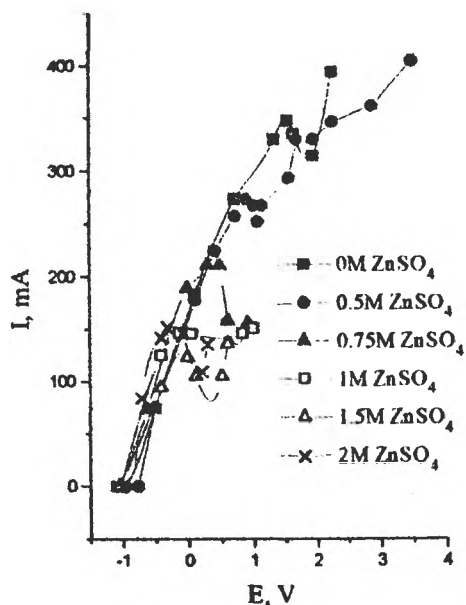


Fig. 1. Polarisation curves for 0.75M Na_2SO_4 with different Zn^{2+} contents, at 20°C.

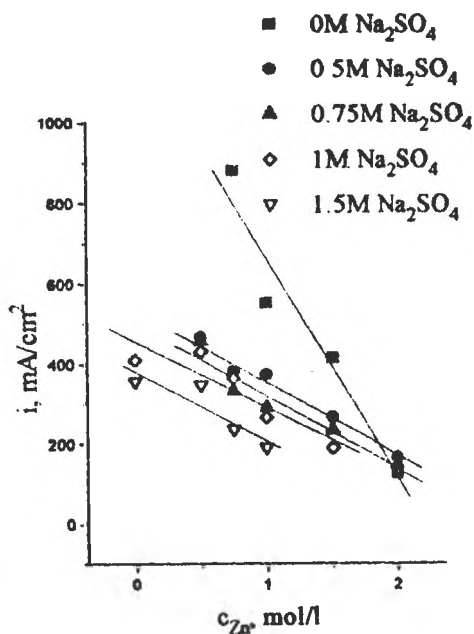


Fig. 2. The i - c dependence for different h at 20°C.

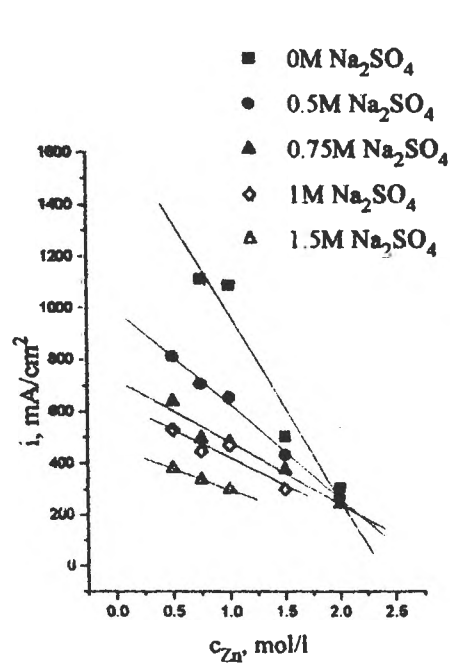


Fig. 3. The i - c dependence for different h at 40°C.

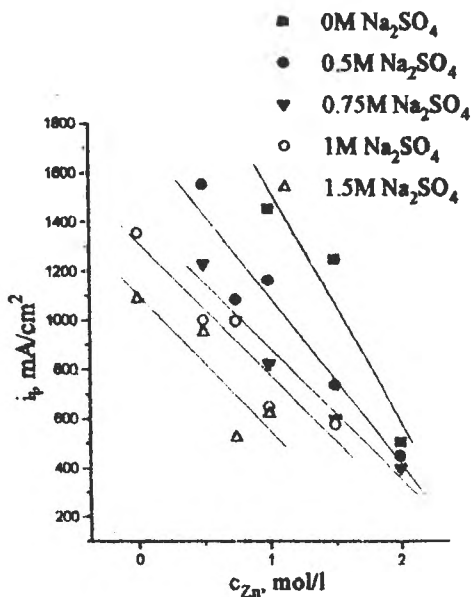


Fig. 4. The i - c dependence for different h at 60°C.

The equations for b are obtained by plotting the logarithm (in fact, the base of the logarithm, that is $-\log(b)$) against the logarithm of the free anion

concentration, h. Considering the general form (fig. 5) for b as $b = -10^{a1} \times h^b$, then, for the studied temperatures the b values are:

$$b_{20} = -173.98 \times h^{-0.058}$$

$$b_{40} = -213.054 \times h^{-0.7119}$$

$$b_{60} = -556.1603 \times h^{-0.1719}$$

The equations for a are obtained by plotting the a values against the free sulphate concentration, h, at constant temperature. The a-h dependencies are shown in fig. 6 for all temperatures; considering the general form for these equations as:

$$a = 10^{a2} \times h^{b2},$$

for the studied temperatures the a values are:

$$a_{20} = 442.895 \times h^{-0.3122}$$

$$a_{40} = 614.879 \times h^{-0.6824}$$

$$a_{60} = 1301.18 \times h^{-0.419}$$

Replacing a and b values in the i equation we find the equations for the limiting anodic dissolution currents for the studied temperatures:

$$i_{20} = 442.985 \times h^{-0.3122} - 173.98 \times h^{-0.0587} \times c;$$

$$i_{40} = 614.88 \times h^{-0.6824} - 213.054 \times h^{-0.7119} \times c;$$

$$i_{60} = 1301.187 \times h^{-0.419} - 556.160 \times h^{-0.1719} \times c$$

Assuming a general form for i as $i = A[1/T] \times h^{B[1/T]} + C[1/T] \times h^{D[1/T]}$, in which the A, B, C and D coefficients are temperature dependent, the values for these coefficients are obtained as following:

the equation for A[1/T] is obtained by plotting the logarithm of the X-intercepts for the straight lines in fig. 5 against 1/T (a2 in fig. 7):

$$A[1/T] = 10^{6.471 - 1130.38/T}$$

the equation for B[1/T] is obtained by plotting the slopes for the straight lines in fig. 5 against 1/T (b2 in fig. 7):

$$B[1/T] = 292.8375 / T - 1.4093$$

the equation for C[1/T] is obtained by plotting the X-intercepts for the straight lines in fig. 6 against 1/T (a1 in fig. 7):

$$C[1/T] = 3246.295 - 915182.6/T$$

the equation for D[1/T] is obtained by plotting the slopes for the straight lines in fig. 6 against 1/T (b1 in fig. 7):

$$D[1/T] = 337.48/T - 1.395$$

Replacing again the A, B, c and d values in the i equation, we obtain the final form for the limiting anodic dissolution currents as a function of the Zn^{2+} concentration (c), free anion concentration (h) and temperature:

$$i = 10^{(6.471 - 1130.3/T)} \times h^{(292.8/T - 1.409)} - (3246.3 - 915182.6/T) \times h^{(337.48/T - 1.395)} \times c(1) \quad (1)$$

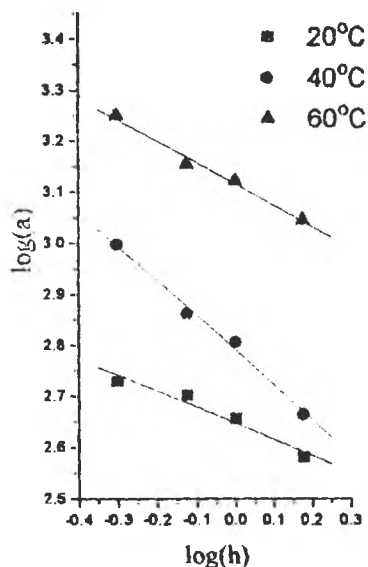


Fig. 5. The dependence of the X-intercepts-a for the straight lines in figs. 2, 3, 4 vs. free anion concentration.

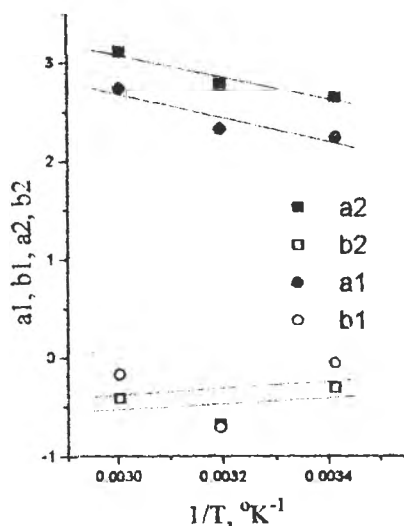


Fig. 7. X-intercepts and slopes for the straight lines in figs. 5 and 6 vs. $1/T$.

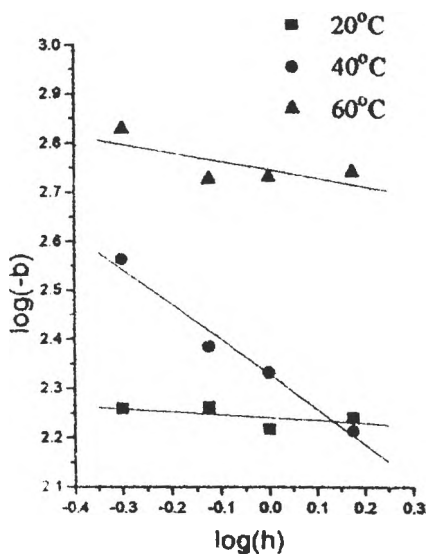


Fig. 6. The dependence of the slopes-b, for the straight lines in figs. 2, 3, 4 vs. free anion concentration.

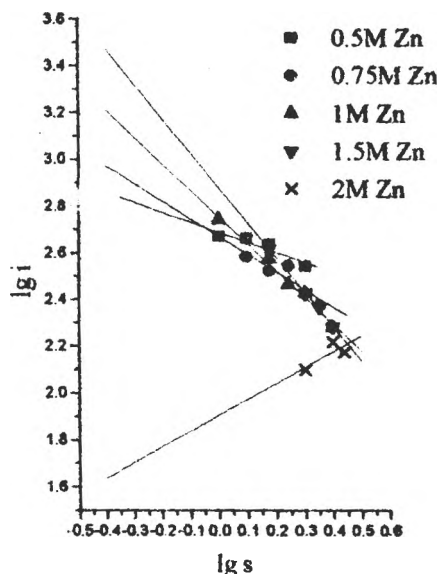


Fig. 8. $lgi-lgs$ dependence for different c at 20°C .

Another way of getting a general equation for the limiting anodic dissolution current is to define the current as a logarithmic function of the free anion concentration, s , for a given temperature (fig. 8, 9, 10).

The total anion concentration is $s=c+h$, where: s -total anion concentration, mol/l, h -free anion concentration, mol/l, $c-\text{Zn}^{2+}$ concentration mol/l. The linear

dependence of $\lg i$ vs. $\lg s$ is shown in figs. 8, 9 and 10, for different Zn^{2+} concentrations and temperatures, and can be written as $\lg i = b \times \lg s + a$, or $i = A \times s^b$, in which b are the slopes of the straight lines in figs. 8-10 and a ($A = 10^a$)-the X-intercepts of the same straight lines. Both a and b are dependent on the Zn^{2+} concentration (c) and temperature.

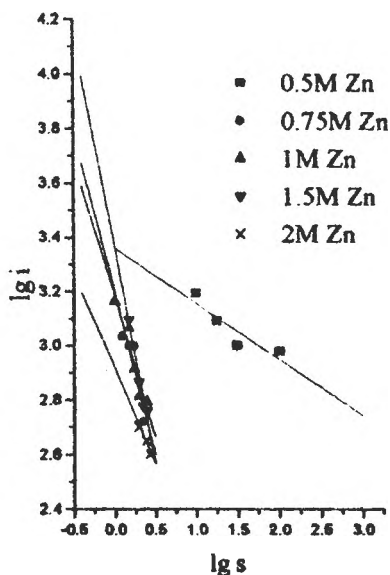
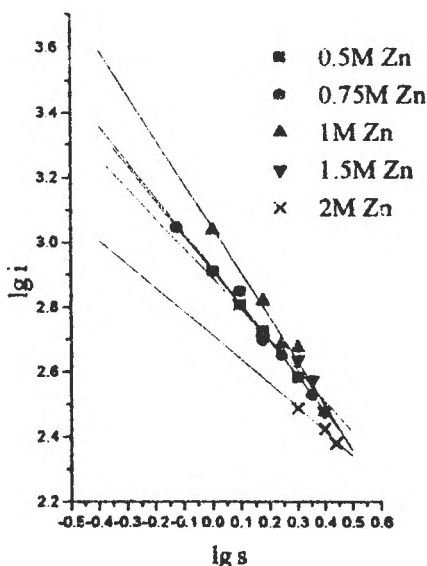


Fig. 9. $\lg i$ - $\lg s$ dependence for different c at 40°C . Fig. 10. $\lg i$ - $\lg s$ dependence for different c at 60°C .

The equations for b are determined by plotting $\lg(1-b)$ against the logarithm of the Zn^{2+} concentration (c) for each temperature, as shown in fig. 11.

For each temperature, the b values are:

$$b_{20} = 1 - 2.0627 \times c^{0.51717}$$

$$b_{40} = 1 - 2.04559 \times c^{-0.12932}$$

$$b_{60} = 1 - 2.16266 \times c^{-0.13712}$$

The equations for a are obtained by plotting their values against the logarithm of c for each studied temperature, as shown in fig. 12. For the studied temperatures the a values are:

$$a_{20} = 592.4613 \times c^{0.41825}$$

$$a_{40} = 871.7862 \times c^{0.01577}$$

$$a_{60} = 1583.215 \times c^{-0.4131}$$

The a and b values are replaced in the i equation, resulting the following dependencies:

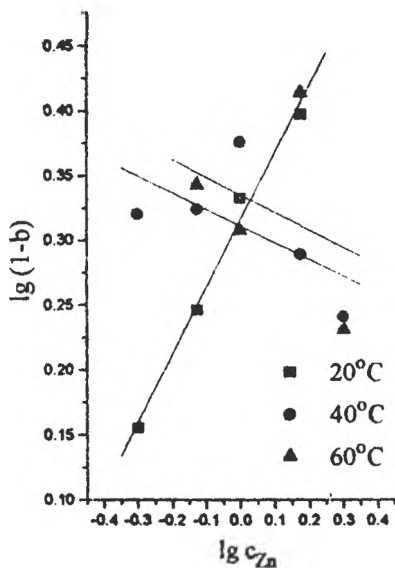


Fig. 11. The dependencies of the slopes of the straight lines in Figs 8-10 vs. c .

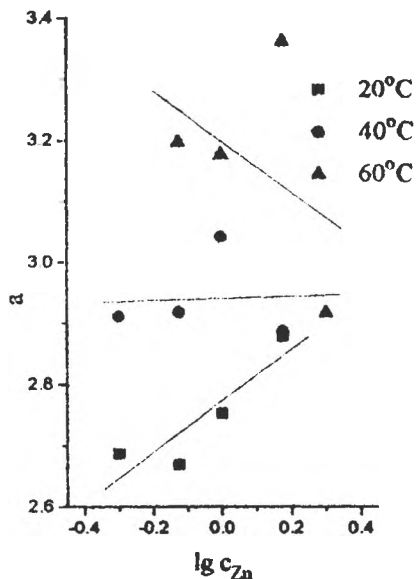


Fig. 12. The dependencies of the X-intercepts of the straight lines in Figs 8-10 vs. c .

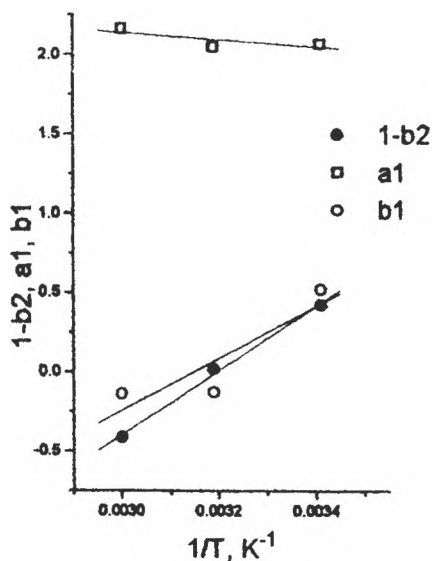


Fig. 13. The dependencies of the slopes and X-intercepts of the straight lines in Figs 11 and 12 vs. $1/T$.

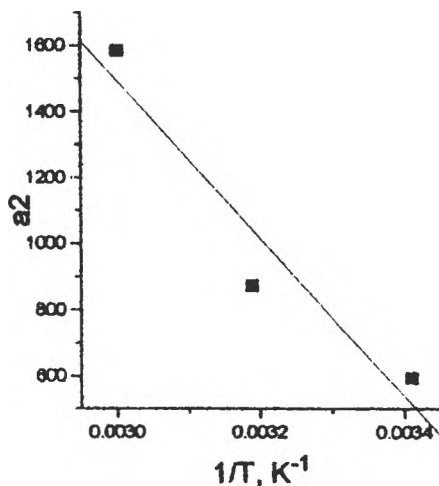


Fig. 14. The dependence of the X-intercepts of the straight lines in Fig. 12 vs. $1/T$.

$$i_{20} = 592.4 \times c^{0.41825} \times s^{1 - 2.0627 \times c^{0.51717}}$$

$$i_{40} = 871.7 \times c^{0.01577} \times s^{1 - 2.04559 \times c^{-0.12932}}$$

$$i_{60} = 1583.2 \times c^{-0.41314} \times s^{1 - 2.162 \times c^{-0.13712}}$$

Assuming again a general equation for i:

$$I = E(1/T) \times c^{F(1/T)} \times s^{1 - G(1/T)} \times c^{H(1/T)}$$

in which E, F, G, H are temperature dependent, the equations for these coefficients are obtained as following:

the equation for E(1/T) is obtained from the plot of the X-intercepts of the straight lines in fig. 12 vs. 1/T (a2 in fig. 14):

$$E(1/T) = 8675.57 - 2390968.4/T$$

the equation for F(1/T) is obtained from the plot of the slopes of the straight lines in fig. 12 vs. 1/T (b2 in fig. 13):

$$F(1/T) = 2023.81/T - 6.4766$$

the equation for G(1/T) is obtained from the plot of the X-intercepts of the straight lines in fig. 11 vs. 1/T (a1 in fig. 13):

$$G(1/T) = 2.848 - 236.532/T$$

the equation for H(1/T) is obtained from the plot of the slopes of the straight lines in fig. 11 vs. 1/T (b1 in fig. 13):

$$H(1/T) = 1628.93/T - 5.128$$

Replacing these values in the I equation we obtain a general equation for the limiting anodic dissolution current, i, as a function of the total anion concentration, s, Zn²⁺ concentration, c, and temperature:

$$I = \left(8675.57 - \frac{2390968.4}{T} \right) \times c^{\frac{2023.81}{T} - 6.4766} \times s^{1 - \left(2.848 - \frac{236.532}{T} \right)} \times c^{\left(\frac{1628.93}{T} - 5.128 \right)} \quad (2)$$

CONCLUSIONS

For the anodic dissolution of Zn in sulphate media two equations for the limiting anodic dissolution current are obtained, that take into account the working parameters that are usually modified in practice, ie the electrolyte composition and temperature.

We can notice that the general form for the obtained equations is similar to those obtained for other metals in their anodic behaviour for different electrolytes, eg Cu and Ag.

Electrochemical Colouring of Anodized Aluminium in AgNO_3 based electrolytes

Liana Anicai*, T.Visan**, Aurelia Meghea**, Carmen Trifu*

*- ICPE-SA, Compartimentul de Produse si Tehnologii Electrochimice, Splaiul Unirii 313,
74204, Bucuresti

** - Universitatea "POLITEHNICA", Facultatea de Chimie Industriala Bucuresti,
Calea Grivitei 132, 78122, Bucuresti

ABSTRACT

Electrochemical colouring of Al anodic films offers special decorative properties, because of their various color palette, as well as protective ones, because of their increased anticorrosive resistance and at light radiation. The final aspect of coloured coating is strongly dependent on involved electrolyte type during initial anodizing and on the applied operating parameters during electrochemical colouring phase.

Initial anodizing electrolytes based on sulfuric acid, nitric acid, phosphoric acid were used, at different current densities against an Al cathode. Electrochemical colouring of the formed anodic films involved a $\text{H}_2\text{SO}_4/\text{AgNO}_3$ solution, at various a.c.voltages and colouring durations, against an aluminium counterelectrode, in stationary conditions.

The final color range depends on the initial anodizing electrolyte, e.g. from yellow-greenish in sulfuric to yellow-bronze in phosphoric ones. Higher values of a.c. voltage and/or colouring time leads to colour darkening.

To analyse electrocoloured anodic films, electronic diffuse reflectance spectra in visible and near infrared domain and also chromatic coordinates in CIELAB system, were recorded.

Electrochemical colouring of Al anodic films is an attractive procedure for various industrial decorative applications, especially in design, architectonic domains, because of their large color palettes using the same electrolyte but different operating conditions.

INTRODUCTION

A great advance has been made in recent times in the use of coloured anodized aluminium, because of its good anticorrosive properties and color fastness, especially by means of electrochemical electrolysis in alternative current. There are several studies dealing with technological improvement of a.c. electrochemical colouring.

According to this method, Al is subjected to an initial anodization, usually done in sulfuric electrolyte, followed by an a.c. electrolysis in a metallic salt solution (e.g. Cu, Ni, Ag, etc.), when as counterelectrode, the corresponding salt metal, or stainless

steel, aluminium, graphite are involved [1, 2, 3, 4, 5]. To characterize the formed coloured anodic film, several techniques were used, such as: SEM, TEM [6], Mossbauer spectroscopy [7], IR spectroscopy and X-ray diffraction [1], etc. Most of those studies revealed the existence of metallic species as Me^0 within coloured anodic film and in some cases, of a mixture of cations in various valence states [5].

The present paper intends to discuss, from visual aspect and existent species points of view, electrochemically coloured Al anodic films in electrolytes based on $AgNO_3$ using different initial anodizing electrolytes.

EXPERIMENTAL

Samples of Al foils (Al min.99.5% purity), with a thickness of 0.2 mm, of 100x40 mm, having a constant surface of 0.4 dm², were used. They were subjected to a surface treatment, as it follows: (a) alkaline degreasing in 2-5 g/l NaOH, 50-100 g/l $Na_2CO_3 \cdot 10 H_2O$, 50-100 g/l $Na_3PO_4 \cdot 12 H_2O$ solution, at 60-80°C, for 1-5 min.; (b) hot water rinsing; (c) chemical pickling in 30% HNO_3 at room temperature for 30 s; (d) cold water rinsing.

The Al specimens were anodized in the three following electrolyte types:

A- 1.5M H_2SO_4 solution, usually recommended at the initial stage of electrochemical colouring of anodic films;

B- 7.5M HNO_3 solution, recommended to obtain porous anodic films that may offer a better absorption capacity in colouring phase, according to our recent researches [8, 9];

C- 2.5M H_3PO_4 solution, usually used to obtain uniformly porous anodic films.

For electrolyte A, anodizing process was performed at a current density of 5A/dm², a bath temperature of 25-30°C, for 10 minutes.

For electrolyte B, anodizing phase was done at 5A/dm², at 25°C, for 15 minutes.

Anodic oxidation in phosphoric electrolyte was conducted at 8.75 A/dm², for 10 minutes.

Electrochemical colouring was effected using an aluminium counterelectrode and an electrolyte with the following composition: 2 g/l $AgNO_3$, 100 g/l H_2SO_4 , in alternative current, at different values of a.c voltage (10, 20 V), for different colouring durations, between 1-30 minutes, at 25°C.

All experiments were done in stationary electrolysis conditions.

The obtained colour was visually noticed, as well as by means of trichromatic coordinates (CIELAB colorimetric space) using a CHROMA SENSOR CS5 spectrophotometer with two fascicules and integrated sphere. To analyse the chromophoric species that may exist in the colored film, electronic diffuse reflectance spectra in the range of 400-1200 nm were recorded, using a VSU-2 type spectrophotometer equipped for reflectance, against an anodized foil in each anodizing electrolyte type, to reveal only the contribution of coloured layer. Absorbance, $A=100-R$ (%) against incident radiation wavelength was recorded to highlight the absorption electronic bands.

RESULTS AND DISCUSSION

Figures 1, 2 and 3 show the colour changes vs. colouring time for anodized Al samples in electrolytes A, B, C.

For an initial anodizing in sulfuric electrolyte (Fig.1), electrochemical colouring in $AgNO_3$ solutions produces yellow to black coloured films. The colour becomes darker when colouring time increases; thus, after 10 minutes the film is black. In all cases, an adherent, uniform, glossy, without blemishes coloured anodic layer, is obtained.

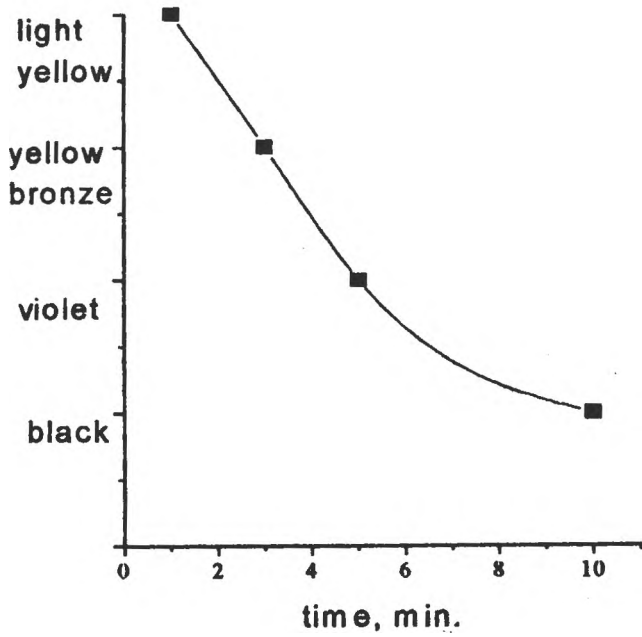


FIGURE 1 - Visual color evolution against colouring time in AgNO_3 based solution, at 10 V a.c., for initial anodizing in 1.5M H_2SO_4

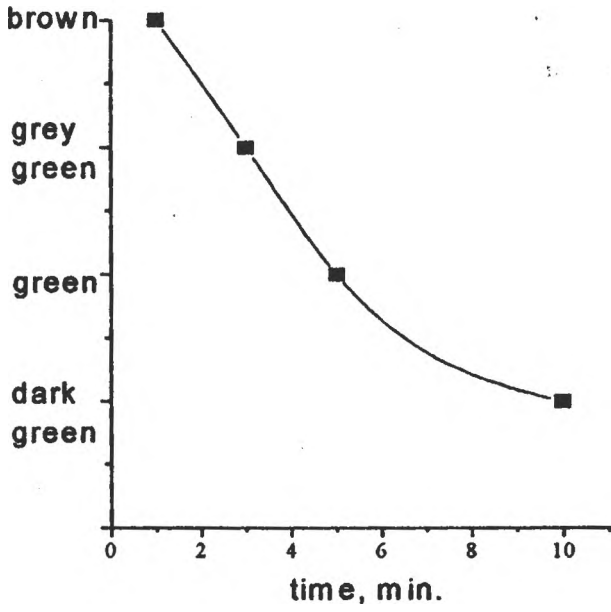


FIGURE 2 - Visual color evolution against colouring time in AgNO_3 based solution, at 10 V a.c., for initial anodizing in 7.5M HNO_3

When initial anodic oxidation involves nitric electrolyte, because of high porosity of the anodic film, the coloured coating is mat and tones of brown to dark green are obtained (Fig.2). An increase of colouring durations determines colour darkening, too.

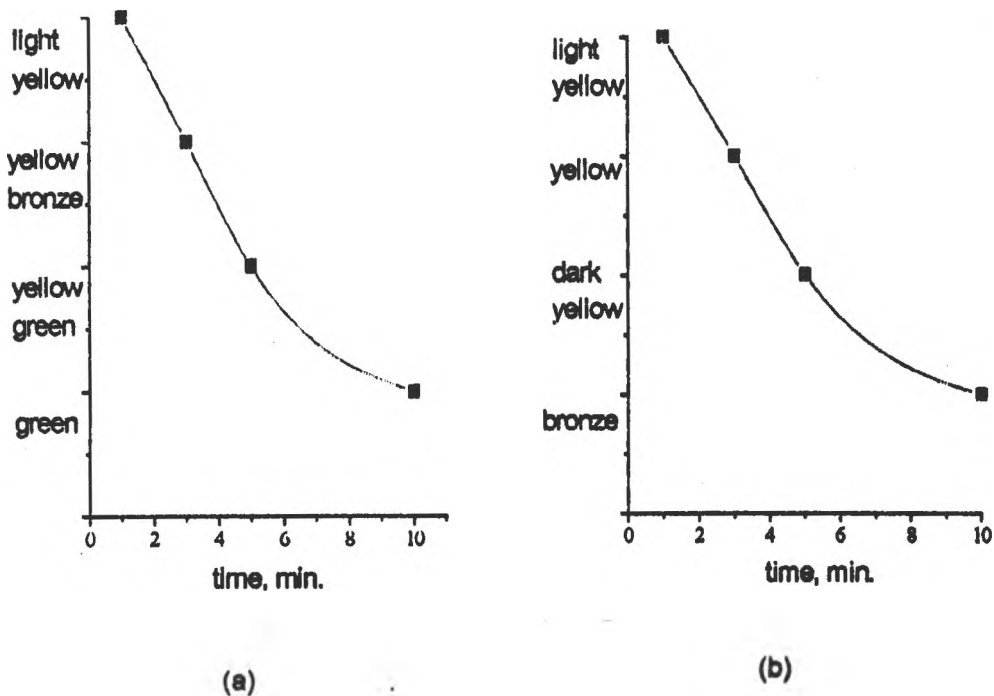


FIGURE 3 - Visual color evolution against colouring time in AgNO₃ based solution, at 10 V a.c.(a) and 20 V a.c (b), for initial anodizing in 2.5M H₃PO₄

Initial anodizing in phosphoric acid electrolyte produces different colour ranges, as a function of colouring time and applied a.c.voltage. Thus, at 10 V a.c , the coloured anodic film has golden -brown-green tones and at 20 V a.c a yellowish palette was obtained (Fig.3).

When higher a.c. voltages were applied, some defects were noticed, rather producing a surface attack.

Comparatively with electrochemical colouring in CuSO₄ solutions, when after initial anodizing in nitric electrolyte was necessary a subsequently long time sealing step [5], in the case of AgNO₃ based colouring , an adequate light stability was noticed; the coloured anodic films remained at the initial shade, even after 15-30 days of natural light exposure.

Figure 4 shows the dependence of colour parameters (L^* , a^* , b^*) in CIELAB trichromatic system against colouring time for Al samples initially anodized in sulfuric electrolyte. It may be noticed again that an increase of colouring duration leads to a colour darkening (L^* value decreases). Also, yellow component is more intense up 5 minutes and for higher durations, the green one.

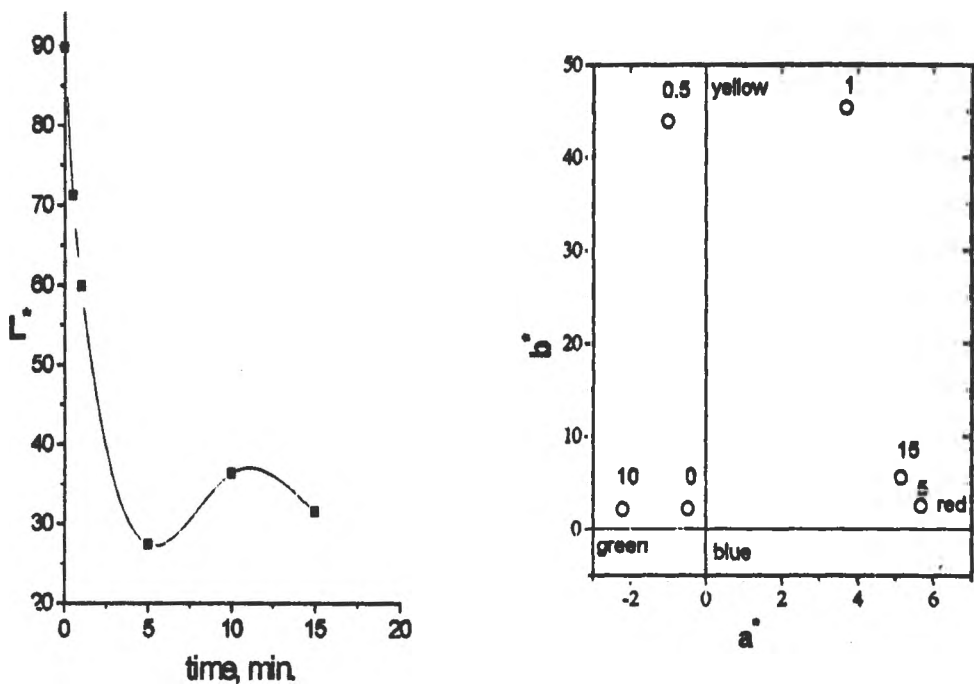


FIGURE 4 - Chromatic coordinates vs. colouring time for Al initially anodized in sulfuric electrolyte

Electronic diffuse reflectance spectra

Figure 5 presents the electronic absorption spectra for Al samples S₁ - S₄, that were initially anodized in sulfuric electrolyte and subsequently electrocoloured in AgNO₃ based solution, at 10 V a.c. and various durations. They have the same sulfuric medium, both for anodizing and colouring phase and with time increasing, a systematic darkening of the color was noticed.

From spectral point of view, this means an intensification and extension of charge transfer band absorption from 400 nm (S₁) to 600 nm (S₂). For S₃ sample, an

intense absorption on the whole visible and near IR range was observed, with a slight predominance between 400-650 nm, while for S4 specimen the absorption intensity is practically constant between 400-1200 nm.

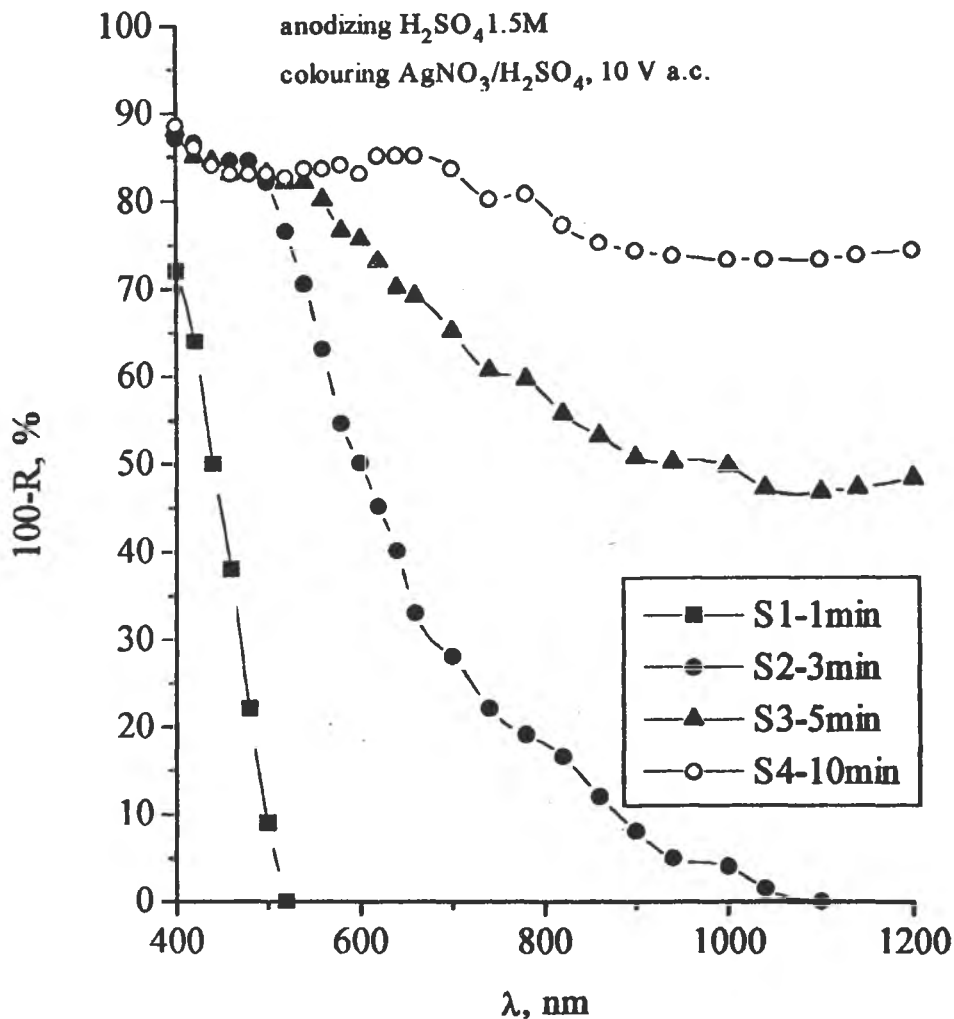


FIGURE 5 - Electronic absorption spectra for Al coloured anodic films at different values of colouring time after initial anodizing in sulfuric electrolyte

Cromophoric species that may be responsible of color darkening are Ag^+ and Ag^0 , the black tone being facilitated by the possible charge transfer between Ag^0 and Ag^+ .

Electronic absorption spectra for coloured anodic films that were initially anodized in nitric electrolyte are shown in Figure 6, for various electrochemical

colouring times. Initial anodizing medium change, from H_2SO_4 to HNO_3 determines different color evolutions, as specimens P5-P8 show. Thus, P5 sample presents a strong absorption on the whole wavelength domain (400 nm-1200 nm), with a maximum in visible range, between 400-750 nm.

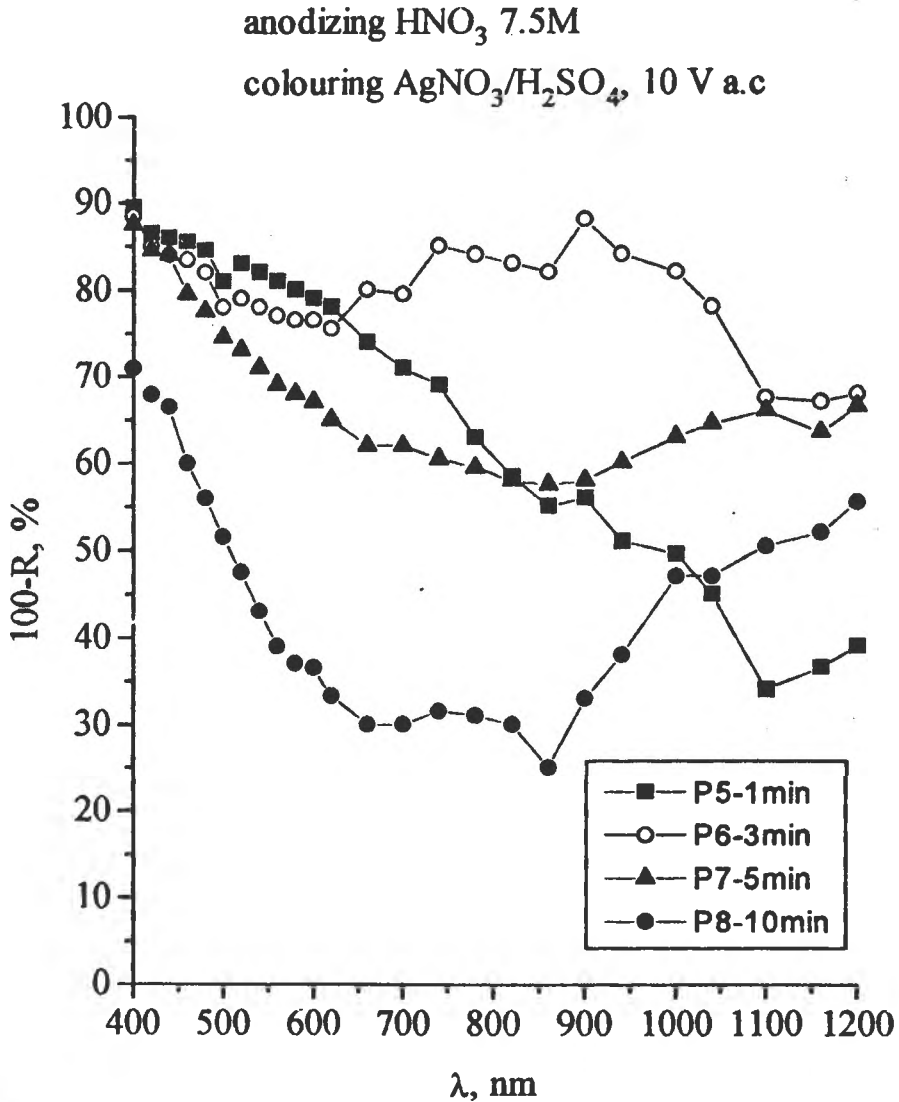


FIGURE 6 - Electronic absorption spectra for Al coloured anodic films at different values of colouring time after initial anodizing in nitric electrolyte

P6 specimen has a similar absorption in 400-600 nm domain, but a maximum in near IR area (750-1000 nm) was noticed, that determines the greenish color.

Subsequently increasing of colouring time, according to P7 and P8 samples, determines absorption diminishing between 400-600 nm with a maximum at 400 nm followed by an intense increase above 1000 nm but without any influence on the color.

Anodic films having yellow-brown tones may also be ascribed to Ag^+ and Ag^0 species, while greenish ones may be determined by certain transient Ag^{2+} species or by some peroxidic compounds with oxygen in a triplet state that have specific absorption over 700 nm.

Figures 7 and 8 present electronic absorption spectra for coloured Al initially anodized in phosphoric electrolyte, at various durations and a.c. voltages..

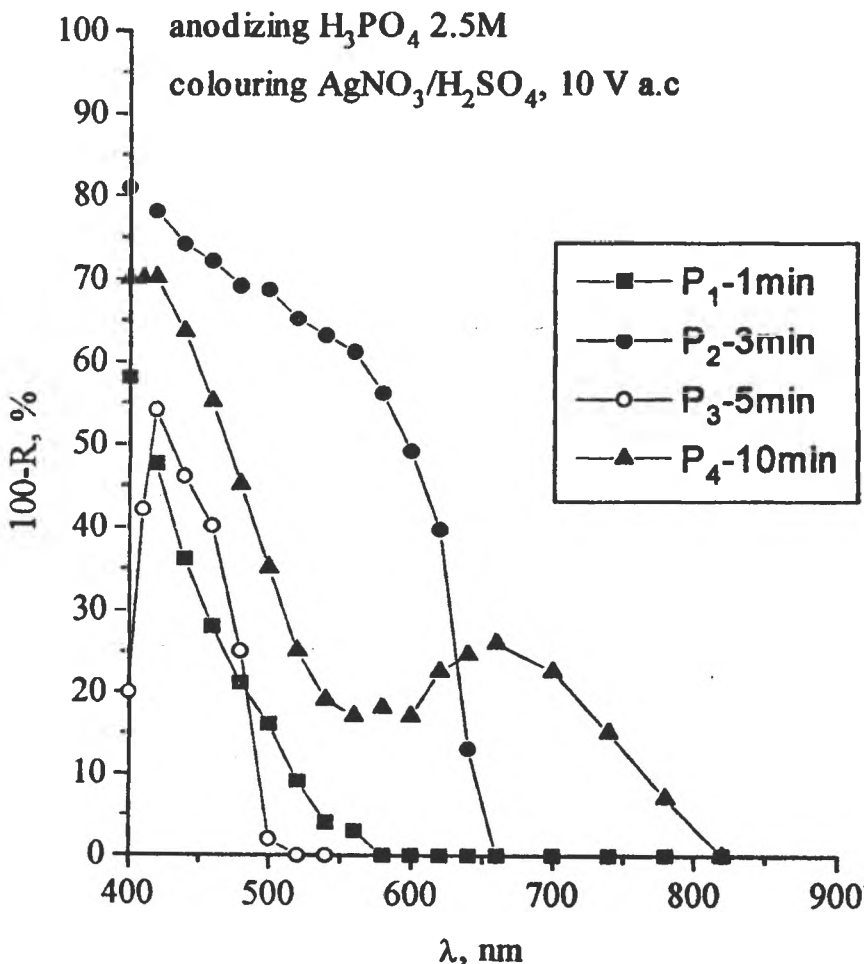


FIGURE 7 - Electronic absorption spectra for Al coloured anodic films at different values of colouring time after initial anodizing in phosphoric electrolyte and a colouring voltage of 10 V a.c.

Thus, at 10 V a.c. a color evolution from golden -brown to green tones was noticed. For P4 specimen, a maximum at 660 nm is revealed, that is characteristic to its greenish tone. Also, the responsible cromophoric species may be Ag^+ , Ag^0 , with possible Ag^{2+} appearance , that determine aleatory and practically non-reproducible color modifications.

anodizing H_3PO_4 30%
 colouring $AgNO_3/H_2SO_4$, 20 V c.a

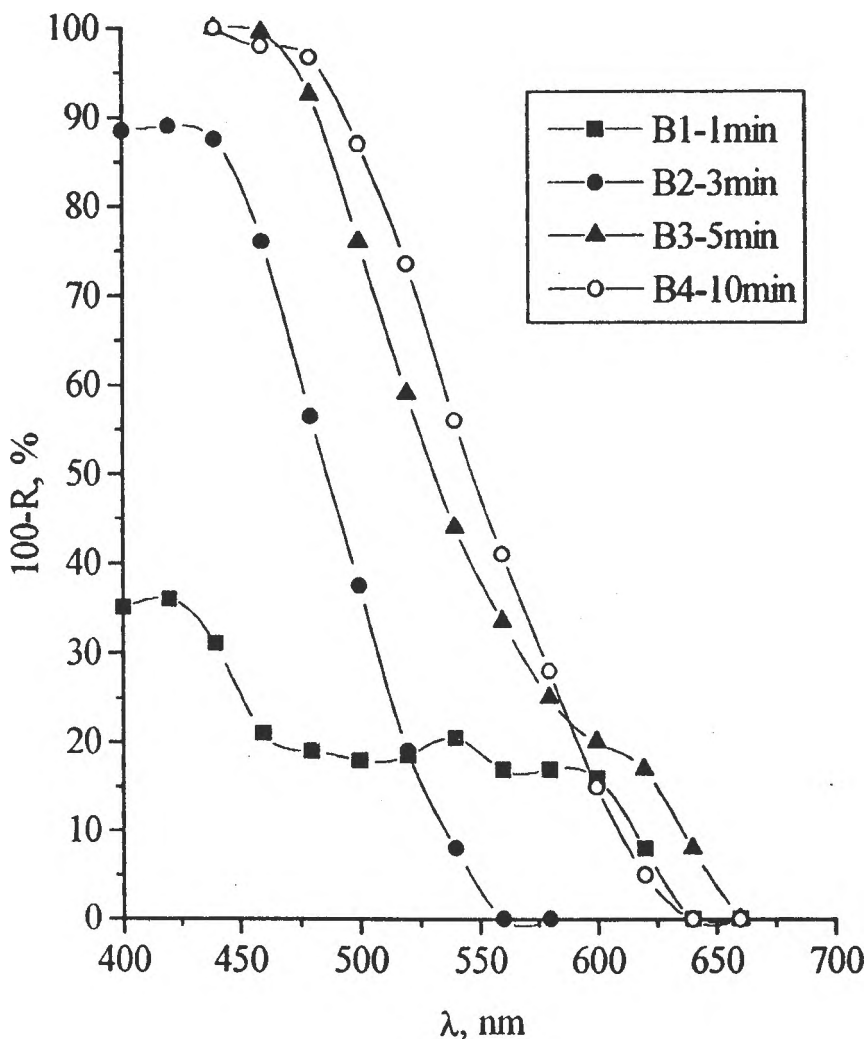


Figure 8 - Electronic absorption spectra for Al coloured anodic films at different values of colouring time after initial anodizing in phosphoric electrolyte and a colouring voltage of 20 V a.c.

For B₁ - B₄ specimens, coloured at 20 V a.c. but with the same initial anodizing in phosphoric electrolyte, the same color evolution, from light yellow to brown-yellow was observed, with colouring time increasing, determined by the existence of Ag⁺ and Ag⁰ species.

Comparing B₁ - B₄ and S₁ - S₄ specimens, a relatively similar behaviour takes place: a systematically color darkening with colouring time, but to relatively different tones; these systems seem to be the most adequate for practical purposes. The greenish colours are very attractive for decorative applications and some supplementary studies are necessary both to establish the optimum conditions for a good reproducibility and existent chromophoric species.

CONCLUSIONS

After the experimentals were done, it was found out that:

- the type of electrolyte involved in initial anodizing step strongly influences the colour range of subsequently electrochemical coloured anodic film in AgNO₃ based solutions;
- a.c. voltage as well as colouring time increasing determines color darkening; in certain cases a high value of a.c. voltage may produce some defects in the coloured anodic film;
- comparatively with electrochemical colouring using CuSO₄ solutions, in the case of AgNO₃ ones there is not necessary a subsequently sealing phase, the final color being stable at light radiation;
- electronic diffuse reflectance spectra revealed the existence of chromophoric species: Ag⁺, Ag⁰ and possible transient Ag²⁺ ions that coexist in the coloured anodic film and produce the final colour;
- electrochemical coloured aluminium anodic films using AgNO₃ based solutions offers a large variety of attractive colours that may be successfully used in decorative applications, involving only a small number of electrolytes but allowing various operating parameters values.

REFERENCES

1. Edith Lichtenberger-Bajza, F.Domolki, I.Imre-Baan, *Metal Finishing*, **72**, 1973, 50.
2. S.A.K.Hsieh, *Metal Finishing*, **79** (10), 1981, 21.

3. M.Wrzecian, *Galvano-Organic*, **499**, 1979, 781.
4. Y.Itoi, A.Hasumi, E.Sato, K.Tachihara, *Electrochim.Acta*, **25**, 1980, 1297.
- 5.Liana Anicai, Aurelia Meghea, Catalina Sirean, L.Dima, *Materials Science Forum*, **185-188**, 1995, 489.
- 6.T.Kawaguchi, S.Ono, T.Sato, N.Masuko, *J. Surf.Finish.Soc.Japan*, **41(6)**, 1990, 690.
7. R.L.Cohen, Ch.J.Raub, T.Muramaki, *J.Electrochem.Soc.*, **125(1)**, 1978, 34.
8. L.Dima, Liana Anicai, Romanian Patent No.98 547, 1989.
9. Liana Anicai, L.Dima, T.Visan, M.Buda, "Aluminium Anodization in Nitric Solutions", in *Studia Universitatis Babes-Bolyai, Series Chemia*, in press.

ELECTROCHEMICAL INVESTIGATION OF IONICALLY ASSEMBLED
MULTILAYER SYSTEMS

Daniel A. Lowy¹

*Babes-Bolyai University
Department of Physical Chemistry
Arany Janos Str. 11
RO-3400 Cluj-Napoca, Romania*

*Present Address: The University of Memphis
Department of Chemistry
Memphis, Tennessee 38152-6060, USA*

Harry O. Finklea

*West Virginia University
Department of Chemistry
Morgantown, West Virginia 26506-6045, USA*

ABSTRACT. - Polycrystalline bulk gold flag electrodes were coated with multilayer systems and various redox were affixed to these assemblies. The multilayer systems were based on self-assembled monolayers of thiol-carboxylic acid molecules, tightly bound to the gold surface via the mercapto groups. The other moiety of the molecules were ionized by alkaline wash to carboxylate ions. To this anionic surface a cationic polyelectrolyte was attached by ionic forces. Such a bilayer system was suitable for binding anionic redox couples (e.g., ferrocyanide, quinone-sulfonic acid, ferrocenecarboxylic acid, etc.) Alternatively, a negatively charged polyelectrolyte layer was attached to the bilayer to form a trilayer system with an outermost anionic layer. To such a trilayer system cationic redox couples were adsorbed (e.g., Co(II) tris(1,10-phenanthroline), trimethylaminomethyl ferrocene, methyl viologen, etc.). In a series of experiments two redox couples were successfully confined to the same electrode surface. Ellipsometry has proven a useful tool for monitoring the layer width of these multilayer systems with and without adsorbed redox couples. Cyclic voltammetry, performed in aqueous supporting electrolytes buffered to a constant pH value, was efficient in probing the electrochemical behavior of multilayer assemblies with adsorbed redox centers.

The "layer-by-layer" deposition technique, introduced in the early nineties by Decher and Lvov [1-4], has become popular in the last years [5]. This method

¹ Author to whom correspondence should be addressed

involves the successive adsorption of oppositely charged polyelectrolytes and/or redox couples. Advantages of the technique are that (i) multilayer systems are easy to assemble, (ii) the process is self-regulating (only one monolayer of charged polyelectrolyte can be attached to the oppositely charged surface) (iii) it is a versatile method to confine various redox couples to the electrode surface, (iv) one or more redox couples can be attached to the same surface, (v) no mechanical manipulation is needed to build up such assemblies, (vi) the multilayer deposition can be automated [5,6].

In our approach [6-9], ionic forces were used to confine redox couples to the gold electrode surface. First, a self-assembled ω -mercapto-carboxylic acid monolayer was deposited at the gold surface, second, oppositely charged polyelectrolytes were confined to the ionized carboxylic groups, then, cationic or anionic redox couples were adsorbed onto these multilayer systems. The obtained bilayer and trilayer assemblies with or without adsorbed redox centers can be efficiently investigated by means of ellipsometry and cyclic voltammetry.

EXPERIMENTAL. Gold mirror electrodes were used for ellipsometric measurements, and bulk gold flags (of approximately 1 cm^2 surface) for cyclic voltammetry. 11-Mercapto-undecanoic acid was obtained from the corresponding bromo-undecanoic acid [6], and re-crystallized from n-heptane. Poly(vinyl-pyridine), Polyscience Inc., was quaternized with a solution of dimethyl sulfate (Fisher Scientific) in methanol and purified by dialysis. Poly(styrene sulfonate), Polyscience Inc., was used as received. Typically, monolayers were deposited from $5.0 \times 10^{-4} \text{ mol L}^{-1}$ mercaptocarboxylic acid solution in acetonitrile, while polyelectrolytes were attached from $1.0 \times 10^{-3} \text{ mol L}^{-1}$ aqueous solutions. Several redox couples were confined to the coated gold surface; some of these were prepared in our laboratory: trimethylaminomethyl ferrocene, $\text{Cr}^{\text{II}}(\text{EDTA})$, and Co^{II} tris(1,10-phenanthroline), while Fe^{II} tris(1,10-phenanthroline), henceforth ferriin, acid, and ferrocyanide, Aldrich, were used without further purification. Cyclic voltammetry was performed in aqueous borate buffer supporting electrolyte (pH 9.0), degassed with argon for at least 30 minutes. The setup consisted of a Voltammograph CV-27, Bioanalytical Systems, Inc., West Lafayette, Indiana, an Omnigraphic 100 Recorder, Houston Instruments, Austin, Texas, and a computerized data collection system, based on the Asystant software, Macmillan Co. A home-made three compartment glass cell was used. The polycrystalline gold flag working electrode was referred to an SCE,

the counter electrode being a platinum wire, with a surface area of 10 cm^2 . Typical experimental conditions were: scan rate of 0.1 V s^{-1} , sensitivity of $2 \mu\text{A V}^{-1}$ (potentiostat), and $2 \mu\text{A cm}^{-1}$ (recorder). For layer width determinations an ellipsometer with manual compensation was used. The home-assembled instrument consisted of a 3 mW maximum output Helium-Neon Laser (Oriel Co., Stratford, Connecticut, and optical components from Oriel Co. and Newport Co., Fountain Valley, California).

RESULTS AND DISCUSSION. The layer width both the mercaptocarboxylic acid and the cationic polyelectrolyte correspond to about one monolayer (see Table). The figures in the Table are mean values for 6 experiments, \pm refers to 90% confidence interval. Ferrocyanide ions adsorbed to the bilayer may cause a slight increase of the layer width or, conversely, a slight decrease of the overall width. Likewise, this decrease is only apparent, and is probably due to the change in the refraction index. Poly(styrene sulfonate) adsorbed to the outermost cationic surface of the bilayer system increases the overall layer width by approximately another monolayer width. To this system an iron-hydroxide based redox center can be attached, by immersion in basic ferroin solution (pH 10.0). Again, the presence of the inorganic redox couple does not affect the overall layer width.

A systematic survey of several cationic and anionic redox couples with redox potentials in the potential window of gold, bound to bilayer or trilayer systems was done. *Strong* binding, i.e. stable attachment of the redox couple to the coated electrode for over 50 potential scans, was obtained for trimethylaminomethyl ferrocene, ferrocyanide, for the Fe^{II} hydroxide redox center, generated with basic ferroin solution, as well as for a Cr^{II} hydroxide redox couple, obtained with Cr^{II} (EDTA). Medium binding, i.e. no significant decrease in the peak areas for 5 to 10 cycles, was achieved for ferrocenecarboxylic acid and Co^{II} tris(1,10-phenanthroline).

Table: Mean values of the layer width for the charged layers in multilayer systems

Examined layer	Total width [nm]
11-Mercapto-undecanoic acid	12 ± 0.3
Bilayer: 11-Mercapto-undecanoic acid + poly(N-methylvinyl pyridine)	26 ± 0.4
Bilayer + [Fe(CN) ₆] ⁴⁻	29 ± 0.4
Trilayer: bilayer + poly(styrene sulfonate)	4.0 ± 0.5
Trilayer + Fe(OH) ³⁺	4.3 ± 0.3

Specific examples of multilayer systems with ionically bound redox couples

Trimethylaminomethyl ferrocene can be ionically bound to a trilayer system formed of a self-assembled ω-mercaptocarboxylic acid monolayer, a quaternized poly(vinylpyridinium) layer and a poly(vinyl sulfonate) layer (Figure 1).

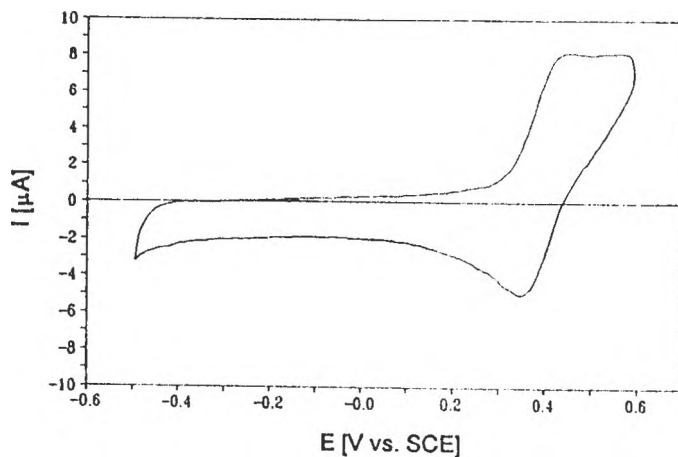


Figure 1. Cyclic voltammetry of trimethylaminomethyl ferrocene attached to a trilayer system (0.1 V s⁻¹, 10 μA V⁻¹, pH 9.6)

An Fe^{II}-complex based redox couple was obtained by soaking the trilayer system in Fe^{II} tris(1,10-phenanthroline) perchlorate (Figure 2). A new redox wave was obtained at E⁰ = -0.34 ± 0.01 V vs. SCE, with a peak splitting of 40 mV. The redox couple responsible for this wave showed an extremely tight adsorption. The concentration of the redox centers was almost unchanged during 50-200 cycles of the electrode potential. These redox waves showed up exclusively when both the deposition and cyclings were performed in an alkaline buffer supporting electrolyte (e.g., borate buffer, at pH 9.0 and 9.6, or in carbonate/bicarbonate buffer, at pH 9.9-10.0). Therefore, the iron-related redox species is probably a form of Fe^{II} hydroxide. The ferrous hydroxide is generated *in situ* by traces of Fe²⁺ or Fe³⁺ ions from the slow decomposition of the iron complex present in the alkaline solution. An approximate composition of such complexes, that involve both the presence of iron hydroxide and of the ionized carboxylic groups can be written as [6,9] [(Au-S-(CH₂)₁₀-COO)_xFe_y(OH)_z], where: x = 1-7, y = 1-3, and z = 1-4.

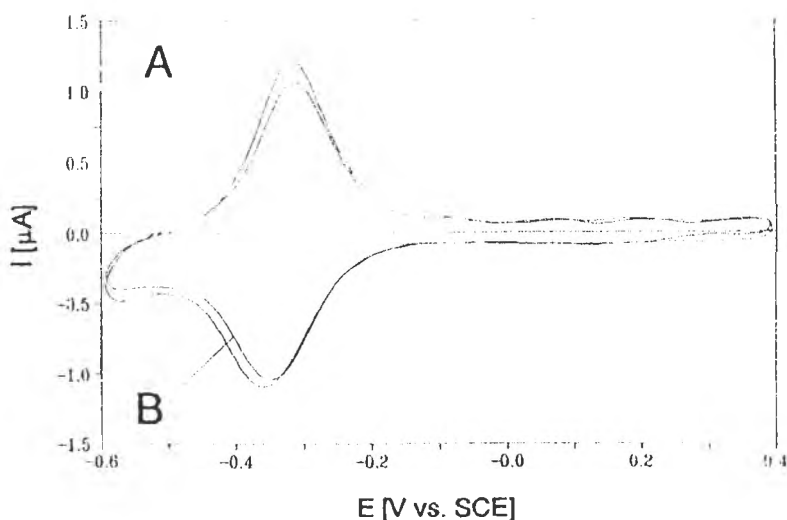


Figure 2. Cyclic voltammetry of the Fe^{II} redox couple attached to a trilayer system (0.1 V s⁻¹, 2 μA V⁻¹, pH 9.6); **A** - 1st scan, **B** - 50th scan.

Construction of a two-terminal bilayer system

The goal of this experiment is to confine two redox groups of different kind to the same electrode surface. The first redox couple is insensitive to the presence of analytes in the sample solution, while the second responds in a Nernstian manner to the analyte concentration in the solution. Such a system can work as a two-terminal voltammetric sensor [10,11]: the analyte-insensitive redox couple, ferrocyanide/ferricyanide, is the internal reference site, while the pH-sensitive Fe^{II} redox couple serves as the sensing site.

1. A self-assembled monolayer of 11-mercaptoundecanoic acid is deposited on the gold flag electrode;
2. Iron(II) redox couple is attached from ferroin solution to the ionized carboxylate groups of the monolayer (cyclic voltammetry is shown in Figure 3a);
3. Poly(4-vinyl-1-methylpyridinium) is attached to the monolayer system with the already confined $\text{Fe}(\text{II})$ redox couple (Figure 3b);
4. Ferrocyanide is adsorbed to the outermost cationic layer (Figure 3c);
5. The $\text{Fe}(\text{II})$ redox couple is regenerated by additional soaking of the system in ferroin solution (Figure 3d).

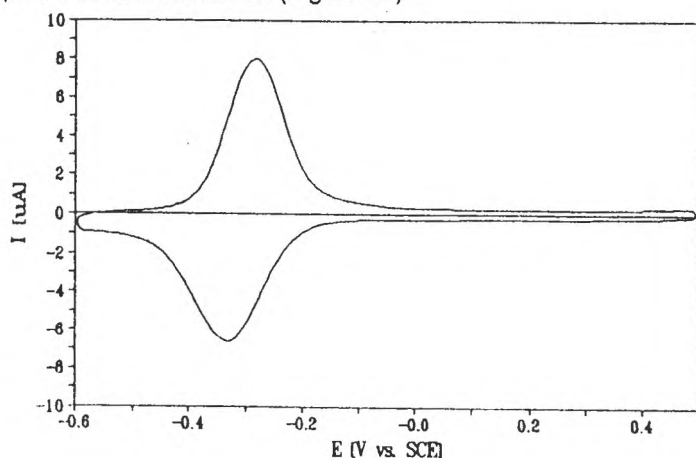


Figure 3a Cyclic voltammetry of the Fe^{II} redox couple attached to an 11-mercapto-undecanoic acid monolayer (0.1 V s^{-1} , $2 \mu\text{A V}^{-1}$, pH 9.0).

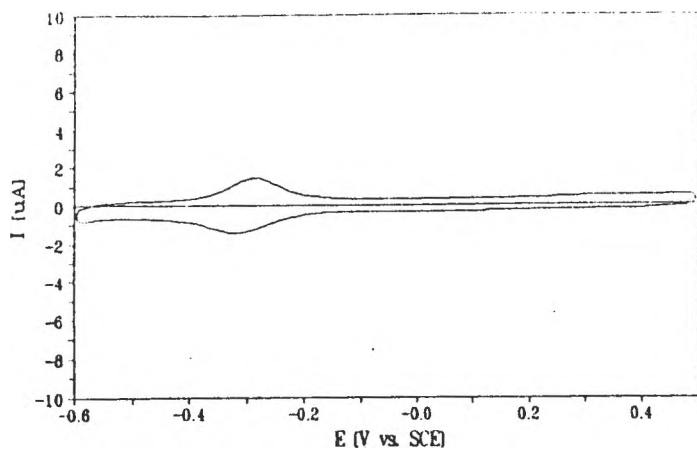


Figure 3b. Cyclic voltammetry of a bilayer system obtained by confining poly(4-vinyl-1-methylpyridinium) to a monolayer of 11- mercaptoundecanoic acid; the Fe^{II} redox couple is attached to the monolayer prior to the adsorption of the cationic polyelectrolyte (same conditions as for Fig.3a).

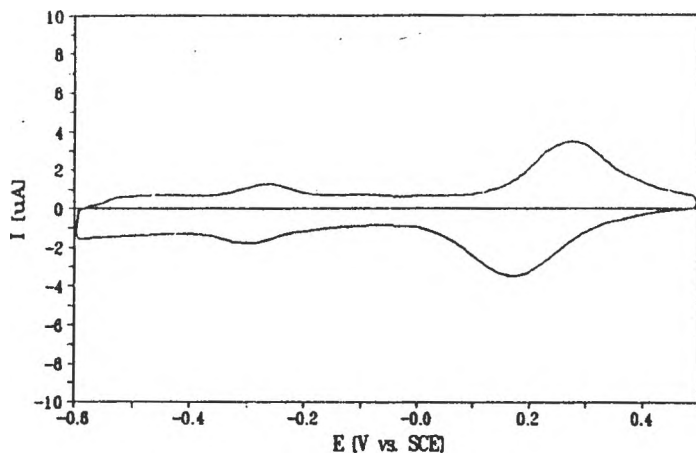


Figure 3c. Cyclic voltammetry of ferrocyanide adsorbed to the outermost cationic layer of a bilayer system with a previously attached Fe^{II} redox center (same conditions as for Fig.3a).

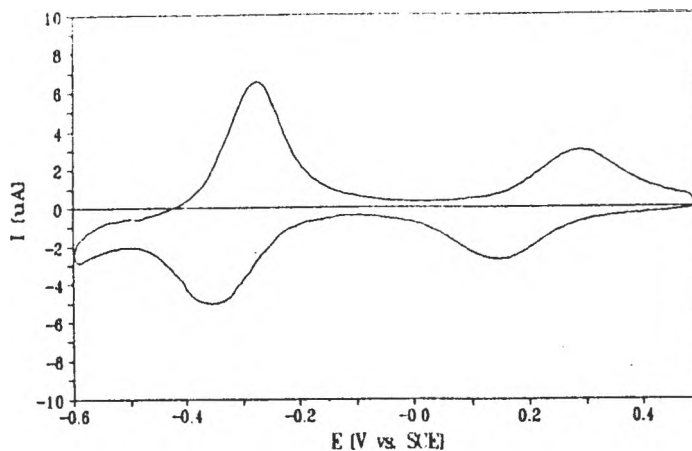


Figure 3d. The Fe(II) redox couple is regenerated by additional soaking of the bilayer system in ferriin solution (same conditions as for Fig 3a).

CONCLUSIONS

The layer-by-layer deposition method was efficient in binding anionic and cationic redox couples to the surface of polycrystalline bulk gold electrodes. These multilayer systems were based on self-assembled monolayers of thiol-carboxylic acid molecules, to which cationic and anionic polyelectrolytes were attached by ionic forces. In a series of experiments one or two redox couples were successfully confined to the same electrode surface. Ellipsometry has proven a useful tool for monitoring the layer width of these multilayer systems, while cyclic voltammetry, was efficient in probing the electrochemical behavior of multilayer assemblies with adsorbed redox centers.

REFERENCES

1. G. Decher, J. D. Hong, *European Patent Appl.*, 1991, 91 113 464.1.
2. G. Decher, J. D. Hong, *Makromol. Chem., Makromol. Symp* 46, 1991, 321.
3. G. Decher, J. D. Hong, *Ber. Bunsenges. Phys. Chem.*, 95, 1991, 1430.
4. G. Decher, J. D. Hong, J. Schmitt, *Thin Solid Films*, 210/211, 1992, 831.
5. D. A. Lowy, "Construction and Use of Electrochemical Sandwiches", Presentation at the University of Mississippi (Ole Miss), Oxford, Mississippi, October 30, 1996.
6. D. A. Lowy, *Ph.D. Dissertation*, West-Virginia University, Morgantown, West-Virginia, 1996.
7. D. A. Lowy, H. O. Finklea, "Construction and Characterization of Bilayer and Trilayer Self-Assembled Monolayers with Ionically Bound Redox Centers", 208th American Chemical Society National Meeting, Washington, D.C., August 21-25, 1994, p. COLL-129.
8. D. A. Lowy, H. O. Finklea, "Two-terminal voltammetric detectors based on ionically bound redox couples", Ninth International Forum Process Analytical Chemistry (Process Analysis & Control) - IFPAC'94, Houston (Montgomery), Texas, January 22-25, 1995, p. I-012.
9. D. A. Lowy, H. O. Finklea, *Electrochim. Acta* (in press).
10. I. Rubinstein, *Anal. Chem.*, 56, 1984, 1135.
11. J. J. Hickman, D. Ofer, P. E. Laibnis, G. M. Whitesides, M. S. Wrighton, *Science*, 253, 1991, 688.

**ELECTROCHEMICAL POLYMERIZATION OF SOME MONOMERS
WITH THIOPHENE UNITS AND SCHIFF BASE STRUCTURE**

C. I. Simionescu¹, Al. Duca¹, Maria Grovu-Ivanoiu¹, I. Cianga², M. Grigoras²

¹*Department of Macromolecular Chemistry, Technical University, Copou Alley, 11, R-6600, Jassy, Romania.*

²*Romanian Academy of Sciences, "Petru Poni" Institute of Macromolecular Chemistry, Gr. Ghica Voda Alley 41/A R-6600 Jassy, Romania*

ABSTRACT

The synthesis and voltammetric characteristics of four monomers with Schiff base-type structure and thiophene moieties (I-IV) and a p-phenylene-di(vinylene thienylene) (V) monomer were performed. The electrochemical polymerization of N,N'-bis(2-thienylmethyl)-1,4-diaminobenzene (II) and bis(2-thienyl-vinyl)-1,4-phenylene (V) proceeds by oxidative coupling reaction and precipitate formation. The polymers result in their *lopecJ* states. The reaction conditions influences the formation of polymer or other undesirable compounds. The spectral characterization of the products confirms the possibility of oxidative coupling of the thiophenes units by their 5-5' positions.

INTRODUCTION

The synthesis of electrically conductive polymers is an area of significant activity [1]. The electrical and non-linear optical properties of polymers containing highly delocalized π -electron systems, continue to be subjects of intense research interest. The investigation in this interdisciplinary field is strongly dependent on the quality of the studied materials. Among these polymers, a great deal of work was devoted to polyheterocycles (polypyrrole, polythiophene), prepared by chemical and electrochemical polymerizations, because they present an increased environmental and thermal stability in both conductive and neutral states.

The introduction of different units belonging to two or three classes of conducting polymers in the same structure of the repeating unit, allows to modify the polymers properties. Thus, monomers containing thiophene as well as vinylene units were obtained and

polymerized electrochemically by Tanaka *et al* [2]. Copolymers containing thiophene and diacetylene units were synthesized using the Glaser coupling reaction from thiophene- based diethynyl monomers [3]. Other polymers containing alternating thiophene and acetylene unit were reported by D'Ilario *et al* [4-6].

Fully aromatic polyazomethines are known as an important class of thermally stable and highly conjugated materials. They are obtained by the conventional melt or solution polycondensation of aromatic diamines with aromatic dialdehydes. Their electrical conductivity varies between $10^{-12} \Omega^{-1} \text{cm}^{-1}$ (neutral state) and $10^{-7} \Omega^{-1} \text{cm}^{-1}$ (oxidized state) [7,8].

Recently there were reported some alternating structures which contain thiophene azomethine and 1,4-phenylene or 4,4'-biphenylene groups [9-11]. The polymers were synthesized by classic polycondensation procedure for the poly(Schiff-base)s type products from the aromatic 5,5'-diformyl-2,2'-dithienyl with the corresponding diamines.

In our works we have applied the oxidative polymerization as a practical method for obtaining poly(Schiff base)s from monomers with -CH=N- preformed function having the general structure: Py-CH=N-R-N=CH-Py , where Py is the 2-substituted pyrrole group and R is an arylene radical [12-15].

In this paper we report some results concerning the synthesis and characterization of monomers that combine the both thiophene and Schiff base functionalities. The monomers contain alternating 2,2'-bithiophene-diyl rings and azomethine units in the main chain. A monomer with thiophene and vinylene units was synthesized, too. Experimentally, the polymers were obtained by oxidative coupling of the corresponding monomers (II or V) at the marginal thiophene units.

EXPERIMENTAL

Materials

2-Thiophenecarboxaldehyde (Merk, 98%), benzene, dichloroethane, dichloromethane, acetonitrile, nitrobenzene, ethanol and N,N'-dimethylformamide (Fluka, p.a.) were distilled before use. p-Toluenesulfonic acid (Aldrich, 99%), hydrazine monohydrate (Fluka, 98%), α,α' -dibromo-p-xylene (Aldrich, 98%), triphenyl phosphine (Merk, 98%) and lithium (Fluka, 99%) were used as received. p-Phenylenediamine (Schuchardt, Munchen, p.a.), benzidine (Merk, p.a.) and 1,5-diaminonaphthalene (Fluka, 98%) were recrystallized from methanol.

Electrolytes: Tetrabutylammonium perchlorate was synthesized and purified (m.p. 143-144°C) according to literature [16]. Tetrabutylammonium tetrafluoroborate (TBAP) was prepared by titration of tetrabutylammonium hydroxide with tetrafluoroboric acid and purified by usual methods (m.p. 161-162°C) [17].

Measurements

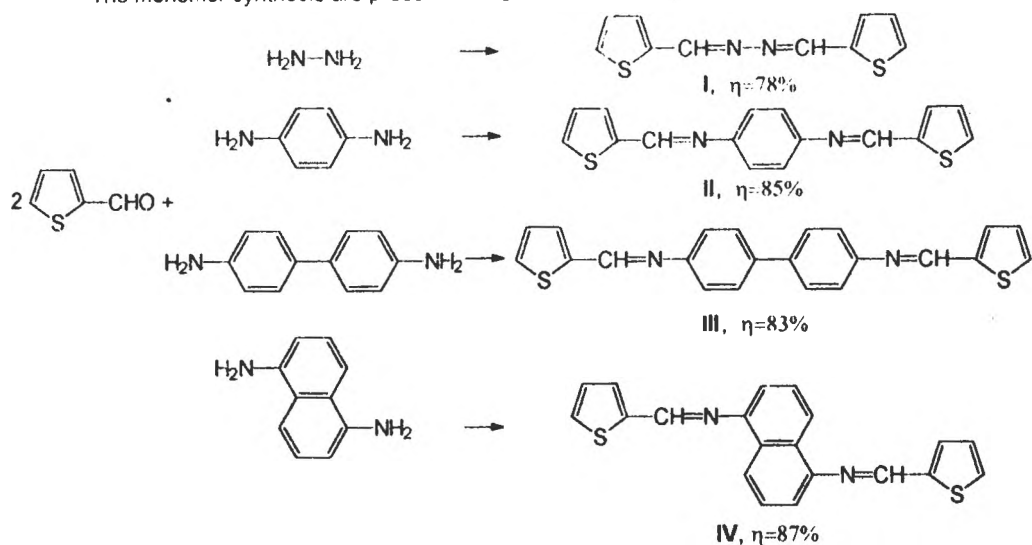
The melting points were determined on a Boetius Microscope. Infrared spectra were obtained on a Perkin Elmer 577 spectrometer using KBr pellets. $^1\text{H-NMR}$ spectral analyses were performed on a JNM-C60 60MHz apparatus, at 20°C using DMSO-d_6 as solvent and tetramethylsilane (TMS), as internal standard. UV spectra were registered with a Specord M80 Carl Zeiss Jena spectrophotometer.

Voltammetric registrations were performed on an OH - 102 Radelkis polarograph.

The electrochemical polymerizations were carried out in a previously described equipment [13].

Monomers

The monomer synthesis are presented in Schemes 1 and 2



2-thiophenecarboxaldehyde concentration: 0.5 mol/l

2-thiophenecarboxaldehyde/diaminemolar ratio: 1/2.2

Solvent: toluene

Reaction time: 6h

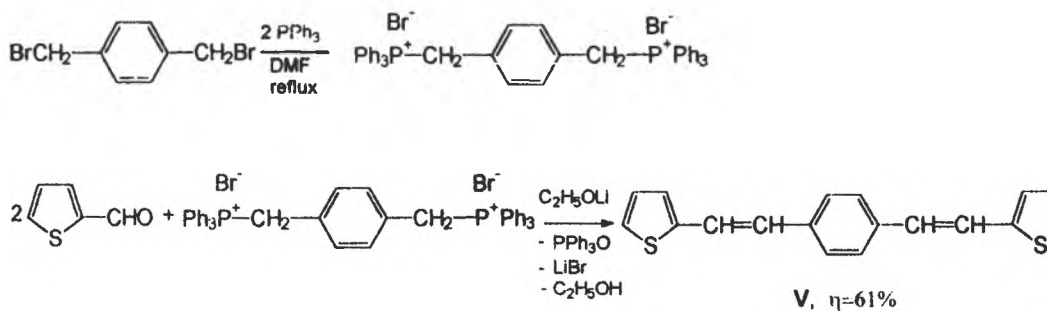
Temperature: reflux

Catalyst: p-toluene sulphonic acid

Purification: recrystallization from dichloroethane; column chromatography

Scheme 1

Synthesis of monomers with
Schiff base structure



2-thiophenecarboxaldehyde concentration: 0.2 mol/l

Solvent: Ethanol

Reaction time: 24h

Temperature: reflux

Catalyst: C_2H_5OLi

Purification: recrystallization from chloroform; column chromatography

Scheme 2

Synthesis of bis(thienyl-vinyl)-
1,4-phenylene

The spectral data (IR, 1H -NMR, UV) and other characteristics of monomers are presented in Table

Table 1 Monomers characterization

Monom.	I	II	III
Colour	green-yellow	light-yellow	orange-yellow
m.p °C	161-162	169-170	248-250
UVdata nm	347	301, 372	303, 371
¹ H-NMR data δ ppm	6.52-6.7, t, 2H poz. 4 from thienyl ring 6.94-7.15, m, 4H poz.3 and 5 from thienyl ring 8.25, s, 2H from CH=N group	6.95-7.3, t, 2H poz. 4 from thienyl ring 7.35, s, 4H from phenylene 7.55-7.7, m, 4H poz.3 and 5 from thienyl ring 8.7, s, 2H from CH=N group	6.58-6.62, t, 2H poz. 4 from thienyl ring 7.08-7.4, m, 4H poz.3 and 5 from thienyl ring 7.6-8.0, m, 8H from biphenylene 8.72, s, 2H from CH=N group
IR data, cm ⁻¹	CH=N gr.: 1610 thienyl: 1430, 1210,1080, 1050, 835, 730	CH=N gr.: 1610. thienyl: 1430, 1200 , 1100, 1050, 850 p-disubstituted phenylene: 1490, 1105, 810	CH=N gr.: 1620 thienyl: 1430, 1200, 1105, 1050, 845 p-disubstituted phenylene:1600, 1500, 1105, 810

IV	V
green-yellow	orange
225-227	161-163
309, 373	360; 373, 398
<p>6.9-7.22, m, 2H poz. 4 thienyl+2H poz.3,7 naphthylene</p> <p>7.3-7.45, d, 2H poz.3 thienyl +2H poz.2,6 naphthylene</p> <p>7.45-7.55, m, 2H poz 5 thienyl</p> <p>7.98-8.1, d 2H poz.4,8 naphthylene</p> <p>8.72, s, 2H, from CH=N group</p>	<p>6.6-7.7, m, 10H overlapping signals from thienylene and vinylene</p> <p>7.78, s, 4H from phenylene</p>
<p>CH=N gr.: 1620</p> <p>thienyl: 1435, 1200, 1100, 1050, 840</p> <p>naphthylene: 1490, 1150, 790</p>	<p>CH=CH gr.:965 (γ CH) 1615 (νCC)</p> <p>thienyl: 1450, 1200, 1185, 1050, 845</p> <p>phenylene: 1495, 1130, 800</p>

RESULTS AND DISCUSSION

Voltammetric study of monomers

The synthesized monomers were characterized by voltammetric method to evaluate redox behavior and the reactivity in electrochemical polymerization reaction. Measurements were performed in one-compartment cell using three electrodes: working electrodes E_W -Pt(wire) or Radelkis, auxiliary electrode E_{AUX} -Pt(band) and standard calomel electrode (SCE) as reference electrode (E_R). There are used different sensibilities $S=2-16 \cdot 10^{-7}$ A. The monomers were analyzed in solution or as a deposit on the electrode by solvent evaporation. The selection of these conditions was necessary due to the poor monomer solubility. The studied potential range was $-1.2 - +2.0$ V and the scan rate 8 mV/s. For solution analysis there was used $(C_4H_9)_4NClO_4$ as supporting electrolyte in CH_2Cl_2 .

A general characteristic of the registrations evidences slow and fast oxidative processes at the electrode. The first slow stages could be attributed to diffusive processes to electrode and the fast ones to the main oxidations.

From the literature data [19], the thiophene, bithiophene or terthiophene oxidation proceeds at 1.65 V, 1.20 V and 1.0 V, respectively. This decrease is attributed to steric and conjugation effects. In the case of monomer I, the oxidation potential is characterized $(E_{1/2})_{a2} = +1.6$ V (Figure 1). This value can be attributed to an irreversible oxidation of thiophene ring. In the conditions of electrode deposit there are evidenced some reduction processes at $(E_{1/2})_c = -0.05$ V.

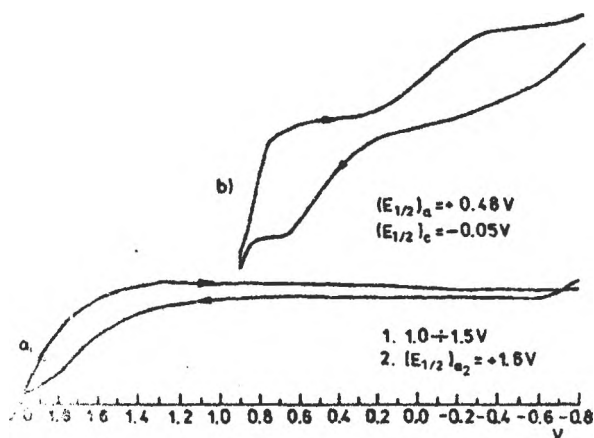


Figure 1

Voltammograms of monomer I

a) E-Pt(Rad)

TBAP 0.1M in CH_2Cl_2

normal, $S=6 \times 10^{-7}$ A, 8mV/s

b) E-Pt(wire) deposit

$LiClO_4$ 0.1M+ $HClO_4$ 0.1M

normal, $S=6 \times 10^{-7}$ A, 8mV/s

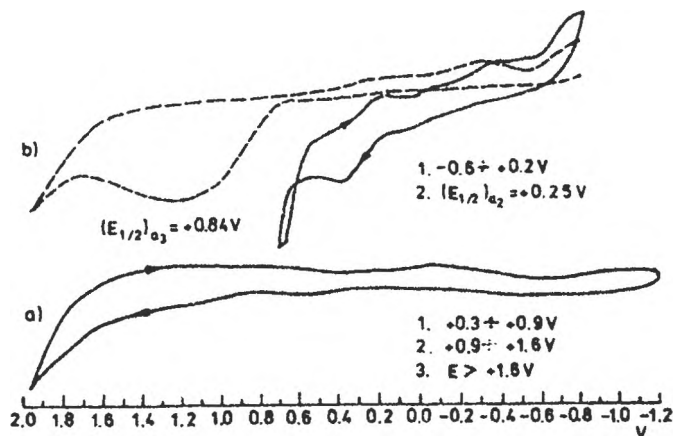
The presence of phenylene radical between azomethinic groups modifies the electrochemical aspect in the range $+0.9 - +1.6$ V, where we consider that the thiophene ring is oxidized (Figure 2).

Figure 2

Voltammograms of monomer II

a) E-Pt(Rad)
TBAP 0.1M in CH₂Cl₂
normal, S=4x10⁻⁷ A, 8mV/s

b) E-Pt(wire)
TBAP 0.05M in CH₂Cl₂
--- normal, S=16x10⁻⁷ A, 8mV/s
— normal, S= 2x10⁻⁷ A, 8mV/s



In the case of monomer III there can be distinguished three successive oxidative steps characterized by $(E_{1/2})_{a1} = +0.6$ V, $(E_{1/2})_{a2} = +0.88$ V and $(E_{1/2})_{a3} = +1.18$ V (Figure 3). The third one can be attributed to the thiophene oxidation, being close to that of bithiophene (+1.2 V) [19]

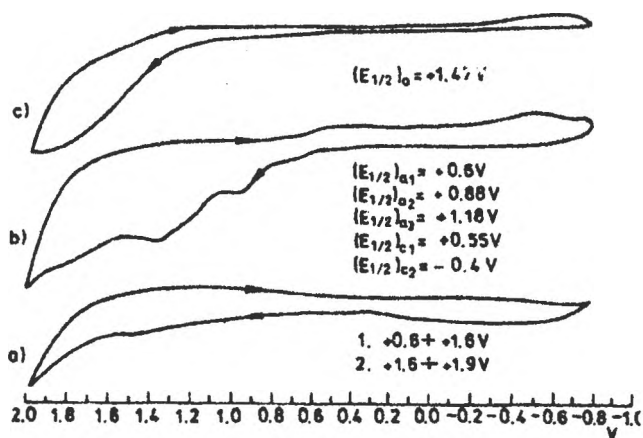
Figure 3

Voltammograms of monomer III

a) E-Pt(Rad)
TBAP 0.05M in CH₂Cl₂
normal, S=4x10⁻⁷ A, 8mV/s

b) E-Pt(wire)
TBAP 0.05M in CH₂Cl₂
normal, S=4x10⁻⁷ A, 8mV/s

c) E-Pt(wire) deposit
LiClO₄ 0.1M
normal, S=16x10⁻⁷ A, 8mV/s



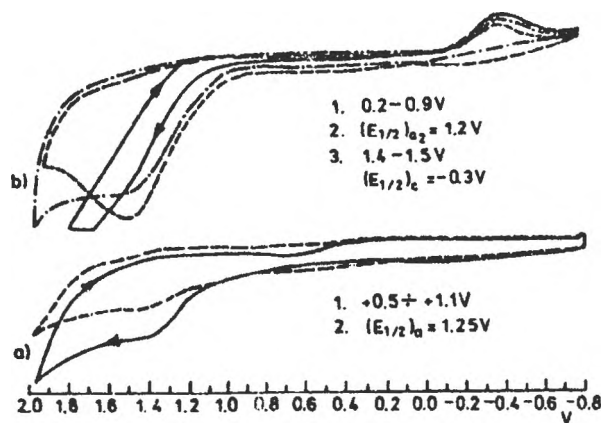
The monomer with 1,5-naphthylene group (IV) shows a faster oxidation step $(E_{1/2})_{a2} = +1.25$ V (Figure 4, a). This value is identical with that found for monomer II ν phenylenic bridge. In this case the reduction stages are present, too.

The voltammograms from Figure 4, b present the successive potential scanings monomer V. We appreciate that the third scanning signal evidences an oxidative degradation process and a light increased reduction peak.

The monomer with bis(2-thienylvinyl)-p-phenylene structure can be placed from the point of view of the oxidative capacity ($(E_{1/2})_{a2} = +1.2 \text{ V}$) before the monomer II with azomethinic group, probably due to the more efficiently conjugation of the vinylene group.

In all the cases the oxidation processes are irreversible.

Figure 4



Voltammograms of monomers IV and V

a) E-Pt(wire)

TBAP 0.05M in CH_2Cl_2

--- normal, $S=6 \times 10^{-7} \text{ A}$, 8mV/s

--- normal, $S=2 \times 10^{-7} \text{ A}$, 8mV/s

b) E-Pt(wire) deposit

LiClO_4 0.1M

TBAP 0.05M in CH_2Cl_2

normal, $S=16 \times 10^{-7} \text{ A}$, 8mV/s

---- 1st scanning; ----- 2nd scanning; — 3rd scanning

For elucidation of the reduction monomers' behavior, it would be necessary to establish the structure of the cathodic products and the redox polymers characteristics.

Electrochemical polymerization

N, N'-bis(2-thienylmethylene)-1,4-diaminobenzene (II) and bis(2-thienylvinyl)-1,4-phenylene (V) were tested in the electropolymerization reaction. For comparison there was polymerized the thiophene, too. The electropolymerization was studied in different conditions due to the particular structure of the monomers and their limited solubility in usual solvents. Taking in account the risks of utilization of perchloric acid salts in organic medium [20], the results were compared using different electrolytes: tetrabutylammonium perchlorate and tetrabutylammonium tetrafluoroborate. For controlling the electrode processes and preventing some secondary reactions, low current densities were used ($1-10 \text{ mA/cm}^2$). The reactions are starting both in the anodic and cathodic compartments. In the first stages they were observed by changing of the solutions' color. After an induction period, the polymers result in the anodic compartment as different colored precipitates (complex mixtures).

In Table 2 there are presented the electrochemical polymerization conditions for monomer II. In the studied processes, the main reaction proceeds in the anodic compartment,

Table 2 The electrochemically polymerizations conditions of monomer II

Exp no.	Electrolyte	Electrolyte conc., mol/l	Solvent	Monomer conc. mol/l	Current, mA	Reaction time, h	Product		Yield %
							Anode	Cathod	
1	(Bu) ₄ NCIO ₄	0,02	nitrobenzene	0,025	4	2	pp	---	14,70
2	(Et) ₄ NCIO ₄	0,1	nitrobenzene	0,025	4	5	pp	---	30,41(a)
3	(Bu) ₄ NBF ₄	0,1	nitrobenzene	0,025	4	7	pp	---	88,78(b)
4	(Bu) ₄ NCIO ₄	0,05	dichloroethane	0,03	4	6	pp	---	31,10
5	(Bu) ₄ NCIO ₄	0,05	dichloroethane	0,05	4	7	pp	---	37,65
6	(Bu) ₄ NCIO ₄	0,1	dichloroethane	0,05	10	8	pp	pp	81,06(c)
7	(Bu) ₄ NCIO ₄	0,1	acetonitrile	0,025	10	8	pp	---	60,36
8	(Bu) ₄ NCIO ₄	0,1	dichloromethane	0,05	10	8	pp	f	(c)
9	(Bu) ₄ NCIO ₄	0,1	dichloromethane	0,025	10	4	pp	pp	(c)
10	(Bu) ₄ NCIO ₄	0,1	dichloromethane	0,025	5	8	pp	pp+f	(c)
11	(Bu) ₄ NCIO ₄	0,1	dichloromethane	0,025	10	8	pp	pp+f	(c)
12	(Bu) ₄ NBF ₄	0,1	dichloromethane	0,025	10	2	pp	---	37,9 (10,11) _p
13	(Bu) ₄ NBF ₄	0,1	dichloromethane	0,05	10	4	pp	---	46,35 (8,75) _p
14	(Bu) ₄ NBF ₄	0,05	dichloromethane	0,05	4	6	pp	---	29,52 (4,42) _p

-temperature 18-20 °C

(a) There is also some organic crystalline product; (b) There is also organic crystalline product; (c) There is also NH₄Cl (separated and identified); pp-precipitate; f-film; p-polymer

were the products result as precipitates. In halogenated solvents, especially in CH_2Cl_2 and $(\text{C}_4\text{H}_9)_4\text{NClO}_4$ as support electrolyte, precipitates and films are formed at the cathode, too. No products are found at the cathode compartment when $(\text{C}_4\text{H}_9)_4\text{NBF}_4$ is used as electrolyte. The deposited films from the cathode are conductive. The Pt modified electrodes were efficient for oxidative electropolymerization of monomer II in other experiments.

Together with polymers, small molecular organic crystalline compounds are formed at the anode. They have to be identified in the future.

In halogenated solvents, undesirable NH_4Cl is formed with any of the two electrolytes. It is favored by the high current densities. We suppose that the solvent is responsible for its formation, being necessary supplementary investigations to prove this hypothesis.

From the anode reaction mixture (Table 2, experiments 1 and 2) there were isolated the following fractions: polymer insoluble in nitrobenzene, polymer precipitated with CH_2Cl_2 and small molecular product soluble in ethanol.

In similar conditions was polymerized monomer V, too.

IR measurements

The IR spectra of some fractions of the products obtained by electrooxidation of monomer II (both at anode and cathode), and of polymer with vinylene groups, in comparison with that of polythiophene, are presented in Figure 5.

The spectra of two fractions of the same product are very close (1 and 2 or 3 and 4 curves), so we suppose they have the same structure. The different solubilities can be due to the molecular weights. The main difference between the spectra of the products obtained with different electrolytes is the presence of the absorption from 1100 cm^{-1} attributed to the dopant anion ClO_4^- . In the 3 and 4 spectra, when $(\text{C}_4\text{H}_9)_4\text{NBF}_4$ was used as electrolyte, we find at that frequency only an absorption shoulder due to the in-plane vibrations of deformations of C-H bonds from aromatic groups (βCH). The signal from 1100 cm^{-1} is present in the spectra of polymer with vinylene groups and of polythiophene, too (6 and 7 curves from Figure 5). The anion ClO_4^- absorption is absent in the cathode fraction spectrum, which is different from those of anode fractions. This is a prove that the cathode product has not the same molecular structure with the anode one.

The absorption from 830 cm^{-1} attributed to the out-of-plane deformation vibrations of C-H in p-disubstituted benzene ring (γCH) is present in all the spectra excepting that of polythiophene. In this case there is a specific signal to polythiophene at 799 cm^{-1} , reported by other authors, too [21-23]. The absorptions from $740\text{-}750\text{ cm}^{-1}$ in the polymers with

Schiff base structure spectra can be attributed to the out-of-plane deformation vibrations of C-H in thiophene ring, and those from 1050 cm^{-1} to the in-plane deformation vibrations of

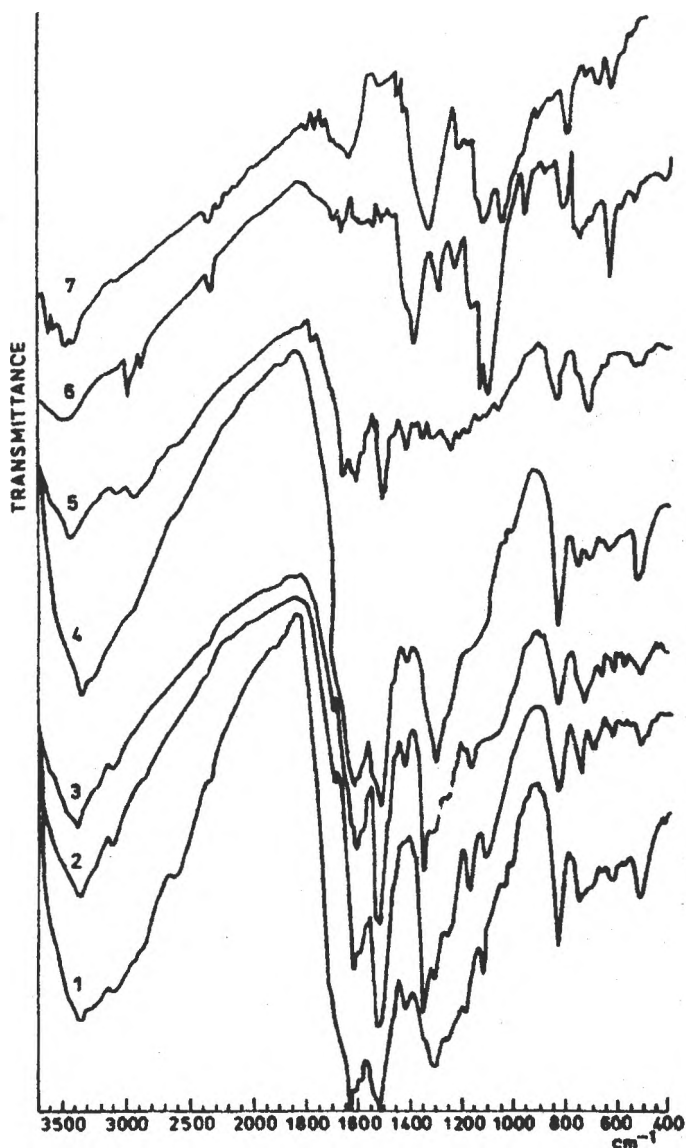


Figure 5
 IR spectra of :
 1- poly(II) (dopant: ClO_4^- , soluble fraction in nitrobenzene);
 2- poly(II) (dopant: ClO_4^- , insoluble fraction in nitrobenzene);
 3- poly(II) (dopant: BF_4^- , soluble fraction in nitrobenzene);
 4- poly(II) (dopant: BF_4^- , insoluble fraction in nitrobenzene);
 5-cathode fraction (monomer II, solvent: CH_2Cl_2 , dopant: BF_4^-);
 6 poly(V) (solvent: CH_2Cl_2 , dopant ClO_4^-);
 7- polythiophene (nitrobenzene, dopant ClO_4^-)

C-H bonds in aromatic rings. The bands from 1330 and 1375 cm^{-1} from monomer II spectrum attributed to the thiophene ring vibrations are found in polymer at 1315 and 1355 cm^{-1} . Other absorptions coming from both thiophene and phenylene rings (ν_{CC}) at 1420 , 1520 and 1580 cm^{-1} (the last value is represented only by shoulder of absorptions) are found. The very intense band from 1620 cm^{-1} is due to the $-\text{CH}=\text{N}-$ group. In the polymer with vinylene groups spectrum there are present some specific absorptions at 960 cm^{-1} (ν_{CH} , trans vinylene) and 1670 cm^{-1} (ν_{CC} , trans vinylene).

¹H-NMR analysis

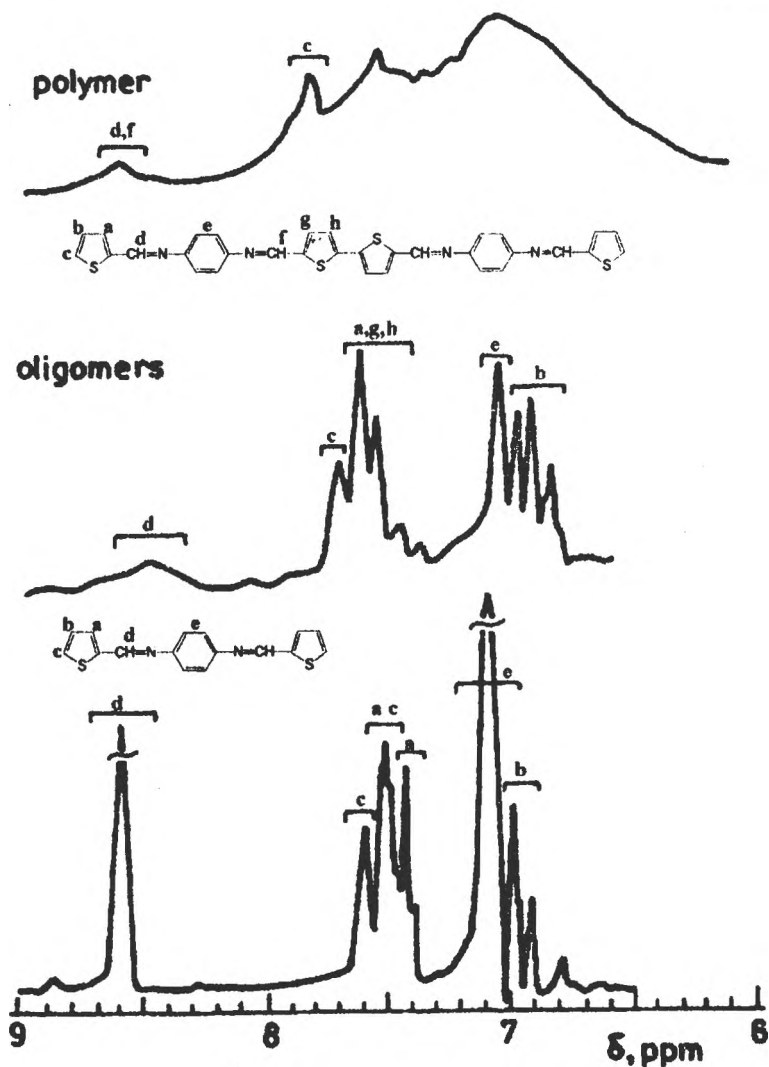


Figure 6 ¹H-NMR spectra of monomer II and of the corresponding oligomeric and polymeric fractions

¹H-NMR spectra of two poly(N,N'-bis(2-thienylmethylene)-1,4-diaminobenzene) fractions in comparison with that of monomer II are presented in Figure 6. The **b** and **e** protons from thiophene and the phenylene rings are found in the monomer spectra at 6.8-7.1 δ ppm. The **a** and **c** protons constitute the second group of signals (7.4 - 7.6 δ ppm). The $(b+e)/(a+c)$ ratio is 1.5 for the monomer. The **g** and **h** protons in dimer are found together with **a** protons. Near the **c** protons are only the phenylene and the **b** protons from the terminal thiophene groups. The theoretical calculated ratio between the two groups of signals is 1.5. In the trimer the ratio would be 1.16, in tetramer 1.12, etc. In the presented

spectrum the ratio calculated from the height of integrals is 1.21. This value is between that of dimer and trimer (55% dimer). However there is possible to have higher oligomers in their mixture, so the percent of dimer could be a little different, but their presence is limited by the low solubility in the fractionating conditions. In the case of polymer spectra the signals lose their individuality due to the nonequivalence of protons from different thiophene and phenylene ring.

CONCLUSIONS

Four monomers with Schiff base structure and thiophene moieties and a p-phenylene-di(vinylene thienylene) one as precursors for obtaining of new conjugated polymers were synthesized and characterized. Their voltammetric registrations evidence some irreversible oxidative electrode processes, in different stages. Also, reductive processes are identified. The electrochemical polymerization of monomers II and V proceeds by oxidative coupling with precipitate formation. The corresponding polymers result in their doped state. The reaction conditions influence the polymers and eventually other undesirable compounds formation. In halogenated solvents, films or precipitates are formed by reduction, too. The cathode deposited films are conductive. The spectral analysis data of the products confirm the possibility of oxidative coupling of the thiophene rings by their 5,5'-positions

REFERENCES

- [1]. T. A. Skotheim, Ed. Handbook of Conducting Polymers; Marcel Dekker: New York, 1986.
- [2]. S. Tanaka, M. Sato and K. Kaeriyama, *Makromol. Chem.*, 186, 1985, 1685.
- [3]. D. R. Rutherford, J. K. Stille, C. M. Elliot and V. R. Reichert, *Macromolecules*, 25, 1992, 2294.
- [4]. F. Chimenti, L. D'Ilario, A. Ettore, E. Muraglia, G. Ortaggi and G. Sleiter, *J. Mat. Sci. Lett.*, 11, 1992, 1532.
- [5]. L. D'Ilario, A. Ettore, E. Muraglia, G. Ortaggi and G. Sleiter, *J. Mat. Sci. Lett.*, 13, 1993, 336.
- [6]. L. D'Ilario, A. Ettore, E. Muraglia, G. Ortaggi and G. Sleiter, *J. Mat. Sci.*, 30, 1995, 4273.

- [7]. K. S. Al-Jumah, K. B. Wagener, T. E. Hogen-Esch, J. L. Musfeldt and D. B. Tanner, *Polym. Preprints*, 31(1), **1990**, 173.
- [8]. G. F. D'Alelio, *Encyc. Polym. Sci. and Eng.*, vol. 10, 1st Edition, John Willey and Sons, New York, **1969**, p.659.
- [9]. S. Bruckner, S. Destri and W. Porzio, *Macromol. Rapid Commun.*, 16, **1995**, 297.
- [10]. S. Destri, M. Mascherpa and W. Porzio, *Synt. Met.*, 69, **1995**, 287.
- [11]. C. Amari, C. Pelizzi, G. Predieri, S. Destri and W. Porzio, *Synth. Met.*, 72, **1995**, 7.
- [12]. C. I. Simionescu, M. Grigoras, I. Cianga, I. Diaconu and A. Farcas, *Polym. Bull.*, 32, **1994**, 257 ().
- [13]. C. I. Simionescu, M. Grovu - Ivanoiu, M. Grigoras and I. Cianga, *Die Andgew. Makrom. Chem.*, **221**, 103 (1994).
- [14]. C. I. Simionescu, M. Grovu - Ivanoiu, I. Cianga, M. Grigoras, Al. Duca and I. Cocârla, *Die Andgew. Makrom. Chem.*, **239**, 1, (1996).
- [15]. M. Grigoras, G. Stoica, I. Cianga, and C. I. Simionescu, *Rev. Roum. Chim.*, in press, (1995).
- [16]. O. F. Olaj, J. W. Breitenbach and B. Buchberger, *Makromol. Chem.*, **3**, 160, (1968).
- [17]. U. Akbulut, R. L. Birke and J. E. Fernandez, *Makromol. Chem.*, **179**, 2507 (1978).
- [18]. H.-P. Weitzel, A. Bohnen and K. Müllen, *Die Makrom. Chem*, **191**, 2815 (1990).
- [19]. R. B. Kaner in *Electrochemical Science and Technology of Polymer-2*, R. G. Linford, ed. (Elsevier Appl. Sci., Essex, England), 1990, p. 97-147.
- [20]. A. Picot and P. Grenouillet, *Actualité Chim.*, avril, 41 (1986)
- [21]. S. Hotta, W. Shimotsuma and M. Taketani, *Synth. Met.*, **10**, 85 (1984).
- [22]. S. Hotta, T. Hosaka, M. Soga and W. Shimotsuma, *Synth. Met.*, **10**, 95 (1984).
- [23]. O. Inganas, B. Liedberg and W. Chang-Ru, *Synth. Met.*, **11**, 239 (1985).

THE ELECTROSTATIC PROPERTIES OF A MULTISPECIES IONOSPHERIC PLASMA

Speranța Coldea

Faculty of Physics, University of Cluj, Cluj-Napoca Ro-3400, Romania

ABSTRACT. The ionospheric and magnetospheric plasmas could be studied either experimentally, theoretically or by the simulation method. By considering for these multicomponent plasma systems two kinds of physical models, the PIC simulation is applied with the aim to analyze the electrostatic and oscillatory properties of such a plasma. The considered models for an infinite, periodic ionospheric plasma system are a 4- and 5- species warm plasma in the magnetic field of the earth. By applying an 1-D electrostatic program of particle simulation the diagnostics for the electrostatic properties, specific energies and oscillatory parameters of the plasma are obtained. From the simulation results the qualitative behavior of the given plasma systems could be described.

1. INTRODUCTION

For knowing the behavior of the Earth ionosphere it is important to have a view on the properties of this ionized part of the atmosphere which could have an important influence on the life conditions on the earth. In ionosphere plasma phenomena heavy ions are also present in abundance's which are not negligible relative to protons and electrons. The mutual streaming between different species of the plasma may give rise to various types of stable or unstable oscillations as are those specific for electrostatic and electromagnetic interactions. In the used models for the ionosphere plasma we consider a totally ionized plasma system. From the point of view of plasma theory an ionosphere plasma could be considered to be an infinite and periodic plasma. A qualitative analysis for the electrostatic and oscillatory properties of 4- and 5- species plasma systems, considered as physical models of a multicomponent ionospheric plasma, is done. The analysis is made by using these models of the plasma systems and the particle simulation method. In the second part of the paper the models for an ionospheric multispecies plasma used to analyze by PIC-simulation the system behavior are presented. In the third chapter a discussion of so obtained results is given together with the conclusions which could be deduced in this stage of the ionosphere study.

2. THE PHYSICAL MODELS FOR AN IONOSPHERE MULTICOMPONENT PLASMA

The first model "w4istream" is that for a four-species plasma, composed from two species of electrons with different temperatures (thermal and superthermal) and two species of ions, one immobile and the other one having a dynamics. Between these four species of particles an electrostatic interaction takes place. The interaction is taken into account as an interaction between four beams. Some input data for this plasma model are given as an example (the indexes will specify the considered beam): the number of particles $n_{the} = n_{sthe} = 512$ and $n_i = 1024$, the specific charge $(q/m)_{the} = (q/m)_{sthe} = -1.00$ and $(q/m)_{i1} = (q/m)_{i2} = 1.00$; the cyclotronic frequencies of the species $\omega_{C_{sthe}} = \omega_{C_{the}} = -4.5 \cdot 10^{-5}$ and $\omega_{ci1} = \omega_{ci2} = 4.5 \cdot 10^{-5}$. The thermal velocities are given as: $v_{the} = 0.5$, $v_{sthe} = 1.00$ and $v_{thi} = 0.05$.

The second model "5nistream" is that made from five species of plasma particles: two of thermal and superthermal electrons, the stationary plasma ions and two species of drifting ions (the specific ions for an ionospheric plasma are: H^+ , He^+ and/or O^+). For these physical plasma models the particle simulation method is applied, using the specific input data and obtaining after running the simulation program some specific diagnostics which describe the behavior of the considered plasma systems.

3. RESULTS OF THE PIC SIMULATION FOR 4- and 5- SPECIES PLASMA MODELS

The specific diagnostics are directly given as diagrams for the electrostatic, energetic and oscillatory properties of the considered multi-component plasma systems: the electric field and potential of the ionospheric plasma model, the charge density and the specific energies: the kinetic energies of the plasma species, the field (potential) energies, the total kinetic energy and the total energy given by: $TE = KE1 + KE2 + \dots + KE5 + FE$. We will give also some diagrams obtained for the Fast Fourier Transformed electrostatic energies of the plasma systems $ESE(k)^j$ from which it is possible to evaluate the linear or growth rates, in case of the unstable oscillations excited in the considered plasma systems, and the bouncing time (frequency) in the case of some stable oscillations. In the Table 1 the specific

(frequency) in the case of some stable oscillations. In the Table 1 the specific energies and the FFT electrostatic field energies are given for the multispecies plasma models. As examples of the obtained diagnostics the diagrams for the mode 1 of the 4- and 5-species models considered for an ionospheric plasma, the ESE1(k) is given in Fig.1. After obtaining the results from applied PIC - simulation method for the multispecies plasma systems considered as different approximations for the ionospheric plasma, the conclusions will be given in the next section.

TABLE 1. The specific energies of the plasma species for the first three oscillation modes in some of the 4- and 5-species models.

Energy type	4i1stream	5n1stream
KE	11.1	10.36
KE1	6.03	4.037
KE2	0.8399	9.136
KE3	4.108	0.00152
KE4	0.0027	0.0115
KE5	-	0.011
FE	0.0117	0.0231
TE	11.1	10.36
ESE1(k)	0.00154	0.0152
ESE2(k)	0.00289	0.00178
ESE3(k)	0.002045	0.00231

4. CONCLUSIONS

From the diagrams for the FFT of the electrostatic energies of the first three modes of oscillation excited by interaction of the various species of particles which compose the used plasma models, considered for such a multispecies plasma system as is the ionospheric plasma, it can be seen the stable or nonstable, linear or nonlinear behavior (growths or not) of the different modes of oscillations. The

oscillatory aspect of a plasma system is important for many other properties which describes phenomena existing in such a physical system. Then new effects of the multi-component species of particles interaction in plasma arise because the various species are mutually coupled through the electromagnetic Lorentz force. In the Fig. 1, one of the diagnostics of the particle simulation applied with an electrostatic 1-D code is given, describing the oscillatory behavior of first mode of the 5-species plasma system. In the same manner, in the other diagrams obtained as diagnostics of the PIC-simulation for the models used to describe an ionospheric plasma, the other two modes of oscillations excited in plasma could be given for the 4- and 5-species systems (not presented).

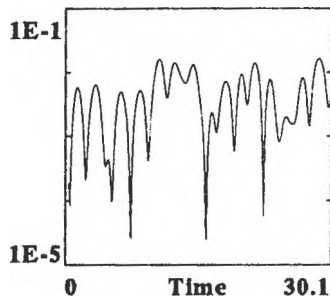


Fig.1 The ESE1(k)-diagnostics of the PIC-simulations for mode-1 of the 4-species plasma model

In both the 4- and 5-species plasma models the first mode of oscillation excited in plasma (mode-1) has a more stable aspect and the other two modes (mode-2 and mode-3) have an unstable behavior, with linear growths from which the linear growth rates could be estimated, as are given in the Table 2, and a nonlinear stage of saturation of the these instabilities. In the case of the nonlinear saturation level of the instabilities the nonlinear growth rates could be estimated and also the nonlinear Landau damping rates. In the nonlinear stage of the unstable oscillation modes the successive nonlinear growths and Landau dampings could be considered as nonlinear fluctuations of the wave amplitude around a mean value which could be also estimated from the ESE(k) diagrams. From the earlier partially presented results of the particle simulation method applied to the ionospheric plasma multi-species systems a first conclusion which may be given is that some electrono-cyclotronic and

iono-cyclotron unstable oscillations will appear in such a warm, magnetized multispecies ionospheric plasma due to the interaction between the different species streams (with different temperatures and different drift velocities). We see that the PIC-simulation method can be applied with good qualitative results, and in a future work, also with quantitative results for describing more accurately the behavior of a multispecies plasma. These results give the possibility to see the stable or unstable behavior of such a complex plasma system, to deduce the basic mechanisms and phenomena which exist in it. As an example we can observe that some of the electrons are captured in the waves potential in the nonlinear stage of the plasma system evolution and they will bounce with a specific frequency that could be eventually estimated. The second conclusion which can be given is that the phenomena in such a multispecies warm magnetized system, as is the ionospheric plasma, are very complex and nonlinear ones, beginning from two- and three-streams instabilities, electrono-cyclotron or iono-cyclotron instabilities and probably containing also compressive modes of oscillations due to differential streaming between various species of the system. Finally it could be stressed that these multicomponent ionospheric plasma systems in which the abundance of heavier ions is not negligible compared to protons (ions of H^+) giving rise to new and interesting effects must be studied further by the particle simulation but using some more accurate data for plasma species parameters, and also by a numerical integration of the corresponding dispersion relations for the various considered models, especially with a larger number of components (a 6-species plasma).

REFERENCES

1. Birdsall Ch.K and Langdon A.K., *Plasma Physics Via Particle Simulations*, Ed. McGraw-Hill, New York, **1985**.
2. Coldea S., *Proceedings of the 8th Joint EPS-APS Int. Conf. on Physics Computing, Krakow, Poland, sept.17-21, 1996*, p. 81.
3. Coldea S., *The interaction of the superthermal, thermal electrons and ions beams systems: a simple model for an ionospheric plasma studied by PIC - simulation 1-D electrostatic code*, *Physica Scripta*, T 63, **1996**, 291.

CYCLIC VOLTAMMETRY OF POLI-*orto*-METOXYANILINE FILMS

M.Sima and M. Buda*

National Institute of Material Physics P.O. Box MG7, Magurele, Bucharest

** "POLITEHNICA" University of Bucharest, Faculty of Industrial Chemistry, Applied*

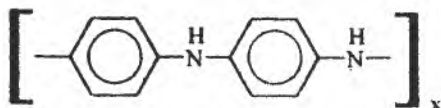
Physical Chemistry & Electrochemistry Dept. Calea Grivitei 132, 78122, Bucharest

ABSTRACT

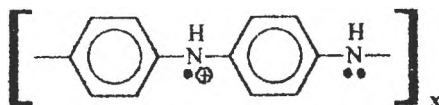
A comparison of the synthesis and conductive properties between polyaniline and poly-*orto*-metoxyaniline is made. Reversibility and air stability of the polymers are discussed. The low air-stability of poly-*orto*-metoxyaniline chain is probably due to the methoxy group, which makes the polymer more reactive.

INTRODUCTION

The electronic conducting polymers are conjugated structures in which the polymer chain consists of alternating simple-double (or triple) bonds; their conductive properties making them extremely useful for electrochemical cells or electronic devices. Electronic conducting polymers are either chemically or electrochemically prepared in oxidized form (p-doped) and they can be repeatedly scanned between the conductive and non-conductive forms in a quasireversible manner [1, 2], through a path that involves the redox reaction of the π electrons system on the polymer chain. The change in the oxidation state of the polymer is associated with a transfer of a counterion in or out the polymer chain. The polymer's conductivity may change with several orders of magnitude during this process; the polymer is electronic conductor only in the doped state [3]. Polyaniline is a typically electronic conductor polymer, which can be prepared by both chemical or electrochemical methods. The completely reduced form of the polyaniline, has the structure:



while the conductive form is:



The oxidized form of the polyaniline is only partially soluble in some solvents like glacial acetic acid or concentrated sulphuric acid. The methoxy substituent in the *ortho* position of the aniline ring gives a soluble polymer in common solvents (e.g. methanol), the poly-*ortho*-methoxyaniline. The practical purpose of using polyaniline films in electrochemical cells or electronic devices requires the optimum chemical and electrochemical stability conditions of the polymer.

The present paper shows the experimental results for the polyaniline and poly-*ortho*-methoxyaniline in air and aqueous solutions.

EXPERIMENTAL

The polymer films were obtained in constant current conditions ($i = 0.125 \text{ mA cm}^{-2}$) and by potential scanning between -0.2 and $+1.05 \text{ V/SCE}$, from 0.06 M monomer (aniline or methoxyaniline respectively) in $1 \text{ M H}_2\text{SO}_4$ solution. The films were deposited onto a platinum foil; all the potentials are SCE referred.

The film conductivity was measured with a conductometer using an ac signal of 200 Hz ; the films were placed in a close, air containing box (fig. 1).

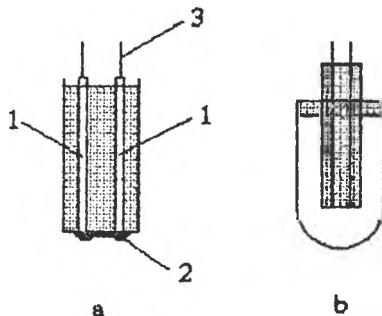


Fig. 1. The cell used for measuring the polymer film conductivity.

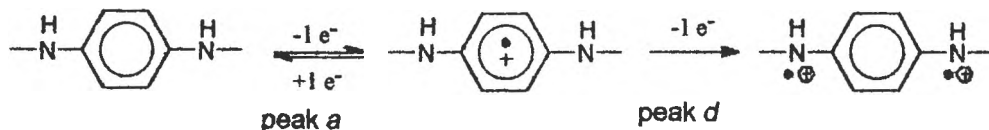
- the two platinum electrodes, insulated with resin, with polymer film. 1-platinum electrode; 2-polymer film; 3-electrical contacts.
- the closed box with the two platinum electrodes.

The cell used for conductometric measurements was made by insulating two platinum wires ($\phi = 0.5 \text{ mm}$, $40 \mu\text{m}$ gap between wires) in epoxy resin. After polishing the two wires with emery paper ($\times 600$), the polymer films were deposited at constant current until the gap between the wires was completely covered with polymer.

RESULTS AND DISCUSSIONS

From the polyaniline synthesis cyclic voltammogram (fig. 2) one can see the presence of an oxidation peak, e , at $+1.05 \text{ V/SCE}$, which was attributed to monomer adsorption and radical-cation formation; this peak disappears in the following scans.

For the polymer film to grow properly, *d* peak potential must be reached. If the potential is scanned only until the base of peak *d*, (that is, +0.62 V) the polymer film stops growing. The process corresponding to this peak is attributed to dication or dication-diradical (bipolaron) formation. The process corresponding to peak *a* (+0.18 V/SCE) is attributed to radical-cation (polaron) formation [4]; the process which persists until the potential of *d* peak is reached.



The bipolaron formed at peak *d* reacts with water from the synthesis solution giving quinonic products which in the following scans will be responsible for new peak occurrence (peak *b* at +0.47 V/SCE [4]). Another impurity peak (*c*, *c'* at +0.54V SCE) is attributed in literature to the *para*-aminophenol/benzoquinonimine redox couple. Peak *f* with the cathodic pair *p'* was attributed to the benzidine/quinoid form of benzidine redox couple [5].

The cyclic voltammogram of poli-*orto*-metoxyaniline synthesis is similar to that for polyaniline synthesis (fig. 3).

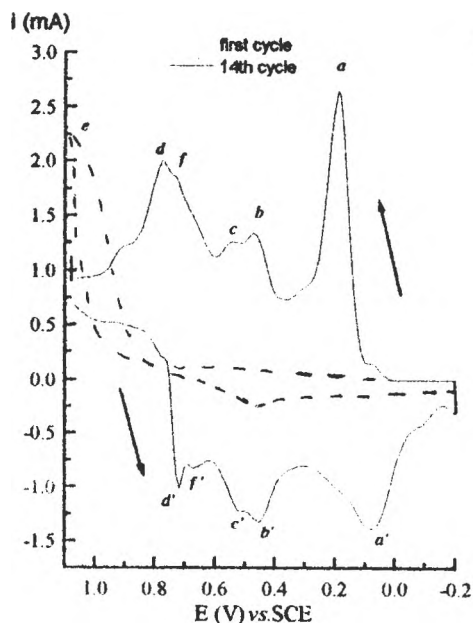


Fig. 2. Cyclic voltammogram for polyaniline electrosynthesis onto Pt electrode (127 mV s^{-1})

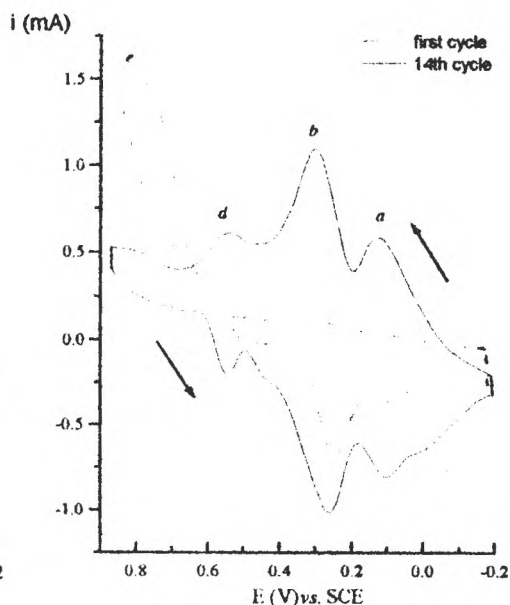


Fig. 3. Cyclic voltammogram for poly-*orto*-metoxyaniline electrosynthesis onto Pt electrode (127 mV s^{-1}).

Some differences however are to be outlined. First, a very large quinone impurities oxidation peak occurs at the poly-*ortho*-metoxyaniline electrosynthesis. These quinonic products are responsible for lowering the chemical and electrochemical activity of the polymer. Second, the region between the polaron and bipolaron peak formation, which is related to the electrochemical stability region of the polymer, is larger for polyaniline (0.58 V) compared to poly-*ortho*-metoxyaniline.

The air stability of the two polymers was monitored by conductivity measurements [6] in a close air containing box (fig. 4).

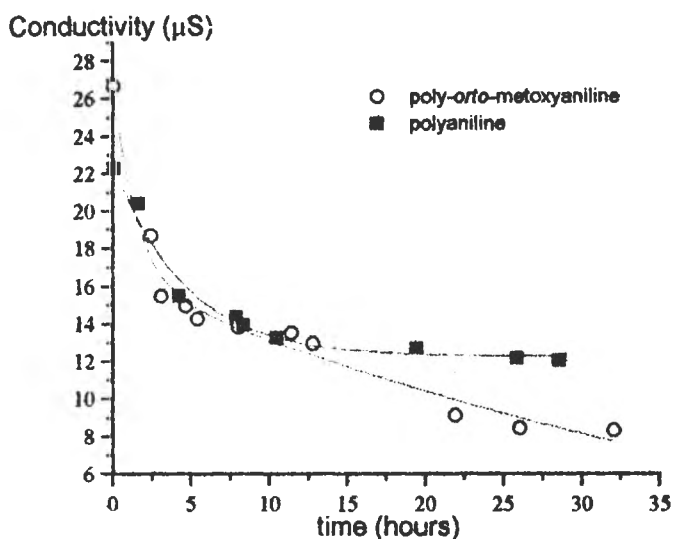


Fig.4. Air conductivity of polyaniline and poly-*ortho*-metoxyaniline.

One can see that the air deactivating process becomes insignificant for polyaniline after 10 hours, while for poly-*ortho*-metoxyaniline this process can still be observed even after times as large as 20 hours. The presence of the metoxy group could be the cause of this low air-stability of the polymer chain.

Figs. 5 and 6 show the cyclic voltammograms of the polymer films in sulphuric acid transfer solution at different scan rates. The peak separation of the first redox process for polyaniline is larger, and $i_{pa} > i_{po}$, indicating a low degree of voltammetric reversibility for this case. For the poly-*ortho*-metoxyaniline case, obtained in the same conditions (0.055M monomer, 1M H₂SO₄ synthesis solution) and having the same thickness ($Q_{\text{synthesis}} = 50 \text{ mC cm}^{-2}$), a peak splitting can be observed for the first redox process (fig 6), proving the existence of some non-homogeneities in the polymer film.

The peak separation (a, a'), ΔE_p , is about 45 mV, in agreement with Hubbard's theory for thin film reversible systems onto electrodes. This peak separation value is much smaller than the value corresponding to peaks (c, c') and is practically the same as for the polyaniline case.

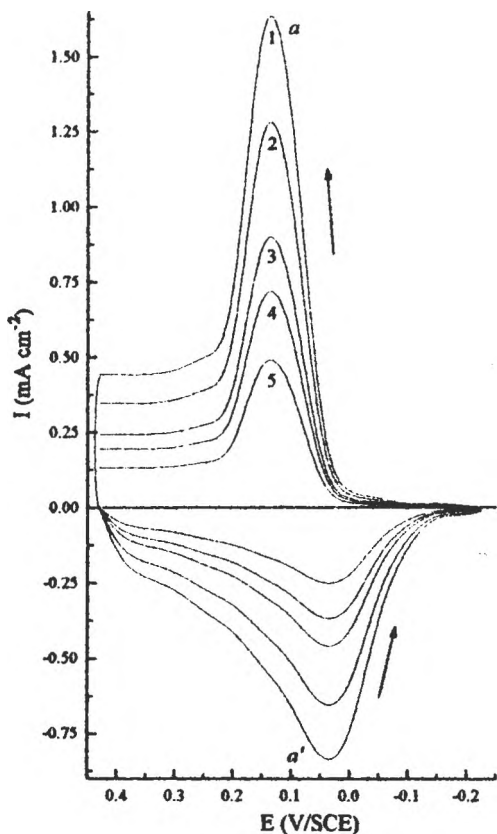


Fig. 5. Cyclic voltammograms for polyaniline film ($Q_{\text{synthesis}} = 66 \text{ mC cm}^{-2}$), onto Pt electrode in H_2SO_4 transfer solution ($H_0 = -1.76$), at different scan rates (mV s^{-1}); 1-16; 2-26; 3-32; 4-50; 5-65.

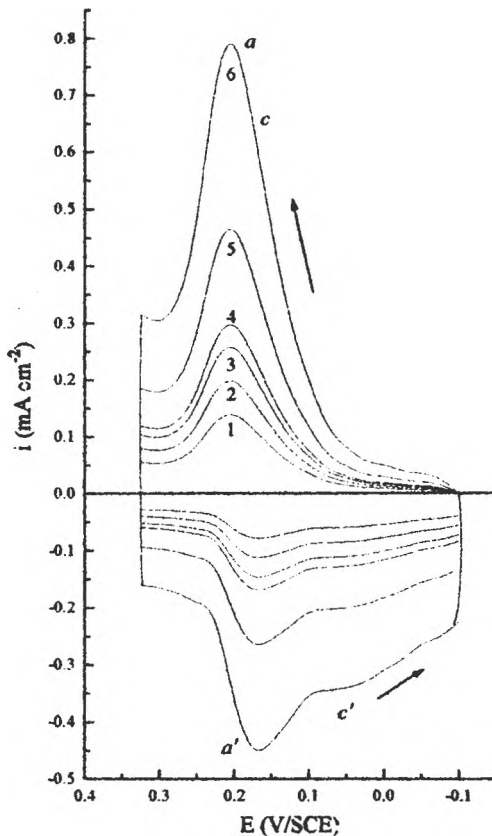


Fig. 6. Cyclic voltammograms for poly-ortho-metoxyaniline film ($Q_{\text{synthesis}} = 66 \text{ mC cm}^{-2}$), onto Pt electrode in H_2SO_4 transfer solution ($H_0 = -1.76$), at different scan rates (mV s^{-1}); 1-11; 2-14; 3-18, 3; 4-22; 5-31, 4; 6-55.

The peak pair (a, a') has $E^0 = 0,178 \text{ V/SCE}$, and the pair (c, c'), $E^0 = 0,11 \text{ V/SCE}$. Although the ΔE_p value for the (a, a') pair is small, still $i_{pa} > i_{pc}$.

Table 1 resumes the main voltammetric characteristics of the first redox process, (a, a') of the poly-ortho-metoxyaniline ($Q_{\text{synthesis}} = 50 \text{ mC cm}^{-2}$) in $1\text{M H}_2\text{SO}_4$ transfer solution.

Table 1. Main voltammetric characteristics of the first redox process, (a, a') of the poly-*ortho*-metoxyaniline ($Q_{\text{synthesis}} = 50 \text{ mC cm}^{-2}$) in 1M H_2SO_4 transfer solution

Scan rate (mV/s)	E_{pa} (V/SCE)	E_{pc} (V/SCE)	ΔE_p (V)	i_{pa} (mA/cm ²)	i_{pc} (mA/cm ²)
11,0	0,200	0,155	0,045	0,140	0,102
14,6	0,200	0,160	0,040	0,189	0,136
18,3	0,200	0,155	0,045	0,268	0,163
22,0	0,200	0,155	0,045	0,310	0,193
31,4	0,200	0,155	0,045	0,468	0,268
55,0	0,210	0,158	0,052	0,795	0,450

REFERENCES

1. A.F Diaz and J.A Logan, *J.Electroanal.Chem.*, **111**, 1980, 111.
2. A.F Diaz and J Castello, *J.Chem.Soc.Chem.Comm.*, 397, **1980**.
3. P.M.McMannus, S.C.Yang and R.J.Cushman, *J.Chem.Soc.Chem.Comm.*, 1556, **1985**.
4. D.E Stilwell and Su-Moon Park, *J.Electrochem.Soc.*, **135**, **1988**, 2254.
5. J Bacon and R.N.Adams, *J.Am.Chem.Soc.*, **20**, **1968**, 6596.
6. C Berggren Kriz, Eva Palqvist and D.Kriz, *Electrochim.Acta*, **40**, **1995**, 1063.

**THE INFLUENCE OF THE LIPOPHILIC SALT ADDED TO THE PVC-BASED
MEMBRANES UPON THE RESPONSE OF A MAGNESIUM-SELECTIVE
ELECTRODE**

Ileana Leoca, Ovidiu Pogăceanu, Ionel C. Ştefan, Emil Cordoş
RESEARCH CENTER FOR ANALYTICAL INSTRUMENTATION
Str. Donath nr.67, 3400 Cluj-Napoca
Tel.: 064/420590, Fax: 064/420667

ABSTRACT

The characteristics of a magnesium-selective electrode with a polymeric membrane and a self-made electrode body are presented. The membranes are based on PVC-HMW, with different plasticizers, N,N'-diheptyl-N,N'-dimethyl-1,4-butanediamide (ETH 1117) as a neutral ligand, and various amounts of lipophilic salt. The electrode exhibits a linear response in the concentration range 10^{-5} - 10^{-1} M Mg^{2+} with a slope of - 23,1 mV/decade. The selectivity coefficient is evaluated by the mixed solution method. The electrode has a good selectivity over sodium and potassium and presents considerable interference from calcium. The pH of the test solution influences the response over pH=10 and under pH=5. The response time, the reproducibility and the life time are also investigated and the results are presented.

INTRODUCTION

The ion-selective electrodes are widely used in clinical chemistry, bioelectrochemistry and industrial laboratories for their ease of handling, precision and short response time [1,2]. The polymeric membrane electrodes with ionophores like neutral macrotetrolide antibiotics or synthetic cyclic or noncyclic carriers as active components, for different alkaline and alkaline earth metal ions were developed in the last 30 years. In the last years there have been made considerable efforts to improve the characteristics of these electrodes by testing new kinds of membrane matrix, new types of ionophores and new designs for the electrodes. The research for the magnesium ion (sometimes called the "forgotten ion") and its interactions with the ligands and the development of magnesium-selective electrodes started later and was conducted in the laboratories of Prof. Wilhelm Simon [3,4]. The most inconvenient aspect of the magnesium electrode is the interference with calcium ion that can not be neglected excepting the intracellular

space where the calcium ion concentration is lower (10^{-6} M) and the magnesium ion concentration is around 10^{-3} M [5].

In this work we present the performances of a magnesium-selective electrode that consists of a self-made electrode body and a PVC-based membrane mounted at one end of the body. The presence of the lipophilic salt in the membrane is beneficial in respect with the facts that this additive reduces interferences by lipophilic anions, leads to changes in selectivity, is able to increase cation-sensitivity and lowers the electrical resistance of the membrane [6]. Our challenge was to find the best ratio between the amount of the lipophilic salt and the amount of the ionophore.

EXPERIMENTAL

Electrode body

The electrode body is made of a PVC tube. The inner reference electrode is a Ag/AgCl electrode. It is made by the electrolytical deposition of AgCl on a silver wire anode in a 10^{-1} M HCl solution at a current density of 8 mA/cm² for 30 minutes.

Membranes

The membranes were prepared from 2% ionophore (N,N'-diheptyl-N,N'-dimethyl-1,4-butanediamide (ETH 1117; Fluka), ca. 33% polyvinyl chloride high molecular weight (PVC-HMW; Fluka), 65% plasticizer (bis(2-ethylhexyl) adipate (DOA), or o-nitrophenyl octyl ether (o-NPOE); Fluka) and various amounts of additive (natriumtetrakis[3,5-bis(trifluoromethyl)phenyl]-borat dehydrate (C₃₇H₁₂BF₂₄Na); Merck) were completely dissolved in a mixture of ciclohexanone and tetrahydrofuran in a 2:8 ratio. The membrane solution was then poured in a glass ring on a glass plate and the solvent was allowed to evaporate. After the evaporation the membranes were cut and fixed at the end of the electrode body. Table 1 presents the compositions of the membranes prepared and tested.

E.m.f. measurements

The measurements were carried out with cells of the following type:

Hg; Hg₂Cl₂; saturated KCl solution; sample solution; membrane; 10^{-2} M Mg(NO₃)₂ solution saturated with AgCl; AgCl; Ag.

E.m.f. measurements were performed with a pH/mV-meter (IAMC Otopeni). As reference electrode a calomel electrode (Institutul de Chimie Cluj) was used.

The selectivity coefficients were determined by the mixed solution method, in the presence of a varying concentration of the determinand and a constant concentration of the interferent. The pH dependence was determined by varying the pH of a 10^{-3} M Mg(NO₃)₂ solution.

Sample solutions

The test solutions were prepared from a 1M Mg(NO₃)₂ stock solution, by serial dilution. We used distilled water and substances of a p.a. grade. For the pH dependence we used pH buffer solutions.

RESULTS AND DISCUSSION

The compositions of the membranes are presented in table 1. The last line presents the calculated slopes of the calibration curves, on the linear domain in the concentration range shown above.

Table 1 - The compositions of the tested membranes and their characteristics

Components; characteristics	Membranes						
	1	2	3	4	5	6	7
ETH 1117(%)	2	2	2	2	2	2	2
C ₃₂ H ₁₂ BF ₂₄ Na (mol%*)	0	10	15	20	33	50	70
DOA(%)						64	64
o-NPOE(%)	65	63	63	64	62		
PVC-HMW(%)	33	34	34	33	34	33	33
Detection limit	-	2,5.10 ⁻⁵	2,5.10 ⁻⁵	10 ⁻⁵	1,6.10 ⁻⁵	2,5.10 ⁻⁵	10 ⁻⁵
Linear concentration range (pMg)	2-4	1-5	1-5	1-5	1-5	1-4	1-4
Slope (mV/decade)	-8,8	-18,9	-21,9	-21,3	-23,2	-19,2	-17,3

*mol% of lipophilic salt relative to the ionophore ETH 1117

The following graphic presents the response curves of the electrodes prepared with the above described membranes.

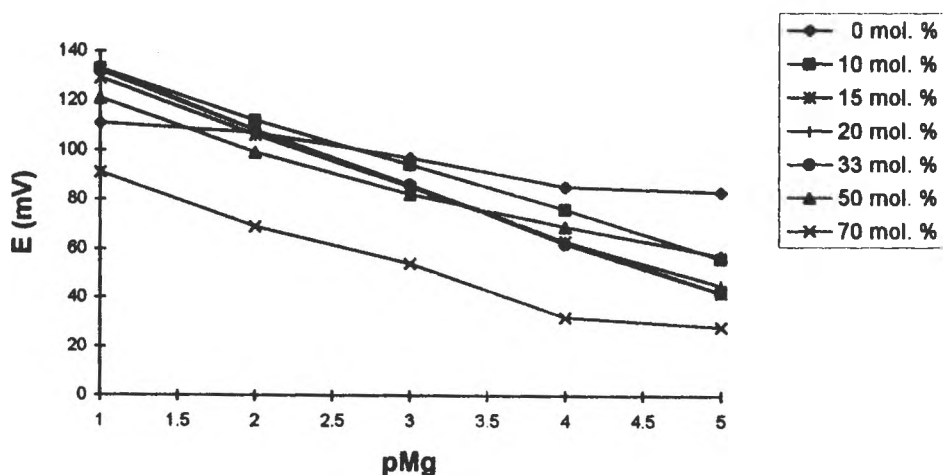


Fig. 1. Response curves of the electrodes based upon the membranes from table 1

We should notice that the membranes that approach the most the nernstian slope of 29,1 mV/decade (at 21°C) are the ones with a molar ratio between the lipophilic salt and the ionophore around 33%. Besides, from the former experiments we concluded that the polar plasticiser (o-NPOE) is better for the divalent cation Mg^{2+} because it has a higher dielectric constant than the nonpolar plasticiser (DOA), fact that is in agreement with the theory [7].

To use this electrode in biological samples we tested the selectivity against the most important interferences: Na^+ , K^+ , and Ca^{2+} . We used the mixed solution method. According to the Nikolski-Eisenmann equation:

$$E = E^0 + \frac{2,303 \cdot R \cdot T}{z_A \cdot F} \lg(a_A + K_{AB} \cdot a_B^{z_A/z_B})$$

the potential of the electrode in a solution is affected by the presence of the determinand ion (A) and interferent ion (B) as well. The selectivity constants were determined graphically and are summarised in the next table:

Table 2 - Selectivity constants of the magnesium electrode prepared with membrane number 5 from table 1

Interferent (B)	K_{AB}	$\lg K_{AB}$
Na^+	$2,48 \cdot 10^{-2}$	-1,61
K^+	$2,79 \cdot 10^{-2}$	-1,55
Ca^{2+}	15,01	1,17

Calcium presents a strong interference upon the response of the magnesium electrode. Hence, this electrode can not be used in solutions with a defined calcium ion concentration.

The influence of the pH of the solution was tested over the response of the magnesium electrode in a $10^{-3}M$ Mg^{2+} solution. The results are shown in the next graphic. In the pH range where the electrode presents considerable interference it is helpful to add an ionic strength adjuster both to samples and calibrating solutions to buffer the electrolytes to a level where there is no interference.

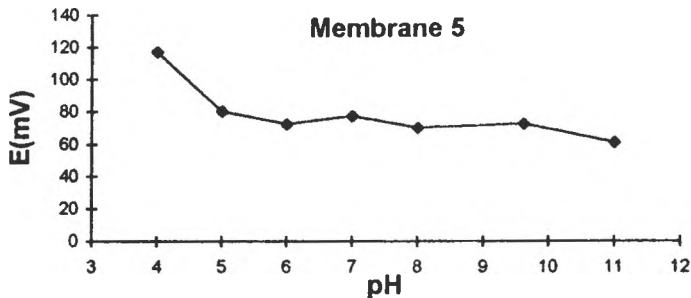


Fig.2. The pH influence over the response of a magnesium electrode in a 10^{-3} M Mg^{2+} solution

The response time (the time after which the e.m.f. reaches 95% from the equilibrium value) is very short, but increases slightly from 1-2 s in a 10^{-1} M Mg^{2+} solution to 10 s in a 10^{-5} M Mg^{2+} solution.

By immersing the electrode ten times in the same solution and washing it with distilled water between the measurements, the reproducibility is evaluated. The maximum relative standard deviation is 2,9% for the most diluted solution (10^{-5} M Mg^{2+}) and the minimum is 0,6% for the 10^{-1} M Mg^{2+} solution.

The short time stability evaluated by the drift of the electrode immersed in a 10^{-2} M Mg^{2+} solution for three hours is 1mV/hour.

The long time stability is evaluated by the drift of the electrode in solutions of different concentrations, and by the change in the slope of the calibration curve during time. The results are presented in figure 3 and table 3, respectively.

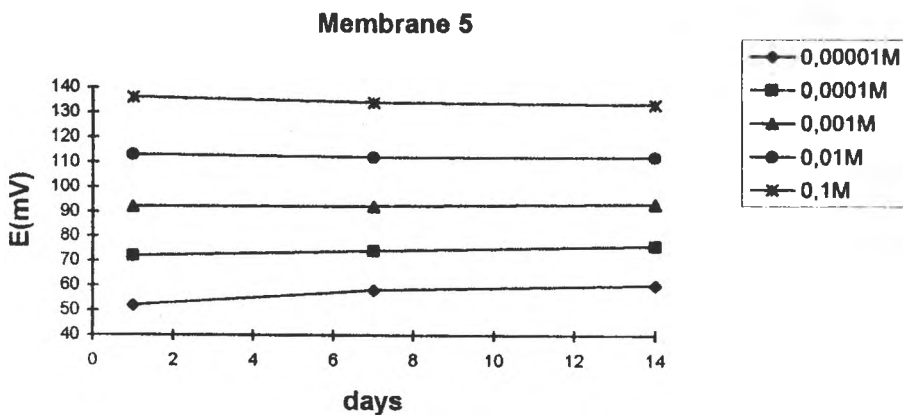


Fig.3. Long time stability of the potential in different Mg^{2+} solutions

Table 3 - Long time stability of the magnesium electrode

Membrane	Slope(mV/decade)	Slope(mV/decade)	Slope(mV/decade)
	Day 1	Day 7	Day 14
5	-23,2	-21,4	-20,02

CONCLUSIONS

This paper outlined the main characteristics of a magnesium-selective electrode with a PVC-based membrane and the ionophore ETH 1117 that was for the first time studied by Prof. W. Simon's research team [10]. The electrode exhibits a nearly nernstian slope, has a good selectivity over sodium and potassium, but is strongly influenced by the presence of calcium ion. The response time, the reproducibility and the short and long time stability are good. This electrode can be used properly to determine the magnesium ion concentration in solutions with a calcium ion concentration more than three orders of magnitude lower.

REFERENCES

1. G.H. Fricke, *Anal. Chem.*, 1980, **52**, 259R-275R
2. R.L. Solsky, *Anal. Chem.*, 1988, **60**, 106R-113R
3. U.E. Spichiger, *Electroanalysis*, 1993, **5**, 739-745
4. M.Huser, P.M. Gehrig, W.E.Morf, W.Simon, E.Lindner, J.Jeney, K.Toth, E.Pungor, *Anal. Chem.*, 1991, **63**, 1380-1386
5. T. Buhner, P. Gehrig, W. Simon, *Anal. Sci.*, Dec.1988, **4**, 27-32
6. D. Ammann, E. Pretsch, W. Simon, E. Lindner, A. Bezegh, E. Pungor, *Anal.Chim.Acta*, 1985, **171**, 119-129
7. R.D.Armstrong, G.Horvai, *Electrochimica Acta*, 1990, 135(1),1-7
8. Y. Umezawa, K. Umezawa, H. Sato, *Pure & Appl. Chem.*, 1995, **67**(3), 507-518
9. U. Spichiger, R. Eugster, W.Simon, *Anal. Chem.*, 1993, **65**, 689-695
10. D.Erne, N.Stojanac, D.Ammann, P.Hofstetter, E.Pretsch, W.Simon, *Helv. Chim. Acta* 1980, **63**, 2271-2275

THE RESPONSE OF A MODIFIED PVC-BASED pH ELECTRODE

Ileana Leoca, Ionel C. Ștefan, Emil Cordoș

RESEARCH CENTER FOR ANALYTICAL INSTRUMENTATION

Str. Donath nr.67, 3400 Cluj-Napoca

Tel.: 064/420590, Fax: 064/420667

ABSTRACT

The characteristics of the H⁺-selective electrodes with modified PVC-based membranes and self-made electrode body are presented. The membranes are based on PVC-COOH and PVC-OH, with different plasticizers, tridodecylamine as a neutral ligand, and potassium tetrakis(4-chlorophenyl)borate as a lipophilic salt. The electrodes exhibit a linear response in the pH range 4 - 10 with a slope of - 55 mV/decade. The selectivity coefficients are evaluated by the fixed interference method. The electrodes have a good selectivity over sodium and potassium but membranes with o-NPOE as plasticizer have a shorter linear response range due the stronger anion interference at low pH values.

INTRODUCTION

In the past 10 years much research has been done in the field of pH measurements using polymeric membrane electrodes [1, 2], even though the traditional pH glass electrodes exhibit outstanding response characteristics. However, in certain applications, the pH-sensitive glass electrodes have shown some disadvantages, such as extremely high resistance of glass microelectrodes as well as the problem of integrating the glass membrane into a multisensor array. In contrast, polymeric membrane electrodes do not suffer from these limitations.

Most of the polymeric membranes of pH sensitive electrodes are PVC-based membranes because PVC, especially PVC-HMW (poly(vinyl chloride) high molecular weight), is a very good matrix for these membranes. It is chemically inert, cheap and easy to use. However, in some cases modified PVCs (aminated PVC (PVC-NH₂), carboxylated PVC (PVC-COOH) and hydroxylated PVC (PVC-OH)) are beneficial as matrices compared with PVC-HMW [3, 4].

Our final goal is to make planar ion-selective electrodes, so the adhesion properties of membrane matrix to the support are very important for the life time of these electrodes. It is known that modified PVCs have better adhesion properties than PVC-HMW, so we have tested the performances of some PVC-

COOH and PVC-OH-based membranes with three different plasticizers: bis(2-ethyl-hexyl)-sebacate (dioctyl-sebacate, DOS), bis(2-ethyl-hexyl)-adipate (dioctyl-adipate DOA) and 2-nitrophenyl-octyl-ether (o-NPOE). Our challenge was to find the optimum composition for a modified PVC-based membrane.

EXPERIMENTAL

Electrode body

The electrode body is made of a PVC tube. The inner reference electrode is a Ag/AgCl electrode. It is made by the electrolytical deposition of AgCl on a silver wire anode in a 10^{-1} M HCl solution at a current density of 8 mA/cm^2 for 30 minutes.

Membranes

The polymeric ion-selective membranes usually contain four components: a polymeric matrix, a plasticizer, an ionophore and a lipophilic salt. We used the classic proportion of components: 33% polymer, 64-66% plasticizer, 1% ionophore and 70 mol.% (compared to the ionophore) lipophilic salt [3]. As polymeric membrane materials we used carboxylated PVC (PVC-COOH, with 1,8% COOH groups) Fluka 81395, and hydroxylated PVC (PVC-OH), a copolymer of 91% vinyl chloride, 3% vinyl acetate and 6% vinyl alcohol, Fluka 27827. As plasticizers, we tested bis(2-ethyl-hexyl)-sebacate (dioctyl-sebacate, DOS) (Fluka 84818), bis(2-ethyl-hexyl)-adipate (dioctyl-adipate, DOA) (Fluka 02138) and 2-nitrophenyl-octyl-ether (o-NPOE) (Fluka 73732). Tridodecylamine (TDDA) (Fluka 95292) was used as an ionophore and potassium tetrakis(4-chlorophenyl)borate (KTPCIPB) as a lipophilic salt. There were tested all possible combinations between polymers and plasticizers. The membrane components were completely dissolved in a mixture of cyclohexanone and tetrahydrofuran in a 1 : 4 ratio. The membrane solution was then poured in a glass ring on a glass plate and the solvent was allowed to evaporate. After the evaporation the membranes were cut and fixed at the end of the electrode body.

E.m.f. measurements

Emf measurements were carried out with a pH/mV-meter (IAMC Otopeni). As reference electrode a saturated calomel electrode (Chemistry Institute Cluj-Napoca) was used.

The selectivity coefficients were determined by the fixed interference method using pH buffer solutions with a constant concentration of interferent ion.

Buffer solutions

To determine the pH sensitivity, the response range, the detection limit and the selectivity coefficients pH buffer solutions were used. The compositions of these solutions are given in the Table 1.

Table 1. Buffer solutions

pH	Substances at 100 ml solution
1,1	4,8ml disodic citrate 0,1M + 95,2ml HCl 0,1N
2,15	0,252g oxalic acid + 0,1gKHCO ₃
3	40,3ml disodic citrate 0,1M + 59,7ml HCl 0,1N or 20,55ml Na ₂ HPO ₄ 0,2M + 79,45ml citric acid 0,1M
4	10ml NaOH 1N + 56,8ml acetic acid 1N or 38,55ml Na ₂ HPO ₄ 0,2M + 61,45ml citric acid 0,1M
5	3,6ml NaOH 0,1N + 96,4ml disodic citrate 0,1M or 51,5ml Na ₂ HPO ₄ 0,2M + 48,5ml citric acid 0,1M
6	10ml NaOH 1N + 10,4ml acetic acid 1N or 63,15ml Na ₂ HPO ₄ 0,2M + 36,85ml citric acid 0,1M
7	61,2ml Na ₂ HPO ₄ 1/15M + 38,8ml KH ₂ PO ₄ 1/15M sau 82,35ml Na ₂ HPO ₄ 0,2M + 17,65ml citric acid 0,1M
8	96,9ml Na ₂ HPO ₄ 1/15M + 3,1ml KH ₂ PO ₄ 1/15M
9,18	0,3812g borax
10	0,84g NaHCO ₃ + 1,06g Na ₂ CO ₃
11	0,168g NaHCO ₃ + 1,908g Na ₂ CO ₃

RESULTS AND DISCUSSION

The compositions of the membranes are presented in Table 2. The calibration curves for the electrodes with these membranes are shown in the graphs of Fig. 1. The last line of Table 2 presents the calculated slopes of the calibration curves, on the linear domains in the concentration range shown above.

Table 2 - The compositions of the tested membranes and their characteristics

Components; characteristics	Membranes					
	1	2	3	4	5	6
TDDA (%)	1	1	1	1	1	1
KTpCIPB (%)	0,7	0,7	0,7	0,7	0,7	0,7
PVC-COOH (%)	33	33	33	-	-	-
PVC-OH (%)	-	-	-	33	33	33
DOS (%)	65,3	-	-	65,3	-	-
DOA (%)	-	65,3	-	-	65,3	-
o-NPOE(%)	-	-	65,3	-	-	65,3
Detection limit (pH)	10	10,5	11	10	10	11
Linear response range (pH)	3-10	3-10	4-11	3-10	3-10	1-11
Slope (mV/decade)	-53,61	-55,05	-54,23	-52,33	-54,74	-53,33

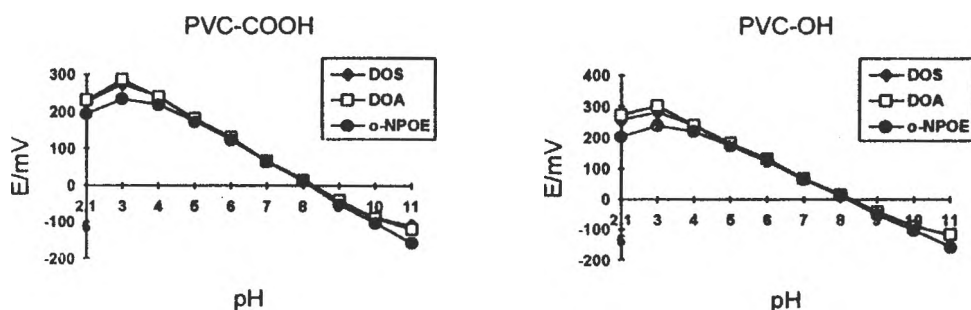


Fig.1. Calibration curves of the electrodes based upon the membranes from table 1

We should notice that all membranes have a linear response at pH values between 4 and 9, so that all are able to be used as membranes for H^+ -selective electrodes. However, PVC-OH - based membranes can hardly be used because of their bad mechanical properties, eventually it is indicated a mixture with

PVC-HMW. Besides, their characteristics are a little worse than those of PVC-COOH - based membranes, they have a lower sensitivity and a shorter linear range. So, although the PVC-OH - based membranes have a little better adhesion than PVC-COOH - based membranes, the other properties of these membranes make them less suitable as electrode membranes.

But the greatest influences on the membranes' characteristics are given by plasticizer. o-NPOE has the highest polarity and the highest dielectric constant of all used plasticizers ($\epsilon_r=21$), so it is expected that the characteristics of o-NPOE plasticized membranes be different. And indeed, it can be noticed that for both polymers the linear range is shorter at low pH values for o-NPOE plasticized membranes than for the other membranes, with at least a pH unit. That means a Donnan failure at rather high pH values and a strong anion interference in acidic solutions [5]. In compensation, the linear range is extended in alcalin solutions till pH=11.

The selectivity of these membranes over alcalin ions, Na^+ și K^+ , was tested by the fixed interference method. In the graphs of Fig. 2 are presented the responses of the PVC-COOH - based membrane electrodes in solutions with a constant concentration of Na^+ or K^+ , and in Fig. 3 the same tests for PVC-OH based membrane electrodes.

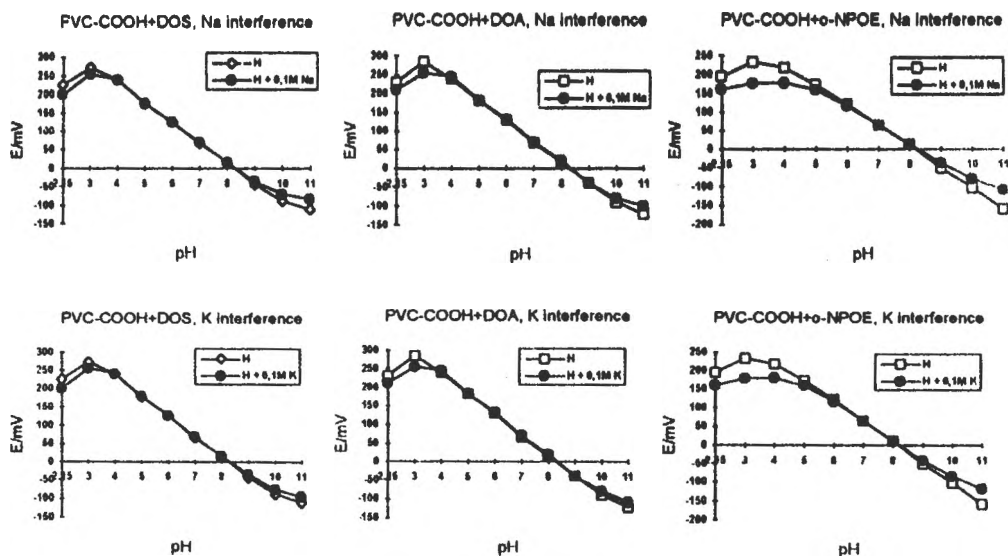


Fig. 2. Selectivity tests for PVC-COOH - based membrane electrodes

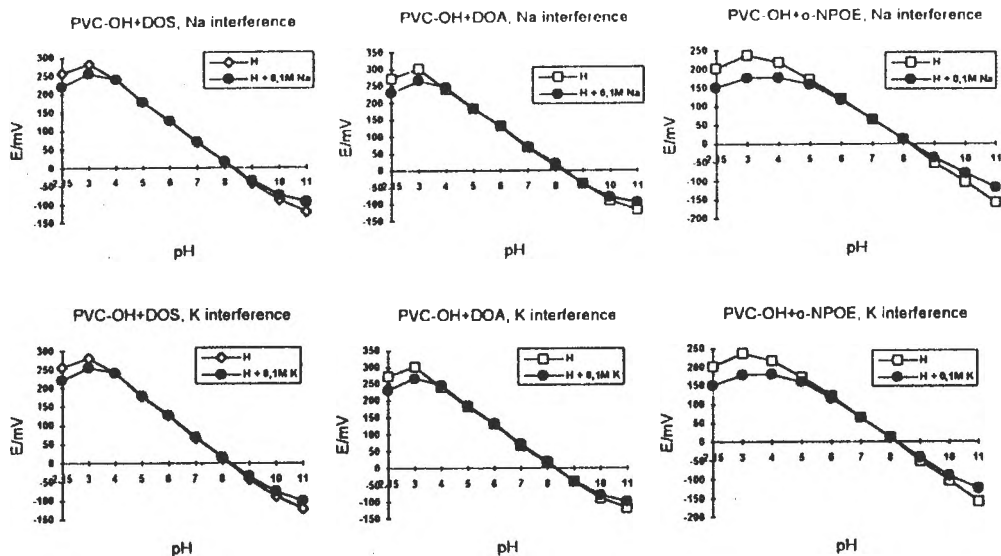


Fig. 3. Selectivity tests for PVC-OH - based membrane electrodes

From the above graphs it can be seen that the response of the electrodes is affected both in acidic and basic solutions, but the responses in acidic solutions are affected identically for both Na⁺ and K⁺ selectivity tests. That means that these deviations are due the anion (Cl⁻) interference, which the same concentration in all solutions. Again, this interference is stronger for o-NPOE plasticized membranes.

The potential of an ion-selective electrode is in accord with Nikolski-Eisenmann equation:

$$E = E^0 + \frac{2,303 \cdot R \cdot T}{z_A \cdot F} \lg(a_A + K_{AB} \cdot a_B^{z_A/z_B})$$

So, the potential of the electrode in a solution is affected by the presence of the determinand ion (A) and interferent ion (B) as well. The selectivity constants were determined by calculation and are summarised in the next table:

Table 3 - Selectivity constants of the H⁺-selective electrodes

Plasticizer Polymer	Na ⁺ interference			K ⁺ interference		
	DOS	DOA	o-NPOE	DOS	DOA	o-NPOE
PVC-COOH	1,73x10 ⁻⁹	1,35x10 ⁻⁹	1,82x10 ⁻⁹	1,16x10 ⁻⁹	1,11x10 ⁻⁹	1,23x10 ⁻⁹
PVC-OH	2,03x10 ⁻⁹	1,75x10 ⁻⁹	2,12x10 ⁻⁹	1,66x10 ⁻⁹	1,41x10 ⁻⁹	1,73x10 ⁻⁹

From these data it can be noticed that the selectivity is better over K^+ ions than over Na^+ ions but all values of selectivity constants are very small. These values are comparable with those for pH sensitive glass membrane electrodes, so the modified PVC based membrane electrodes can be used at least for the same purposes like glass membrane electrodes.

CONCLUSIONS

This paper outlined the main characteristics of modified PVC based membrane H^+ -selective electrodes. The electrodes exhibit a nearly nernstian slope and have a good selectivity over sodium and potassium. From our experiments we can conclude that PVC-COOH based membranes have good analytical and mechanical performances and can be used for ion-selective electrodes. O-NPOE is less indicated as plasticizer for H^+ -selective electrodes and DOS or DOA should be used for the best performances.

REFERENCES

1. U. Oesch, Z. Brzozka, A. Xu, b. Rusterholz, G. Suter, H.V. Pham, H. Welti, D. Ammann, E. Pretsch, W. Simon, *Anal. Chem.*, 1986, **58**, 2285-2289
2. V.V. Egorov, Y.F. Lushchik, *Talanta*, 1990, **37**(5), 461-469E.
3. Lindner, V.V. Coşofreţ, R.P.Kusy, R.P. Buck, T. Rosatzin, U. Scaller, W. Simon, J. Jeney, K. Toth, E. Pungor, *Talanta*, 1993, **40**(7), 957-967
4. V.V. Coşofreţ, T.M. Nahir, E. Lindner, R.P. Buck, *J.Electroanal.Chem.*, 1992, **327**, 137-146
5. S.C. Ma, N.A. Chaniotakis, M.E. Meyerhoff, *Anal. Chem.*, 1988, **60**, 2293-2299
6. D. Ammann, F. Lanter, R.A. Steiner, P.Schultess, Y.Shijo, W. Simon, *Anal. Chem.*, 1981, **52**, 2267-2269

ELECTROCHEMICAL STUDY OF VANADIUM CONTAINING KEGGIN -TYPE HETEROPOLYTUNGSTATE AND HETEROPOLYMOLYBDATE ACIDS

Alexandra Fodor*, Liana Muresan**, A. Suteu*** and I.C. Popescu**

**Facultatea de Medicina si Farmacie, Universitatea Oradea, 3700 Oradea, Romania*

***Facultatea de Chimie si Inginerie Chimica, Universitatea Babes-Bolyai, 3400 Cluj-Napoca, Romania*

****Facultatea de Energetica, Universitatea Oradea, 3700 Oradea, Romania*

ABSTRACT

Cyclic voltammetric measurements were performed in acidic media (0.5 M Na₂SO₄ + H₂SO₄) in the pH range 1-3 and at different voltage scan rates for H₅[PW₁₀V₂O₄₀]·24H₂O, H₆[PMo₁₀V₂O₄₀]·30H₂O and H₅[SiMo₁₀V₂O₄₀]·25H₂O on Pt electrodes. The features of the W/Mo oxo-cage electrochemical activity were found in accordance with the previously reported data, in spite of the deleterious effect of hydrogen evolution reaction on Pt electrode. An electrochemical reversible wave was observed for V. Its formal redox potential is shifted towards more negative potentials as compared with the VO₂⁺ / VO₂²⁺ couple and is more influenced by the nature of the central heteroatom (P, Si) as by the transition metal (W, Mo) from the peripheral octahedra. Thus, changing the identity of the central heteroatom, (P with Si), a slight shift of the formal potential of the [XMo₁₀V₂O₄₀]ⁿ⁺ / [XMo₁₀V₂O₄₀]⁽ⁿ⁻¹⁾⁺ redox couple was observed, while the replacement of W from the host oxo-matrix with Mo, practically does not change the formal potential of the [PM₁₀V₂O₄₀]⁵⁻ / [PM₁₀V₂O₄₀]⁶⁻ redox couple.

INTRODUCTION

Heteropolyacids and their salts have been studied extensively owing to their interesting catalytic properties [1]. Several metal-substituted heteropolyoxometalates have been the subject of electrochemical studies in order to investigate their electrochemical [2-7] or electrocatalytical [8-16] behavior.

A class of these compounds, presenting a Keggin structure with mixed addenda, is represented with the general formula [XM₁₀V₂O₄₀]^{m-}, where X is a tetrahedral coordinated heteroatom such as P or Si and M is a transition metal (W, Mo). Taking into account that vanadium could modify the redox activity of parent anions with single species addenda, [XM₁₂O₄₀]ⁿ⁻, it might be expected that this class of polyoxometalates will offer new possibilities to perform electrocatalytical processes.

The aim of this paper is to study the electrochemical behavior of three vanadium substituted heteropolyacids: H₅[PW₁₀V₂O₄₀]·24H₂O (I), H₆[PMo₁₀V₂O₄₀]·30H₂O (II) and H₅[SiMo₁₀V₂O₄₀]·25H₂O (III). Cyclic voltammetric measurements, performed in different experimental conditions, allowed us to obtain information about the electrochemical reversibility of the involved redox processes and the pH dependence of the corresponding formal potentials.

EXPERIMENTAL

Reagents

$H_5[PW_{10}V_2O_{40}] \cdot 24H_2O$, $H_6[PMo_{10}V_2O_{40}] \cdot 30H_2O$ and $H_7[SiMo_{10}V_2O_{40}] \cdot 25H_2O$ were synthesized by a modification of the Kokorin's method [17-21] using the following molar ratios between the reagents: for compound (I) $NaH_2PO_4/NaVO_3/Na_2WO_4 = 1: 10: 5$, for compound (II) $Na_3PO_4/NaVO_3/Na_2MoO_4 = 1: 6: 10$ and for compound (III) $Na_2SiO_3/NaVO_3/Na_2MoO_4 = 1: 1.5: 5$. The three heteropolyacids were separated by double ether extraction and recrystallised at room temperature in darkness.

All chemicals were reagent grade and used as received. 0.5 M buffer solutions (pH = 1-3) were prepared from Na_2SO_4 (Reactivul Bucuresti) and H_2SO_4 (Merck). All solutions were prepared with distilled water. Their pH was measured with a combined glass electrode (Metrohm, Switzerland) and a digital pH-meter (MV-Präcitronic, GDR).

Electrochemical experiments

Electrochemical experiments were performed using a potentiostatic set-up consisting of a potentiostat (PS 3 Meinsberg, GDR), a signal generator (PV2 Meinsberg, GDR) and a XY-recorder (Endim 620.02, Meinsberg, GDR). A conventional three electrodes cell was used. The working electrode was a Pt disk ($\phi=5$ mm). The reference electrode was a saturated calomel electrode (SCE). The Pt counter electrode was separated from the test solution by a glass frit. All measurements were performed at room temperature.

RESULTS AND DISCUSSIONS

The voltammograms for the three vanadium containing heteropolyanions are presented in figures 1 and 2.

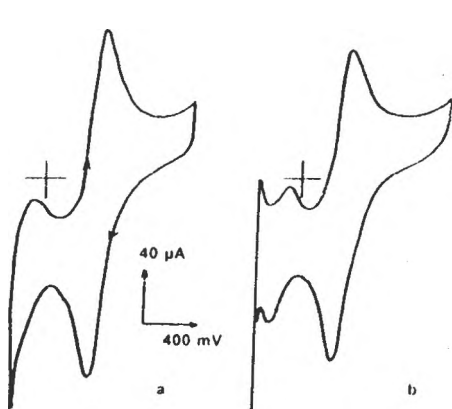


Figure 1. Cyclic voltammograms of 0.5 mM $H_5[PW_{10}V_2O_{40}]$ a) pH =1.2; b) pH =2.4; Experimental conditions: supporting electrolyte, 0.5M Na_2SO_4 ; scan rate 100 mV/s

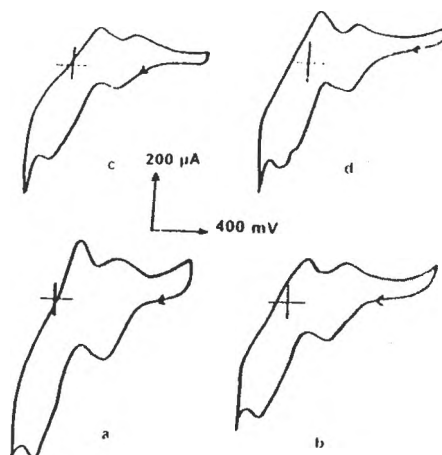


Figure 2. Cyclic voltammograms of 0.5 mM $H_6[PMo_{10}V_2O_{40}]$ (a, b) and of 0.5 mM $H_6[SiMo_{10}V_2O_{40}]$ (c, d); (a) and (c), pH =1.7; (b) and (d), pH =2.5. Experimental conditions as in figure 1.

Irrespective of the compound identity, at least two reduction waves and the corresponding reoxidation waves are observed. Thus, for compound (I), due to the low overpotential for the hydrogen evolution reaction (HER) on Pt electrode, the more negative potential wave, clearly visible at pH =2.5 (figure 1b), is not completely developed at pH 1.2 (figure 1a). The one electron wave ($\epsilon^0 = -0.17$ V/SCE) was identified with the most positive wave of the three waves set characterizing, as previously reported in [2,6,16], the oxidation/reduction of the tungsten-oxo cage. The wave with $\epsilon^0 = 0.37$ V/SCE was attributed to $V^{VI/V}$ couple from (I). The negative shift of about 300 mV existing between the formal redox potential corresponding to VO_2^+/VO_2^{2+} couple [22] and that for $[PW_{10}V_2O_{40}]^{5-}/[PW_{10}V_2O_{40}]^{6-}$ is due to its insertion in the tungsten-oxo cage [2].

The comparison of the redox behavior of compound (I) (fig.1) and compound (II) (fig. 2a and b) shows that the replacement of W from the host oxo-matrix with Mo, does not change the formal potential of the $[PM_{10}V_2VO_{40}]^{5-}/[PM_{10}V_2VO_{40}]^{6-}$ redox couple (table 1), as was pointed out also for other Keggin-type anions [6]. In the same time, the reduction waves corresponding to molybden-oxo cage appear at more positive potentials than those corresponding to tungsten-oxo cage (figures 1 and 2a, b) [6].

Table 1. Formal redox potentials for $[XM_{10}V_2VO_{40}]^{m-}/[XM_{10}V_2VO_{40}]^{(m+1)-}$ couple for the investigated compounds

Compound	ϵ^0 , V/SCE
$H_5[PW_{10}V_2O_{40}]$	0.35*
$H_5[PMo_{10}V_2O_{40}]$	0.41*
$H_5[SiMo_{10}V_2O_{40}]$	0.36*

*estimated from the recorded voltammograms (fig. 1, 2) as an average, for pH 1.2-2.4

However, changing the identity of the central heteroatom, (P with Si), a slight shift of the formal potential of the $[XMo_{10}V_2VO_{40}]^{m-}/[XMo_{10}V_2VO_{40}]^{(m+1)-}$ redox couple was observed (figure 2c and d compared with 2a and b). This effect was attributed to the difference between the overall ionic charge of the two corresponding anions [6, 13].

Beside the $[XM_{10}V_2VO_{40}]^{m-}/[XM_{10}V_2VO_{40}]^{(m+1)-}$ wave, the other waves existing in the voltammograms for compounds (II) and (III), were attributed to oxidation-reduction of molybdenum-oxo cage, more or less overlapped with HER [16]. As expected, the position of these waves is influenced by the nature of the heteroatom, being shifted towards more negative potentials with the increase of the overall ionic charge [6].

The cyclic voltammograms recorded for the three compounds at different scan rates and constant pH, showed that the peak potentials (ϵ_p) for $[XM_{10}V_2VO_{40}]^{m-}/[XM_{10}V_2VO_{40}]^{(m+1)-}$ were independent of the voltage scan rate in the range 0.01-0.1 $V \cdot s^{-1}$, suggesting reversible or quasi-reversible electron transfer. Taking into account that, irrespective to the scan rate, $\Delta\epsilon_p$ is slightly higher than $0.059/n$ V [18] and that $i_{p,a}/i_{p,c} \approx 1$, it is most probable that the redox process corresponding to vanadium couple involves one electron and is quasi-reversible.

On the other hand, for all compounds, the V^{VIV} current peaks are proportional to the square root of the voltage scan rate in the range 0.01-0.1 $V \cdot s^{-1}$, as can be seen in figure 3 for compound (I), indicating that the electrode process is diffusior controlled.

The compounds (I)-(III) are stable in aqueous media in the investigated pH range [4]. As previously reported [5-7, 24], protons are involved in V^{VIV} redox process for all investigated compounds. The ϵ^0 value for V^{VIV} couple is linearly dependent on pH as can be seen in figure 4 for compound (III). The slopes of ϵ^0 vs pH plots (table 2) show a H^+/e^- ratio of about 1.5/1, in the investigated pH range. It is interesting to note that the slopes of ϵ^0 vs. pH plots are, in the limit of experimental errors, almost identical and are corresponding to parallel lines. This shows once again, that the oxo cage has an influence upon the ϵ^0 for V^{VIV} couple.

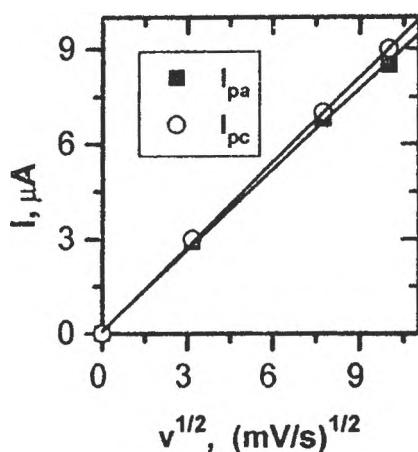


Figure 3. Anodic ($I_{p,a}$) and cathodic ($I_{p,c}$) peak currents vs. square root of scan rate ($v^{1/2}$) corresponding to V^{VIV} redox couple in $H_5[PW_{10}V_2O_{40}]$

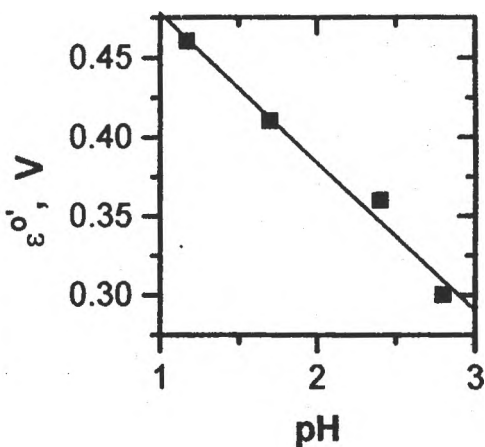


Figure 4. pH dependence of formal redox potential for (V^{VIV}) couple in $H_6[SiMo_{10}V_2O_{40}]$.

Table 2. Dependence on pH of the formal redox potentials for V^{VIV} couple in the investigated compounds

Compound	$\Delta \epsilon^0 / \Delta pH$ (V/pH)	<u>Correlation coefficient</u> no. of points
$H_5[PW_{10}V_2O_{40}]$	0.074	<u>0.940</u> 4
$H_5[PMo_{10}V_2O_{40}]$	0.084	<u>0.969</u> 4
$H_6[SiMo_{10}V_2O_{40}]$	0.093	<u>0.990</u> 4

CONCLUSIONS

Cyclic voltammetric measurements were performed in acidic media (0.5 M Na₂SO₄ + H₂SO₄) in the pH range 1-3 and at different voltage scan rates for H₅[PW₁₀V₂O₄₀]·24H₂O, H₆[PMo₁₀V₂O₄₀]·30H₂O and H₅[SiMo₁₀V₂O₄₀]·25H₂O, on Pt electrodes. The features of the W/Mo-oxo cage electrochemical behavior were found in accordance with the previously reported data, in spite of the deleterious effect of hydrogen evolution reaction on Pt electrode. An electrochemical reversible wave was observed for V. Its formal redox potential is shifted towards more negative potentials as compared with the VO₂⁺/VO²⁺ couple and is more influenced by the nature of the central heteroatom (P, Si) as by the transition metal (W, Mo) from the peripheral octahedra.

REFERENCES

1. M.T. Pope, "Heteropoly and Isopoly Oxometalates", Springer, Berlin, 1983
2. C. Rong and M.T. Pope, *J. Am. Chem. Soc.*, 1992, **114**, 2932
3. J.C. Bart and F.C. Anson, *J. Electroanal. Chem.*, 1995, **390**, 11
4. H. Wang, Z. Yu and E. Wang, *J. Electroanal. Chem.*, 1995, **380**, 69
5. S. Himeno, K. Maeda, T. Osakai, A. Salto and T. Hori, *Bull. Chem. Soc. Jpn.*, 1993, **66**, 109
6. K. Maeda, H. Katano, T. Osakai, S. Himeno and A. Saito, *J. Electroanal. Chem.*, 1995, **389**, 167
7. A.M. Bond, J.B. Cooper, F. Marken and D.M. Way, *J. Electroanal. Chem.*, 1995, **396**, 407
8. O. Savadogo and D.L. Piron, *Int. J. Hydrogen Energy*, 1990, **15**, 715
9. B. Keita, L. Nadjo, G. Krier and J.F. Muller, *J. Electroanal. Chem.*, 1987, **223**, 287
10. O. Savadogo and S. Levesque, *J. Appl. Electrochem.*, 1991, **21**, 457
11. B. Keita, L. Nadjo and J.M. Saveant, *J. Electroanal. Chem.*, 1988, **243**, 105
12. P. Wang, Y. Li, *J. Electroanal. Chem.*, 1996, **408**, 77
13. J.E. Toth and F.C. Anson, *J. Am. Chem. Soc.*, 1989, **111**, 2444
14. P.J. Kulesza, G. Rosnolek and L.R. Faulkner, *J. Electroanal. Chem.*, 1990, **280**, 233
15. S. Dong and M. Liu, *J. Electroanal. Chem.*, 1994, **372**, 94
16. C. Rong and F. Anson, *Inorg. Chem. Acta*, 1996, **242**, 11
17. A.I. Kokorin and N.A. Polotebnova, *Zhur. Obsehehei Khim.*, 1954, **24**, 967
18. A.I. Kokorin and N.A. Polotebnova, *Zhur. Obsehehei Khim.*, 1954, **24**, 1573
19. A.I. Kokorin and N.A. Polotebnova, *Zhur. Obsehehei Khim.*, 1954, **24**, 1718
20. A.I. Kokorin and N.A. Polotebnova, *Uchenye Zapiski Kishinev Univ.*, 1953, **6**, 63
21. A.I. Kokorin and P.L. Diamant, *Zhur. Obsehehei Khim.*, 1954, **24**, 971
22. M.S. Antelman, "The Encyclopedia of Chemical Electrode Potentials", Plenum Press, N. York, 1982
23. R.S. Nicholson, I. Shain, *Anal. Chem.*, 1964, **36**, 706
24. B. Keita, L. Nadjo, *J. Electroanal. Chem.*, 1987, **227**, 7 and references cited therein

ELECTROCHEMICAL PROCESSES AT THE $\text{Cu}_6\text{PS}_5\text{I}$
ELECTROLYTE INTERFASE.

S.K.Kovach, Yu.M.Stasyuk, V.V.Panyko.

Uzhgorod State University, Pidgirna, 46, 249000, Uzhgorod, Ukraine.

ABSTRACT.

The copper-selective electrode based on $\text{Cu}_6\text{PS}_5\text{I}$ stable in H_2SO_4 -medium was developed. The Nernstian response of electrode remains in the range of concentration $10^{-1} - 10^{-5}$ M CuSO_4 at $\text{pH}=0$. The detection limit, selectivity coefficients and long-time stability were determined. Electrochemical investigation demonstrated, that $\text{Cu}_6\text{PS}_5\text{I}$ electrode behaved as the semiconductor of p-type.

INTRODUCTION.

Binary chalcogenides are widely used as materials of the ion-selective electrodes [1]. The chemical stability of common chalcogenides in the acidic media is limited because of decomposition in it. The chemical stability of complex chalcogenides is higher than of common one, especially for the complex chalcogenides containing elements with covalent bonds. Recent time we have been investigating the electrochemical properties of "argyrodite"-family materials with general formula [2] $\text{A}_{(12-n-m)}\text{BX}_{(6-x)}\text{Y}_x$ (A-Cu,Ag,Cd,Hg; B - Si, Ge, Sn; X - S, Se, Te; Y- Cl, Br, I; $0 < x < 1$). Results of these investigations [3 -5] opened the possibility of using argyrodite-family materials as membrane of ion-selective electrodes. The electrochemical properties of the copper-selective electrode based on $\text{Cu}_6\text{PS}_5\text{I}$ will be discussed.

RESULTS AND DISCUSSION.

Electrode characteristics were investigated in the 0.1M H_2SO_4 -medium. The Nernstian response of the electrode remained in the range of the concentration $10^{-1} - 10^{-5}$ M CuSO_4 at $\text{pH}=0$ and slope was 28 ± 2 mV/decade (Fig. 1).

Fig. 1. Calibration curve of $\text{Cu}_6\text{PS}_3\text{I}$ - electrode in the CuSO_4 solutions at $\text{pH}=0$ ($0.5 \text{ M H}_2\text{SO}_4$).

The detection limit of Cu (II) was $8 \times 10^{-6} \text{ M}$. Selectivity coefficients of electrodes were determined by two-solution method. The results of measures are presented in table 1.

The experiments demonstrated that monocrystalline membrane was not corroded in the H_2SO_4 -medium and only oxidants destroyed the electrode response. Investigations of long-term stability of copper-selective electrode in this medium showed that the slope of Nernstian response slightly decreased within time (1000 hours).

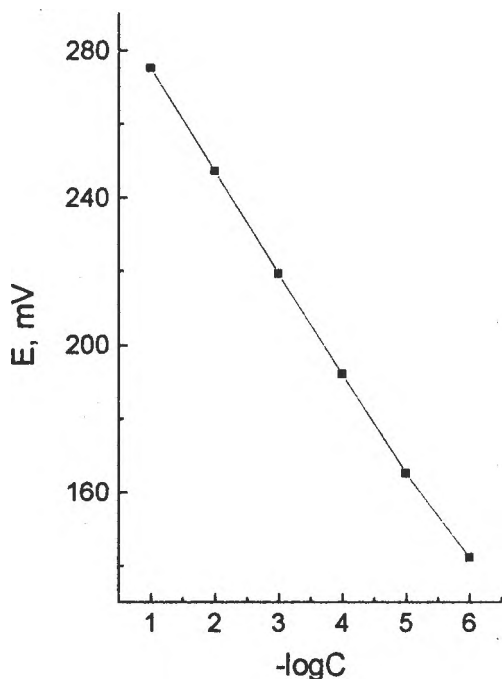


Table 1. Selectivity coefficients of $\text{Cu}_6\text{PS}_3\text{I}$ -electrode.

Ion Me	Fe^{2+}	Co^{2+}	Ni^{2+}	Zn^{2+}	Cd^{2+}	Mn^{2+}	Al^{3+}	Fe^{3+}
log K	-3.00	-4.04	-4.14	-4.82	-4.10	-4.80	-3.89	0.70

Current-voltage investigation in the solution of different concentration of Cu(II) demonstrated that the $\text{Cu}_6\text{PS}_3\text{I}$ -electrode behaved as the p-type semiconductor.

The anodic current did not limited by electrochemical process and the electrode in this case showed a property of simple resistor. Specific resistivity was measured on linear segment of current-voltage curve (Fig. 2).

In the cathodic region of the cyclic voltammogram the current saturation was observed, that transformed into cathodic maximum when concentration of Cu(II) in the solution was increased (Fig. 2). Potential of this maximum move into cathodic direction with increasing of the scanning rate (Fig. 3) and of the concentration of Cu(II) (Fig. 2).

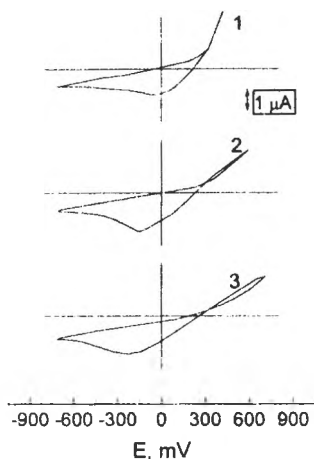


Fig. 2. Current-voltage curves of $\text{Cu}_6\text{PS}_5\text{I}$ -electrode in the solutions contained 10^{-3} M Cu(II) (1), 10^{-2} M Cu(II) (2), 10^{-1} M Cu(II) (3) at the H_2SO_4 -medium.

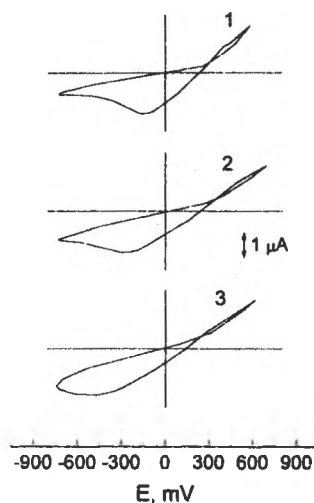


Fig. 3. Current-voltage curves of $\text{Cu}_6\text{PS}_5\text{I}$ -electrode with 20 mV/s (1), 40 mV/s (2), 80 mV/s (3) scanning rates. The electrolyte is 0.01 M $\text{CuSO}_4/0.5$ M H_2SO_4 .

On the basis of the experimental results we can conclude that the $\text{Cu}_6\text{PS}_5\text{I}$ -electrode is the copper-selective electrode and is stable in H_2SO_4 -medium. Equilibrium between $\text{Cu}_6\text{PS}_5\text{I}$ and solution containing Cu(II) is reversible. Cyclic voltammograms demonstrate, that electrochemical reaction is not the limiting process. The electrode behaves the semiconductor of p-type. These results are in accordance with the investigations in organic solution [6].

EXPERIMENTAL

$\text{Cu}_6\text{PS}_5\text{I}$ single crystals were grown by chemical vapor transport method in a closed silica tube. The transporting agent was copper iodide. The temperature of the transport and growth zones were, respectively, 670-750 and 600-700°C. Red and dark-red crystals ($3 \times 5 \times 5 \text{ mm}^2$) were obtained. Chemical and phase composition of the obtained crystals were controlled by chemical and X-ray analyses. The ion-selective electrodes were constructed by mounting of single crystals on the top of PVC-tube by means of epoxy resin. The crystals used in the experiments were plates with an area $3\text{-}5 \text{ mm}^2$.

Potential of the ion-selective electrode was measured using silver-chloride double-junction reference electrode. Electrochemical experiments were performed in a three-electrode cell with silver-chloride double-junction electrode as a reference electrode and platinum counterelectrode. Current-voltage characteristics were obtained with a potentiostat P-5827M and registered on a XY-Recorder-A3. Electrochemical cell was thermostated by water thermostat UTU-4.

REFERENCES

1. K. Camman, *Springer-Verlag, Berlin-Heidelberg-New-York*, 1977, 283.
2. W. F. Kuhs, R. Nitsche, K. Sheunemann, *Mat. Res.Bull.*, 14, 1979, 241-248.
3. S. Kovach, A. Kokhan, S. Motrya, *Europacat-1, Montpellier September, 12-17, 1993*, 734.
4. S. Kovach, A. Kokhan, Yu. Voroshilov, *Ukrainski Khim. Zhurnal, (Ukr.)* 59, 1993, 396-398.
5. S. Kovach, S. Motrya, E. Semrad, *Electrokhimiya (Russ.)*, 28, 1992, 1000-1005.
6. G. Betz, H. Tributsch, S. Fiechter, *J. Electrochem. Soc.*, 1984, 640-644.

CYCLIC VOLTAMMETRY STUDY OF POWDER SULFIDE ORES DISSOLUTION

M. Buda, N. Ibris, Mariana Pali[†] and T. Visan

*Dept. of Appl. Phys. Chem. and Electrochem., "POLITEHNICA" University,
Bucharest, Roumania*

Mining Research and Design Institute, Baia Mare, Roumania

ABSTRACT

The results of cyclic voltammetry experiments concerning the electrochemical behaviour of galena, pyrite and chalcopyrite powders in the flotation solutions are presented. The sulfide ore particles were immobilized in a paraffin film onto the electrode surface of PIGE (paraffin impregnated graphite electrodes). The presence of xanthate ion in these alkaline solutions has required a distinct voltammetric study using various cathodic limits of potentials. The corresponding mechanisms for electrochemical dissolution of sulfide ores are proposed in agreement with previous literature data for acid dissolution. The occurrence of several current peaks on both anodic and cathodic branches was also discussed.

INTRODUCTION

The main interest in electrochemical studies of sulfide minerals under conditions similar to those used in flotation arises from the information such studies provide concerning the mechanism of separation and dissolution (leaching). The oxidative leaching of galena, pyrite and chalcopyrite is an important step in the hydrometallurgical extraction of metals from their ores. Moreover, pyrite, FeS_2 , is frequently present in coal, so that the wet cleaning of coal leaves behind aqueous slurries of refuse containing millions tons of pyrite per year. The recent application of stripping voltammetry for analysis of solid sulfides used as pigments (sulfides of mercury, cadmium, silver, arsen, etc.) showed the importance of knowing their electrochemical spectra for archeologists, art restores, criminologists and other researchers.

In mining industry the sulfide mineral flotation is performed in a solution with complex composition, each component having a specific role in this process. An example of the usual content in flotation reagents is given in Table 1.

Table. 1 Composition of the flotation solution used in the treatment of roumanian sulfide ores (mainly, galena, pyrite and chalcopyrite ores).

Substance	Concentration (M)	PbS	FeS ₂	CuFeS ₂
Na ethylxanthate	2.3×10^{-4}	x	x	x
Ca(OH) ₂	1.3×10^{-2}	x	x	x
CuSO ₄	2×10^{-3}		x	
Na ₂ SO ₃	9.4×10^{-4}			x
Na ₂ S ₂ O ₃	1×10^{-3}		x	x
NaCN	9.4×10^{-4}	x	x	x
K ₂ Cr ₂ O ₇	2.3×10^{-3}	x	x	x
ZnSO ₄	4.1×10^{-3}			x
Na ₂ S	8.6×10^{-3}	x		x
Na ₂ CO ₃	9.4×10^{-3}	x		

Because powder materials are always involved in the flotation processes a variety of electrodes were developed. Among these, the paste electrodes (especially carbon paste electrodes) were employed in many electrochemical investigations [1]. Other approach to study the electrochemical behaviour of powder solids included the immobilization of small solid particles in a paraffin film onto the electrode surface. The most satisfying results were obtained using PIGE electrodes [2,3] (paraffin - impregnated graphite electrodes) where even traces of solid samples (less than 1µg, for example) could be transferred. The paraffin is an electric insulator which does not alter the shape of voltammograms; it is also an easily handled and cheap material, so that an advantage of PIGE electrodes is the low cost of manufacture.

In this paper we present the cyclic voltammetry investigation of galena, pyrite and chalcopyrite dissolution in various compositions of the flotation solution. Both anodic and cathodic processes in these alkaline media are investigated and qualitatively interpreted.

EXPERIMENTAL

PIGE electrodes were prepared as previously described in literature [2,3]. A spectral graphite rod (6 mm in diameter) was dipped for several seconds in molten paraffin in order to obtain an adherent non-conductive film. Separately, small amount of powder ore was distributed on a glass plate with a spatula to produce a finely dispersed spot. The bottom disc surface of PIGE was rubbed and pressed gently onto that spot to transfer the sulfide particles (about 0.5 - 1 mg) in the paraffin film and to contact the graphite body; a supplementary shaking or wiping on a clean filter paper provided the removal of non-adherent particles. The electrode surface can easily renewed after each experiment by vigorously rubbing on emery paper to remove the remaining sample or reaction products. The procedure of paraffin film deposition on the fresh graphite surface was taken again.

Cyclic voltammetric experiments were performed at 25°C using conventional instrumentation

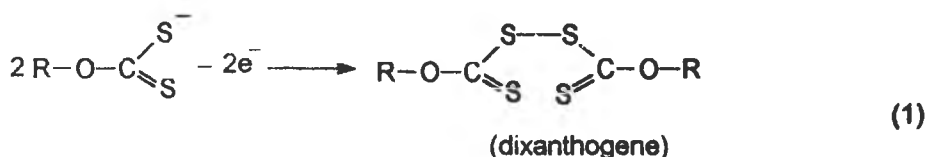
(PAR Model 173 potentiostat, pulse generator, X - Y recorder). The reference electrode was a saturated calomel electrode (SCE) whereas the counterelectrode was a cylindrical Pt sieve around PIGE. Because the surface area of adherent powder grains on PIGE electrode is difficult to be established, the cyclic voltammograms have on the ordinate axis an arbitrary current.

The electrolytes used contained various components of flotation solution depending on the nature of mineral. The pH value measured using a pH - meter was usually 12.5.

RESULTS AND DISCUSSION

The use of xanthate as flotation collectors for sulfide minerals is due to their surface - active properties and capacity of oxidation on a hydrophobic surface. Firstly, we have performed a series of cyclic voltammetric experiments with simple graphite electrodes in the absence of paraffin film and without mechanically attached mineral. Figure 1 shows several obtained voltammograms using a simple component solution of ethylxanthate, i.e. a 2.34×10^{-4} M solution of Na ethylxanthate (pH = 7.5). Starting from low negative values of cathodic limit, a distinct oxidation peak (A_1) is observed during the forward scan in the positive potential direction. No peak was registered at the reverse scan in cathodic direction.

The oxidation peak at 0.52 - 0.58 V on these voltammograms may be attributed to the electrochemical dimerization of xanthate ion according to the process:



The presence of this peak at about the same value as the potential scan is changed from 30 to 100 mV/s suggested a predominantly diffusion control.

However, a large anodic shift (of about 600 mV), in the oxidation peak occurs when the cathodic limit of potential scan is extended at potentials where H_2 evolution takes place (Figure 2). The anodic overpotential of xanthate discharge is surely explained in terms of partial blocking, of the graphite porous surface due to adsorbed H_2 molecules.

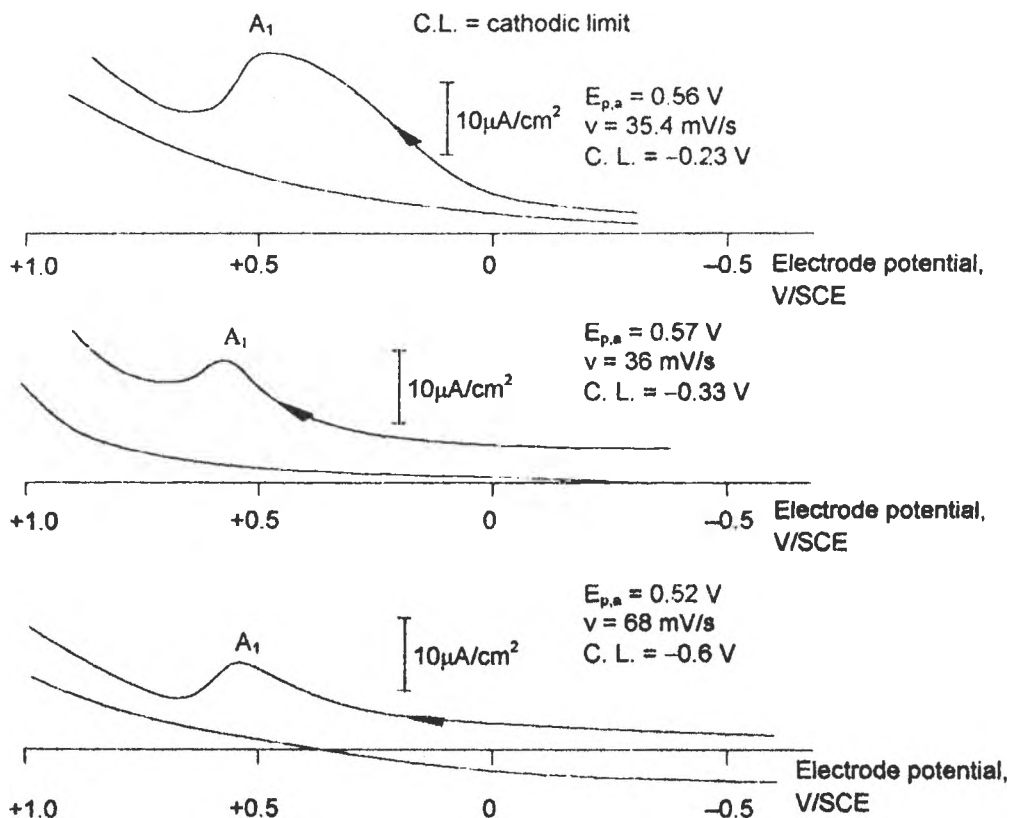


Fig. 1. Cyclic voltammograms of xanthate solution (2.34×10^{-4} M, pH = 7.5)

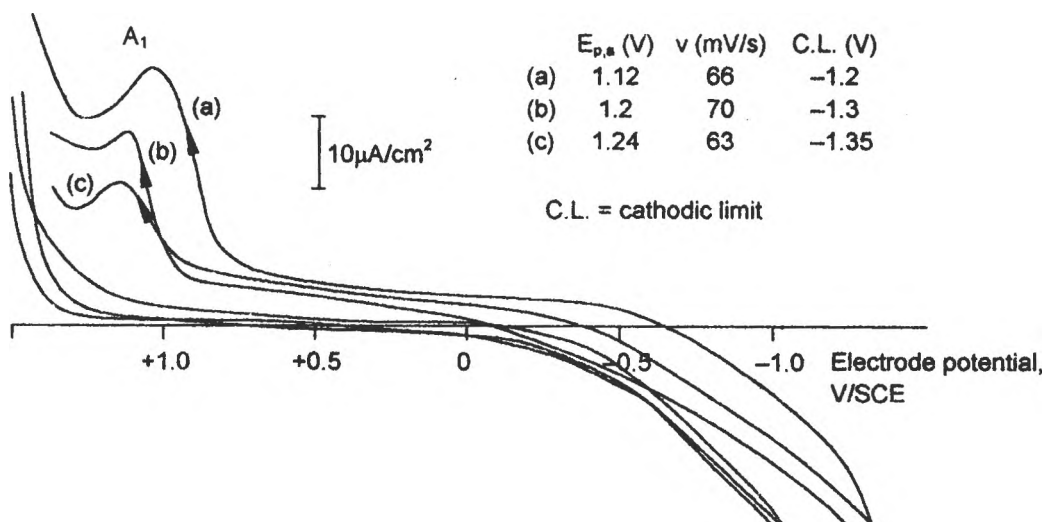


Fig. 2. Cyclic voltammograms of xanthate solution (2.34×10^{-4} M, pH = 7.5)

Figure 3 presents comparatively two voltammograms obtained using the flotation solution in the absence (curve 1) and presence (curve 2) of xanthate ions. The measured pH value (of 12.5) was not significantly influenced by the change in composition but remarkable differences both on anodic and cathodic branches of voltammograms were noticed.

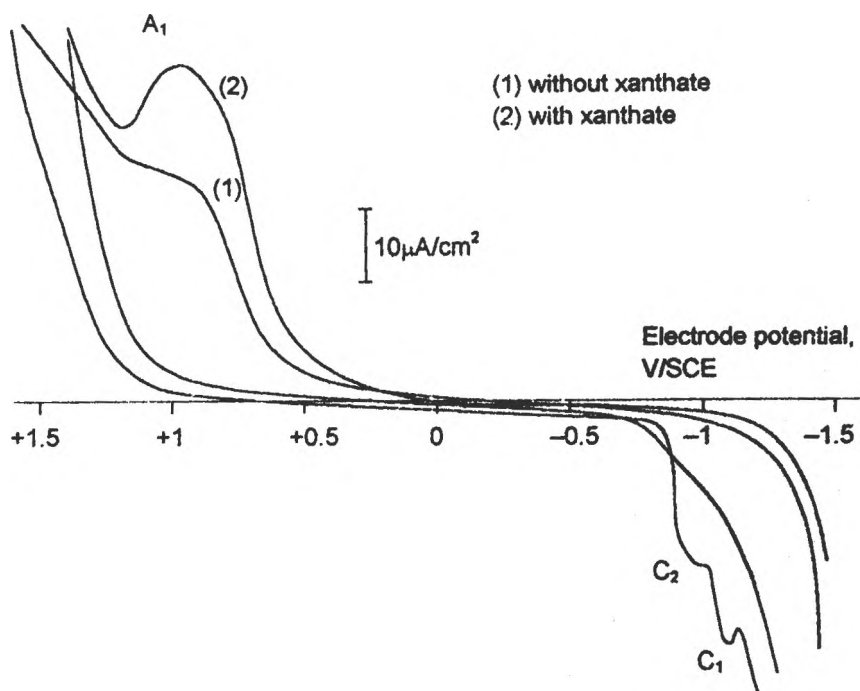


Fig. 3. Cyclic voltammograms of solutions containing flotation reagents without (1) and with (2) xanthate

So, in the absence of ethylxanthate the current rises gradually as the potential is anodically changed until the peak of O_2 evolution was reached. A pre-peak of adsorption of resulted oxygen was sometimes obtained. In a flotation solution containing ethylxanthate the corresponding oxidation peak, above discussed, occurs at about the same potential values as in single xanthate solutions, being followed by the increasing of current due to oxygen evolution.

On the other hand, a reverse situation is concerning about the cathodic branches: the curve for solution without xanthate (curve 1) exhibits clearly one peak C

(or a couple of peaks C_1 and C_2) whereas the formation of dixanthogene in the second solution impedes the occurrence of any cathodic processes until hydrogen discharge at very negative potential. The lack of cathodic peaks on curve 2 suggests a strong adsorption of dixanthogene on graphite surface.

In the following the results of using PIGE electrodes with small amounts of galena, pyrite or chalcopyrite will be discussed. The interpretation of electrochemical processes will be done in agreement with the mechanisms described in literature (usually for the behaviour in acid media).

Behaviour of galena electrode

A number of authors have studied the electrochemical behaviour of galena electrode, in acid media [4-7]. A detailed investigation in alkaline media was undertaken by Lamache *et al.* [8-11].

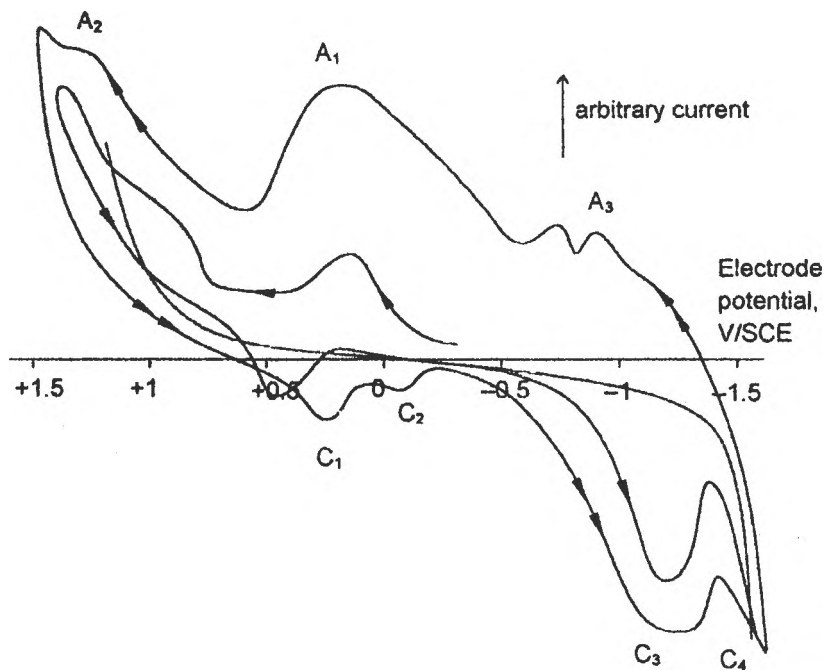


Fig. 4 Cyclic voltammogram of galena electrode in the flotation solution (see Table 1)

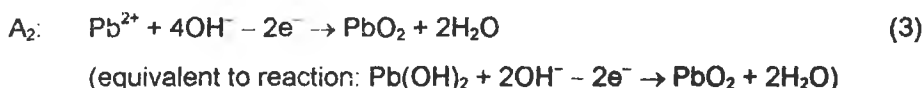
In the voltammogram presented in Figure 4 the electrochemical behaviour of galena particles was investigated within "the window of potentials" between oxygen and hydrogen evolution. Starting from stationary potential in anodic direction two peaks

were recorded. The first peak (A_1) clearly represents the anodic dissolution of galena

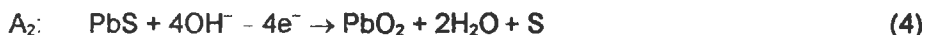


and its mechanism contains a step of xanthate chemisorption, as has been demonstrated by Richardson and O'Dell [12]. These authors showed that ethylxanthate can be chemisorbed on galena and complexed over a narrow potential range between -0.4 and -0.2 V. This is in excellent agreement with the position of peak A_1 in our records.

The second peaks (A_2) correspond to a transition at a high oxidation state of lead, described either by equation:



or by directly oxidation:

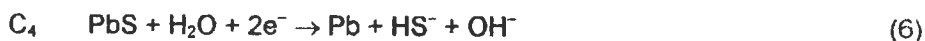


The electrochemical production of PbO_2 (probably in a hydrated form of $\text{PbO}_2 \cdot n\text{H}_2\text{O}$) may favour its solubilization by a chemical reaction with calcium hydroxide present in solution in high concentration; a solution of calcium plumbate, $\text{CaPb}(\text{OH})_6$, may occur.

In the cathodic direction, after the O_2 reduction peak (C_1) and a small peak of xanthate desorption (C_2), the next two cathodic processes are attributed to the following reactions: sulfur reduction



and galena reduction at cathodic limit of voltammogram:



So, in the proposed mechanism both anodic and cathodic electrochemical decomposition of galena was presumed.

During the second scan the appearance of two new anodic peaks was related to the electrochemical formation of $\text{Pb}(\text{OH})_2$ (peak A_3) and polysulfides (peak A_4). The occurrence of $\text{Pb}(\text{OH})_2$ may be described by the reaction:



Systematic studies of the influence of scan rate and pH changes has demonstrated a relatively high irreversibility of the main peaks A_1 and C_2 : the peak potentials are shifted when the scan rate increases from 60 mV/s to 300 mV/s, whereas the decreasing of pH from 12.6 at 7.2 and even 2.5 produced a drastic reduction in the intensity of peak current (especially for C_2). The repetitive deposition/dissolution of metallic lead according to the processes proposed for the peaks C_4 and A_3 has been demonstrated by performing the voltammograms in a narrower range, of negative potentials (Figure 5).

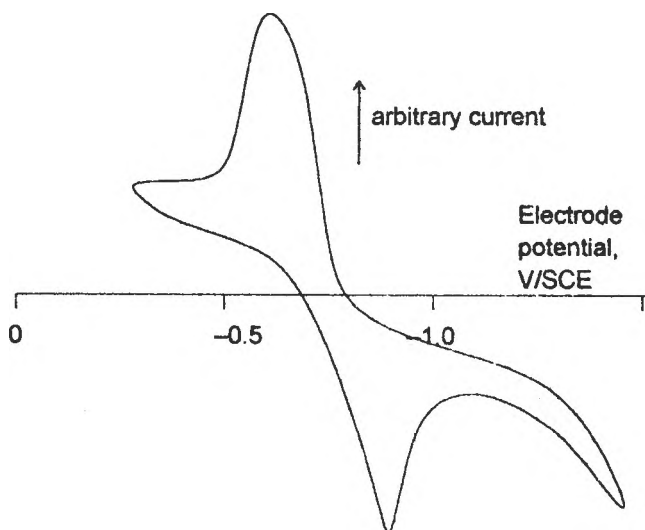


Fig. 5. Cyclic voltammogram of galena electrode in a narrower range of potential

The characteristic features of the voltammogram from this figure suggest a relatively reversible deposition/dissolution process, although the cathodic and anodic reactions are not exactly the same.

Behaviour of pyrite electrode

The pyrite is the most common of the sulfide minerals and its electrochemical oxidation is frequently studied in acid media [13]. Therefore, by using the alkaline flotation solution our study extends the existing knowledge of pyrite anodic behaviour. From typical voltammogram illustrated by Figure 6 it can be seen that the first scan starting either anodically or cathodically from the steady state potential shows the absence of any peak; only an abruptly increasing of cathodic current occurs, due to the pyrite electrochemical dissolution:

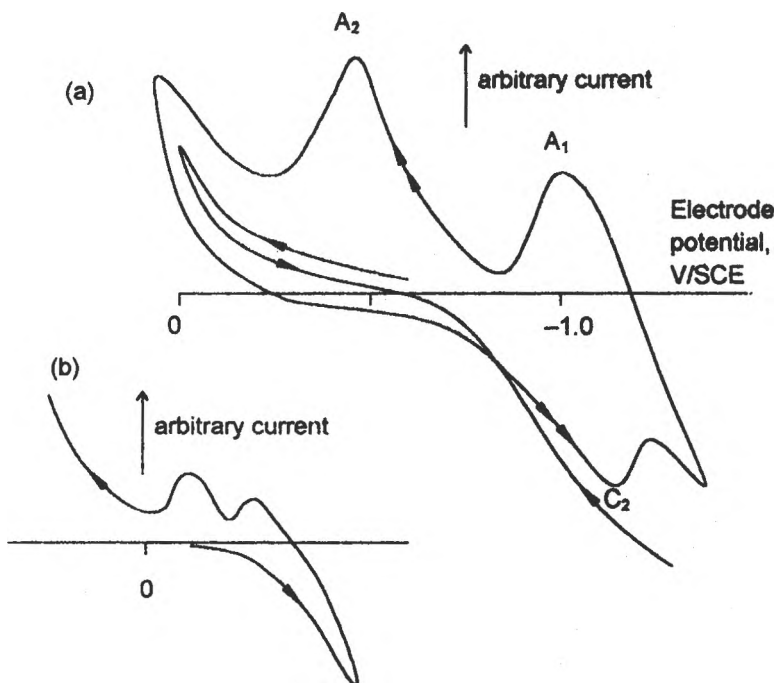
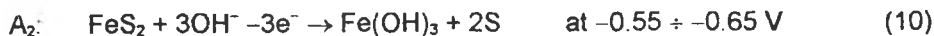


Fig. 6. Cyclic voltammograms of pyrite electrode
 (a) first scan anodically, (b) first scan cathodically

At subsequent scanning, other two anodic peaks were observed in the region of negative potentials. The following electrochemical reactions were proposed:





The peak A_2 may be also described in terms of electrochemical corrosion mechanism given in literature [13].



Nevertheless, we consider that the first equation is more plausible, because it requires a transfer of less number of electrons ($3e^-$ instead of $15e^-$). Furthermore, the diffusion control of the anodic process was demonstrated by using the chronoamperometric technique and obtaining the $i - t^{-1/2}$ straightlines passing through origin.

On the cathodic branch of voltammogram from Figure 6 a new peak is also evidenced at -0.8 V , which may be assumed to the process:

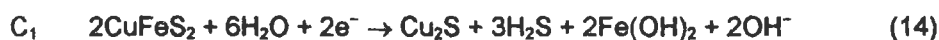


It is supposed that in the presence of basic medium of flotation the ferrous hydroxide is easily converted into soluble hydroxide iron compounds (ferrates) according to reaction:



Behaviour of chalcopyrite electrodes

Since chalcopyrite dissolution is the primary step in many hydrometallurgical processes for copper extraction it is important to establish which processes take places in alkaline media. In spite of previous results that indicated a slow dissolution rate and even a passivation of chalcopyrite particles [14], the typical voltammogram showed in Figure 7 exhibits relative high values of both anodic and cathodic current responses. The electrochemical process attributed is as follows:



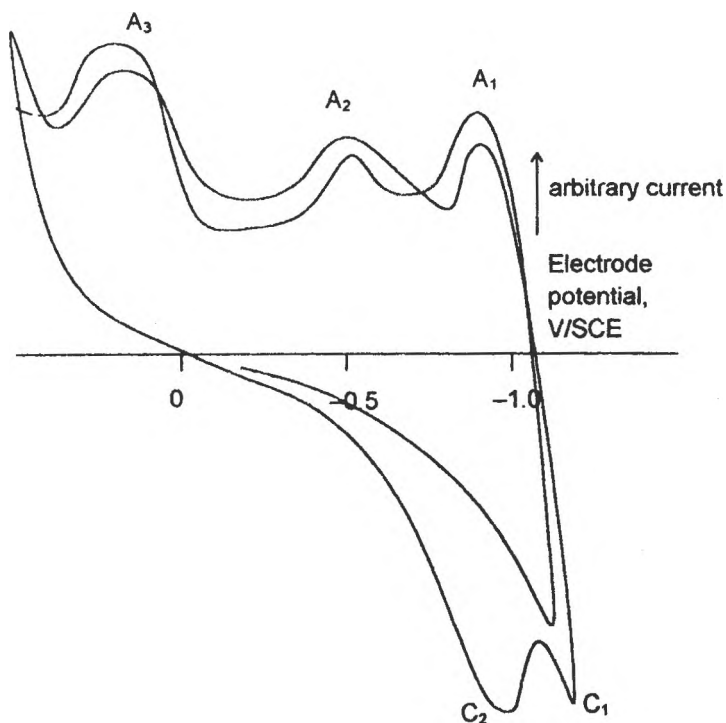
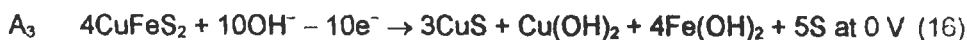
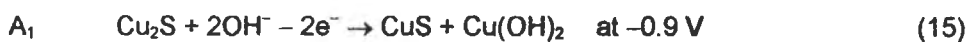


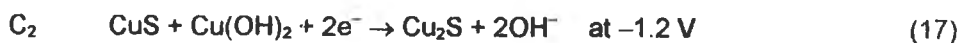
Fig. 7. Cyclic voltammogram of chalcopyrite electrode

By returning in anodic direction the two peaks (denoted by A_1 and A_3 , respectively) correspond to the processes:



The intermediate peak A_2 represents an oxidation reaction of $\text{Fe}(\text{OH})_2$ to $\text{Fe}(\text{OH})_3$ at -0.55 V potential.

During the second scan a supplementary cathodic peak appears indicating the reduction:



and the process C_1 may proceed with $\text{Cu}(\text{OH})_2$ participation according to the reaction:



It seems that a couple of peaks referring to the oxidation/reduction of copper sulfides (CuS and Cu₂S) occurs reversibly.

CONCLUSIONS

In solutions of pH higher than 10, galena, pyrite and chalcopyrite have given reproducible (in shape) cyclic voltammetry curves. The occurrence of an anodic peak for dimerization of xanthate ion was evidenced, although its position on the potential axis depends on cathodic H₂ formation. The proposed mechanisms have taken into account both anodic and cathodic dissolution of sulfide ores. No attempts were made quantitatively to analyse the experimental data.

LITERATURE

1. M. Lamache, *Electrochim. Acta*, **24**, (1979) 79-84
2. B. Lange, F. Scholtz, A. Weiß, G. Schwedt, J. Behnert, K. Raetzke, *International Laboratory*, June, (1993) 23-26
3. A. M. Bond, F. Scholtz, *J. Phys. Chem.*, **95**, (1991) 7460-7465
4. R. L. Paul, M. J. Nicol, J. W. Dieggle, A. P. Saunders, *Electrochim. Acta*, **23**, (1978) 625-633
5. R. L. Paul, M. J. Nicol, J. W. Dieggle, A. P. Saunders, *Electrochim. Acta*, **23**, (1978) 635-639
6. T. Biegler, D. A. Swift, *Electrochim. Acta*, **24**, (1979), 415-420
7. B. Dandapdani, E. Ghali, *J. Electrochem. Soc.*, **129**, 2, (1982), 271-276
8. M. Lamache, D. Bauer, J. Pegouret *Electrochim. Acta*, **26**, 12, (1981), 1845-1850
9. P. O. Lam-Thi, M. Lamache, D. Bauer *Electrochim. Acta*, **29**, 2, (1984), 217-226
10. O.H.Thi, M.Lamache, D.Bauer *Electrochim. Acta*, **26**, (1981), 33-44
11. A. Andriamanana, M. Lamache *Electrochim. Acta*, **28**, 2, (1982), 177-183
12. P. E. Richardson, C. S. O'Dell *J. Electrochem. Soc.*, **132**, 6, (1985), 1350-1356
13. S. B. Lalvani, M. Shami *J. Electrochem. Soc.*, **133**, 7, (1986), 1364-1368
14. T. Biegler, M. D. Home, *J. Electrochem. Soc.*, **132**, 6, (1985), 1363-1369

ANODIC BEHAVIOUR OF ZINC IN CYANIDE SOLUTIONS

Daniela Bughiu[†] M.Buda^{††} L.Dima^{*}

^{*} ICPE - SA, Splaiul Unirii 313, Bucharest, ROMANIA

[†] "POLITEHNICA" University of Bucharest, Applied Physical Chemistry & Electrochemistry Dept., Calea Grivitel 132, 78122, Bucharest, ROMANIA

ABSTRACT: Anodic behaviour of zinc is studied in cyanide electrolytes, using classical electrochemical experiments: voltammetry, chronoamperometry and chronopotentiometry. The results show two anodic processes for low cyanide content and only one for high cyanide content; in high cyanide content, solutions periodic current oscillations occur, in a narrow potential region, when using a relatively large Zn electrode (0.64 cm²). A dissolution mechanism is proposed, taken into account the voltametric data, and the current oscillations are discussed by means of a simple oscillator model that uses as a critical parameter for onsets current oscillation: the product between the uncompensated cell resistance (R_u) and the double layer capacity (C_d).

INTRODUCTION

Although the anodic behaviour of zinc has been extensively studied, especially in alkaline [1-4], its anodic behaviour in cyanide solutions was far less paid attention.

The anodic behaviour of zinc in cyanide solutions might be useful in plating processing, even if the general tendency is to abandon, for ecological reasons, the plating baths using cyanides. On the other hand, this study offer a large field of theoretical investigation of the complex processes that take place in such electrolytes: dissolution-precipitation, current oscillations, metal ion complexing, passivation, etc. The presence in large concentrations of a strong complexing agent, that may also adsorb strongly on the zinc electrode, can affect the processes that take place on the zinc anode.

EXPERIMENTAL

We performed classical electrochemical experiments: potentiodynamic polarization curves (at 500 mV min⁻¹), cyclic voltammetry, chronoamperometry and chronopotentiometry in cyanide solutions, with and without Zn(CN)₄²⁻ content. The electrolytes were prepared using NaCN and Zn(CN)₂ of analytical grade according to the following reaction:



Thus, at the NaCN quantity needed for totally complexing the Zn(CN)₂, the exact excess amount was added to give the desired CN⁻ concentration: in the following, the CN⁻ concentrations are referred to the free CN⁻ and the "Zn" concentrations are referred to the complex Na₂[Zn(CN)₄]. The NaCN amount added for totally complexing the Zn(CN)₂ was calculated according to the above reaction, and from stability constants of zinc-cyanide complexes we found that, practically, only the Na₂[Zn(CN)₄] complex is

[†] Author to whom correspondence should be addressed.

present for the studied electrolytes.

The concentration and temperature range for which potentiodynamic polarization curves were taken is given in Table 1. The voltametric, chronoamperometric and chronopotentiometric experiments were performed only on some of the mentioned electrolytes at $20 \pm 1^\circ\text{C}$.

Because we have used only cyanide electrolytes, without any supporting electrolyte, the ohmic drop for this set of experiments can be significant, especially for high current values. For this reason we performed two sets of voltammograms, using either a 0.64 or 0.032 cm^2 99.99% working zinc electrode. Prior to each determination the zinc electrode was polished with emery paper (600) and $1\text{ }\mu\text{m}$ diamond powder until "mirror" surface was attained. The counterelectrode was a platinum mesh ($\sim 10\text{ cm}^2$), and the reference electrode was a saturated calomel electrode (all potentials are referred to the SCE). The electrochemical measurements were performed using a PAR 173 potentiostat-galvanostat, a wave generator and an X-Y recorder.

Table 1. Experimental parameters for studying the anodic behaviour of zinc in cyanide solutions ($t = 20, 40, 60^\circ\text{C}$).

NaCN (mol/L)	0	0.1	0.25	0.5	1	2
$[\text{Zn}(\text{CN})_4]^{2-}$ (mol/L)	0	0.1	0.25	0.5	0.75	1

RESULTS AND DISCUSSIONS

Potentiodynamic polarization curves

The shape of the potentiodynamic polarization curves are practically the same for all studied temperatures and concentrations; in the figure below are presented three polarization curves (for one CN^- and "Zn" concentration) at three different temperatures (Fig. 1).

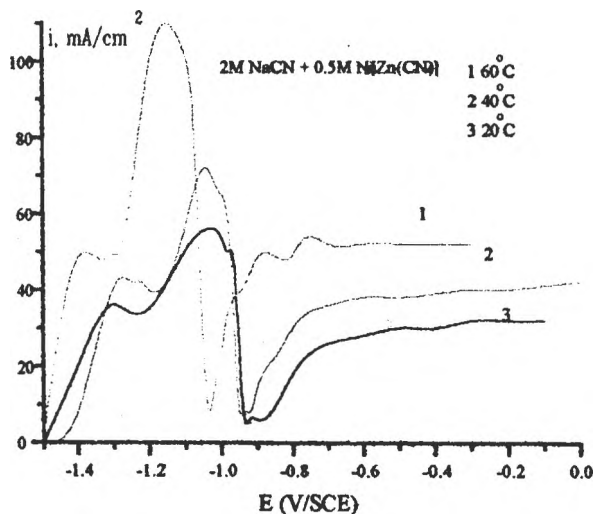


Fig. 1. Potentiodynamic polarization curves for Zn in cyanide electrolytes at 20, 40 and 60°C $S = 0.64\text{ cm}^2$, 500 mV min^{-1} .

The polarization curves show three main regions: the first one is the dissolution region (where the dissolution peak occurs), the second one (just after the dissolution peak) is the "passive-like" region, where the current drops significantly (but not to a zero value) and the electrode starts covering with a layer (probably an oxide layer) and the third one is the "oxidation region" (when the current is rising again), where two

simultaneous processes take place: the oxide precipitation and its dissolution in the cyanide electrolyte

The main experimental values obtained from the polarization curves for the studied electrolytes are presented below (Table 2)

This set of results is also published elsewhere [5], in our attempt to find an empirical correlation between the anodic current (mA cm^{-2}), temperature (T/K), free (L), total ($s = L + 4c$) cyanide and "Zn" (c) concentration. These equations are given below.

$$i = \left[\left(-\frac{18311}{T} + 7539 \right) \times L + \left(-\frac{2587}{T} + 21.733 \right) \right] \times c + \left[\left(-\frac{58946}{T} + 272.535 \right) \times L + \left(-\frac{32228}{T} + 98.672 \right) \right] \\ i = 10^{-4} \left(-\frac{4.58 - \frac{837.5}{T}}{T} \right) \times c + \left(-5.021 + \frac{406.532}{T} \right) \times s \left(\frac{2.876 + \frac{292.3}{T}}{T} \right) - \left(\frac{2.501 - \frac{402.58}{T}}{T} \right) \times c$$

However, here we want to complete the study of the anodic behaviour of zinc-cyanide system and for a better interpretation of the results we preferred to split them into two major categories:

1. Electrolytes with low cyanide content (0.1, 0.25, 0.5 M).

For a given concentration of CN^- the current peak increases with temperature and $\text{Na}[\text{Zn}(\text{CN})_2]_4$ content. For the electrolyte containing 0.5M CN^- the current peak is somehow not correlated with temperature and $\text{Na}[\text{Zn}(\text{CN})_2]_4$ content.

2. Electrolytes with high cyanide content (1 and 2M).

For a given CN^- concentration the first current peak decreases with the $\text{Na}[\text{Zn}(\text{CN})_2]_4$ content and increases with temperature.

For all the studied solutions the current peak increases with CN^- content (at constant "Zn" concentration), the increase being proportional to the CN^- concentration; this fact indicates that the dissolution process is strictly related to the CN^- concentration and is diffusion-controlled.

The different behaviour of the electrolytes with low and high cyanide concentration can be ascribed to a very large non-ideality for the high cyanide content electrolytes, since we correlated the current peaks with the concentrations. The case of the 0.5M solution, where the data are not so well correlated with the CN^- and "Zn" concentration, is somewhere just at the limit between the low and high cyanide contents.

Table 2. Data for the anodic dissolution of zinc in cyanide electrolytes.

0.10M NaCN		20°C		40°C		60°C	
"Zn" (mol/l)	i_{max} (mA)	E_{max} (V)	i_{max} (mA)	E_{max} (V)	i_{max} (mA)	E_{max} (V)	
0	2.7	-0.92	4.4	-0.78	3.9	-0.75	
0.1	4.0	-0.94	5.6	-0.95	9.3	-0.89	
0.25	4.3	-0.91	5.1	-0.8	9.0	-1.04	
0.5	4.4/	-0.78	6.0	-1.09	12.2	-1.12	
0.75	4.9/	-1.04	6.6/	-0.81	13.9	-1.2	
1	5.4/	-1.15	6.0	-0.9	13.0	-1.12	
0.25M NaCN		20°C		40°C		60°C	
Zn (mol/l)	i_{max} (mA)	E_{max} (V)	i_{max} (mA)	E_{max} (V)	i_{max} (mA)	E_{max} (V)	
0.1	6.7/	-0.9	8.3/	-0.84	14/	14/	
0.25	7.4	-0.7	8.5	-0.95			
0.5	7.7	-1.01	9.8	-1.04	18.8	-1.04	
0.75	7.6	-0.9	11.8	-1.06	2.0	-1.07	
1	8.1	-1.09	10	-1.1	14.6	-1.14	
0.50M NaCN		20°C		40°C		60°C	
Zn (mol/l)	i_{max} (mA)	E_{max} (V)	i_{max} (mA)	E_{max} (V)	i_{max} (mA)	E_{max} (V)	
0.1	16.0	-0.90	20.8	-0.74	27.7	-0.74	
0.25	16.4	-0.94	24.0	-0.94	27.0	-1.00	
0.5	11.1	-1.20	16.6	-1.04	22.0	-1.08	
0.75	16.6	-1.00	18.4	-1.02	26.0	-1.18	
1	11.4	-1.08	14.2	-1.10	26.2	-1.00	
1.0M NaCN		20°C		40°C		60°C	
Zn (mol/l)	i_{max} (mA)	E_{max} (V)	i_{max} (mA)	E_{max} (V)	i_{max} (mA)	E_{max} (V)	
0.1	34.4	-0.9	44.0	-0.8/	62.0	-0.8	
0.25	31.6	-0.92	43.0	-0.94	58.0	-0.96	
0.5	23.4	-0.9	38.0	-0.95	56.0	-1.04	
0.75	22.0	-1.06	27.0	-1.00	54.0	-0.98	
1	21.2	-1.0	23.2	-0.90	51.0	-1.50	
2.0 M NaCN		20°C		40°C		60°C	
Zn (mol/l)	i_{max} (mA)	E_{max} (V)	i_{max} (mA)	E_{max} (V)	i_{max} (mA)	E_{max} (V)	
0.1	88	-0.90	112	-0.90	134	-0.80	
0.25	74	-0.92	88	-0.90	106	-0.90	
0.5	63	-1.00	71	-0.92	94	-0.91	
0.75	49	-1.12	65	-1.00	87	-0.90	
1	32	-1.04	52	-1.00	72	-0.94	

Cyclic voltammetry

Using the same electrode ($S = 0.64 \text{ cm}^2$) we performed voltammograms for 0.1, 0.5 and 1M NaCN electrolytes ("Zn" free) for 20°C and different scan rates (Fig. 2, a, b,c).

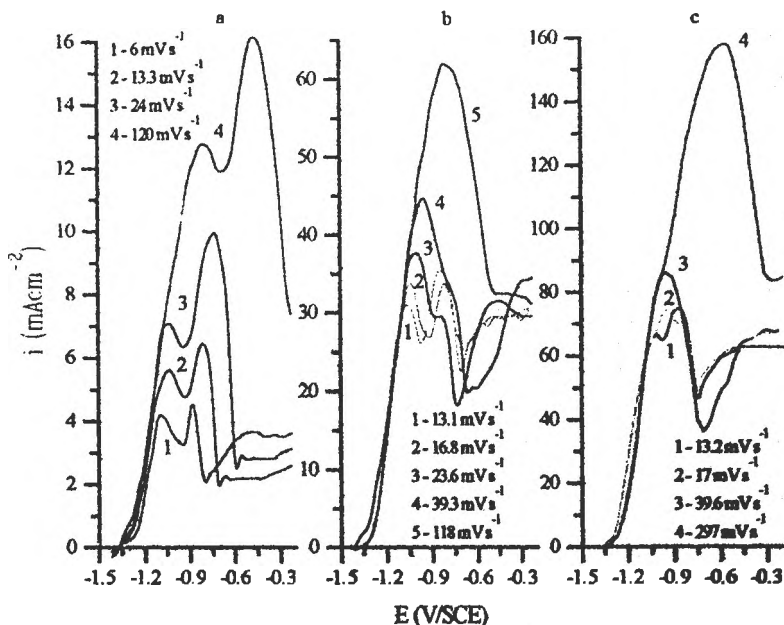


Fig. 2. Voltammograms for 0.64 cm^2 Zn electrode in (a) 0.1M NaCN; (b) 0.5M NaCN and (c) 1M NaCN at different scan rates.

The voltammograms show two anodic peaks: the first peak in the $-1.15 - -0.65 \text{ V}$ potential range and the second one, which is observable only for 0.1M and 0.5M electrolytes, in the $-0.92 - -0.45 \text{ V}$ potential range. The cathodic sweep shows no reduction peak and therefore we did not present as well the cathodic branch of the voltammograms. However, a peak may be observable at sufficiently negative potentials, but the contribution of hydrogen evolution to this current peak is significant. Because we wanted to study only the anodic behaviour of the zinc electrode, trying to simplify the processes that occur on the zinc electrode, we avoided hydrogen evolution on the zinc electrode and thus we did not sweep the cathodic potential in this potential range.

Fig. 3 presents the $i_p - v^{1/2}$ and the $E_{p1} - \ln(v)$ dependencies for the first current peak. One can see that the $i_p - v^{1/2}$ dependence is linear, but the y intercept differs significantly from the zero value; this y intercept is proportional with the CN⁻ concentration; the slopes of these dependencies are also proportional with the CN⁻ concentration. The first peak potential shifts towards positive values as the scan rate

increases; the $E_{p1}-\ln(v)$ dependence is linear only for low scan rates, and relatively low cyanide contents (0.1 and 0.5M), indicating that for higher scan rates and cyanide contents the uncompensated ohmic drop can affect the voltammogram's shape.

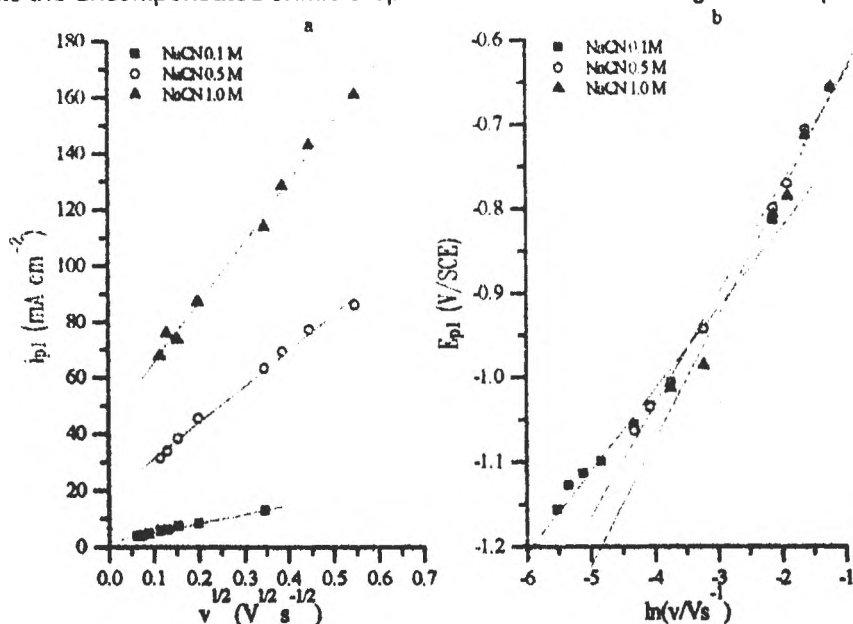


Fig. 3. First current peak voltammetric plots for 0.64 cm² Zn electrode.

For very low scan rates and relatively high CN⁻ concentrations (0.5 and 1M), reproducible current oscillations occurs in a narrow potential range. As the scan rate is lowered, the potential range in which oscillations occurs widens and their amplitude increases; an example is shown in fig. 4. After this potential region, irregular and small amplitude current oscillations occurs.

The second current peak, as it can be seen from fig. 2, appears only for 0.1 and 0.5M NaCN solutions; for 1M NaCN this second peak cannot be observed. At 0.1M NaCN this second current peak increases with increasing scan rate and it can be observed in a wide scan rate domain; the peak potential is also shifting towards positive values as the scan rate increases. At 0.5M NaCN the second current peak decreases as the scan rate increases and it can be observed only for relatively low scan rates.

We performed cyclic voltammetry experiments for 2M NaCN solutions having either 1M or 0.5M "Zn"; the typical voltammograms are shown in fig. 6. The voltammograms show a single current peak and they look like "polarization curves", even for relatively high scan rates, with a limiting current. Therefore, the peak current and potential can be

observed only for high scan rates. The voltammograms show the same two oscillation potential regions. The i_{p1} vs. $v^{1/2}$ and E_{p1} vs. $\ln(v)$ dependencies are shown in fig. 7.

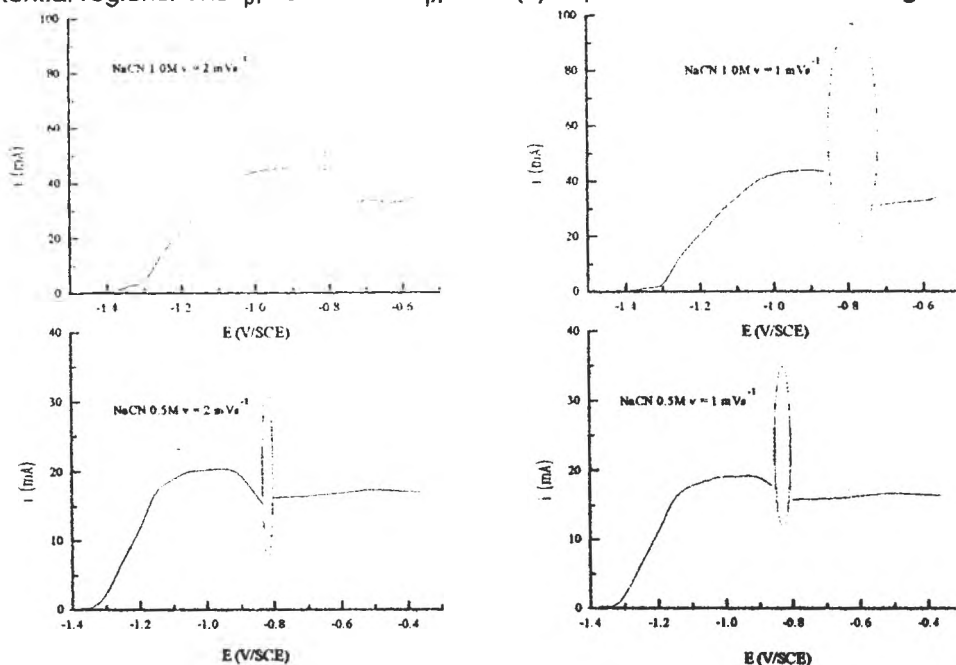


Fig. 4. Potentiodynamic polarization curves for 0.64 cm^2 Zn at very low scan rates for 0.5 and 1M NaCN; the regions where current oscillations occurs are denoted with an oval.

The voltametric data for the 0.64 cm^2 Zn electrode are summarized in Table 3.

Table 3. Voltammetric data for the 0.64 cm^2 Zn electrode. The parameters A and B are for $i_p = A + Bv^{1/2}$ and for $E_p = A + B\ln(v)$, with v in Vs^{-1} .

XM NaCN + YM Na ₂ [Zn(CN) ₄]		i_{p1} (mA cm ⁻²)		E_{p1} (V)		E_{p2} (V)	
X	Y	A	B	A	B	A	B
0.1	0.0	1.84	32.2	-0.63	0.096	-0.45	0.085
0.5	0.0	18.2	128.5	-0.51	0.131	—	—
1.0	0.0	43.4	215.7	-0.49	0.146	—	—
2.0	0.5	17.6	286.3	-0.60	0.118	—	—
2.0	1.0	44.8	186.5	-0.74	0.069	—	—

For high CN⁻ concentrations, where the currents involved are very high, the uncompensated ohmic drop influences strongly the process on the electrode surface. For this reason we performed cyclic voltammograms experiments using a Zn electrode with a smaller surface area (0.032 cm^2), trying to avoid the effect of uncompensated ohmic drop.

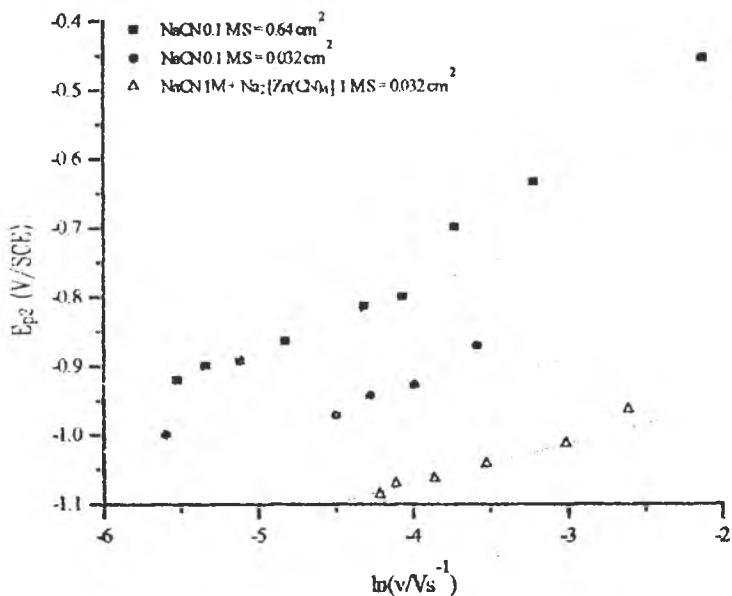


Fig. 5. The $E_{p2} - \ln(v)$ plots for the 0.64 and 0.032 cm^2 Zn electrode.

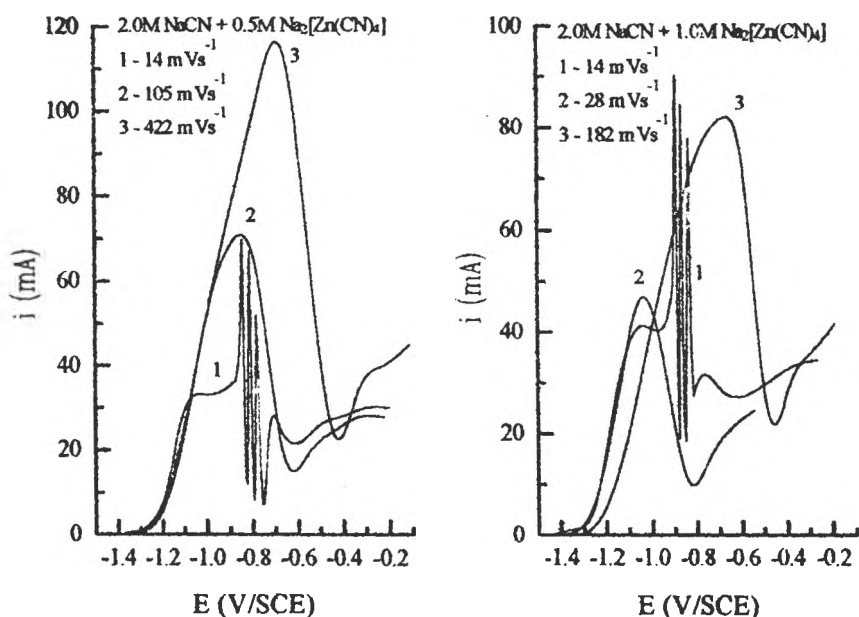


Fig. 6. Voltammograms for 0.64 cm^2 Zn electrode in 2M cyanide electrolytes.

The voltammograms' shape is qualitatively the same, but, as it was expected, the peak potentials are shifted towards negative values (at the same scan rate). At the same time, the slopes for the E_p vs. $\ln(v)$ are considerably smaller and the slopes of i_p vs. $v^{1/2}$ are larger than those obtained with the 0.64 cm^2 Zn electrode. For example, for the 0.1M NaCN solution, the $E_{p1} - \ln(v)$ slope is 0.04 (compared to 0.096 for the 0.64 cm^2 electrode) and is practically the same as for the 0.5M (0.032 cm^2) case.

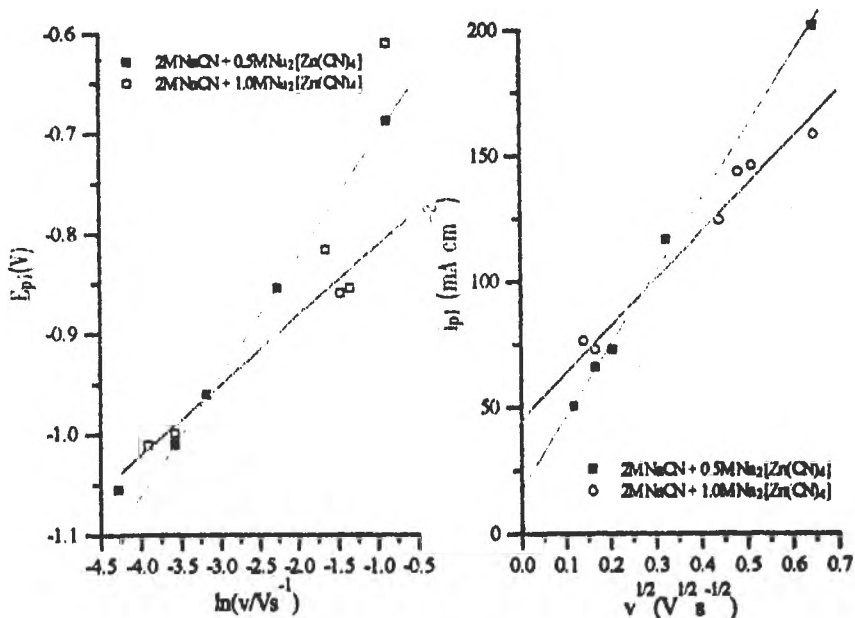


Fig. 7. $E_{p1} - \ln(v)$ and $i_{p1} - v^{1/2}$ dependencies for the 0.64 cm^2 electrolytes in 2M cyanide solutions.

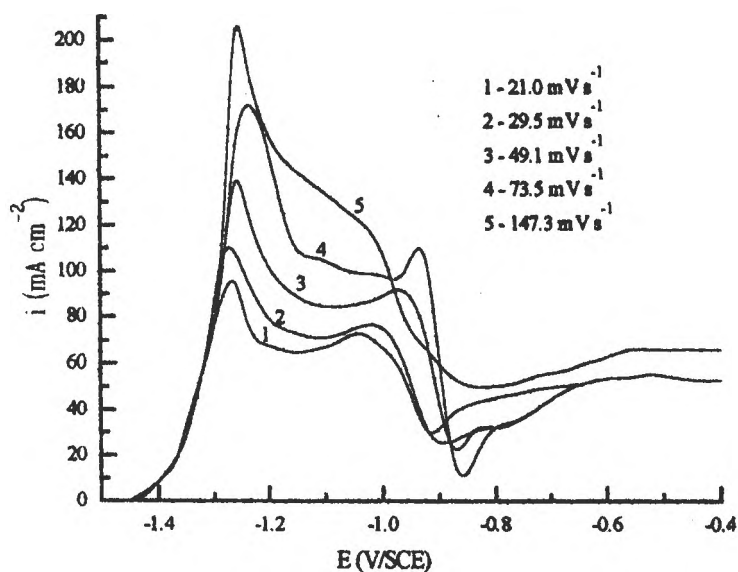


Fig. 8. Voltammograms for the 0.032 cm^2 in 1M NaCN + 1M $\text{Na}_2[\text{Zn}(\text{CN})_4]$.

The E_p vs. $\ln(v)$ slope is greater for 1M NaCN solution than those for 0.1 and 0.5M NaCN, which indicates that, even for this case, the uncompensated ohmic drop still plays an important role at high CN^- concentrations. For NaCN 1M with 1M "Zn", the E_p vs. $\ln(v)$ slope is lower (0.027); in this case the presence of the highly dissociated $\text{Na}_2[\text{Zn}(\text{CN})_4]$ complex may improve the electrolyte conductivity and, therefore, diminishing the influence of the uncompensated ohmic drop. It is very interesting that

the second anodic peak can be observed (fig. 8) for 1M NaCN + 1M "Zn" solution, with a current peak decreasing as the scan rate increases (the second current peak is measured from the base line of the first current peak). In this case no current oscillations can be observed in the potential range where those oscillations occurred when using the 0.64 cm² Zn electrode, but the region where irregular and small amplitude current oscillations occurs still exists. Therefore, the ohmic drop plays a very important role in onsetting high amplitude current oscillations (this fact is also revealed by other authors, see e.g. Kleinke [6]). In fig. 9 are presented the $E_{p1} - \ln(v)$ and $i_{p1} - v^{1/2}$ dependencies for the 0.032 cm² electrode.

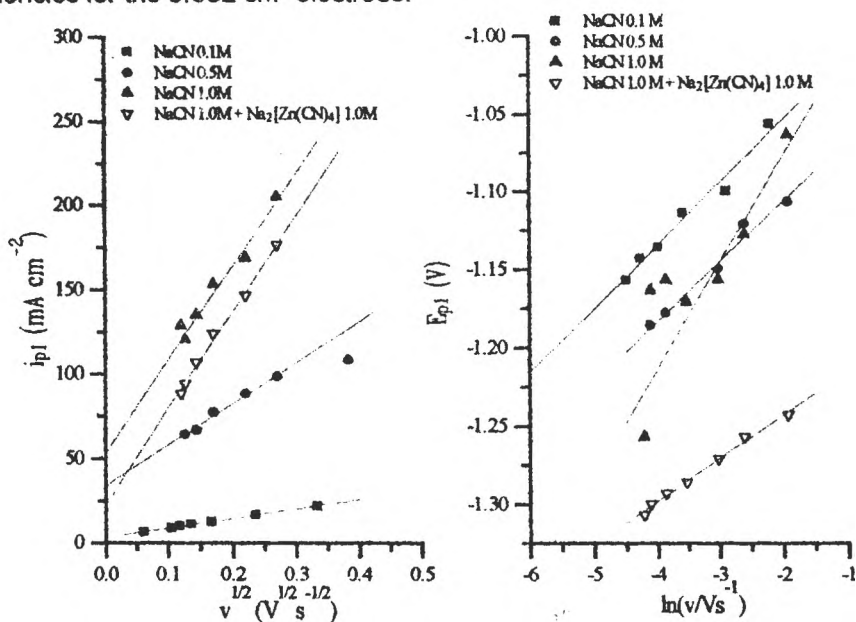


Fig. 9. $E_{p1} - \ln(v)$ and $i_{p1} - v^{1/2}$ plots for 0.032 cm² Zn electrode.

The voltammetric data for the 0.032 cm² Zn electrode are summarized in Table 4.

Table 4. Voltammetric data for the 0.032 cm² Zn electrode. The parameters A and B are for $i_p = A + Bv^{1/2}$ and for $E_p = A + B\ln(v)$, with v in Vs⁻¹.

XM NaCN + YM Na ₂ [Zn(CN) ₄]		i_{p1} (mA cm ⁻²)		E_{p1} (V)		E_{p2} (V)	
X	Y	A	B	A	B	A	B
0.1	0.0	3.06	56.9	-0.97	0.040	-0.68	0.059
0.5	0.0	33.6	242.2	-1.03	0.038	--	--
1.0	0.0	71.5	446.6	-0.94	0.068	--	--
1.0	1.0	52.8	550.5	-1.19	0.027	-0.84	0.057

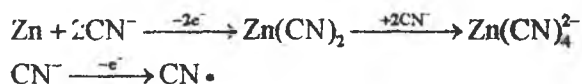
From the E_p vs. $\ln(v)$ slopes we calculated [7] the αn products for both anodic

peaks, only in the case of the 0.032 cm² electrode, trying to avoid the influence of the uncompensated cell resistance upon these slopes; one can see that the first anodic process can be considered as a two-electron charge transfer and the second one as a one-electron charge transfer (table 5).

Table 5. Calculated αn values for the two anodic processes occurring on Zn in cyanide solutions.

Electrolyte	$(\alpha n)_1$	$(\alpha n)_2$
NaCN 0.1M	0.31	0.21
NaCN 0.5M	0.33	--
NaCN 1.0M	0.20	--
NaCN 1.0M + Na₂[Zn(CN)₄] 1.0M	0.46	0.18

Therefore, the two main processes that may take place onto the Zn electrode in cyanide solutions can be:



For dilute cyanide electrolytes, both processes can take place, which might explain the two anodic peaks observed for 0.1M NaCN voltammograms. In more concentrated solutions (0.5M NaCN) the first process becomes more important, consuming thus the CN⁻ ions, so the second process cannot be observed for high scan rates (where diffusion cannot bring enough CN⁻ near the electrode surface). In even more concentrated solutions (1M NaCN), the Zn dissolution is very substantial and consumes probably all the CN⁻ ions, so the second anodic process cannot take place any more. For the 1M NaCN + 1M Na₂[Zn(CN)₄] solution, the presence of the zinc complex in high concentration may determine the first reaction to occur at some equilibrium state, so the second process is allowed to take place.

The second process could be considered as the oxidation of CN⁻ adsorbed onto Zn electrode surface; the data found in literature shows that CN⁻ is strongly and specifically adsorbed onto Au [8], Ag [9] and Ni [10] electrodes, metals that form very stable complexes with CN⁻ ions. We assumed that CN⁻ is also strongly adsorbed onto the Zn electrode, and that this adsorption plays a very important role in the anodic behaviour of Zn in cyanide solutions. The non-zero value of the y intercept of i_{p1} vs. $v^{1/2}$ dependencies can be attributed to a very large limiting current in such concentrated

electrolytes.

Chronopotentiometry

We performed several chronopotentiometric experiments, using the 0.032 cm^2 electrode in NaCN 0.1, 0.5 and 1M (zinc free) and NaCN 1M + $\text{Na}_2[\text{Zn}(\text{CN})_4]$ 1M. The curves are shown in fig. 9. The chronopotentiograms' shapes show two clear processes for 0.1 and 0.5 M solutions and only one for the 1M solution, in accordance with the voltammetric data.

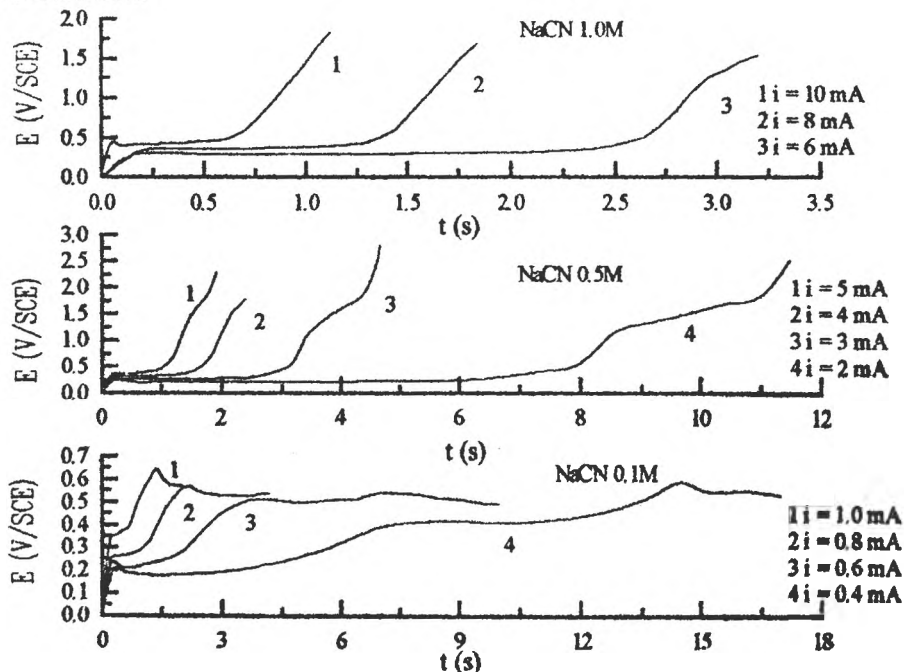


Fig. 10. Chronopotentiograms for 0.032 cm^2 Zn electrode in 0.1M, 0.5M, 1M NaCN electrolytes.

Chronoamperometry

We performed several chronoamperometric experiments for 2M NaCN solutions, in the potential range where current oscillations appears. For determining the potential regions where current oscillations occurs we performed polarization curves (taken at 1 mV s^{-1}), shown in fig. 11. One can see that the potential region where current oscillation occur is narrowing as the "Zn" concentration increases, probably due to an increase of the electrolyte conductivity. The current oscillation are very large (amplitude of about 90 mA) and very reproducible.

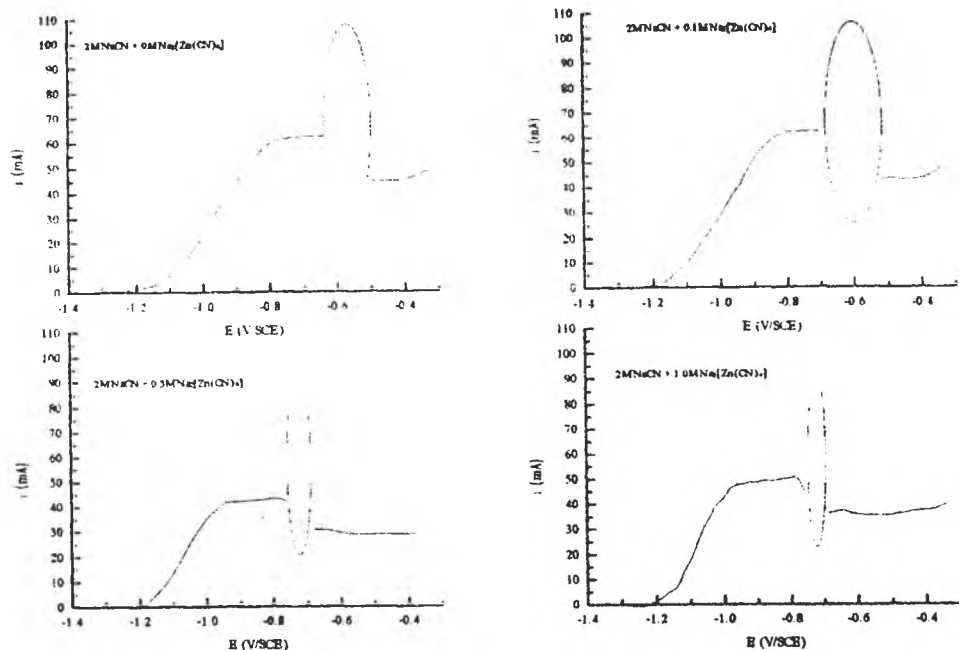


Fig. 11. Polarization curves for 0.64 cm^2 Zn electrode in 2M NaCN solutions; the region where current oscillations occurs is denoted with an oval.

We have taken chronoamperograms; two of them, for 2M NaCN, are shown in fig. 12. The oscillations' shape is very similar to those found in literature for Zn in KOH solutions [11] and for Au in acidic solutions [12]. We saw that the ohmic drop is very important for onsets current oscillations: the current oscillations occur only when using the 0.64 cm^2 Zn electrode and only for relatively high CN^- concentrations (0.5, 1 and 2M), where the currents involved are relatively large. In our opinion, the CN^- and $\text{Zn}(\text{CN})_4^{2-}$ concentrations effect upon the electrolyte's conductivity, and the resulting current, are the determining factor that onsets current oscillations. The oscillation shape (and amplitude) changes with changing the potential: as the potential is more anodic, the oscillation's frequency lowers and the amplitude is slightly increasing (this fact is valid for oscillations observed for all 2M NaCN solutions). As the potential increases, the oscillations' shape becomes more and more similar to those simulated with the model described below (at parameters value shown in the following). The oscillations are periodic and last for at least 20 minutes. If the model holds, then the adsorption and oxidation of CN^- plays an important role in this oscillator behaviour. We intend to pay attention, in detail, to the current oscillation of zinc in cyanide solutions in another paper [13].

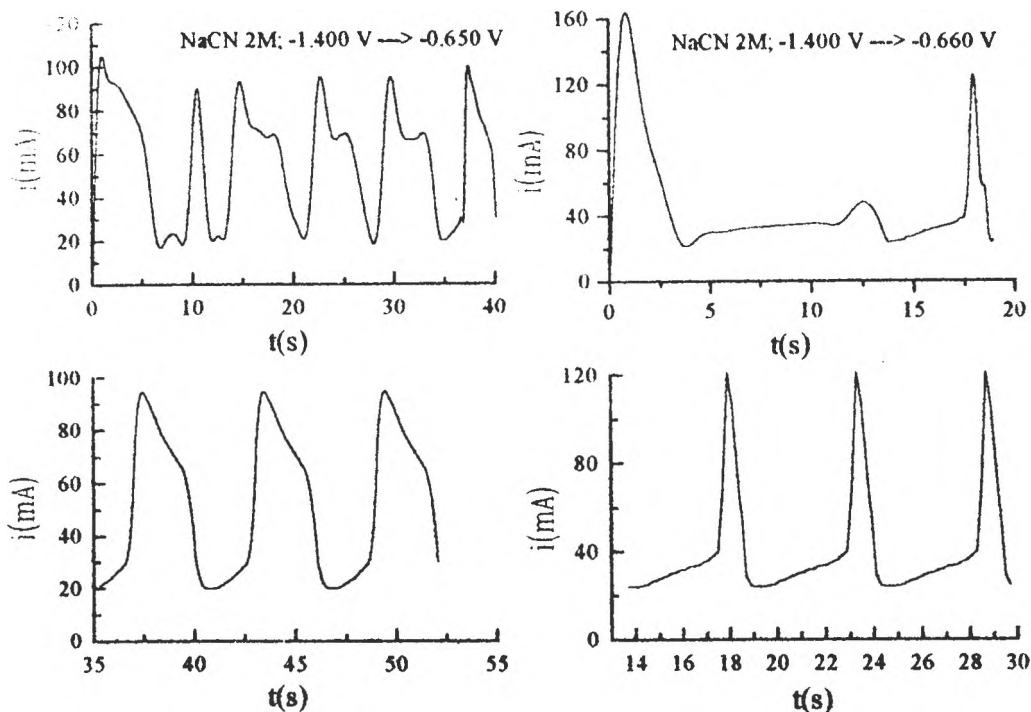


Fig. 12. Cronoamperograms for 0.64 cm^2 Zn at two potential values in the oscillation region for 2M NaCN ("Zn" free).

The theoretical description of current oscillations seems to be very difficult, but the simple model proposed by Koper and Gaspard [14] gives current oscillations very similar to those obtained in our case. This model takes into account the ohmic drop (in fact, the "time constant" - the product between the uncompensated cell resistance R_u and the double layer capacity C_d) as a critical parameter for onsets of current oscillations. Even if this model was created starting from the current oscillations observed for the reduction of In^{3+} catalyzed by the specific adsorption of SCN^- ions, its generality makes it suitable for other processes too, and it proves to give satisfactory results in our case. The single problem remains that the adsorption isotherm can hardly be extrapolated in our case, since we studied an anodic process and not a cathodic one. The model is briefly described below [14]

$$\frac{de}{dt} = \frac{v - e}{r} - mk(e)u$$

$$\frac{du}{dt} = -k(e)u + \alpha(w - u)$$

$$\frac{dw}{dt} = \frac{19}{333} \alpha(16 - 25w + 9u)$$

where e is the dimensionless electrode potential, v is the circuit potential, r the series resistance (ohmic solution resistance included), m a dimensionless parameter proportional to the bulk concentration, d is a parameter proportional to the diffusion coefficient, and $k(e)$ is the dimensionless heterogeneous rate constant:

$$k(e) = k_1 \theta^2 + k_2 \exp[\alpha n(e - e^0)],$$

$$\theta = \begin{cases} 1 & \text{for } e \leq e_d \\ \exp[-b(e - e_d)^2] & \text{for } e > e_d \end{cases}$$

assuming that $Zn(CN)_2$ intermediate can also be formed via the CN species. The simulated current oscillations are given in fig. 13. One can see a good agreement between the experimental and simulated chronoamperograms. The correlation between the experimental data and the simulation parameters is however not yet well established; this will be the subject of another paper [13].

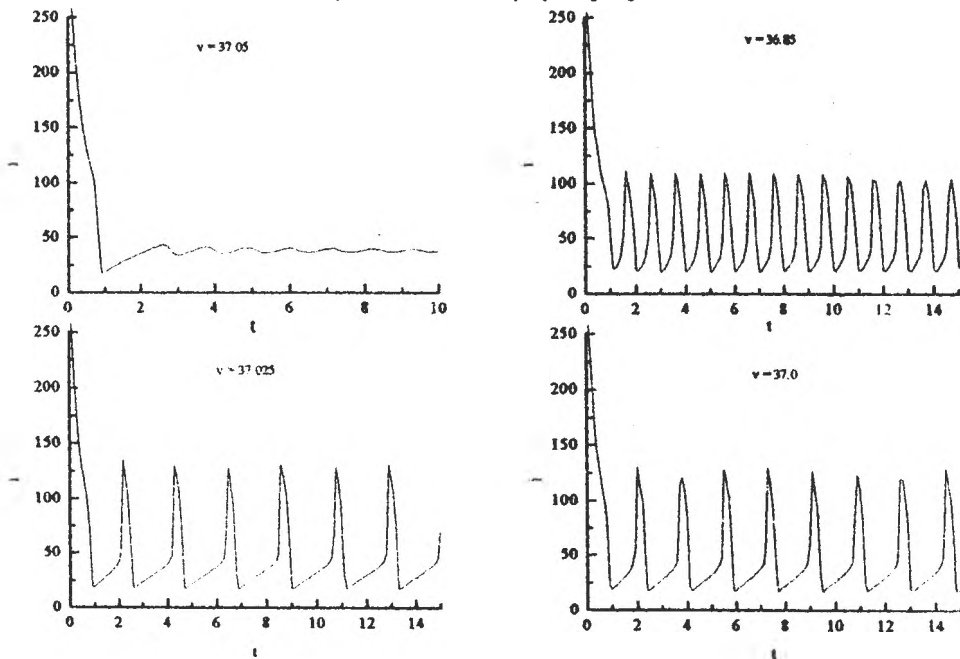


Fig. 13. Simulated chronoamperograms for different potential values (v); $d = 1$, $m = 120$, $k_1 = 2.5$, $k_2 = 0.01$, $e_d = 35$, $b = 0.5$, $\alpha n = 0.5$, $e^0 = 30$, $r = 0.01774$.

CONCLUSIONS

We found general relationships that links the dissolution current, temperature and free and total cyanide concentration for anodic dissolution of zinc in cyanide electrolytes, with and without $Na[Zn(CN)_4]$ content. The voltametric show that in dilute cyanide electrolytes (up to 0.5M) two anodic processes occurs, the first with two-

electrons charge transfer and the second with one-electron charge transfer, while for concentrated cyanide electrolytes (1 and 2M) only the first process is observable. For concentrated cyanide electrolytes, high amplitude current oscillations occurs in a narrow potential region; this potential region is dependent on the $\text{Na}[\text{Zn}(\text{CN})_4]$ content. The current oscillations can be explained, with certain limitations, by the general model proposed by Koper and Gaspard [14].

REFERENCES

1. M.A.Devanathan and S.Lakshaman, *Electrochim.Acta* **13**, 667 (1968).
2. J.Euler, *Electrochim.Acta* **11**, 701 (1966).
3. H.Kaesche, *Electrochim.Acta* **9**, 383 (1964).
4. P.LL.Calbot, M.Cortes, F.A.Centellas, J.A.Garrido and E.Perez, *Electrochim.Acta* **32**, 1321 (1987).
5. L.Dima, Daniela Bughiu, Liana Anicai, M.Buda, accepted paper for 47th Annual Meeting of ISE, Veszprem-Balatonfured, Hungary, September 1-6, 1996.
6. M.U.Kleinke, *J.Phys.Chem.* **99**, 17403 (1995).
7. A.J.Bard, L.R.Faulkner, *Electrochemical Methods* p. 222-223, John Wiley&Sons, New York (1980).
8. T.Sawaguchi, T.Yamada, Y.Okinaka and K.Itaya, *J.Phys.Chem.* **99**, 14149 (1995).
9. W.Plieth, R.Boy and H.Bruckner, *Ber.Bunsenges.Phys.Chem.* **86**, 273 (1982).
10. M.R.Mucalo, R.P.Cooney and G.A.Wright, *J.Chem.Soc.Faraday Trans.* **86**(7), 1093 (1990).
11. R.C.V.Piatti, J.J.Podesta and A.J.Arvia, *Electrochim.Acta* **25**, 827 (1980).
12. J.J.Podesta, R.C.V.Piatti and A.J.Arvia, *Electrochim.Acta* **24**, 633 (1979).
13. Daniela Bughiu, M.Buda, L.Dima, to be published.
14. M.T.M.Koper and P.Gaspard, *J.Chem.Phys.* **95**, 4945 (1991).

ELECTROCHEMICAL CHARACTERIZATION
OF SOME METAL PHTHALOCYANINES ELECTRODES

Elena Maria Pica^{*}, Maria Jitaru, I.Marian, and N.Santa^{**}

*Babes-Bolyai University, Faculty of Chemistry and Chemical Engineering
St. Arany Janos No.11, RO-3400 Cluj-Napoca, Roumania*

^{} Technical University of Cluj-Napoca, Roumania*

*^{**} C.A.C.S., St. Donath, 3400 Cluj-Napoca, Roumania*

ABSTRACT. Metal-phtalocyanines are square planar complexes and show electrocatalytic activity, especially in aqueous media. Next we explored the electrocatalytic activity of the obtained electrodes for the oxygen discharge reaction. Experiments were performed in aqueous solution, (0.1 M NaClO₄ ; 0.1M KCl ; 0.25 M H₂SO₄ ; 1 M KCl + 0.01 M KOH) in the pH range from 2 to 10.

A comparative study of the electrocatalytic activity of carbon paste electrode (CPE) with cobalt phtalocyanine (Pc-Co) and lead phtalocyanine films (Pc-Pb) deposited in vacuum on indium or bronze (Cu/Sn) supports was made. Given the large volume of the Pb²⁺ ions the lead phtalocyanine complex was prepared by performing the ring closure reaction of the ligand in the presence of lead ions. Disk electrodes with In or Cu/Sn, with a surface area of 12 mm², were coated with phtalocyanine films. Typically, phtalocyanine films were deposited in vacuum (6x 10⁻³ torr) under argon atmosphere, to yield uniform, 300-400 μm thick coatings.

The magnitude of the redox potential and the electrocatalytic activity of metal phtalocyanines depends on the pH, the composition of the supporting electrolyte and the identity of the conductive support.

Therefore, the Pc-Pb and the Pc-Co complexes can act as a redox mediator and the electrodes may be useful in mediated electrochemical reductions of oxygen molecules and of various organic substrates.

Key words: electroreduction, phtalocyanine film, cyclic voltammetry, chemical modified electrodes.

INTRODUCTION. The metal chelates, especially phtalocyanines complex, which is similar in structure to the heme in the blood pigment, hemoglobin, **Figure 1**, has been found to be active in electrocatalysis [1]. Organic N₄ macrocycles have been used in the reduction of oxygen since 1964, when Jasinski [2] introduced phtalocyanines in the electroreduction of oxygen in alkaline medium. Later a vast

number of papers has been published on this subject, mainly because of the possible applications of these materials as catalysts for fuel cell cathode materials. The topic

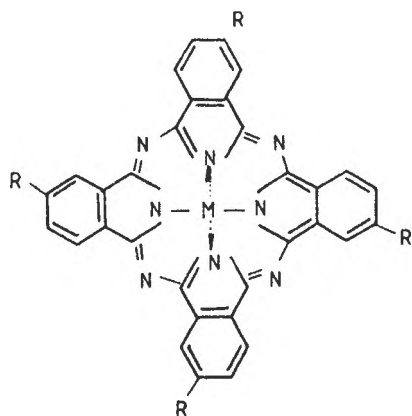


Figure 1. Phtalocyanine cycle.

has been reviewed by various authors [3,4]. The relation between redox properties and catalytic activity was first pointed out by Randin [5]. According to the concept of redox catalysis [6,7] the metal in the macrocycle is oxydized upon interaction with oxygen, which is partially reduced, and in this way the catalytic cycle is started.

As catalysts in oxygen reduction have been used the phtalocyanines of cobalt [8-11], iron [8], rhodium [12], in acid [9,10] and alkaline [1,8-11] medium.

In this paper we have studied comparatively the carbon paste electrode with phtalocyanines of cobalt and lead and the phtalocyanine films [13] deposited in vacuum on indium or bronze (Cu/Sn) supports. The influence of the photoexcitation was also reported.

EXPERIMENTAL. **Pc-Pb and Pc-Co film deposition on indium and bronze** is carried out and has been reported previously -vacuum (6×10^{-3} torr) under Ar atmosphere, to yield uniform, 300-400 μm thick coatings [13].

Chemicals and solutions. For the polarographic and cyclic voltammetric measurements all chemicals were obtained from Fluka Chemical Company. All the solutions were deoxygenated (Ar 99.9%) for 4 min., before the recording of the current-voltage curves.

Cyclic voltammetry. The voltammetric curves were recorded with a Taccussel Potentiostat with X-Y Recorder BD 90 Kipp and Zonen. An electrolytic cell (Kalousek cell) with a liquid junction was used, with a helix made of platine counter electrode and a saturated calomel reference electrode. Two types of the working electrodes were utilized: carbon paste electrode with metal phtalocyanines, CPE/Me-Pc, and the phtalocyanine films deposited in vacuum on indium or bronze disk supports (conditions: $6 \cdot 10^{-7}$ torr, Ar 99.97%; disk surface 4.52 mm^2 ; $I = 50 \text{ A}$ for 5 mn and $I = 100 \text{ A}$ for 5 mn.)

Microphotographs of the electrodes were taken before and after their utilization by using a Tesla type BS 340 scanning electronic microscope with a resolution of 4 nm.

RESULTS AND DISCUSSIONS.

The potentiodynamic response of the metal - phtalocyanine and of the H₂ Pc, depends on the metal-ligands interactions, electronic structure of metal ions, supporting electrolyte, chemical nature of the support, and photoexcitation, **Table 1**.

Table1. Electroreduction potentials of the oxygen for the metal phtalocyanines of cobalt and lead on Pb/bronze in KCl 1M, in Ar ; S = 30 mA; v_x = 0.5 · 100 mV/s; v_y = 5 mV/s.

Electrode	v [mV/s]	ε _{p,c} [mV/SCE]	ε _{p,a} [mV/SCE]
Pc-Pb/bronze	0.66	-0.542	-0.525
	1.70	-0.560	-0.500
	3.33	-0.582	-0.480
	10.00	-0.640	-0.450
Pc-Pb/bronze*	0.66	-0.645	-0.460
Pc-Co/bronze	0.66	-0.812	-0.775
	1.70	-0.500	-0.420
	3.33	-0.560	-0.510
	10.00	-0.570	-0.520
Pc-Co/bronze*	0.66	-0.575	-0.530

* in the presence of the photoexcitation, the process is intensified.

Carbon electrodes were used because not only binds Pc-Me, but also exert an influence upon their redox potential. The electrochemical response of the H₂Pc, **Figure 2**, curve a) presents a reversible current peak at -0.912 V SCE, attributed to a reversible redox process taking place on the phtalocyanine ring, according to Lever [14]. The carbon paste electrodes with Pc-Co (**Figure 2**, curve b) and Pc-Pb (**Figure 2**, curve c) present a similar peak at more positive potentials, which has been assigned to the metal ion in the macrocycle.

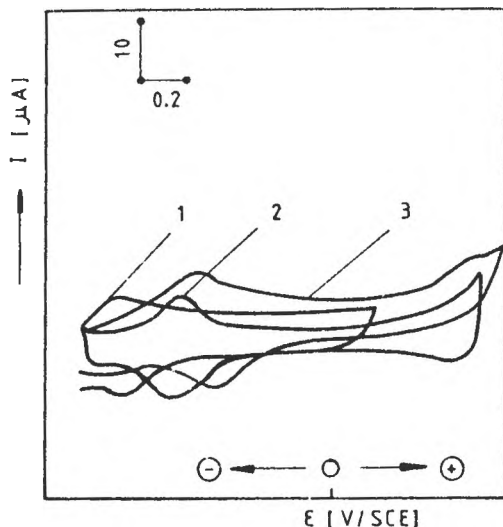


Figure 2.
Cyclic voltammograms for carbon paste electrodes with: Pc (curve a); Pc-Co (curve b); Pc-Pb (curve c); 0.25 M H₂SO₄; v=10 mV/sec ;

The presence of the O₂ molecules modifies the redox potential of the macrocycle interacting *via* axial coordination to the metal ion and/or *via* peripheral bonding to the macrocycle ring, **Figure 3** .

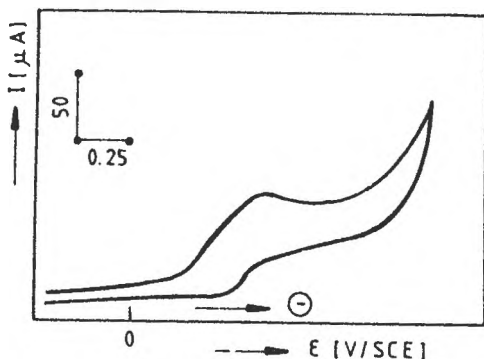


Figure 3.
Voltammogram of the reduction of oxygen on carbon paste + 10% Pc-Co electrode in 1M KCl + 0.01 M KOH and 3% H₂O₂ ; v = 300 mV/sec.

The metal phthalocyanine films on In and bronze are not very stable in time; pores and cracks are developed during polarization, **Figure 4** .

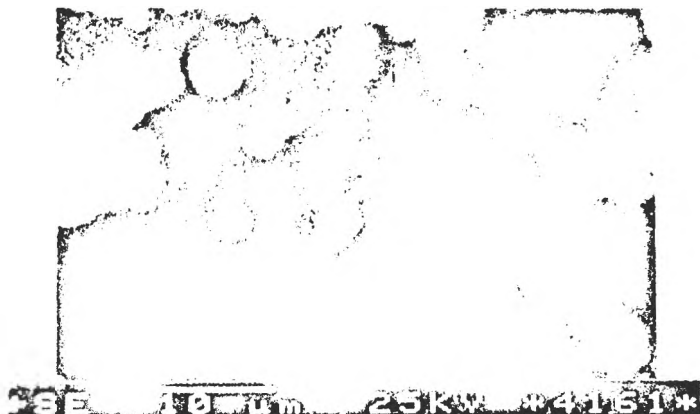


Figure 4.
SE photomicrograph of the Pc-Co film on Indium

CONCLUSIONS

The metal phthalocyanines of cobalt and lead are both active in the reduction of the oxygen molecule. The difference between their electrocatalytic activity (appreciated by the potential at the constant current) should be correlated with the ability of the complex to bind extraplanar ligands (O_2 , CO_2 and other molecules); these charge-transfer intermediates depend on the electronic structure of the metal and are obviously related to the redox potential.

ACKNOWLEDGEMENTS

This work has been supported by a GRANT from the Roumanian Academy.

REFERENCES

1. H.Jahnke, M.Schönborn and G.Zimmermann in "Topics in Current Chemistry" Springer-Verlag Berlin Heidelberg, 1996, p. 135-180.
2. R. Jasinski, *J. Electrochem. Soc.*, 112, 1965, 1212.
3. R. Tarasevich and K.A. Radyushkina, *Russ. Chem. Rev.*, 49, 1980, 718.
4. J. Zagal, M.Perez, A.A.Tanaka, J.R. dos Santos, and C.A. Linkous. *J.Electroanal. Chem.*, 339, 1992, 13-20.
5. J.P.Randin, *Electrochim. Acta*, 19, 1974, 83.
6. F. Beck, *J.Appl. Electrochem.*, 7, 1977 191.
7. L.Oniciu, Maria Jitaru and G.Bocea in "Electrocataliza" Ed.Stiințifică București 1991, p.205.
8. M. Musilova, J.Mrha and J.Jindra, *J.Appl. electrochem.*, 3, 1973, 213.
9. L. Galicia, I.Gonzales, and Y.Meas, *Reaction Kinetics and Catalysis*, 44, 1991, 109.
10. M.A. Elmorsi, M. Gabor and E. Barendrecht, *J. Appl. Electrochem.*, 21, 1991, 1005.
11. E.M. Pica, C. Popescu, and I. Teuca, *Acta Tehnica Napocensis*, 1993, 38-44.
12. N. Kobayashi, H.Lam and C.C. Leznoff, *Inorg. Chem.*, 30, 1991, 973.
13. M.Jitaru, I. Marian, M.Pica, N.Santa, *Symposium " Electrochemistry- a Frontier Field of Theoretical and Practical Interest"*, Cluj-Napoca, 1996, p.29.
14. A.B.P. Lever, S. Liccocia, K.Magnell, P.C. Minor and B.S. Ramaswamy, *Am.Chem.Soc. Symp.*, Ser., 202, 1982, 237.

ELECTRODEPOSITION OF ZIRCONIUM OXIDE AND SILICON CARBIDE WITH NICKEL

Lidia Benea¹, Olga Mitoseriu¹ and Magda Lakatos-Varsanyi²

¹. Department of Metallurgy and Materials Science, "Lower Danube"
University, 47 Domneasca st., R-6200 GALATZI, Romanie

². Department of Physical Chemistry, Eötvös Lorand University,
Budapest 112 P.O. Box 32, H-1518 Hungary

ABSTRACT

Composite coatings obtained by metal, codeposition of various disperse phases during electrocrystallization have been given special attention in recent years. Advanced results have been reported both from the fundamental research and industrial application implementation.

The paper reviews the information from literature on the disperse phase electrochemical deposition in metals and also outlines the author's own experimental results in this field.

The study is focused on the composite system in nickel matrix with zirconium oxide and silicon carbide disperse particles. The cathodic polarization curves in electrolytes have been determined and plotted both in the presence and absence of insoluble disperse particles by means of a computer controlled potentiostat galvanostat type PAR 273 (USA). The electrochemical impedance spectroscopy method was used to obtain additional information on the early steps of nickel and nickel matrix composite electrodeposition. Measurement of impedance data were performed with Solartron type electrochemical interface and frequency response analyzer. A codeposition mechanism with its influencing to the disperse phase concentration in the composite layer is studied too.

The electrochemical cell of cylindrical shape with the anode and cathode cylindrically shaped too have provided good uniformity to the composite layers, enabling a proper structural analysis.

The effect of the operating parameters (current density, concentration of the disperse phase in the electrolyte) on the concentration of the disperse phase in the composite layer is correlated by means of simple mathematical equations.

A comparative study of the pure metal and the composite electrodeposits with the help of an electronic microscope revealed important morphological differences.

1. INTRODUCTION

Composite layer electrodeposition makes it possible for new materials to be obtained by incorporating different disperse particles into a metallic matrix reducing at the same time with the metal during the electrolyses [1].

The electrochemical codeposition (ECC) is one of the most important methods of providing composites with metallic or non-metallic compounds, as a second phase, inside metallic matrix (ECCM) or non-metallic matrix (ECCP).

Little research was carried out in this field, although Fink and Prince investigated the use of electrochemical deposition to obtain self lubricating copper graphite coatings in 1928 [2], until 30 years ago. In the last years the researches and interests in electrochemical codeposition have increased resulting in a better understanding of the process itself and in finding new industrial applications [3-19]. Materials are tested for resistance to wear, corrosion, lubrication, a longer service life of the materials in contact while moving [20] and even electrocatalysis [21].

The literature refers to composite coatings obtained through electrodeposition, characterised in terms of their mechanical properties. There is however a lack of comparative data with respect to the properties and influence of different disperse phases on the metallic matrix electrocrystallization.

Composite layer electrodeposition essentially consists in codeposition (inclusions) of solid disperse particles, which are in suspension in an electrodeposition bath, into the metal being deposited and which represents the really metallic matrix. These particles are generally considered insoluble. The electrochemical codeposition cannot be regarded as an electrochemical process separate from the metal itself electrocrystallisation [22].

Various metals were used as matrix, such as nickel considered an inert metal, copper for being an intermediate metal and zinc considered a normal metal from the electrocrystallization point of view.

2. EXPERIMENTAL CONDITIONS

For the investigation of particles codeposition with metals in order to obtain composite layers in metal matrix we have used two types of disperse particles: zirconium oxide (ZrO_2) and silicon carbide (SiC) for comparison purpose, both types of particles are semiconductors.

To ensure an even current distribution during the electrodeposition process, a 300 cm^3 cylindrical electrochemical cell was used having the cylindrically-shaped anode 20 mm from the cathode surface [22]. The cell provides a good uniformity to the metallic and composite coating, which is necessary for a better study of electrodeposition. The disperse particles have uniform access to the cathode surface and the effects of the different densities and therefore different coating compositions existing in the edges are thus eliminated. Holes of 5 mm diameter are drilled in the anodes 10 mm part to ensure uniformity of the suspension in the electrolyte and reduce the effective anode surface. This electrochemical cell excludes any forced codeposition by sedimentation and the influence of the particles on the metal electrodeposition as well as the influence of the operating parameters on codeposition can be properly investigated.

Electrodeposition was made on carbon steel, stainless steel, copper and nickel as supports (cathodes) having cylindrical shape and an effective area of 6 to 10 cm^2 .

The electrochemical cell used to obtain composite coatings is schematically illustrated in Fig.1

Cathodic polarisation experiments were performed on a potentiometer-galvanostate type EG & G PAR model 273 (USA), at the Physical Chemistry Department at Budapest University by

means of a computer program of cyclic voltametry for current voltage diagram plotting. The value of the metal reducing voltage (E) is given in connection with the calomel saturated electrode (ESC).

The particles were kept in suspension by mechanical or magnetic stirring at a speed 100-1500 rot/ min. A saturated calomel electrode was used as reference electrode (SCE) only to determine the influence of the disperse phase on polarisation curves. Nickel matrix codeposition were made in common nickel plating electrolytes, only the effect of dilution on the amount of disperse phase included in the coating was studied. The electrolytes were prepared from reactive p.a. and distilled water which provided the required purity for the potentiodynamic investigations and characterisations of the coatings obtained.

To determine the influence of the working parameters (electrolyte concentration, disperse phase concentration, current density) on the inclusion of the disperse phase into the composite layer, electrodeposition was performed on platinum cathodes, thus eliminating the possibility for the support to dissolve and errors to occur, when determining the disperse phase concentration.

To plot the curves of cathodic polarisation in electrolytes, with and without disperse phase and to characterise the composite layers obtained, electrodepositions were carried out on supports made from steel, nickel and copper.

To analyse the layer thickness and particle concentrations inside the composite layer, the layers were dissolved and subsequently weighed in an analytical microbalance of 10^{-5} accuracy. After dissolving the layers, the particles were separated on a filter type ME24-0.2 μ m. After rinsing and drying in vacuum at 80°C (10^{-2} torr), the particles were weighed again. The weight percentage of the particles in the composite deposition was calculated by the formula:

$$p\% = \frac{m_p}{m_s} 100 \quad (1)$$

where: $p\%$ - stands for the weight percentage of the particles in the composite layer; m_p - is the particle weight, in grams; m_s - is the dissolved composite layer mass, in grams

The following solutions were used to dissolve the metallic and composite layers:

- 15% nitric acid and composites in nickel matrix (for chemical dissolution),

-10% sulphuric acid (for electrochemical anodic dissolution). In this latter case, platinum was used as cathode. Electrochemical dissolution is more favourable since it takes less time (approximate 1/4) than the chemical dissolution.

3. RESULTS AND DISCUSSION

3.1. Cathodic polarisation curves

To investigate the disperse phase influence on the metal electrodeposition, the curves of cathodic polarisation, with and without disperse phase, were plotted, i.e. the variation of the current density with the metal reducing overvoltage was studied in the presence and absence of the disperse phases. No such measurements could be found in the literature for comparison purpose and diagram interpretations are based on exiting theories about metal and alloy electrocrystallisation [23, 24, 25].

From the analysis of cathode polarisation in the presence and absence of disperse phases the following remarks can be made:

* Hydrophilic particles (zirconium oxide) and hydrophobic particles (silicon carbide) have different effects on the cathodic polarisation curves in nickel electrodeposition.


* Disperse phases do not alter the shape of the cathodic polarisation curves in nickel electrodeposition they are only slightly shifted to lower values of the metal reducing voltage for zirconium oxide (Fig.2) and to higher values in the case of silicon carbide (Fig.3).

* Zirconium oxide as disperse phase in the nickel deposition electrolyte, does not change the electrocrystallization of nickel, but it does take part in the process by increasing the metal

deposition rate. For the same current density, metal reducing overvoltage is lower in the presence of oxides in electrolytes

The larger amount of metal being deposited in the presence of oxides as disperse phases, can also be due to the electroactive metal species which are absorbed or formed on the particle surface to be subsequently reduced on the cathode.

In increasing the layer thickness of metal being deposited, and which is the result of a competition between the nucleation steps and crystal growth, the oxides act as catalysts of metal reducing leading to an increase in the number of active nucleation sites.

As is well known, an increase in the current density leads to an increase in the nucleation centres so that the crystal size gets smaller within the electrodeposited metal structure. At the same current density the effect of the oxides involved in electrochemical metal deposition induces the same growth of the active nucleation sites. This conclusion further suggests that **the oxides involved in the metal electrodeposition will change their structure towards lower crystallite sizes**. The modification in the size of crystallites during composite oxide electrodeposition was checked by investigating the surfaces with respect to the pure metals electrodeposited at the same current density by means of the electronic microscope.  The decrease in the crystallite size will have a different influence on the reactivity of phase composite surfaces for the three types of metals directly related to their surface tension and the corrosive environment.

* Silicon carbide, a hydrophobic material, has an opposite effect on the nickel electrodeposition acting like an inhibitor. For the same current density, the metal deposition overvoltage increases which means that the silicon carbide particles blocks the cathode surface and needs an extra amount of energy to activate the electrodeposition.

The zirconium oxide as disperse phase in the metal electrodeposition electrolyte does not induce modifications to their electrocrystallization mechanism; it only influences the increase of the metal deposition speed. In the presence of zirconium oxide, the layer amount of metal

deposited as due to the electroactive metal species which are adsorbed or accumulate on the particle surface to be further reduced on the cathode.

The electrochemical spectroscopy impedance method was used to obtain additional information on the early steps of nickel electrodeposition (ESI) [26].

The electrodepositions of pure nickel in the presence of zirconium oxide have taken place at the same overvoltage, -1150 mV (ESC). For the same cathode surface, the current was 50 mA in the case of pure nickel electrodeposition and it subsequently increased to 87 mA in the case of zirconium oxide electrolyte. This is in good agreement with the cathode polarisation diagrams showing the increase in the deposition current at the same overvoltage in the case of zirconium oxide codeposition in a nickel matrix

This method allows for the calculations of the equivalent circuit for the intermediate steps with electron transfer during electrodeposition and therefore the estimation of the time constant.

The complex plane impedance diagrams for nickel matrix with zirconium oxide composite coatings and pure nickel electrodeposition are illustrated in Fig. 4. In Fig. 5(A) and 5(B) are presented the capacitance and conductance curves vs. frequency, plotted in the same conditions. Full circles on the capacitance vs. frequency curves represent its negative values.

3.2. Estimation of the equivalent circuit

As it can be seen, the impedance diagrams for the pure nickel and composite electrodeposition have the same shape while the time constants for the intermediate steps take the same values as shown in Table 1. This confirms that the disperse particles do not modify the metal electrocrystallization mechanism.

Table 1. Impedance data calculated for intermediate steps for pure nickel electrodeposition and composite coating with ZrO₂, from the same electrolyte and the same reducing overvoltage

Type of coating ⇒ Calculated data ↓	Pure Ni	ZrO ₂ /Ni-AC
Double layer capacity $C_{dl} [\mu\text{Fcm}^{-2}]$	59	53
Charge transfer resistance $R_{TS} [\Omega\text{cm}^2]$	5.2	3,8
$C_1 [\mu\text{Fcm}^{-2}]$	13	5,2
$R_1 [\Omega\text{cm}^2]$	40	40
$\tau_1 [s]$	$6,2 \times 10^{-4}$	2×10^{-4}
$C_2 [\mu\text{Fcm}^{-2}]$	1200	857
$R_2 [\Omega\text{cm}^2]$	58	30,3
$\tau_2 [s]$	$6,9 \times 10^{-2}$	$2,6 \times 10^{-2}$
$C_3 [\text{mFcm}^{-2}]$	249	74
$R_3 [\Omega\text{cm}^2]$	19.8	27
$\tau_3 [s]$	4,9	1,9

From the conductance vs. frequency curves and capacitance vs. frequency curves, three steps of intermediate electronic transfer were of interest with their time constants shown in the Table 1. The curves were estimated after the electrolyte resistance had been removed. The charge transfer resistance is $R_{TS}=3.8\Omega\text{cm}^2$ for composite coating, and higher for pure nickel electrocrystallization, $R_{TS} = 5.2 \Omega\text{cm}^2$ respectively. The equivalent circuit proposed is presented in Fig. 6. Reaction paths for the dissolution of divalent species involving univalent intermediates must exhibit pseudo capacitance effects in transient or ac phenomena. This is due to the fact that the change in potential must be accompanied by a corresponding change in the concentration of

the intermediate. This can be done only by exchanging charge with the electrode. The method of evaluating of the impedance spectra was described in the works [27, 28, 29].

Further experiments during composite electrodeposition can be done in the low frequency range for obtaining information about structural aspects and grain sizes of metal matrix in presence of disperse phase

3. 2. Codeposition mechanism and steps

In the absence of an electric field, on the cathode surface there is a layer absorbed by ion species which include hydrated metal ions and ions from the particle adsorption area. Particles are absorbed on the cathode surface due to the ions absorbed at their surface.

Bivalent metal transition from ion state to metal state takes places in two steps of ion transfer which call for a lower energy barrier than only one step of two ion changing.

In poor acid or neutral solutions they form chemical species with the hydroxyl ions (OH^-) of type (MOH^+) and $\text{M}(\text{OH})_2$ which exist in enough concentration on the cathode surface to compete with the free metal ion during the mass transfer.

Nickel electrodeposition is strongly influenced by hydrogen discharge and can take place according to the following intermediate formulas [30, 31]:



Adion Ni_{ads}^+ , more or less solvated or complexed, in the surface species, NiOH_{ads} , proposed as intermediate element in the nickel dissolution and deposition mechanism [32].

Hydrogen, H^* _{ads}, can be much adsorbed on the deposited nickel surface due to the presence of Ni^+ _{ads} which may be born by recombination or inclusion into the electrodeposition , according with the reactions:



Hydrogen adsorption and inclusion into the deposition inhibits hydrogen development according to reaction (2 d). The effect of zirconium oxide and silicon carbide particles on the cathodic polarisation curves (Fig. 2 and 3) reveals the difference between the two types of particles during the nickel electrocrystallization, the silicon carbide acting as inhibitor of the cathodic nickel reducing reaction and decreasing the current efficiency.

It is possible that reaction (2e) should be catalysed due to the hydrogen adsorbed into the silicon carbide particles and therefore the hydrogen included into the composite deposition should be catalysed as well. The analyses revealed a hydrogen content 10 times higher in the silicon carbide composite layers as compared with the pure nickel [33]. The first step, having the fastest time constant can be related to the hydrogen evolution on the nickel deposit surfaces, the charge transfer for its reduction being known as a fast process.

The other two time constants belong to reactions (2a) and (2b) of the nickel electrodeposition mechanism. During the electrochemical codeposition the zirconium oxide particles catalyses the adsorbed intermediate element according to reaction (2a) , thus decreasing the influence of charge transfer for the final reaction (2b). This can be easily noticed on the impedance diagrams plotted in the complex plane (Fig. 4) and in Table 1.

The oxide acts as catalyst for the metal reduction , resulting in a larger number of active nucleation sites. The oxide codeposited during the metal electrodeposition process will induce

structural modifications in these metals, i.e. smaller crystal grains. Modification of crystal size in zirconium oxide composite coating as compared with pure metals electrodeposited in the same conditions were checked with the electronic microscope (Fig. 7 a and b).

The silicon carbide, a hydrophobe material, has an opposite effect on nickel electrodeposition, acting like inhibitor. For the same current density, the metal deposition overvoltage increases which indicates that the silicon carbide particles block the cathode surface requiring on extra amount of energy to activate the electrodeposition (Fig.7 c).

Metal electrodeposition rate and crystallite growth is a function of the overvoltage (deposition potential) just like other electrode processes. The basic elements of their relation were found by Erdey- Gruz and Volmer [23] who determined the way in which the rate of the entire process of incorporating the hydrated metal ion into the metal network affects the shape of the current-potential curve. In general, far enough from the equilibrium potential where metal electrocrystallization usually takes place, the essential step of metal electrodeposition rate is the neutralisation of the metal ion by transferring the electron from the cathodic to the metal ion.

Many interdependent experimental factors affect the codeposition process. The models able to predict the amount of particles included into the composite layer under experimental conditions are promising but still require a lot of study and correlation for each individual composite system.

Codeposition of disperse particles in the metal electrodeposition can be schematised in the following steps:

- (1) a double layer of adsorbed species is formed round each particle after their introducing in the electrolyte;
- (2) particles are carried , by stirring, to the limit of the hydrodynamic layer;

(3) under the influence of an electric field, only the positively charged particles will be diffused to the cathode surface. The adsorbed particles above all negative ions will be diffused back in the electrolyte solution.

(4) free or adsorbed electroactive species are reduced at the cathode;

(5) the particle is included into the deposition when the adsorbed ion species on it are reduced at the cathode surface.

Particle codeposition through the five steps occurring on parallel with the pure metal electrodeposition is schematically illustrated in Fig. 8.

Experimental data demonstrated a strong dependence of particle codeposition on solution composition, type and concentration of disperse phases, current density and another influencing factors in electrocrystallization of metals. All of these influencing factors will be presented in further papers.

5. CONCLUSIONS

Electrochemical codeposition of inert disperse particles into a metal matrix is a favourable technique for providing composite materials. Codeposition represents a good alternative above all in terms of coatings as compared with other techniques and provides composite layers of unique properties.

The experiments have shown the possibility of obtaining composite layers in nickel, copper and zinc matrix by metal electrodeposition with inert particles of oxides and silicon carbide, featuring different effects in the intermediate steps of electrocrystallization which are further to be found in the different structures and properties .

The various effects during codeposition showed a good correlation with various structures and different properties of the corresponding composite layers.

The experiments carried out for the codeposition of oxides and silicon carbide disperse phase in nickel matrix lead to the following conclusions:

- the electrodeposition was carried out to see the influence of the disperse phase on metal electrodeposition process on the cathodic polarisation curves, since no references were found in the literature.
- correlations were made between the working parameters and the electrolyte composition and the disperse phase concentration for the composite layers in nickel, copper and zinc matrix.
- the SEM morphologies of nickel matrix composite coatings comparative with pure nickel electrodeposition were in agreement with the influences of the disperses phases in the nicel plating.

REFERENCES

- [1] Benea L.; Ph.D. Thesis "*Obtinerea si analiza structurală a peliculelor protectoare din materiale compozite*" University "Dunărea de Jos" of Galati, 1995, pp. 10-15.
- [2] Fink C. G. and Prince J. D.; *Trans. Am. Electrochem. Soc.* **54**, 315 (1928).
- [3] Roos J. R., Celis J.P., Fransaer J. and Buelens C.; *J. Metals*, **42**, 60 (1990).
- [4] Fransaer J., Celis J. P. and Roos J. P.; *Met. Finish.* **91**, 97 (1993).
- [5] Greco V. P. and Baldauf W.; *Plating* **55**, 250 (1968).
- [6] Keddam M., Senyarich S., Takenouti H. and Bernard P.; *J. Appl. Electrochem.* **24**, 103 (1994).
- [7] Sautter F. K.; *J. Electrochem. Soc.* **110**, 557 (1963).
- [8] Guglielmi N. ; *J. Electrochem. Soc.* **119**, 1009 (1972).
- [9] Celis J. P. and Roos J. R. ; *J. Electrochem.Soc.* **124**, 1508 (1977).
- [10] Suzuki Y. and Asai O ; *J. Electrochem. Soc.*; **134**, 1905 (1987).
- [11] Haayashi H., Izumi S. and Tari I.; *J. Electrochem. Soc.*, **140**, 362 (1993).
- [12] Lee C. C. and Wan C. C.; *J. Electrochem. Soc.*, **135**, 1930 (1988).
- [13] Lakshminarayanan G. R., Chen E. S. and Sautter F. K.; *Plat. Surf. Finish.*; **63**, 38 (1976).
- [14] Yeh S. H. and Wan C. C.; *J. Appl. Electrochem.* **24**, 993 (1994).

- [15] Celis J. P., Roos J. R. and Buelens C.; *J. Electrochem. Soc.* ; **134**, 1402 (1987)
- [16] Hwang B. J. and Hwang C. S.; *J. Electrochem. Soc.*, **140**, 979 (1993).
- [17] Sonneveld P. J., Visscher W and Barendrecht E.; *J. Appl. Electrochem.*, **20**, 563 (1990).
- [18] Gibbons D. W., Muller R. H. and Tobias C. W.; *J. Electrochem. Soc.*; **138**, 3255 (1991).
- [19] Degrez M. and Winand R.; *Electrochimica Acta*, **29**, 365 (1984).
- [20] Hovestad A. and Janssen L. J. J. ; *J. Appl. Electrochem.*, **25**, 519-527 (1995).
- [21] Anani A., Mao Z., Srinivasan S. and Appelby A. J. ; *J. Appl. Electrochem.*, **21**, 683 (1991).
- [22] Benea L.; Ph. D. Thesis "*Obtinerea si analiza structurală a peliculelor protectoare din materiale compozite*" University "Dunărea de Jos" of Galati, 1995, pp. 30-60.
- [23] Erdey-Grúz T.; "*Kinetics of Electrode Processes*", Ed. Akadémiai Kiadó, Budapest, English Ed. Published by A. Hilger Ltd. London, 1972, pp. 350-430.
- [24] Radovici O. ; "*Tratat de Chimie Fizică, Vol 4, Electrochimie*", Ed. Academy, Bucuresti, 1986.
- [25] Bockris J. O 'M. ; "*Fundamental Aspects of Electrocrystallization*", Plenum Press, New-York, 1967.
- [26] Benea L.; Ph. D. Thesis "*Obtinerea si analiza structurală a peliculelor protectoare din materiale compozite*" University "Dunărea de Jos" of Galati, 1996, pp. 112-121.

- [27] R.D. Armstrong, and M.Henderson ; *J.Electroanal. Chem.*, **39**, 81-90 (1972).
- [28] A. Pirnát, L. Mészáros, and B. Lengyel ; *Electrochimica Acta*, **35**, 515-522 (1990)
- [29] L. Mészáros; "*Evaluation of Impedance Diagrams In Corrosion Measuring Technique*",
Paper in press (1995).
- [30] A.J. bard, *Encyclopedia of Electrochemistry of the Elements* Vol. III (1973), Dekker,
Bard
- [31] V.V. Skorchelleti, in "*Theory of Metal Corrosion*", Leningrad 1973, Translated from
Russian by R.Kondov 1976, p.108.
- [32] Wiart R.; *Electrochimica Acta* , **35** , 1587-1593 (1990).
- [33] Watson S. W. ; *J. Electrochem Soc.* , **140**, 2235 (1993).

FIGURES CAPTION

- Fig. 1. Scheme of the experimental set-up for the electrodeposition of composite coatings : (1) electrolytic cell; (2) electrolyte and disperse phase suspension, (3) anode; (3') anode surface cross-section; (4) cathode; (5) copper electrical contact with taper inside the cathode; (6) reference electrode; (7) insulating system for maintaining the cathode; (8) stirring device.
- Fig. 2. Cathodic polarisation curves for obtaining composite layers in a nickel matrix; (a) nickel-plating electrolyte; b) nickel-plating electrolyte + 100g/l zirconium oxide
- Fig. 3. Cathodic polarisation curves for obtaining composite layers with silicon carbide in a nickel matrix; a) chloride sulphate nickel-plating electrolyte; b) nickel-plating electrolyte + 100g/l silicon carbide.
- Fig. 4. Complex plane representation of the impedance diagrams at the same reduced overvoltage: (NiD-7) composite coating codeposition with ZrO_2 particles in a nickel matrix; (NiD-1) pure nickel depositions
- Fig. 5 (A). Impedance data for the composite layer electrodeposition ZrO_2 /Ni-AC: [b] (D) $1/R_p$ depending on frequency ; [c] (o) C_p depending on frequency
- Fig. 5 (B). Impedance data for pure Ni electrodeposition; [b] (Δ) $1/R_p$ depending on frequency ; [c] (o) C_p depending on frequency
- Fig. 6. Equivalent circuit for the nickel and nickel matrix composite electrodeposition
- Fig. 7. SEM morphology of coatings: (a) pure nickel electrodeposited; (b) composite coating with ZrO_2 particles; (c) composite coating with SiC particles
- Fig. 8. The five steps of disperse particle codeposition in metal matrix for obtaining composite layers by electrolysis



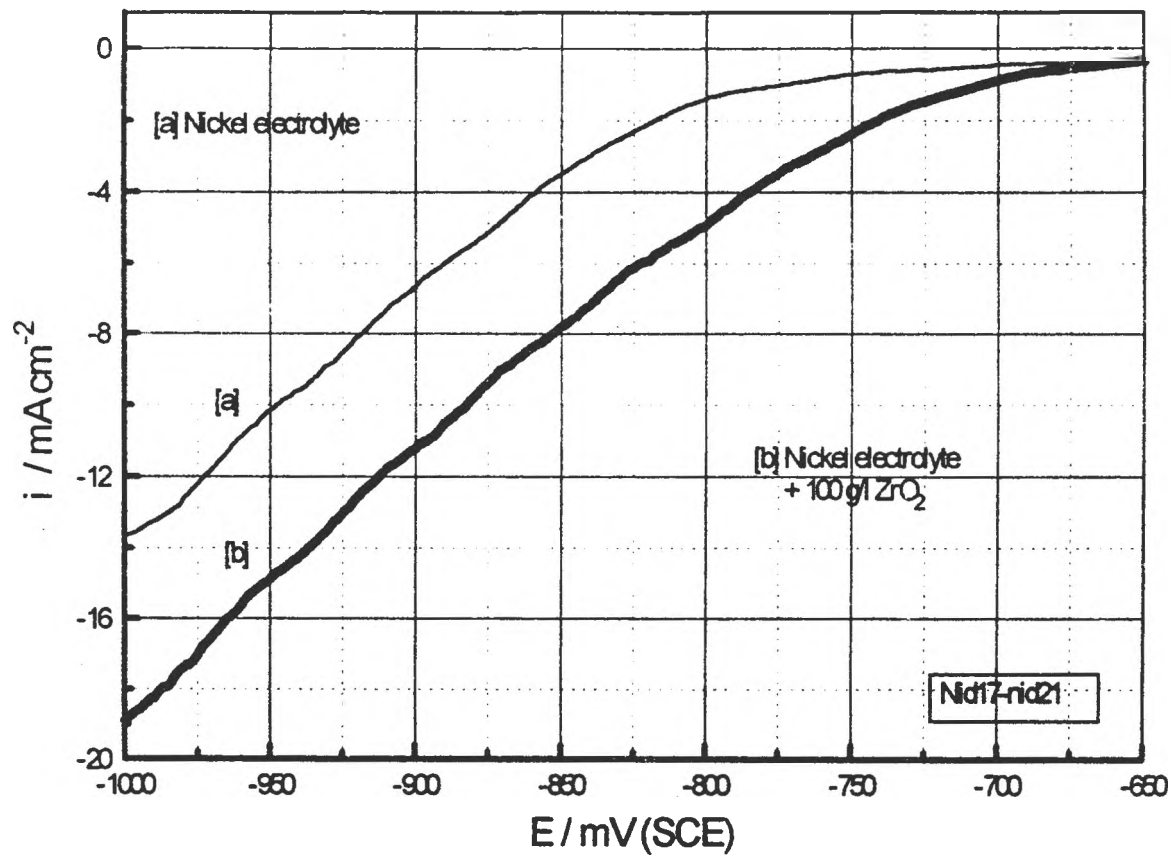


Fig. 2. Cathodic polarisation curves for obtaining composite layers in a nickel matrix;
 (a) nickel-plating electrolyte; b) nickel-plating electrolyte + 100g/l zirconium oxide

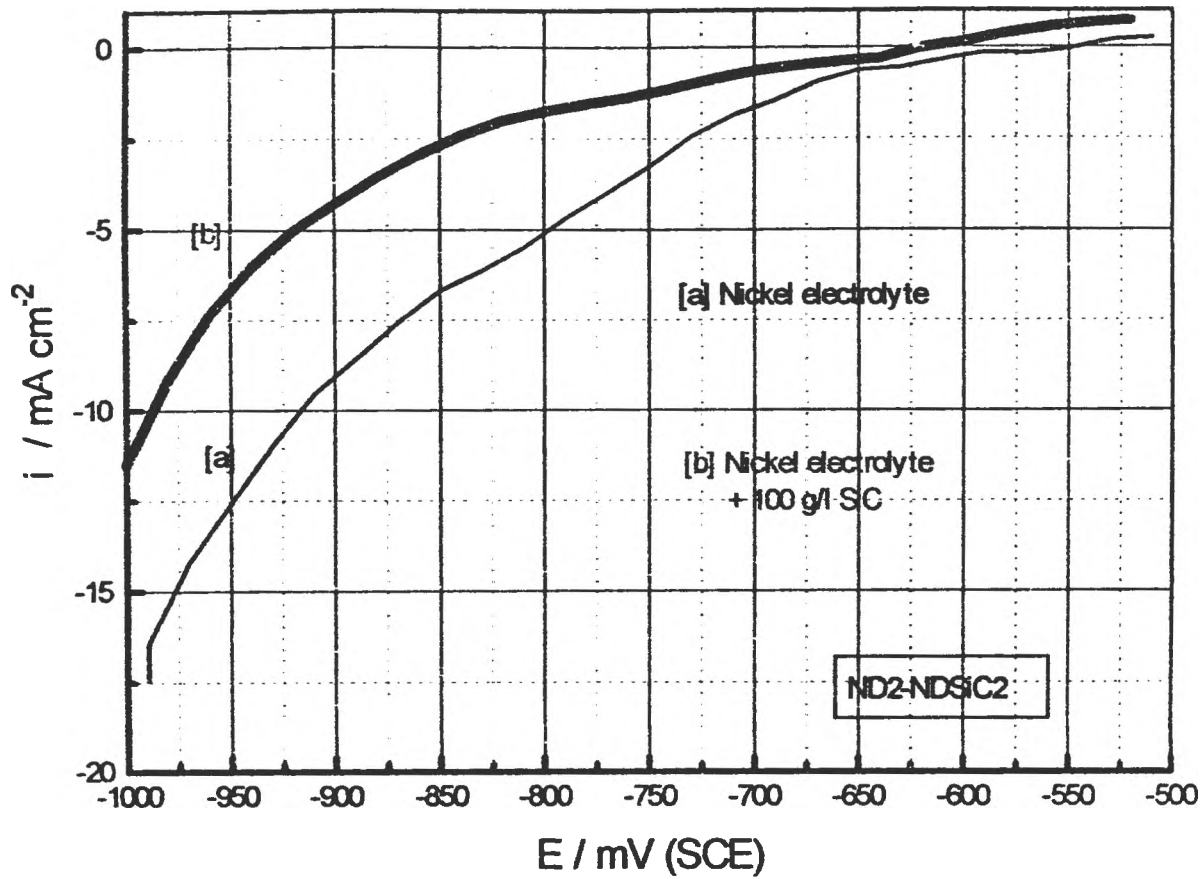


Fig. 3. Cathodic polarisation curves for obtaining composite layers with silicon carbide in a nickel matrix; a) nickel-plating electrolyte. b) nickel-plating electrolyte + 100 g/l silicon carbide.

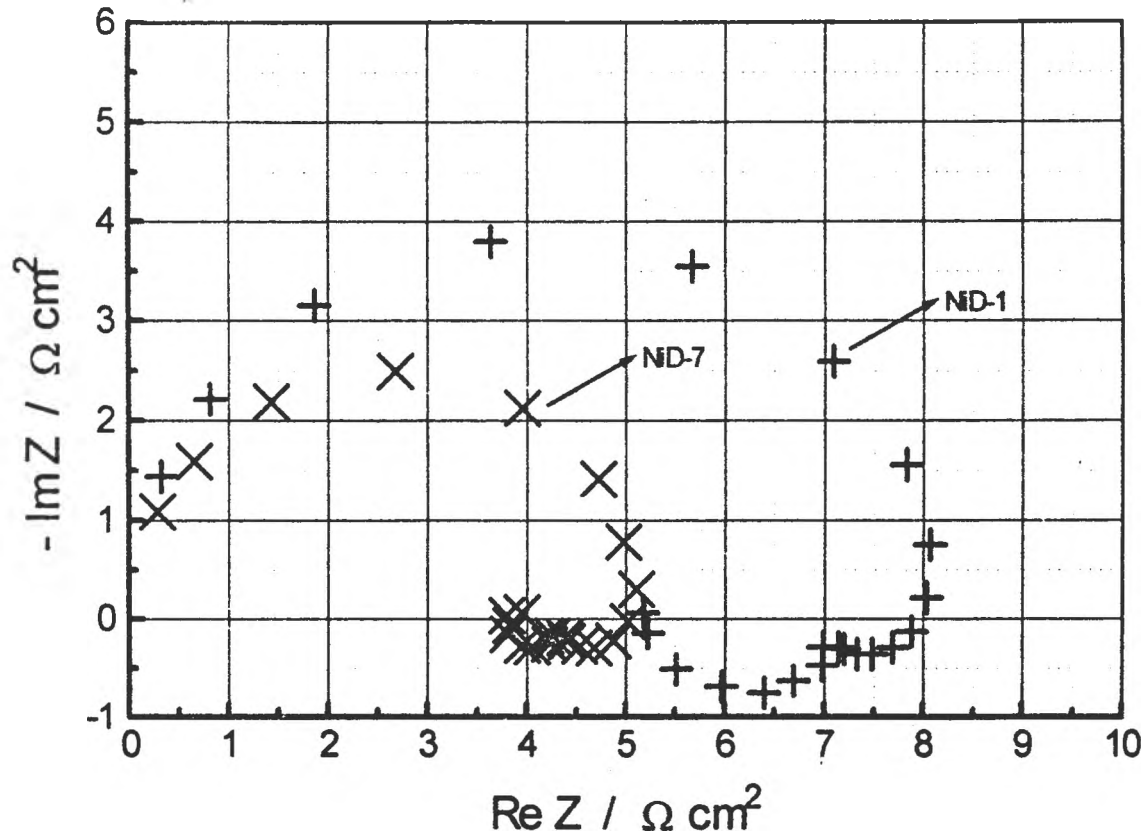


Fig. 4 Complex plane representation of the impedance diagrams at the same reduced overvoltage: (NiD-7) composite coating codeposition $ZrO_2 / Ni-CC$; (NiD-1) pure nickel deposition

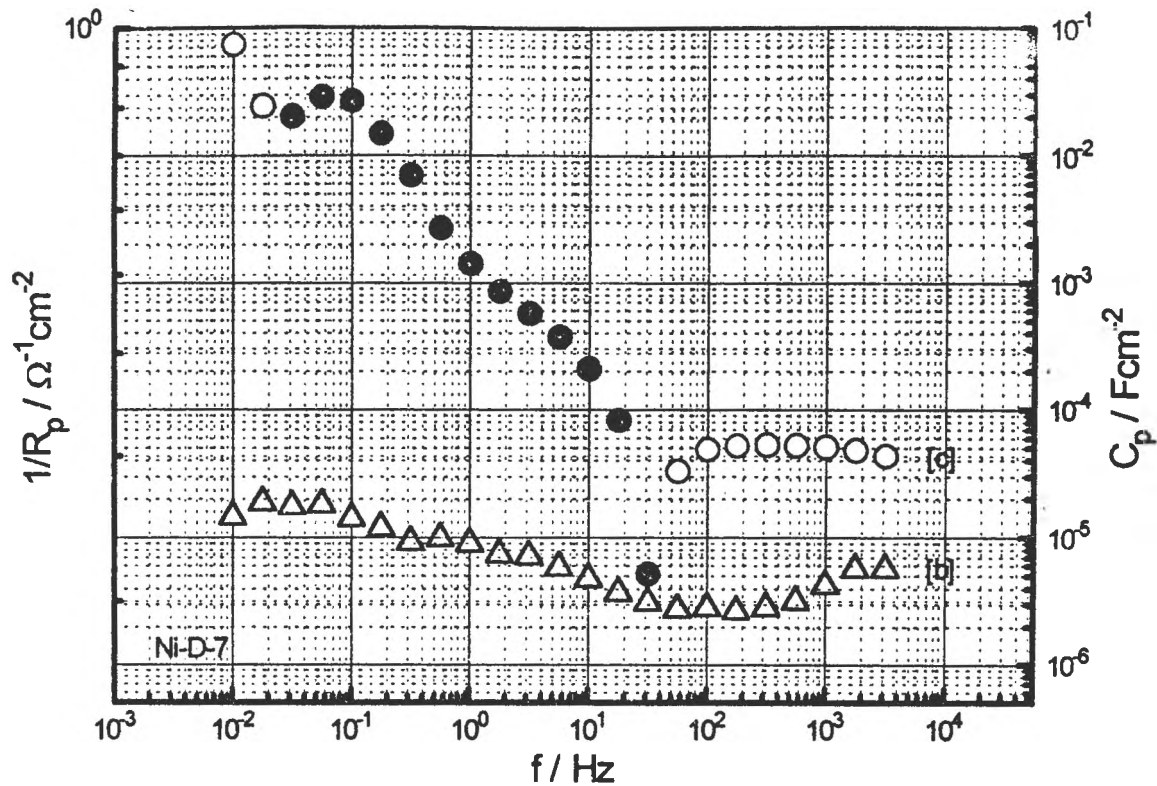


Fig. 5 (a) Impedance data for composite coating codeposition ZrO₂ /Ni-CC
 [b] (Δ) $1/R_p$ vs. frequency ; [c] (o) C_p vs. frequency

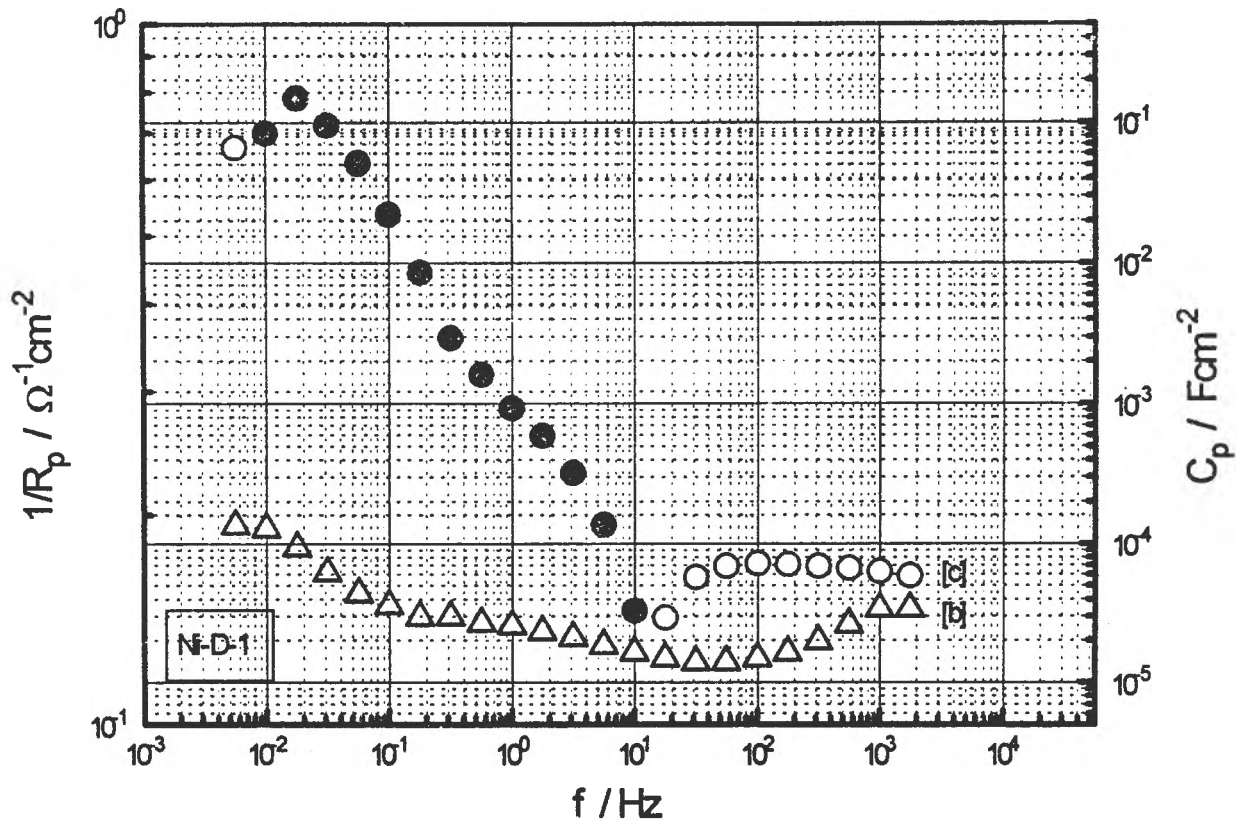


Fig. 5 (b) Impedance data for pure Ni electrodeposition:
 (Δ) $1/R_p$ vs. frequency ; [c] (o) C_p vs. frequency;

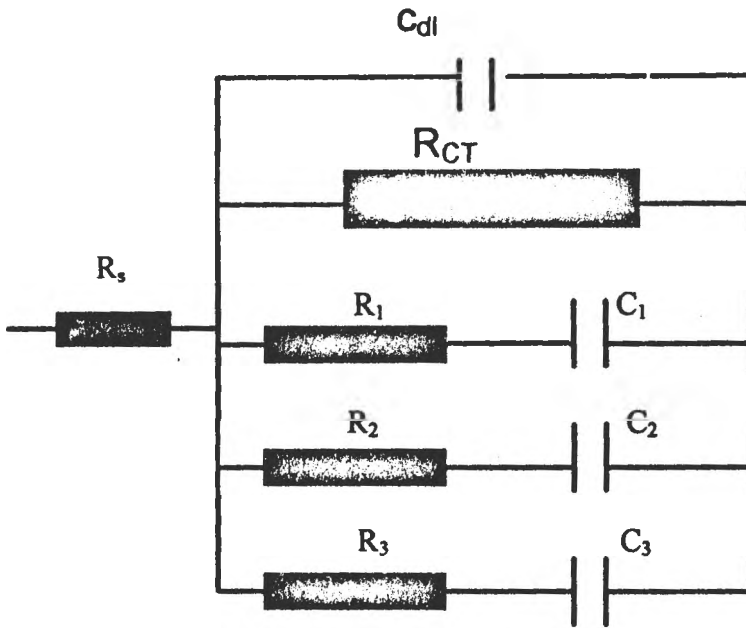


Fig. 6

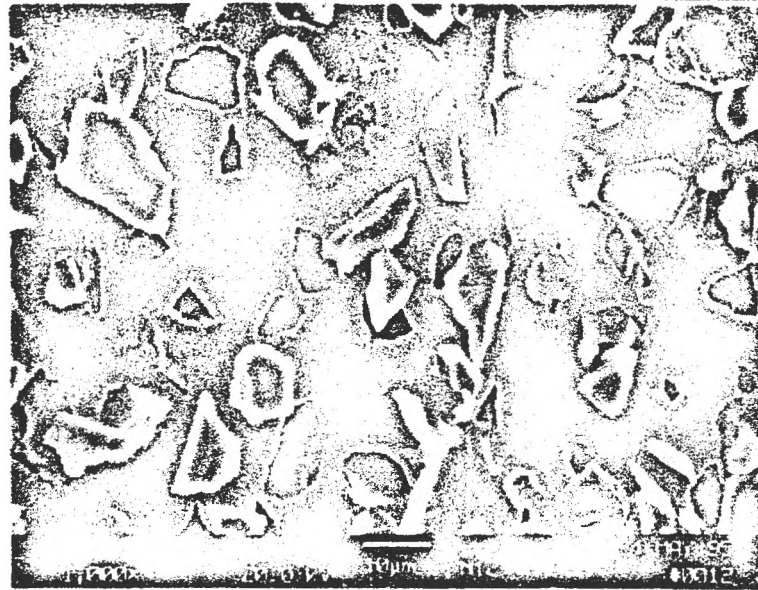


(a)



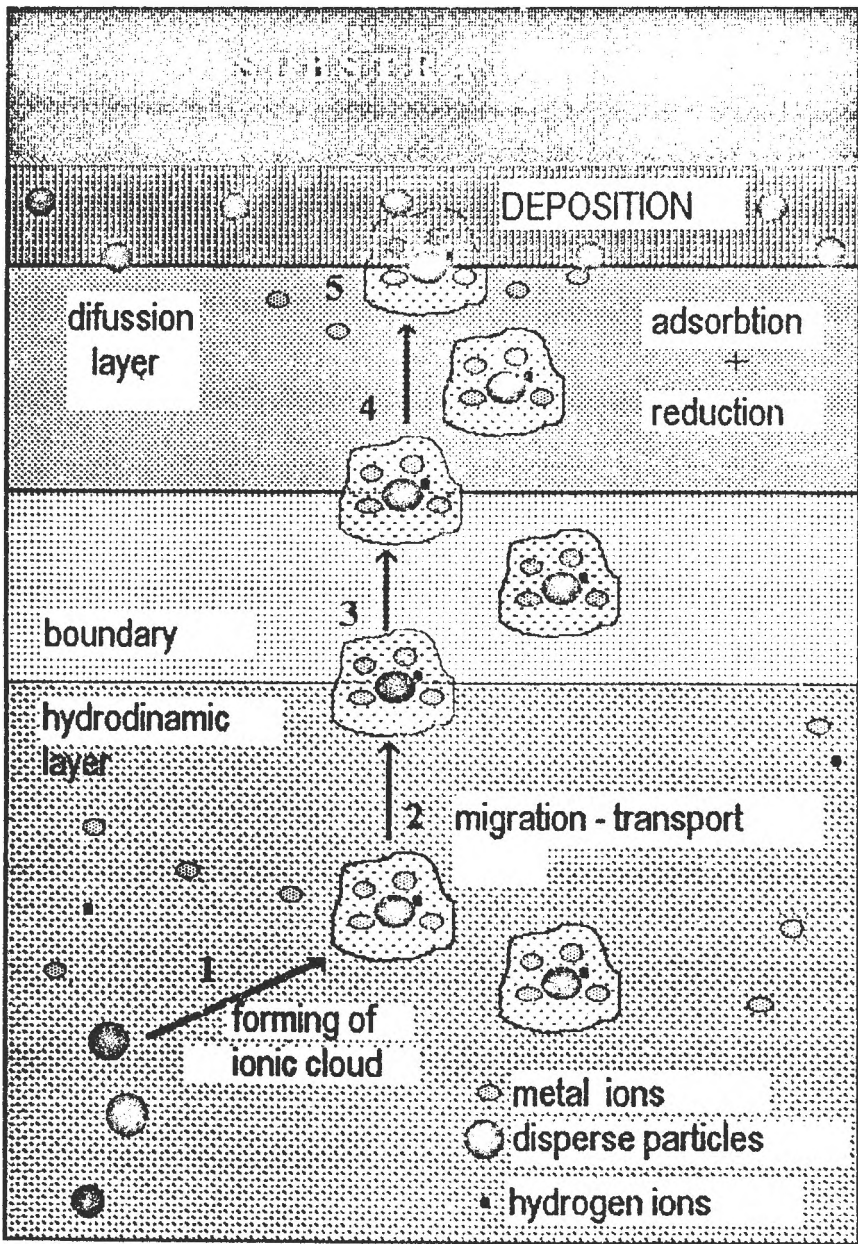
(b)

Figure 7. SEM morphology of coating: (a) Electrodeposited pure Ni; (b) ZrO_2 / Ni



(d)

Figure 7 (d). SEM morphology of coating: (c) SiC / Ni-CC,



THE FIVE STEPS OF DISPERSE PARTICLE CODEPOSITION
 IN A METAL MATRIX FOR OBTAINING COMPOSITE
 LAYERS BY ELECTROLYSIS

Fig. 8

THE EFFECT OF ANTIMONY ON ELECTROCHEMICAL BEHAVIOUR OF LEAD/ACID GRIDS

Eleonora Maria Rus and Della Constantin

DEPARTMENT OF PHYSICAL-CHEMISTRY, FACULTY OF CHEMISTRY AND
CHEMICAL ENGINEERING, "BABEŞ-BOLYAI" UNIVERSITY, 3400 CLUJ-NAPOCA,
ROUMANIA

ABSTRACT

Cyclic voltammetry, under rigorously controlled conditions (scan rates, positive and negative reversal potentials, polarizations at definite potentials and times) has been used to obtain more details on the effect of antimony presence upon the electrochemical properties of lead-antimony alloys in lead-acid battery grids. The composite lead sulfate-oxide passive layer produced anodically in the potential range 0 to 800 mV, on pure Pb and Pb with 1.7, 3.0, 8.5 and 11.27 wt% Sb alloys respectively in 3.83 and 2.32 M H₂SO₄ solutions have been investigated. The effects of antimony on the electrochemical behaviour of the alloys has been found to be beneficial only at Sb contents lower than 11.27wt%.

INTRODUCTION

Although, the influence of antimony within the acid battery grids upon its operation has been extensively investigated, its role has not been totally clarified in the speciality literature, some contradictory opinions still exist [1-10]. The presence of Sb in the alloys of battery grids was proved to significantly influence both the mechanical properties and the electrochemical behaviour of electrodes [11-15].

The antimony is considered to strengthen the cohesion between the grid and the inner corrosion layer which is formed at the positive plates on charging, and it improves, at the same time, its integrity implicitly the integrity of the PbO₂ layer [5].

Through their high resistance to passivation the Pb-Sb alloys confer a high charge acceptance and a high structural stability to plates on deep charge-discharge cycles. Pavlov and coworkers suggest a cathalitical effect of antimony on the oxidation process of PbO₂→PbO_n, demonstrating that it causes a potential range between 0.8 and 1.3V/Hg, Hg₂SO₄ to be set up, wherein nonstoichiometric oxides of Pb_{1-x}Sb_xO_n would be formed[1]. The mixt oxides are structurally cristalline or amorphous, similar to those formed on pure lead [11]. Nevertheless, the formation of mixt oxides as a result of the high affinity of antimony ions for water, changes the hydrating degree of PbO₂ which was found to be 20- 30% on alloys against only 10% on pure Pb.

The increased discharging capacity of Pb-Sb grid batteries is at some extent, determined by this high hydrating degree which confers also a remarkable integrity and elasticity to the corrosion layer against the stress induced by volume variation accompanying oxides products formation.

It has been found that the multi-phase structure layer which is formed on lead below 0.8 V/ Hg, Hg_2SO_4 , between the PbSO_4 passive membrane and metallic lead, consists mainly of tetra-PbO and contains a few basic lead sulfates ($3\text{PbO}\cdot\text{PbSO}_4\cdot\text{H}_2\text{O}$ and $\text{PbO}\cdot\text{PbSO}_4$)[1,9,12]. The electrochemical behaviour of the tetra-PbO film plays an important role in the performances of lead acid battery. Both the formation and the reduction of the tetra-PbO and of the basic lead sulfates, according to Guo, occur via a dissolution-deposition mechanism and are controlled by HO^- ion diffusion through the PbSO_4 membrane[9,12].

On the Pb-Sb electrodes a smaller amount of tetra- PbO and a thicker layer of basic lead sulfates are formed compared with Pb electrodes. This fact was explained by the more microporous structure PbSO_4 membrane formed by dissolution of Sb into H_2SO_4 solution [1, 12, 13]. According to Guo the greater diffusion rates of ions (H^+ and SO_4^{2-} from the bulk of the solution to the inner layer of PbSO_4 membrane and HO^- ion in the opposite direction) cause a drop of the pH in inner layer and promote the basic lead sulfates to be formed.

Once formed, these thick layers of basic lead sulfates reduce the migration rate of H^+ , SO_4^{2-} and HO^- ions and prevent the formation of consistent tetra-PbO layers. In these conditions the corrosion layers formed in alloys become less sensitive to stresses caused by the formation of anodic products[16].

The present paper compares the results of investigation by cyclic voltammetry in strictly controlled conditions on the electrochemical behaviour of lead and some Pb-Sb alloys, in various concentrations of sulfuric acid.

EXPERIMENTAL CONDITIONS

The disk-shaped 1cm^2 area test electrodes were 99.998wt% Pb(A) and Pb-Sb alloys with a content of 1.7(B), 3.0(C), 8.5(D) and 11.3wt% Sb(E). The counter electrode was a Pt spiral 5cm^2 in area. All potential values were measured and expressed in this paper, versus the $\text{Hg}/\text{Hg}_2\text{SO}_4$, K_2SO_4 (sat.) reference electrode. Prior to each test, the electrode surface was mechanically cleaned with emery paper, washed with distilled water and polarized for a determined time at potentials below -1.3V in order to provide a totally oxide-free surface. In view of results reproducibility, all experiments were started after maintaining the electrodes for 5 minutes at the stationary installed potential, after immersion in electrolyte. The 2.32 and 3.83 M H_2SO_4 solutions were prepared of concentrated p.a. H_2SO_4 .

The cyclic voltammograms and the potentiodynamic cathodic curves were recorded at room temperature using a PCA-72H Wenking potentiostat, a PV-2 Meinsberg voltage scan generator, an MV-87 multimeter and a X-Y 7911 NE 230 recorder.

RESULTS AND DISCUSSIONS

1. Cyclic Voltammetry on Pure Lead

The recorded voltammograms, within the potential of hydrogen evolution and that of oxygen evolution range, in 2.3 M and 3.83 M H_2SO_4 solutions on pure lead electrode presented the peak A, in anodic sweep, at -980mV, corresponding to $PbSO_4$ formation (Fig. 1).

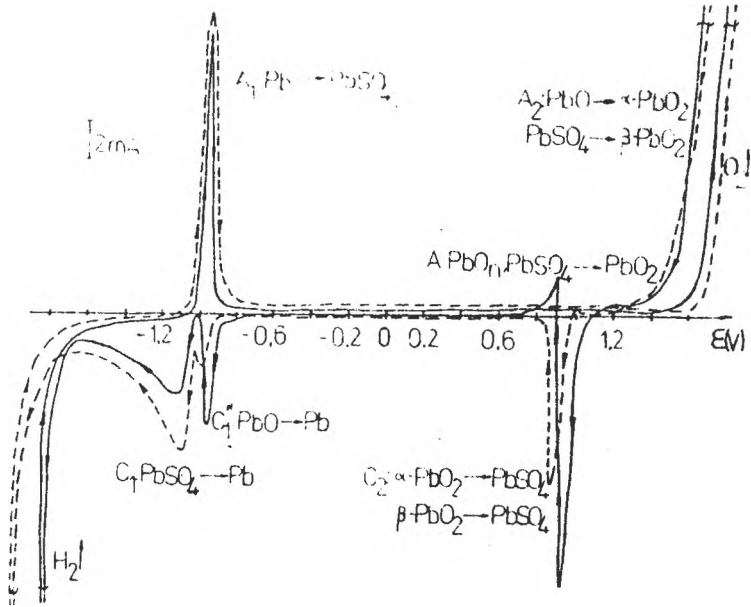


Fig 1. Cyclic voltammograms of Pb in 2.32 (- - -)and 3.83M(—) H_2SO_4 solutions; $v=20mV/s$

A passive range up to approximately 1600mV follows after this peak, where the appearance of peak A_2 is attributed to the oxidation of tetra-PbO and $PbSO_4$ to α - and β - PbO_2 concomitantly with the oxygen evolution. In cathodic potential sweep a mixt cathodic and anodic activity is recorded within 1000:900 mV, which is due, one hand, to the reduction of α - and β - PbO_2 to $PbSO_4$ (peak C_2) and, on the other hand, to further oxidation of lead and/or some incompletely oxidized compounds of lead (peak A) [16,17].

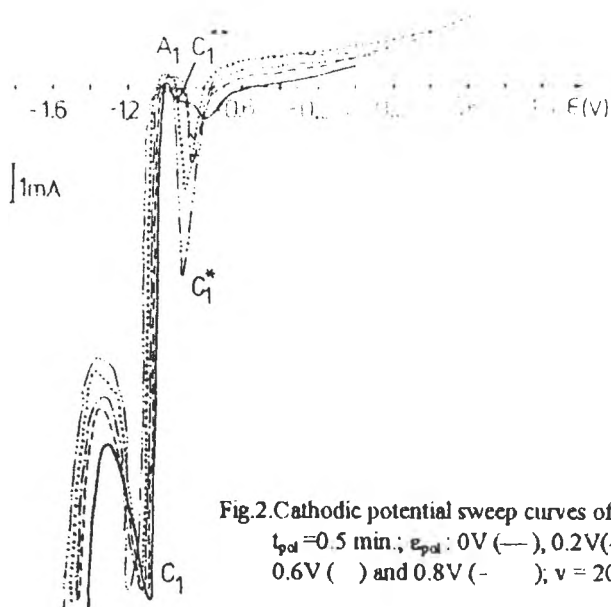


Fig.2. Cathodic potential sweep curves of Pb in 3.83M H₂SO₄; $t_{pox}=0.5$ min.; e_{pox} : 0V (—), 0.2V(---), 0.4V(-.-), 0.6V (·) and 0.8V(- - -); $v = 20$ mV/s.

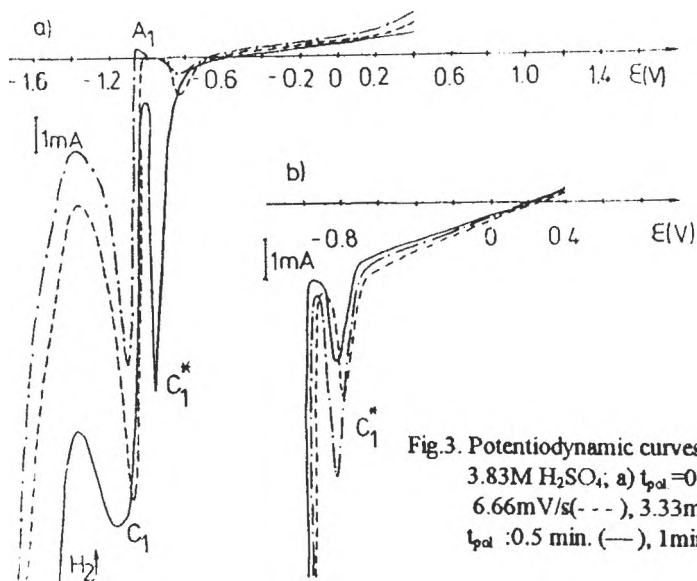


Fig.3. Potentiodynamic curves of Pb; $e_{pox} = 0.4$ V; 3.83M H₂SO₄; a) $t_{pox}=0.5$ min.; v : 20mV/s(—), 6.66mV/s(---), 3.33mV/s(-.-); b) $v=20$ mV/s; t_{pox} : 0.5 min. (—), 1 min. (---), 2 min. (-.-).

THE EFFECT OF ANTIMONY

As the oxidation products associated with this peak(A) is concerned, the literature is still contradictory. It was suggested to be a divalent[18,19], trivalent[20] or even tetravalent [21] product of lead. The evolution of such processes is favoured by the decrease of thickness or partial destruction (cracks appearance) of inner layer as a result of PbO₂ reduction.

On more negative potentials, in cathodic sweep the peak C₁' was recorded at -850mV subsequent to reducing the tetra-PbO, a fact recently confirmed by Guo and co. by X-rays diffraction[22]. At -1150mV, the peak C₁ sets into evidence the reduction of PbSO₄ to Pb, a process followed by hydrogen evolution. In order to obtain more information about the composition of anodic layer formed on lead at potentials below 0.8V, the negative potential sweep curves, after polarization at different potentials and times, with different sweep rates were recorded. Fig. 2 shows the cathodic sweep curves after the Pb electrode has been polarized for 0.5 minute at 0, 0.2, 0.4, 0.6 and 0.8V respectively.

At polarization potentials up to 0V only two reduction peaks (C₁' at -850mV and C₁ at -1150mV) and an oxidation peak (A₁ at -1000mV) in the potentiodynamic curves between the polarization potential(E_{pol}) and -2000mV are clearly visible.

We can say that if during the anodic polarization basic lead sulfates are formed, their amount is so small that their reduction peak current cannot appear in this curves. The anodic peak A₁ which appears in cathodic potential sweep corresponds to the oxidation of the freshly formed metallic lead on the reduction of tetra-PbO (peak C₁') underneath the PbSO₄ layer[9,12]. On the polarization of 0V, a small cathodic peak C₁'', at approximately -900mV corresponding to the reduction of an basic lead sulfate was recorded[6]. The potentiodynamic curves denote that the height of peak C₁' significantly increases with the increase of polarization potential value and concomitantly the reduction potential (of C₁') shifts in the negative direction increasing the reduction of tetra-PbO overpotential. The more negative the C₁' peak potential, the greater the amount of the tetra-PbO formed in the anodic layer. It seems that on pure lead, in our experimental conditions at anodic polarization potential above 0V, the growth of tetra-PbO is the main process.

Great changes of peak C₁' current and potential take place when after the electrode was polarized at 0.4V for 0.5 minute, the cathodic potentiodynamic curves at different sweep rates were recorded, Fig. 3a.

The faster the sweep rate is, the higher the peak current and the more negative the reduction peak potential of tetra-PbO. Although the duration of the potentiostatic oxidation is the same in each case the charge contained in peak C₁' is smaller at slower cathodic potential sweep rates. It is possible that, a major part of tetra-PbO has been transformed underneath the PbSO₄ membrane into lead sulfate in the slower potential sweep. Stronger C₁' cathodic currents were recorded after longer anodic polarization at the same potential values (Fig 3b), but no basic lead sulfates were recorded.

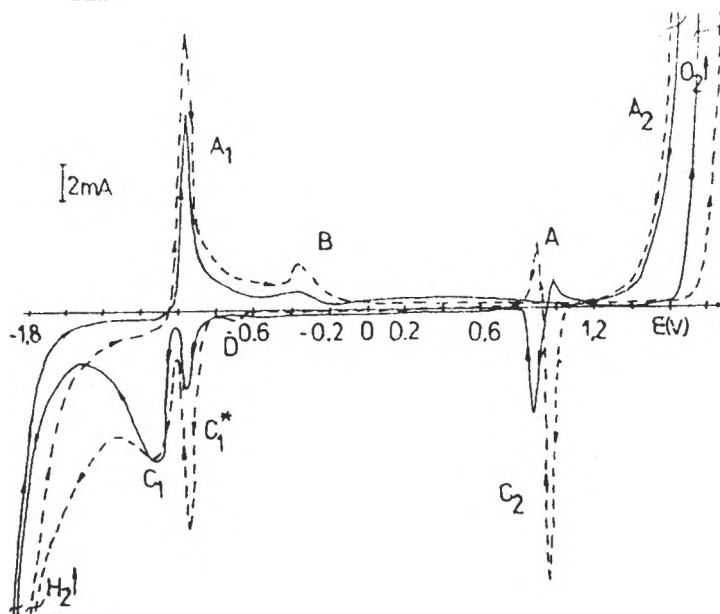


Fig.4. Cyclic voltammograms of Pb - 3% Sb electrode. $v = 20 \text{ mV/s}$; $2.32 \text{ M H}_2\text{SO}_4$ (—), $3.83 \text{ M H}_2\text{SO}_4$ (---).

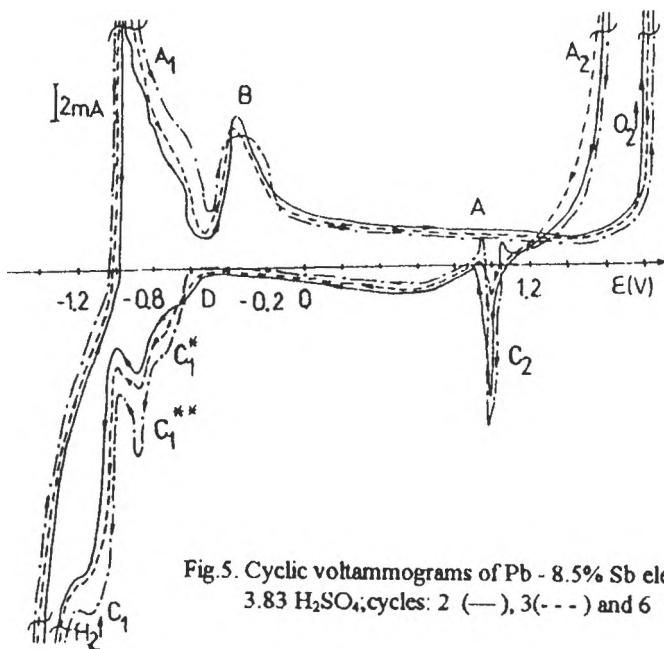


Fig.5. Cyclic voltammograms of Pb - 8.5% Sb electrode; $v=20 \text{ mV/s}$; $3.83 \text{ H}_2\text{SO}_4$, cycles: 2 (—), 3(---) and 6 (-.-).

2 Cyclic Voltammetry on Antimony-Lead Alloys

On Pb-Sb alloys, in anodic potential sweep, the evolution of an oxidation process at approximately -360mV is noticed (peak B in all figure) which stops the passivation initiated after the formation of $PbSO_4$ (peak A.) In conformity with data from literature peak B is associated with the dissolution of Sb at the electrode/electrolyte interface [8,13]. With the increase of the number of cycles and of the electrolyte concentration peak B becomes more proeminent enabling us to suppose that the passage of antimony from alloy into electrolyte is quicker. The existence of an appreciable current almost constant in the passivation range indicates the presence of some electrochemical processes which do not occur on pure lead, and which are conspicuous for anodic layer structure being formed in the passivation range. The growth of electrolyte concentration visibly affects the behaviour of C-type electrodes (Pb-3wt% Sb), Fig.4. Thus, the forming overpotential of PbO_2 and oxygen evolution (peak A_2) is higher than on pure lead. In concentrated electrolyte the reduction peak current of PbO_2 is higher (peak C_2) the same as the tetra-PbO reduction current peak (peak C_1). In cathodic potential sweep the front and rear position of peak C_2 is to be remarked with respect to peak A. If in conformity with Sharpe's point of view [18] peak C_2 is the result of two cathodic processes: β - $PbO_2 \rightarrow PbSO_4$ (at more noble potential) and α - $PbO_2 \rightarrow PbSO_4$ (at less noble potential) we can assert that on this alloy, in the concentrated solution, the predominant species is β - PbO_2 formed by the oxidation of $PbSO_4$. The peak D recorded in cathodic sweep at -650mV is associated with the reduction of the oxidized species of antimony formed in anodic sweep [7, 11].

The essential changes, both concerning the forms of the voltammograms and peak currents height were on alloys with high Sb contents; electrode D (Pb-Sb 8.5wt%, Fig.5) and electrode E (Pb-11.3 wt%Sb, Fig.6).

Thus: I. The dissolution of antimony occurs at much higher rates reaching a stationary value after approximately 6 cycles (peak B, Fig.5). The greater area of the anodic peak B as compared with that of the corresponding cathodic peak D is a result of the formation of some soluble antimony complexes or ions which passing through the $PbSO_4$ membrane pores leave the electrode remaining in the electrolyte and are not reduced.

II. The passivation current is appreciable and nearly constant on alloy D (Fig.5) and variable on E (Fig. 6) suggesting a better ionic conductivity of corrosion anodic film as compared with that formed on pure lead. The constance of this current may be due to setting up an equilibrium between the rate of anodic layer formation at alloy/layer interface and that of its dissolution at layer/ H_2SO_4 solution interface [13]. We cannot tell too much about the composition, but it is obvious that it influences the further behaviour of the interface. On repeated cyclings, the height of peak B decreases but extending to more positive values the passivation range is further characterized by a stronger current. It is evident that the anodic layer formed after antimony dissolution on alloy D in a much less degree pasivates the surface of the electrode than that formed on alloy E. We believe that it is due to the less porous corrosion layer which is formed on alloy E, and which is not totally reduced in cathodic sweep. Thus it covers quite a major part of electrode surface.

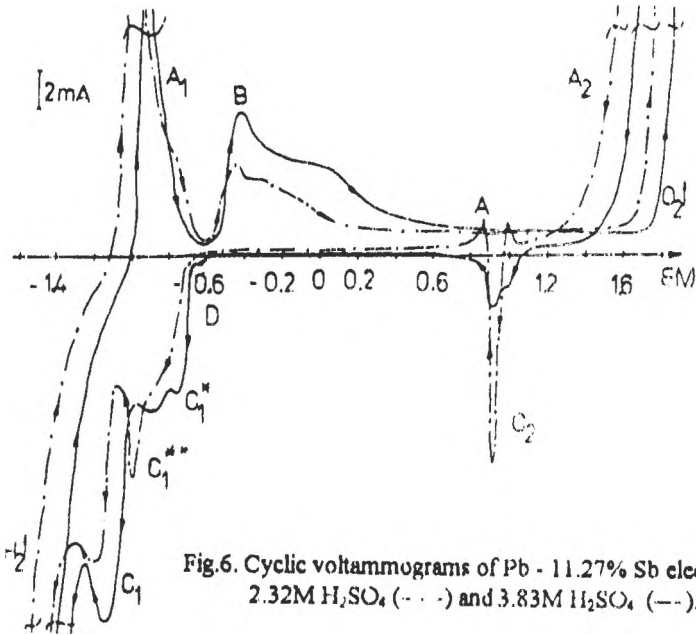


Fig.6. Cyclic voltammograms of Pb - 11.27% Sb electrode, $v=20\text{mV/s}$; $2.32\text{M H}_2\text{SO}_4$ (---) and $3.83\text{M H}_2\text{SO}_4$ (—).

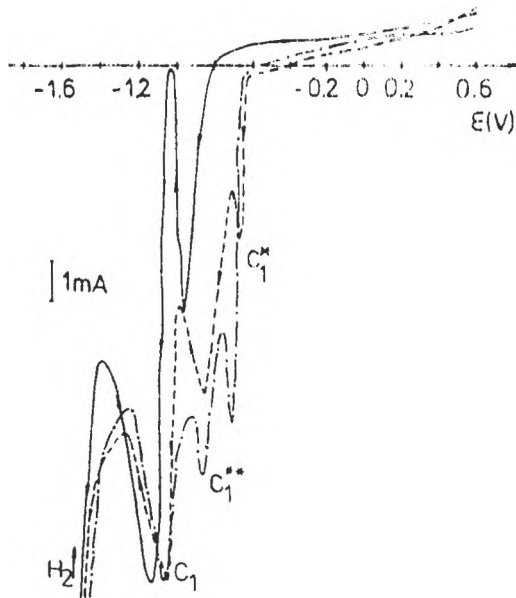


Fig. 7. Potentiodynamic curves; $v = 20\text{mV/s}$; $t_{\text{pot}} = 2 \text{ min.}$; $e_{\text{pot}} = 0.6\text{V}$; Pb (—), Pb - 8.5% Sb (---) and Pb - 11.27% Sb (-.-).

THE EFFECT OF ANTIMONY

iii) The formation processes of species α - and β -PbO₂, as well as the evolution of oxygen occur at much higher potentials (1.8V) on alloys as compared with pure lead

IV. On both alloys, the reduction rate of PbO₂ (peak C₂) is lower (quite very low on electrode E) in more concentrated solutions

V. The current of peak D, associated with a reduction process in which species of antimony (more probably SbO⁻ ions in solution [14]) are implied is higher in concentrated solutions.

VI. The C₁' and C₁ peak potentials are more positive on alloys than on pure lead and their exact values depend on experimental conditions. The reduction peak C₁' which appears between peak C₁' and C₁ indicates the presence of some basic lead sulfates whose formation is aided by the presence of antimony in alloys.

On the cathodic potentiodynamic curves recorded on Pb-Sb alloys after the electrodes were polarized at 600 mV for 0.5 minute the reduction peak C₁' also appears, at -780mV, Fig. 7. This potential value corresponds to the reduction of PbO, PbSO₄ which is formed between PbSO₄ and tetra-PbO during the polarization [7, 12, 13]. We have found that more basic lead sulfate is formed on Pb-8.5 wt% Sb alloys on longer polarization times while the amount of tetra-PbO was unchanged. It seems that the tetra-PbO \rightarrow PbO PbSO₄ transformation occurs at a high enough rate which prevents the deep passivation of electrode.

A different behaviour was observed with Pb-11.27wt% Sb alloy, where the amount of tetra-PbO, formed in different conditions, was greater than with the other alloys. It is supposed that the porosity of the anodic layer formed on this alloy at potentials lower than 800mV is, for certain reasons, smaller and prevents an appreciable amount of tetra-PbO to be converted into basic lead sulfates. The formation of some more compact oxidation layers on this alloy is also aided by the lower more variable value of the current in the passivation range, Fig. 6.

CONCLUSIONS

In the oxidation of pure lead in H₂SO₄ solutions at potentials above 0V, underneath the PbSO₄ membrane, tetra-PbO rather than basic lead sulfates is formed. At polarization potentials below 0V a small part of tetra-PbO is converted into lead sulfate, at slower sweep potentials.

The reduction tetra-PbO \rightarrow Pb peak potential and current depend on the polarization potential and time and on the electrolyte concentration.

The longer the anodic polarization time the more negative the reduction of tetra-PbO peak potential is and the higher the peak becomes.

The presence of Sb in the alloys can greatly reduce the amount of tetra-PbO which is in anodic corrosion layer and at the same time decreases the reduction overpotential. The existence of a greater anodic passive state current on Pb-Sb alloys as compared with that on pure lead is explained by a greater layer porosity which promotes the conversion of a major part of tetra-PbO into PbSO₄.

Generally, the amount of tetra-PbO which is formed on Pb-Sb alloys decreases when the antimony content of the alloy increases, excepting the Pb-11.27wt% Sb.

Taking into account the results of our investigations we think that alloys with Sb contents lower from 11.27wt% are recommendable to use in acid battery grids.

REFERENCES

1. B. Monahov și D. Pavlov, *J. Electrochem. Soc.* **141**, 2316 (1994).
2. Y. Yamamoto, K. Fumino, T. Ueda și M. Nambu, *Electrochem. Acta* **37**, 199 (1992).
3. L. J. Li, M. Fleischmann și L. M. Peter, *Electrochim. Acta* **34**, 459 (1989).
4. J. S. Buchanan și L. M. Peter, *Electrochim. Acta*, **33**, 127 (1988)
5. Y. Guo, J. Yue și C. Liu, *Electrochim. Acta*, **38**, 1131 (1993)
6. Y. Guo, *J. Electrochem. Soc.* **138**, 1222 (1991).
7. T. Laitinen, K. Salmi, G. Sundholm, B. Monahov și D. Pavlov, *Electrochim. Acta* **36**, 605 (1991).
8. R. Babic, M. Metikos-Hukovic, N. Lalqy, S. Brinic, *J. Power Sources* **52**, 17 (1994)
9. Y. Guo, *Electrochim. Acta* **37**, 495 (1992).
10. T. Laitinen, B. Monahov, K. Salmi și G. Sundholm, *Electrochim. Acta* **36**, 953 (1991).
11. D. Pavlov, B. Monahov, G. Sundholm și T. Laitinen, *J. Electroanal. Chem.* **305**, 57 (1991).
12. Y. Guo, *J. Electrochem. Soc.* **140**, 3369 (1993).
13. D. Pavlov, M. Bojinov, T. Laitinen și G. Sundholm, *Electrochim. Acta* **36**, 2081 (1991).
14. T. Laitinen, H. Revotzer, G. Sundholm, J. Vilhunen, D. Pavlov și M. Bojinov, *Electrochim. Acta* **36**, 2093 (1991).
15. A. G. Gaad Allah, H. A. A. El-Rahman, S. A. Salih și M. A. El-Galil, *J. Appl. Electrochem.* **22**, 571 (1992).
16. L. A. Avaca, E. R. Gonzales și G. Tremiliosi-Filho, *J. Power Sources* **30**, 161 (1990)
17. E. M. Rus, *Studia Univ. Babeş-Bolyai, Seria Chemia*, in press
18. T. F. Sharpe, *J. Electrochem. Soc.* **122**, 845 (1975).
19. T. F. Sharpe, *J. Electrochem. Soc.* **124**, 168 (1977).
20. J. G. Sunderland, *J. Electroanal. Chem.* **71**, 341 (1976).
21. D. Pavlov, *J. Electrochem. Soc.* **139**, 3075 (1992)
22. Y. Guo, *J. Electrochem. Soc.* **139**, 2114 (1992).

THE ELECTROCHEMICAL BEHAVIOUR OF SINTERED CADMIUM ELECTRODES IN ALKALINE ELECTROLYTE

Della Constantin, L. Oniclu, Eleonora Maria Rus

DEPARTMENT OF PHYSICAL-CHEMISTRY, FACULTY OF CHEMISTRY AND CHEMICAL ENGINEERING, "BABES-BOLYAI" UNIVERSITY, 3400, CLUJ-NAPOCA, ROUMANIA

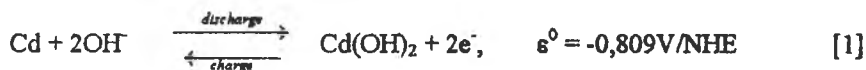
ABSTRACT

The electrochemical behaviour of sintered cadmium electrode in 6N KOH electrolyte has been investigated by cyclic voltammetry. The anodic and cathodic curves were recorded at different sweep rates and the peaks were associated with the electrooxidation and electroreduction processes which occurred. The performances of sintered cadmium electrodes (70 x 35 x 1 mm) were investigated in a half-cell by charge-discharge curves. The different forms of active material (uncycled, charged and discharged) were characterized by X-ray diffraction.

INTRODUCTION

The electrochemical behaviour of cadmium electrodes in alkaline solutions has been the object of many studies because of their wide applications in nickel-cadmium and silver-cadmium batteries [1-8].

Cadmium can be reversibly charged and discharged through the reaction formally written as:



Two different mechanisms have been proposed: the dissolution-precipitation mechanism involving solution phases [9,10] and the solid state mechanism involving ionic transport through the $\text{Cd}(\text{OH})_2$ active material film [11,12].

In this paper are presented the results obtained by electrochemical and structural investigations of cadmium electrodes, prepared by cathodical deposition of active material on sintered nickel supports.

EXPERIMENTAL

Cadmium electrodes were prepared by cathodical polarization, in 25% KOH solution, of sintered nickel supports impregnated with $\text{Cd}(\text{NO}_3)_2 \cdot 4 \text{H}_2\text{O}$ [13]. The sintered nickel plates were realised from nickel powder obtained by thermolysis of $\text{Ni}(\text{NO}_3)_2 \cdot 6 \text{H}_2\text{O}$ [14].

The cyclic voltammetry was applied to study the electrochemical behaviour of sintered cadmium electrodes in 6N KOH electrolyte. The measurements were made in a conventional three-electrodes cell using SCE as reference, connected through a Luggin capillary, and a platinum wire as counter electrode. All the potentials given in this paper are referred to SCE. The apparent surface area of the working electrode was 1cm². The 6N KOH electrolyte was prepared from analytical grade KOH and distilled water. The experiments were performed by means of an Wenking HP 72 potentiostat, a PV 2 programmer and an Endim 620.02 X-Y recorder.

Before the investigations, the cadmium electrode was polarized in the net hydrogen evolution reaction (HER) region, at -1.75 V/SCE, for 5 minutes, to eliminate the impurities from its surface.

The charge-discharge curves were performed in a half-cell consisting of the sintered cadmium electrode (70 x 35 x 1 mm) as working electrode, a SCE as reference and a nickel plate as counter electrode. All experiments were conducted at room temperature.

X-ray diffractograms were obtained with a Dron 3 powder diffractometer, using CuK_α radiation.

RESULTS AND DISCUSSION

Cyclic Voltammetry

The stabilized form of voltammograms for sintered cadmium electrode was attained after 6 oxidation-reduction cycles, in 6N KOH electrolyte, at $v = 20$ mV/s, corresponding to the formation of active material.

The potential was scanned between anodic value 0.440 V/SCE, at which oxygen evolution reaction (OER) occurs, and cathodic value -1.400 V/SCE, corresponding to hydrogen evolution reaction (HER).

Fig.1 shows the voltammograms of sintered cadmium electrode in 6N KOH, at three potential sweep rates: 20, 6.66 and 3.33mV/s, respectively.

In the negative potentials range, two current peaks were recorded. The anodic peak A was associated with the oxidation of Cd to Cd(OH)₂ (discharge process) and the peak B with the reduction of Cd(OH)₂ to Cd (charge process). At extreme cathodic potentials, HER represents an overcharge process.

In the positive potentials range, before OER, a corrosion process of the sintered nickel support, in which NiOOH is formed, (anodic peak C) occurred. These processes (OER and corrosion) take place only at overdischarge of the electrode, which must be avoided by constructive and operation measures.

The cathodic peak D represents the reduction of NiOOH to Ni(OH)₂.

From anodic and cathodic peak potential values were calculated the average potential, ϵ' , and the difference of peak positions, $\Delta\epsilon_{a,c}$ [15]:

$$\epsilon' = \frac{\epsilon_{a,p} + \epsilon_{c,p}}{2} \quad (2)$$

THE ELECTROCHEMICAL BEHAVIOUR OF SINTERED CADMIUM

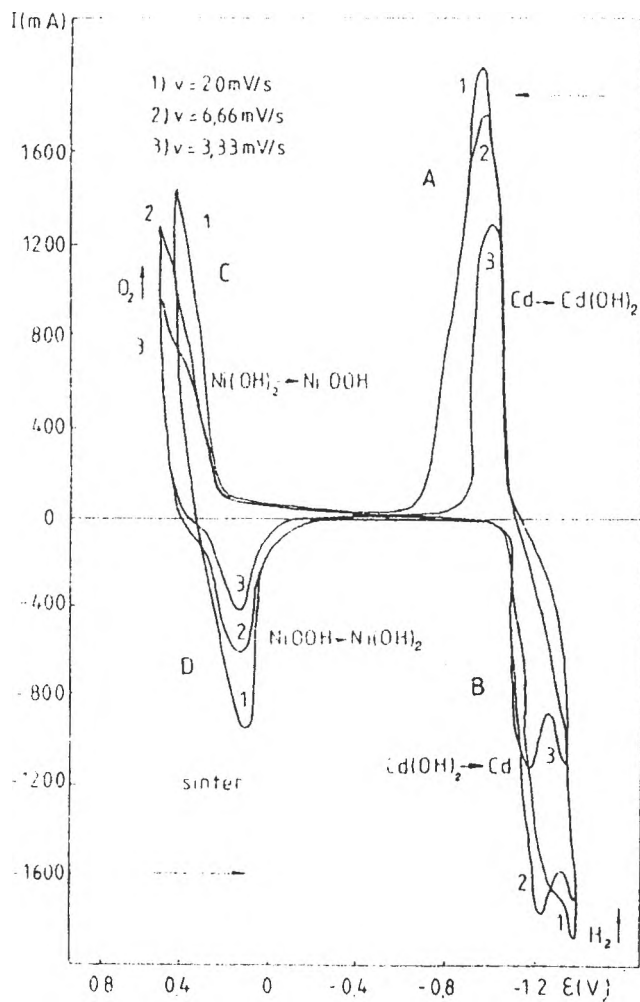


Fig.1. Cyclic voltammograms of sintered cadmium electrode in 6N KOH at :
 $v = 20 \text{ mV/s}$ (1), $v = 6.66 \text{ mV/s}$ (2) and $v = 3.33 \text{ mV/s}$ (3)

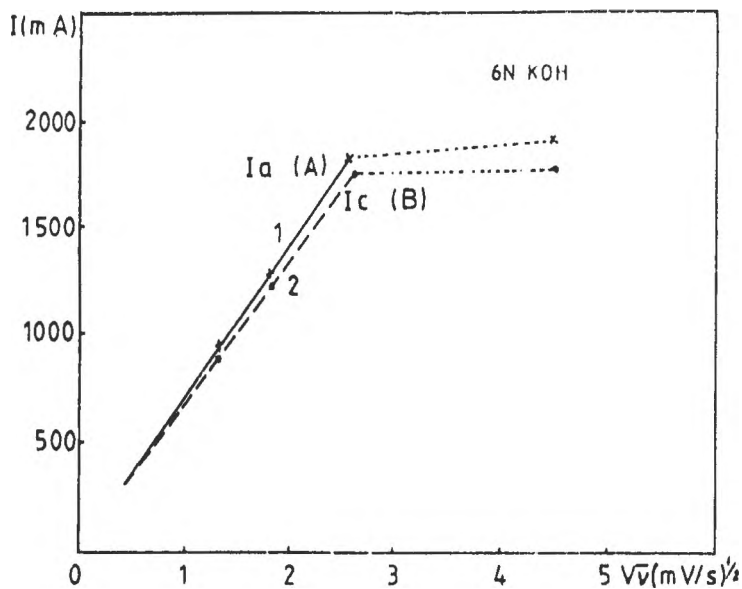


Fig. 2. The dependence of the anodic (1) and cathodic (2) peak current intensity of $v^{1/2}$

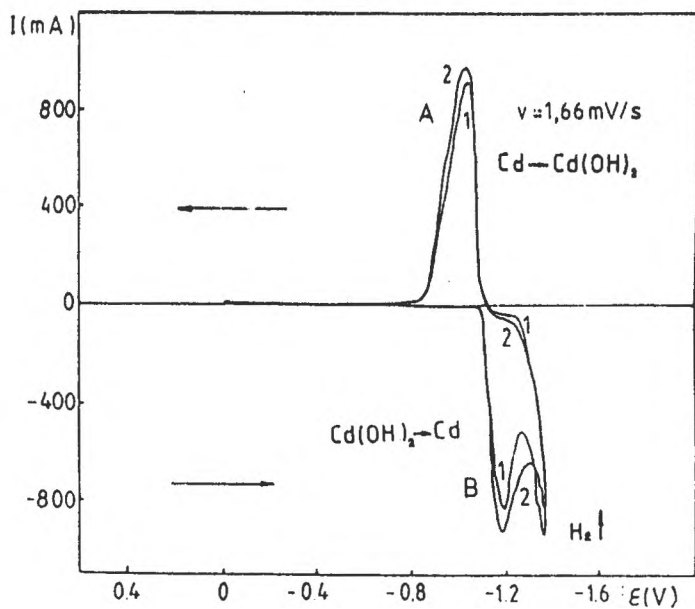


Fig. 3. Voltammograms of cadmium sintered electrode in 6N KOH, at $v = 1.66 \text{ mV/s}$, in unstirred (1) and in stirred (2) electrolyte

THE ELECTROCHEMICAL BEHAVIOUR OF SINTERED CADMIUM

$$\Delta E_{a,c} = E_{a,p} - E_{c,p} \quad (3)$$

The results of cyclic voltammetry measurements of sintered cadmium electrode, related to the peaks A and B, are tabulated in Table I.

Table I. Cyclic voltammetry measurements of sintered cadmium electrode, in 6N KOH.

Sweep rate (mV/s)	$E_{a,p}$ (A) (V/SCE)	$E_{c,p}$ (B) (V/SCE)	$\Delta E_{a,c}$ (V)	E' (V/SCE)	$I_{a,p}$ (A) (mA)	$I_{c,p}$ (B) (mA)	$\frac{I_{c,p}}{I_{a,p}}$
20	-0.980	-1.320	0.340	-1.150	2000	1760	0.88
6.66	-0.990	-1.260	0.270	-1.125	1820	1760	0.96
3.33	-1.010	-1.210	0.200	-1.115	1275	1220	0.96
1.11	-1.050	-1.170	0.120	-1.110	840	820	0.98

The average potential, E' , is taken as an estimation of the reversible potential. The theoretical value of the reversible potential, calculated for 6N KOH electrolyte and $t = 20^\circ\text{C}$ is $E_r = -1.088 \text{ V/SCE}$ [16].

If the difference in the anodic and cathodic positions, $\Delta E_{a,c}$ is taken as an estimation of the reversibility of the reaction, it is evident that the reversibility of process increases with decreasing of sweep rates.

The ratio of the cathodic to anodic peak currents tends to value 1 with decreasing of sweep rates. This demonstrates that the charge recovered on the cathodic sweep was very close with that of the previous anodic sweep, suggesting the high efficiency of processes on sintered cadmium electrode.

The current intensities of the peaks were plotted against the square root of sweep rates (Fig.2).

The linear dependence suggests that the involved reactions behave as diffusion controlled electrochemical processes for $v \leq 6.66 \text{ mV/s}$, according to Randles-Sevcik equation :

$$I_p = 2.69 \times 10^5 \times z^{2/3} \times A \times D^{1/2} \times c \times v^{1/2} \quad (4)$$

- where: I_p = current intensity of the peak;
 z = the number of electrons exchanged;
 A = area of the electrode;
 D = diffusion coefficient;
 c = concentration;
 v = sweep rate.

The voltammograms depicted in Fig.3 were recorded in order to investigate the effect of solution stirring on the mechanisms of processes.

Under stirring, the height of peaks is changed, suggesting the involvement of precipitation-dissolution mechanism in the formation of $\text{Cd}(\text{OH})_2$ and its reduction.

According to Will's investigations [17] the oxidation of Cd to $\text{Cd}(\text{OH})_2$ occurs through a complex mechanism involving 2 steps:

- the dissolution of Cd with the formation of complex cadmate ions, at the electrode surface:



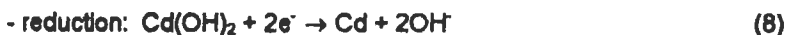
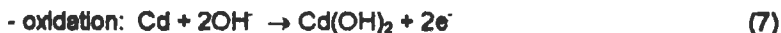
- the precipitation of $\text{Cd}(\text{OH})_2$ after saturation with $[\text{Cd}(\text{OH})_3]$:



The reduction of $\text{Cd}(\text{OH})_2$ during the cathodic sweep occurs by eq. (5) and (6) in reverse order.

From the slopes of the plots presented in Fig.2 were determined the diffusion coefficients of cadmate ions for oxidation process, $D_o = 8.985 \times 10^{-5} \text{ cm}^2/\text{s}$, and for reduction process, $D_r = 8.046 \times 10^{-5} \text{ cm}^2/\text{s}$. The considered solubility of cadmium in 6N KOH, at $t = 25^\circ \text{C}$, is $1 \times 10^{-4} \text{ mol/liter}$ [18].

For $v > 6.66 \text{ mV/s}$, the plots suggest a modification of reaction mechanism, being very probably the involvement of solid state processes:



Galvanostatic Charge-Discharge Curves

The electrochemical processes that occur on sintered cadmium electrode were also investigated by charge-discharge curves.

The cadmium electrodes ($70 \times 35 \times 1 \text{ mm}$) were charged and discharged in galvanostatic regime ($I=100, 400$ and 500 mA), in 6N KOH electrolyte.

In Fig.4 are shown the different regions exhibited by charge-discharge curves, in cathodic and anodic processes. These regions were corroborated with voltammetric findings.

The anodic curve 2 presents three regions:

- ◆ the plateau A corresponds to discharge process (oxidation of Cd to $\text{Cd}(\text{OH})_2$);
- ◆ the region B indicates the end of discharge process by an abrupt modification of potential, which arrives in positive range;
- ◆ the region C corresponds to overdischarge of electrodes, manifested by corrosion of sintered support and OER.

The cathodic curve 1 presents four distinct regions:

- ◆ the region D corresponds to reduction of NiOOH , formed by corrosion of nickel support;

THE ELECTROCHEMICAL BEHAVIOUR OF SINTERED CADMIUM

- ◆ the region E represents an abrupt modification of potential to negative values, when the reduction process of NiOOH to Ni(OH)₂ is finished;
 - ◆ the plateau F indicates the reduction of discharged active material Cd(OH)₂, to charged form, Cd;
- the region G is related to HER (overcharge).

From galvanostatic charge-discharge curves were determined the discharge capacities and the coulombic efficiencies of the sintered cadmium electrodes (Table II)

Table II. Coulombic efficiencies of sintered cadmium electrodes.

I_{charge} (mA)	t_{charge} (h)	C_{charge} (mAh)	$I_{\text{discharge}}$ (mA)	$t_{\text{discharge}}$ (h)	$C_{\text{discharge}}$ (mAh)	Coulombic efficiency (%)
100	5.50	550	100	5	500	90.91
400	1.32	528	400	1.16	464	87.88
500	0.930	465	500	0.80	400	86.02

It is clearly that sintered cadmium electrodes function with high coulombic efficiencies even for great charge-discharge rates.

X-Ray Characterization

The different forms of active material (uncycled, charged and discharged) were characterized by X-ray diffraction (Fig.5).

The X-ray diffraction patterns in the $2\theta = 4 - 63^\circ$ range, obtained on the powder scraped from the electrode surface, show two characteristic lines for nickel, (111) and (200), proceeded from sintered support.

The active material of uncycled electrode consists largely of Cd(OH)₂, but there are some lines of small intensity corresponding to CdCO₃ (curve a). It should be pointed out that the active material was impregnated in sintered support, by cathodical polarization, in discharge form.

The charge active material consists largely of Cd, but there are a small number of lines corresponding to uncharged Cd(OH)₂ and traces of CdO (curve b).

In the discharged active material Cd(OH)₂, there are Cd undischarged and CdCO₃, (curve c).

The presence of Cd(OH)₂ remained unreduced in charged active material and of Cd remained unoxidized in discharged active material can be explained by the higher capacity of sintered cadmium electrode than of nickel plate electrode, used as counter electrode. The presence of CdCO₃ in active material is a result of the action of CO₂ from air on KOH electrolyte solution and of the pronounced tendency of substitution of NO₃⁻ ions, remained from the preparation step, by CO₃²⁻ ions.

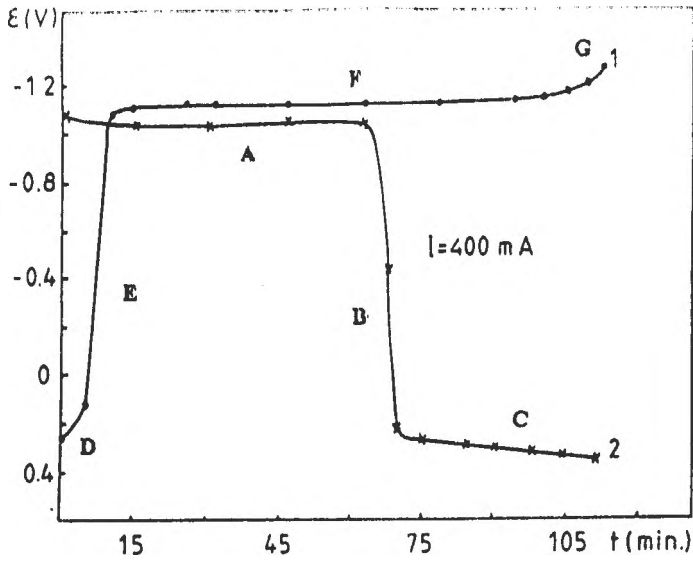


Fig.4. Charge-discharge curves of sintered cadmium electrode, in 6N KOH electrolyte, at $I = 400 \text{ mA}$

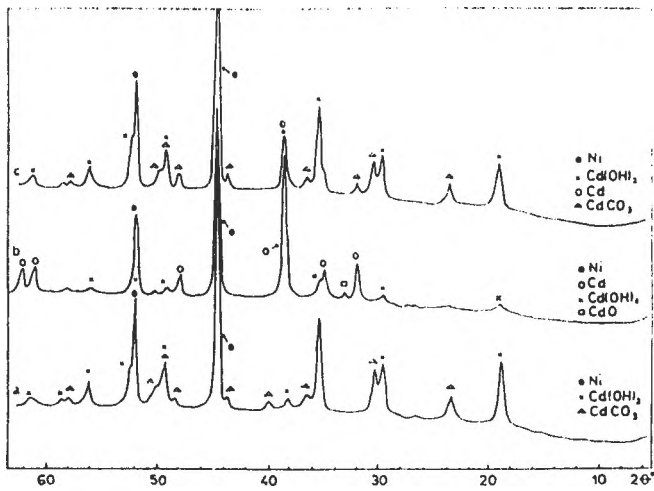


Fig.5. X-ray diffractograms of sintered cadmium electrode : a) uncycled, b) charged and c) discharged

CONCLUSIONS

The uncycled active material, impregnated in sintered support by cathodic polarization, is in discharged form, $\text{Cd}(\text{OH})_2$. Six oxidation-reduction cycles were necessary for the formation of active material.

By cyclic voltammetry has been demonstrated that the oxidation-reduction processes of active material can occur by different mechanisms :

- at low sweep rates, the processes take place by cadmate soluble specie, $[\text{Cd}(\text{OH})_3]$, and are controlled by diffusion;
- at higher sweep rates, it is very probably the involvement of solide state processes.

At the overdischarge of sintered cadmium electrode, before OER, a corrosior process of nickel support occured.

The sintered cadmium electrodes functioned with high coulombic efficiencies.

REFERENCES

1. B.S.Hobbs, T. Keily, A.G. Palmer, *J.Appl.Electrochem.*, **10**, 721 (1980)
2. J.A. Garrido, F. Centellas, P.L. Cabot, R.M. Rodríguez, E.Perez, *J.Appl.Electrochem.*, **17**, 1093 (1987).
3. J.A.de Urraza, C.A. Gervasi, S.B. Saidman, J.R. Vilche, *J.Appl.Electrochem.*, **23**,1207 (1993)
4. S.T. Selvan, R. Sabapathi, N. Venkatakrishnan, *J.Appl.Electrochem.*, **21**, 646 (1991).
5. R. Barnard, *J.Appl.Electrochem.*, **11**, 217 (1981).
6. D. Fan, R.E. White, *J.Electrochem.Soc.*, **138**, 17 (1991).
7. M. Hamdani, J.F. Koenig, P. Chartier, *J.Appl.Electrochem.*, **14**, 247 (1984)
8. Y. Okinaka, C.M. Whitehurst, *J. Electrochem.Soc.*, **5**, 583 (1970).
9. M.Z.A. Munshi, A.C.C. Tseung, J. Parker, *J.Appl.Electrochem.*, **17**, 427 (1987).
10. J.O. Zerbino, S.B. Saidman, J.R. Vilche, A.J. Arvia, *Electrochim.Acta*, **35**, 605 (1990).
11. Y. Duhirel, B. Beden, J.M. Leger, C. Lamy, *Electrochim.Acta*, **37**, 665 (1992).
12. S.B. Saidman, J.R. Vilche, A.J. Arvia, *J.Appl.Electrochem.* **189**, 633 (1988).
13. L. Oniciu, Eleonora Maria Rus, Delia Constantin, Florentina Ciomos, *Revista de Chimie*, **37**, 44 (1986).
14. L. Oniciu, Eleonora Maria Rus, P.Ilea, Violeta Voina, *Delia Constantin, Revista de Chimie*, **36**, 340 (1985).
15. P.T. Kissinger, W.R. Heineman, *J.Chemical Education*, **60**, 702 (1983).
16. G. Halpert, *J.Power Sources*, **15**, 119 (1985).
17. F.G. Will, *J.Electrochem.Soc.*, **136**, 2194 (1989).
18. B.S. Hobbs, T. Keily, A.G. Palmer, *J.Appl.Electrochem.*, **10**, 721 (1980).

CATHODE MATERIALS FROM LITHIUM BATTERIES CHARACTERIZED BY CYCLIC VOLTAMMETRY

L. Oniciu, Silvia Avram, Georgeta Țarălungă, L.D. Boboș, Cs. Bolla

DEPARTMENT OF PHYSICAL-CHEMISTRY, FACULTY OF CHEMISTRY AND
CHEMICAL ENGINEERING, "BABEȘ-BOLYAI" UNIVERSITY, 3400, CLUJ-NAPOCA,
ROUMANIA

ABSTRACT

Cathodes based on CuO and MnO₂ were prepared and characterized by XRD and cyclic voltammetry. To improve the behaviour of these cathodes, we tried to establish the most propitious ratio between the components of cathode mixture (active materials, teflon and graphite).

INTRODUCTION

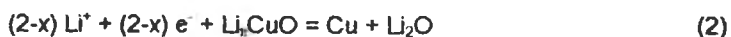
The rapid development of sophisticated, small-size electronic devices and portable equipment such as: video cameras, cordless telephones, watches, calculators, toys, peace-makers, electric vehicles and so on, has favoured the study and the characterization of new types of electrochemical power sources with high power, high energy density, and long cycle life. Among these, lithium batteries based on the lightest and most electropositive metal, have received particular attention [1]. This has resulted in the development of lithium cells using various non-aqueous electrolyte media and various kinds of active cathode materials.

The technology of primary lithium batteries production was accomplished more than 15 years ago, and presently lithium batteries are used for many applications [2], but their mechanism has not yet been satisfactorily elucidated. Various types of reaction mechanisms were therefore proposed in the literature [3,4] involving chemical, electrochemical and intercalation reactions and diffusion in the solid state. However, it remains to be decided which is the rate controlling step.

Recent studies [5,6], suggest that the cathodic reaction involves intercalation of Li⁺ ions into the CuO lattice. PODHAJECKY and SCROSATI [7] wrote the cathodic reaction in the form:



followed by further reactions:



Both reaction steps are electrochemical in nature, since complete discharge of the cathode gives almost 100% of the theoretical charge necessary for a two-electron reduction of CuO[8].

Primary lithium batteries has reached a wide commercial market being produced in different sizes and capacities in Europe, Japan, and in the United States.

EXPERIMENTAL

Amorphous MnO_2 synthesized electrolytically, was heat-treated at $400^\circ C$ for 0.5, 2.5, and 5 hours to obtain the β - MnO_2 crystalline structure [9]. The structure was confirmed by X-ray diffraction. Powder X-ray diffraction profiles were collected using a Dron diffractometer with CuK_α radiation. The X-ray spectra for the MnO_2 heat-treated at $400^\circ C$ for 0.5, 2.5, and 5h are shown in Fig. 1a, b, and c. From the figure it can be seen that only the structure of MnO_2 treated at $400^\circ C$ for 5h is favorable for the intercalation process.

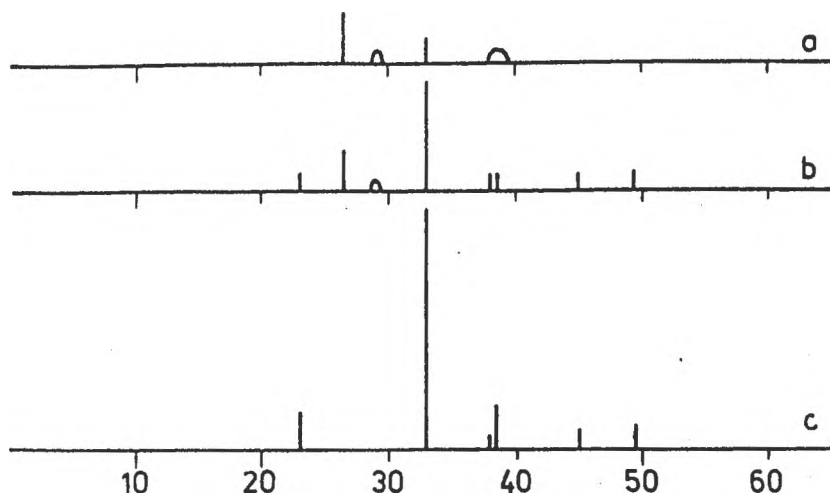


Fig.1. X-ray spectra for MnO_2 heat-treated at $400^\circ C$ for: a) 0.5 h; b) 2.5 h; c) 5h.

CuO was prepared from $Cu(NO_3)_2$ by rising the temperature slowly to $400^\circ C$ and maintaining this temperature for another 2h on air [10]. The product was then calcinated at $800^\circ C$ for 8h. The purity of prepared CuO was confirmed by X-ray diffraction showed in Fig. 2.

To estimate the influence of the different components, we prepared cathode mixtures containing different weight per cent (w/o) of active materials, teflon (as binder), and graphite (as electronic conductor). We prepared 35 samples based on MnO_2 containing 4 to 12% binder, and 6 to 40% graphite, and 20 samples based on CuO with 6 to 14% binder, and 10 to 40% graphite. In each case, the difference until 100% was active material (MnO_2 or CuO).

Samples were sieved under $71\mu m$, mixed with binder and graphite and pressed into pellets ($\phi = 20 mm$) and 0.8-1 mm thick.

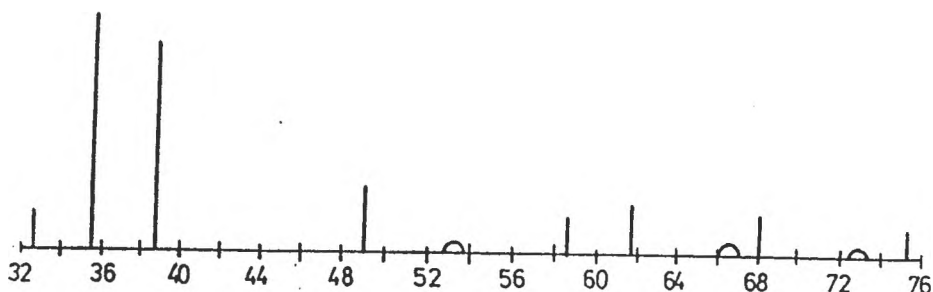


Fig.2. X-ray diffraction for CuO.

Electrochemical measurements were done in a three electrode glass cell at room temperature. A large Pt counter-electrode was placed near the working electrode. The potential of the working electrode was measured against a Li reference electrode. The electrolyte, 1 M LiClO₄ in propylene carbonate, was in excess, and contained less than 50 ppm H₂O. The cell was assembled in a dry box in argon atmosphere containing less than 20 ppm H₂O [11]. The cell was evacuated for several hours prior to the measurements to remove gases from electrolyte [12].

Electrodes prepared only from teflonized graphite (94% graphite and 6% teflon) were tested in the same way for comparison.

The cyclic voltammetry experiments were performed by means of a classical potentiostatic circuit.

RESULTS AND DISCUSSION

The aim of this work is to estimate the influence of different components from the cathode mixture on the performances of batteries. We tried to establish the most propitious ratio between the components of cathode mixtures (active materials, teflon, and graphite), and to estimate how they interfere in the discharge mechanism. The optimum composition needs to be determined since too much binder will lead to lower specific energy, poor rate capability and inadequate Li intercalation later, and insufficient binder cannot hold the carbon particles together. Further, low porosity and nonuniform loading of active material in the electrode will also reduce the rate capability and intercalatable Li capacity.

a) CuO: from the cyclic voltammograms, it can be seen that the discharge reaction is irreversible. There are three peaks on the cyclic voltammograms for CuO:

- the main peak, close to 1.15 V vs. Li/Li⁺ (see Fig.3), corresponds to reduction of CuO (intercalation of Li⁺ into the crystal lattice), according with [7]:

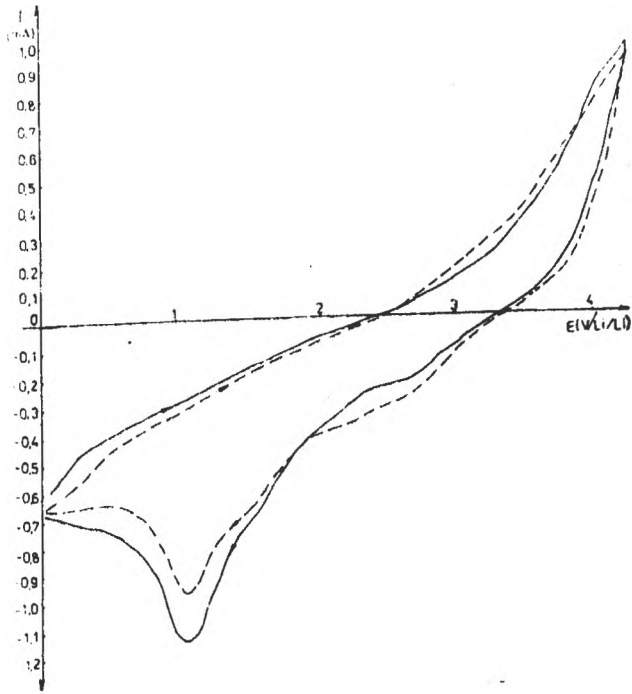


Fig.3. Cyclic voltammograms for cathode containing: 75% CuO, 20% graphite, 5% teflon; — cycle 1; - - - cycle 2; electrolyte 1M LiClO₄ in propylene carbonate; sweep rate $v = 20\text{mV/s}$.

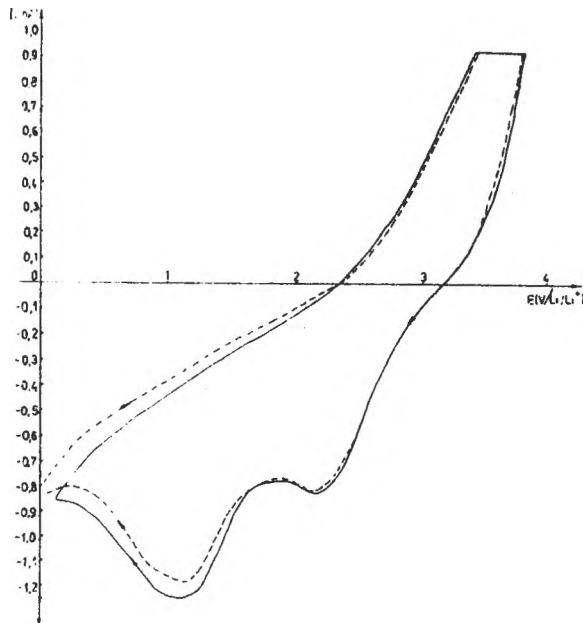


Fig.4. Cyclic voltammograms for cathode containing: 72% CuO, 20% graphite, 8% teflon; — cycle 1; - - - cycle 2; electrolyte 1M LiClO₄ in propylene carbonate; sweep rate $v = 20\text{mV/s}$.

CATHODE MATERIALS FROM LITHIUM BATTERIES



- there is another peak, close to 2.15 V vs. Li/Li^+ (see Fig.4). We believe that this peak is due to traces of adsorbed oxygen and H_2O [13]. The participation of O_2 and H_2O cannot be excluded, since these species are known to be strongly adsorbed on the CuO surface;

- for samples containing too much graphite (>30%), there is only a peak at 0.75 V vs. Li/Li^+ that corresponds to the reaction of lithium with graphite (see Fig.5);

- from the values of i_{max} it can be seen that electrodes containing 72% CuO , 20% graphite, and 8% teflon are more appropriate as cathodic depolarisants based on CuO .

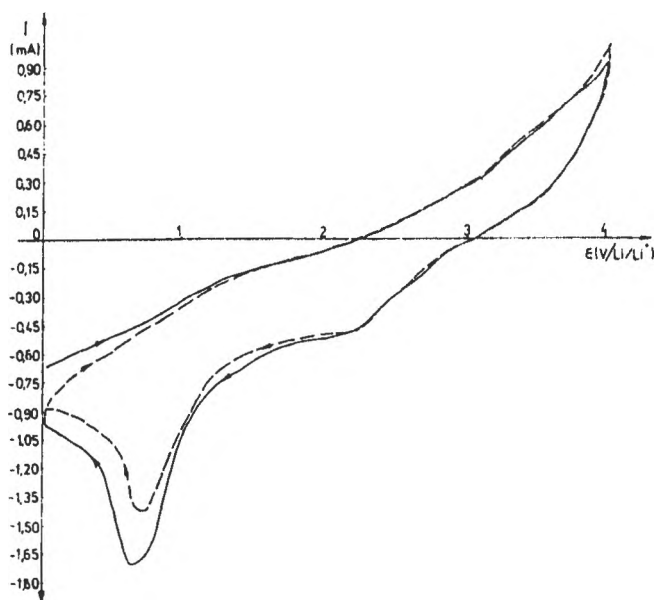


Fig.5. Cyclic voltammograms for cathode containing: 54% CuO , 40% graphite, 6% teflon; — cycle 1; - - - cycle 2; electrolyte 1M LiClO_4 in propylene carbonate; sweep rate $v = 20\text{mV/s}$.

b) MnO_2 : the behaviour of MnO_2 cathode is irreversible, too;

- the main peak for reduction of MnO_2 lies close to 2.2 V vs. Li/Li^+ ;

- for samples with high content of teflon (>9%), the intercalation is inhibited because the binder fill many gaps of the crystallographic structure, and the intercalation process is blocked (see Fig.6);

- because the conductivity of MnO_2 is not so good, a content above 15% graphite in the cathode mixture is necessary;

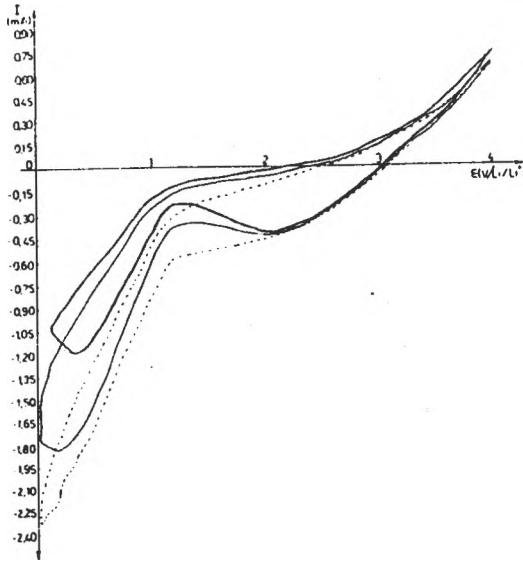


Fig.6. Cyclic voltammograms for cathode containing: 60% CuO, 30% graphite, 10% teflon; --- cycle 3; — cycle 5; — cycle 7; electrolyte 1M LiClO₄ in propylene carbonate; sweep rate $v = 20\text{mV/s}$.

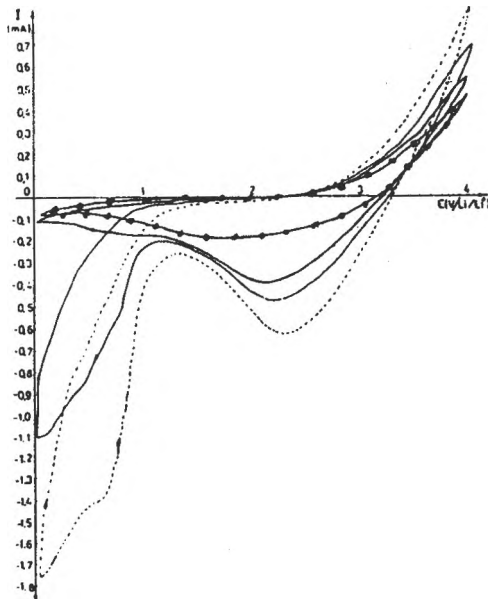


Fig.7. Cyclic voltammograms for cathode containing: 52% CuO, 40% graphite, 8% teflon; ... cycle 20; — cycle 30; — cycle 55; —●— cycle 85; electrolyte 1M LiClO₄ in propylene carbonate; sweep rate $v = 20\text{mV/s}$.

CATHODE MATERIALS FROM LITHIUM BATTERIES

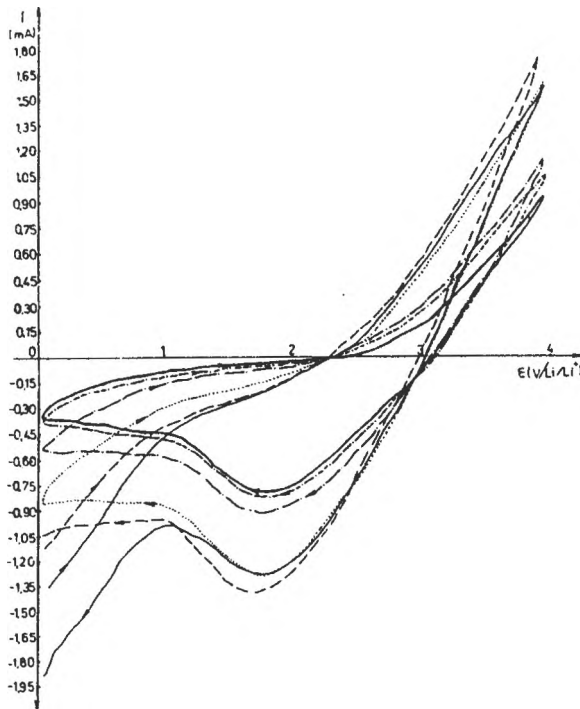


Fig.8. Cyclic voltammograms for cathode containing: 74% CuO, 15% graphite, 11% teflon; — cycle 1; --- cycle 5; cycle 10; - · - · - cycle 15; - - - - cycle 20; — cycle 35; electrolyte 1M LiClO₄ in propylene carbonate; sweep rate $v = 20\text{mV/s}$.

- after 30-35 cycles, the peak corresponding to the intercalation of Li⁺ into graphite disappear (see Fig. 7). For the cathodes with high content of binder, relative to graphite content, this peak quickly disappear (see Fig. 8).

- from the peak height we establish the most appropriate composition for cathode mixture: 70% MnO₂, 20% graphite, 10% teflon.

CONCLUSIONS

- only after a heat-treatment of electrolytically MnO₂ it is possible to achieve a structure close to that which is favourable to intercalation process;

- the discharge reaction is irreversible for both CuO and MnO₂ cathodes;

- the intercalation of Li⁺ into the lattice (CuO or MnO₂) is high during the first cycle and decreases with following cycles.

REFERENCES

1. B. Scrosati, *Electrochim. Acta*, **26**, 1559 (1981).
2. Z-i. Takehara, K. Kanamura, *Electrochim. Acta*, **38**, 1169 (1993).
3. H. Ikeda, S. Narukawa, *J. Power Sources*, **9**, 329 (1983).
4. R. Fournie, R. Messina, J. Perichon, *J. Appl. Electrochem.*, **9**, 329 (1979).
5. X. Xing, M. Xiao, Ch. Li, H.Wu, *Huaxue Xuebao*, **42**, 220 (1984) [cited in *Chemical Abstracts* **100**, 173 (1984)].
6. T. Iijima, Y. Toyoguchi, J. Nishimura, H. Ogawa, *J. Power Sources*, **5**, 99 (1980).
7. P. Podhajecky, B.Scrosati, *J. Power Sources*, **16**, 309 (1985).
8. P. Novak, B.Klapste, P. Podhajecky, *J. Power Sources*, **16**, 309 (1985).
9. T. Ohzuku, J. Kato, K. Sawai, T. Hirai, *J. Electrochem. Soc.*, **138**, 2556 (1991).
10. P. Podhajecky, Z. Zabransky, P. Novak, Z. Dobiasova, R. Cerny, V. Valvoda, *Electrochim. Acta*, **35**, 245 (1990).
11. P. Novak, *Electrochim. Acta*, **30**, 1687 (1985).
12. P. Novak, *Electrochim. Acta*, **31**, 1167 (1986).
13. P. Podhajecky, B.Klapste, P. Novak, J. Mrha, R. Moshtev, V. Manev, A. Nassalevska, *J. Power Sources*, **14**, 269 (1985).

THE ELECTROCHEMICAL BEHAVIOUR OF ZINC IN KOH SOLUTIONS,
UNDER POTENTIODYNAMIC TECHNIQUE (RDE)

VIOLETA VOINA *
LIANA MURESAN **
L. ONICIU **

* BABES-BOLYAI UNIVERSITY, LABORATORY OF ELECTROCHEMISTRY 3400
CLUJ-NAPOCA, ROMANIA

** BABES-BOLYAI UNIVERSITY, DEPT. OF PHYSICAL CHEMISTRY 3400
CLUJ-NAPOCA, ROMANIA.

Abstract

A potentiodynamic study of electrochemical behaviour of zinc in alkalyne solutions under controlled hydrodynamic condition was carried out. A rotating disk electrode (RDE) was used in order to elucidate some aspects related to behaviour of zinc anodes in Ni-Zn batteries.

The voltammograms recorder on zinc RDE in KOH solution (with and without LiOH) exhibit several current variations situated in the region corresponding to the transition from active dissolution to passivation.

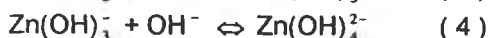
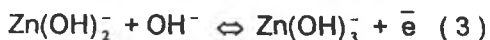
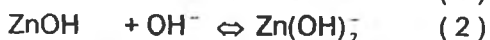
The failure of curves was attribute to the diffusion of OH⁻ ions through these more or less soluble compounds, specially in conditions of slow agitation. The mechanism changes in KOH 6N.

A beneficial catalytic effect of LiOH was put on evidence which justifies its use in alkaline Ni-Zn batteries in order to improve their performances.

1. Introduction

The electrochemical behavior of zinc in alcalyne media continues to be a field of considerable importance because of its interest in batteries and its potential application in advanced energy storage devices.

The mecanism of zinc dissolution into zincate has been studied previously using the galvanostatic, potentiostatic, potentiodynamic, RDE and impedance techniques [1-8]. Recent work agrees with the mechanism proposed already by Bockris et all [1,2,4,7]:



Under potentiodynamic conditions mass transport effects have been invoked to explain the deviation of the exponential dependence of current with potential in the anodic dissolution of the metal [4,7,9,-14].

The aim of our work was to study the electrochemical behaviour of zinc in alcalyne solutions under controlled potentiodynamic and hydrodynamic

conditions, using a rotating disk electrode (RDE) in order to elucidate some aspects related to working of zinc anodes in Ni-Zn batteries.

The influence of RDE rotation speed, of KOH concentration and of Li^+ ions, on zinc electrochemical behaviour, was studied.

2. Experimental

All reagents used in the experiments were of analytical degree and the solutions were prepared using bidistilled water.

Electrochemical experiments were performed using a potentiostatic set-up consisting of a potentiostat (PS 3, Meinsberg), a signal generator (Polarograph LP 7e, Praha) and an X-Y recorder (Endim 620.02, Meinsberg). The potential was scanned between -2 and -1 V/SCE.

A conventional three electrode cell was used. The working electrode was a rotating disk electrode made of Zn 99,99% ($S=0,07065 \text{ cm}^2$). The reference electrode was a saturated calomel electrode (SCE). The Pt counterelectrode was separated from the test solution by a glass frit.

Before each experiment, the working electrode was polished on emery paper and rinsed with distilled water.

3. Results and discussion

The voltammograms recorded in a 1N KOH solution on stationary zinc electrode ($\omega = 0$) using a scan rate of 60 mV/s (v) exhibit four anodic and one cathodic peak. (Figure 1).

Peaks 1 and 2 appeared during the anodic scan, while the others during the cathodic scan.

After the first peak (1), which appears at -1,4 V/ECS, the current decreases to a value of about 2,5 mA and then increases again forming another peak at -1,25 V/ECS, followed by a strong decrease of the current to a residual value of 0,1 mA suggesting a passivation of the electrode.

Peaks 3 and 4, which appear during the cathodic scan, indicate the presence of some non-electrochemical processes, while peak 5 corresponds to cathodic reduction of Zn^{2+} ions to Zn.

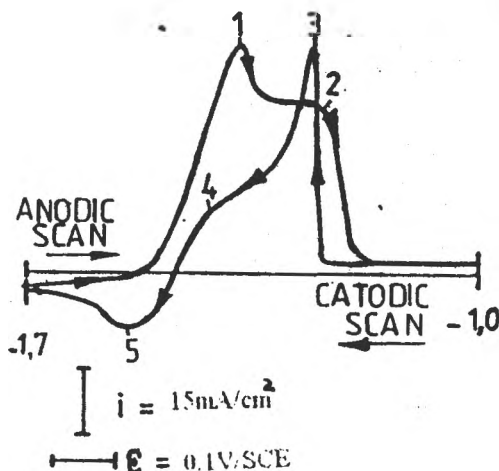


Figure 1 The voltammogram in 1N KOH solution at $\omega = 0$ and $v = 60 \text{ mV/s}$

Influence of RDE rotation speed

As the anodic currents increase with the rotation speed, ω , one can conclude that these are controlled by the diffusion of OH^- ions, because accumulation of zincate ions of $\text{Zn}(\text{OH})_2$, or of zinc oxides (which result by zinc dissolution) near the electrode surface, is diminished by electrode rotation and thus, the local concentration of OH^- ions increases.

Three main reaction mechanisms were proposed in the literature for zinc passivation process: This could take place by:

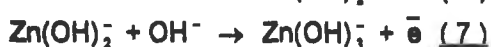
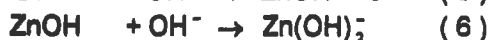
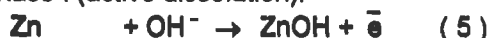
a) dissolution - precipitation processes [4,9,15,16]

b) adsorption - processes [17,18]

c) nucleation - growth processes [19,20]

The shape of potentiodynamic curves recorded by us in 1N KOH solutions, using RDE technique, suggest the applicability of mechanism proposed by Sabater and Victorri [21] involving the following steps:

- Phase I (active dissolution):



- Phase II (prepassive dissolution):



- Phase III (passivation)

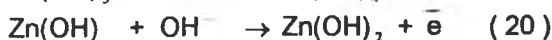
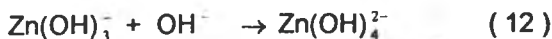


- Phase IV (oxide growth)

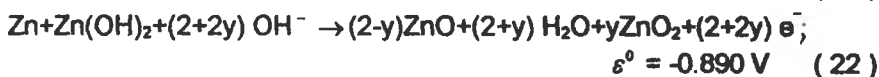
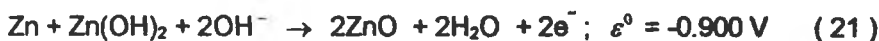


Prentice and Chang [22] consider reaction (7) as rate determining step for initial dissolution phase. Applying Langmuir's treatment, they proposed a model for zinc dissolution in KOH solutions, based on coupled elementary steps that partially cover the electrode surface with soluble species. Chang and Prentice consider that the most important are the following reactions:





The curves registered during our experiments suggest that the first anodic peak corresponds to the formation of a porous, less soluble film of Zn(OH)_2 (zinc oxide of first type after Powers and Breiter [23]) corresponding to the second phase of Sabater and Victori mechanism. This film ensures a partial passivation of Zn, illustrated by the slight decrease of the current. The second anodic peak (corresponding to phase IV Sabater - Victori) appears because of ZnO formation (zinc oxide of second type after Powers and Breiter) which leads to electrode passivation. ZnO is less porous and more adherent than Zn(OH)_2 and thus leads to better passivation. We consider that beside ZnO, other superior nonstoichiometric oxides may appear, contributing to the passivation involving following reactions [22]:



Reactions (22) shows that the Zn(OH)_2 film generated on the electrode may react with OH^- ions that penetrate the pores, generating oxides and peroxides combinations. Generally, the nonstoichiometric compounds may appear following similar reaction schemes.

The existence of zinc peroxyde (ZnO_2) is pointed out in Pourbaix diagram [24] and in the works of Popova et al [25]. Reaction (22) is valid also in the absence of peroxydes. For $y = 0$, one retrieves equation (21). The apparition of peroxydes could be suggested also by the shift of the second anodic peak potential towards more positive values (Table 1) at higher rotation speeds, when OH^- transport is favoured.

The experiments carried out at various rotation speeds of the RDE, showed an increase of the height of peaks 1, 2, 3 and 4 with the rotation speed and the transformation of peak 5 in a plateau. The maintenance of peaks 1-4 even in stirring conditions could be explained by the formation on the electrode surface of adherent, less soluble products which limit the diffusion of electroactive species towards and from the electrode.

The deviation of the exponential dependence of current with potential under potentiodynamic conditions in the anodic dissolution of Zn was generally attributed to mass transport effects [4, 7, 9-11].

The dependences of peak currents, 1 and 2 on $\omega^{1/2}$ are linear, as well as the $(I)^{-1}$ vs. $\omega^{-1/2}$ plots.

The $1/I_1 = f(\omega^{-1/2})$ plot, (Figure 2a) intersects the origin, denoting diffusion control of process when the $1/I_2 = f(\omega^{-1/2})$ plot not intercepting the origin, a mixed control of charge transfer and diffusion in the case of the second anodic process is denoting (Figure 2b).

So, it seems that the second peak corresponds to the formation of a film on electrode surface is controlled both by diffusion and charge transfer.

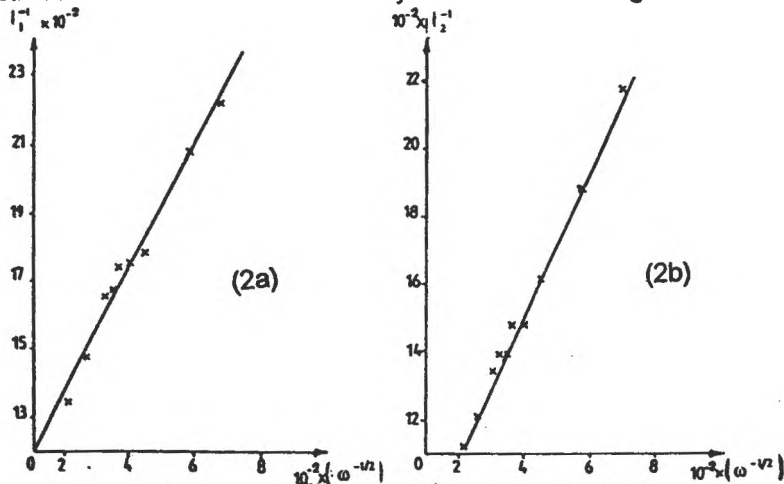


Figure 2. The plots of representations I_1^{-1} versus $\omega^{-1/2}$ (2a) and I_2^{-1} versus $\omega^{-1/2}$ (2b)

With increase of the rotation speed, the relative height and the shape of the peaks 1 and 2 changes; peak 2 becomes dominant at rotation speeds $\omega > 400$ rpm and at $\omega \geq 2000$ rpm, peak 1 changes into a shoulder. (Figure 3).

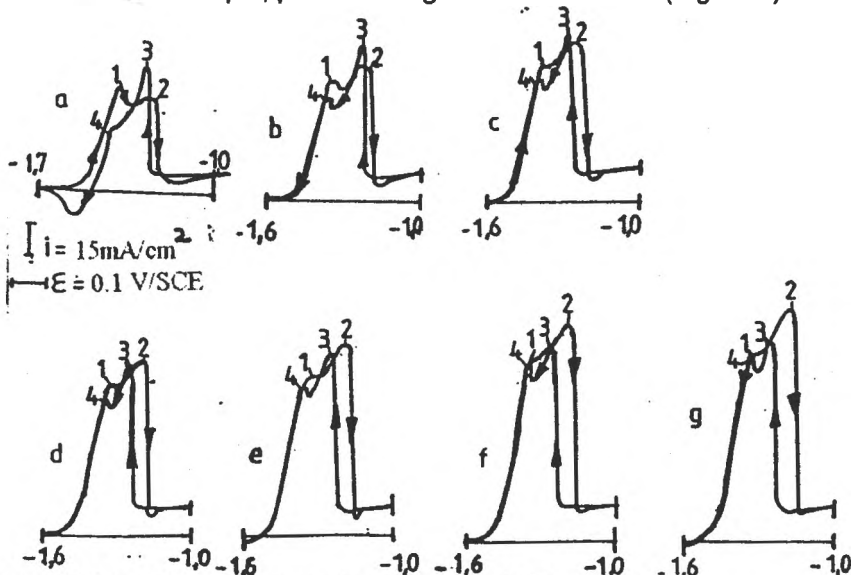


Figure 3. The voltammograms at various ω in KOH 1N solutions.

- a) $\omega = 100$ rpm b) $\omega = 300$ rpm
- c) $\omega = 500$ rpm d) $\omega = 700$ rpm
- e) $\omega = 1000$ rpm f) $\omega = 1500$ rpm
- g) $\omega = 2000$ rpm

At the same time with the increase of peak 1 and 2 at higher rotation speeds, a corresponding increase of peak 3 and 4 takes place, suggesting a correlation between processes 1 and 2 and the non-electrochemical ones, corresponding to peaks 3 and 4. It is plausible that processes 3 and 4 correspond to an arrachement from the electrode surface of less soluble products formed during the anodic scan.

In Table 1, the current and potential values corresponding to the peaks recorded at different rotation speeds of RDE, are presented.

Table 1

The values of currents and potentials for peaks 1, 2, 3, 4, 5, at various ω in 1N KOH solution.

ω (rpm)	i_1 (mA)	E_1 (V/ SCE)	i_2 (mA)	E_2 (V/ SCE)	i_3 (mA)	E_3 (V/ SCE)	i_4 (mA)	E_4 (V/ SCE)	i_5 (mA)	E_5 (V/ SCE)
0	3.70	-1.38	2.70	-1.25	3.70	-1.27	1.10	-1.42	1.05	-1.55
100	4.20	-1.37	3.80	-1.23	5.20	-1.27	2.60	-1.41	0.90	-1.54
200	4.50	-1.37	4.60	-1.22	5.80	-1.25	3.40	-1.40	0.30	-1.55
300	4.80	-1.35	5.32	-1.20	6.00	-1.23	4.00	-1.36	-	-
400	5.50	-1.36	6.20	-1.20	6.70	-1.23	4.90	-1.38	-	-
500	5.30	-1.36	6.20	-1.23	6.50	-1.27	4.80	-1.40	-	-
600	5.70	-1.36	6.75	-1.22	6.80	-1.27	5.30	-1.39	-	-
700	5.75	-1.32	6.75	-1.19	6.70	-1.24	5.30	-1.36	-	-
800	6.00	-1.32	7.20	-1.18	6.90	-1.23	5.65	-1.35	-	-
900	6.05	-1.33	7.20	-1.19	6.90	-1.24	5.70	-1.36	-	-
1000	6.10	-1.33	7.45	-1.18	7.05	-1.23	5.80	-1.36	-	-
1500	6.80	-1.33	8.20	-1.18	7.70	-1.25	6.60	-1.36	-	-
2000	7.45	-1.32	9.00	-1.18	8.00	-1.24	7.35	-1.34	-	-*

Influence of (Li⁺ ions) additives

The addition of 35 g/l LiOH to 1N KOH solutions results in significant changes of the $i - E$ curves registered by RDE. Thus, the first anodic peak is no more clearly delimited and the area of the anodic peaks is much more higher than in absence of Li⁺ ions, while the peak potential values are slightly shifted towards more positive values (figure 4 and table 2). During the cathodic sweep only one anodic peak appears also higher than in the absence of Li⁺ ions.

The important increase of anodic currents in the presence of LiOH shows that this has a strong influence upon the anodic oxidation of zinc. It seems that Li⁺ ions exert a catalytical effect on zinc oxidation, which could be beneficial in Ni - Zn alkaline batteries, because the LiOH addition improve their performances. It is possible that some intercalation of Li in nonstoichiometric ZnO lattice takes

place, leading to more conductive oxide layer, leading to changes in the reactional mechanism.

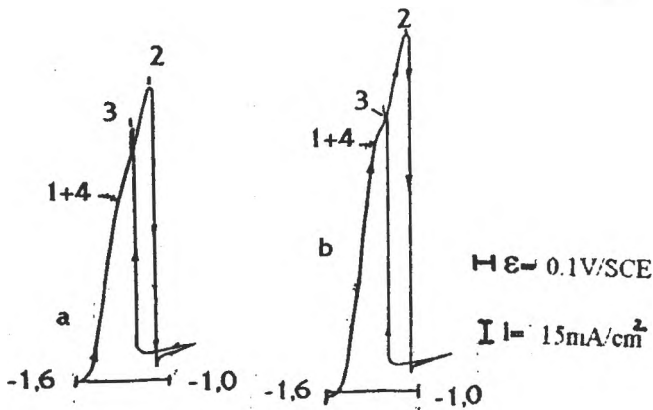


Figure 4. Voltammograms of Zn electrode in KOH 1N + 35 g/l KOH
 a) $\omega = 500$ rpm; b) $\omega = 1000$ rpm

Table 2. The values of currents and potentials for peaks 2 and 3 at $\omega = 500$ rpm, $\nu = 60$ mV/sec.

Nr. crt.	Electrolyte	i_2 (mA)	ϵ_2 (V/SCE)	i_3 (mA)	ϵ_3 (V/SCE)
1	KOH 1N	6.20	-1.23	6.50	-1.27
2	KOH 1N +35 g/l LiOH	18.30	-1.105	15.50	-1.22

It is of interest to mention that the curves recorded in KOH 6N (the same concentration as in the batteries) in the presence of various concentrations of LiOH (Figure 5) exhibit only one anodic peak with different shape during the anodic scan and another during the cathodic one, showing that Zn electrooxidation takes place differently as in KOH 1N. The residual current after passivation decreases with increasing Li^+ concentration and the distance between the two peaks increases, showing that the arrachement of the oxidation products from the electrode surface becomes more difficult while passivation is better.

As a slight increase of anodic peak potential with LiOH concentration takes place, a too high concentration of LiOH in electrolyte is not recommended. At the

same time an increase of solution viscosity with Li^+ ions concentration is mentioned [26].

Therefore, an optimum concentration of 35 g / l Li^+ ions is recommended for use in alkaline batteries.

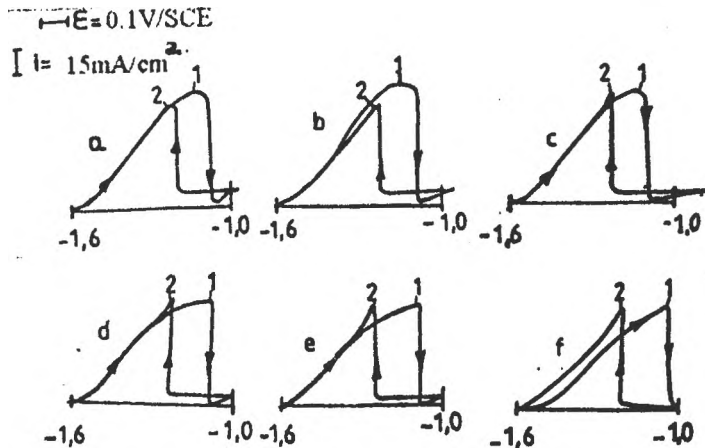


Figure 5. Voltammograms in KOH 6N and various LiOH concentration

- a) KOH 6N; b) KOH 6N + 10g/l LiOH; c) KOH 6N + 20 g/l LiOH
- d) KOH 6N + 35 g/l LiOH; e) KOH 6N + 50 g/l LiOH;
- f) KOH 6N + 70 g/l LiOH

4. Conclusions

The voltammograms recorded on zinc RDE in KOH solutions exhibit several current variations situated in the region corresponding to the transition from active dissolution to passivation.

Four anodic peaks were registered in KOH 1N, two during anodic and two during cathodic scan, and one cathodic peak visible only at $\omega = 0$, which disappears in presence of stirring. The two first anodic peaks were attributed to less soluble oxidation products formation, such as $\text{Zn}(\text{OH})_2$ and ZnO , on the electrode surface. The diffusion of OH^- ions through these more or less soluble compounds especially in conditions of slow stirring, becomes rate determining step and leads to the apparition of above mentioned peaks in the voltammograms. The mechanism changes in KOH 6N.

A beneficial catalytic effect of LiOH was put on evidence which justifies, its use in alkaline Ni - Zn batteries in order to improve their performances.

References

1. J.O'M. Bockris, Z. Nagy , A. Damjanovic
J. Electrochem Soc, 1972, **119**, 285.
2. J. Hendriks. Van Der, Putten, W. Visscher , E. Barendrecht
J. Electrochim Acta 1984, **29**, 81.
3. J. Hendriks, W. Visscher, E. Barendrecht
Electrochim Acta 1985, **30**, 999.
4. P.L. Cabot , M. Cortes, F. Centellas, J.A. Garrido, E. Perez
J. Electroanal Chem. 1986, **201**, 85.
5. R.D. Armstrong G.M. Bulman
J. Electroanal Chem. 1970, **25**, 121.
6. R.D. Armstrong, M.F. Bell
J. Electroanal Chem. 1974, **55**, 201
7. Y.C. C, G. Prentice
J. Electrochem Soc. 1985, **132**, 375.
8. Y.C. Chang G. Prentice
J. Electrochem Soc. 1989, **136**, 3398.
9. M.C.H. Mc Kubre , D.D. Mac Donald
J. Electrochem Soc. 1981, **128**, 524.
10. L.M. Baugh , A. Higginson
Electrochim Acta 1985, **30**, 1163.
11. P.L. Cabot , M. Cortes , F. Centellas , E. Perez
J. of Appl Electrochem 1993, **23**, 371.
12. J.J. Podesta , R.C.V. Piatti , A.J. Arvia
J. Electrochem Soc. 1979, **128**, 1363.
13. M.N. Hull , J.E. Ellison , J.E. Toni
J. Electrochem Soc. 1970, **117**, 192.
14. R.C.V. Piatti , J.J. Podesta , A.J. Arvia
Electrochim Acta 1980, **25**, 827.
15. M. Eisenberg, H.F. Bauman , D.M. Brettner
J. Electrochem Soc. 1961, **108**, 909.
16. M.B. Liu , G.M. Cook , N.P. Yao
J. Electrochem Soc. 1981, **128**, 1663.
17. M.N. Hull J.E. Toni
Trans. Faraday Soc, 1971 **67**, 1128.
18. L.M. Baugh , A.R. Baikie
Electrochim Acta 1985, **30**, 1173.
19. R.D. Armstrong , G.M. Bulman , H.R. Thirsk
J. Electroanal Chem. 1969, **22**, 55.
20. H. Kaesche
Electrochim Acta. 1964, **9**, 383.
21. J. Sabater , L. Victoril
36-th Meeting ISE, Extended Abstracts Salamanca (Spain), 1985,
23-28 sept, 11.230.

22. G. Prentice Y. C. Chang , X. Shan
J. Electrochem Soc. 1991, **138**, 890.
23. R.W. Powers, M.W. Breiter
J. Electrochem Soc. 1969, **116**, 719.
24. M. Pourbaix
"DIAGRAMES" chap. IV. p. 409, 1962
25. T.Y. Popova , N.A. Simonova , B.N. Fabanov
Soviet Electrochem 1967, **3**, 1273.
26. S.Uno Falk , Alvin S. Salkind
"Alcaline Storage Batteries", 1969, Ed. J. WILEY & SONS,
New York p. 517.

În anul de al XLI - an (1996) *STUDIA UNIVERSITATIS BABEȘ-BOLYAI* apare următoarele serii:

matematică (trimestrial)	studii europene (semestrial)
informatică (semestrial)	business (semestrial)
fizică (semestrial)	psihologie-pedagogie (semestrial)
chimie (semestrial)	științe economice (semestrial)
geologie (semestrial)	științe juridice (semestrial)
geografie (semestrial)	istorie (trei apariții pe an)
biologie (semestrial)	filologie (trimestrial)
filosofie (semestrial)	teologie ortodoxă (semestrial)
sociologie (semestrial)	teologie catolică (anual)
politică (anual)	educație fizică (anual)
efemeride (anual)	

In the XLI - year of its publication (1996) *STUDIA UNIVERSITATIS BABEȘ-BOLYAI* is issued in the following series:

mathematics (quarterly)	european studies (semesterily)
computer science (semesterily)	business (semesterily)
physics (semesterily)	psychology - pedagogy (semesterily)
chemistry (semesterily)	economic sciences (semesterily)
geology (semesterily)	juridical sciences (semesterily)
geography (semesterily)	history (three issues per year)
biology (semesterily)	philology (quarterly)
philosophy (semesterily)	orthodox theology (semesterily)
sociology (semesterily)	catholic theology (yearly)
politics (yearly)	physical training (yearly)
ephemerides (yearly)	

Dans sa XLI - e année (1996) *STUDIA UNIVERSITATIS BABEȘ-BOLYAI* paraît les séries suivantes:

mathématiques (trimestriellement)	études européennes (semestriellement)
informatiques (semestriellement)	affaires (semestriellement)
physique (semestriellement)	psychologie - pédagogie (semestriellement)
chimie (semestriellement)	études économiques (semestriellement)
géologie (semestriellement)	études juridiques (semestriellement)
géographie (semestriellement)	histoire (trois apparitions per année)
biologie (semestriellement)	philologie (trimestriellement)
philosophie (semestriellement)	théologie orthodoxe (semestriellement)
sociologie (semestriellement)	théologie catholique (annuel)
politique (annuel)	éducation physique (annuel)
ephemerides (annuel)	

